AD NUMBER

ADB008943

LIMITATION CHANGES

TO:

Approved for public release; distribution is unlimited.

FROM:

Distribution authorized to U.S. Gov't. agencies only; Test and Evaluation; 01 MAR 1975. Other requests shall be referred to Aeronautical Systems Division, ATTN: ASD/XRG, Wright-Patterson AFB, OH 45433.

AUTHORITY

ASD ltr dtd 11 Jun 1980

NUCLEAR AIRCRAFT FEASIBILITY STUDY

VOLUME I. FINAL REPORT

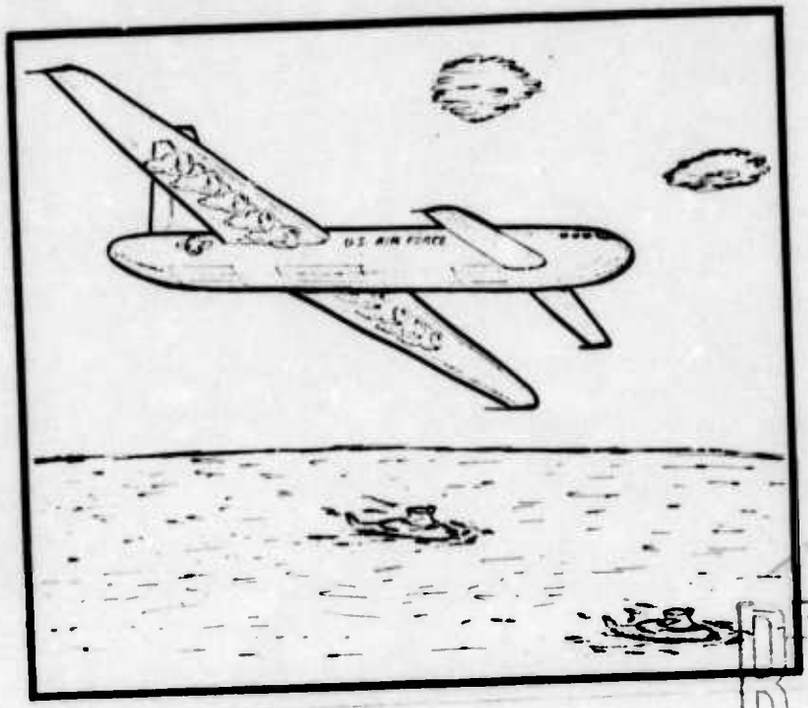

1975
GRADUATE CLASS
OF
SYSTEMS ENGINEERING

MARCH 1975

SCHOOL OF ENGINEERING
AIR FORCE INSTITUTE OF TECHNOLOGY
WRIGHT-PATTERSON AIR FORCE BASE, OHIO

NOTICE

This effort was accomplished for the purposes of illuminating problem areas in the context of a total weapon system concept and assessing the impact of different propulsion system design approaches upon the total aircraft system weight and performance. It was performed as a thesis research effort by AFIT students, and the resultant weapon system design concept is the product of the design constraints selected by the students. The influences of two of these constraints, the fuselage volume alloted per crew member, and the design wing loading are such that the resulting aircraft system size, weight, and power requirements are considerably larger than those obtained during previous in-house studies or those reported by other competent investigators examining similar mission requirements. Thus, it is important to note that the design constraints, subsystem tradeoffs, aircraft configuration selection and subsystem integration tasks were totally accomplished by the students and are, therefore, not to be construed in any way as reflecting the opinion or thinking of the Air Force or the Deputy for Development Planning.

Dr. Larry W. Noggle
ASD/XR (AFSC)
Wright-Patterson AFB OH 45433

ABSTRACT

The objective of this study was to assess the feasibility of applying nuclear propulsion to aircraft in performance of the Air Force mission. This was accomplished by using a systems approach with the system divided into six areas: (1) Mission Selection, (2) Required Mission Avionics, (3) Aircraft Design, (4) Propulsion System Design, (5) Public Safety, and (6) Cost.

From several missions requiring a long endurance aircraft, the antisubmarine warfare (ASW) mission was selected for the purpose of establishing point design parameters. Since the mission avionics package was required to be relatively large, the weight was minimized using a constraint of 0.95 reliability for a 14 day mission. The aircraft was designed utilizing standard aerodynamic design techniques, considering mission constraints but optimizing to require minimum thrust. From the several aircraft configurations analyzed, a canard configuration was chosen for final design consideration. The propulsion system, consisting of the reactor, the heat transfer system, and the engines, was analyzed for various configurations, including liquid metal and gas cooled reactors and indirect and direct cycle engines. A probabilistic risk analysis was performed to determine the hazard to society in terms of deaths caused by radiological exposure. Several cost modeling techniques were coupled with expert opinion to form a probabilistic assessment of the life cycle cost of the point design aircraft.

The overriding constraint of the study was the assumption that technology would limit an aircraft gross weight to 2,000,000 lbs in the 1990s. At this gross weight, an aircraft built using conventional construction methods and powered by a liquid metal cooled nuclear reactor, but using only chemical fuel for takeoff, would have a negative payload of 120,000 lbs. If the aircraft were constructed using advanced composites and a liquid metal cooled reactor with chemical augmentation for takeoff, the payload would be 470,000 lbs. By switching the liquid metal reactor for a similarly constructed helium cooled reactor, the payload would drop from 470,000 lbs to 210,000 lbs. For each individual in the U.S., the risk of being killed by the radioactive particles associated with one of the airborne 574 MW reactors, would be 9.34×10^{-8} per year, which is less risk than that of being struck by lightning. The 62,000 hr airframe life cycle cost was estimated to be $26.4 billion for 60 aircraft.

~~UNCLASSIFIED~~
SECURITY CLASSIFICATION OF THIS PAGE (When Data Entered)

REPORT DOCUMENTATION PAGE

READ INSTRUCTIONS BEFORE COMPLETING FORM

1. REPORT NUMBER: GSE/SE/75-1- Vol-1	2. GOVT ACCESSION NO.
3. RECIPIENT'S CATALOG NUMBER	
4. TITLE (and Subtitle): NUCLEAR AIRCRAFT FEASIBILITY STUDY, (VOL I) Volume I.	5. TYPE OF REPORT & PERIOD COVERED: MASTERS THESIS
6. PERFORMING ORG. REPORT NUMBER	
7. AUTHOR(s): M. W. AMOS, J. S. BUTT, B. L. CAMPBELL, R. G. DIEHL W. J. FANNING, JR., G. M. LACY, R. J. LUCZAK, E. H. HOORMAN, JR., J. W. SHATTUCK, V. K. WILKINSON	8. CONTRACT OR GRANT NUMBER(s): (13) 415 p.
9. PERFORMING ORGANIZATION NAME AND ADDRESS: AIR FORCE INSTITUTE OF TECHNOLOGY (AFIT/EN) WRIGHT-PATTERSON AFB OH 45433	10. PROGRAM ELEMENT, PROJECT, TASK AREA & WORK UNIT NUMBERS: P.E. 6 3737F
11. CONTROLLING OFFICE NAME AND ADDRESS: AERONAUTICAL SYSTEMS DIVISION (ASD/XR) WRIGHT-PATTERSON AFB OH 45433 (11)	12. REPORT DATE: Mar 75
	13. NUMBER OF PAGES: 426
14. MONITORING AGENCY NAME & ADDRESS (if different from Controlling Office): Distribution limited to U.S. Gov't. agencies only; Test and Evaluation; 1 MAR 75. Other requests for this document must be referred to	15. SECURITY CLASS. (of this report): UNCLASSIFIED
	15a. DECLASSIFICATION/DOWNGRADING SCHEDULE

16. DISTRIBUTION STATEMENT (of this Report)

[redacted] of ASD/XR, Wright-Patterson AFB OH 45433.

17. DISTRIBUTION STATEMENT (of the abstract entered in Block 20, if different from Report)

Approved for public release; distribution unlimited.

(9) Final rept. 1 Mar 74—7 Feb 75

18. SUPPLEMENTARY NOTES

(10) Michael W. /Amos, James S. /Butt, Bruce L. /Campbell, Richard G. /Diehl, William J. /Fanning, Jr

19. KEY WORDS (Continue on reverse side if necessary and identify by block number)

Nuclear propulsion, fault tree analysis, event tree analysis, heat transfer, life cycle cost, nuclear aircraft, weight estimation, anti-submarine, reactor power, large aircraft design, long endurance aircraft, nuclear safety, helium cooled reactor, liquid-metal cooled reactor.

20. ABSTRACT (Continue on reverse side if necessary and identify by block number)

The objective of this study was to assess the feasibility of applying nuclear propulsion to aircraft in performance of the Air Force mission. This was accomplished by using a systems approach with the system divided into six areas: (1) Mission Selection, (2) Required Mission Avionics, (3) Aircraft Design, (4) Propulsion System Design, (5) Public Safety, and (6) Cost.

The overriding constraint of the study was the assumption that technology would limit an aircraft gross weight to 2,000,000 lbs in the 1990s. At this

DD FORM 1 JAN 73 1473 EDITION OF 1 NOV 65 IS OBSOLETE

UNCLASSIFIED
SECURITY CLASSIFICATION OF THIS PAGE (When Data Entered)

012225

gross weight, an aircraft built using conventional construction methods and powered by a liquid metal cooled nuclear reactor, but using only chemical fuel for takeoff, would have a negative payload of 120,000 lbs. If the aircraft were constructed using advanced composites and a liquid metal cooled reactor with chemical augmentation for takeoff, the payload would be 470,000 lbs. By switching the liquid metal reactor for a similarly constructed helium cooled reactor, the payload would drop from 470,000 lbs to 210,000 lbs. For each individual in the U.S., the risk of being killed by the radioactive particles associated with one of the airborne 574 MW reactors, would be 9.34×10^{-8} per year, which is less risk than that of being struck by lightning. The 62,000 hr airframe life cycle cost was estimated to be $26.4 billion for 60 aircraft.

TABLE OF CONTENTS

Section			Page
Abstract			
Table of Contents			i
List of Figures			vii
List of Tables			xiii
Preface			xvii
1	INTRODUCTION		1-1
	1.1	Background	1-1
	1.2	Objective	1-1
	1.3	Approach	1-1
2	MISSION		2-1
	2.0	Background	2-1
	2.1	Mission Requirements	2-1
3	AVIONICS		3-1
	3.0	Introduction	3-1
		3.0.1 Background	3-1
		3.0.2 Statement of Problem	3-1
		3.0.3 Symbols	3-1
	3.1	Method of Analysis	3-2
		3.1.1 System Definition	3-2
		3.1.2 Estimation of System Parameters	3-4
	3.2	Results	3-12
		3.2.1 System Definition	3-12
		3.2.2 Estimation of Total System Parameters	3-23
	3.3	Conclusions	3-28
		3.3.1 Redundancy	3-28
		3.3.2 Alternatives to Redundancy	3-29
		3.3.3 Recommendations for Additional Study	3-29
4	AIRCRAFT		4-1
	4.0	Introduction	4-1
	4.1	Initial Weight Estimation	4-6
		4.1.1 Structural Weight	4-7
		4.1.2 Chemical Engine Weight	4-7
		4.1.3 Chemical Fuel Weight	4-10
		4.1.4 Fixed Equipment Weight	4-12
		4.1.5 Nuclear Propulsion System Weight	4-12
		4.1.6 Payload	4-16
		4.1.7 Initial Weight Estimation Results	4-20
	4.2	Aircraft Configuration	4-22
		4.2.1 Candidate Configurations	4-22
		4.2.2 Configuration Selection	4-28

TABLE OF CONTENTS (Continued)

4.3 Sizing Analysis 4-28
4.3.1 Tail/Canard Surfaces 4-30
4.3.2 Structural Component Weights 4-32
4.3.3 Composite Weight Savings 4-34
4.3.4 Wing 4-36
4.3.5 Fuselage 4-49
4.3.6 Reactor Mounting 4-49
4.3.7 Landing Gear 4-56
4.3.8 Sizing Results 4-57
4.4 Aircraft Performance 4-61
4.4.1 Takeoff Requirements 4-62
4.4.2 Climb Requirements 4-62
4.4.3 Service Ceiling 4-63
4.4.4 Cruise Performance 4-64
4.4.5 Descent 4-67
4.4.6 Landing 4-68
4.4.7 Aircraft Performance 4-70
4.5 Aircraft Recommendations 4-71
4.5.1 Chemical Capability 4-71
4.5.2 Composite Weight Savings 4-71
4.5.3 Reactor Mounting and Ground Handling 4-71
4.5.4 Aircraft Landing Systems 4-72
4.5.5 Aircraft Configuration 4-72
5 NUCLEAR REACTOR 5-1
5.0 Introduction 5-1
5.0.1 Approach 5-1
5.0.2 Technology 5-1
5.1 Reactor Design Requirements 5-3
5.1.1 Power Requirements 5-3
5.1.2 Environmental Requirements 5-3
5.2 Reactor Designs 5-4
5.2.1 Westinghouse High Temperature Gas Reactor (WHTGR) 5-4
5.2.2 Mills High Temperature Gas Reactor (MHTGR) 5-10
5.2.3 Westinghouse Liquid Metal Reactor 5-13
5.3 Evaluation of the Reactors 5-15
5.3.1 Environmental Effects 5-15
5.4 Potential Weight Savings 5-23
5.4.1 Separation Distance 5-23
5.4.2 Crew Ratio 5-26

TABLE OF CONTENTS (Continued)

6 ENGINES 6-1
6.0 Introduction 6-1
6.0.1 Background 6-1
6.0.2 Propulsion Concepts 6-2
6.0.3 Safety 6-4
6.0.4 State-of-the-Art Assessment 6-4
6.0.5 Nuclear Cycles 6-4
6.0.6 Nuclear Powered Engines System Concepts 6-6
6.0.7 Design Constraints 6-9
6.1 Indirect Cycle 6-11
6.1.1 Cycle Analysis 6-11
6.1.2 Overall Engine Pressure Ration (R_p) 6-16
6.1.3 Bypass Ratio 6-16
6.1.4 Horsepower Requirements 6-18
6.1.5 Pressure Losses 6-20
6.1.6 Core Mass Flow ($\dot{m}_c$) 6-20
6.1.7 Turbine (T_{t4}) and Bypass Stream (T_{ef}) Temperatures 6-22
6.1.8 Engine Sizing 6-24
6.1.9 Off-Design Considerations 6-29
6.1.10 Results and Recommendations 6-32
6.2 Direct Cycle 6-36
6.2.1 Regenerative Cycle 6-36
6.2.2 Helium Mass Flow 6-42
6.2.3 Fan Pressure Ratio 6-42
6.2.4 Regenerative Cycle Application 6-43
6.2.5 Brayton Cycle Application 6-46
6.2.6 Central Turbine System 6-49
6.2.7 System Sizing 6-50
6.2.8 Primary and Secondary Loop Turbine Pumps 6-51
6.2.9 Results 6-55
6.3 Summary 6-56
6.3.1 Results 6-56
6.3.2 Conclusions 6-58
6.3.3 Recommendations 6-59
7 HEAT TRANSFER 7-1
7.0 Introduction 7-1
7.0.1 Heat Transfer Systems Descriptions 7-4
7.0.2 Point Design Selection 7-7
7.1 Heat Transfer Fluid Parameters 7-8
7.1.1 Helium 7-8
7.1.2 NaK Indirect Cycle 7-15

TABLE OF CONTENTS (Continued)

7.2 The Reactor Heat Exchanger 7-16
7.2.1 Design Parameters of Reactor Heat Exchanger 7-17
7.2.2 Liquid Metal Reactor Heat Exchanger 7-23
7.3 Piping Specifications 7-24
7.3.1 Two Pipe Configuration 7-25
7.3.2 Concentric Configuration 7-27
7.4 Engine Heat Exchangers 7-30
7.4.1 Indirect Cycle Heat Exchangers 7-30
7.4.2 Direct Cycle Heat Exchangers 7-49
7.5 Working Fluid Circulation 7-54
7.5.1 Primary Loop Pumping System Heat Exchangers 7-56
7.5.2 Secondary Loop Pumping System Heat Exchangers 7-58
7.5.3 Pumping System Summary 7-60
7.6 Fast Acting Valves 7-61
7.6.1 Design Parameters 7-62
7.6.2 Design Proposals 7-63
7.6.3 Orifice Reduction to Save Weight 7-66
7.6.4 Summary 7-67
7.7 Results and Comparisions 7-68
7.7.1 Conclusions 7-70
7.7.2 Areas Recommended for Further Study 7-70
8 SAFETY ANALYSIS 8-1
8.0 Introduction 8-1
8.0.1 Background 8-1
8.0.2 Objective 8-1
8.0.3 Overview of Methodology 8-1
8.1 Release Probability 8-2
8.1.1 Event Trees 8-2
8.1.2 Fault Trees 8-4
8.1.3 Impact Event Tree 8-8
8.1.4 Transient Event Tree 8-28
8.1.5 Loss of Coolant 8-36
8.1.6 Total Release Probabilities 8-36
8.1.7 Application of Results to a Liquid-Metal Cooled System 8-38
8.2 Consequence Model 8-39
8.2.1 Magnitude of Release 8-40
8.2.2 Dispersion Model 8-44
8.2.3 Evacuation 8-49
8.2.4 Health Effects Model 8-50
8.2.5 Population Density Model 8-57

TABLE OF CONTENTS (Continued)

8.2.6 Risk Comparison 8-59
8.2.7 Sensitivity 8-60
8.3 Conclusions and Recommendations 8-61
8.3.1 Conclusions 8-61
8.3.2 Recommendations 8-61
8.4 Summary 8-62
9 LIFE CYCLE COST 9-1
9.0 Introduction 9-1
9.1 Methodology 9-2
9.1.1 Cost Estimating Techniques 9-2
9.1.2 SIMPAK Computer Program 9-4
9.2 Airframe 9-5
9.3 Propulsion 9-9
9.3.1 Fossil Fueled Engines 9-9
9.3.2 Nuclear Engines 9-10
9.4 Reactor 9-14
9.5 Isolation Safety Valve 9-15
9.6 Avionics 9-16
9.7 Flyaway Cost 9-16
9.8 Total Recurring Cost 9-18
9.9 Initial Spares, Peculiar Support, and Training Equipment 9-19
9.10 Procurement Cost 9-20
9.11 Research, Development, Test, and Evaluation 9-20
9.12 Acquisition Cost 9-23
9.13 Ten Year Operating and Support Cost 9-23
9.14 Life Cycle Cost 9-28
10 SUMMARY 10-1
10.1 Background 10-1
10.1.1 Mission (Section 2) 10-2
10.1.2 Avionics (Section 3) 10-3
10.1.3 Aircraft (Section 4) 10-4
10.1.4 Reactor (Section 5) 10-10
10.1.5 Engines (Section 6) 10-13
10.1.6 Heat Transfer (Section 7) 10-16
10.1.7 Safety (Section 8) 10-19
10.1.8 Life Cycle Cost (Section 9) 10-20
10.2 Weapon System 10-21
10.2.1 Propulsion System 10-21
10.2.2 Total Aircraft System 10-23
10.2.3 Mission Application 10-25

TABLE OF CONTENTS (Continued)

10.3 Conclusions and Recommendations 10-26
10.3.1 Avionics 10-26
10.3.2 Reactor 10-27
10.3.3 Nuclear Propulsion System 10-27
10.3.4 Chemical Propulsion System 10-28
10.3.5 Payload 10-29
10.3.6 Safety 10-29
Bibliography B-1

LIST OF FIGURES

Figure		Page
3.1.1.2-1	Avionic System Definition	3-4
3.1.2.2-1	Assumed Failure Distribution	3-6
3.1.2.2-2	Parallel Components Model	3-7
3.1.2.2-3	Series-Parallel Model	3-9
3.2.1.2-1	Avionic Categories	3-14
3.2.1.3-1	Common Functional Areas	3-14
3.2.1.3-2	Navigation Subsystems	3-15
3.2.1.3-3	Mission Traffic and Control Subsystems	3-16
3.2.1.3-4	Instruments and Aircraft Systems Subsystems	3-16
3.2.1.3-5	Controls and Displays Subsystems	3-17
3.2.1.3-6	Tactical Functional Areas	3-18
3.2.1.3-7	Penetration Aids Subsystems	3-18
3.2.1.3-8	Sensor Subsystems	3-19
3.2.1.3-9	Power Generation Subsystems	3-20
3.2.2.1-1	Avionic System Weight vs Mission Length	3-25
3.2.2.1-2	Redundancy Required to Meet System Reliability and Mission Length	3-26
3.2.2.2-1	Avionics Volume vs Mission Length	3-27
3.2.2.3-1	Power Requirements	3-28
4.0-1	Design Tasks Relationship	4-1
4.0-2	Aircraft Design Methodology	4-3
4.1.1-1	Structural Weight as a Function of Gross Weight	4-8
4.1.2.1-1	Takeoff Chart: Thrust Loading as Determined by Takeoff Distance	4-9
4.1.2.1-2	Structural Weight/Takeoff Thrust as a Function of Gross Weight	4-11
4.1.2.1-3	Takeoff Thrust/Structural Weight as a Function of Wing Loading	4-11
4.1.5.1-1	Thrust and L/D as a Function of Wing Loading	4-14
4.1.5.1-2	Thrust and L/D as a Function of Wing Loading	4-14
4.1.5.1-3	L/D as a Function of Velocity and Wing Loading	4-15
4.1.5.1-4	L/D as a Function of Velocity and Wing Loading	4-15
4.1.5.2-1	Reactor System Weight vs Reactor Power	4-17
4.1.6-1	Payload vs Wing Loading	4-17
4.1.6-2	Payload vs Wing Loading	4-18
4.1.6-3	Payload vs Wing Loading — Gas Reactor	4-18
4.1.6-4	Payload vs Wing Loading — Liquid metal Reactor	4-19
4.1.6-5	Payload vs Gross Weight	4-19
4.1.6-6	Payload as Percent of Gross Weight	4-20
4.1.7.2-1	Aircraft Weight Trends	4-21
4.2.1.1-1	Conventional Aircraft	4-23
4.2.1.2-1	Straight Wing Canard	4-24
4.2.1.2-2	Sweep Aft Canard	4-25

LIST OF FIGURES (Continued)

4.2.1.2-3	Sweep Forward Canard	4-25
4.2.1.3-1	Flying Wing	4-26
4.2.1.4-1	Twin Body Aircraft	4-27
4.2.2-1	Point Design Configuration	4-29
4.3.1.1-1	Canard Area	4-30
4.3.1.2-1	Vertical Tail Area	4-31
4.3.4-1	NACA Airfoil Sections	4-36
4.3.4.2-1	Lift Distribution	4-38
4.3.4.3-1	Wing Loading	4-38
4.3.4.4-1	Wing Beam Loading, Shear Force, Bending Moment	4-39
4.3.4.4-2	Shear Loads	4-40
4.3.4.4-3	Bending Moments	4-40
4.3.4.5-1	Beam Section Envelopes	4-41
4.3.4.5-2	Beam Section Notation	4-42
4.3.4.5-3	Beam Cap Thickness	4-43
4.3.4.5-4	Beam Cap Area	4-43
4.3.4.7-1	Geometry for Divergence Speed Calculation	4-46
4.3.4.7-2	Multhopp Wing Stations	4-47
4.3.4.7-3	Divergence Speeds	4-48
4.3.6-1	Trunnion Arrangement	4-51
4.3.6-2	Truss Framework	4-52
4.3.6-3	Shear Beam Analysis	4-54
4.3.8.2-1	Point Design Configuration	4-60
4.4.2-1	Airplane Forces in Level and Climbing Flight	4-62
4.4.3-1	Rate of Climb and Total Required Thrust vs Altitude	4-63
4.4.4-1	L/D Curve	4-64
4.4.4-2	Drag Curve	4-64
4.4.4-3	Cruise Speed vs Altitude	4-65
4.4.4.3-1	Stall Speed/Maximum Speed vs Altitude	4-67
4.4.5-1	Airfoil with Speed Brakes Open ϕ Degrees	4-68
4.4.6-1	Flight Path in Landing	4-69
4.4.7-1	Nuclear Powered Aircraft Performance — 2,000,000 lbs Gross Weight	4-70
5.2.1-1	Preliminary Drawing — WHTGR	5-4
5.2.1-2	WHTGR Temperature vs Heat Exchanger Temperature	5-5
5.2.1-3	WHTGR Reactor Power vs Reactor Weight	5-6
5.2.1-4	WHTGR Reactor Power vs Reactor Weight	5-6
5.2.1-5	WHTGR Reactor Power vs Reactor Weight	5-7
5.2.1-6	WHTGR/Reactor Power vs Outer Diameter	5-7
5.2.1-7	WHTGR Reactor Power vs Outer Diameter	5-8
5.2.1-8	WHTGR Reactor Power vs Outer Diameter	5-8
5.2.1-9	Westinghouse Revised Reactor System Weight vs Reactor Power	5-9
5.2.2-1	Cutaway Drawing of MHTGR	5-10

LIST OF FIGURES (Continued)

5.2.2.1-1	MHTGR Reactor Power vs Reactor Weight	5-14
5.3.1.1-1	Flights per Year	5-16
5.3.1.2-1	Total Dose as a Function of Distance from Full Power Reactor	5-20
5.3.1.2-2	Geometric Model	5-21
5.4.1-1	Spheroid Volume	5-25
6.0.2-1	Three Basic Engine Concepts	6-3
6.0.2-2	Comparison of Turboprop, Turbofan, and Turbojet Air Mass-Velocity Relationship	6-4
6.0.5-1	Open Cycle Air Turboprop	6-5
6.0.5-2	Closed Cycle Turbofan	6-6
6.0.6-1	Indirect Cycle, Heat Exchanger Turbofan Engine	6-6
6.0.6-2	Closed Loop Independent Turbine System with Helium Expanded Directly Over the Turbine	6-8
6.0.6-3	Direct Cycle Central Turbine Ducted Fan	6-8
6.0.6-4	Engine Systems Summary	6-9
6.1.1-1	T-S Diagram of Ideal Brayton Cycle	6-13
6.1.1-2	T-S Diagram of Brayton Cycle for Turbofan Engine	6-15
6.1.2-1	Comparison of Thrust for Various Overall Engine Pressure Ratios and Fan Pressure Ratio for Bypass Ratio = 4.0 and a Core Mass of 200 lbs/sec	6-17
6.1.3-1	Comparison of Net Thrust for Various Bypass Ratios Having an Overall Engine Pressure Ratio = 16.8 and Core Mass Flow of Air = 200 lbs/sec	6-18
6.1.4-1	Net Thrust as a Function of Horsepower Extracted Off the Engine for Various Fan Pressure Ratios; Bypass Ratio = 4.0 with an Overall Engine Pressure Ratio of 16.8 and a Core Mass Flow of 200 lbs/sec	6-19
6.1.5-1	Pressure Loss Effects of Net Thrust Where Bypass Ratio = 4.0, Overall Engine Pressure Ratio = 16.8, Fan Pressure Ratio = 1.6, and Core Mass Flow is 200 lbs/sec	6-20
6.1.6-1	Comparison of Increased Mass Flow of Air through the Core on Net Thrust for Various Fan Loading and Overall Engine Pressure Ratios, with Bypass Ratio = 4.0	6-21
6.1.6-2	Effect of Horsepower Extraction on Net Thrust Where Bypass Ratio = 3.0, Core Mass Flow is 250 lb/sec, and Overall Engine Pressure Ratio is 16.8	6-22
6.1.6-3	Pressure Loss Effects on High Core Mass Flow Engine Thrust with Overall Engine Pressure Ratio = 16.8, Bypass Ratio = 3.0 ($\dot{m}_c$ = 250 lbs/sec), 4.0 ($\dot{m}_c$ = 200 lbs/sec)	6-23
6.1.7-1	Turbine Inlet Temperature Effects on Thrust Where Bypass Ratio = 4.0, Fan Pressure Ratio = 1.4, and Overall Engine Pressure Ratio is 16.8	6-24
6.1.7-2	Bypass Heat Addition	6-25

LIST OF FIGURES (Continued)

6.1.8-1	Mass Flow per Unit Frontal Area as a Function of Mach Number and Hub-Tip Radius	6-26
6.1.8-2	Functional Relationship Between Mass Flow and Fan Diameter	6-27
6.1.8-3	Sea Level Static Thrust-to-Weight Relationship	6-28
6.1.9-1	Mach Number and Inlet Air Mass Flow for Various Altitudes Based on Bypass Ratio = 4.0 at 30,000 ft and Core Mass Flow of 200 lbs/sec	6-29
6.1.9-2	Off-Design Method of Analysis	6-30
6.1.9-3	Thrust vs Altitude for Off-Design Analysis	6-31
6.1.10-1	Effects of Three Engine Parameters on Net Thrust	6-33
6.1.10-2	Effects of Three Engine Parameters on Net Thrust	6-34
6.2.1-1	Regenerative Cycle	6-37
6.2.1-2	Schematic of Regenerative System	6-38
6.2.1-3	Pressure Ratio and Thermal Efficiency of Regenerative Cycle	6-40
6.2.1-4	Pressure Ratio Function vs Mass Flow of Air	6-42
6.2.4-1	Thrust as a Function of Compressor and Regenerator Temperatures	6-44
6.2.4-2	Net Thrust for Ideal Cycle Analysis	6-45
6.2.4-3	Optimum Fan Pressure Ratio for Maximum Net Thrust Within Given Temperature Limitations	6-46
6.2.4-4	Regenerative Cycle Designed with T_{t1} = 500 R	6-47
6.2.4-5	Regenerative Cycle Designed with T_{t1} = 700 R	6-48
6.2.4-6	Thrust as a Function of Pressure Ratio and Work/lb (Thrust Based on 70 lbs/sec of Helium and Fan Pressure Ratio of 1.6)	6-49
6.2.5-1	Brayton Closed Cycle Thermodynamic Analysis	6-50
6.2.8-1	Indirect Cycle Gas Circulation System	6-53
6.2.8-2	Gas Turbine Generator — Pump Cycle Analysis	6-54
7.0.1-1	Energy Flow	7-4
7.0.1.1-1	Two-Loop Indirect Cycle System	7-5
7.0.1.2-1	Two-Loop Direct Cycle System	7-6
7.1.1.1-1	Helium Parameters	7-13
7.1.1.2-1	Direct Cycle	7-13
7.1.1.2-2	Direct Cycle Helium Parameters	7-14
7.1.2-1	NaK Parameters	7-15
7.2-1	Reactor Heat Exchanger Core	7-16
7.2.1.1-1	Effectiveness for Cross-Flow Exchanger with Fluids Unmixed (Ref. 74, p. 313)	7-21
7.3.1-1	Pipe Velocity vs Pipe Weight and Pump Power	7-25
7.3.2-1	Concentric Pipe Cross Section	7-28
7.4.1.1-1	Wraparound Heat Exchanger Assembly (Ref. 111, p. 69)	7-31
7.4.1.1-2	Cross-Counterflow Arrangements with Two Passes on the NaK Side (Ref. 111, p. 95)	7-32
7.4.1.1-3	Geometry of Helical Disc Fins on Round Tubes (Ref. 111, p. 97)	7-33

LIST OF FIGURES (Continued)

7.4.1.1-4	Cross Sectional View of U-Tube Arrangement (Ref. 111, p. 29)	7-34
7.4.1.1-5	Air Flow through Nuclear Engine (Ref. 111, p. 269)	7-35
7.4.1.1-6	Nuclear Turbofan Engine Layout Showing Heat Exchanger Manifolds (Ref. 111, p. 69)	7-36
7.4.1.2-1	Helium Heat Exchanger Engine	7-37
7.4.1.2-2	Section of Heat Exchanger Looking in Direction of Air Flow	7-39
7.4.1.2-3	Effectiveness — N_{tu} Relationship (Ref. 87, p. 51)	7-42
7.4.1.2-4	Capacity Ratio Variations	7-43
7.4.1.2-5	Air Mass Flow Variations	7-44
7.4.1.2-6	Schematic of Shaped Inlet Header with a Box Exit Header	7-46
7.4.1.2-7	Mass Flow Air (lbs/sec)	7-46
7.4.2-1	Direct Cycle System Engine	7-50
7.4.2.1-1	Precooler	7-53
7.5.1-1	Primary Loop Pumping System	7-56
7.5.1-2	Reactor Heat Exchanger Temperatures	7-57
7.5.2-1	Indirect Cycle Engine and Secondary Loop Pumping System	7-59
7.6-1	Sandia's Proposed Design (Ref. 154)	7-62
7.6.2-1	Proposed Slide Valve	7-63
7.6.2-2	Proposed Pin Valve	7-64
7.6.3-1	Resistance Due to Sudden Enlargements and Contractions (Ref. 35, A26)	7-68
7.6.4-1	Valve Weight as a Function of Pipe Size	7-69
8.1.1-1	Event Tree Construction	8-3
8.1.2-1	Fault Tree Construction	8-5
8.1.2-2	Typical Failure Rate Pattern of Complex Equipments	8-6
8.1.2-3	Fault Tree Solution	8-7
8.1.3.2-1	Electrical Power Failure Fault Tree	8-9
8.1.3.3-1	Pre-Impact Sensing Fault Tree	8-11
8.1.3.4-1a	Reactor Shutdown Fault Tree	8-12
8.1.3.4-1b	Reactor Shutdown Fault Tree	8-13
8.1.3.4-1c	Reactor Shutdown Fault Tree	8-14
8.1.3.4-1d	Reactor Shutdown Fault Tree	8-15
8.1.3.4-2	Reactor Control	8-16
8.1.3.5-1	Safety Valve Fault Tree	8-18
8.1.3.8-1	Impact Event Tree	8-28
8.1.4.2-1	Electrical System Fault Tree	8-29
8.1.4.6-1	Transient Event Tree	8-37
8.2.2-1	Cloud Expansion Stability Classification: Pasquill F	8-45
8.2.2-2	Standard Deviation of the Vertical Concentration Distribution, σ_z, as a Function of Travel Distance from a Continuous Source (A-F are Pasquill's Diffusion Categories) (Ref. 160, p. 409)	8-46
8.2.2-3	Cloud Concentration Corrected for Deposition	8-49

LIST OF FIGURES (Continued)

8.2.2-4	Cloud Concentration Corrected for Deposition (Pasquill Stability Classification F)	8-50
8.2.4-1	Assumed Probability Distribution for Fatalities vs Radioactive Dose	8-51
8.2.4-2	Cumulative Whole Body Dose for the 4500 Meter Interval	8-56
9.0-1	Cost Outline	9-2
9.1-1	Relation of Weapon System Stage to Input and Estimating Methods	9-3
9.2-1	C-5A Total Program Cost vs Quantity	9-6
9.3.1-1	Production Cost for Fossil Fueled Engines in $74 vs Quantity	9-10
9.3.2-1	Production Cost for Nuclear Engines in $74 vs Quantity	9-11
9.3.2-2	Cost of Nuclear Engine Heat Exchangers for Liquid Sodium System vs Quantity	9-13
9.7-1	Flyaway Cost in Millions of $74 vs Cumulative Probability	9-18
9.8-1	Total Recurring Cost (Flyaway Cost for 60 Aircraft) in Billions of $74 vs Cumulative Probability	9-19
9.10-1	Procurement Cost in Billions of $74 vs Cumulative Probability	9-21
9.12-1	Acquisition Cost in Billions of $74 vs Cumulative Probability	9-23
9.14-1	Ten Year Life Cycle Cost for 60 Production Nuclear Aircraft vs Cumulative Probability	9-28
10.1.2-1	Redundancy Required to Meet System Reliability and Mission Length	10-4
10.1.3-1	Nuclear Powered Aircraft — C-5A Comparison	10-8
10.1.3-2	Nuclear Powered Aircraft Performance — 2,000,000 lbs Gross Weight	10-9
10.1.4-1	Number of Flights vs Distance from Reactor	10-12
10.1.4-2	3.5 Mrem/Hr Iso Dose	10-12
10.1.4-3	Absorption Cross Section Ratio	10-14
10.1.5-1	Engine Systems Study Diagram	10-15
10.1.8-1	Life Cycle Cost for 60 Nuclear Aircraft — Cumulative Probability	10-21

LIST OF TABLES

Table		Page
2.1-1	Aircraft Parameters	2-2
3.0.3-1	List of Symbols	3-2
3.1.1.1-1	System Definition Assumptions	3-3
3.1.2.1-1	System Parameter Estimate Assumptions	3-5
3.2.1.4-1	Avionic Components and Parameters	3-21
3.2.2-1	Avionic Requirements for a 0.95 Reliable System 14 Day Mission	3.24
4.0-1	Aircraft Parameters	4-2
4.0-2	Symbols List	4-4
4.2.2-1	Configuration Comparison	4-28
4.3.3-1	Candidate Airframe Structural Materials (Ref. 2, p. 752)	4-34
4.3.3-2	Possible Structural Weight Reduction with Composite Materials (Ref. 2, p. 753)	4-35
4.3.4.6-1	Preliminary Design Weight Estimate (lbs)	4-45
4.3.4.7-1	Divergence Speed Results	4-48
4.3.7.1-1	Aircraft Tire Summary	4-56
4.3.7.2-1	Landing Gear Strut Summary	4-57
4.3.8.1-1	Possible Structural Weight Reduction with Composite Materials	4-58
4.3.8.1-2	Aircraft Weight and Balance Summary — 2,000,000 lbs Gross Weight	4-59
4.3.8.2-1	Aircraft Dimensions and Configuration — 2,000,000 lbs Gross Weight	4-61
5.2.1-1	Component Weights for a 275 MW(th) WHTGR	5-9
5.2.1-2	Westinghouse High Temperature Gas Reactor — Gamma Radiation Data (Ref. 175)	5-10
5.2.2-1	Component Weights for a 200 MW(th) MHTGR	5-11
5.2.2-2	Dimensions of MHTGR	5-11
5.2.2-3	Mills High Temperature Gas Reactor Gamma Radiation Data (Ref. 122, p. 133)	5-11
5.2.2.1-1	MHTGR Weight Estimation at 200 MW(th)	5-12
5.2.2.1-2	MHTGR Weight Estimation at 574 MW(th)	5-14
5.2.2.1-3	MHTGR Weight Estimation at 700 MW(th)	5-14
5.3.1-1	Reactor Radiation Data	5-15
5.4.1-1	WHTGR Weight Estimation for 275 MW(th)	5-25
5.4.1-2	WHTGR Weight Estimation for 700 MW(th)	5-26
5.4.1-3	WHTGR Weight Estimation for 700 MW(th) Reduced Shielding	5-26
5.4.1-4	MHTGR Weight Estimation for 700 MW(th) Reduced Shielding	5-27
6.0.1-1	Table of Symbols	6-1
6.0.4-1	State-of-the-Art Assessment of Present Engine Concepts	6-5
6.0.6-1	Comparison of Dedicated vs Dual-Mode Nuclear Powered Engines	6-7

LIST OF TABLES (Continued)

6.0.7-1	Design Constraints	6-10
6.1.10-1	Effects of Engine Parameter Variation on the Net Thrust of the Heat Exchanger Turbofan Engine	6-35
6.1.10-2	Summary of Engine Design Parameters	6-36
6.2.7-1	Engine System Weight Comparison	6-52
6.2.8-1	Turbine-Pump Parameters	6-55
6.2.9-1	Regenerative Engine Parameters	6-56
6.3.1-1	Engine System Summary	6-58
7.0-1	Symbols List	7-2
7.1.2-1	Physical Properties of Helium and NaK	7-15
7.2.1.1-1	Core Geometry Specifications	7-18
7.2.1.1-2	Heat Exchanger Parameters	7-22
7.3.2-1	Pipe Parameter Summary	7-29
7.4.1.1-1	Heat Exchanger Construction Parameters (Ref. 111, p. 33)	7-35
7.4.1.2-1	Heat Transfer Parameters	7-47
7.4.1.2-2	Helium Side Pressure Drop	7-48
7.4.1.2-3	Gas Heat Exchanger Weights (lbs)	7-49
7.4.1.2-4	Parameters for Two Assembly High Temperature Helium Gas Heat Exchanger	7-49
7.4.2.1-1	Recuperator Specifications	7-50
7.4.2.1-2	Precooler Parameters	7-52
7.4.2.1-3	Precooler Weights (lbs)	7-53
7.4.2.1-4	Heat Transfer Parameters	7-53
7.4.2.1-5	Pressure Drops (psi)	7-53
7.4.2.2-1	Precooler Specifications	7-54
7.4.2.2-2	Recuperator Specifications	7-54
7.5-1	Pump Power Required	7-55
7.5.1-1	Primary Pump System Recuperator Parameters	7-57
7.5.1-2	Primary Pump System Precooler Parameters	7-58
7.5.2-1	Secondary Pump System Recuperator Parameters	7-59
7.5.2-2	Secondary Pump System Precooler Parameters	7-60
7.5.3-1	Pump Power and Weight Requirements	7-60
7.6.2-1	Slide Valve and Pin Valve Results for 10 in. Diameter Fluid Line	7-65
7.7-1	Weight and Power Comparisons	7-70
8.1.3.1-1	Crash Probability Distribution per Flight	8-8
8.1.3.2-1	Electrical Power Failure Probability Distribution	8-10
8.1.3.3-1	Pre-Impact Sensing Failure Probability Distribution	8-11
8.1.3.4-1	Reactor Shutdown Failure Probability Distributions	8-17
8.1.3.5-1	Safety Valve Failure Probability Distribution	8-19
8.1.3.6-1	Impact Integrity Failure Probability Distribution	8-22

LIST OF TABLES (Continued)

8.1.3.7-1	Post-Impact Integrity Failure Probability Distribution	8-25
8.1.3.8-1	Impact Event Tree Sequence Probabilities	8-26
8.1.4.1-1	Transient Probability Distribution	8-28
8.1.4.2-1	Electric Power Failure Probability Distribution	8-30
8.1.4.3-1	Heat Removal Failure Probability Distributions	8-34
8.1.4.6-1	Transient Event Tree Sequence Probabilities	8-35
8.1.6-1	Total Release Probability per Flight	8-38
8.1.6-2	Total Release Probability per Year	8-38
8.2.1	Amount of Radioactive Isotopes Released when Fissioned UO_2 Melts	8-41
8.2-2	Set of Initial Activity of Fission Products Used in the Wash-1400 Report for a 3200 MW Reactor	8-42
8.2.2.1-1	Angular Widths for Pasquill's Stability Classifications	8-45
8.2.2.3-1	Meteorological Parameters	8-48
8.2.4-1	Average Decay Energies and Dose Factors for Ground Deposition and Cloud Shine	8-52
8.2.4-2	Inhalation Dose Factors (REM/CI) x 10^3	8-54
8.2.4-3	K Factors for a 574 MW Reactor	8-58
8.2.5-1	Population Density Probability Distribution	8-58
8.2.5-2	Fatalities per Release of Radioactive Material Probability Distribution	8-58
8.2.6-1	Deaths per Year Probability Distribution	8-59
8.2.6-2	Individual Risk of Acute Fatality by Various Causes (U.S. Population Average 1969)	8-59
8.2.7-1	Probability Distribution of the Three Reactors Considered	8-61
9.0-1	Parameters Used to Estimate Nuclear Aircraft Cost	9-1
9.2-1	Price Index with 1974 as Base Year	9-7
9.2-2	Airframe Total Program Cost	9-7
9.2-3	Prototype Airframe Cost for a Nuclear Aircraft	9-8
9.2-4	Average Airframe Cost	9-8
9.3.1-1	Production Cost for Six Fossil Fueled Engines	9-9
9.3.2-1	Production Cost for Ten Nuclear Engines	9-11
9.3.2-2	Production Cost for First Ten Engine Heat Exchangers	9-12
9.3.2-3	Production Cost for Ten Nuclear Engine Heat Exchangers	9-13
9.4-1	Production Cost for 200 MW Helium Cooled Nuclear Reactor	9-14
9.4-2	Cost for One 475 MW Liquid Sodium Cooled Reactor	9-15
9.4-3	Cost for One 500 MW Liquid Sodium Cooled Reactor with Redundant Instrumentation	9-15
9.5-1	Heavy Safety Valve Cost per Reactor	9-16
9.6-1	Avionics Subsystem Cost for a 0.95 Reliable System	9-17
9.6-2	Cost for Avionics Package for a 14 Day Mission	9-17
9.9-1	Initial Spares, Peculiar Support, and Training Equipment Cost per Aircraft	9-20

LIST OF TABLES (Continued)

9.9-2	Initial Spares, Peculiar Support, and Training Equipment Cost for Fleet	9-20
9.11-1	Engine Development Cost	9-22
9.11-2	Total Development Cost	9-22
9.13-1	PACE Model Inputs	9-25
9.13-2	PACE Model Summary	9-26
9.13-3	Discount Factor at 10%	9-27
9.13-4	Operating and Support for 20 Aircraft, Discounted Over 10 Years	9-27
9.13-5	Operating and Support Cost for 60 Aircraft, Discounted Over 10 Years	9-27
10.1.1-1	Aircraft/Mission Parameters	10-3
10.1.3-1	Aircraft Weight and Balance Summary — 2,000,000 lbs Gross Weight	10-6
10.1.3-2	Aircraft Dimensions and configuration — 2,000,000 lbs Gross Weight	10-7
10.1.4-1	Reactor Weights (lbs)	10-11
10.1.4-2	Reactor Weights: Original vs Reduced Shielding	10-13
10.1.5-1	Effects of Engine Parameter Variations on the Net Thrust of the Heat Exchanger Turbofan Engine	10-16
10.1.5-2	Engine System Study Summary	10-17
10.1.6-1	Gas Circulation Power Requirements	10-18
10.1.6-2	Weight and Power Comparisons	10-19
10.1.7-1	Total Release Probability per Flight	10-19
10.1.7-2	Fatalities per Release of Radioactive Material Probability Distribution	10-20
10.1.7-3	Deaths per Year Probability Distribution	10-20
10.2.1-1	Nuclear Propulsion Systems	10-22
10.2.2-1	Predicted Payload for 2,000,000 lbs Gross Weight Aircraft	10-24
10.2.3-1	Aircraft Parameters for Selected Missions	10-26
10.3.3-1	Propulsion System Weights and Power Requirements (2,000,000 lbs Aircraft)	10-28

PREFACE

This report was prepared by the 1975-M Graduate Systems Engineering Class (GSE-75M) at the Air Force Institute of Technology (AFIT), Wright-Patterson AFB, Ohio, in partial fulfillment of requirements for the Master of Science degree. This is not an official Air Force Design Study. The work was sponsored by the Propulsion and Energy Division, Deputy for Development Planning, Aeronautical Systems Division, Air Force Systems Command, Wright-Patterson AFB, Ohio. Authors of this report are the following 10 members of the AFIT GSE-75M class:

- Capt. Michael W. Amos, USAF
- Maj. James S. Butt, USAF
- Lt. Bruce L. Campbell, USAF
- Capt. Richard G. Diehl, USAF
- Maj. William J. Fanning, Jr., USAF
- Capt. George M. Lacy, Jr., USAF
- Capt. Ralph J. Luczak, USAF
- Maj. Edwin M. Moorman, Jr., USAF
- Capt. Julian W. Shattuck, USAF
- Maj. Vance K. Wilkinson, USAF

AFIT faculty members who advised and assisted the class are:

- Dr. D. Wallace Breuer
- Dr. Charles J. Bridgman
- Capt. James T. Karam, Jr., USAF
- Maj. Louis T. Montulli, USAF
- Dr. Lynn E. Wolaver
- Dr. Norman K. Womer

Technical work was conducted during the period 1 March 1974 to 7 February 1975. The final report was submitted on 14 March 1975.

Special appreciation is given to Col. James H. Hall, Deputy for Development Planning, ASD, and Dr. Larry W. Noggle, Nuclear Propulsion Technology Program Manager, ASD, for their close support and cooperation in all phases of the study.

Special recognition is given to the following for their cooperation in providing technical assistance in all phases of the study:

- Mr. Gary Averill, Naval Air Development Center.
- Maj. George T. Babbitt, USAF
- Mr. & Mrs. William Bustard, AFIT
- Mr. George Eck, Naval Air Development Center
- Dr. William C. Elrod, AFIT
- Mr. Anthony R. Hakl, Westinghouse Astronuclear Laboratory
- Dr. James E. Hitchcock, AFIT
- Prof. Harold C. Larsen, AFIT
- Capt. King L. Mills, III, USAF
- Mr. David Panetta, Naval Air Development Center.
- Mr. Robert E. Thompson, Westinghouse Astronuclear Laboratory
- Maj. Jack L. Wolff, USAF

The report consists of three volumes: Volume I, *Final Report*; Volume II, *Appendices*; and Volume III, *Classified Annex*.

SECTION 1
INTRODUCTION

1.1 BACKGROUND

The last major effort to develop a nuclear powered airplane was the Aircraft Nuclear Propulsion (ANP) Development Program which was terminated in 1961. The design objectives of that program and the technology of that time were such that the program was unable to meet its design objectives.

Since 1961, a combination of several factors has served to renew interest in the concept of a nuclear powered airplane. First, the United States is no longer self-sufficient in meeting its energy needs in that it is now dependent on foreign sources to supply a portion of its total oil demand.

Second, nuclear technology has seen significant improvements since 1961. Developments in high temperature, gas cooled and liquid metal cooled reactors and refinements in fuels for higher power density and longer life are examples of improvements which have given support to the concept of a relatively lightweight nuclear power system for airborne application.

Finally, changes in the performance requirements for a nuclear powered aircraft have made the concept much more viable. In particular, the ANP program sought an aircraft with supersonic speed capability, but no such requirement exists today. In fact, the guidance given for this study said, "Pick an Air Force mission(s) and determine whether or not nuclear power can be utilized to perform that mission(s)."

1.2 OBJECTIVE

The objective of this study was to assess, through a comprehensive systems engineering analysis, the feasibility of applying nuclear propulsion to aircraft in the performance of the Air Force mission(s).

1.3 APPROACH

Since the ANP program, the several studies which have considered various aspects of the nuclear powered airplane concept have been cursory in nature, or studied only a small part of the problem, or both. For example, individual studies of mission application, aircraft design, lightweight reactors, engines, and heat transfer systems have been made, but no study has addressed the full scope of the concept in detail. No comprehensive nuclear aircraft safety study has previously been accomplished. In order to address the full scope of the nuclear powered airplane concept, a systems approach was used, with the system divided into six major areas: (1) Mission Selection; (2) Required Mission Avionics; (3) Aircraft Design; (4) Propulsion System Design; (5) Public Safety; and (6) Cost.

Mission selection (Annex 2, Volume III) was the logical starting point for the study, since the feasibility of a nuclear powered aircraft hinges on having a viable mission to perform. Beginning with assumptions that the aircraft would be at least as large as the C-5A and that the unique features which must be exploited are long endurance and/or long range, several missions were analyzed for the applicability of nuclear power. One mission, antisubmarine warfare (ASW), was eventually selected for the purpose of establishing point design parameters.

The required mission avionics (Section 3, Volume I) was studied for two reasons: (1) the mission selection had identified the ASW mission as one requiring a relatively large avionics package, even for current mission durations; (2) the long endurance nature of the nuclear airplane was expected to place extraordinary demands on the avionics package in order to maintain an acceptable mission reliability. This study assumed a one order of magnitude improvement in avionics mean time between failure (MTBF) and then assessed the system and subsystem redundancies that would be required to satisfy the mission reliability requirements.

Aircraft design (Section 4, Volume I) was accomplished using standard aerodynamic design techniques, but within the constraints of the mission requirements and the desire to use the nuclear capability to its greatest advantage. An iterative approach, employing all known parameters, was used for each of several aircraft configurations, with a canard configuration finally being utilized for the point design.

The propulsion system [consisting of the reactor, the engines, and the heat transfer system, is analyzed in Sections 5, 6, and 7 (Volume I), respectively, with additional reactor analysis provided in Annex 5, Volume III] was analyzed for various configurations, including liquid metal and gas cooled reactors, and two different types of engines. Also included in the analysis are such interface items as valves, piping, pumps, turbines, and heat exchangers.

Safety analysis (Section 8, Volume I) provides a two-phase, probabilistic analysis of the risk of a nuclear powered airplane to the general public. The first phase, utilizing Fault Tree and Event Tree techniques, analyzes the probability of releasing radioactive material to the environment. The second phase, utilizing Monte Carlo simulation of dispersal of radioactive material, analyzes the probability of death to any member of the public, given that a release of radioactive material has occurred.

The last major area of analysis, cost (Section 9, Volume I) utilizes three methods of estimating cost (cost estimating relationships, expert opinion, and cost of analagous items on other aircraft), coupled with probabilistic modeling techniques to give a probabilistic estimate of the life cycle cost (LCC). Specifically, the result is presented as the LCC, discounted over a 10 year period, in terms of 1974 dollars.

The result is a detailed analysis of the applicability of a nuclear powered aircraft to the ASW mission. It is believed that the results can be used for a wider range of evaluations by serving as a basis from which to evaluate other missions and/or configurations.

SECTION 2
MISSION

2.0 BACKGROUND

In the early phase of the study, it was found that a large, subsonic, nuclear powered aircraft could conceivably perform several Air Force missions. These missions were: (1) antisubmarine warfare (ASW), (2) strategic airlift, (3) command and control, (4) airborne warning and control, and (5) airborne missile launch. The ASW mission was chosen as the point design mission because it readily lent itself to the operational nuclear safety considerations and the aircraft designed for this mission could most easily be adapted to perform other missions.

2.1 MISSION REQUIREMENTS

Mission requirements were estimated from an analysis of projected enemy submarine capabilities. Design parameters were developed using the aircraft performance that was necessary to fulfill the mission requirements. A summary of the aircraft and mission parameters is presented in Table 2.1-1. Parameters were selected using the following bases:

1) The two week mission duration is based on human factors. It was felt that fatigue, boredom, vibration, etc., would impair flight safety after two weeks.

2) The crew component of 36 men assumes three shifts of 12 men each, performing mission related jobs for eight hours per day. The 12 man crew is based on Navy studies for an advanced ASW aircraft and is comprised of a four man flight crew and an eight man tactical crew.

3) The 150 to 350 kts airspeeds are based on airspeeds currently used by the Navy during ASW operations. It was anticipated that there would be no significant increase in the speed of a submarine in the time frame addressed in this report. Consequently, current Navy ASW operations speeds were deemed sufficient.

4) The requirement that the aircraft be able to operate from sea level to 30,000 ft is compatible with projected ASW sensor capabilities.

5) The 130,000 to 200,000 lbs payload is based on projected weights of avionics and expendables as outlined in Section 3 and Volume III.

6) The takeoff and landing distances insure that the nuclear aircraft will be capable of using existing DoD airfields.

7) The nuclear powered aircraft was assumed to have unlimited range, therefore, the radius of action was not of concern in this design study.

8) The fleet size of 60 aircraft is based on an assumption that no more aircraft will be built than the number of Submarine-Launched Ballistic Missile submarines allowed by the Strategic Arms Limitations Talks.

9) It was assumed that at least 20 years would be required to develop a nuclear powered aircraft. The initial operational capability would then occur during the decade of the 1990s.

10) The aircraft lifetime of 62,000 hrs is based on the current high airframe time experience of large commercial transports as discussed in Volume III.

The complete mission discussion is contained in Volume III.

TABLE 2.1-1 AIRCRAFT PARAMETERS

MISSION DURATION (HRS)	**336 (2 WEEKS)**
CREW COMPONENT	**36 MEN (3 SHIFTS OF 12 MEN)**
AIRSPEED (KTS)	**150 AT SEA LEVEL 250-350 AT 30,000 FEET**
ALTITUDE (FT)	**SEA LEVEL TO 30,000**
PAYLOAD (LBS)	**MINIMUM 130,000 MAXIMUM 200,000**
TAKEOFF DISTANCE	**CLEAR A 35 FT OBJECT IN 12,000 FEET**
LANDING DISTANCE	**CLEAR A 50 FT OBJECT AND STOP IN 12,000 FEET**
FLEET SIZE	**60 AIRCRAFT**
IOC	**1990-2000**
LIFETIME	**62,000 FLYING HOURS**

SECTION 3
AVIONICS

3.0 INTRODUCTION

This study examines the avionic requirements for a large aircraft performing a long duration antisubmarine warfare (ASW) mission in the 1990s.

3.0.1 BACKGROUND: One of the more obvious advantages of a nuclear powered aircraft is its inherent long mission duration capability, because nuclear power makes it possible to consider mission length in terms of days rather than hours. This particular advantage, however, does have a serious impact on the total avionic system. Specifically, given the capability to remain airborne for periods of days, what kind and how much avionics are required to make the mission viable? Certainly the type of avionics will be strongly influenced by the mission to be performed by the aircraft. The amount of avionics, however, is directly a function of the amount of aircraft space available to carry the equipment, the amount of aircraft payload which can be dedicated to avionics, the reliability of individual subsystems, and the total system cost.

While system costs are one of the driving factors of any development, the purpose of this particular section was not to investigate individual avionic systems costs, but rather to concentrate on the avionic system as a package to perform a specific mission. Estimates of avionic cost can be found in Section 9 of this report.

Avionic systems reliability has traditionally been an area of intense interest, because mission success usually depends upon individual systems operating when they are called upon. Military avionics evolved as useful *black boxes* — first a radio, then navigation equipment, then bombing systems and so forth. As each new generation of aircraft was developed, the avionics became increasingly more sophisticated and complicated. Advances in solid-state technology resulted in individual components generally becoming more reliable than their earlier counterparts. However, because of the increased sophistication, the newer systems tended to be less reliable than their predecessors (Ref. 99, p. 55-56). To alleviate this situation, designers have turned to redundancy for some subsystems to insure that the desired reliability is obtained.

3.0.2 STATEMENT OF THE PROBLEM: The areas investigated by this study are twofold. First, identify those avionic subsystems, along with their parameters, required to perform a long duration ASW mission. Second, assuming a growth in reliability of individual subsystems, estimate total avionic system parameters. These parameters include system weight, volume, power required, and redundancy.

3.0.3 SYMBOLS: The symbols listed in Table 3.0.3-1 will be used throughout this section.

TABLE 3.0.3-1. LIST OF SYMBOLS

a	PROPORTIONALITY CONSTANT
C	COST FUNCTION
F(t)	CUMULATIVE DISTRIBUTION FUNCTION
f(t)	PROBABILITY DENSITY FUNCTION
H	PAYOFF FUNCTION
M	TOTAL NUMBER OF SUBSYSTEMS
MTBF	MEAN TIME BETWEEN FAILURE
n	NUMBER OF COMPONENTS IN PARALLEL
R(t)	RELIABILITY FUNCTION
RP(t)	RELIABILITY FUNCTION FOR PARALLEL SYSTEM
RS	SPECIFIED SYSTEM RELIABILITY
RT(t)	RELIABILITY FUNCTION FOR A SERIES-PARALLEL SYSTEM
S	SET OF ALL POSSIBLE STRATEGIES
λ	NONNEGATIVE REAL NUMBER
ν	DUMMY VARIABLE
μ	MEAN VALUE

3.1 METHOD OF ANALYSIS

As indicated in Section 3.0.2, two problems, system definition and parameter estimation, were considered. In order to maintain clarity, the background information, the assumptions, and the problem solution methodology for each problem are presented separately in this section.

3.1.1 SYSTEM DEFINITION: This section presents the methodology used to define the individual systems which will comprise the avionic package for the nuclear powered aircraft. Since it is assumed that the avionic equipment for this aircraft will not be developed for another 15 to 20 years, there will be no attempt to identify specific requirements for individual components. For example, if a radar set were required for this system, this study would not identify requirements for transmitter frequency, power output, signal-to-noise ratios, etc. Rather the effort is directed toward identifying functions which must be satisfied, and then listing a type of equipment which can satisfy that function. When listing the types of equipment to be used, the tendency will be to list the equipment in terms of present day technology. This is not to suggest, however, that systems fulfilling functional requirements 20 years hence will bear any resemblance to today's technology. It would be unreasonable to assume that electronics development will stagnate over the next 20 years. It is expected that new developments will continue to occur, and that these new developments will have just as profound an impact on avionics as did solid-state technology and miniaturization. These expected developments may well change avionics as presently defined, yet the functional requirements for various types of equipment should still exist.

3.1.1.1 ASSUMPTIONS: Several basic assumptions were made which impact the definition of the avionic package. The first assumption relates to the length of the mission performed by the aircraft and highlights one of the major advantages of nuclear power for aircraft. It was assumed that the mission duration is measured in terms of days rather than in terms of hours.

Section 2 of this study indicates that the principal threat to the United States are Soviet submarines. It is assumed that these submarines will be capable of operating deeper, faster, and quieter than present day submarines (Ref. 68, p. 1).

Enemy submarines are assumed to operate in any of the earth's oceans. This assumption impacts the navigational requirements for the aircraft.

It is assumed that the equipment that will make up the avionic package will not be developed for at least 15 or 20 years. During this time period, it is assumed that refinements in manufacturing techniques and advances in technology will result in increases in equipment reliability.

As indicated in the statement of the problem, Section 3.0.2, the parameters of interest for the avionic system are weight, volume, power and reliability. Estimates for these parameters were assumed to have the same values as present day equipment performing similar functions. Recognizing that electronic equipment has tended to become smaller and lighter, it is assumed that these estimates for the parameters of the equipment will provide a pessimistic or a worse case estimate of the avionic parameter 20 years from now. A summary of assumptions for the system definition section of the study is provided in Table 3.1.1.1-1.

TABLE 3.1.1.1-1. SYSTEM DEFINITION ASSUMPTIONS

1. MISSION LENGTH IS GREATER THAN 24 HOURS.
2. SOVIET SUBMARINES ARE THE PRINCIPAL THREAT.
3. SUBMARINES WILL OPERATE DEEPER, FASTER, AND QUIETER.
4. ENEMY SUBMARINES WILL OPERATE IN ANY OCEAN ON THE EARTH.
5. AVIONICS EQUIPMENT FOR THE NUCLEAR POWERED AIRCRAFT WILL NOT BE DEVELOPED FOR AT LEAST 15 YEARS AND DURING THIS TIME EQUIPMENT RELIABILITY WILL INCREASE.
6. THE PARAMETERS OF INTEREST ARE WEIGHT, VOLUME, POWER, AND RELIABILITY.
7. THE USE OF CURRENT SYSTEM PARAMETERS WILL PROVIDE A WORSE CASE ESTIMATE FOR FUTURE SYSTEMS.

3.1.1.2 METHODOLOGY: Having made some basic assumptions relating to the aircraft and its mission, avionic requirements were then defined. These requirements were based on mission, threat, and enemy capabilities. It must be emphasized that these requirements are not requirements in the strictest sense of the word. They are not demands or obligations which must be met. Rather, these requirements simply define the limits on the types of equipment which may be required to satisfy the mission and the threat. The requirements then were translated into types of systems and equipment. In order to insure that the total avionic package was considered, the avionic requirements were broken down into categories, functional areas, and subsystems. Figure 3.1.1.2-1 illustrates this process. Each category includes a broad spectrum of requirements. The divisions between these categories are independent of the requirements for the remaining categories. Each category was then divided into functional areas. A functional area is defined to be those elements of the avionic system which satisfy specific mission or aircraft requirements. Finally, each functional area is divided into specific subsystems. These subsystems are the units which perform the required operations and are the units which make up the avionic package. Having defined an avionic system, weight, volume, power, and reliability parameters were associated with each one of the subsystems.

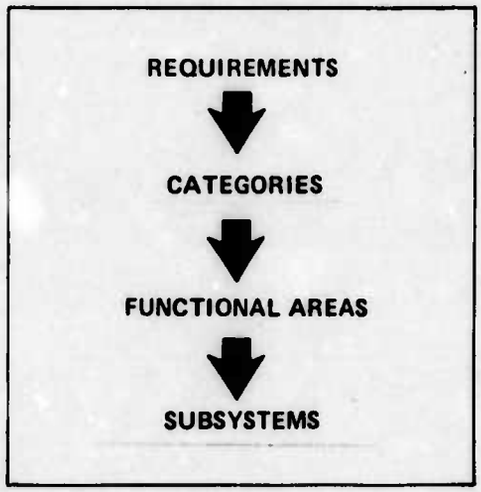

Figure 3.1.1.2-1. Avionic System Definition

3.1.2 ESTIMATION OF SYSTEM PARAMETERS: The method of estimating the avionic system parameters was accomplished by developing a system model and then applying optimal estimate to this model. The objective was to determine what effect changes in component reliability, overall system reliability, and mission duration would have on the system parameters of weight, volume, and power. Dynamic programming and LaGrange Multipliers were both considered as methods to accomplish this task. However, the Dynamic Programming technique required substantial amounts of computer resources and was dropped in favor of the LaGrange Multiplier method. For continuity purposes, both methods are discussed.

3.1.2.1 ASSUMPTIONS: The estimation of avionic system parameters required that further assumptions be made in addition to those made in Section 3.1.1.1. First, it was assumed that the aircraft would be assigned to a geographical region and would patrol in that

region for its entire mission. This assumption implies that the time spent patrolling is much greater than the time spent traveling to and from the patrol region. Therefore, the avionic utilization rate was assumed to approach one. In Section 3.1.1.1 it was assumed that avionic equipment reliability will improve during the next 20 years. For the purpose of this study, it is assumed that this improvement in system component reliability will be reflected in a tenfold increase in mean time between failure (MTBF). This assumption is made to determine what effect, if any, increased component reliability will have on avionic system parameters such as weight, volume, and power. Keep in mind that the total avionic system reliability for the long duration was to be achieved through the application of redundancy.

It was assumed that the component failures, as a function of time, can be modeled by an exponential function. This function has found widespread acceptance in the area of reliability theory (Ref. 30, p. 183). Implied in the use of this function is that each component has an operating life. This operating life is characterized by a burn-in period, a useful life period, and a wearout period. During the burn-in period, weak components die out and the failure rate decreases. During the useful life period, the failure rate is at its lowest and remains constant. During the wearout period, the component has exceeded its useful life and the failure rate increases (Ref. 13, Ch. 5). The exponential function models the random failures that occur during the useful life of the component and not the wearout or burn-in failure. Implicit, then, is that preventive maintenance has assured that the system components are neither in the burn-in or wearout period.

As shown in Section 4, the aircraft itself is physically large. As a result, volume requirements for the avionics were not considered critical, as in previous aircraft. However, reduction in avionic system weight could provide additional usable payload for other systems. Therefore, it was assumed that minimizing avionic weight will provide the greatest payoff. A summary of these assumptions is contained in Table 3.1.2.1-1.

TABLE 3.1.2.1-1. SYSTEM PARAMETER ESTIMATE ASSUMPTIONS

1. TIME ON STATION IS MUCH GREATER THAN TIME IN TRANSIT.
2. EQUIPMENT UTILIZATION APPROACHES 1.
3. MTBF WILL INCREASE BY A FACTOR OF 10 OVER PRESENT SYSTEMS.
4. FAILURES ARE MODELED BY AN EXPONENTIAL FUNCTION.
5. MINIMIZING SYSTEM WEIGHT WILL PROVIDE THE GREATEST PAYOFF.

3.1.2.2 PROBABILITY DISTRIBUTION FUNCTION: Recall from Section 3.1.2.1 that the probability of a failure for any avionic component is modeled by an exponential function. Implied in this assumption is that, at time, t, equal to zero, the probability of failure is zero

and as t becomes very large, the probability of failure approaches 1 (Ref. 13, p. 39). This function can be modeled by the equation:

$$F(t) = 1 - e^{-at} \qquad (3.1.2\text{-}1)$$

Graphically, this equation would appear as shown in Figure 3.1.2.2-1.

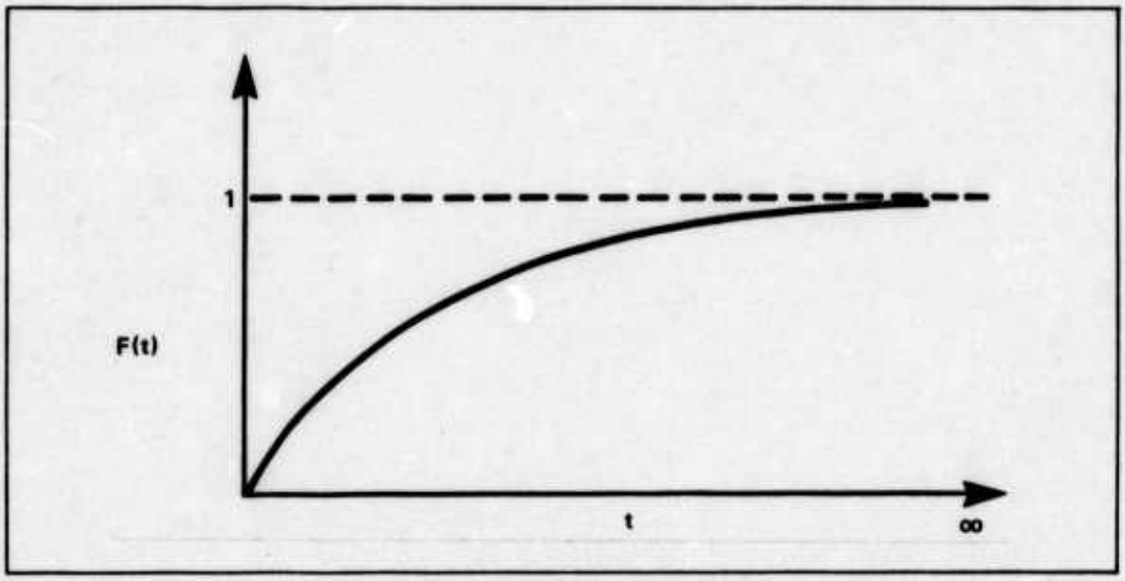

Figure 3.1.2.2-1. Assumed Failure Distribution

Taking the first derivative of Eq. 3.1.2-1 yields the probability density function (PDF) for the avionics failure model.

$$\frac{dF(t)}{dt} = f(t) = ae^{-at} \qquad (3.1.2\text{-}2)$$

The mean value of the PDF is the expectation of Eq. 3.1.2-2:

$$\mu = \int_0^\infty t\, f(t)\, dt$$
$$= 1/a$$

If the mean value for the system is the MTBF, then:

$$\mu = MTBF = 1/a$$

Next define the reliability, R(t), of an avionic system as the probability that the system will be operating at some time $\tau > 0$. Then the probability that the system is operating at τ is:

$$R(\tau) = \int_{\tau}^{\infty} ae^{-at}\, dt$$
$$= e^{-a\tau}$$

Thus the reliability for any one component can be modeled by:

$$R(\tau) = e^{-\tau/MTBF} \qquad (3.1.2\text{-}3)$$

where τ is the time interval of interest.

Consider now that redundancy has been introduced into the system. Suppose, for example, that several of the same kind of systems are placed in parallel to increase the reliability of that system. Figure 3.1.2.2-2 illustrates this concept.

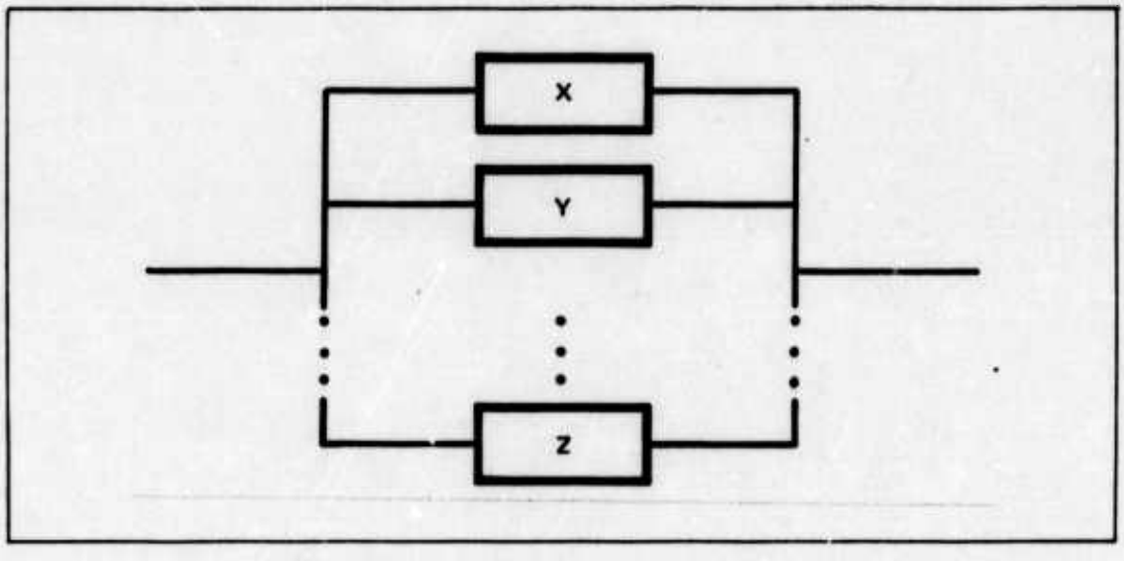

Figure 3.1.2.2-2. Parallel Components Model

The probability of failure for the parallel system, then, is:

Pr[(x fails) and (y fails) and . . . and (z fails)]

However, if each unit in the parallel system operates independently of the remaining units, then a failure in any one unit will in no way affect the operation of the remaining units. By independence then:

$$\Pr[(x \text{ fails}) \cap (y \text{ fails}) \cap \ldots \cap (z \text{ fails})] = \Pr[(x \text{ fails})] \Pr[(y \text{ fails})] \ldots \Pr[(z \text{ fails})] \quad (3.1.2\text{-}4)$$

However, recall that each of the units in the parallel system is identical, then Eq. 3.1.2-4 reduces to:

$$\Pr[\, x \text{ fails} \,]^n$$

where n is the number of units in parallel.

From basic probability theory, it can be shown that:

$$\Pr[\text{System Failure}] = 1 - \Pr[\text{System Operating}] \quad (3.1.2\text{-}5)$$

Therefore, if the system is made up of n units in parallel, then:

$$(\Pr[\text{System Failure}])^n = (1 - \Pr[\text{System Operating}])^n$$

From Eq. 3.1.2-3:

$$\Pr[\text{System Operating}] = e^{-\tau/\text{MTBF}}$$

Therefore, the probability of system failure for n units in parallel is:

$$(1 - e^{-\tau/\text{MTBF}})^n \quad (3.1.2\text{-}6)$$

Eq. 3.1.2-6 gives the "worst case" prediction of a redundant network for the following reasons:

1) It assumes all units are operating all of the time.

2) It assumes that the whole network is needed for the entire mission.

The reliability of a parallel system, RP(t), can then be defined as the probability that the parallel system is operating at time, τ.

From Eq. 3.1.2-5:

$$RP(\tau) = 1 - (1 - e^{-\tau/\text{MTBF}})^n \quad (3.1.2\text{-}7)$$

Eq. 3.1.2-7 models the avionic system as if it were made up of one component with n units in parallel. Consider now that the avionic system is made up of many components, and each of the components had n units in parallel. Figure 3.1.2.2-3 illustrates this concept.

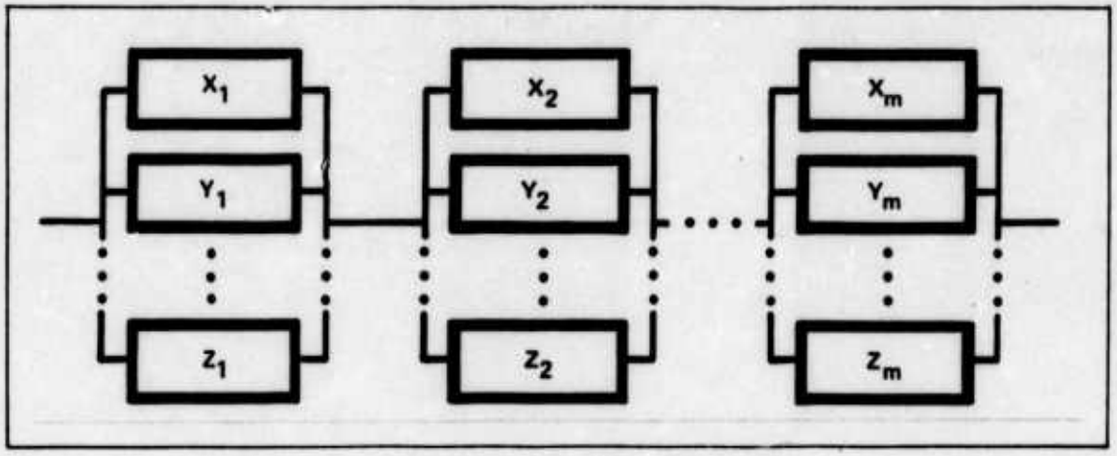

Figure 3.1.2.2-3. Series-Parallel Model

Note that there is no restriction on n for the M components. It is assumed that a failure of any one group of components is independent of the failures of any other group of components. The reliability of the total system, RT(t), is defined as the probability that the total system has at least one unit of each component operating at time τ. By independence:

$$RT(\tau) = \prod_{i=1}^{M} RP(\tau)_i = \prod_{i=1}^{M} [1 - (1 - e^{-\tau/MTBF_i})^{n_i}] \qquad (3.1.2\text{-}8)$$

Eq. 3.1.2-8 models the reliability function for the total avionic package. The possibility arises, however, that all n components in the i^{th} subsystem might fail! Implicit in the model is that the avionic system reliability RT(t) may not be met. It would be a matter of command policy and criticality toward the mission of the failed subsystem to determine if mission abort were warranted.

3.1.2.3 DYNAMIC PROGRAMMING: Dynamic Programming was the first technique considered to solve the constrained avionic weight-minimization problem. The problem was to find the combination of parallel components that minimize the overall system weight subject to a system reliability constraint for a fixed mission duration. Essentially, the method presents a means of systematically examining combinations of series-parallel systems and selecting that combination which satisfies the problem. The algorithm was tested against a sample problem. Based on those results, it was estimated that excessive computer time would be required to solve the avionic problem. As a result of the computational requirements, this technique was dropped in favor of an algorithm which required less computer resources. Detailed information concerning the Dynamic Programming technique, along with applications, sample problems, and computer techniques can be found in References 90, 142, and 162.

3.1.2.4 LAGRANGE MULTIPLIERS: As with Dynamic Programming techniques, the problem to be solved by the LaGrange Multiplier is to find the combination of parallel components which would minimize the overall weight, subject to a reliability constraint. Unlike Dynamic Programming, however, the LaGrange Multiplier algorithm provides a direct

solution to the problem. In addition, some LaGrange techniques require less computer resources than Dynamic Programming (Ref. 50, p. 412). The problem is to minimize a scaler function H(x) of an n-dimensional vector x, which is defined on some closed n-dimensional region R, subject to the side conditions:

$$\phi_k(\bar{x}) = 0 \qquad k = 1, 2, \ldots p<n$$

It is no longer possible to vary x freely. In minimizing H(x), only those x which satisfy the constraints may be considered. Let S denote the set of points x which satisfy all the side conditions $\phi_k(x) = 0$. It is assumed that S is a non-empty set, that is, a set in which the constraints are not inconsistent with each other. The problem then is to:

$$\text{Minimize } H(\bar{x})$$

subject to

$$\phi_k(\bar{x}) = RS - RT(\tau) = 0$$

By the method LaGrange .tipliers, an augmented function is defined as:

$$L(\bar{x}) = H(\bar{x}) + \sum_{k=1}^{R} \lambda_k \phi_k(x)$$

where λ , k= 1, 2, . . . p<n are non-negative real numbers corresponding to the number of side conditions or constraints which must be satisfied. To apply this method to the avionic parameter estimation problem, recall from Eq. 3.1.2-8 that the total system reliability function is defined to be:

$$RT(\tau) = \prod_{i=1}^{M} [1 - (1 - a_i)^{n_i}]$$

where:

$$a_i = e^{-\tau/MTBF_i}$$

The total system weight is:

$$W = \sum_{i=1}^{M} n_i C_i \qquad (3.1.2\text{-}9)$$

where C is the weight of the i^{th} unit and n is the number of parallel components in the i^{th} unit. The problem is to minimize the total system weight subject to the constraint that the total system reliability, RT(τ), is equal to a specified reliability, RS. If the total system weight, W, is considered to be the scalar function H(n), and the system reliability the constraint, then the problem can be put in the form of an augmented LaGrangian:

$$L = \sum_{i=1}^{M} n_i C_i + \lambda \left[RS - \prod_{i=1}^{M} (1 - (1 - a_i)^{n_i})\right] \qquad (3.1.2\text{-}10)$$

Thus, by the method just described, it is only necessary to minimize L for each h independently. This is accomplished analytically by taking the first derivative of Eq. 3.1.2-10 and setting it equal to zero:

$$\frac{\partial L}{\partial n_i} = C_i + [\lambda\, RS\, (1 - a_i)^{n_i} \ln (1 - a_i)]/[1 - (1 - a_i)^{n_i}] = 0 \qquad (3.1.2\text{-}11)$$

The value of n can be found by taking the log of the equation and solving algebraically:

$$n_i = \{\ln (C_i/RS\lambda) - \ln [C_i/RS\lambda - \ln (1 - a_i)]\}/\ln (1 - a_i) \qquad (3.1.2\text{-}12)$$

The interpretation of Eq. 3.1.2-12 is that, for some λ, the n_i calculated will give the minimum total system weight for a specified reliability. The procedure is to select an initial value for λ and compute the augmented LaGrangian function L from Eq. 3.1.2-10. A new value of λ is then selected and the computations repeated until L is minimized, i.e.,

$$\frac{L_1 - L_2}{L_1} < 10^{-R}$$

This yields the optimum numbers n_i. However, the solution will not always yield integer values for n_i and it is meaningless to consider a fractional component. Therefore, the technique used is to find the solution that minimized the LaGrangian, L, and then round the values of n_i to the nearest integer value. The LaGrangian was then recomputed and the percent difference between the integer and noninteger solution was found. The error which resulted from rounding the values of n_i varied from less than 1% to as much as 8% for various solutions. It was reasoned that the error in the LaGrangian was within the limits of the errors for the estimates of individual component weights and consequently was an acceptable solution for an estimate of total system weight.

In order to obtain an initial value of λ it was assumed that each of M components had an equal reliability. This means that Eq. 3.1.2-8 can be written as:

$$RS = [1 - (1 - a_i)^{n_i}]^M \qquad (3.1.2\text{-}13)$$

Solving for n_i:

$$n_i = \{\ln [1 - EXP\ (\ln RS/M)]\}/\ln (1 - a_i) \qquad (3.1.2\text{-}14)$$

Substituting this value of n_i into Eq. 3.1.2-12 and solving for λ gives:

$$\lambda_i = - C_i \text{ EXP } [(\ln RS)/M]/\{RS [1 - \text{EXP } [(\ln RS)/M]] \ln (1 - a_i)\}$$

An initial estimate of λ was found by obtaining the arithmetic mean of all the λ . λ is then iterated around this initial value until a minimum value of the augmented LaGrangian is found. A computer code was written to perform these operations. Execution time for this set of equations on a Control Data Corporation 6600 computer system is approximately 400 milliseconds. The results are given in Section 3.2.2.

3.2 RESULTS

This section discusses the finding for the two problems posed in Section 3.0.2. Results for each problem are considered separately.

3.2.1 SYSTEM DEFINITION: As explained in Section 3.1.1.2, the definition of the components that would make up the avionic package for the nuclear powered aircraft required that several steps be taken. These steps included developing requirements and establishing categories, functional areas, subsystems, and parameters.

3.2.1.1 AVIONIC REQUIREMENTS: When considering avionic requirements, one must keep in mind the mission of the aircraft and the threat it may encounter. Although the mission and threat have been discussed elsewhere in this report, they will be highlighted here as they pertain to the avionics. As stated in Section 2, the mission is to search for and identify enemy submarines and surface ships, and then to take whatever military action is necessary. As noted in Section 3.1.1, it is assumed that Soviet submarines will have the capability of operating with increased speed, at greater depths, and quieter than present day submarines. These capabilities will place greater demands, in terms of sensitivity and responsiveness, on the sensors in future avionic packages. In addition, the mission requires that the aircraft locate surface ships as well as submarines. Therefore, the sensors must be capable of locating enemy vessels either on or below the ocean surface.

Several tactics may be employed when searching for enemy vessels. One tactic is to observe the enemy while he performs routine activities, which suggests that the observer remain covert for as long as possible and, in turn, suggests the use of passive sensors. Passive sensors allow the observer to gather information about the enemy without giving away his own presence. This can be a distinct advantage if, for example, the ASW effort during a cold war situation is one of intelligence gathering. Passive sensors can be either acoustic or nonacoustic. Nonacoustic sensors gather information in the geomagnetic and electromagnetic spectra. However, operation need not be limited only to passive sensors.

Active sensors can provide additional information in terms of range, bearing, size, etc., of the target when covert operation is not possible. As with passive sensors, active sensors can be either acoustic or nonacoustic. The nonacoustic sensors operate in the electromagnetic spectrum. Since it was assumed that mission duration for this aircraft is measured in terms of days, the capability of gathering information should not be severely hampered by darkness, fog, haze, or other low light conditions.

In addition to the sensor requirements, general aviation avionics are required, including communications, navigation, flight controls, controls and displays. Communications are required to provide command and control and other information to the air crew. The capability of a nuclear powered aircraft to remain in flight for extended periods of time and to have virtually unlimited range demands a requirement for reliable long range communications. Also, reliable short range communications are required for critical operations of the flight, such as takeoff and landing. Because of the long mission durations, situations may arise where secure communications may be required. Thus, some form of encrypting may be needed. Also, some raw data from the sensors may be of such a nature that it would be desirable to transmit these data to headquarters prior to completion of the mission requiring a data link.

Since it is assumed that enemy submarines and ships can operate in any of the earth's oceans, it would be desirable that the aircraft be capable of navigating to any position on the earth. Inertial navigation is desirable since, during any period of hostilities, the aircraft would not be dependent on external navigational aids. Navigational errors can accumulate during a long duration mission. Consequently, a method of updating the navigation system to minimize accumulated errors is desirable. Navigational updates can be accomplished by either active or passive devices. Passive devices are desirable in the event that the aircraft is operating in a covert mode.

Returning to the long duration mission, automatic flight controls are desirable to help alleviate fatigue which may result from long periods of routine flight. In addition, in the presence of aerodynamic changes, automatic flight controls can help to provide a more stable platform in which to work.

Controls and displays are required to effectively display all pertinent information in a form readily usable by the operators.

In addition to all of the foregoing, the nuclear power plant will require its own avionics. This equipment is needed to insure that reactor power levels are accurately maintained; to monitor reactor and aircraft radiation levels; and to maintain surveillance of critical temperatures, pressures, and flow rates. Also, this equipment must be capable of protecting the reactor, the aircraft crew, and the populace in the event of malfunction or emergency.

Finally, to insure proper operation of the avionic equipment, it is desirable that all of the avionics have sufficient amounts of built-in test equipment that can detect a malfunction or an out-of-tolerance condition. This test equipment would detect when any function was not being properly performed by the avionic device and would switch to an alternate or back-up device.

3.2.1.2 CATEGORIES: The avionic requirements were broken down into three categories (Figure 3.2.1.2-1): Common, Tactical, and Power Generation. As indicated in Section 3.1.1.2, ideally each category would be independent of the others. However, in a large integrated system, the division line between categories is not distinct, and some overlap may occur. Overlap occurs when one piece of equipment is capable of fulfilling requirements in more than one category. For example, a multipurpose display unit could present information from all categories.A description of the categories used in this study follows.

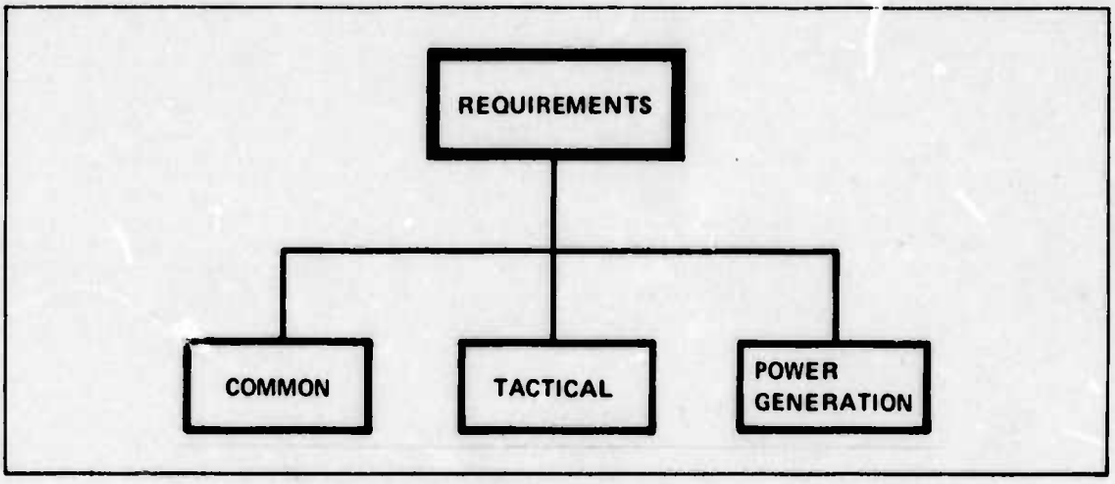

Figure 3.2.1.2-1. Avionic Categories

The Common equipment is that avionics which would be found on any modern aircraft. It is the equipment which is required for operation of the aircraft and is generally not associated with the aircraft's mission.

The Tactical equipment is that avionic equipment which is peculiar to the aircraft's mission, including all the sensors and other devices that allow the aircraft to perform its assigned mission.

The Power Generation avionics is that equipment which is associated with the nuclear reactor and its peripheral equipment.

3.2.1.3 FUNCTIONAL AREAS: Each category was broken down into functional areas, each of which satisfies specific requirements. Each functional area was then broken down into individual subsystems to satisfy the requirements.

Functional areas for the Common category are Navigation, mission and traffic control, instruments and aircraft systems, computers and controls and displays (Figure 3.2.1.3-1).

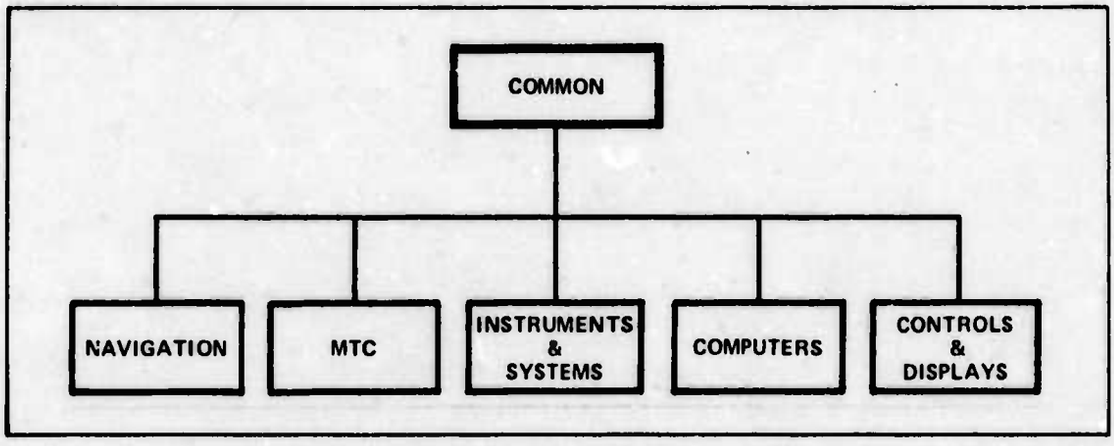

Figure 3.2.1.3-1. Common Functional Areas

Navigation equipment provides accurate data regarding aircraft position, altitude, velocity, and other parameters. The subsystems which will support the navigation functional area shown in Figure 3.2.1.3-2 are: inertial navigation set (INS); radar; Doppler radar; radar altimeter; and astrotracker. The basic navigation function is provided by the INS. Updates to the INS are provided by passive and active sensors; the passive device is the astrotracker. Note that the radar set is a device which transcends two categories. It is used for the enroute navigation functions for weather avoidance, and also can be used tactically to locate enemy vessels.

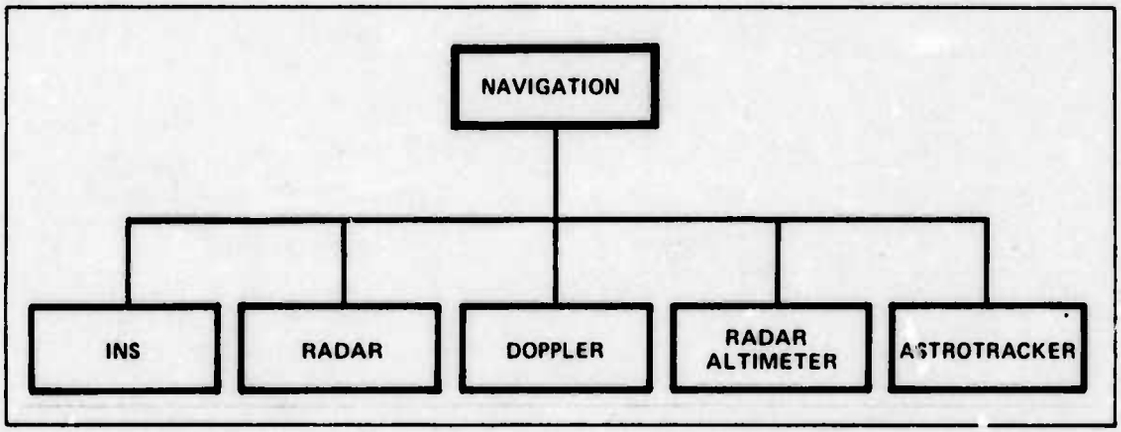

Figure 3.2.1.3-2. Navigation Subsystems

Mission and traffic control (MTC) equipment provides the means of coordinating with ground stations and other members and elements through radio frequency communication. This includes voice, navigation aid, and information or identification communication. (Ref. 24, p. 4-73). The mission and traffic control equipment is shown in Figure 3.2.1.3-3. UHF and HF radios provide short and long range communications, respectively. The VHF equipment, used as a communications link with sonobuoys, will be discussed later, The secure speech set provides a means of encrypting and decrypting voice communications. The data link provides a means of communicating information which may be awkward or impossible to accomplish through voice communications. This information might include such items as aircraft position and status reports and sensor data. The navigation aids include tactical air navigation (TACAN), instrument landing set (ILS), automatic direction finder (ADF), and long range navigation (LORAN). In future systems, the LORAN may be replaced or complemented by the global positioning system (GPS). For the purpose of this study, only LORAN is considered; but, it is assumed that, if the GPS system is realized, the weight, volume, and power requirements will be essentially the same as present day LORAN. The functions provided by beacons and identification friend or foe (IFF) are evidenced by their names and will not be discussed.

Instruments and aircraft systems are avionic equipment which are aids necessary for the pilot to perform flight functions. The subsystems which make up this area are automatic flight controls, air-data system and standby altitude indicating system (Figure 3.2.1.3-4). The functions provided by these subsystems are self-explanatory.

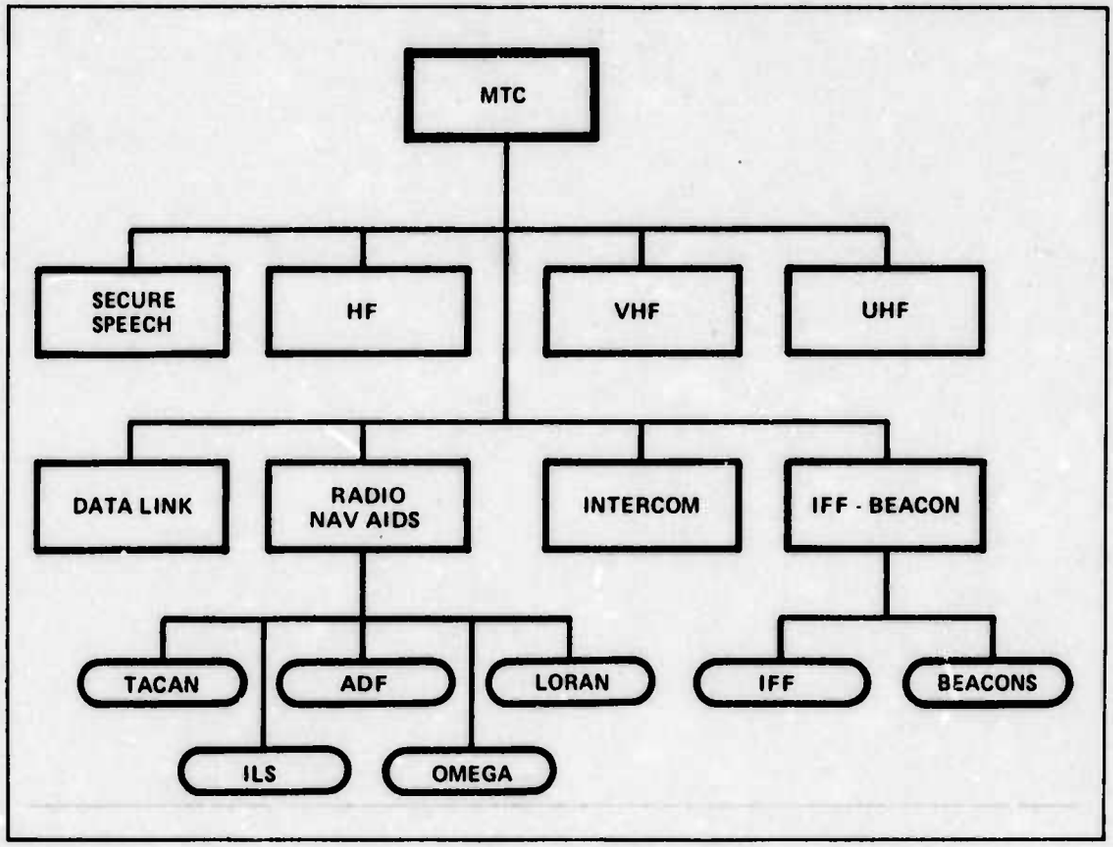

Figure 3.2.1.3-3. Mission Traffic and Control Subsystems

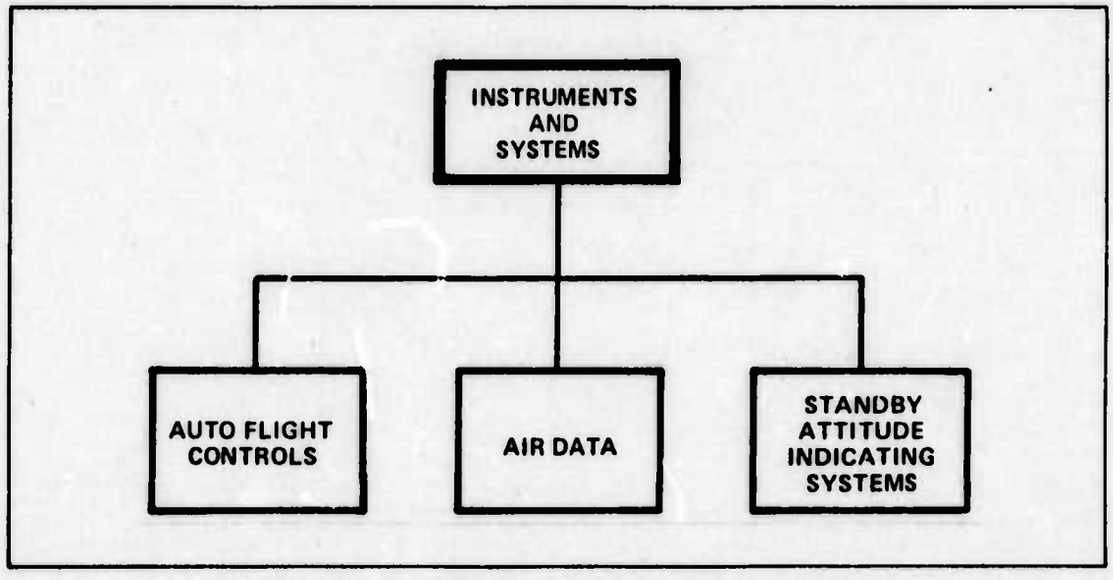

Figure 3.2.1.3-4. Instruments and Aircraft Systems Subsystems

Although it was not specifically required, a digital computer complex was included in the avionic package because digital techniques lend themselves to efficiently manage, store, retrieve, manipulate, and format the vast amounts of data that are collected by the sensors and systems of the avionic package. In addition, digital techniques aid in system integration and provide greater flexibility to modify the equipment to suit mission requirements (Ref. 99). The computer complex functional area was not broken down into individual subsystems, but was treated as a subsystem in itself.

Controls and displays provide the necessary devices for an operator to interface with the avionics equipment. The controls permit the operator to enter data into and make requests from the avionic system. The use of digital techniques for data handling permit great flexibility in display format. Display faces include warning lights, electromechanical displays, video displays, and digital discrete displays. The subsystems of this functional area are shown in Figure 3.2.1.3-5.

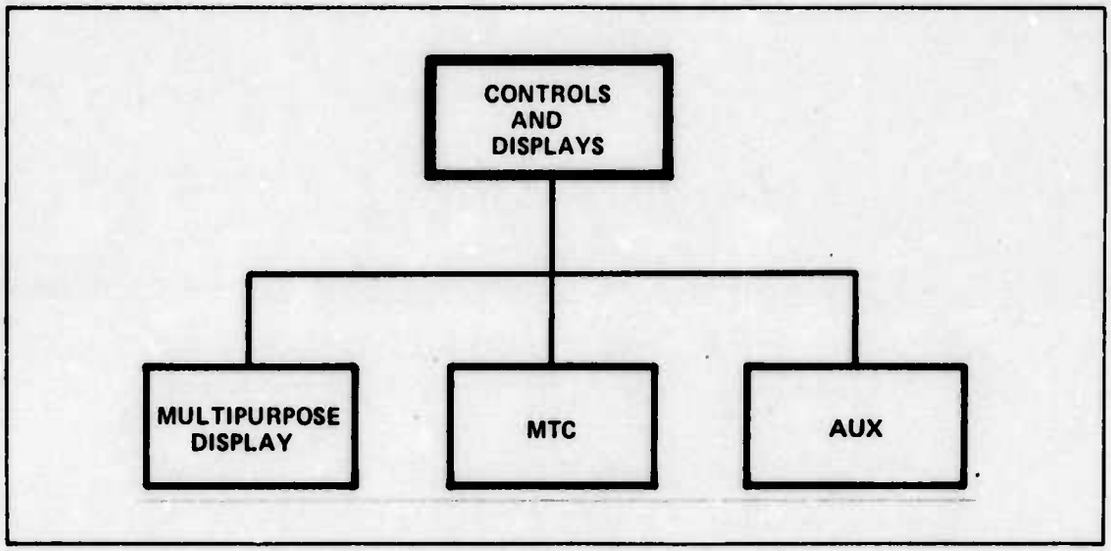

Figure 3.2.1.3-5. Controls and Displays Subsystems

The multipurpose display is a device that allows the operator to select desired information and display it in a video format. Since it was assumed that digital techniques are used, it would only be necessary to format the data to fit the video device. Thus, all information would be available at each crew station equipped with this display. Information which is presently displayed on an ADI and NSI would be displayed on devices of this type. This study calls them HSD and VSD. The MTC subsystem are those controls and displays necessary to operate the mission and traffic control equipment. The auxiliary subsystem consists of those controls and displays that are not included in the previous two subsystems.

The Tactical category is broken down into the following functional areas: penetration aids; sensors; and controls and displays. These are shown in Figure 3.2.1.3-6.

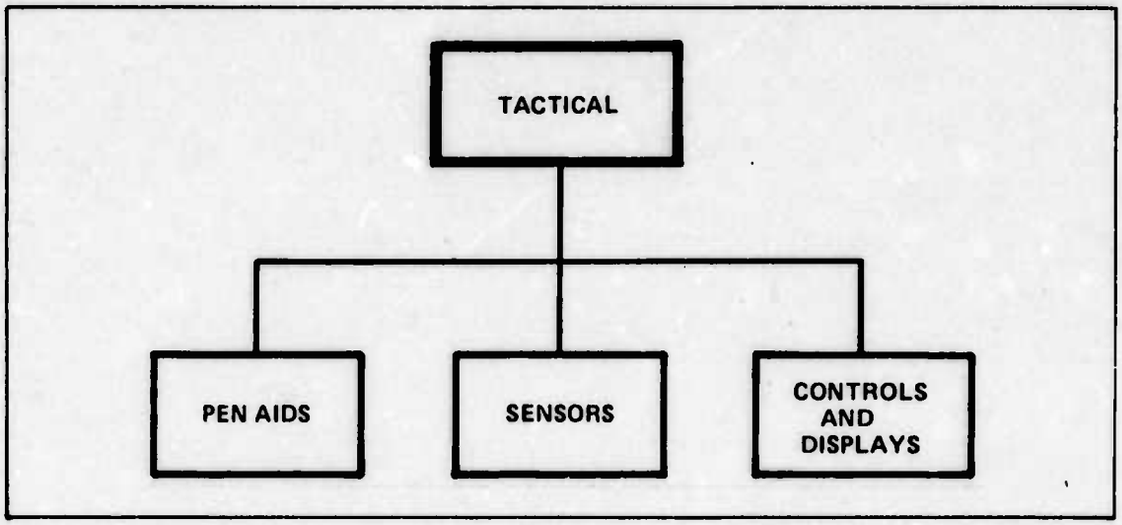

Figure 3.2.1.3-6. Tactical Functional Areas

The penetration aids subsystems consist of radar homing and warning (RHAW) and electronic countermeasures (ECM). RHAW equipment detects airborne or ground based threat radars, analyzes the received signals, and presents the information to the aircraft crew for evaluation. The ECM is used to degrade the performance of enemy air defense systems. This equipment provides increased aircraft survival during hostile activities by destroying the enemy's sensor capability of determining the aircraft's true range and angle (Ref. 26, p. 29). The interference blanker keeps the aircraft's own radiated emissions from interfering with the aircraft sensors. These subsystems are displayed in Figure 3.2.1.3-7.

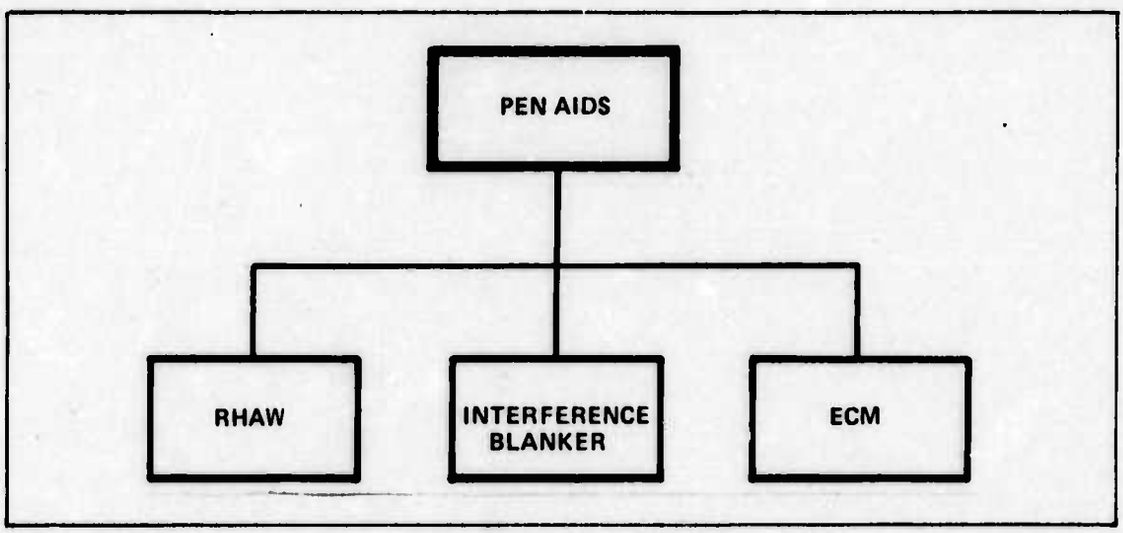

Figure 3.2.1.3-7. Penetration Aids Subsystems

The sensors subsystems include search radar, acoustic sensors, electro-optical sensors, and magnetic anomaly detector (MAD) which are shown in Figure 3.2.1.3-8. The search radar provides relative range, bearing, and azimuth to an enemy vessel. This subsystem, however, is included in the Common category, in the navigation functional area.

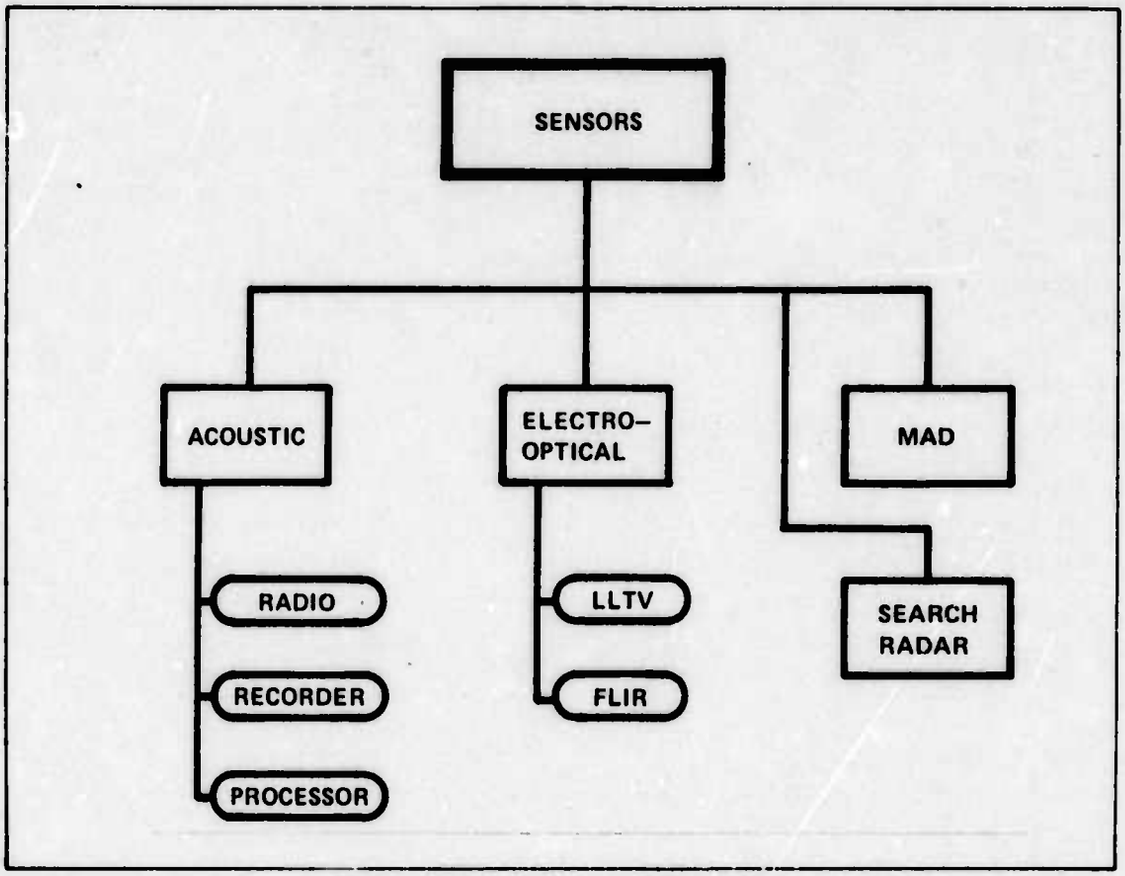

Figure 3.2.1.3-8. Sensor Subsystems

The acoustic sensors provide information about enemy submarines by analysis of sounds that either emanate or are reflected from the vessels. Devices are deployed in the ocean to collect this audio information and transmit it, by radio, to the aircraft where it is stored and analyzed. The radio link is considered in the Common category under MTC. Processing of the information is accomplished by the computer complex. Storage is accomplished on an audio recorder.

The electro-optical subsystem includes forward looking infrared (FLIR) and low light television (LLTV). These devices provide target identification information. LLTV provides visual information during night of low light level conditons. FLIR provides a visual representation of the thermal contrast in a ground scene (Ref. 24, p. 4-28). FLIR can be used as an adjunct to LLTV during fog or haze conditions.

Finally, the MAD subsystem detects perturbations, caused by metallic objects, in the earth's magnetic field. This equipment is used in the terminal phase of the ASW activity to refine the position and confine the classification of the target (Ref. 68, p. 5).

Tactical communications are accomplished using the same equipment as presented in the Common category under the heading MTC.

The controls and displays are essentially the same as those previously presented. A multimode video display set is envisioned for the display of sensor data. This device allows the operators to select the desired information which is then presented in a video format. Thus each sensor operator would be using the same type of equipment, only the information displayed at each station would be different.

The Power Generation avionics is that equipment associated with the nuclear reactor. The subsystems are sensors, processors, and controls and displays (Figure 3.2.1.3-9). The sensors monitor the reactor and associated equipment for proper operation, including power levels, radiation, temperatures, pressures, and flow. The processor works in conjunction with the computer complex, interfacing the sensors with the computer and performing any reactor safety or monitor functions. The controls and displays are of the multimode type previously discussed.

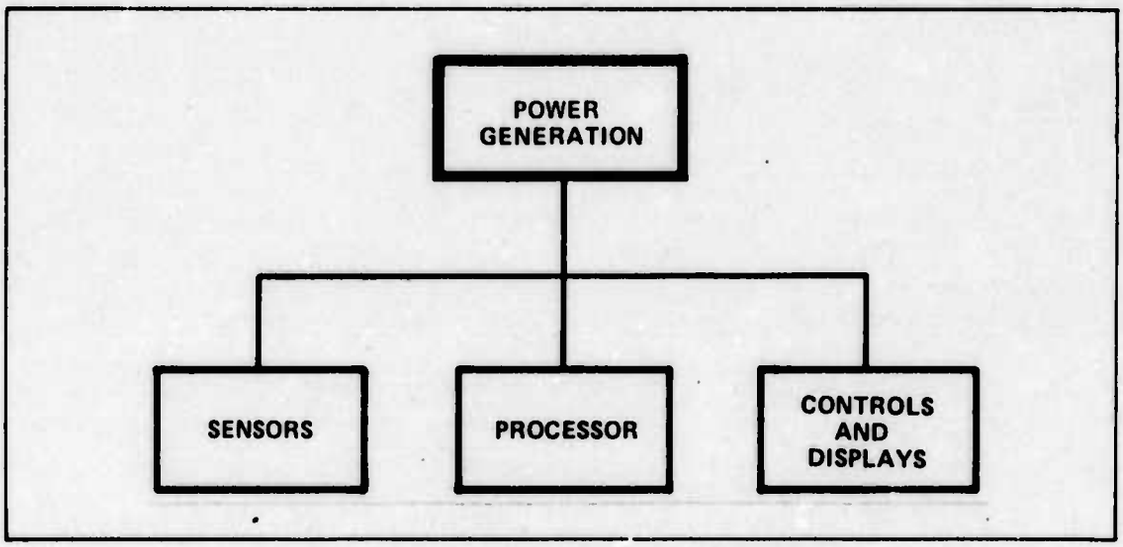

Figure 3.2.1.3-9. Power Generation Subsystems

3.2.1.4 AVIONIC COMPONENTS AND PARAMETERS: A complete list of the avionic subsystems and their associated weight, volume, power, and assumed MTBFs is contained in Table 3.2.1.4-1. These parameters were obtained by examining present day systems which perform similar functions, including systems from the B-1, C-5A and FB-111 aircraft, and from manufacturer data. Some reliability information was obtained through the use of MIL-STD-756A, *Military Standard for Reliability Prediction*. Recall, from Section 3.1.2.1, that the MTBF for the avionics was assumed to have improved by a factor of 10. Weight and volume estimates consider only the subsystems themselves and do not include estimates for mounting racks or interconnecting wiring. Also, it is assumed that the reactor sensor parameters are included in these estimates of the overall reactor parameters. Reactor parameters can be found in Section 5 of this report.

TABLE 3.2.1.4-1. AVIONIC COMPONENTS AND PARAMETERS

UNIT	SUBSYSTEM	VOL (FT^3)	POWER (VA)	WEIGHT (LBS)	MTBF (HRS)
1	INERTIAL	0.80[a]	245[a]	30[a]	30[d]
2	RADAR	6.00[a]	5500[a]	350[a]	66[b]
3	DOPPLER	1.90[c]	50[c]	15[c]	40[d]
4	R ALTIMETER	0.30[a]	110[a]	11[a]	70[d]
5	ASTROTRACKER	1.90[f]	50[f]	15[f]	30[d]
6	SECURE SPEECH	0.25[a]	30[a]	7[a]	150[g]
7	HF RADIO	1.20[a]	800[a]	54[a]	50[d]
8	VHF RADIO	0.56[h]	425[h]	33[h]	40[h]
9	UHF RADIO	0.56[a]	425[a]	33[a]	40[d]
10	DATA LINK	0.54[a]	120[a]	17[a]	150[g]
11	INTERCOM	1.20[i]	800[i]	54[i]	350[g]
12	TACAN	0.37[a]	160[a]	29[a]	60[d]
13	ADF[x]	0.30[a]	51[a]	15[a]	60[a]
14	ILS[y]	0.12[a]	51[a]	8[a]	150[d]
15	LORAN	0.80[a]	250[a]	22[a]	60[d]
16	IFF	0.33[a]	150[a]	22[a]	90[d]
17	BEACONS	0.10[j]	16[j]	3[j]	150[d]
18	OMEGA[z]	1.10[k]	200[k]	60[k]	150[k]
19	AIR DATA	0.28[a]	45[a]	12[a]	350[m]
20	AUTOPILOT	1.40[a]	235[a]	61[a]	30[d]
21	STBY ATTITUDE	0.39[a]	160[a]	25[a]	50[d]
22	RHAW[aa]	0.91[a]	225[a]	85[a]	50[g]
23	ECM[bb]	3.84[a]	7200[a]	218[a]	50[g]
24	INTERFERENCE	0.10[a]	100[a]	5[a]	150[g]
25	COMM/NAV DISP	0.21[a]	20[a]	15[a]	278[g]
26	MTC C&D[cc]	0.49[a]	835[a]	30[a]	50[d]
27	AU C&D[dd]	0.49[p]	835[p]	30[p]	50[p]
28	VSD[ee]	0.89[a]	473[a]	43[a]	40[d]
29	HSD[ff]	0.89[q]	473[q]	43[q]	40[q]
30	AUDIO RECORDER	___[r]	___[r]	___[r]	___[r]
31	MAD[gg]	___[r]	___[r]	___[r]	___[r]

TABLE 3.2.1.4-1. AVIONIC COMPONENTS AND PARAMETERS (Cont.)

UNIT	SUBSYSTEM	VOL (FT^3)	POWER (VA)	WEIGHT (LBS)	MTBF (HRS)
32	LLTV[hh]	1.22[a]	230[a]	67[a]	25[g]
33	FLIR[ii]	1.22[s]	230[s]	67[s]	25[s]
34	MULTI-DISPLAY	4.75[t]	385[t]	80[t]	278[t]
35	COMPUTERS	___[r]	___[r]	___[r]	___[r]
36	MISC C&D[jj]	0.49[q]	835[q]	30[q]	50[q]
37	R PROCESSOR[kk]	4.40[u]	200[u]	60[u]	4400[v]

FOOTNOTES

a) Weight, volume, and power estimates are based on ASD/XR avionics estimates for similar equipment on an advanced aircraft (Ref. 10).

b) Failure rates based on equipment performing similar functions on the C-5A aircraft (Ref. 108).

c) Estimates based on the Kearfott SKD-2100 Doppler Set (Ref. 158).

d) Failure rates based on equipment performing similar functions on the FB-111 aircraft (Ref. 67).

f) Assumed physical parameters to be approximately the same as a doppler set.

g) Failure rates based on estimates using MIL-STD-756A (Ref. 123).

h) Assumed physical parameters to be approximately the same as a UHF radio.

i) Assumed the intercom had station-to-station addressing and full duplex capabilities. Assumed the physical parameter to be approximately the same as the HF radio.

j) Estimates based on Motorola SST-131 transponder (Ref. 126).

k) Estimates based on Northrop AN/ARN-99(V)2 Omega (Ref. 133).

m) Estimates based on C-5A Air Data System (Ref. 156).

p) Parameters assumed to be the same as Mission and Traffic Control controls and displays.

q) Parameters assumed to be the same as Vertical Situation Display.

r) See Annex 3 of Volume III.

s) Parameters assumed to be the same as Low Light Television.

t) Estimates based on Tektronics Video Display (Ref. 37).

u) Estimates made by Dr. T. Blakley, Ohio State University, Reactor Facility (Ref. 17).

TABLE 3.2.1.4-1. FOOTNOTES (Continued)

v) Failure rates are based on failure data from Handbook For Nuclear Power Facilities and WASH-1400 report (Ref. 185, p. 19-20; 98, p. 1-445).

w) These MTBF do not include the assumed IOX improvement, i.e., these are the present values.

x) ADF - Automatic Direction Finder

y) ILS - Instrument Landing Set

z) Omega - Worldwide radio navigation system

aa) RHAW - Radar Homing and Warning

bb) ECM - Electronic Countermeasures

cc) MTC C&D - Mission and Traffic Control Controls and Displays

dd) AUX C&D - Auxiliary Control and Displays

ee) VSD - Vertical Situation Display

ff) HSD - Horizontal Situation Display

gg) MAD - Magnetic Anomaly Detector

hh) LLTV - Low Light Television

ii) FLIR - Forward Looking Infrared

jj) MISC C&D - Miscellaneous Controls and Displays

kk) R Processor - Reactor Processor

3.2.2 ESTIMATION OF TOTAL SYSTEM PARAMETERS: This section presents the results of applying the data in Table 3.2.1.4-1 to the methods outlined in Section 3.1.2.4, *LaGrange Multipliers*. For example, consider a worse case condition where a 14 day mission is specified to be 0.95 reliable. The allocation of components for each subsystem would be as shown in Table 3.2.2-1. The numbers in the quantity required column indicate the number of redundant components for each subsystem. It is important to emphasize that this list is the combination of components that will minimize overall system weight and yet achieve a 0.95 reliability for a period of 14 days. There has been no effort toward placing a priority or weighting factor on the importance

TABLE 3.2.2-1. AVIONIC REQUIREMENTS FOR NOMINAL 0.95 RELIABLE SYSTEM 14 DAY MISSION

SYSTEM	QUANTITY REQ	SYSTEM	QUANTITY REQ
INERTIAL	18	AIR DATA	4
RADAR	6	AUTO PILOT	17
DOPPLER	15	STBY ATTITUDE	11
RADAR ALTIMETER	9	RHAW	10
ASTROTRACKER	20	ECM	8
SECURE SPEECH	6	INTERFERENCE BLANKER	7
HF RADIO	10	COMM/NAV DISPLAYS	4
VHF RADIO	13	MTC DISPLAYS	11
UHF RADIO	13	AUX DISPLAYS	11
DATA LINK	6	VSD	13
INTERCOM	4	HSD	13
TACAN	10	MAD	16
ADF	10	AUDIO RECORDER	8
ILS	6	LLTV	20
LORAN	10	IR	20
IFF	7	TACTICAL DISPLAYS	4
BEACONS	7	COMPUTER	16
OMEGA	5	MISC DISPLAYS	11
SYSTEM WEIGHT — 28,867 LBS SYSTEM RELIABILITY — 0.947			

The reactor processor MTBF, as listed in Table 3.2.1.4-1, was estimated to be in excess of 4000 hours. This high MTBF would probably force the computer model to allow only single allocations of redundancy to this unit. Because of its critical function, this device was assumed to have triple redundancy, and its weight, volume, and power requirements were added to the totals manually. Triple redundancy was assumed in order to allow the built-in test equipment to vote between the three systems to determine which system has failed.

3.2.2.1 MISSION LENGTH vs RELIABILITY: Figure 3.2.2.1-1 presents the results of minimizing system weight using the LaGrange technique. In this figure, the system reliability is held constant, while system weight is plotted as a function of mission duration. This figure provides an indication of how the system weight increases as mission duration increases. However, these figures do not provide an insight into the overall composition of the avionic package. Consequently, an average component redundancy was found. This was accomplished by the application of

$$Z = \sum_{i=1}^{M} n_i/M$$

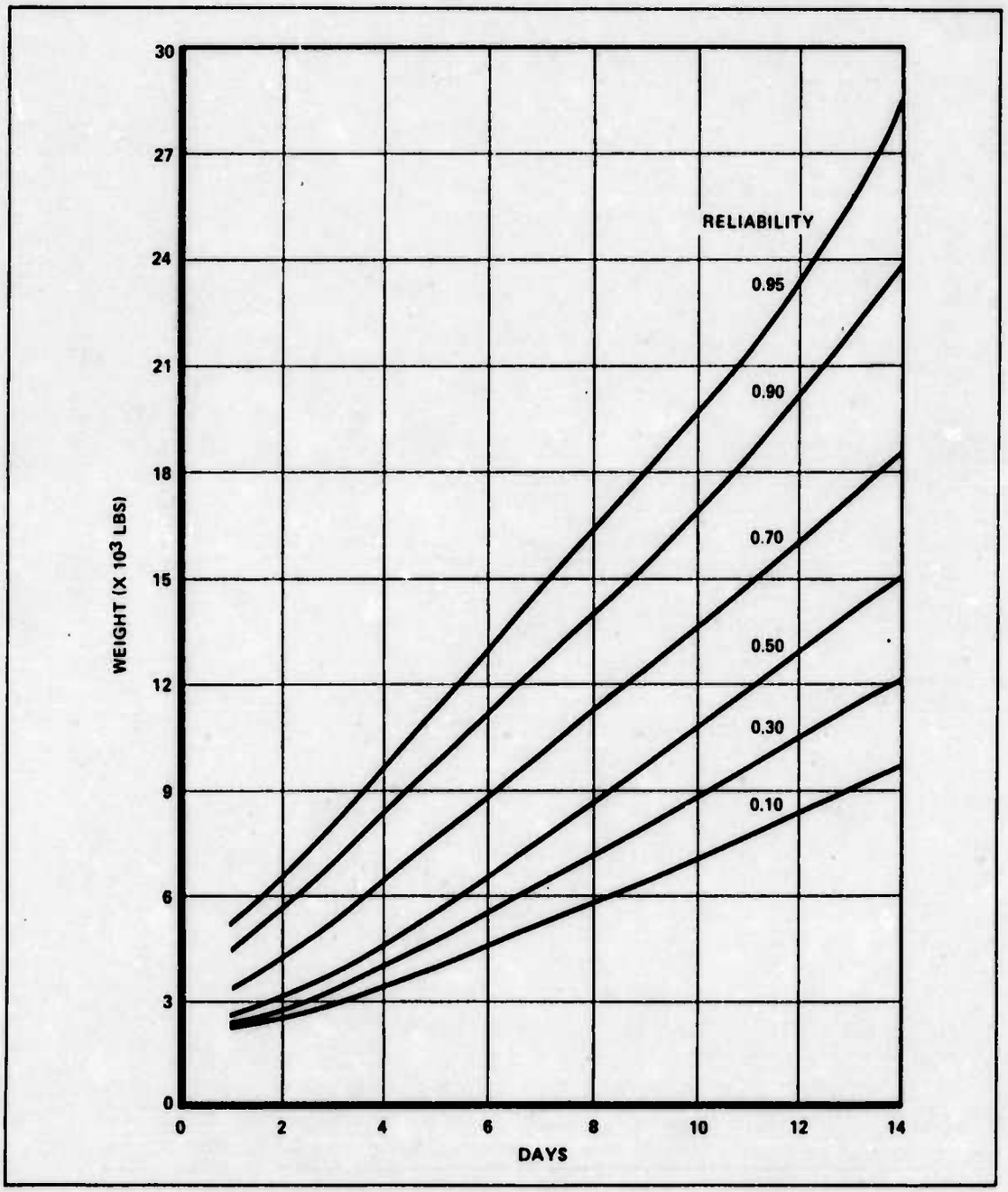

Figure 3.2.2.1-1. Avionic System Weight vs Mission Length

for various system reliabilities and mission durations. Z was rounded to an integer and results were plotted (Figure 3.2.2.1-2). The dashed line in the figure represents Z. Intuitively, one would expect Z to be a horizontal line indicating a constant weight. However, recall that Z is an average and that the algorithm may vary the parallel resource allotments to achieve a different system reliability. Consequently, the resources allocated to achieve a 50% reliable system may be different from the resources allocated to achieve a 90% reliable system. For example, suppose an avionic package is to be designed such that, on the average, each subsystem would have quadruple redundancy and the total system is specified to be 95% reliable. Then the system weight would be approximately 8,700 lbs and the mission duration would be about 3 days. If the mission were extended to 4 days, with the 8,700 lbs of equipment, then the system reliability would drop to slightly less than 90%.

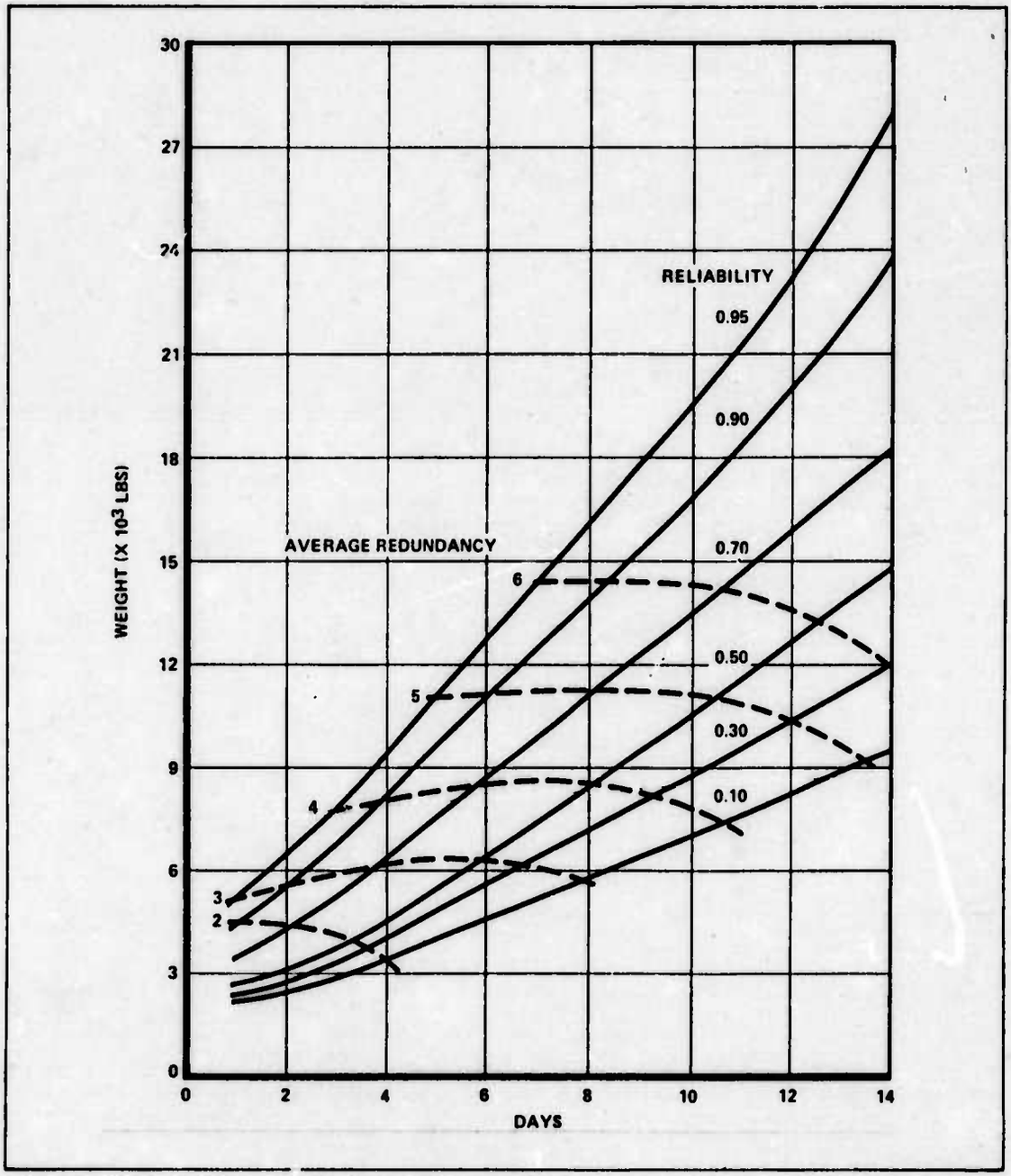

Figure 3.2.2.1-2. Redundancy Required to Meet System Reliability and Mission Length

3.2.2.2 VOLUME REQUIREMENTS: The volume of the avionic equipment associated with the weight, system reliability, and mission duration presented in the previous section is contained in Figure 3.2.2.2-1. In Section 4, the volume of fuselage was estimated to be about 540,000 cu ft. From Figure 3.2.2.2-1, the greatest volume required for the avionics is 600 cu ft. This estimate does not include mounting racks. Even if the mounting racks quadrupled the total avionic volume, it would still be less than 1% of the total aircraft volume.

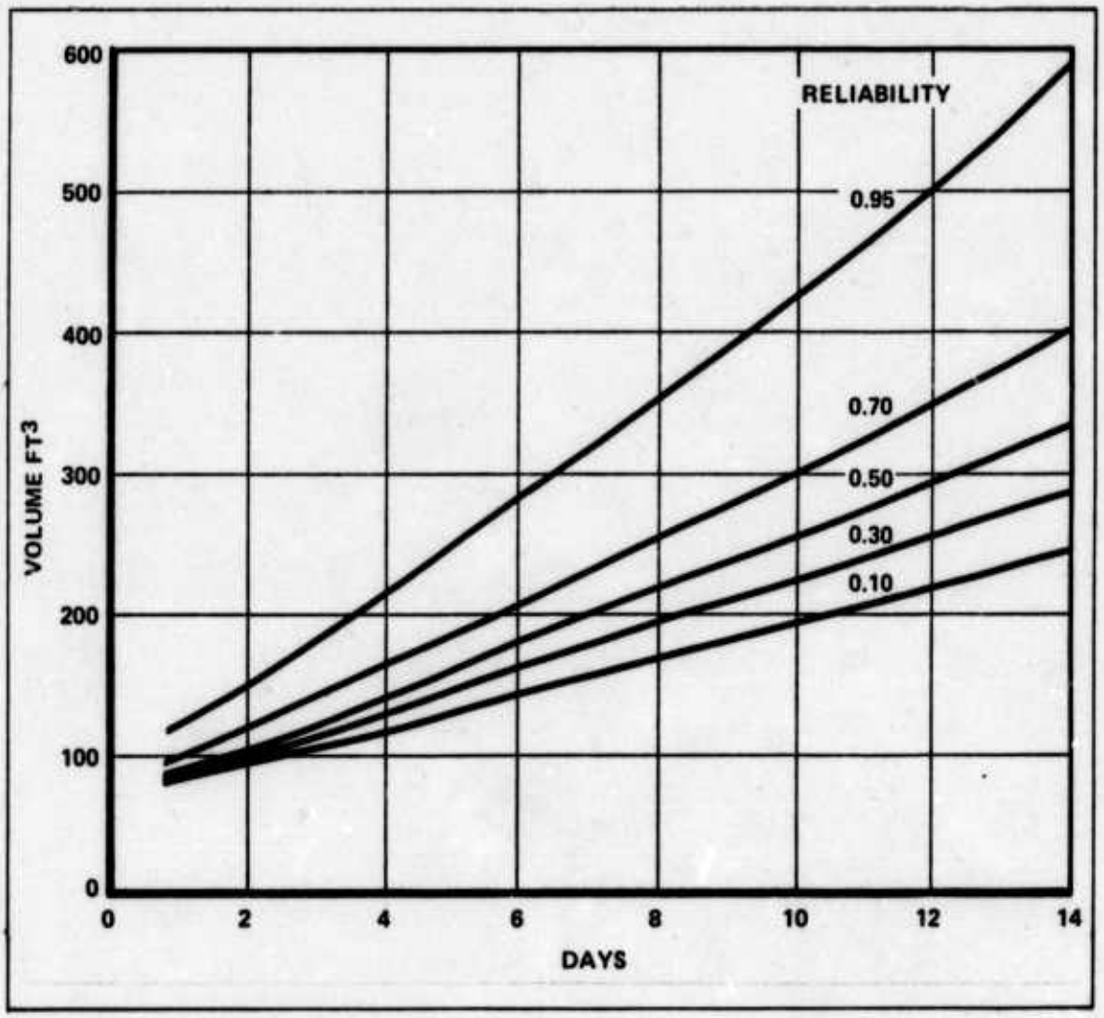

Figure 3.2.2.2-1. Avionics Volume vs Mission Length

3.2.2.3 POWER REQUIREMENTS: Power requirements for the avionics are displayed in Figure 3.2.2.3-1. These estimates represent a worse case situation, in which all subsystems are in an operate mode.

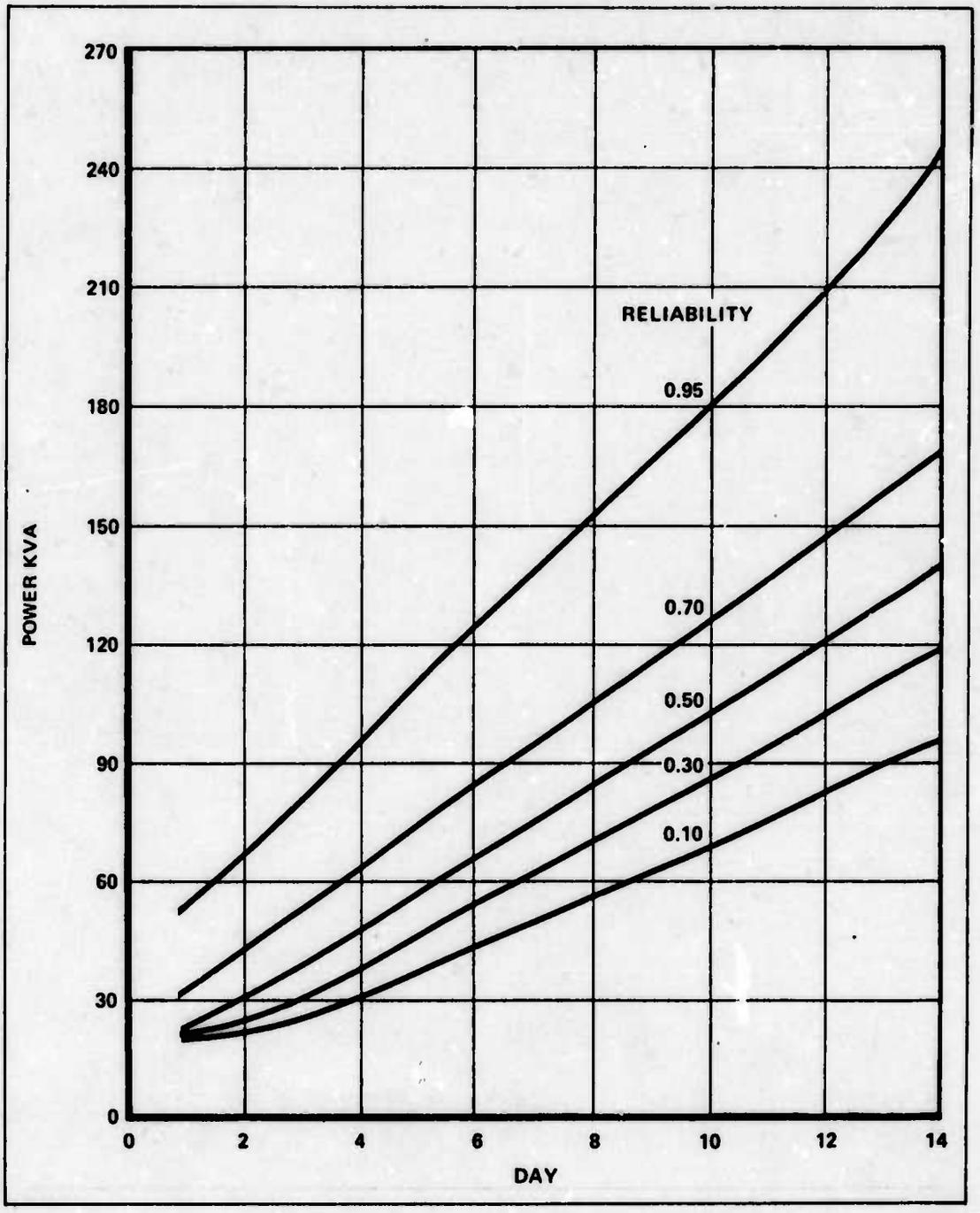

Figure 3.2.2.3-1. Power Requirements

3.3 CONCLUSIONS

3.3.1 REDUNDANCY: As indicated in Figure 3.2.2.1-2, greater than quadruple system redundancy is required to achieve a 90% reliable system which can operate more than 4 days. The redundancy for the avionics is bought at the expense of aircraft payload. This payload could

be utilized more efficiently for expendables or even for reducing aircraft gross weight. It would seem that, to achieve a long duration mission, an alternative to redundancy would be desirable.

3.3.2 ALTERNATIVES TO REDUNDANCY: Redundancy achieves reliability by providing spares at the subsystem level. One alternative to redundancy is to provide the crew with the capability to perform in-flight repair of the avionics. This notion presumes that sufficient testing capability and spare parts are on board the aircraft to correct any avionics malfunction. However, this idea presents some formidable problems. The first relates to testing and isolation of the malfunction. In order to make a redundancy scheme feasible, built-in test equipment was included. This test equipment performs end-to-end test of each subsystem. The end-to-end tests of a subsystem determine if that system is operating properly; however, little if anything can be said about the nature of the malfunction. If in-flight repairs are to be included, then it will be necessary to isolate the malfunction to some level lower than the subsystem level. If each subsystem is assumed to be a *black box*, then the next level down is the module. The testing then must isolate the malfunction to module level. If sufficient amounts of test equipment were included in the avionics to isolate the malfunction to module level, then in-flight repair could be accomplished. To provide the capability of in-flight repair to the module level will require substantial changes in testing capability and maintenance philosophy. The in-flight test equipment would have to perform the same functions as performed by ground equipment, yet weigh less than this redundant avionic system previously discussed.

3.3.3 RECOMMENDATIONS FOR ADDITIONAL STUDY: Determine what impact in flight repair would have, if any, on the weight of the total avionic package.

SECTION 4
AIRCRAFT

4.0 INTRODUCTION

A study to determine the feasibility of a nuclear powered airplane is primarily a study of the aircraft's propulsion system. The requirements that the propulsion system must meet are determined by aircraft size and weight and mission performance requirements. The relationship between these three areas is shown schematically in Figure 4.0-1. As indicated in the figure, the design process entails both interaction between the subsystem designs and iteration of system parameter estimates to arrive at a final acceptable system design. The primary purpose of this section is to describe the process by which the propulsion system requirements were determined and to enumerate those requirements. The airframe design itself, however, does provide inputs to determine the feasibility of a nuclear powered airplane. A secondary purpose of this section is to investigate those airframe related aspects of feasibility.

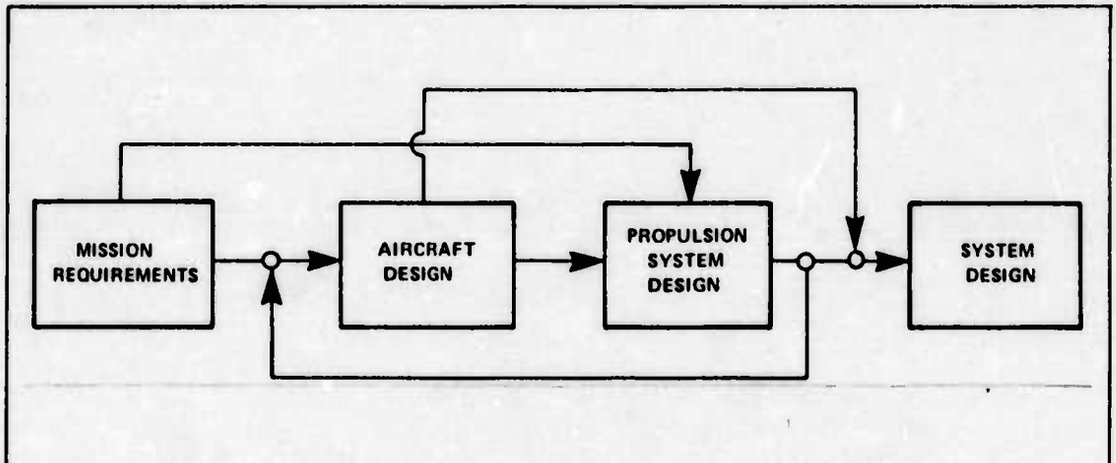

Figure 4.0-1. Design Tasks Relationship

The mission requirements were determined in Section 2 and are summarized in Table 2.1-1. The table is reproduced here, as Table 4.0-1, for the convenience of the reader. Mission parameters of primary importance to the aircraft design were airspeed, altitude, payload, and takeoff and landing distances.

The airframe design methodology is shown in the flow chart of Figure 4.0-2. The section numbers on the chart refer to other major sections of this report. The dashed-line box of Figure 4.0-2 represents the aircraft design box of Figure 4.0-1.

TABLE 4.0-1. AIRCRAFT PARAMETERS

MISSION DURATION (HRS)	336 (2 WEEKS)
CREW COMPONENT	36 MEN (3 SHIFTS OF 12 MEN)
AIRSPEED (KTS)	150 AT SEA LEVEL 250-350 AT 30,000 FEET
ALTITUDE (FT)	SEA LEVEL TO 30,000
PAYLOAD (LBS)	MINIMUM 130,000 MAXIMUM 200,000
TAKEOFF DISTANCE	CLEAR A 35 FT OBJECT IN 12,000 FEET
LANDING DISTANCE	CLEAR A 50 FT OBJECT AND STOP IN 12,000 FEET
FLEET SIZE	60 AIRCRAFT
IOC	1990-2000
LIFETIME	62,000 FLYING HOURS

The design of a nuclear powered aircraft posed a problem somewhat different from that of designing a conventional chemical powered aircraft. Not only did the aircraft have to fulfill the antisubmarine warfare (ASW) mission requirements, but it also had to use nuclear power to its best advantages. Standard aerodynamic design techniques were used throughout the design process, but were modified as necessary because of this difference.

The initial problem in the aircraft design was to make an estimate of the aircraft gross weight. Because of the large weight of the reactor, the gross weight will be quite high. Theoretically, the gross weight could be determined as a function of the payload, airspeed, and altitude requirements. In practice, however, that function is very complex and usually cannot be determined in a closed form. Therefore, the design method used was a parametric analysis in which aircraft gross weights were assumed and wing loadings and payloads were calculated as a function of gross weight. Then it was an easy matter to determine the wing loading with the best payload potential consistent with mission requirements. The aircraft gross weight was broken down into component weight elements to determine the weight available for the nuclear propulsion system and the payload. With the wing loading determined, performance estimates were made which dictated the aircraft power requirements. These power requirements were used to estimate nuclear propulsion systems weights. With all aircraft component weights estimated, the required payload dictated the point design aircraft gross weight.

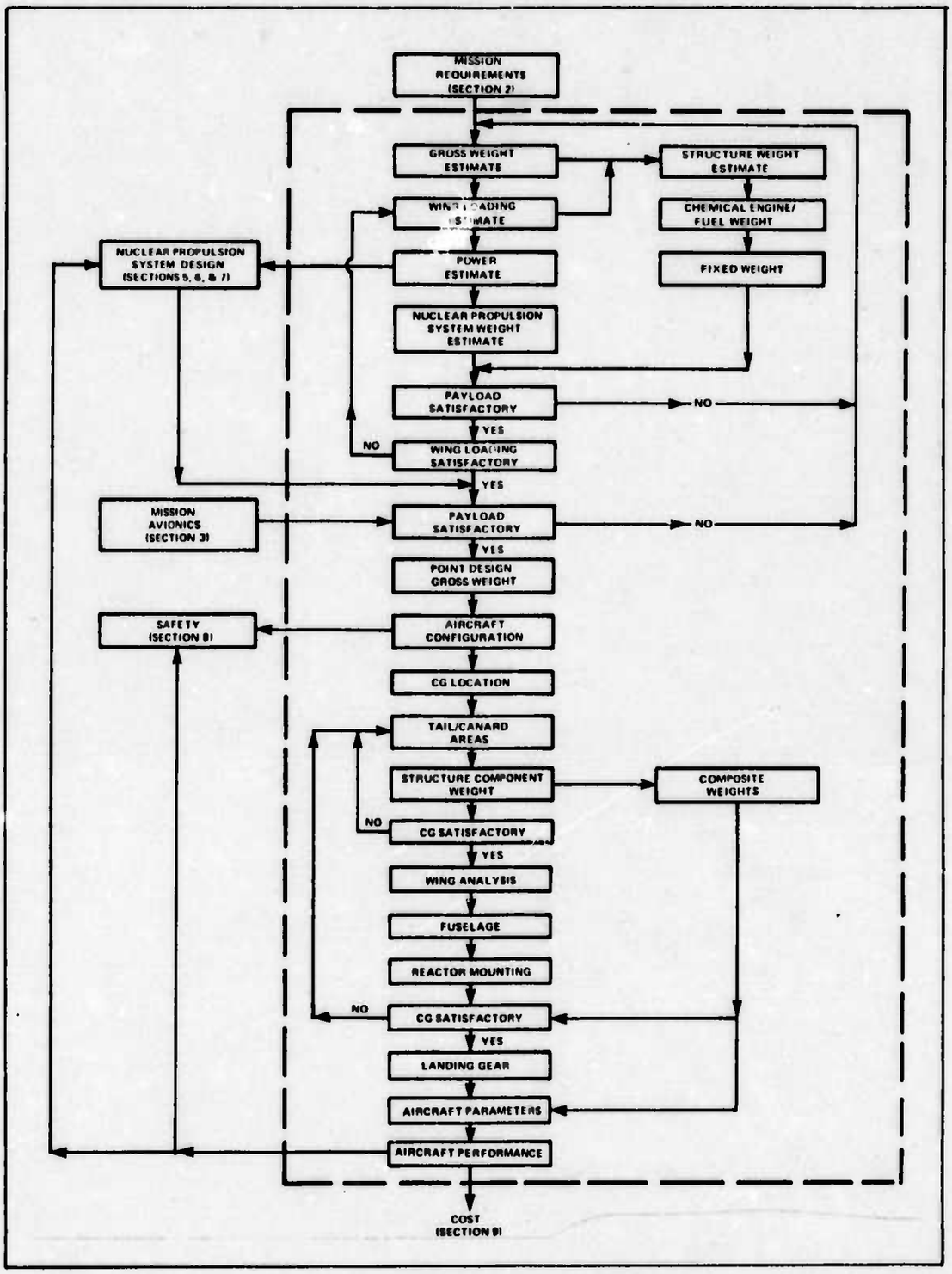

Figure 4.0-2. Aircraft Design Methodology

Several candidate aircraft configurations were considered and the most appropriate configuration was selected in light of the concept of airborne nuclear power and mission requirements. Among the configurations considered were a conventional wing and tail, a canard with the horizontal tail forward of the wing, a flying wing, and a twin body type aircraft.

Following configuration selection, a sizing analysis was conducted on the critical aircraft components to insure the feasibility of that configuration. An estimate of overall aircraft parameters such as weight and balance, aircraft dimensions, and aircraft performance was made for the selected point design aircraft.

Appendix A.4.1 contains numerical examples of the aircraft design method for most of the subsections that follow. Two computer programs were developed to aid in investigation of the aircraft design. One program was used to perform the parametric gross weight analysis and to determine aircraft parameters. The logic flow chart for that program is contained in Appendix A.4.2.1. The second program was developed to analyze the wing as a critical substructure of the airframe. The logic flow chart for the program is contained in Appendix A.4.2.2.

The symbols list shown in Table 4.0-2 is presented as an aid to understanding this section. In those cases where a symbol is used only once in the section and explained there, it is not included in this list.

TABLE 4.0-2. SYMBOLS LIST

a	ACCELERATION
AR	ASPECT RATIO = (WING SPAN)^2/WING AREA
b_C	CANARD SPAN
b_W	WING SPAN
c	LOCAL CHORD
C_D	COEFFICIENT OF DRAG
C_{DC}	COMPRESSIBILITY DRAG COEFFICIENT
C_{DI}	INDUCED DRAG COEFFICIENT
C_{DP}	PARASITE DRAG COEFFICIENT
C_{DS}	SPEED BRAKE DRAG COEFFICIENT
C_L	COEFFICIENT OF LIFT
C_{LMAX}	MAXIMUM LIFT COEFFICIENT
C_{LTO}	TAKEOFF LIFT COEFFICIENT
C_R	ROOT CHORD
C_T	TIP CHORD
D	DRAG
d	DISTANCE
D/T	DRAG TO THRUST RATIO
e	DISTANCE FROM QUARTER CHORD TO ELASTIC AXIS
E	MODULUS OF ELASTICITY
F	FORCE

TABLE 4.0-2. SYMBOLS LIST (Continued)

g	GRAVITATIONAL CONSTANT
G	MODULUS OF RIGIDITY
GW	AIRCRAFT GROSS WEIGHT
I	AREA MOMENT OF INERTIA
J	TORSIONAL STIFFNESS
L	LIFT
L/D	LIFT TO DRAG RATIO
LF	LOAD FACTOR
m	MASS
M	BENDING MOMENT
MAC	MEAN AERODYNAMIC CHORD = $2/3\ C_R \left[\frac{1 + \lambda + \lambda^2}{1 + 2} \right]$
MW	MEGAWATT
nm	NAUTICAL MILE
P	SHEAR FORCE
Q	DYNAMIC PRESSURE = $\frac{1}{2}\rho V^2$
Q_{MAX}	MAXIMUM DYNAMIC PRESSURE
R/C	RATE OF CLIMB
R/D	RATE OF DESCENT
S_C	CANARD AREA
S_{HT}	HORIZONTAL TAIL AREA
S_S	SPEED BRAKE AREA
S_{VT}	VERTICAL TAIL AREA
S_W	WING AREA
t	THICKNESS
T	THRUST
T_C	CLIMB THRUST
T_{CRUISE}	CRUISE THRUST
T_T	TOTAL THRUST
t/c	THICKNESS RATIO = THICKNESS/CHORD
V	VELOCITY
V_D	DIVERGENCE SPEED
V_{SO}	STALL SPEED
V_{TD}	TOUCHDOWN VELOCITY

TABLE 4.0-2. SYMBOLS LIST (Continued)

w	WING BEAM LOADING
[W]	MATRIX OF WEIGHTING FACTORS
W_W	WING STRUCTURE WEIGHT
W/S	WING LOADING
W/T	GROSS WEIGHT TO THRUST RATIO
α	ANGLE OF ATTACK
λ	TAPER RATIO = C_t/C_R
ρ	DENSITY, RADIUS OF GYRATION
σ	DENSITY RATIO = ρ @ ALTITUDE/ρ @ SEA LEVEL
τ	STRESS

4.1 INITIAL WEIGHT ESTIMATION

An initial weight estimation was made to determine a point design aircraft gross weight and wing loading. The point design gross weight was determined by estimating the weight of the following component parts of aircraft gross weight:

1) structural weight
2) chemical engine weight
3) chemical fuel weight
4) fixed equipment weight
5) nuclear propulsion system weight
6) payload

The difference between the sum of the first five and the aircraft gross weight resulted in the sixth, payload.

This approach determined possible aircraft gross weights which would satisfy the mission payload requirements of 130,000 to 200,000 lbs. Results of the above calculations were then compared to the findings of the nuclear propulsion system analysis (Sections 5, 6, and 7) to determine the point design aircraft gross weight.

These calculations also resulted in the selection of an optimum wing loading consistent with the mission requirements of operating altitudes from sea level to 30,000 ft at speeds of 150 to 350 kts. The aircraft speed and altitude determined the lift to drag ratio (L/D) of the study aircraft which, in turn, dictated the propulsion system power required. This power is directly related to the nuclear propulsion system weight, which is a major component of gross weight. Both L/D and structural weight are functions of wing area; therefore, the wing loading has a direct relationship to potential payload for any aircraft gross weight.

The initial weight estimation was only the first step in the preliminary aircraft design. Two of the major components of gross weight, structural weight and nuclear propulsion system weight, are reexamined after the aircraft configuration selection. Component parts of the aircraft structure are evaluated in Section 4.4, *Sizing Analysis*, and the total weights of the nuclear propulsion system are computed in Sections 5, 6, and 7.

An initial weight analysis of the six component parts of aircraft gross weight is made in the remainder of Section 4.1. A numerical example of this analysis is contained in Appendix A.4.1, Sections A.4.1.1 through A.4.1.8.

4.1.1 STRUCTURAL WEIGHT: The structure consists of the wing, fuselage, landing gear, engine nacelles, and empennage. Using weight data from a study of jet transports, Gerald Corning developed the following formula for structural weight estimation (Ref. 33, p. 29):

$$\text{STRUCTURAL WEIGHT} = \left[0.16\ GW + \frac{9.8\ GW}{(100/W/S)^{0.63}\ W/S}\right] K_{t/c}\, K_{AR}\, K_{\lambda} \qquad (4.1.1\text{-}1)$$

where:
- GW = aircraft gross weight
- W/S = wing loading = GW/wing area
- t/c = wing thickness ratio = thickness/chord
- λ = wing taper ratio = tip chord/root chord
- *A*R = wing aspect ratio = (wing span)^2/wing area
- K = correction factors for t/c, *A*R, and λ (Ref. 33, p. 32)

Corning's method was used for the initial structural weight estimation because it takes into account wing loading and wing planform. Eq. 4.1.1-1 was checked against the C-5A and Boeing 747 structure weight and the results indicated a 15 to 20% error, which was deemed acceptable for an initial estimate. The results of Eq. 4.1.1-1 are shown in Figure 4.1.1-1 for aircraft gross weights of 800,000 to 3,000,000 lbs and wing loadings of 20 and 150 lbs/sq ft.

4.1.2 CHEMICAL ENGINE WEIGHT: The second component of aircraft gross weight is the weight contributed by the chemical engines. An assumption of the study was that takeoff and landing will be accomplished with chemical power only. This operating restriction will be discussed further in Section 4.1.3, *Chemical Fuel Weight*.

The size and weight of an aircraft jet engine depends on many variables. The most prominent of these variables is the sea level static thrust of the engines. Other variables, such as manufacture and designer, have only minor influence on the weight. Therefore, this study used the required takeoff thrust as the one variable which determined engine weight.

4.1.2.1 TAKEOFF THRUST ESTIMATION: For a transport type aircraft, the highest gross weight to thrust ratio, or thrust loading (W/T), will be required at takeoff. It was assumed that the thrust would be required to lift off the aircraft over a 35 ft obstacle in a 10,000 ft distance. This 10,000 ft distance will allow the study aircraft to use existing Air Force runways.

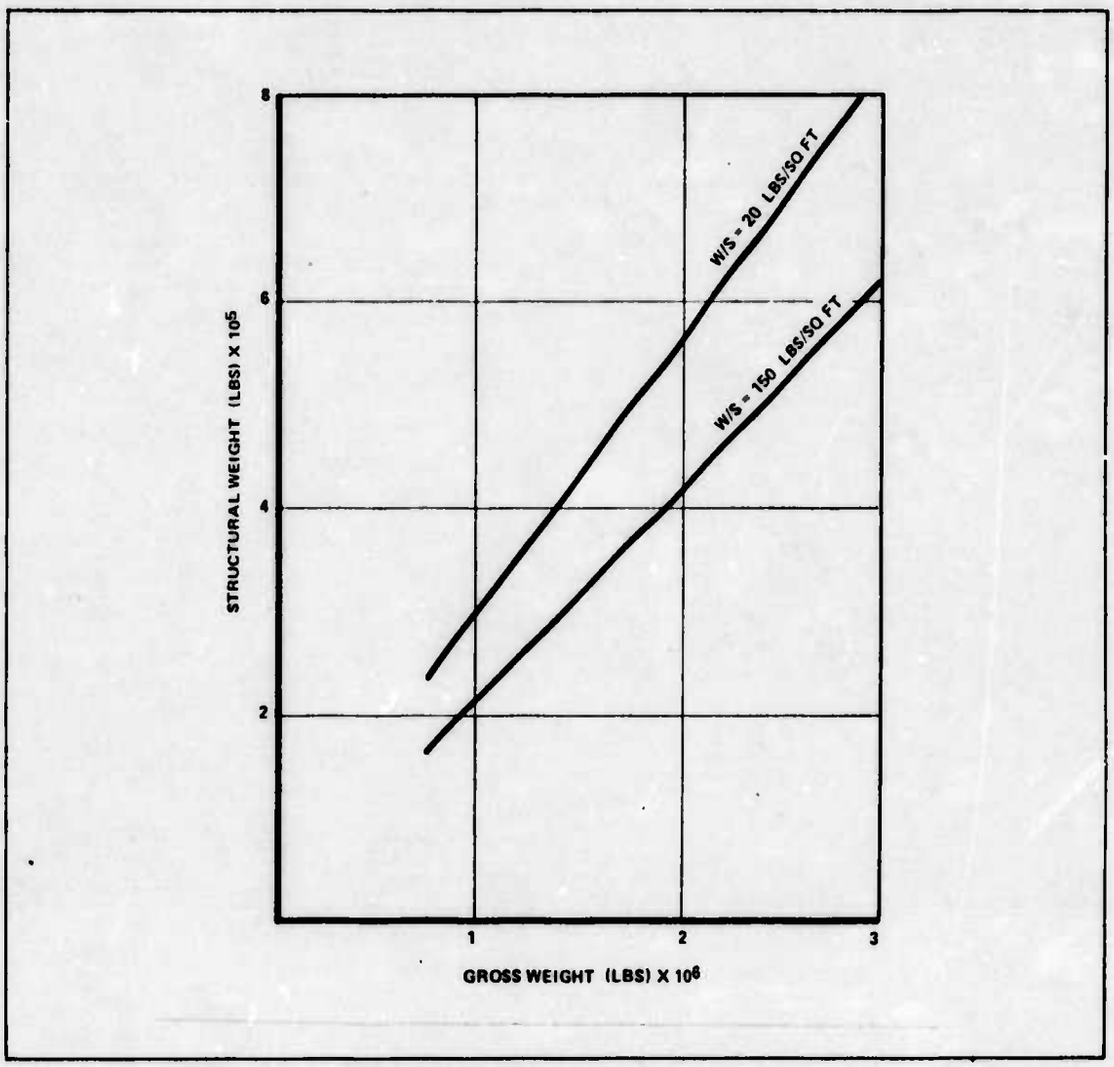

Figure 4.1.1-1. Structural Weight as a Function of Gross Weight

Corning used empirical data for subsonic jet aircraft values of drag to thrust ratios (D/T) to derive a relationship between takeoff distance and a parameter K (Ref. 33, p. 24). Figure 4.1.2.1-1 is a plot of this relationship. The parameter K is related to aircraft parameters such that:

$$K = (W/S)(W/T)(1/C_{LTO})(1/\sigma) \qquad (4.1.2\text{-}1)$$

where: W/S = wing loading
W/T = thrust loading
C_{LTO} = takeoff lift coefficient
σ = air density ratio

To avoid stall conditions during takeoff, C_{LTO} was assumed to be 75% of C_{LMAX}. C_{LMAX} is the maximum lift coefficient with full flaps, which was assumed to be 2 for initial estimation. A value of 2 for C_{LMAX} is well within the parameters of a number of subsonic airfoils.

With the assumed takeoff distance, K was obtained from Figure 4.1.2.1-1 and the required thrust loading calculated from Eq. 4.1.2-1 such that:

$$W/T = \frac{K \sigma C_{LTO}}{W/S}$$

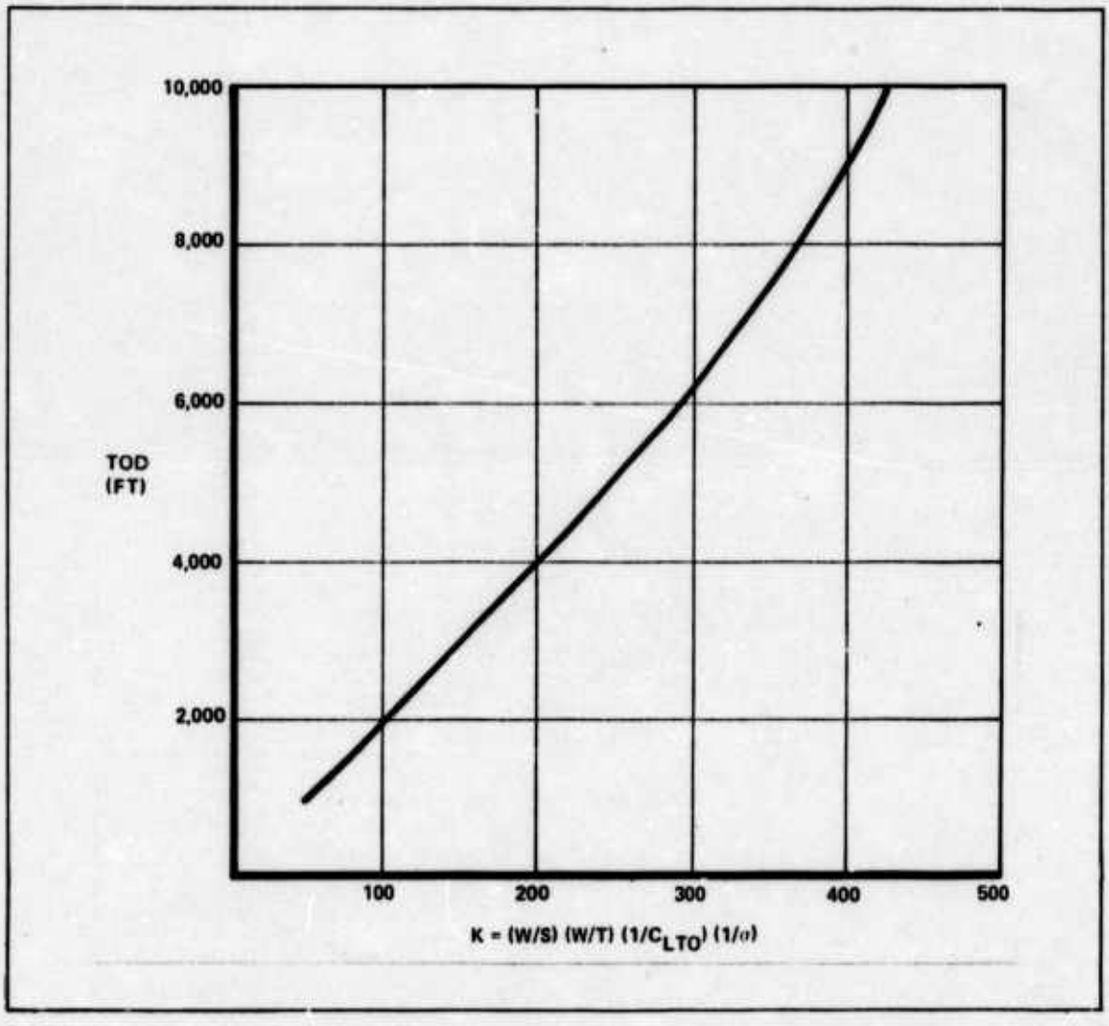

Figure 4.1.2.1-1. Takeoff Chart: Thrust Loading as Determined by Takeoff Distance

The air density ratio accounts for hot day conditions. This study used a hot day takeoff at 100°F, at which the value of the air density ratio is 0.926.

Since the thrust of a jet engine is reduced by about 10% due to this high temperature, the W/T obtained above was reduced by 10% to assure that enough thrust was available for takeoff.

therefore: takeoff thrust required = $$\frac{GW\ W/S}{0.9\ K\ \sigma\ C_{LTO}}$$

Figures 4.1.2.1-2 and 4.1.2.1-3 show graphically how gross weight and wing loading affect takeoff thrust and structural weight. Note that gross weight and wing loading have a major effect on the required takeoff thrust while wing loading has a minor effect on structure weight.

4.1.2.2 ENGINE WEIGHT AS A FUNCTION OF THRUST: The weight of the chemical engines was determined as a function of the required takeoff thrust calculated above. The method used in this study was empirical and was based on the weights and sea level static thrusts of presently available jet engines. A plot of engine weight vs sea level static thrust was made for 26 current high thrust jet engines. A curve was then fitted through the data points by the least squares method which resulted in the following formula for engine weight:

$$\text{Engine Weight} = \text{EXP}\left[\frac{\ln(\text{thrust}) + 1.36}{1.349}\right] \qquad (4.1.2\text{-}2)$$

with one standard deviation 18% of the mean.

Details and development of Eq. 4.1.2-2 are contained in Section 6.1 of this study.

Eq. 4.1.2-2 was applied with the takeoff thrust estimation to estimate chemical engine weight. For example, the TF-39, C-5A engine, has a sea level static thrust of 40,000 lbs. By use of Eq. 4.1.2-2, the estimated weight of this engine is 7039 lbs. The actual weight of the TF-39 is 7311 lbs, which is within 5% of the estimate. Note that thrust in Eq. 4.1.2-2 must be thrust per engine which results in weight per engine.

4.1.3 CHEMICAL FUEL WEIGHT: Dr. Larry Noggle, Nuclear Propulsion Program Manager, Deputy for Development Planning, Aeronautical Systems Division (ASD), predicts that a nuclear powered aircraft will be restricted to chemical takeoff and landing with the reactor shut down below a certain altitude. Further, Dr. Noggle states that the aircraft should have a limited chemical cruise capability in case of reactor failure (Ref. 134). These restrictions are a natural extension of today's concern over nuclear power plant safety.

Based on data assembled by Corning, chemical fuel weight was estimated at 16% of aircraft gross weight (Ref. 33, p. 20). This chemical fuel weight is the amount of JP-4 which would be required for takeoff, landing, a 500 to 1000 nm emergency cruise, and required reserve.

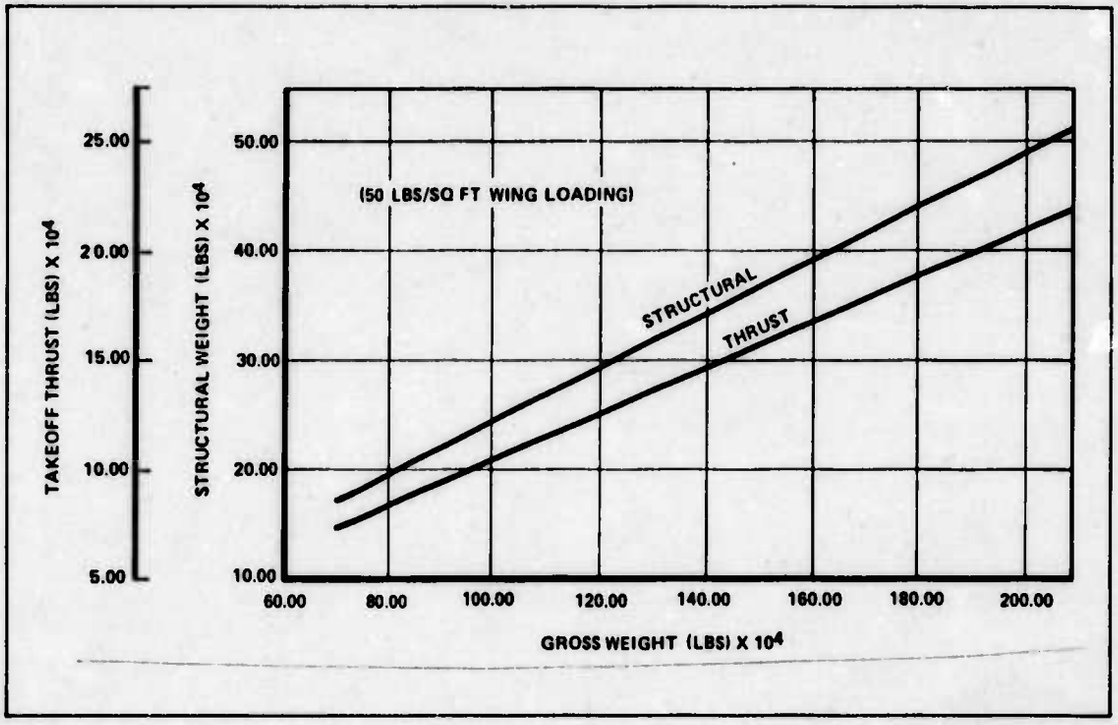

Figure 4.1.2.1-2. Structural Weight/Takeoff Thrust as a Function of Gross Weight

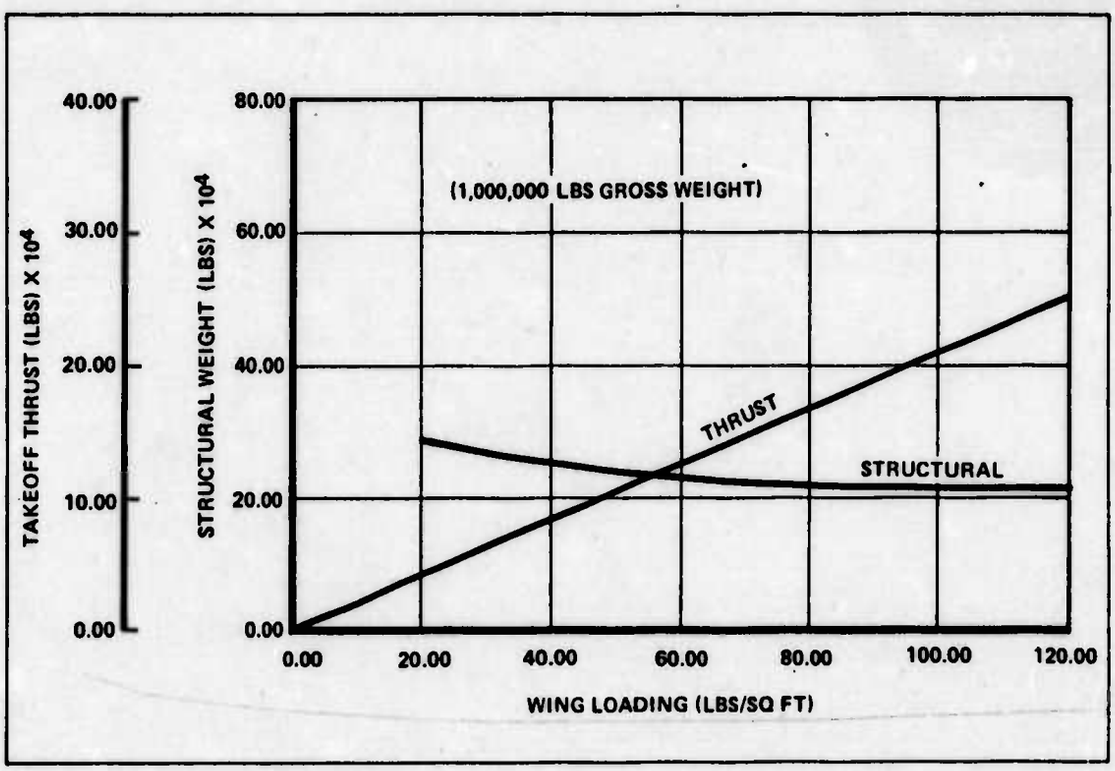

Figure 4.1.2.1-3. Takeoff Thrust/Structural Weight as a Function of Wing Loading

If it were permissible to use nuclear power for takeoff and landing, and the chemical cruise capability were eliminated, the chemical fuel weight could be greatly reduced. Chemical power used only to supplement the nuclear power available for takeoff and initial climb would reduce the weight of chemical fuel required to approximately 4% of gross weight. This estimation is based on the specific fuel consumption of two 40,000 lb thrust TF-39 engines during takeoff and climb to 30,000 ft. This 80,000 lbs supplementary thrust is the additional thrust required for a 2,000,000 lb aircraft to take off on nuclear power.

If the reactor is to operate at full power during takeoff and landing, a complete evaluation of the safety aspects of both aircraft crash and ground radiation is required (Sections 5 & 8).

4.1.4 FIXED EQUIPMENT WEIGHT: The fourth part of aircraft gross weight was defined as fixed equipment. Fixed equipment consists of the crew weight and all the weight directly related to crew comfort and many miscellaneous items. The miscellaneous items, such as hydraulic and electrical systems, instruments, and emergency equipment are subject to considerable variation.

The method used to determine this weight was to examine modern large transport aircraft to find the percent of gross weight that could be classified as fixed equipment. With *Jane's All The World Aircraft* as a guide, aircraft component weights of the DC-10, Boeing 747, and C-5A were estimated (Ref. 171, p. 274, 336, 353). The result of this analysis was that fixed equipment comprised about 7 to 9% of the three aircraft's gross weights. This rationale resulted in the selection of 10% of aircraft gross weight as the fixed weight estimation.

The above analysis may be compared to a Corning estimation technique. This technique allots 4½% of gross weight to miscellaneous and 390 lbs per crew member (Ref. 33, p. 34). Applied to the study aircraft this would result in about 6% of gross weight for fixed equipment. With the length of mission envisioned for the study aircraft, the 10% allotment was considered the more realistic.

4.1.5 NUCLEAR PROPULSION SYSTEM WEIGHT: The last item of aircraft gross weight required to find an estimated payload is the nuclear propulsion system weight. This weight estimation is only intended as a rough approximation. A refined nuclear propulsion system weight will be found in the results of the analyses of reactor, heat transfer, and engines (Sections 5, 6, and 7).

The preliminary estimation of the nuclear propulsion system weight was found by estimating the aircraft power required at cruise:

At cruise: thrust (T) = drag (D) & lift (L) = GW

Therefore: $L/D = GW/T$ or $T = GW/(L/D)$ (4.1.5-1)

And: power = thrust x velocity (V)

From Eq. 4.1.5-1 it is apparent that the determining factor in the thrust required for a given gross weight is L/D. Therefore, it is necessary to digress and determine the aircraft's L/D.

4.1.5.1 LIFT TO DRAG RATIO (L/D): The method used to estimate the study aircraft's L/D was again developed by Corning (Ref. 33). Corning's technique is to estimate the lift and drag coefficients (C_L and C_D) from basic definitions and historical data on transport aircraft such that:

$$\text{Lift/Drag} = C_L/C_D \qquad (4.1.5\text{-}2)$$

$$\text{Lift} = \tfrac{1}{2}\,\rho\, S_W\, V^2\, C_L$$

where: S_W = Wing Area = GW/(W/S)
at cruise lift = GW

and:
$$C_L = (2GW)/(\rho\, S_W V^2) \qquad (4.1.5\text{-}3)$$

$$\text{Total Drag Coefficient } C_D = C_{DP} + C_{DI} + C_{DC} \qquad (4.1.5\text{-}4)$$

C_{DP}, C_{DI}, C_{DC} are defined and calculated below.

$$C_{DP} = \text{Parasite Drag} = F/S_W \qquad (4.1.5\text{-}5)$$

where F = sum of wetted area times friction coefficient

The friction coefficient for the size and speed of the study aircraft should be approximately 0.003 for wing, 0.0024 for fuselage, 0.006 for nacelles and 0.0025 for empennage (Ref. 33, p. 36).

The tail surface areas are a function of the wing area, the nacelle area a function of the engine thrust, and the fuselage area a function of the number of passengers the aircraft could carry if it were an airliner. Therefore, (F) can be written as a function of these variables. From a Corning study of jet transports the following equation was evolved (Ref. 33, p. 36):

$$F = 1.1 + 0.128\,NP + 0.007\,S_W + 0.0021\,NE\,(T)^{.7} \qquad (4.1.5\text{-}6)$$

where: NP = number of passengers
NE = number of engines
T = static sea level, takeoff thrust per engine

The size aircraft required for this study will be about twice the size of the Boeing 747, so 1000 passengers were assumed for NP in the parasite drag estimation.

C_{DI}:
$$C_{DI} = \text{Induced Drag} = C_L^2/(\pi\, AR\, e) \qquad (4.1.5\text{-}7)$$
where: e = wing efficiency factor ≈ 0.8 (Ref 33, p. 37)

C_{DC}: Mission requirements specify a cruise speed of Mach 0.6 at 30,000 ft. At this Mach, the aircraft was assumed to cruise very near critical Mach speed.

Therefore: C_{DC} = Compressibility Drag = 0.002 (Ref. 33, Ch. 2, p. 44). C_{DC} only contributes about 6% of the total drag; therefore, a large error in the C assumption will only have a small effect on the overall L/D result.

This L/D estimation technique was checked against the Boeing 747 and less than 5% error resulted.

Wing loading, lift-to-drag, thrust, altitude, and air speed are compared graphically in Figures 4.1.5.1-1 through 4.1.5.1-4. From Eq. 4.1.5-1 thrust is equal to gross weight divided by L/D; therefore, the minimum cruise thrust is at the maximum L/D for a given air speed and altitude. This is shown in Figures 4.1.5.1-1 and 4.1.5.1-2.

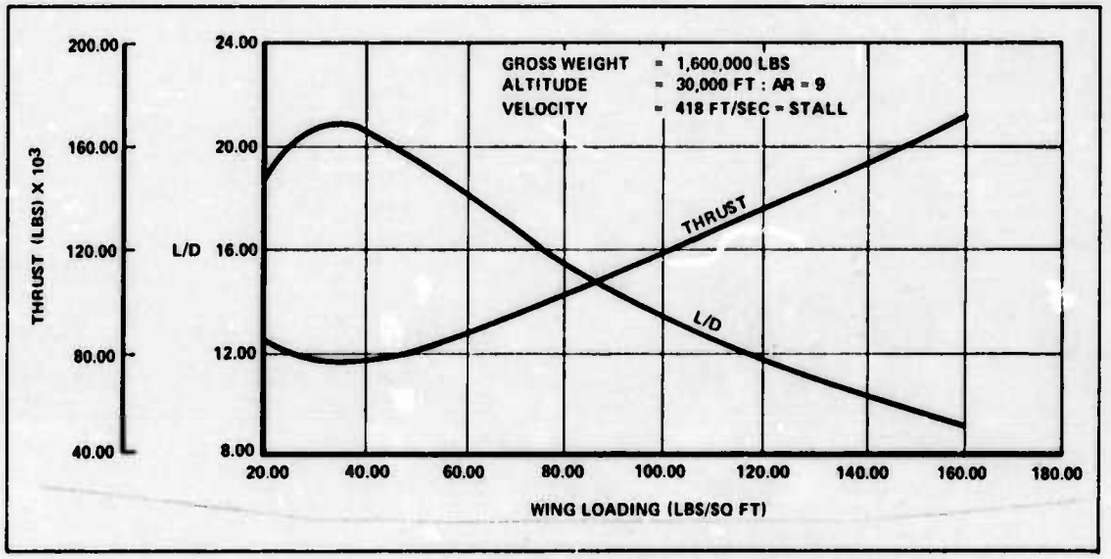

Figure 4.1.5.1-1. Thrust and L/D as a Function of Wing Loading

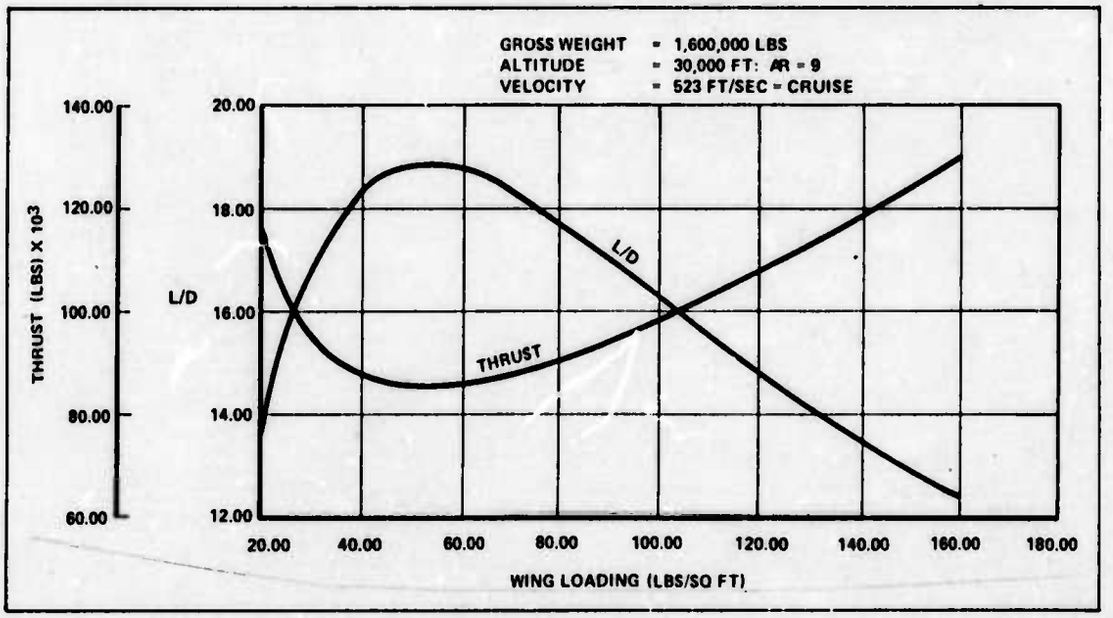

Figure 4.1.5.1-2. Thrust and L/D as a Function of Wing Loading

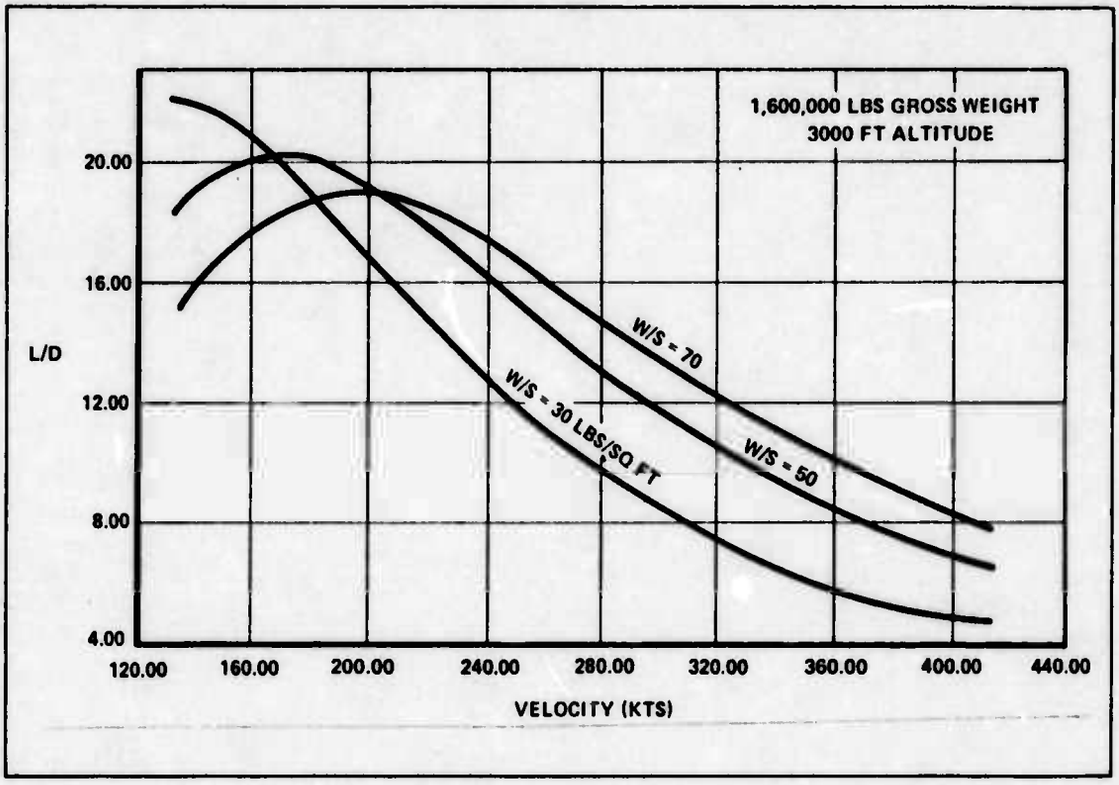

Figure 4.1.5.1-3. L/D as a Function of Velocity and Wing Loading

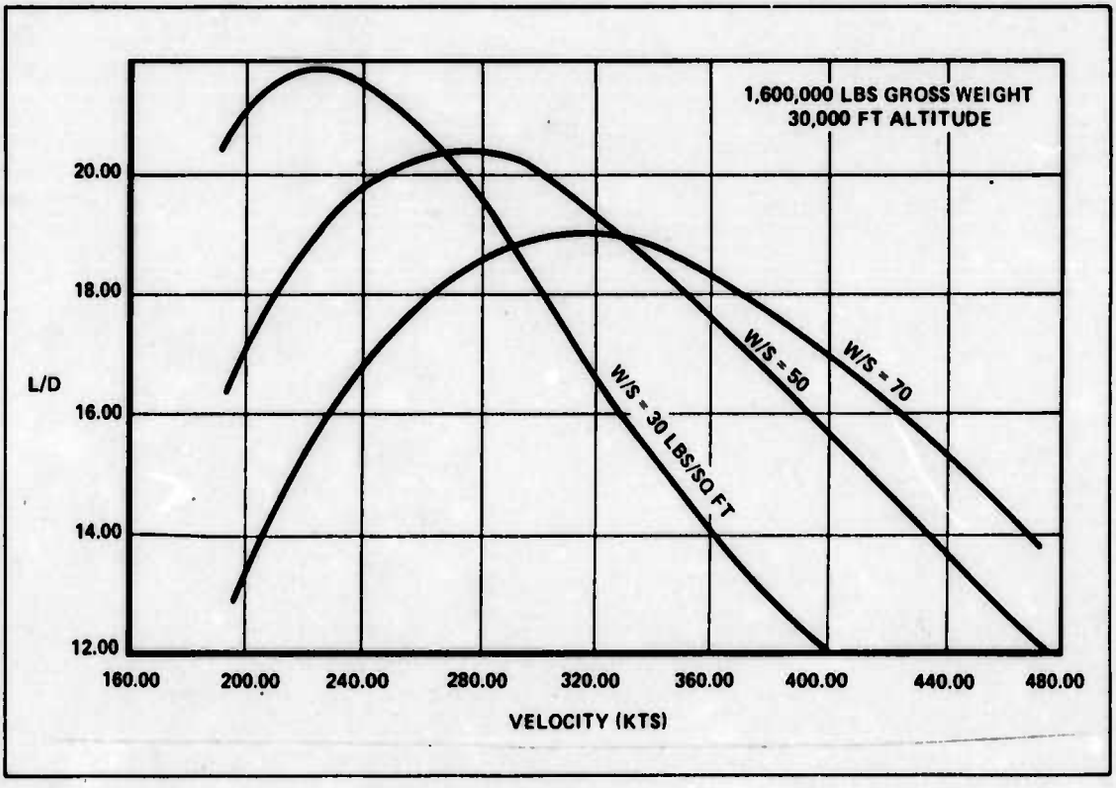

Figure 4.1.5.1-4. L/D as a Function of Velocity and Wing Loading

In addition to determining thrust, the aircraft L/D is instrumental in determining optimum wing loading. This wing loading will be determined by the required cruise speeds and altitudes. After discussions with Prof. Larsen, Head of AFIT's Aero Design Center, it was concluded that the cruise speed should be at about 80% of maximum L/D and at a speed greater than that speed which yields the maximum L/D (Ref. 94). The cruise L/D will be discussed further in Section 4.4.4, *Cruise Performance*. Figures 4.1.5.1-3 and 4.1.5.1-4 indicate that the optimum wing loadings for mission air speeds and altitudes is about 60 lbs/sq ft. The optimum wing loading will be examined again in Section 4.1.7.1, *Optimum Wing Loading*.

4.1.5.2 NUCLEAR PROPULSION SYSTEM WEIGHT AS A FUNCTION OF REACTOR POWER: It was assumed that the nuclear reactor weight would be 95 to 98% of the total nuclear propulsion system weight. This small weight difference was ignored for the preliminary estimate and the weight of the nuclear reactor was assumed to be the total nuclear propulsion system weight. Recall that this estimation is only intended to be a rough approximation.

The power calculated by Eq. 4.1.5-1 and the cruise velocity was converted to nuclear reactor power required by using a 35% efficiency factor for thermal to mechanical power conversion. This efficiency is consistent with the efficiencies achieved in today's nuclear power plants. Fifteen percent additional power was assumed and added to this power estimate for additional aircraft power requirements (hydraulics, etc.) Fifteen percent is based on the C-5A's 12 to 15% auxiliary power requirement. This resulted in the nuclear reactor power required to fly the aircraft at cruise conditions.

The resulting reactor power was applied to the most recently available aircraft reactor data, the Westinghouse Low Specific Weight Powerplant (LSWP) data shown in Figure 4.1.5.2-1, to estimate the nuclear propulsion system weight for both gas and liquid metal reactors (Ref. 190).

4.1.6 PAYLOAD: The estimated available payload for each aircraft gross weight was the difference between the gross weight and the sum of the structural, chemical engine, chemical fuel, fixed equipment, and nuclear propulsion system weights required for that gross weight. This method of estimating payload required iteration of aircraft gross weight and wing loading, at the required mission speed and altitudes, over a range of values. The gross weight was examined from 800,000 to 2,400,000 lbs. and wing loading was iterated from 20 to 150 lbs/sq ft. These results can best be compared in graphical form.

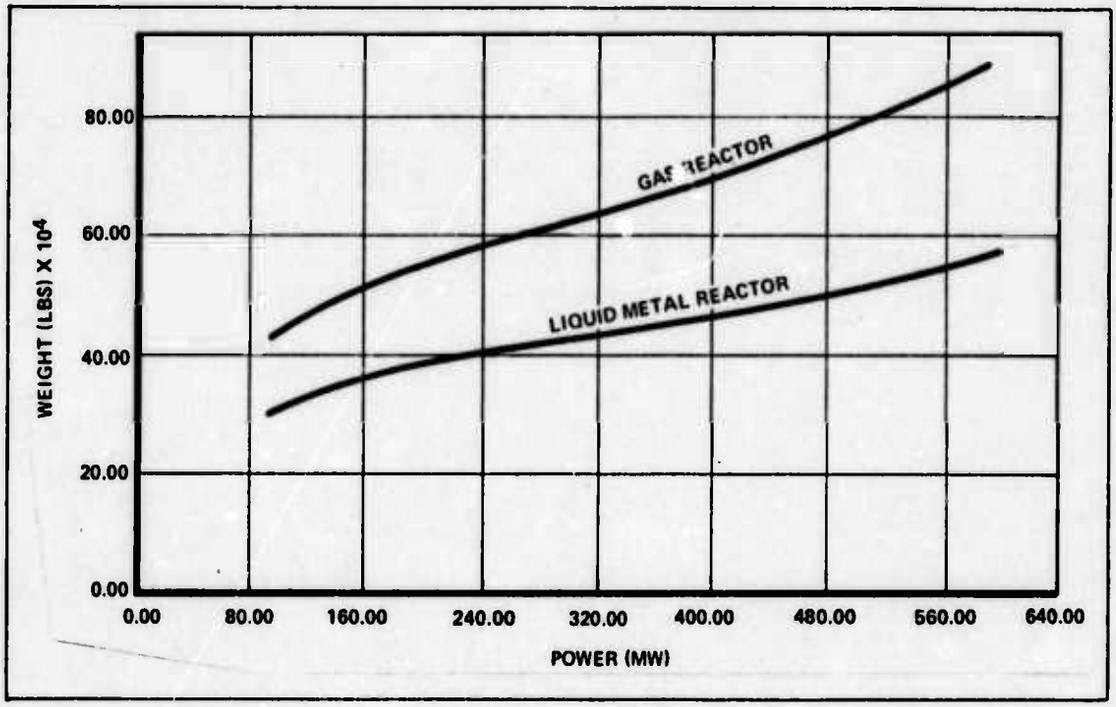

Figure 4.1.5.2-1. Reactor System Weight vs Reactor Power

Wing loading, gross weight, and payload are compared in Figures 4.1.6-1 through 4.1.6-6. Figures 4.1.6-1 and 4.1.6-2 show that the best payload potential for an 800,000 and 1,600,000 lb gross weight aircraft is at a wing loading of 50 to 60 lbs/sq ft. Figures 4.1.6-3 and 4.1.6-4 are a summary of the payload for three different weight aircraft (800,000, 1,600,000, and 2,400,000 lbs). Figure 4.1.6-3 is the result with a gas reactor, and Figure 4.1.6-4 is for a liquid metal reactor. Again the best payload is at a wing loading of 50 to 60 lbs/sq ft.

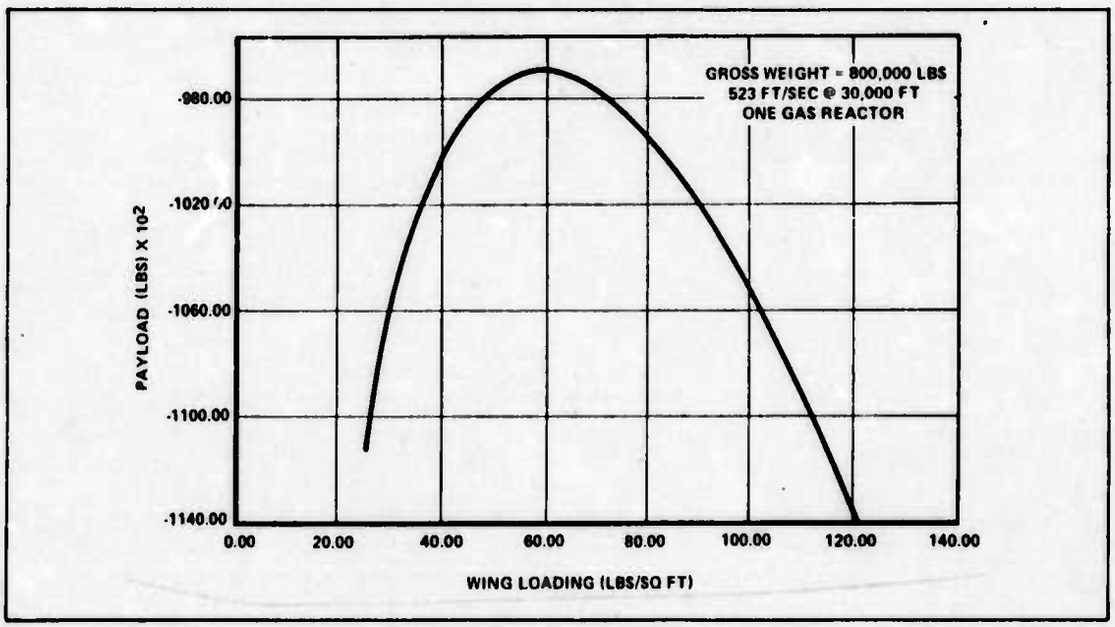

Figure 4.1.6-1. Payload vs Wing Loading

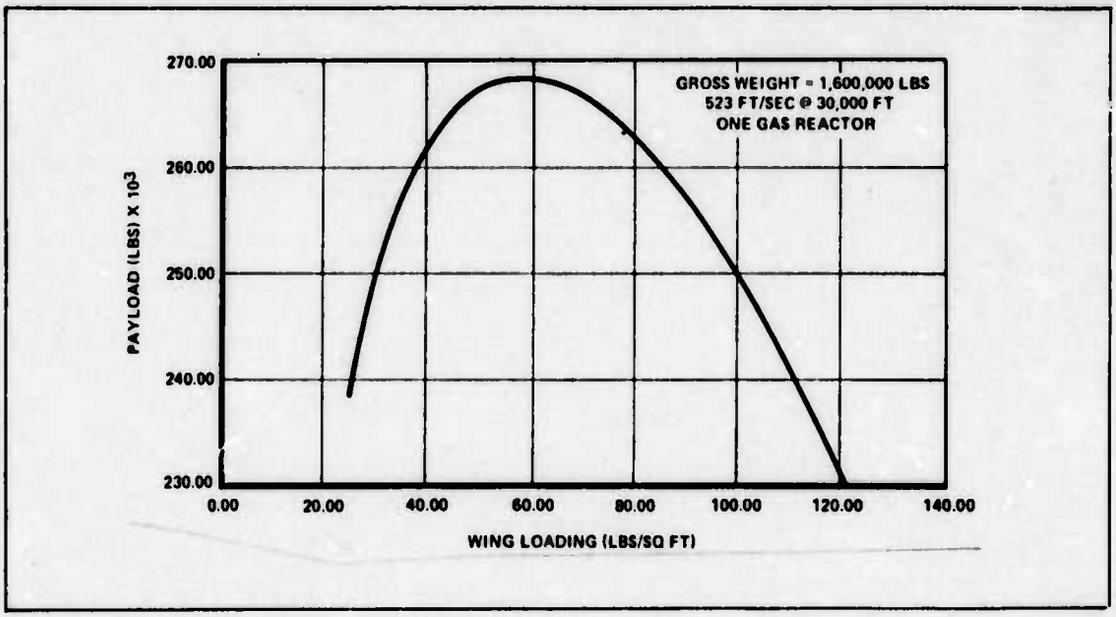

Figure 4.1.6-2. Payload vs Wing Loading

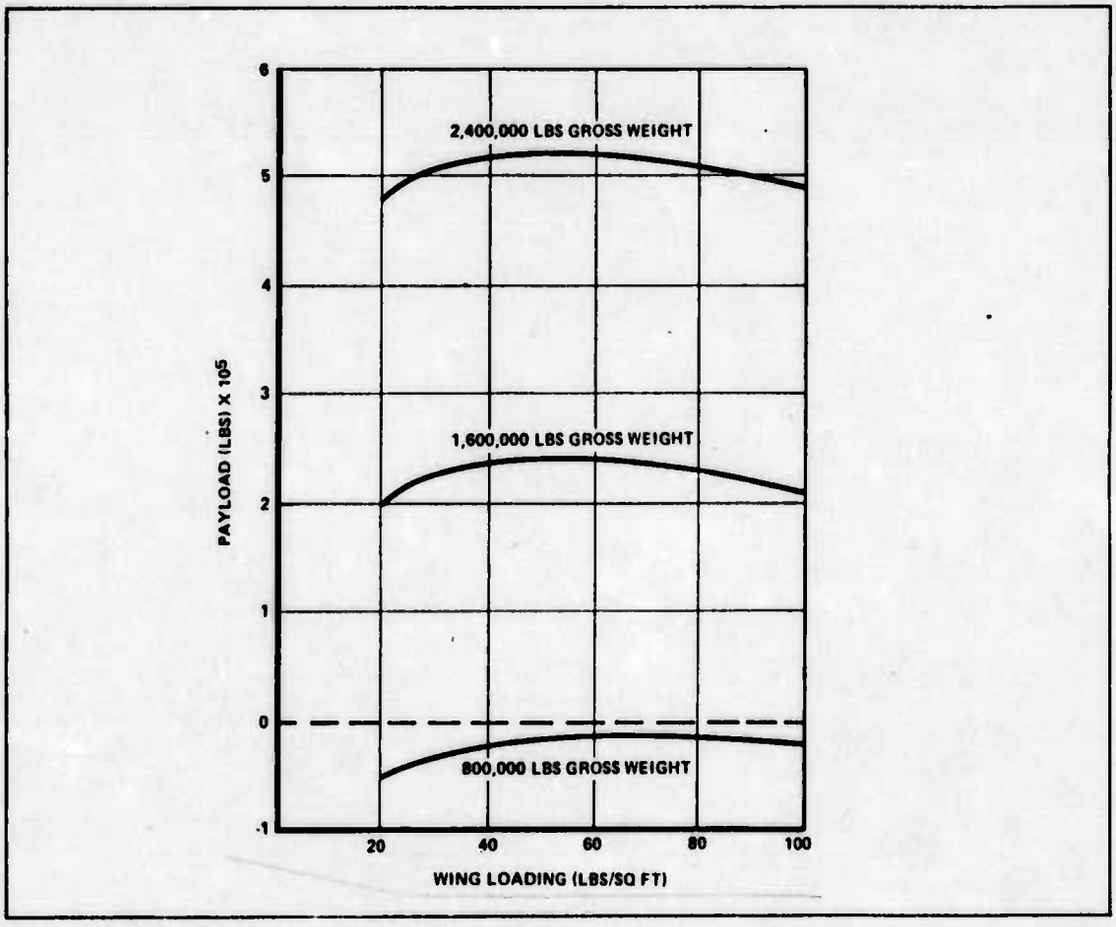

Figure 4.1.6-3. Payload vs Wing Loading — Gas Reactor

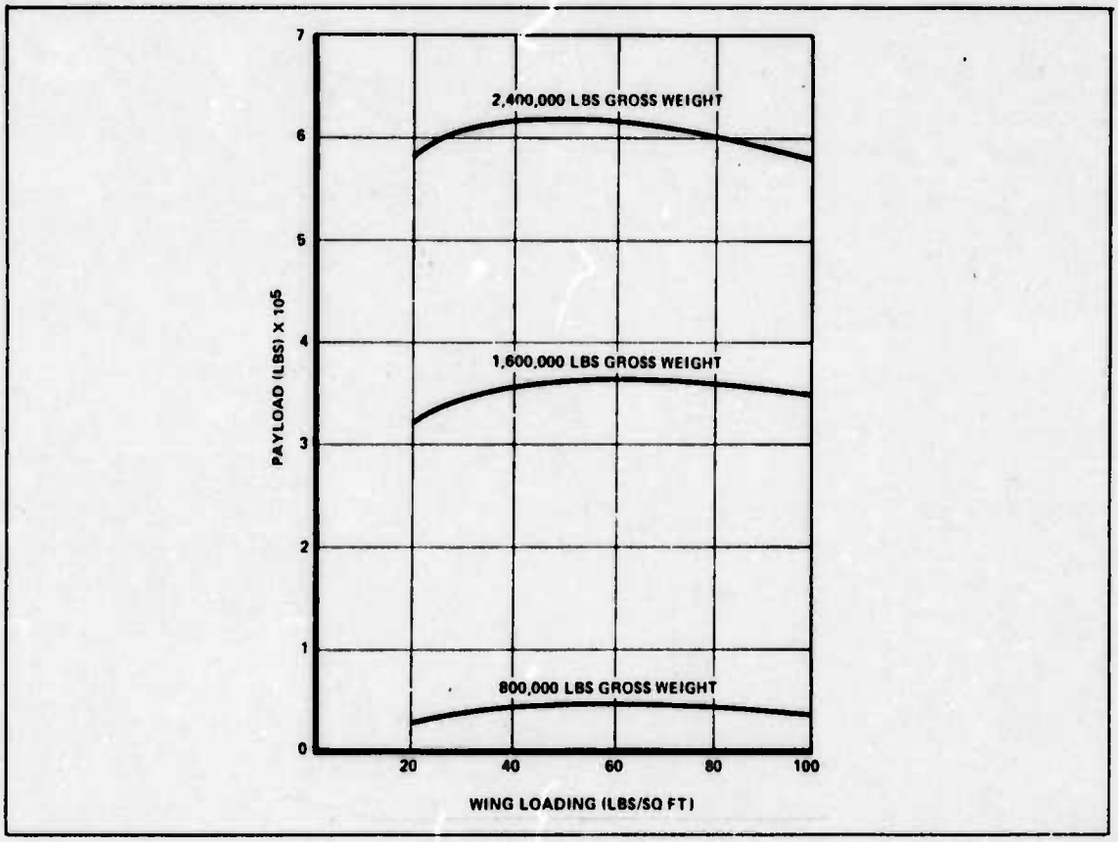

Figure 4.1.6-4. Payload vs Wing Loading — Liquid Metal Reactor

Figure 4.1.6-5 shows a comparison of payload and aircraft gross weight for four reactor configurations at a wing loading of 50 lbs/sq ft. Figure 4.1.6-6 shows the payload expressed as percent of aircraft gross weight. Note that the payload percent appears to approach an asymptote as the gross weight approaches eight to ten million lbs.

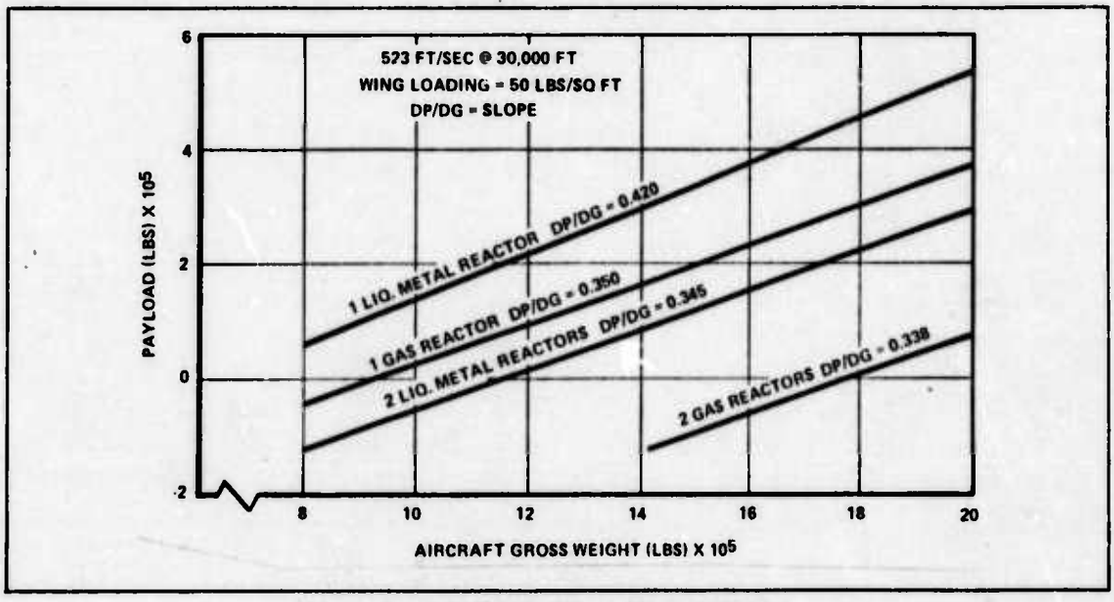

Figure 4.1.6-5. Payload vs Gross Weight

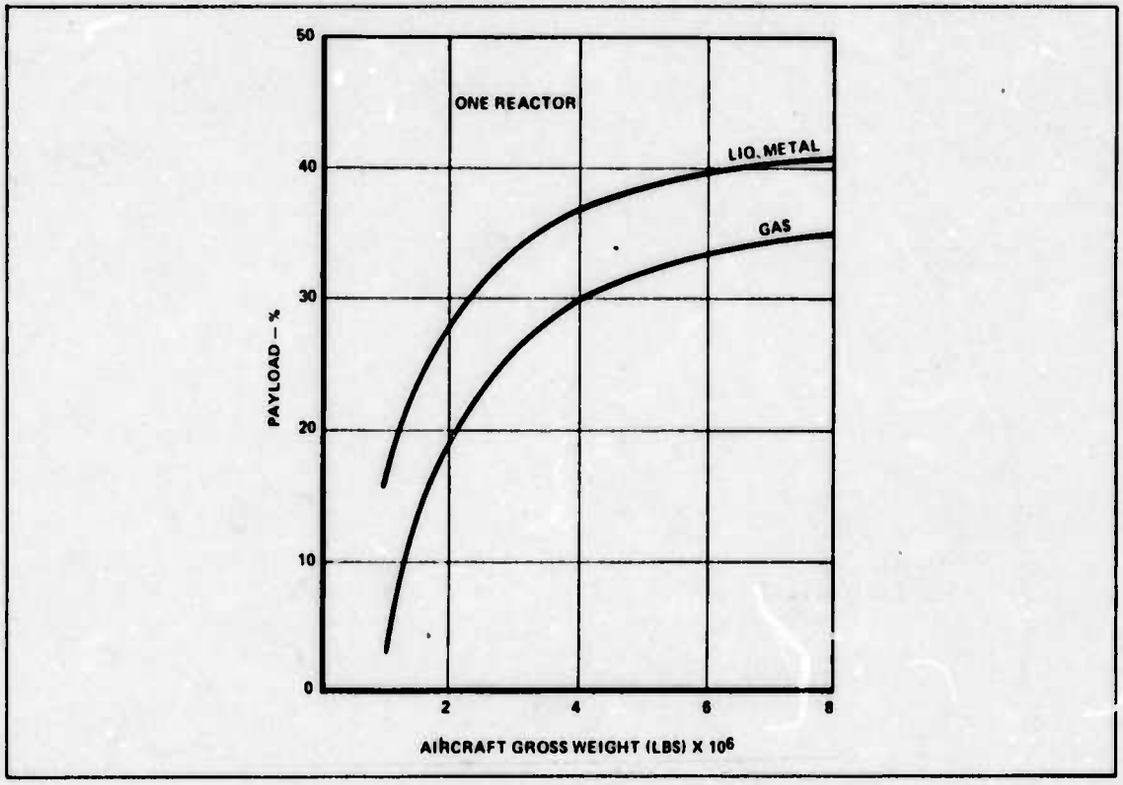

Figure 4.1.6-6. Payload as Percent of Gross Weight

4.1.7 INITIAL WEIGHT ESTIMATION RESULTS: The preceding weight analysis resulted in optimum wing loading and a point design aircraft gross weight. The optimum wing loading was derived from L/D estimation and potential payload at mission speeds and altitudes. The point design gross weight selection resulted from analysis of the nuclear propulsion system component weights, initial aircraft weight estimation, and discussions with aircraft design experts.

4.1.7.1 OPTIMUM WING LOADING: The initial weight estimation resulted in the selection of an optimum wing loading consistent with mission requirements of operating altitudes from sea level to 30,000 ft at speeds of 150 to 350 kts.

In Section 4.1.5, *Nuclear Propulsion System Weight*, it was shown that the aircraft's L/D has a direct relationship to the potential payload. This relationship is shown graphically as a payload-wing loading comparison in Figures 4.1.6-1 through 4.1.6-4. The result of both Sections 4.1.5 and 4.1.6 was that the optimum wing loading for the study aircraft should be between 50 and 60 lbs/sq ft.

The physical size of the wing was also a consideration. The wing size should be as small as practicable. Wing area is inversely proportional to wing loading. Therefore, at the mission speeds and altitudes, the optimum wing loading should be 60 lbs/sq ft.

4.1.7.2 POINT DESIGN AIRCRAFT GROSS WEIGHT: Preliminary nuclear propulsion system weight estimates (Section 4.1.5) proved to be underestimated by 50 to 70% as a result

of the reactor, heat transfer, and nuclear engine analysis (Section 5, 6, and 7). Therefore the aircraft's gross weight will be required to be as large as is considered practicable.

Discussions were held with Prof. Larsen of AFIT, Maj. Koob, Mr. Diggs and Mr. Armstrong of the Air Force Flight Dynamics Laboratory, and Mr. Maas of ASD's Deputy for Development Planning to determine what is a practicable size aircraft for the 1990-2000 year timeframe (Refs. 9, 40, 94, and 105). The consensus of the discussions was that the technology limit for this timeframe was about 2,000,000 lbs gross weight. As a result of these discussions and the analysis of this study, the point design aircraft gross weight was set at 2,000,000 lbs for the following reasons:

1) LANDING GEAR: A 2,000,000 lb gross weight is considered the upper limit for conventional land based landing systems. For gross weights in excess of 2,000,000 lbs, water and/or surface effects landing systems may prove to be more effective.

2) LANDING FIELDS: An aircraft in excess of 2,000,000 lbs may require takeoff and landing distances exceeding conventional runway dimensions.

3) STRUCTURE WEIGHT AND COST ESTIMATES: Present structure weight and cost estimation techniques may not be viable for gross weights in excess of 2 to 2½ times current technology.

4) REACTOR PARAMETERS: Reactor weight and power parameters have not been developed for the size reactors required for aircraft in excess of 2,000,000 lbs (Ref. 190). For example, a 2,400,000 lb gross weight aircraft will require in excess of 600 MW of reactor power.

5) TECHNOLOGY LIMIT: The Lockheed Georgia Company has projected a technology limit of about 2,000,000 lbs for the 1990 to 2000 year timeframe (Ref. 127, p. 14). Figure 4.1.7.2-1 depicts the history of aircraft gross weights and Lockheed's technology limit.

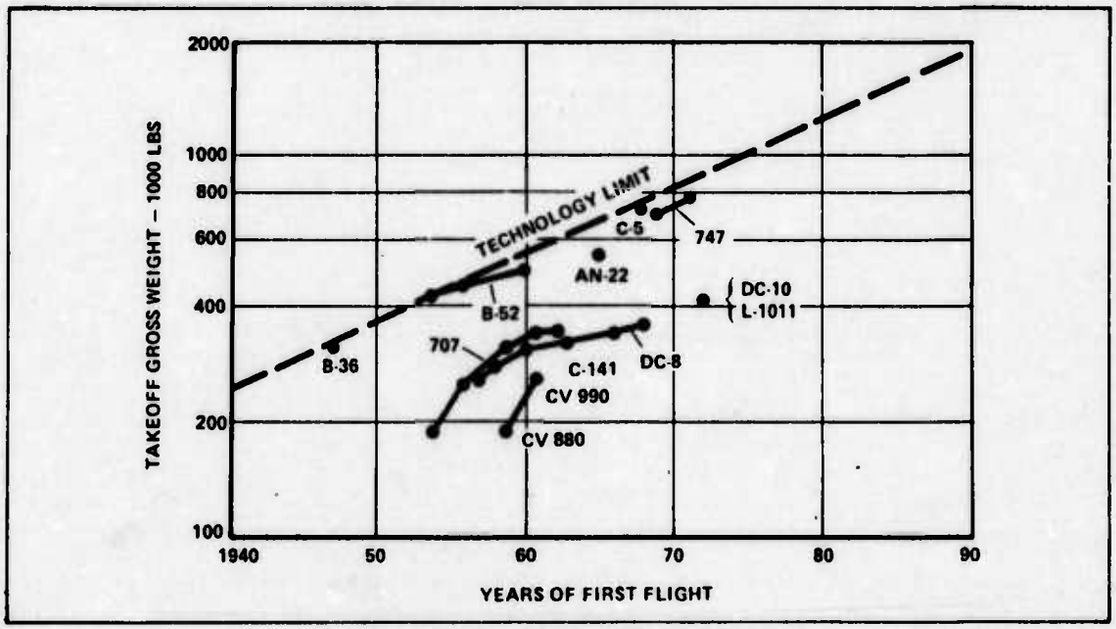

Figure 4.1.7.2-1. Aircraft Weight Trends

4.2 AIRCRAFT CONFIGURATION

The aircraft analysis techniques presented thus far apply to any configuration of aircraft. The question arose whether the propulsion system design and the total weapon system design were sensitive to aircraft configuration. The best approach in answering that question would have been to design and optimize each candidate configuration aircraft and then choose that configuration which best met the design objectives and requirements. However, limited manpower resources for aircraft design necessitated a qualitative sensitivity analysis of the several candidates and a more detailed design of the configuration that appeared to be most promising.

Each configuration was considered in relation to the following set of criteria:

1) performance
2) radiation hazard
3) structural risk
4) crew comfort
5) stability and control
6) maintainability

A configuration which reduced reactor power required, reactor weight, and airframe weight over another configuration was considered to be a better configuration. Therefore the first three criteria were considered more important than the last three.

4.2.1 CANDIDATE CONFIGURATIONS: Four candidate configurations were examined: conventional wing and tail, canard with horizontal tail first, flying wing, and twin body. The three variations of the canard which were examined are explained in Section 4.2.1.2. Dominant advantages and disadvantages of each configuration are discussed in the following subsections. The configurations are shown in Figures 4.2.1.1-1 through 4.2.1.4-1.

4.2.1.1 CONVENTIONAL AIRCRAFT: Figure 4.2.1.1-1 shows the overall configuration required in a conventional wing and tail design. The conventional aircraft presents the classical design problem. Almost all large aircraft designs are of this type.

4.2.1.2 CANARD AIRCRAFT: The canard configuration was selected as a candidate because it offers several advantages over a conventional aircraft. The canard configuration offers a possible reactor shielding weight reduction due to the reactor radiation attenuation over the large distance from the reactor to the crew compartment. It offers a probable structural weight savings over a conventional aircraft because the canard surface provides lift. That means that the wing may be smaller than the wing for a conventional aircraft and, thus, lighter. Also, the canard lift acts counter to the weight of the fuselage, thus reducing the loads that the fuselage structure must carry. According to Corning, canard configured aircraft have shorter takeoff and landing rolls; the horizontal control surface is out of the wing wake, so its behavior is much more predictable; and the engines are far back from the crew compartment and thus decrease the noise to the crew (Ref. 33, Section 9-15). One disadvan-

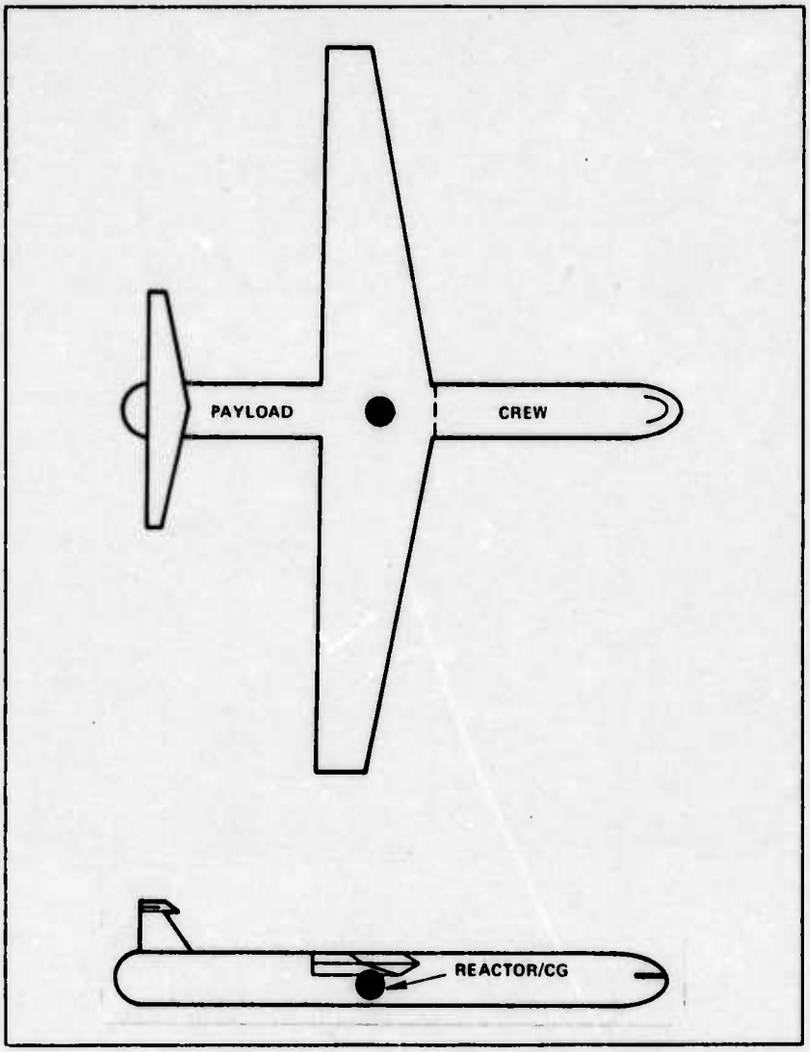

Figure 4.2.1.1-1. Conventional Aircraft

tage of the canard configuration is that the long distance from the aircraft center of gravity to the crew compartment makes the effects of yaw and pitch rates on the crew worse than those in conventionally configured aircraft.

Figure 4.2.1.2-1 shows the overall configuration required in a straight wing canard aircraft design. This configuration provides greater accessibility to the reactor than the conventional layout and offers the possibility of a modularized propulsion system. It does require an extremely large vertical tail area for stability.

In an effort to reduce this large vertical tail area, the effects of wing sweep were investigated. In general, a swept wing has greater weight than a straight wing, but it does reduce the vertical tail area considerably. Figure 4.2.1.2-2 shows the overall configuration of a canard aircraft design with the wings swept aft. This layout retains the advantages of reactor accessibility and prospects for a modularized propulsion system, but it presents a rather

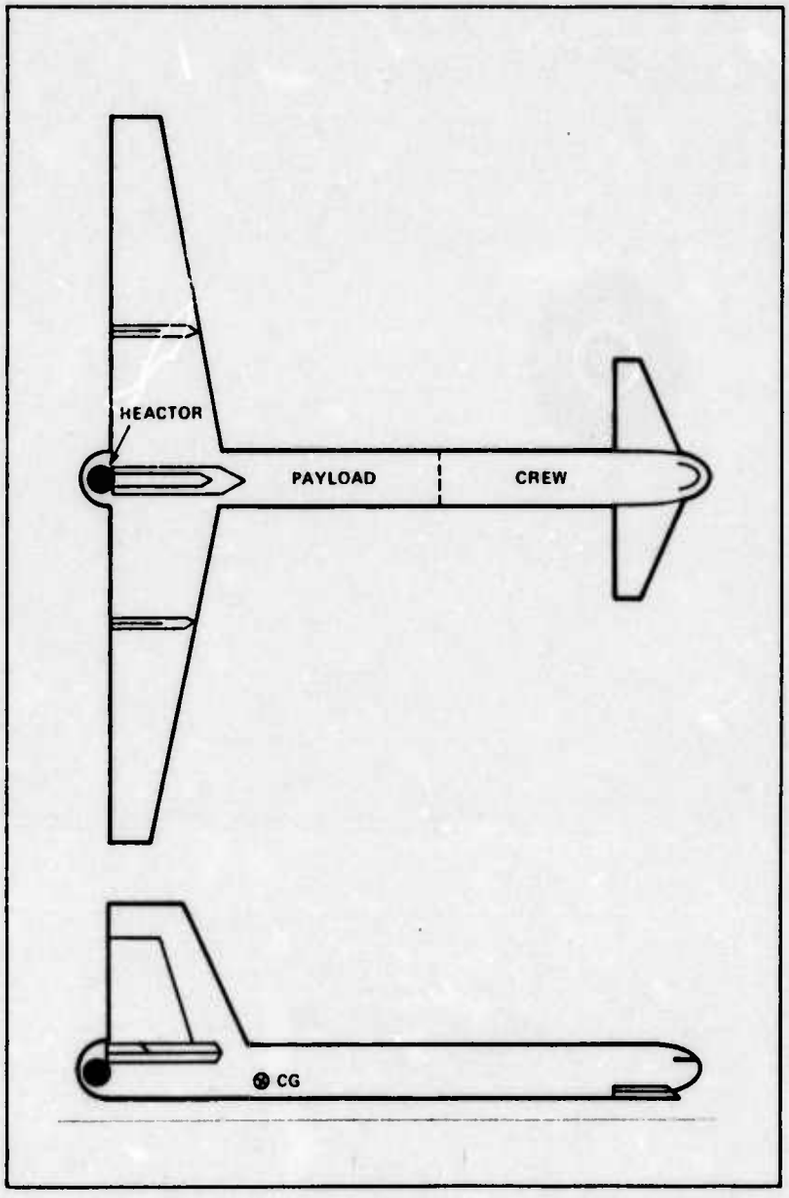

Figure 4.2.1.2-1. Straight Wing Canard

glaring disadvantage. The incidence angle of the wing with the fuselage axis, combined with the aft sweep, acts to droop the wing tips very close to the ground. With enough sweep to reduce the vertical tail area, the wing tips may actually touch the ground.

Figure 4.2.1.2-3 shows the overall configuration of a canard aircraft design with the wings swept forward. This configuration is different from the sweep aft configuration, in that it moves the wing tips up from the height in the straight wing layout. It does have two disadvantages: it obviates reactor accessibility by moving the reactor forward of the wing; and, a forward swept wing, in general, has a low divergence speed.

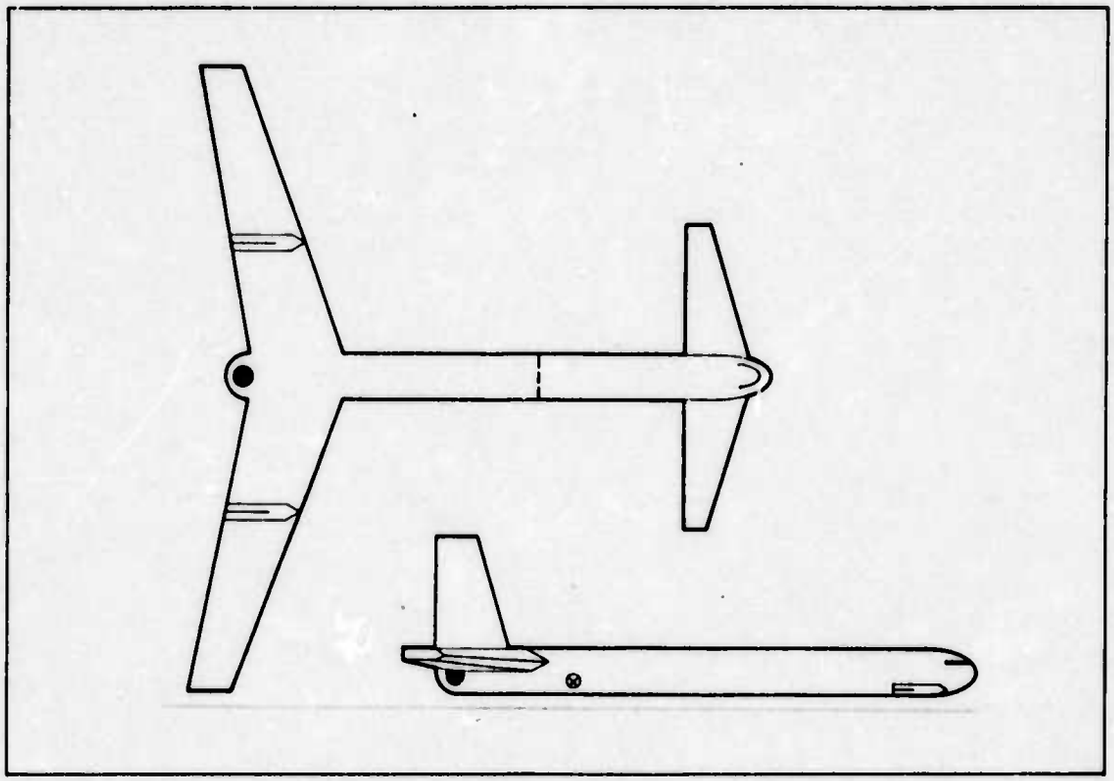

Figure 4.2.1.2-2. Sweep Aft Canard

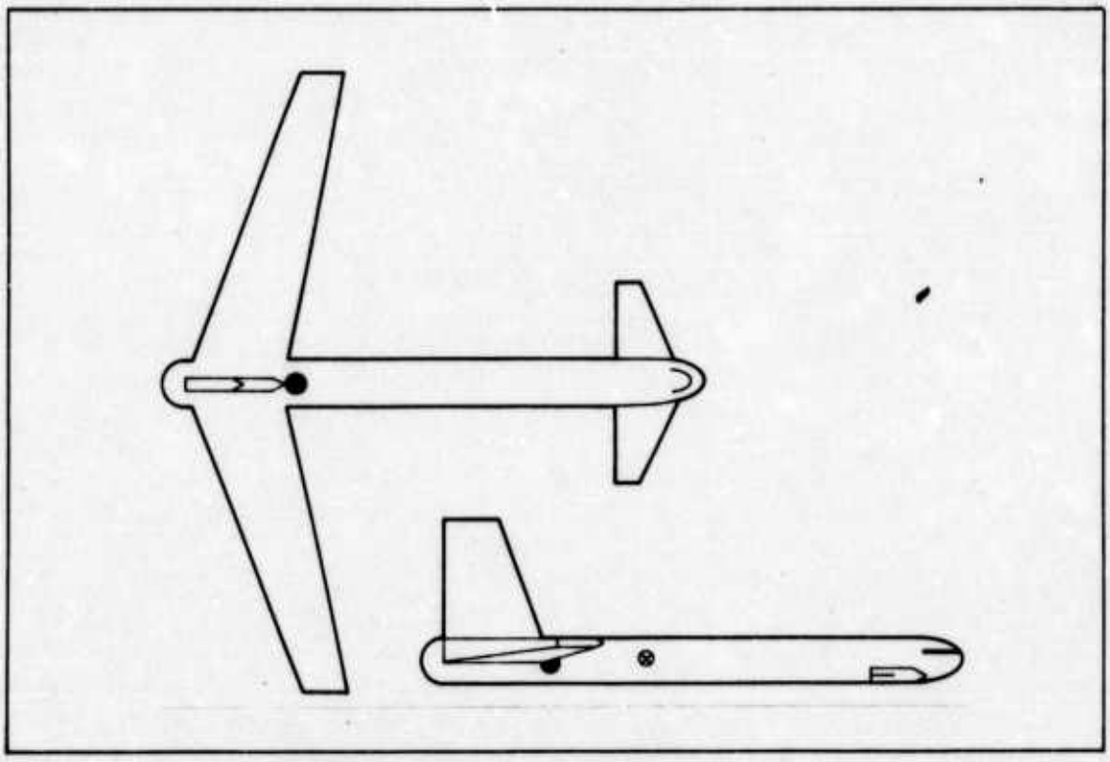

Figure 4.2.1.2-3. Sweep Forward Canard

4.2.1.3 FLYING WING AIRCRAFT: Figure 4.2.1.3-1 shows the overall configuration required in a flying wing design. The flying wing design offers some advantage in greatly reduced parasite drag which would reduce the thrust requirement. This, in turn, would act to reduce the required reactor size and weight. However, this layout has the shortest distance between the reactor and the crew compartment, and would require thicker and heavier reactor shielding. It would have the minimum fuselage structural weight of the several configurations, and the minimum pitch and yaw effects on the crew. Another advantage is the replacement of the fuselage weight point load with a distributed wing load, thereby providing an inertia relief effect and decreasing the maximum wing shear force and bending moment. However, flying wing designs historically have had severe stability and control problems.

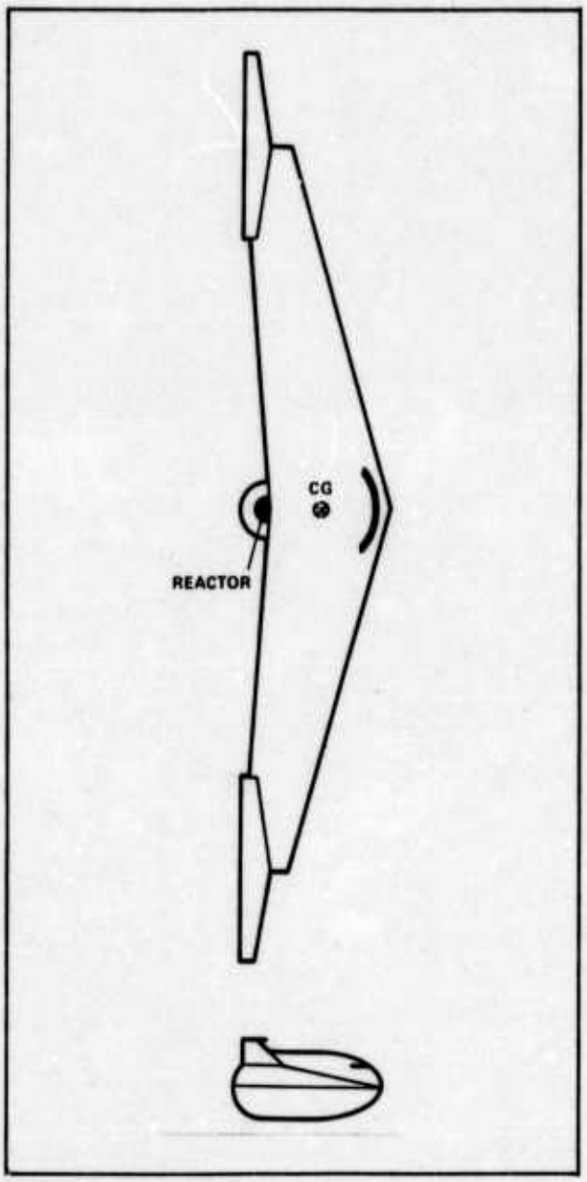

Figure 4.2.1.3-1. Flying Wing

4.2.1.4 TWIN-BODY AIRCRAFT: Figure 4.2.1.4-1 shows the overall configuration of a twin-body aircraft design. The twin-body design is based on the Virtus aircraft designed by Turbo Three Aircraft Corporation (Ref. 182), and offers ease of maintenance and increased aircraft availability with its modularized, pod-mounted reactor. The reactor pod could be removed and replaced much faster on this design than on the other candidate configurations, thus making it available to fly with much less maintenance time. With the use of dedicated nuclear and chemical fuel engines, the aircraft could be flown without the reactor pod or with a cargo pod. This design has smaller wing moments than either the conventional or flying wing configurations; therefore, the wing structure could be somewhat lighter. The twin-body configuration is the only one that lends itself to use of an air cushion landing system, since the twin fuselages give a great deal of roll stability during takeoff and landing.

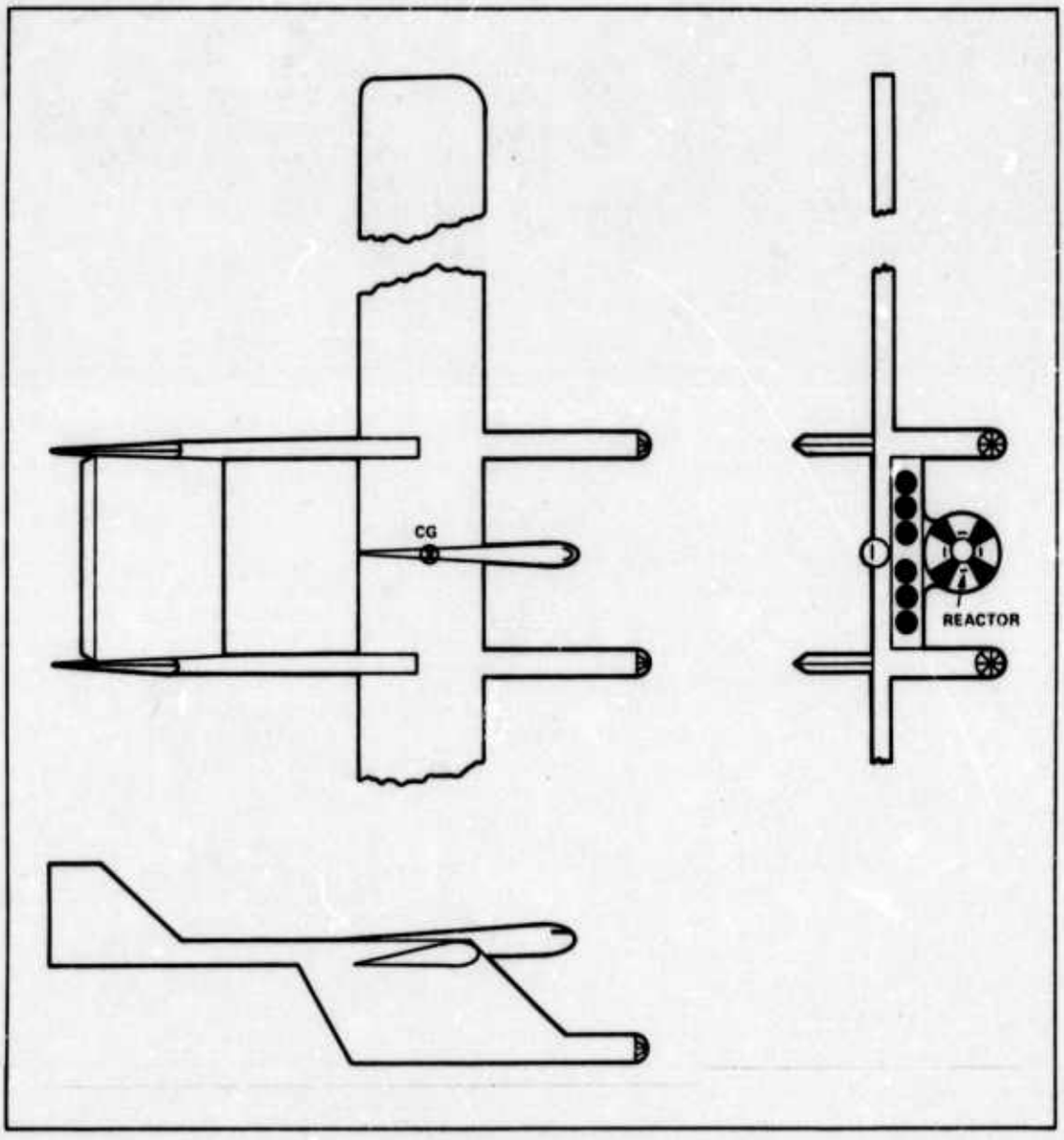

Figure 4.2.1.4-1. Twin Body Aircraft

This configuration would probably have the greatest drag and would, therefore, require more power to attain cruise performance. Crew members in the twin bodies would experience roll rate effects not inherent in the other configurations. Landing impact loads would be somewhat more severe and the design would require a more complex structural analysis.

4.2.2 CONFIGURATION SELECTION: The merits of each of the other configurations relative to the conventional configuration are shown in Table 4.2.2-1. Each configuration was rated as having increased, decreased, or no change in capability from the conventional aircraft in the six criteria listed at the beginning of Section 4.2.

TABLE 4.2.2-1. CONFIGURATION COMPARISON

	CANARD	FLYING WING	TWIN-BODY
PERFORMANCE	INCREASED	INCREASED	DECREASED
RADIATION HAZARD	DECREASED	INCREASED	NO CHANGE
STRUCTURAL RISK	DECREASED	DECREASED	NO CHANGE
CREW COMFORT	DECREASED	INCREASED	DECREASED
STABILITY AND CONTROL	INCREASED	DECREASED	NO CHANGE
MAINTAINABILITY	NO CHANGE	INCREASED	INCREASED

After comparing the advantages and disadvantages of the several candidate configurations, it appeared that the straight wing canard design offered the best total system. It offered the advantages of requiring a somewhat smaller wing (saving on structure weight and required thrust) and of requiring somewhat less reactor shielding (saving on shielding weight). The only major disadvantage to the straight wing canard was the large vertical tail area required. By locating the wing and reactor somewhat forward on the fuselage, the vertical tail area was reduced to a reasonable size. Figure 4.2.2-1 shows the point design configuration. Subsequent detailed aircraft analyses are based on this aircraft configuration.

4.3 SIZING ANALYSIS

After the aircraft wing loading, gross weight, and configuration were selected, the overall aircraft was sized. A preliminary sizing analysis was conducted on the aircraft subsystems which determine aircraft dimensions and redefine structural weight. This weight analysis included a refined structural weight estimation, wing weight buildup to compensate for aeroelastic effects, and additional fueslage weight required for reactor mounting. A simplified landing gear analysis was also conducted to examine the number and size of aircraft tires and struts required on the point design aircraft.

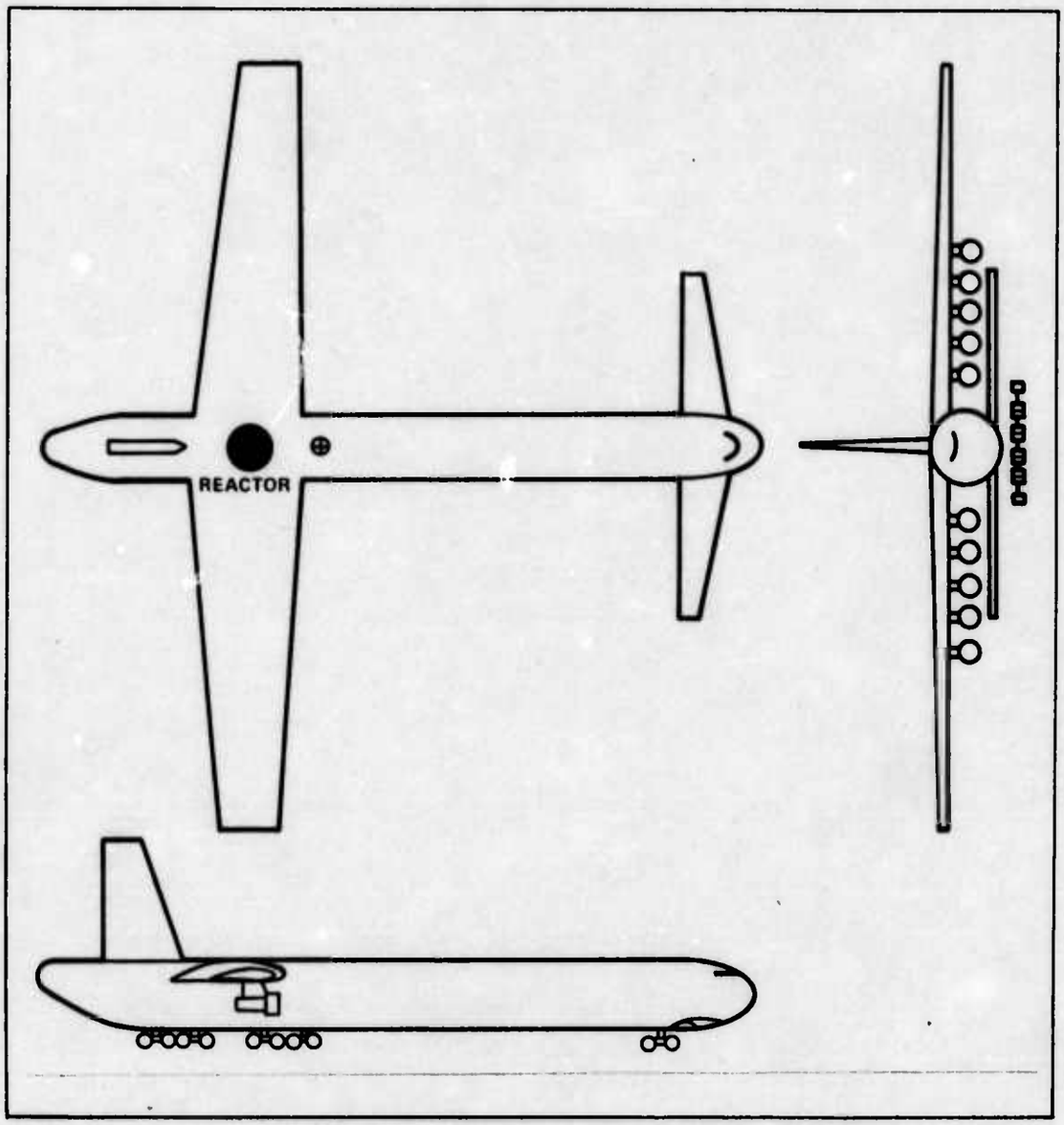

Figure 4.2.2-1. Point Design Configuration

This preliminary analysis was conducted only on:

1) tail/canard surface areas
2) structural component weights
3) composite weight savings
4) aircraft wing
5) aircraft fuselage
6) reactor mounting
7) aircraft landing gear

Other critical aircraft subsystems, such as hydraulic, electrical, air conditioning, and control surfaces, were not included due to lack of time.

The sizing analysis was again an iterative process. Each change in the size and/or weight of an aircraft component required another iteration through the sizing analysis until the structural components and aircraft center of gravity were in balance.

4.3.1 TAIL/CANARD SURFACES: The tail/canard aid in controlling the aircraft in flight and provide aircraft stability. This control and stability is accomplished by producing pitching and yawing moments about the aircraft's center of gravity (CG). For a first approximation of the canard and vertical tail areas, the method of moments was used to determine aircraft balance. The more refined stability derivatives ($\partial C_m/\partial\alpha$ and $\alpha C_N/\partial\beta$) were not addressed in this study.

The CG was initially located by the use of structural component weight as a percent of the total structural weight found by the method outlined in Section 4.1.1. An example of the component weight is shown in Appendix A.4.1.16. With an estimate of individual airframe component weights, the CG was located by the standard method where:

$$\text{cg moment arm} = \frac{\text{Sum of (component weights x moment arms)}}{\text{total weight}}$$

Results shown in this section are for a CG location 260 ft from the nose.

4.3.1.1 CANARD AREA: The canard will control the pitching moment about the aircraft's CG. In straight and level flight, the sum of the moments must be zero for aircraft trim. Figure 4.3.1.1-1 depicts the vertical lift forces and their associated moment arms. The sum of these moments must be zero.

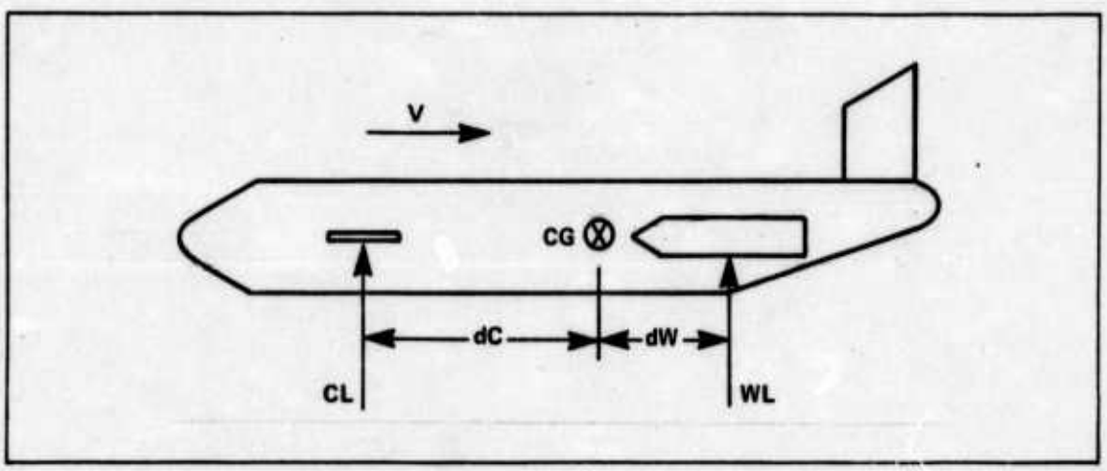

Figure 4.3.1.1-1. Canard Area

Therefore: Lift on canard times canard moment arm equals lift on wing times wing moment arm.

where: CL = lift on canard
WL = lift on wing
dC = canard moment arm = 200 ft
dW = wing moment arm = 40 ft

$$\text{Lift} = \tfrac{1}{2}\,\rho\, S\, V^2\, C_L$$

thus: $\tfrac{1}{2}\,\rho\, S_C\, V^2\, C_{LC}\, dC = \tfrac{1}{2}\,\rho\, S_W\, V^2\, C_{LW}\, dW$

therefore:
$$S_C = \frac{S_W\, C_{LW}\, dW}{C_{LC}\, dC} = 5600 \text{ sq ft} \qquad (4.3.1\text{-}1)$$

where:
- S_C = canard area
- S_W = wing area = 27,800 sq ft
- C_{LC} = canard lift coefficient (assumed $C_{LC} = C_{LW}$)
- C_{LW} = wing lift coefficient

4.3.1.2 VERTICAL TAIL AREA: The vertical tail will control the yaw moment about the CG. In straight and level flight the sum of these moments must also be zero for aircraft trim.

Figure 4.3.1.2-1 depicts the side forces due to a side gust and their associated moment arms. The sum of the moments must be zero.

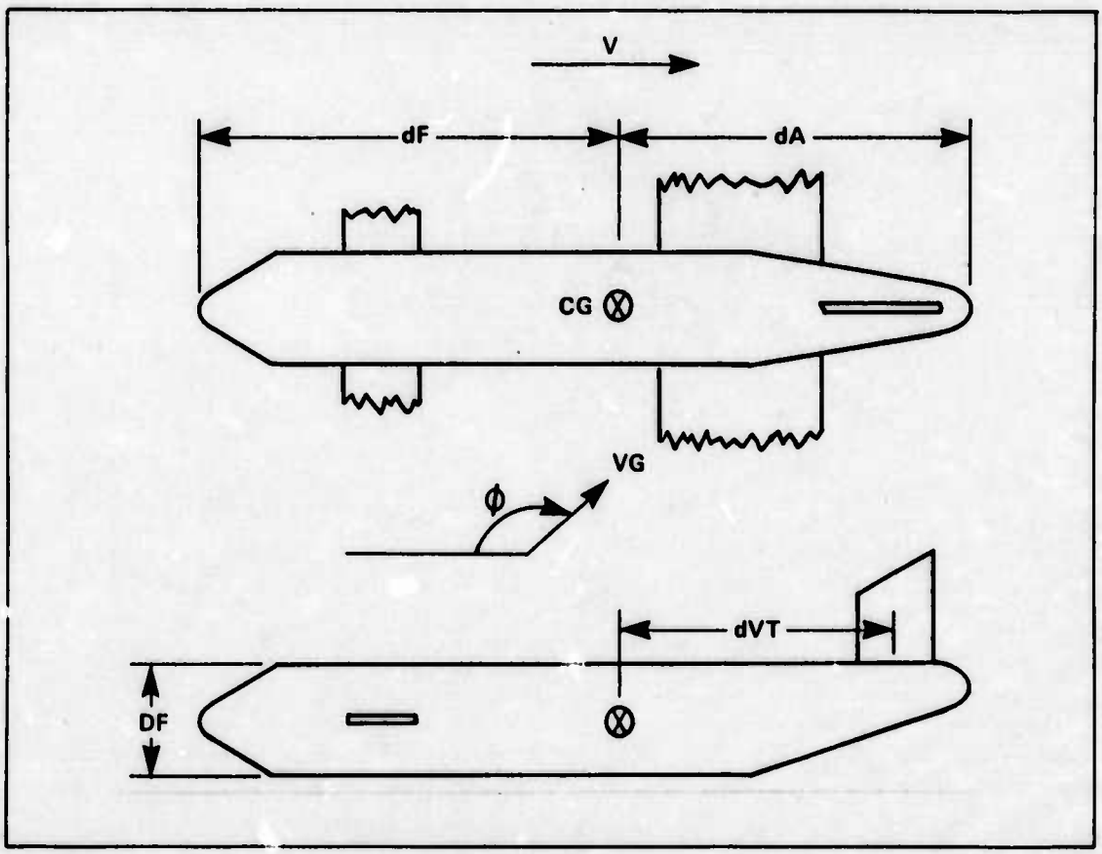

Figure 4.3.1.2-1. Vertical Tail Area

where: dA = distance aft of CG = 170 ft
dF = distance fwd of CG = 260 ft
DF = fuselage diameter = 40 ft
dVT = distance from CG to vertical tail quarter chord = 100 ft
VG = wind gust at velocity V
ϕ = angle of gust

and: Gust Force = $\frac{1}{2} \rho (V \sin \phi)^2$ AREA C_D

where: AREA = area the gust acts on
C_D = drag coefficient

Moment arms: ½ dF; ½ dA; dVT
Areas: DF by dA; DF by dF; S_{VT} (vertical tail area)

therefore:
$$S_{VT} = \frac{0.5 \text{ DF } C_{DF} (dF^2 - dA^2)}{C_{DVT} \text{ dVT}} = 4300 \text{ sq ft} \qquad (4.3.1\text{-}2)$$

where: C_{DF} = fuselage drag coefficient = 0.5 (Ref. 155, p. 410)
C_{DVT} = vertical tail drag coefficient = 0.91 (Ref. 155, p. 360)

With the wing and tail/canard areas determined, the structural component weights were calculated. After this weight calculation the CG and tail/canard areas were recomputed with the new weight data and the process iterated again.

4.3.2 STRUCTURAL COMPONENT WEIGHTS: The final structural weight was computed on individual component weights by a method developed by the Aerophysics Research Corporation (Ref. 3). The Aerophysics weight estimation method is based on statistical analysis of historical weight data for low to moderately swept wing transport and bomber aircraft. Included in the data base are 15 transports from the C-118A, C-123A through the C-141A and C-5A. The six bomber aircraft in the data base range from the B-66B to the B-52B.

The following is a summary of component weight estimation equations used for final weight analysis and possible composite weight savings (Ref. 3, p. 6-22, 33-35). All sizes and weights are in feet and pounds.

$$\text{Wing weight} = 1624 \left(\frac{\text{GW LF } b_W S_W}{\text{root thickness x } 10^9} \right)^{0.584} \qquad (4.3.2\text{-}1)$$

where: LF = load factor b_W = wing span
S_W = wing area

$$\text{Horizontal tail weight} = 0.0055 \left[(W/S)^{1.21} (S_{HT})^{.814} (Q_{MAX})^{.467} \right] \qquad (4.3.2\text{-}2)$$

where: S_{HT} = horizontal tail area

Q_{MAX} = maximum dynamic pressure

$$\text{Vertical tail weight} = 1.197\,(S_{VT})^{1.24} \qquad (4.3.2\text{-}3)$$

where: S_{VT} = vertical tail area

Fuselage weight =

$$0.273\left[\left(\frac{\text{length x LF}}{\text{height}}\right)^{0.15}(Q_{MAX})^{0.16}(\text{wetted area})^{1.05}\right]^{0.88} \qquad (4.3.2\text{-}4)$$

$$\text{Landing gear weight} = 0.00916\,(GW)^{1.124} \qquad (4.3.2\text{-}5)$$

The canard aircraft was selected as the point design configuration. In a canard aircraft the horizontal tail is replaced by the canard surface which supplies a force upward (lift) in flight, and not a force downward as a conventional aircraft's horizontal tail does. Therefore, Eqs. 4.3.2-1 and 4.3.2-2 must be modified due to the fact that the wing and canard both supply lift. Thus, the total required wing area is the sum of the wing and the canard areas.

The canard was treated as a wing so that:

$$S_T = S_W + S_C$$

$$\text{Wing lift} = (W/S)\,S_W$$

$$\text{Canard lift} = (W/S)\,S_C$$

where: Wing lift + canard lift = GW

S_W and S_C are determined as shown in Section 4.3.1

Eq. 4.3.2-1 was modified for canard aircraft such that:

$$\text{Wing weight} = 1624\left(\frac{W/S\;S_W\;LF\;b_W\;S_W}{\text{wing root thickness x } 10^9}\right)^{0.584} \qquad (4.3.2\text{-}6)$$

$$\text{Canard weight} = 1624\left(\frac{W/S\;S_C\;LF\;b_C\;S_C}{\text{canard root thickness x } 10^9}\right)^{0.584} \qquad (4.3.2\text{-}7)$$

where: S_C = canard area $\quad b_C$ = canard span

4.3.3 COMPOSITE WEIGHT SAVINGS: A preliminary analysis was made of the use of composites for the study aircraft's construction. This analysis was done to find the magnitude of weight savings which may be possible with current and advanced composite technology. The following discussion is based on a similar analysis made by D. F. Adams of the Universtiy of Wyoming (Ref. 2, p. 751).

Use of composite material in airframe construction offers a potential structural weight savings for the study aircraft. No consideration was given to the possibility of resizing the entire aircraft because of the reduced airframe weight; it was assumed that any weight savings would be used for increased payload.

The candidate materials which were considered are compared to aluminum alloy in Table 4.3.3-1. This list is representative of the wide variety of new materials now being developed (Ref. 2, p. 752).

TABLE 4.3.3-1. CANDIDATE AIRFRAME STRUCTURAL MATERIALS (REF. 2, P. 752)

MATERIAL	DENSITY LB/CU IN.	ULTIMATE TENSILE STRENGTH 10^3PSI	ELASTIC STIFFNESS 10^6PSI	SPECIFIC TENSILE STRENGTH 10^6IN.	SPECIFIC STIFFNESS 10^9IN.
ALUMINUM ALLOY 2024-T6	0.100	57.0	10.5	0.570	1.050
TITANIUM ALLOY Ti-Al-4V	0.160	129.2	15.8	0.810	0.988
BERYLLIUM HOT ROLLED	0.067	70.0	44.0	1.050	6.597
BORON/EPOXY COMPOSITE UNIDIRECTIONAL (50% FILAMENT VOLUME)	0.073	190.0	30.0	2.603	4.110
GRAPHITE/EPOXY COMPOSITE UNIDIRECTIONAL THORNEL 75S (60% FILAMENT VOLUME)	0.058	210.0	45.0	3.621	7.759
ORGANIC/EPOXY COMPOSITE UNIDIRECTIONAL PRD-49-III (65% FILAMENT VOLUME)	0.050	250.0	11.0	5.000	2.200

Eight different material/construction combinations were considered. These combinations are shown in Table 4.3.3-2 along with the estimated weight reduction for each combination. The percent reduction shown uses aluminum conventional sheet and stringer construction component weights as the basis for comparison to the use of the weight savings materials. For example: a 100,000 lb aluminum wing could be reduced in weight by 10,000 lbs (10%) with the use of combination 2, or by 58,000 lbs (58%) with combination 6.

TABLE 4.3.3-2. POSSIBLE STRUCTURAL WEIGHT REDUCTION WITH COMPOSITE MATERIALS (REF. 2, P. 753)

MATERIAL/CONSTRUCTION COMBINATION	COMPONENT WEIGHT REDUCTION (% REDUCTION)			
	WING	FUSELAGE	HORIZONTAL STABILIZER/ CANARD	VERTICAL STABILIZER
1. ALUMINUM — CONVENTIONAL CONSTRUCTION	BASE CASE			
2. TITANIUM ALLOY (50% Ti, 50% Al) CONVENTIONAL CONSTRUCTION	10	15	10	10
3. BERYLLIUM (50% Be, 50% Al) CURRENT CONSTRUCTION	36	23	26	26
4. BORON/EPOXY (50% B/Ep, 50% Al) CURRENT CONSTRUCTION	19	23	19	19
5. GRAPHITE/EPOXY (50% Gr/Ep, 50% Al) CURRENT CONSTRUCTION	31	29	29	29
6. GRAPHITE/EPOXY (80% Gr/Ep, 20% Gl/Ep) ADVANCED CONSTRUCTION	58	54	53	53
7. ORGANIC FILAMENT/EPOXY (50% Org/Ep, 50% Al) CURRENT CONSTRUCTION	13	23	13	13
8. ORGANIC FILAMENT/EPOXY (80% Org/Ep, 20% Gl/Ep) ADVANCED CONSTRUCTION	30	45	30	30

Conventional construction as used in combinations 1 and 2 refers to conventional sheet and stringer construction which has dominated metal airframe technology for many years.

Current composite construction, as used in combinations 3, 4, 5, and 7, refers to using new materials on a direct substitution basis with only minor changes in construction details.

Advanced composite construction, as used in combinations 6 and 8, is still in the development stage. This construction technology involves the use of unitized construction to reduce the number of subassembly parts, and almost total use of polymer matrix composite materials. Adhesive bonding is used for joining composites, and is essentially the same as the basic compcsite process. Thus it is possible to fabricate a complex structure in almost one step, eliminating most of the riveted and bolted joints typical of a conventional structure (Ref. 2, p. 753).

4.3.4 WING: A preliminary structural design of the wing was performed for three reasons: to determine wing section properties, to provide a check on the wing weight estimate, and to determine aeroelastic effects. A preliminary design based upon static loads was performed to determine the thickness of the wing skins and shear webs of the wing box structure. These material thicknesses provided an indication of the producibility of the wing structure. With all the material dimensions, a calculation of the wing weight based on material volume gave a check on the wing weight estimated in Section 4.3.2. With the preliminary wing design completed, preliminary estimates of major aeroelastic effects were made to determine whether or not they would significantly affect the design.

The weight and performance analyses provided most of the information required for the structural analysis of the wing. This information included gross weight, lift of the wing, wing loading, aspect ratio, taper ratio, wing weight, and load factor. In short, it included all of the data required to determine the wing planform and dimensions. Two other pieces of information were required for the wing analysis: material properties and airfoil geometry. The material selected was 2024-T3 aluminum which, according to MIL-HDBK-5, has a relatively low yield stress in tension of 40,000 psi and a weight density of 0.1 lb/cu in. (Ref. 119, Ch. 3.2.3). This material has reasonably good fatigue and fracture mechanics properties which permit a long service life for the system. The airfoils were selected in keeping with the high lift, low drag criteria from the performance analysis. The airspeed requirements of 250-350 kts were also a factor in the airfoil selections. The airfoils selected were the NACA 65_3-618 at the wing root tapering uniformly to the NACA 65-410 at the wing tip (Refs. 1, p. 434, 439; and 94). These airfoils satisfy the aerodynamic requirements and are certainly sufficient for the purpose intended here. The airfoil shapes are shown in Figure 4.3.4-1. The aerodynamic characteristics of the airfoils are presented in Appendix A.4.3.

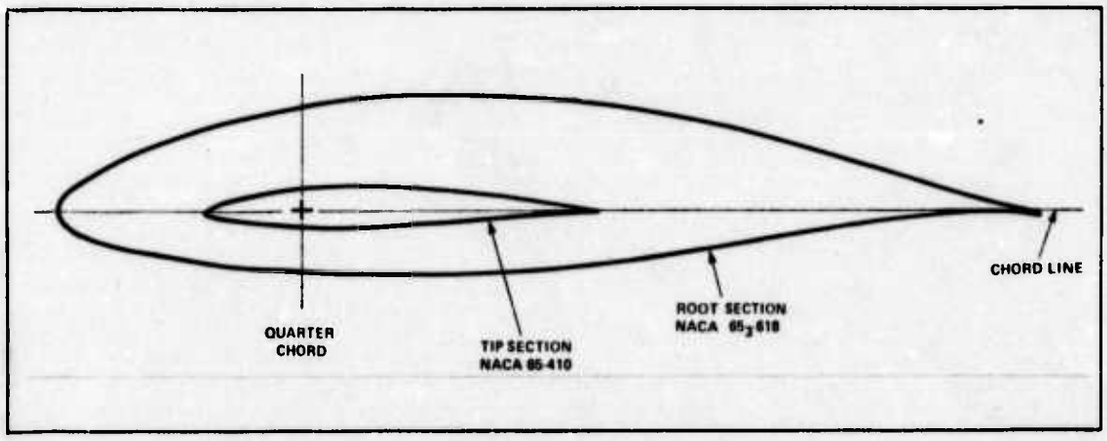

Figure 4.3.4-1. NACA Airfoil Sections

A synopsis of the method of analysis is given here and is followed by details of the mathematics involved. Schrenk's approximation was used to determine the spanwise lift distribution of the wing. The wing weight distribution was subtracted from the lift distribution to determine a wing beam loading. The wing beam loading was numerically integrated twice to

give both the shear and moment at each wing station. Engineering beam theory was employed to determine the wing section geometry required to carry the loads. This information, in turn, was used to perform a weight estimate for the wing structure. The wing section properties designed to carry the lift and bending moments were used to calculate torsional influence coefficients used in the divergence speed calculation. The divergence speed was calculated using matrix methods. The analysis was performed as described below, although most of it was accomplished using a digital computer program (See Appendix A.4.2.2). All numerical results in this section are for a 2,000,000 lb gross weight airplane.

4.3.4.1 PLANFORM DATA: The wing area, S_W, is equal to the lift, L, that the wing must provide, divided by the wing loading (W/S) = 60 lbs/sq ft.

$$S_W = L/(W/S) = 27{,}800 \text{ sq ft} \qquad (4.3.4\text{-}1)$$

where L = 0.833 GW = 1,666,000 lbs.

The wing span, b_W, is equal to the square root of the product of the wing area and the aspect ratio, AR = 9.

$$b_W = (S_W AR)^{1/2} = 500 \text{ ft} \qquad (4.3.4\text{-}2)$$

The root chord, C_R, is a function of the taper ratio, λ = 0.4, the wing area, and the aspect ratio for a trapezoidal planform.

$$C_R = \left(\frac{2}{1+\lambda} \right) \left(\frac{S_W}{AR} \right)^{1/2} = 79 \text{ ft} \qquad (4.3.4\text{-}3)$$

The tip chord, C_T, is equal to the product of the taper ratio and the root chord.

$$C_T = \lambda C_R = 32 \text{ ft} \qquad (4.3.4\text{-}4)$$

The mean aerodynamic chord (MAC) is a function of the taper ratio and the root chord for a trapezoidal planform (Ref. 33, p. 4).

$$MAC = 2/3\, C_R \left(\frac{1+\lambda+\lambda^2}{1+\lambda} \right) = 59 \text{ ft} \qquad (4.3.4\text{-}5)$$

4.3.4.2 SPANWISE LIFT DISTRIBUTION: Schrenk's approximation to the lift distribution as stated by Kuethe and Schetzer is based on strip theory (Ref. 92, p. 114-115). It says that the lift can be approximated by the average of two lift distributions. One is the pure strip theory result that the lift is proportional to the chord. For this design, the lift distribution is trapezoidal along the semispan. The other distribution is an elliptical distribution providing

the equivalent amount of lift. The average of the two distributions has historically provided good results compared to experimental results. The average acts to shift the lift distribution outboard while still accounting for tip effects. The spanwise lift distribution derived using Schrenk's approximation is shown in Figure 4.3.4.2-1. At the wing root, the lift per unit span is 4500 lbs/ft and at the wing tip it is 952 lbs/ft.

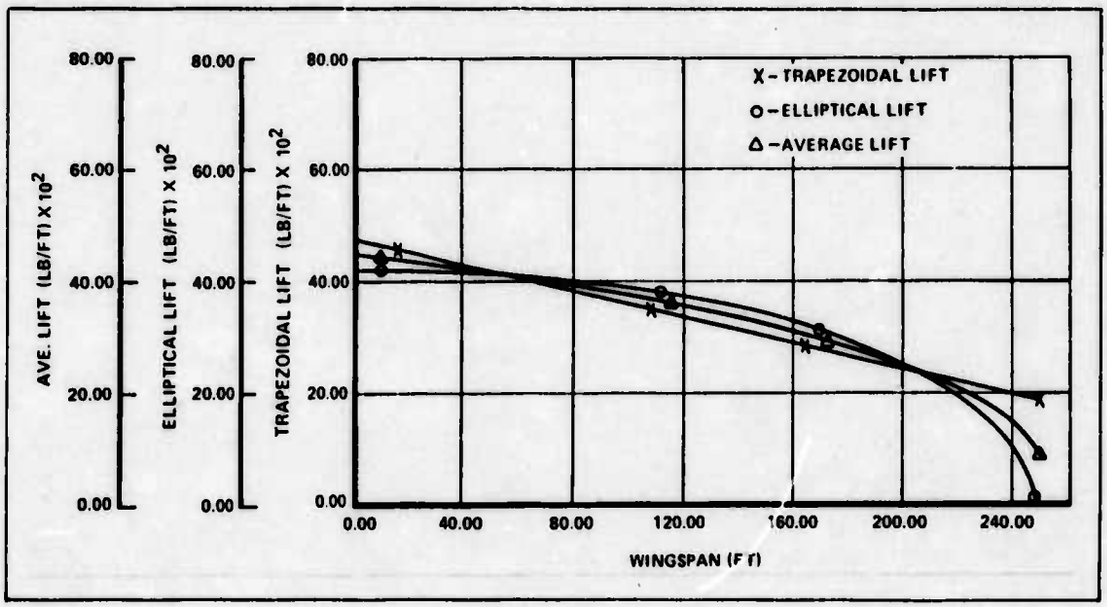

Figure 4.3.4.2-1. Lift Distribution

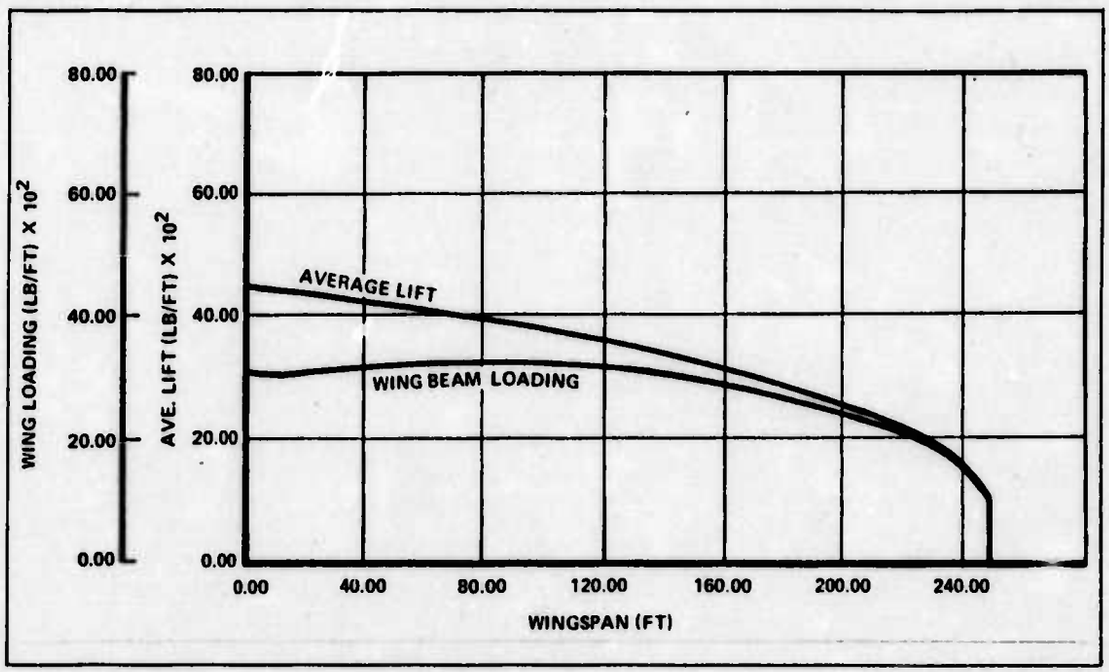

Figure 4.3.4.3-1. Wing Loading

4.3.4.3 WING WEIGHT DISTRIBUTION: The estimated wing weight was distributed along the span in parts. One part was distributed according to the wing area. It was assumed that the wing skins were 0.040 in. on both the projected upper and lower surfaces of the wing. The assumed thickness times the wing area times the weight density of aluminum yielded the skin weight. The second part of the wing weight was assumed to be distributed according to the bending moments at each wing station. The wing weight distribution was subtracted from the lift distribution to yield the wing beam loading. The lift distribution and the wing beam loading are shown in Figure 4.3.4.3-1. The maximum wing beam loading is 3250 lbs/ft and occurs at 80 ft from the wing root.

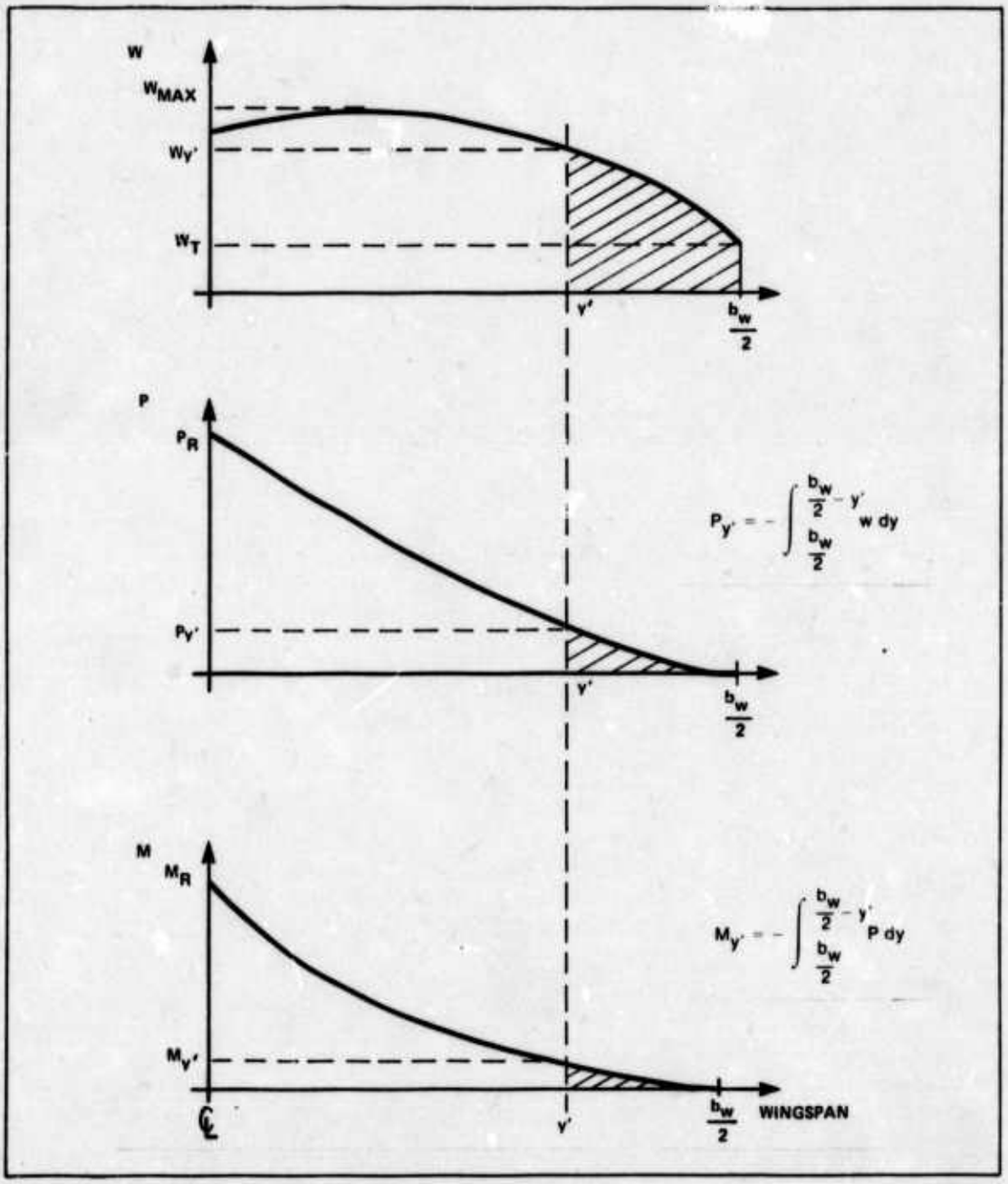

Figure 4.3.4.4-1. Wing Beam Loading, Shear Force, Bending Moment

4.3.4.4 SHEAR FORCES AND BENDING MOMENTS: The wing shear forces, P, and bending moments, M, were determined by numerical integration of the wing beam loading, w, diagram in accordance with Crandall and Dahl (Ref. 36, Ch. 3). The first integral yields the shear forces. The second integral yields the bending moments.

$$P_{y'} = -\int_{\frac{b_w}{2}}^{\frac{b_w}{2} - y'} w \, dy \qquad (4.3.4\text{-}6)$$

$$M_{y'} = -\int_{\frac{b_w}{2}}^{\frac{b_w}{2} - y'} P \, dy \qquad (4.3.4\text{-}7)$$

The process is shown schematically in Figure 4.3.4.4-1. The maximum shear load is 705,500 lbs and occurs at the wing root as shown in Figure 4.3.4.4-2. The maximum bending moment is 80,300,000 foot-pounds and also occurs at the wing root as shown in Figure 4.3.4.4-3. These loads were determined from the static equilibrium (+ 1g) condition.

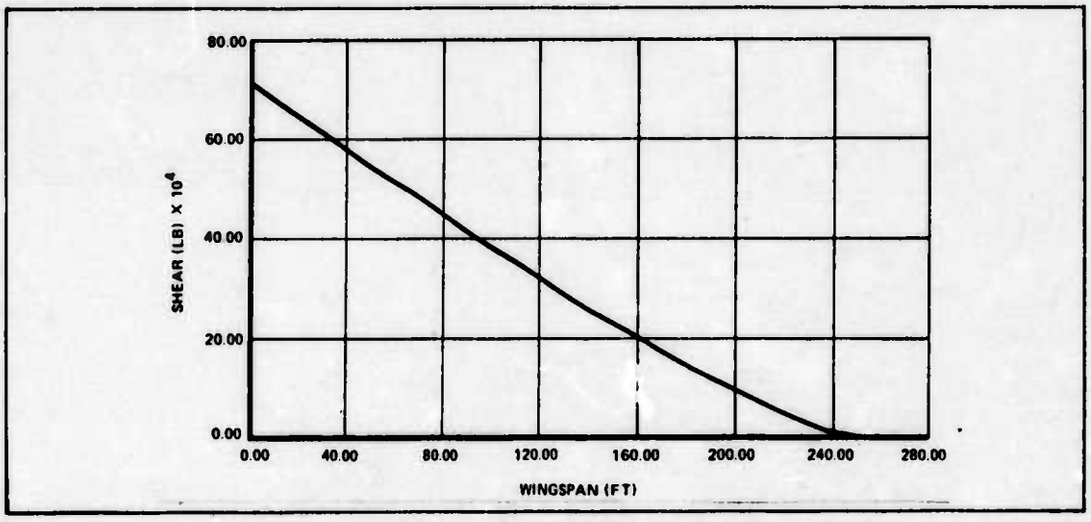

Figure 4.3.4.4-2. Shear Loads

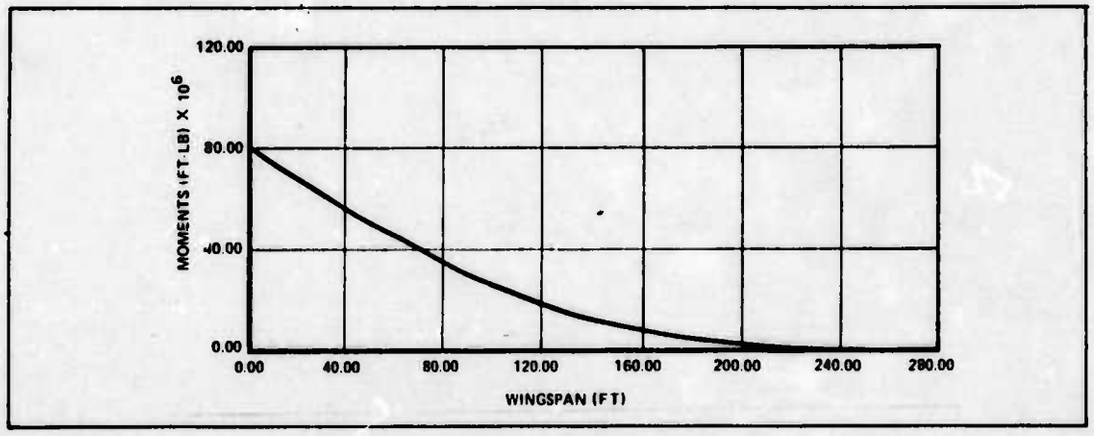

Figure 4.3.4.4-3. Bending Moments

4.3.4.5 WING BEAM SECTION PROPERTIES: The wing section geometries and properties were determined using engineering beam theory which assumes that the wing can be treated as a cantilever beam and that one dimension of the beam is much greater than the other two dimensions (Ref. 36, Ch. 7). Root and tip airfoil sections were used to develop root and tip beam section envelopes (Figure 4.3.4.5-1). Since the airfoil section tapers linearly from the root to the tip, so does the beam envelope.

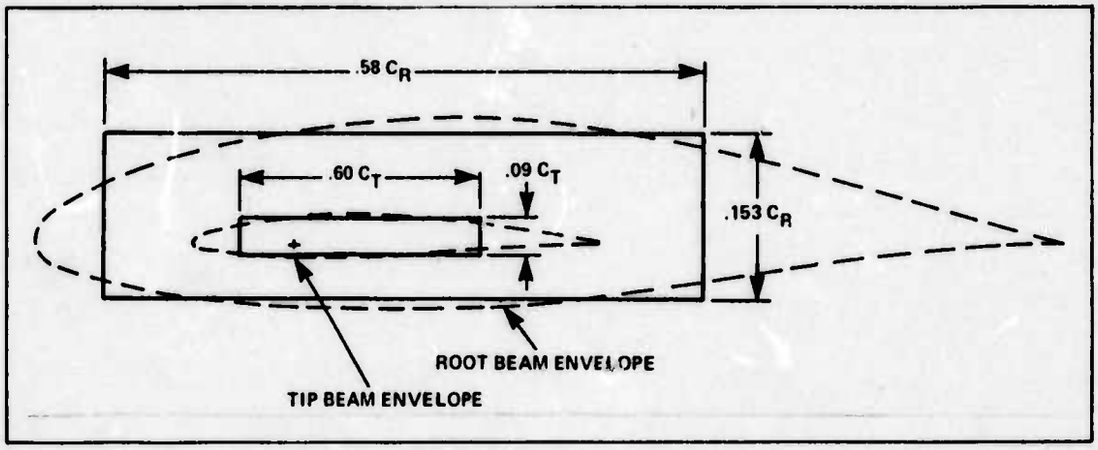

Figure 4.3.4.5-1. Beam Section Envelopes

The beam section was assumed rectangular for this analysis. The notation used in the beam section analysis is shown in Figure 4.3.4.5-2. Beam caps were designed to carry the bending moments and the webs were designed to carry the shear forces. The working stress, τ, due to bending in a beam section is given by the formula:

$$\tau = \frac{(LF)\, M\, (h_1/2)}{I} \qquad (4.3.4\text{-}8)$$

where I is the beam section area moment of inertia and (LF) is the design load factor. This equation can be rearranged to give an expression for the moment of inertia required to carry the bending moment when τ is the allowable material stress. The moment of inertia is a function only of the geometry of the section, so an expression for it can be used to determine the inside dimensions of the section.

$$I = \frac{\ell_1}{12}(h_1^3 - h_2^3)$$

$$h_2 = \sqrt[3]{h_1^3 - \frac{12\, I}{\ell_1}} \qquad (4.3.4\text{-}9)$$

The beam cap thickness, t_c, is given by the expression:

$$t_c = \tfrac{1}{2}(h_1 - h_2) \qquad (4.3.4\text{-}10)$$

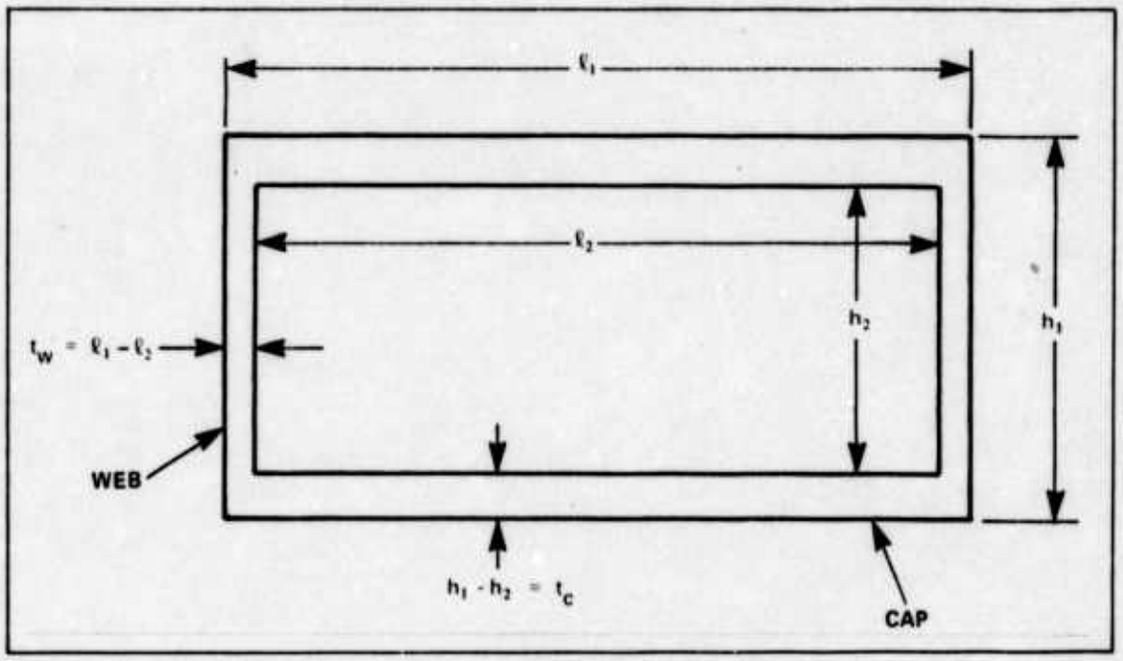

Figure 4.3.4.5-2. Beam Section Notation

The working stress due to shear force in a beam section is given by

$$\tau = \frac{(LF)\,P}{A} \qquad (4.3.4\text{-}11)$$

where A is the effective shear area.

Using the notation of Figure 4.3.4.5-2, the area A is given by

$$A = 2\,h_2\,t_w$$

The thickness, t_w, can be found by rearranging the equations and using an allowable stress for τ.

$$\tau_w = \frac{(LF)\,P}{2\,h_2\,\tau} \qquad (4.3.4\text{-}12)$$

In those instances where the calculations for t_c and t_w gave values of less than 0.040 in., t_c and t_w were defined to be 0.040 in. as a lower practical limit on the material thickness.

The beam cap thickness of one cap is shown in Figure 4.3.4.5-3. The maximum cap thickness required is 0.757 in. at the wing root and tapers almost linearly to 0.125 in. at 200 ft from the centerline. This minimum one-eighth in. thickness will be explained more fully later.

One other plot of some interest is the spanwise distribution of beam cap area for one cap as shown in Figure 4.3.4.5-4. The cap area was found by multiplying the cap thickness by the chordwise length at each station. The maximum area is 2.90 sq ft at the wing root. The minimum cap area is 0.20 sq ft at the wing tip. A comparison of this plot with the wing bending moment plot shows that they have the same general shape, but that the average cap area is farther outboard than the average bending moment. Although the bending moments were used to determine the major portion of the wing weight distribution, the cap areas would have provided a more accurate wing weight distribution. The method used gave a wing beam loading which yielded a slightly conservative structure.

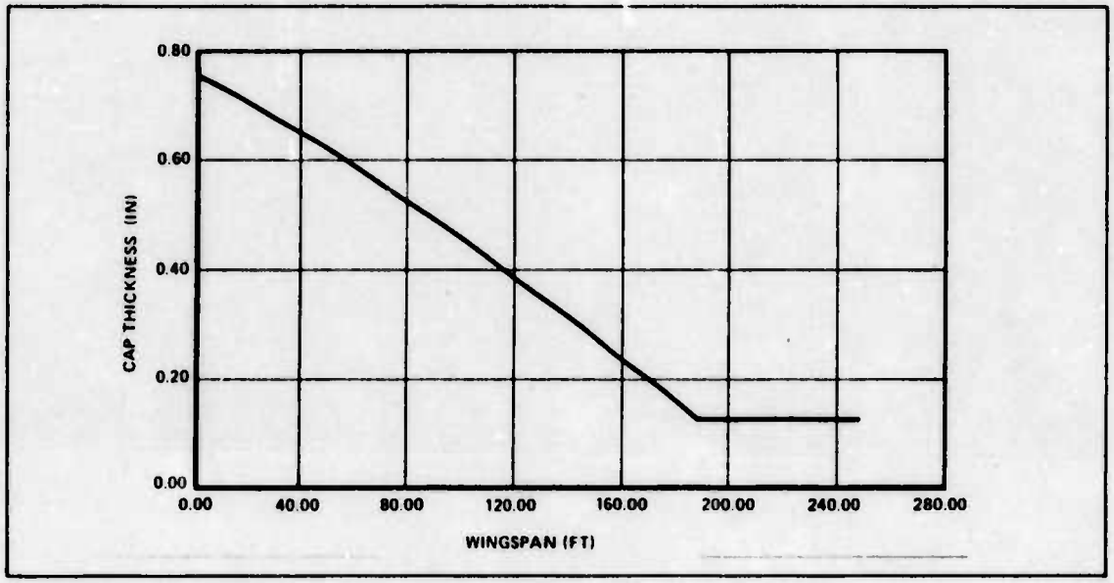

Figure 4.3.4.5-3. Beam Cap Thickness

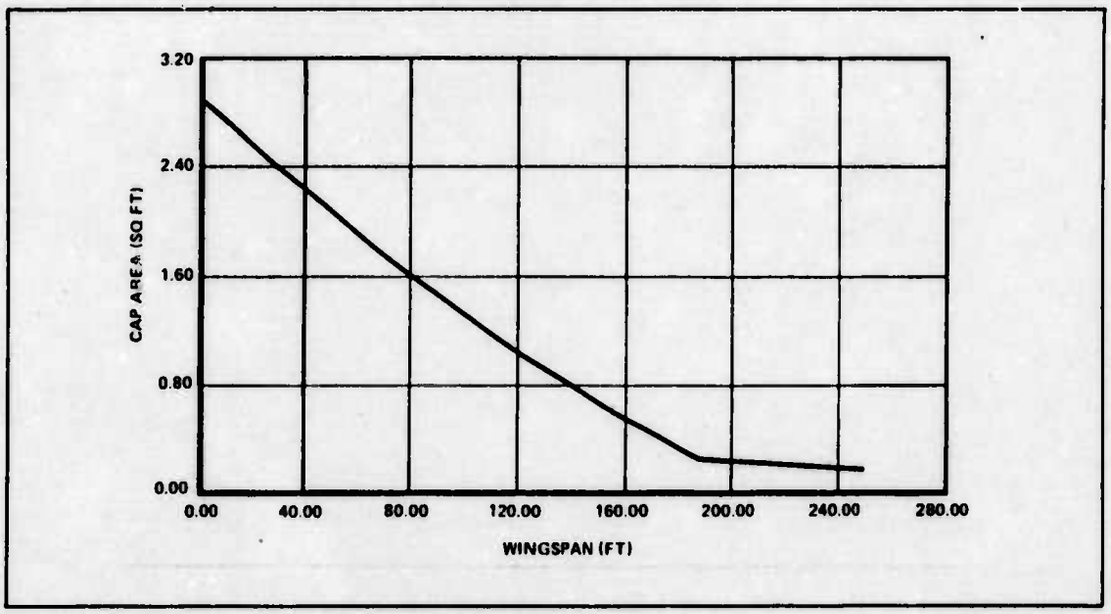

Figure 4.3.4.5-4. Beam Cap Area

4.3.4.6 CHECK ON WING WEIGHT ESTIMATE: In performing the wing weight estimate, the wing was modeled as having five major contributing elements: beam caps, beam webs, beam ribs, the skin of the wing covering structure not occupied by the beam, and flap weight. No attempt was made to account for the weight of stiffeners or fasteners. Using guidance from Corning, a flap area of 20% of the wing area was selected to increase C_{LMAX} from a value of 1.0 with no flaps to a value of 2.0 with flaps fully extended (Ref. 33, p. 16). Flap weight was calculated using 3 lbs/sq ft of flap area (Ref. 6). The other four elements were found by calculating the material volume and then multiplying the volume by the weight density to get the weight. For both the caps and the webs of the beams, the thickness decreased from the root to the tip. An increment of material volume for the beam caps between two wing stations was calculated by multiplying the average length of the cap times the distance between the two wing stations, Δy, times the thickness of the cap at the inboard station, t_c.

$$\Delta \text{ vol} = \frac{\ell_{1\ \text{inboard}} + \ell_{1\text{outboard}}}{2} \times \Delta y \times t_{c\ \text{inboard}}$$

A similar calculation was performed for increments of volume of the beam webs. The wing skin weight was calculated using a thickness of 0.040 in. over twice the panform area excluding the projected beam area.

A rough calculation of the wing rib weight was made using the rib spacing required to prevent buckling of the upper beam cap due to the compressive stresses it is required to carry. The rib spacing required at the mean aerodynamic chord was used to determine the number of ribs in the wing. For this calculation, the beam cap is considered as consisting of panels separated by ribs and stiffeners. Stiffeners run approximately parallel to the wing axis and are spaced chordwise a distance, b, apart. Ribs run perpendicular to the wing axis and are spaced spanwise a distance, a, apart. The object was to determine the dimension, a, and therefore the number of ribs in the wing. The plate buckling criteria for panels loaded in compression is, according to Peery (Ref. 137, p. 368-372):

$$\tau_{CCR} = K E_c (t_c/b)^2 \qquad (4.3.4\text{-}13)$$

where:

τ_{CCR} is the allowable compressive stress
E_c is the modulus of elasticity in compression
t_c is the panel (beam cap) thickness
K is a buckling factor that is a function of the ratio of dimensions a/b and the edge fixity conditions. Here K = 6.35.

All the terms in the expression are known except the dimension b. This dimension was found and was used with the a/b ratio to determine the rib spacing, a. The ratio a/b was assumed to be 4/1 for this calculation. The rib area at the mean aerodynamic chord was used to determine the total rib area for the wing. An average rib thickness of 0.063 in. was used to determine the rib volume and hence the rib weight for the wing.

A computer program was used to perform most of the above calculations, since they were repeated at each wing station. One of the initial problems was to determine what size increment in wing station would yield sufficiently accurate answers. Examples were calculated using increments of 50, 40, 25, 10, 5, and 2.5 ft. For the 2,000,000 lb airplane they are 20, 16, 10, 4, 2, and 1% of the wing span. It was found that the difference in weight estimates given by using 10 ft and 2.5 ft was about 2% for the size airplane being investigated, so 10 ft was used. The results of the wing weight check calculations are shown in Table 4.3.4.6-1.

TABLE 4.3.4.6-1. PRELIMINARY DESIGN WEIGHT ESTIMATE (LBS)

BEAM CAP	**203,600**
BEAM WEB	**12,400**
BEAM RIB	**19,100**
WING SKIN	**15,400**
FLAP	**16,700**
TOTAL WING WEIGHT	**267,200**

The wing weight found in this manner was 267,200 lbs. The original wing weight estimate from Section 4.3.2 was 210,200 lbs. The ratio of the two weights is 1.27. So the original estimate was low and the wing structure weight was revised up to 267,200 lbs.

4.3.4.7 WING DIVERGENCE SPEED: Because the wing was designed with the relatively large aspect ratio of 9, it was important to examine aeroelastic effects on the wing performance. Wing divergence speed, V_D, is essentially a check on the effects of torsion about a spanwise axis. Each wing section has a torsional stiffness which generally varies along the wing span. It was assumed that only the beam section provided this stiffness. Since the lift acts through the quarter chord and the shear center of each beam section is aft of the quarter chord, a torque acts on each wing station. As the airspeed increases, the lift, and hence the torque, increases to the point where the beam can no longer carry the torque and fails catastrophically. According to MIL-A-008870, the design requirement is that the divergence speed be 15% greater than the maximum speed over the range of operating altitudes (Ref. 118, p. 2).

The purpose of this analysis was to determine whether aeroelastic effects would cause a significant structural weight penalty. Bisplinghoff's text on aeroelasticity outlines a method to calculate the divergence speed which has a solution by matrices using strip theory (Ref. 16, Ch. 8). Figure 4.3.4.7-1 shows the construct of the problem. The matrix equation to be solved can be written in the form:

$$\frac{G}{\rho/2\, V_D^2 \left(\frac{\partial C_L}{\partial \alpha}\right)} \{C\, C_L^{\bullet}\} = [c]\left[\int \frac{1}{J}\, dy\right][e][W]\{C\, C_L^{\bullet}\} \qquad (4.3.4\text{-}14)$$

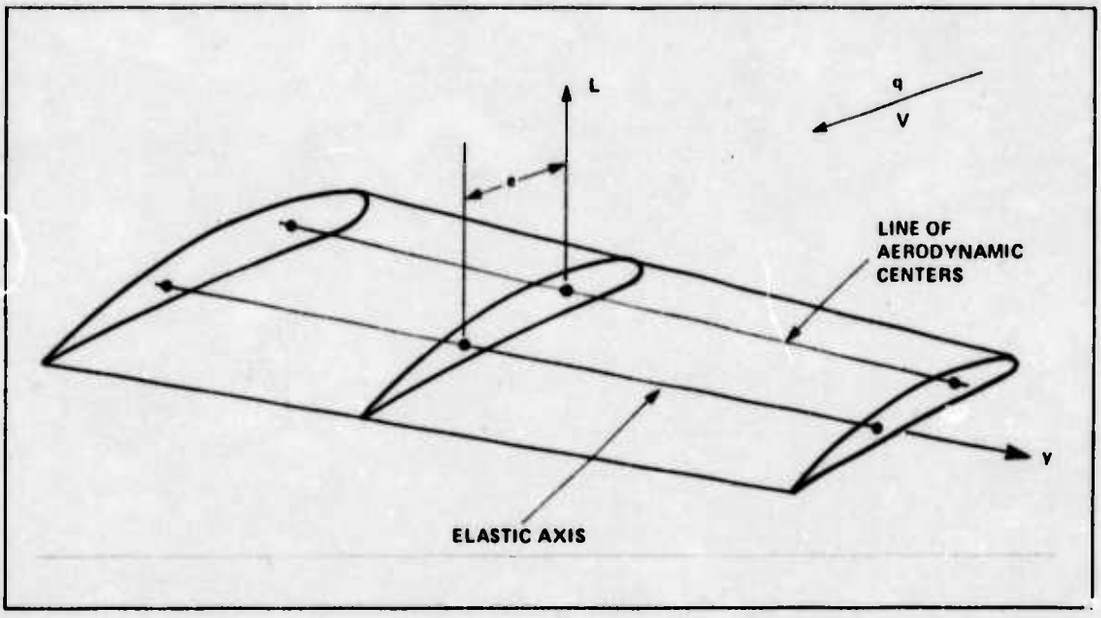

Figure 4.3.4.7-1. Geometry for Divergence Speed Calculation

where: G = modulus of rigidity of the material (4×10^6 psi for 2024 aluminum)

ρ = air density

$\frac{\partial C_L}{\partial \alpha}$ = slope of lift coefficient curve of the wing = 4.94 = $a_o \frac{AR}{AR + 3}$

$\{C\ C_L^e\}$ = vector of products of chord and section lift coefficient due to elastic twist

$[c]$ = diagonal matrix of local chords

$[\int \frac{1}{J} dy]$ = matrix of influence coefficients

$[e]$ = diagonal matrix of distances from quarter chord to elastic axis

$[W]$ = diagonal matrix of weighting factors

The matrix quantities above are dependent upon the choice of a coordinate system along the wing span. Figure 4.3.4.7-2 shows the coordinate system used in this analysis. This system of coordinates was derived from Multhopp's quadrature formula (Ref.)6, App. B), resulting in six wing stations and requires the solution for the eigenvalue of a 5 x 5 matrix. The matrix of weighting factors, [W], is given by:

$$[W] = \frac{\pi\, b_w}{24} \begin{bmatrix} \sin \pi/12 & 0 & 0 & 0 & 0 & 0 \\ 0 & \sin \pi/6 & 0 & 0 & 0 & 0 \\ 0 & 0 & \sin \pi/4 & 0 & 0 & 0 \\ 0 & 0 & 0 & \sin \pi/3 & 0 & 0 \\ 0 & 0 & 0 & 0 & \sin 5\pi/12 & 0 \\ 0 & 0 & 0 & 0 & 0 & \tfrac{1}{2} \sin \pi/2 \end{bmatrix} \quad (4.3.4\text{-}15)$$

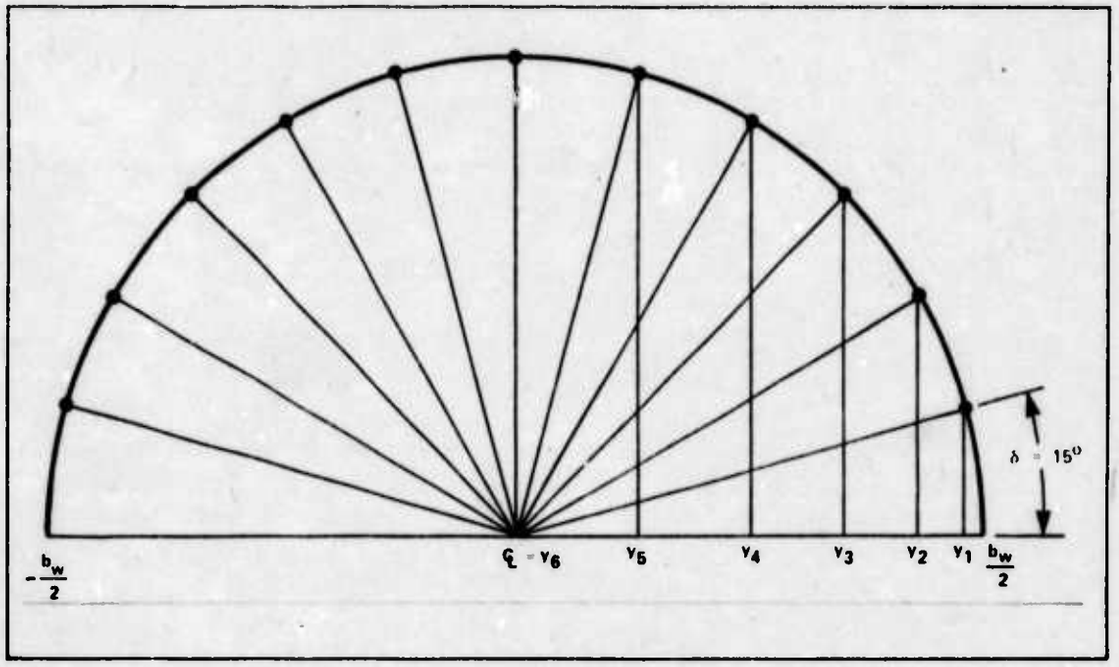

Figure 4.3.4.7-2. Multhopp Wing Stations

The matrices [c], [e], and $[\int \frac{1}{J} dy]$ consist of values for these parameters at each wing station. The wing stations were found from the expression:

$$y_i = \frac{b_w}{2} \cos \frac{i\pi}{12} \qquad i = 1, 6$$

The influence coefficients $\int \frac{1}{J} dy$ were found by first calculating the values of $\frac{1}{J}$ along the whole wing and then numerically integrating from the center line to station y_i. The torsional stiffness, J, is given by:

$$J = \frac{4 A^2}{\Sigma \frac{\ell}{t}} \qquad (4.3.4\text{-}16)$$

where: A = area enclosed by the beam section

$\Sigma \frac{\ell}{t}$ = the sum over the four sides of the length of the side divided by the thickness of the side

The solution for the divergence speed was accomplished in two steps. First the eigenvalue of the matrix product on the right hand side of Eq. 4.3.4-14 was found. The eigenvalue, r, found in this manner was set equal to the group of constants on the left hand side of Eq. 4.3.4-14. The terms were rearranged to solve for the divergence speed:

$$V_D = \sqrt{\frac{2 G}{\rho r \left(\frac{\partial C_L}{\partial \alpha}\right)}} \qquad (4.3.4\text{-}17)$$

The initial calculation of the wing divergence speed gave a value of 253 kts at sea level, which is only 16 kts above the cruise speed at sea level, and is well below the 310 kts maximum sea level speed. Examination of Eq. 4.3.4-14 indicates that the divergence speed increases as the eigenvalue, r, decreases. If all of the elements of the matrix product $[c]\left[\int \frac{1}{J}\, dy\right][e][W]$ are decreased, then the eigenvalue decreases.

It turned out that the value of the influence coefficients increased very rapidly near the wing tip where the material thicknesses initially were a minimum gauge of 0.040 in. By increasing the minimum gauge, the value of the influence coefficients dropped off and the value of the elements of the matrix product decreased. This increase in minimum material thickness also caused a weight penalty. Three minimum gauges were investigated. The results are shown in Table 4.3.4.7-1.

TABLE 4.3.4.7-1. DIVERGENCE SPEED RESULTS

MIN GAUGE (IN.)	WEIGHT PENALTY (LBS)	DIVERGENCE SPEED AT SEA LEVEL (KTS)
0.040	0	253
0.100	3500	320
0.125	5900	343

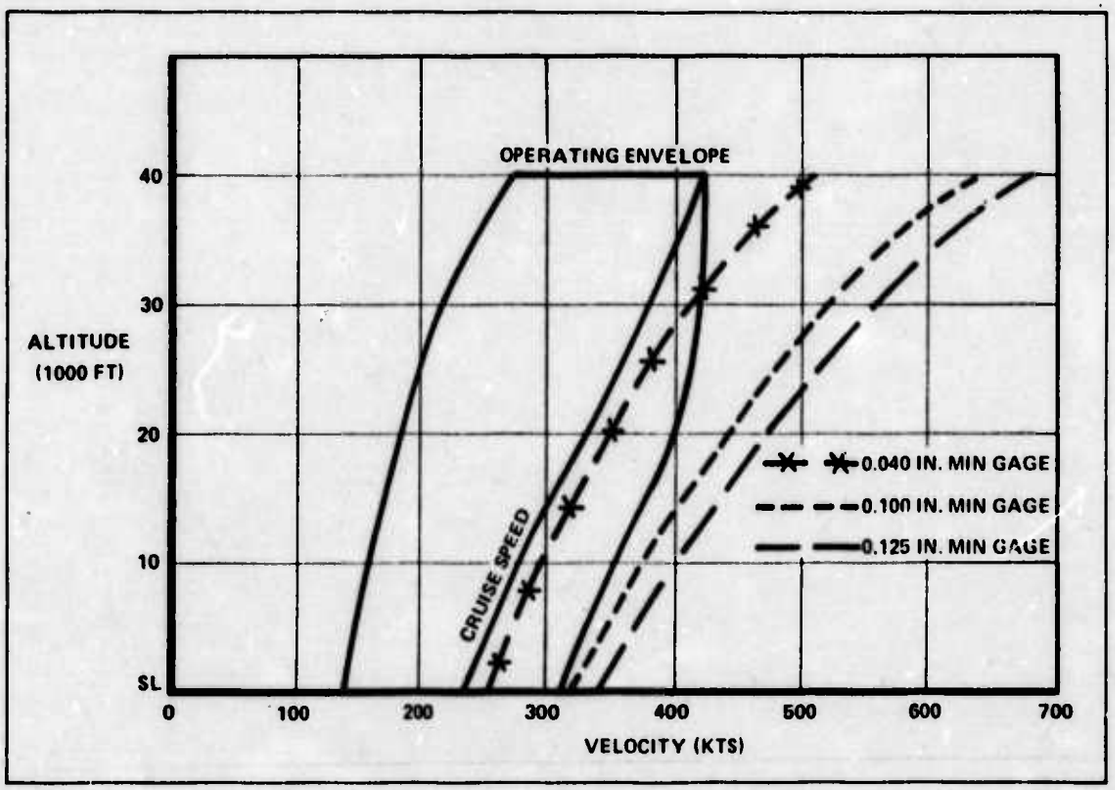

Figure 4.3.4.7-3. Divergence Speeds

There was a dramatic increase in divergence speed as the wing tips were stiffened by increasing the minimum gauge of the beam structure material. The 343 kts speed is 11% greater than the 310 kts maximum speed at sea level, so the divergence speed was not quite within acceptable limits. The weight penalty of 5900 lbs is only 2% of the wing weight estimate of 267,200 lbs. It appears, then, that divergence speed is not a severe problem for this wing planform. A detail designer should be able to increase the divergence speed a few more percent into an acceptable range. The results of the divergence speed investigation are shown in Figure 4.3.4.7-3 superimposed on the operating envelope for the aircraft. The operating envelope is discussed in Section 4.4.7.

4.3.5 FUSELAGE: The fuselage diameter was determined by the nuclear reactor and reactor associated equipment size. As shown in Sections 5 and 6, the estimate for the size was 30 to 40 ft in diameter. The fuselage length was determined from two considerations:

1) It may be possible to reduce the reactor shielding if crew members are stationed no closer than 200 ft from the reactor.

2) A recommendation by Col. Beers, Chief Medical officer ASD's Life Support Office, that, for a 14 day mission, each crew member have 6,000 cu ft or more of living/working volume (Ref 14).

The above analysis of fuselage diameter and length resulted in a 40 ft diameter fuselage, 430 ft long. This fuselage volume is almost five times that of the C-5A's fuselage.

4.3.6 REACTOR MOUNTING: One aspect of the nuclear powered aircraft that does not appear to have been very carefully investigated is the problem of mounting the reactor and containment vessel in the aircraft. Some of the feasibility studies have addressed the problem of absorbing the kinetic energy of the reactor containment vessel during a crash. But those schemes do not provide for the degree of rigid support required to keep the containment vessel in place during flight maneuvers.

It also seems reasonable to let the aircraft structure provide for a considerable fraction of the kinetic energy absorption required in the event of a crash landing. But that requires that the inertia of the containment vessel be transmitted to the aircraft structure.

A method for implementing this philosophy is described below. Many aircraft engines are mounted in the airframe through the use of trunnions and bearings. That is one possible method for mounting the containment vessel in the airframe. The trunnions would be an integral part of the containment vessel. The loads are transmitted from the trunnions to bearings, or trunnion rings, which are built into the airframe structure. The loads from the trunnion rings may be carried to the fuselage structure or the wing-carry-thru structure in several ways. One is through the use of a truss framework consisting of bars and tubular columns. The other is through the use of stiffened shear beams.

All of this extra structure is essentially a weight penalty that the nuclear powered aircraft must pay which is not incurred by conventionally powered aircraft. This analysis was performed to determine the extent of the weight penalty.

The location of the containment vessel in the aircraft is shown in Figure 4.2.2-1. The center of the containment vessel is at the same fuselage station as the wing quarter chord. This enables the containment vessel loads to be transferred most efficiently to the wing during flight. The main landing gear trucks are located just in front of and just behind the containment vessel. This enables the containment vessel loads to be transmitted most efficiently to the landing gear during landing and ground operations.

One of the first tasks was to determine the load conditions that the structure must carry. There were four classes of load conditions considered: (1) straight and level flight, (2) sitting on the ramp, (3) symmetric flight maneuvers, and (4) crash landings. The symmetric flight maneuver load factors were taken from MIL-A-8861 as + 2.5 and -1.0 (Ref. 116, Table 1). The crash landing load factors were taken from MIL-A-8865 as 20 forward, 10 aft, 10 up, 20 down and 10 laterally (Ref. 117, Table I). Each of the load conditions was considered separately and in combination with other load conditions to determine the maximum loads in the structure.

For this analysis the reactor containment vessel was assumed to be a 20 ft diameter sphere weighing 800,000 lbs. The containment vessel is made of Haynes Alloy No. 188. The following physical and mechanical properties were taken from the *Aerospace Structural Metals Handbook* (Ref. 193, Article 4310, Table 3.011):

density = 0.330 lbs/cu in.
τ_{tu} = 125,000 psi ultimate tensile strength
τ_{ty} = 73,000 psi yield tensile strength

The following mechanical properties were estimated:

τ_{sy} = 67,000 psi yield shear strength
τ_{bry} = 125,000 psi yield bearing strength

The material selected for the support structure was 4130 steel. It is a common aircraft structural material and has a higher specific strength than 2024 aluminum. The physical and mechanical properties were taken from MIL-HDBK-5 (Ref. 119, Table 2.2.2.0):

E = 29.0 x 10^6 psi modulus of elasticity
density .283 lbs/cu in
τ_{tu} = 180,000 psi
τ_{ty} = 163,000 psi
τ_{cy} = 179,000 psi yield compressive strength
τ_{bry} = 230,000 psi
τ_{sy} = 73,000 psi

The trunnions were assumed to be an integral part of the containment vessel and made of the same material, Haynes Alloy No. 188. At least three trunnions are required to completely restrain the containment vessel. As many as six might reasonably be used. The number of trunnions used would determine the magnitude of the loads imparted to the supporting structure at each trunnion. The analysis here used four trunnions as shown in Figure 4.3.6-1. Four trunnions were used as a compromise between reducing loads and unduly restraining the geometry of the heat transfer piping out of the containment vessel. The diameter of each

trunnion was determined by the shear load that the trunnion was required to carry. The thickness of each trunnion was determined by the bearing load each trunnion was required to carry. The top and bottom trunnions were 10.4 in. in diameter by 4.4 in. thick. The side trunnions were 13.0 in. in diameter by 5.5 in. thick. No attempt was made to determine how much extra containment vessel structure would be required to react the bending stresses in the containment vessel wall caused by the trunnions.

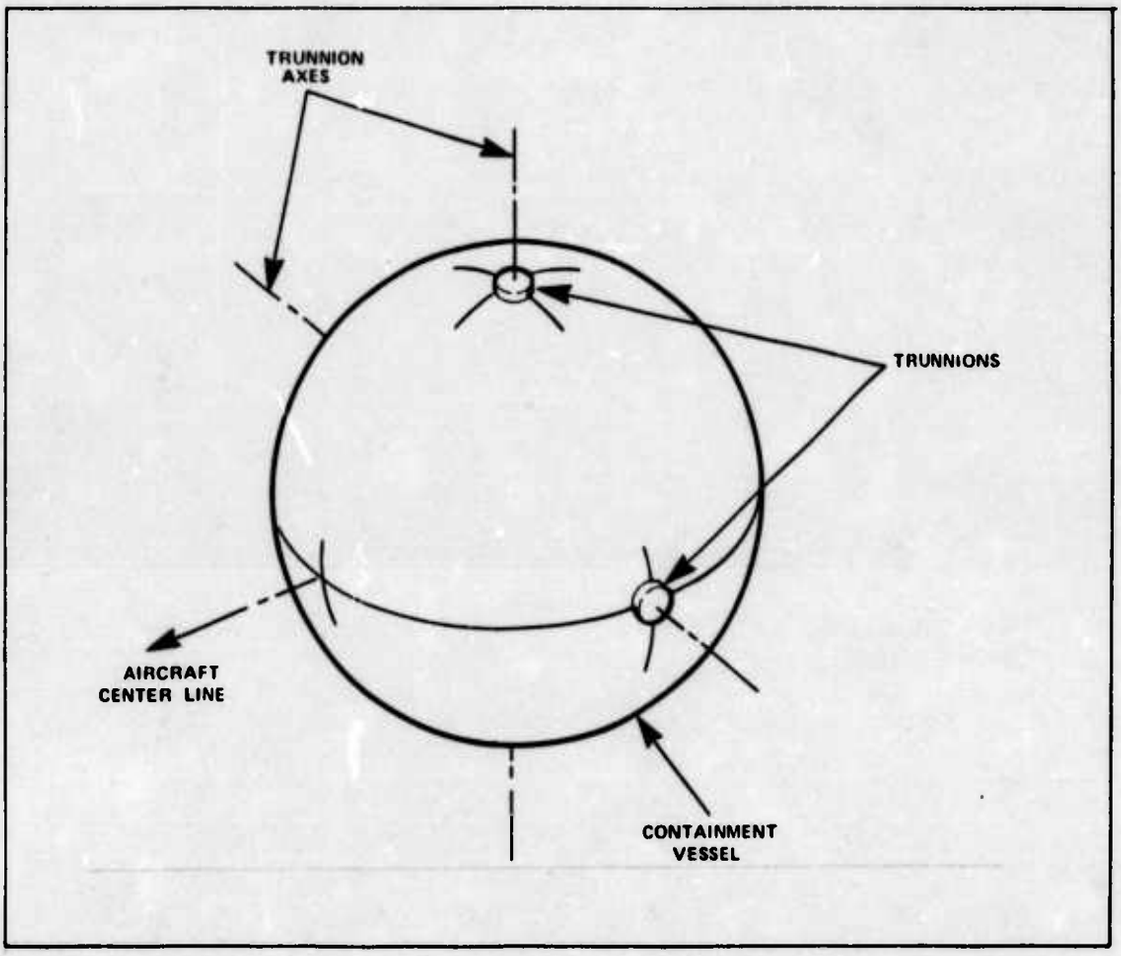

Figure 4.3.6-1. Trunnion Arrangement

The trunnion rings were assumed to be made from the 4130 steel. Since the bearing strength of the Haynes Alloy No. 188 is considerably less than the bearing yield strength of the 4130 steel, the trunnion is the critical part and the thickness of the ring must match the thickness of the trunnion. The inside diameter of the ring must match the diameter of the trunnion. The outside diameter of the ring was determined from the standard empirical relationship that the distance from the edge of a part to the center of the hole must be one and one-half times the diameter of the hole. In other words, the outside diameter is three times the inside diameter. The outside diameter of the top and bottom trunnion rings was 31.1 in. The side trunnion rings had an outside diameter of 39.1 in.

As mentioned earlier, one of the ways to transmit the containment vessel loads is through a truss framework made up of tubular columns. The framework used in this analysis is shown in Figure 4.3.6-2. The structure shown is statically indeterminate. To simplify the analysis for this feasibility study, each load condition was examined and it was assumed that all of the load was reacted by one primary triangle of the frame. After the loads in each column for each load condition were determined, the principle of superposition was used to determine the total load each column was required to carry. Most of the members act as columns carrying compressive loads. Some of the columns were required to support both tensile and compressive loads, depending upon the load condition acting. The most efficient column for this frame is a round tube, since each column is not constrained to fail in a certain direction.

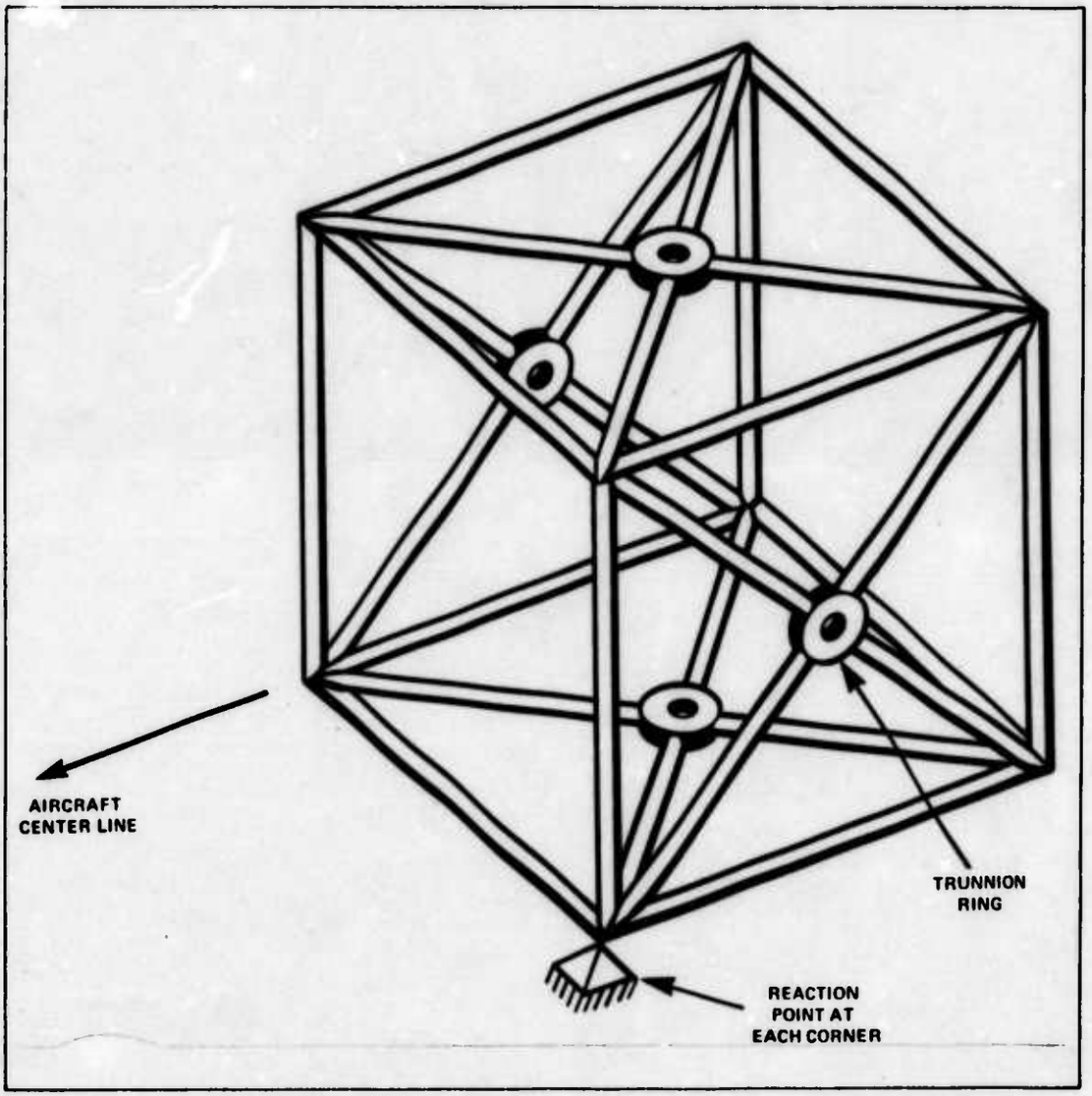

Figure 4.3.6-2. Truss Framework

A column can fail in two ways. The primary mode of failure is a lateral deflection of the entire column essentially causing it to bow from straight. The secondary mode of failure is a local collapse or wrinkling of the tube wall. This secondary mode of failure is precluded when

the ratio of tube diameter to wall thickness is less than or equal to 50 (Ref. 119, Table 2.4.2.1). An initial value for the area, A, of the column is given by dividing the load, F, by the yield stress, τ_{cy}.

$$A = F/\tau_{cy} \tag{4.3.6-1}$$

Properties for a circular ring cross section are taken from *Mechanics of Materials* by Timoshenko and Gere (Ref. 179, App. B). The area, $A = 2\pi rt$. The area moment of inertia, $I = \pi r^3 t$. Since $r/t = 25$ these formulas may be rewritten. Since the area was already estimated, the area relation can be solved to find the average radius, r.

$$r = \left(\frac{2\pi}{25} A\right)^{1/2} \tag{4.3.6-2}$$

Then the moment of inertia, I, is given by the expression

$$I = \frac{\pi}{25} r^4 \tag{4.3.6-3}$$

The radius of gyration, ρ, is the square root of the quotient of the moment of inertia divided by the area.

$$\rho = \sqrt{I/A} \tag{4.3.6-4}$$

Then the column buckling stress is given by the equation:

$$\tau_{CR} = 179{,}000 - 27.95\,(\ell'/\rho)^2 \tag{4.3.6-5}$$

where ℓ' is the effective length of the column and is dependent upon the actual length, ℓ, and the end fixity conditions (Ref. 119, Table 2.4.2.1). All columns were assumed to have one end fixed and the other end pinned. The relation between the effective length and actual length is

$$\ell' = K\ell \tag{4.3.6-6}$$

where "K" is the factor indicating the end fixity. For this case, K = 0.7. With the buckling stress, a better estimate of the tube area can be made.

$$A_{CR} = F/\tau_{CR} \tag{4.3.6-7}$$

The largest column had an average diameter of 27.5 in. and a wall thickness of 0.56 in. The smallest column had an average diameter of 9.1 in. and a wall thickness of 0.18 in.

The other method of transmitting the loads from the trunnion rings into the fuselage is through the use of stiffened plates. The load condition that caused the largest loads in each panel was examined. For ease of analysis it was assumed that only one fourth of the 20 ft square panel carried all of the load (See Figure 4.3.6-3). The 10 ft square panel carries a combined load in shear and compression. The panel was designed to withstand buckling under this load using methods in Peery's *Aircraft Structures* (Ref. 137, p. 368-372, 393-394). The combined loading may be analyzed using the interaction equation:

$$R_S^{1.5} + R_C \leq 1 \qquad (4.3.6\text{-}8)$$

where the R's are the stress ratios of the working stresses, f, in the plates to the critical buckling stresses, τ_{CR}.

$$R_S = f_S/\tau_{SCR},\ R_C = f_C/\tau_{CCR} \qquad (4.3.6\text{-}9)$$

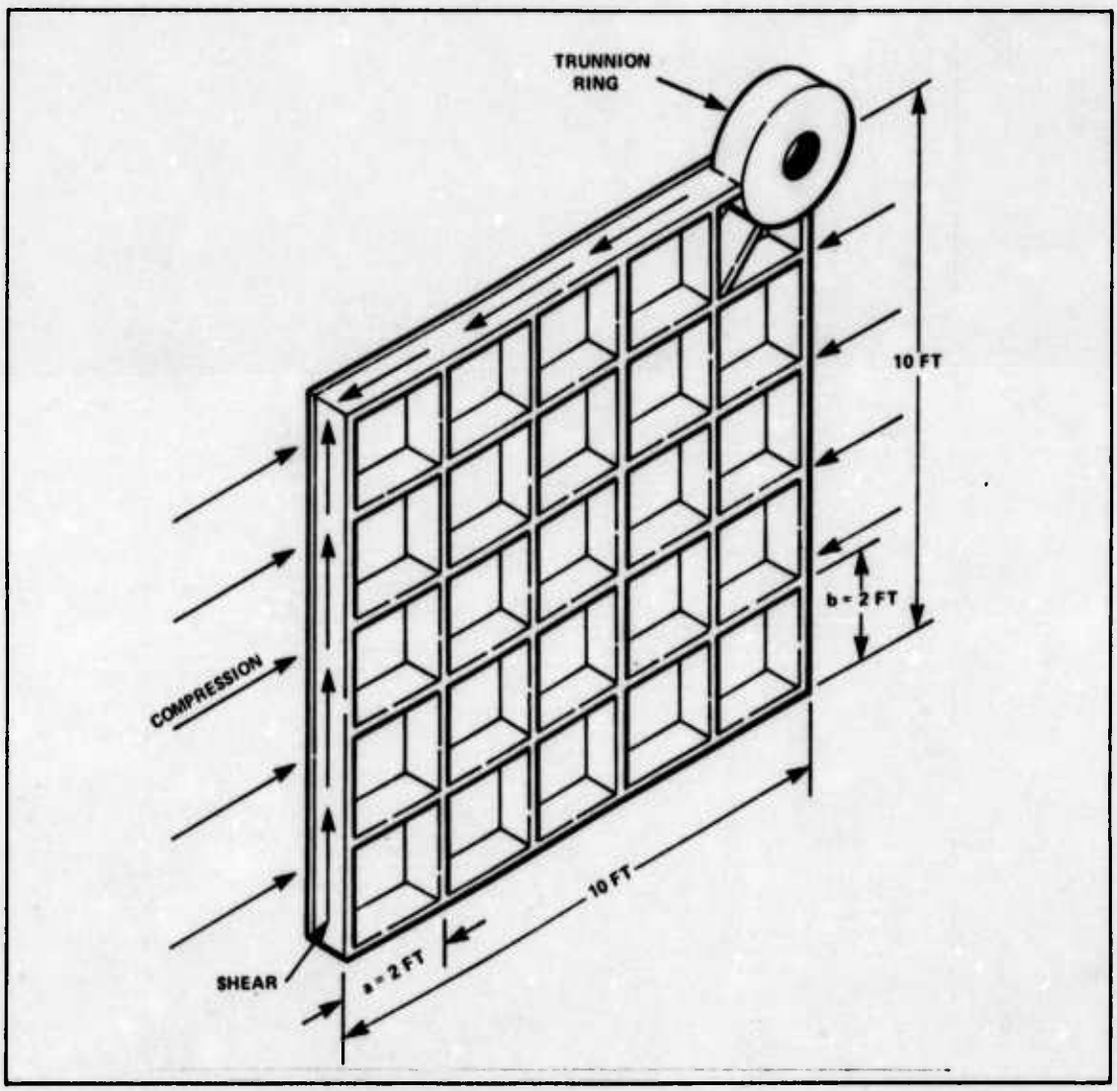

Figure 4.3.6-3. Shear Beam Analysis

The subscript s represents shear and the subscript c is for compression. The working stress is the load divided by the area. The critical buckling stresses are given by the following equation:

$$\tau_{CR} = K E (t/b)^2 \qquad (4.3.6\text{-}10)$$

where τ_{CR} = buckling stress
K = fixity coefficient
= 6.35 for compression
= 8.00 for shear
E = modulus of elasticity
= 29.0 X 10^6 psi
t = plate thickness
b = minimum bay dimension

The dimensions a and b in Figure 4.3.6-3 were arbitarily chosen as 2 ft.

The method used was as follows. Initially the thickness of material required to prevent yielding was determined for shear and compression separately. The larger of the two thicknesses thus found was increased by 10% and new working stresses and buckling stresses were calculated. These values were then substituted into the interaction equation to see if it was satisfied. If the equation was not satisfied the thickness was increased and another check was made. When the calculated buckling stress was greater than the yield stress, the yield stress was used as the critical stress. The vertical plates required a thickness of 1.05 in. The horizontal plates required a thickness of 0.65 in.

It was further assumed that the volume of stiffener material was equal to the volume of plate material. Since it was assumed that one-fourth of the panel carried all of the load, an additonal factor of 10% was used to calculate the total volume of material in one 20 ft by 20 ft panel.

With the dimensions of all components of the support structure, it was a simple matter to calculate the material volume and, hence, the weight of the structure. The weight was calculated for both the stiffened plate structure and the truss frame structure. Then an average of the two was used to arrive at an estimate of the final support structure weight. The truss frame structure weighed 27,000 lbs, and the stiffened plate structure weighed 36,000 lbs. The average weight of 31,500 lbs was used in structural weight calculations for the fuselage of the airplane.

One of the concerns with the nuclear powered airplane is with reactor accessibility and/or removal when the reactor required refurbishing. Either of the two support structures analyzed

could be adapted to permit removal of the reactor. One method would be to remove it through the bottom of the aircraft. Another would be to remove it through the rear of the aircraft

4.3.7 LANDING GEAR: The aircraft landing gear is considered to be a critical structural component in an aircraft of the size required for nuclear propulsion application. A preliminary analysis was made to determine the size and number of tires required for a 2,000,000 lb aircraft. A first order approximation was also made to determine the relative size and the amount of energy the aircraft's strut must absorb.

As stated in Sections 2 and 4.1, the aircraft was assumed to use conventional Air Force runways and taxiways. No analysis was attempted on water takeoff and landing, air cushion landing systems, or other non-conventional landing systems.

4.3.7.1 AIRCRAFT TIRES: As stated above, the study aircraft assumed the use of conventional runways and taxiways. AFM-88-6 defines Air Force taxiway working stress as 250 psi for heavy load rated taxiways (Ref. 4, p. 12-18).

Therefore: minimum aircraft footprint = GW/taxiway working stress

For the point design aircraft, the minimum aircraft footprint is 8000 sq in.

For comparison: 747 footprint = 3890 sq in.; stress = 197 psi
C-5A footprint = 6083 sq in.; stress = 120 psi

With the aircraft footprint the type and number of tires were found with the use of MIL-T-5041 *Aircraft Tire Specifications* (Ref. 124, p. 12).

where: footprint per tire = 85% of tire rated load/tire pressure

and: number of tires = total footprint/tire footprint.

Table 4.3.7.1-1 summarizes the aircraft tire analysis results for the 2,000,000 lb gross weight point design aircraft.

TABLE 4.3.7.1-1. AIRCRAFT TIRE SUMMARY

TIRE SIZE	**56 X 16**
NUMBER OF TIRES	**36**
LANDING GEAR BOGIES	**4 MAIN — 8 TIRES EACH** **1 NOSE — 4 TIRES**
AIRCRAFT FOOTPRINT	**8700 SQ IN.**

4.3.7.2 LANDING GEAR STRUT: The aircraft struts must absorb the change in aircraft energy due to the rate of descent (R/D). The energy of the landing was found by assuming a constant vertical deceleration from an initial vertical velocity to a final, zero vertical velocity.

So that energy = $\frac{1}{2}$ m V^2 (4.3.7-1)

where: V = max R/D = 500 fpm
m = GW/g (4.3.7-2)

The strut will absorb the energy due to the change in strut pressure and internal strut volume change.

or: $E = \int PdV$ (4.3.7-3)

where: E = energy absorbed
P = strut pressure
dV = internal strut volume change

With this information, the strut size and wall thickness were estimated.

Table 4.3.7.2-1 summarizes the landing gear strut analysis results for the 2,000,000 lb gross weight point design aircraft.

TABLE 4.3.7.2-1. LANDING GEAR STRUT SUMMARY

TYPE STRUT	TRIPLE OLEO
INTERNAL STRUT DIA (IN.)	5.25
EXTERNAL STRUT DIA (IN.)	11.25
STRUT DEFLECTION (FT)	2
STRUT PRESSURE (PSI)	12,500

4.3.8 SIZING RESULTS: The sizing analysis resulted in the final aircraft parameters. The following parameters are for the 2,000,000 lb gross weight-point design-canard aircraft.

Weight and balance, dimensions, and configuration are dependent on many variables, such as weight of the nuclear propulsion system, airframe construction, and the weight of chemical fuel required. Weight and balance are summarized for standard aluminum construction, advanced composite construction, and fuel weights of 4% and 16% of gross weight. Dimensions and configuration are presented in tabular form for overall aircraft and individual components.

4.3.8.1 WEIGHT AND BALANCE: The exact weight and balance is dependent upon the material used, construction method employed, the nuclear power plant weight, the amount of chemical fuel required, and the number and size of chemical engines required. Table 4.3.8.1-1 summarizes possible structural weight reduction with the use of composite materials outlined in Section 4.3.3.

TABLE 4.3.8.1-1. POSSIBLE STRUCTURAL WEIGHT REDUCTION WITH COMPOSITE MATERIALS

MATERIAL	WEIGHT OF STRUCTURAL COMPONENT					
	FUSELAGE	WING	VERTICAL STABILIZER	CANARD	TOTAL STRUCTURE WEIGHT*	TOTAL REDUCTION
ALUMINUM	219,500	267,200	38,000	31,200	555,900	—
TITANIUM	186,575	240,480	34,200	28,080	489,335	66,565
BERYLLIUM	169,015	171,008	28,120	23,088	391,231	164,669
BORON/EPOXY	169,015	216,432	30,780	25,272	441,449	114,401
GRAPHITE/EPOXY (CURRENT TECHNOLOGY)	155,845	184,368	26,220	21,528	389,961	167,939
GRAPHITE/EPOXY (ADVANCED TECHNOLOGY)	100,970	112,224	17,860	14,664	245,718	310,182
ORGANIC/EPOXY (CURRENT TECHNOLOGY)	169,015	232,464	33,060	27,144	461,683	94,217
ORGANIC/EPOXY (ADVANCED TECHNOLOGY)	120,725	187,040	26,600	21,840	356,205	199,695

* Does not include landing gear weight.

Table 4.3.8.1-2 summarizes the point design weight and balance and the weights available for nuclear propulsion system and payload. The CG location, found by the method outlined in Section 4.3.1, is an approximation and is given as distance from the aircraft nose. The CG location depends upon the nuclear power plant weight, the required chemical capability, and the type of material and construction. For illustrative purposes, the nuclear propulsion system weight was assumed to be 820,000 lbs (500 MW gas reactor) for all configurations. Six 50,000 lb thrust chemical engines with 16% of the gross weight in chemical fuel were used in configurations A and C. Two 40,000 lb thrust chemical engines with 4% of the gross weight in chemical fuel were used in configurations B and D. The 300,000 lbs total static, sea level thrust (configurations A and C) will give the point design aircraft the capability to complete takeoff if one chemical engine is lost during takeoff (Ref. 116, p. 13). As outlined in Section 4.1.3, the two 40,000 lb thrust chemical engines (configurations B and D) will only be used to supplement nuclear power for takeoff and initial climb.

TABLE 4.3.8.1-2. AIRCRAFT WEIGHT AND BALANCE SUMMARY 2,000,000 LBS GW

	COMPONENT WEIGHT (LBS)			
	A	B	C	D
WING WEIGHT	267,200	267,200	112,224	112,224
CANARD WEIGHT	31,200	31,200	14,664	14,664
VERTICAL STABILIZER WEIGHT	38,000	38,000	17,860	17,860
FUSELAGE WEIGHT	219,500	219,500	100,970	100,970
LANDING GEAR WEIGHT	111,000	111,000	111,000	111,000
TOTAL STRUCTURAL WEIGHT	666,900	666,900	356,718	356,718
FIXED EQUIPMENT WEIGHT	200,000	200,000	200,000	200,000
CHEMICAL ENGINE WEIGHT	50,000	14,000	50,000	14,000
CHEMICAL FUEL WEIGHT	320,000	80,000	320,000	80,000
TOTAL LESS NUCLEAR PROPULSION SYSTEM & PAYLOAD	1,236,900	960,900	926,718	650,718
AVAILABLE FOR NUCLEAR PROPULSION SYSTEM & PAYLOAD	763,100	1,039,100	1,073,282	1,349,282
CG LOCATION (FT)	265	250	260	255

A - STANDARD ALUMINUM CONSTRUCTION (SEC. 4.3.2) — TAKEOFF WITH CHEMICAL POWER (SEC. 4.1.3)

B - STANDARD ALUMINUM CONSTRUCTION — TAKEOFF WITH NUCLEAR POWER (SEC. 4.1.3)

C - GRAPHITE/EPOXY ADVANCED CONSTRUCTION (SEC. 4.3.3) — TAKEOFF WITH CHEMICAL POWER

D - GRAPHITE/EPOXY ADVANCED CONSTRUCTION — TAKEOFF WITH NUCLEAR POWER

4.3.8.2 DIMENSIONS AND CONFIGURATION: Table 4.3.8.2-1 details the dimensions and Figure 4.3.8.2-1 shows the configuration of the point design aircraft. The 60 lbs/sq ft wing/canard loading was found to be optimum considering the mission requirements (Section 2), the L/D (Section 4.1.7.1), the required thrust (Section 4.4.4), and wing size (Section 4.3.4). This wing loading yielded a large wing area with a canard area almost the same as a C-5A wing (6000 sq ft). The required reactor power was found to be 475-700 MW, depending upon the type of nuclear propulsion system (Sections 5, 6, and 7).

The landing gear consists of triple oleo struts with thirty-six 56 X 16 tires mounted on four 8 tire main bogies, centered about the reactor and a 4 tire nose bogey. This configuration compares to the C-5A's twenty-eight 49 X 17 tires on four 6 tire main bogies and a 4 tire nose bogey. The resulting 8700 sq in. footprint compares to the C-5A's 6083 sq in. and the 747's 3890

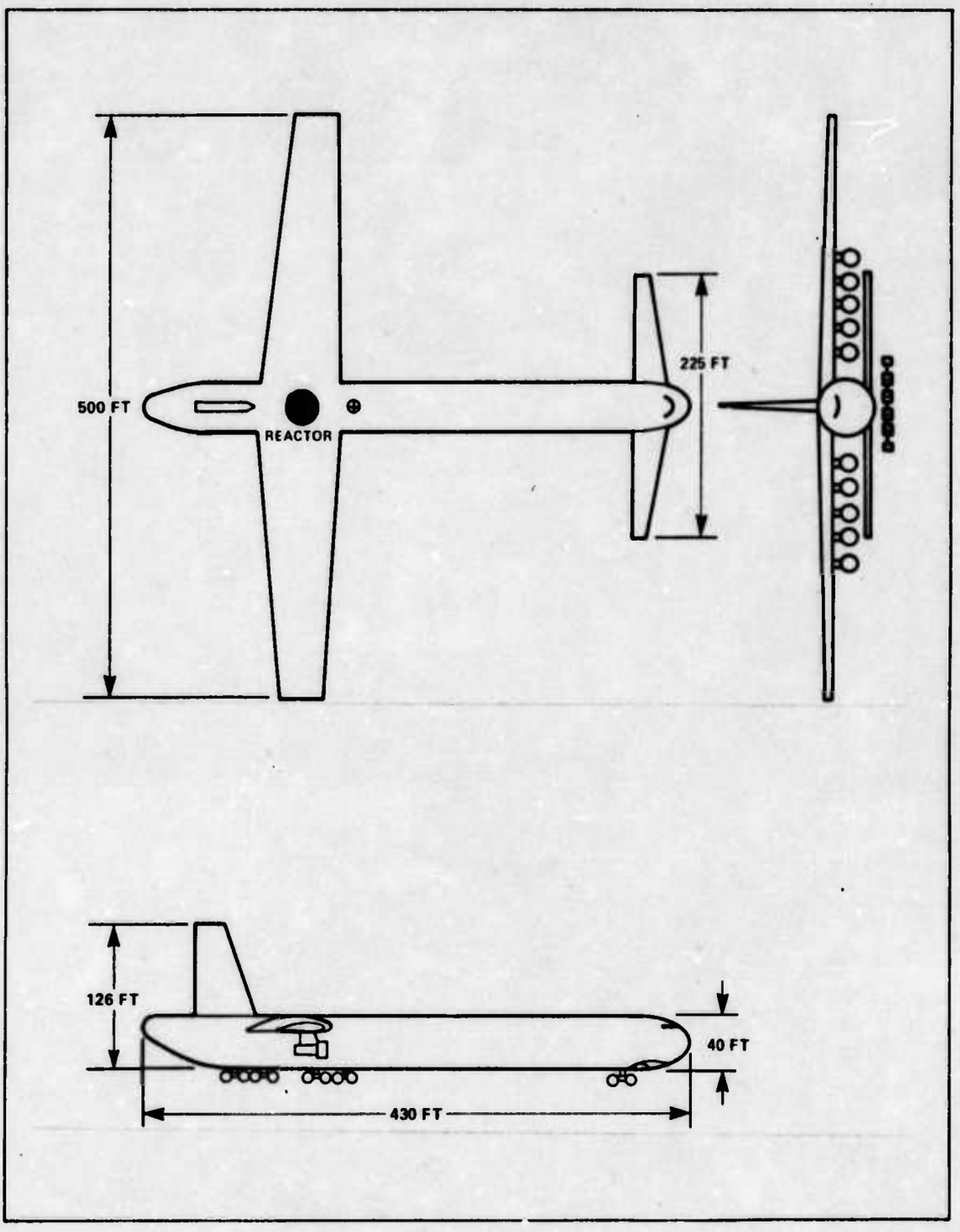

Figure 4.3.8.2-1. Point Design Configuration

sq in. This results in a pressure of 230 psi which is comparable to the B-52's 250 psi. This pressure print will allow the point design aircraft to use any runway and taxiway presently rated for B-52 use.

TABLE 4.3.8.2-1. AIRCRAFT DIMENSIONS AND CONFIGURATION 2,000,000 LBS GROSS WEIGHT

WING/CANARD LOADING (PSF)	60
ASPECT RATIO	9
TAPER RATIO	0.4
THICKNESS RATIO	0.18
WING QUARTER CHORD LOCATION (FT)	300
WING AREA (SQ FT)	27,800
WING SPAN (FT)	500
WING ROOT (FT)	79
WING TIP (FT)	32
WING MAC (FT)	59
FLAP AREA (% OF WING AREA)	20
SPEED BRAKE AREA (% OF WING AREA)	13
CANARD QUARTER CHORD LOCATION (FT)	60
CANARD AREA (SQ FT)	5600
CANARD SPAN (FT)	225
CANARD ROOT (FT)	36
CANARD TIP (FT)	14
CANARD MAC (FT)	27
VERTICAL TAIL QUARTER CHORD LOCATION (FT)	360
VERTICAL TAIL AREA (SQ FT)	4300
VERTICAL TAIL HEIGHT (FT)	86
VERTICAL TAIL ROOT (FT)	70
VERTICAL TAIL TIP (FT)	30
VERTICAL TAIL MAC (FT)	53
MAX FUSELAGE DIAMETER (FT)	40
FUSELAGE LENGTH (FT)	430
REACTOR LOCATION (FT)	300
REACTOR POWER (MW)	475 - 700
LANDING GEAR LOCATION (FT)	60, 265, & 335
NUMBER OF TIRES	36
TIRE SIZE	56 X 16
AIRCRAFT FOOTPRINT (SQ IN)	8700
AIRCRAFT PRESSURE PRINT (PSI)	230

NOTE: ALL LOCATIONS MEASURED FROM AIRCRAFT NOSE.

4.4 AIRCRAFT PERFORMANCE

As the last step in the design process, the general aircraft performance was estimated. The performance is presented in the form of a mission profile. This profile takes the point design aircraft from takeoff through climbout, into a performance envelope, and then to descent and landing. The results of this performance analysis are presented as an aircraft flight envelope with takeoff and landing parameters.

The use of existing Air Force runways (12,000-13,000 ft in length) and the mission requirements govern all performance requirements.

Numerical examples of this analysis are presented in Appendices A.4.1.9 through A.4.1.13.

4.4.1 TAKEOFF REQUIREMENTS: Takeoff thrust estimation was examined in Section 4.1.2.1 of this study. The assumed takeoff distance was 10,000 ft over a 35 ft obstacle on a hot day (100°F). C_{LTO} was assumed to be $0.75C_{LMAX}$; where $C_{LMAX} = 2$ with full flaps (Ref. 92, p. 369). If the takeoff was accomplished at maximum C_L and the aircraft encountered a gust that increased the angle of attack, an undesirable stall condition could be encountered. It is necessary that the flaps be positioned and the angle of attack be such that $C_{LTO} = 0.75\ C_{LMAX}$ for aircraft stability.

At takeoff: Lift = GW = $\frac{1}{2}\rho SV^2C_{LTO}$

so that V at lift off = $(2GW/(\rho S_T C_{LTO}))^{0.5}$ = 186 ft/sec (4.4.1-1)

4.4.2 CLIMB REQUIREMENTS: In level flight at constant speed, the engine thrust is equal to the drag of the aircraft. With additional thrust the aircraft can climb at a rate determined by the amount of additional thrust available and altitude. Figure 4.4.2-1 shows the aircraft forces in level unaccelerated flight and the aircraft climbing in unaccelerated flight.

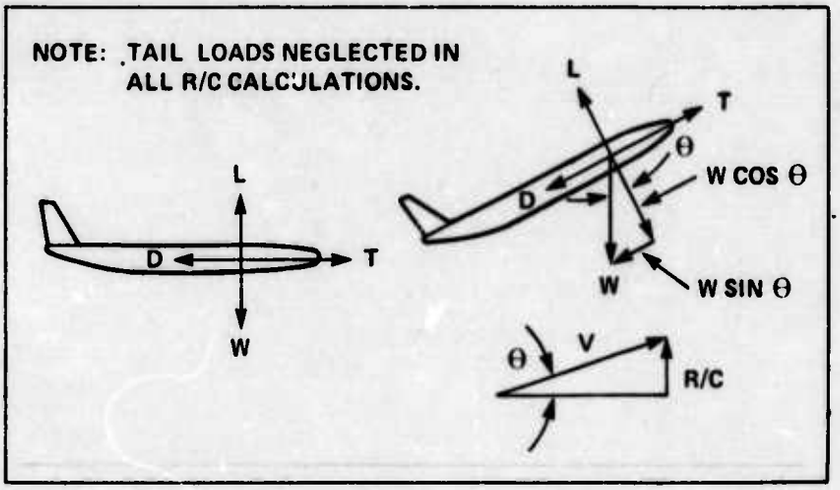

Figure 4.4.2-1. Airplane Forces in Level and Climbing Flight

In level flight, lift is equal to gross weight. It is desired to use all the additional thrust to climb while maintaining the same speed. To reach equilibrium the aircraft is rotated until T = D + W sin θ

where: D = total drag
W = GW for estimation
θ = angle of climb
T = minimum total aircraft thrust available

SIN θ = R/C/V where R/C = rate of climb
and V = $(2GW/(\rho SC_L))^{0.5}$

$$\text{so that } T = \frac{GW}{L/D} + \frac{GW\ R/C}{V} \qquad (4.4.2\text{-}1)$$

The first right hand term is the cruise thrust and the second term is the additional trust required to maintain a specified rate of climb.

Additional thrust required for climb (T_C) =

$$T_C = \frac{GW\ R/C\ (\rho\ S_T\ C_L)^{0.5}}{(2\ GW)^{0.5}} \qquad (4.4.2\text{-}2)$$

therefore: Total required thrust =

T_C + the maximum of (stall or cruise thrust) (4.4.2-3)

This study used a rate of climb of 600 fpm at sea level as that desired for the ASW mission (Section 2).

4.4.3 SERVICE CEILING: Service ceiling is the altitude at which an aircraft's maximum rate of climb is 100 fpm. This study assumed a service ceiling which conformed to the mission requirements of 40,000 ft. With the assumed service ceiling and the rate of climb at sea level, the required total thrust for all altitudes was computed by Eq. 4.4.2-3. Figure 4.4.3-1 shows the resulting total thrusts and rates of climb for the point design aircraft gross weight of 2,000,000 lbs.

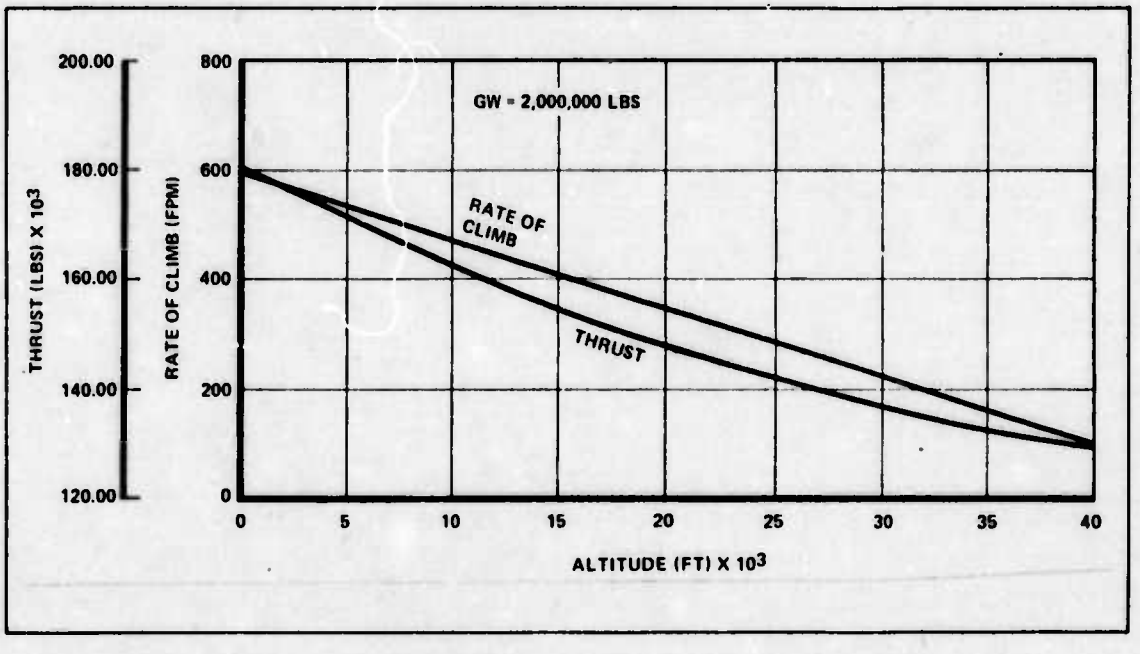

Figure 4.4.3-1. Rate of Climb and Total Required Thrust vs Altitude

4.4.4 CRUISE PERFORMANCE: Cruise requirements were dictated by the mission requirements. These requirements specified a high altitude cruise speed of 250 to 350 kts at an altitude of 30,000 ft and a low altitude cruise at sea level with a speed of 150 to 250 kts. For velocity stability, the cruise must be at a speed that will yield less than the maximum lift to drag ratio (Point B in Figure 4.4.4-1) and at a speed greater than that which will yield maximum lift to drag (L/D), in other words, on the right hand side or down slope of the L/D curve. This is shown as Point C in Figure 4.4.4-1. As a further example, consider that at cruise lift is constant. This fact results in Figure 4.4.4-2, the drag curve.

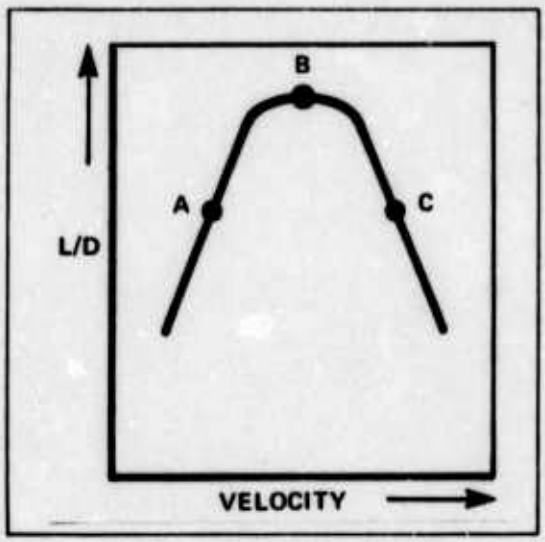

Figure 4.4.4-1. L/D Curve

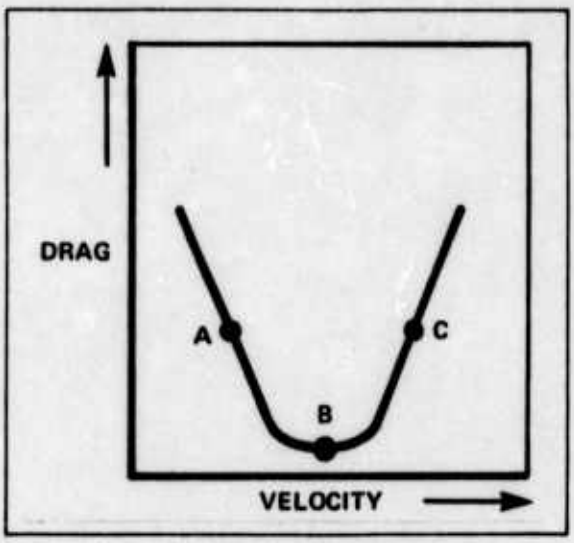

Figure 4.4.4-2. Drag Curve

For velocity stability: $dD/dV > 0$

where: dD = change in drag due to change in velocity dV.

For example:

At point A (Fig. 4.4.4-2):	if $dV > 0$ then $dD < 0$ - unstable
	if $dV < 0$ then $dD > 0$ - unstable
At point B: (minimum D)	if $dV > 0$ then $dD > 0$ - stable
	if $dV < 0$ then $dD > 0$ - unstable
At point C	if $dV > 0$ then $dD > 0$ - stable
	if $dV < 0$ then $dD < 0$ - stable

The following must be considered in determining the L/D value:

1) Point C must be at a value such that the difference between L/D at cruise and maximum L/D will allow the aircraft to remain stable during normal flight velocity fluctuations. If cruise L/D is too high, velocity fluctuations, such as wind shifts, may cause the aircraft's flight L/D to reach or pass maximum L/D and result in instability.

2) If cruise L/D is too low, excessive power requirements may result.

After discussions with Prof. Larsen, it was concluded that point C should be about 80% of maximum L/D for a conservative estimate of cruise L/D (Ref. 94). Therefore a cruise L/D = 80% of maximum L/D was assumed for cruise performance estimation. Cruise thrust was computed as a function of gross weight and cruise L/D.

thus: cruise thrust = GW/(cruise L/D)

where: L/D was computed as in Section 4.1.5.1.

Cruise speeds for all altitudes were computed by solving the basic L/D equation for velocity:

$$L/D = \frac{C_L}{C_{DP} + C_{DC} + C_L^2/(2.51\,AR)}$$

and:

$$C_L = \frac{2\,GW}{\rho\,S_T\,V^2}$$

therefore:

$$V = \left[\frac{GW \left\{ 1 + \left[1 - 4\,(L/D)^2 \left(\frac{C_{DP} + C_{DC}}{2.51\,AR} \right) \right]^{1/2} \right\}}{\rho\,S_T\,L/D\,(C_{DP} + C_{DC})} \right]^{1/2} \qquad (4.4.4\text{-}1)$$

where: C_{DP} and C_{DC} are as computed in Section 4.1.5.1

and: If L/D is cruise L/D then V is cruise V.

Cruise speeds for all operating altitudes are shown in Figure 4.4.4-3 for the point design aircraft.

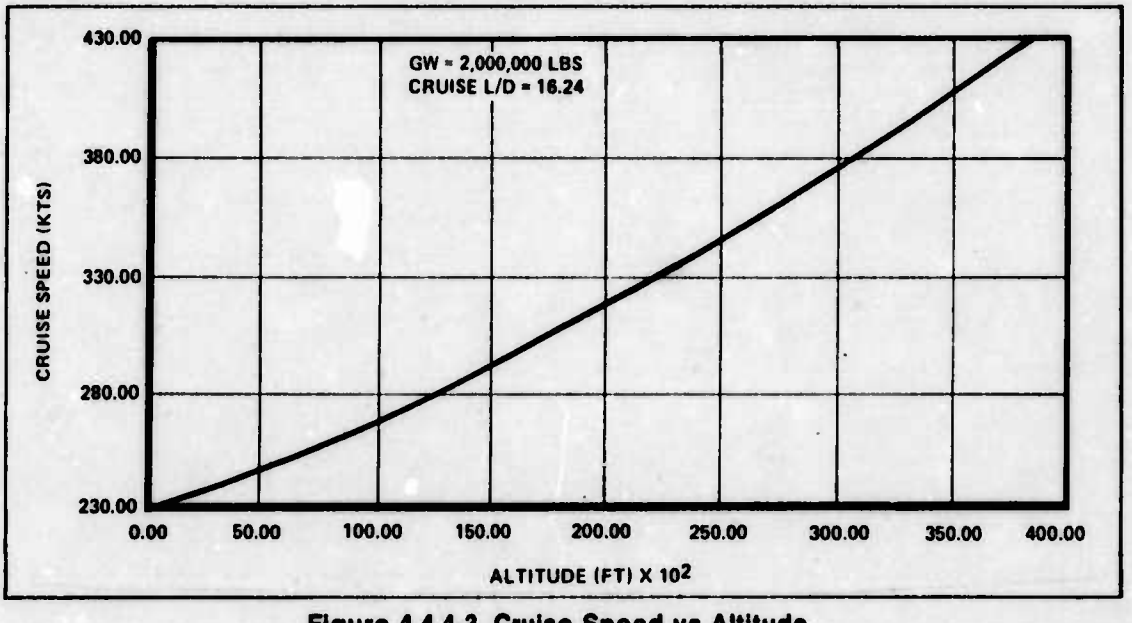

Figure 4.4.4-3. Cruise Speed vs Altitude

4.4.4.1 STALL SPEED: Stall speed is the speed at maximum C_L. The study aircraft was assumed to have C_{LMAX} equal to 1.

therefore: $\text{Lift} = GW = \frac{1}{2} \rho S_T V^2 C_L$

and:
$$V = \left(\frac{2\,GW}{\rho\, S_T\, C_{LMAX}} \right)^{1/2} \qquad (4.4.1\text{-}1)$$

where: V = Stall speed @ ρ

4.4.4.2 STALL THRUST: Stall thrust is the minimum thrust required to keep the aircraft at or above stall speed:

Since $T = GW/(L/D)$ (4.1.5-1)

and: $C_{LMAX} = 1$ at all altitudes

therefore:
$$L/D_{STALL} = \frac{C_{LMAX}}{C_{DP} + C_{DC} + \dfrac{C_{LMAX}^2}{\pi\, AR\, e}} \qquad (4.4.4\text{-}2)$$

Stall L/D is constant for all altitudes

For example:

At sea level: Cruise thrust = 126,000 lbs
Stall thrust = 115,000 lbs
Climb thrust = 56,000 lbs
Total thrust at sea level = 182,000 lbs

At 30,000 ft: Cruise thrust = 123,000 lbs
Stall thrust = 115,000 lbs
Climb thrust = 15,000 lbs
Total thrust required at 30,000 ft = 138,000 lbs

4.4.4.3 MAXIMUM SPEED: The aircraft's maximum straight and level speed will be determined by the L/D at that speed: L/D @ maximum speed = GW/T_T

where: T_T is the total available thrust

therefore: V@ maximum speed is found by Eq. 4.4.4-1.

The aircraft structure configuration will limit the aircraft's maximum speed. Therefore, a structural speed limit of Mach 0.7 was assumed for the study aircraft (Ref. 9).

Stall speed and maximum speed as a function of altitude are shown in Figure 4.4.4.3-1 for the point design aircraft. The maximum speed is the minimum of the speed found by Eq. 4.4.4-1 or Mach 0.7. For the study aircraft the Mach 0.7 limit is applicable above 20,000 ft altitude.

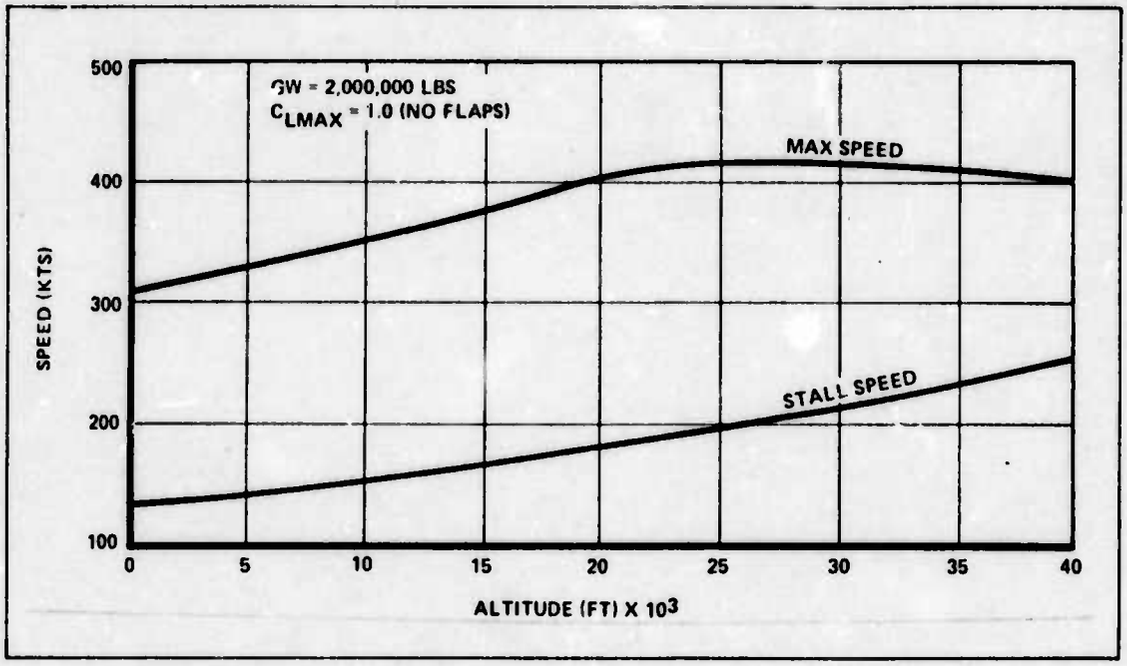

Figure 4.4.4.3-1. Stall Speed/Maximum Speed vs Altitude

4.4.5 DESCENT: The rate of descent (R/D) was specified to be 8000 fpm from 30,000 ft for the selected mission.

Let R/D = -R/C and T = 0

From Section 4.4.2: $O = \frac{GW}{L/D} + \frac{GW\ R/C}{V}$

and: $\frac{GW}{L/D} = -\frac{GW\ R/C}{V} = T_{CRUISE} = D$

therefore: $D = \frac{GW\ R/C}{V}$ where: V = Velocity at cruise

let: D_S = Speed brake drag

Total drag for descent = $D + D_S = T + D_S$

where: T = thrust at cruise V prior to the start of descent

therefore:

$$D_S = \frac{GW\ R/D}{V} - T$$

$$D_S = \tfrac{1}{2}\,\rho\, S_S\, V^2\, C_{DS} \sin\phi \qquad (4.4.5\text{-}1)$$

where: S_S = area of speed brakes

C_{DS} = speed brake drag coefficient

ϕ = speed brake angle as shown in Figure 4.4.5-1

therefore:

$$S_S = \frac{2\ GW}{\rho\ V^2\ C_{DS} \sin\phi} \left(\frac{R/D}{V} - \frac{1}{L/D} \right) \qquad (4.4.5\text{-}2)$$

This resulted in a speed brake area of 3321 sq ft, or less than 6% of the wing area.

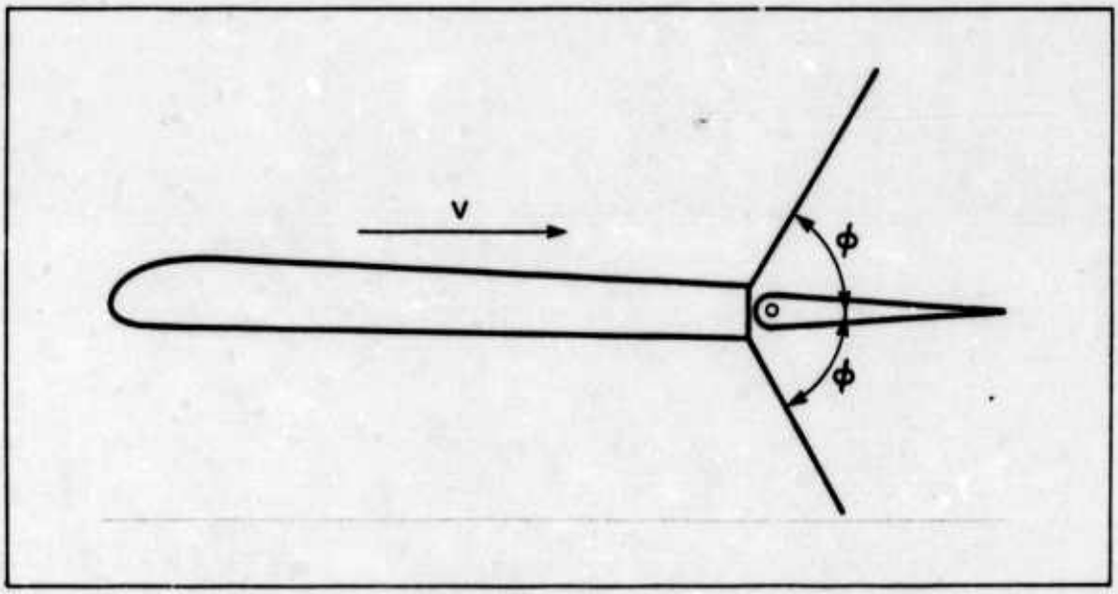

Figure 4.4.5-1. Airfoil with Speed Brakes Open ϕ Degrees

4.4.6 LANDING: The landing distance specified by the Civil Air Regulations is the horizontal distance required to clear a 50 ft obstacle and come to a complete stop. As shown in Figure 4.4.6-1, the distance can be divided into two parts, the descent from the 50 ft altitude to touchdown, and the deceleration distance required to come to a complete stop. Civil Air Regulations require that, at the 50 ft altitude, a steady gliding approach be maintained at a true airspeed equal to 1.30 of the stall speed and at touchdown the speed shall equal 1.15 of the stall speed. These factors are used as safety factors to prevent a stall if, for any reason, the angle of attack of the aircraft is increased.

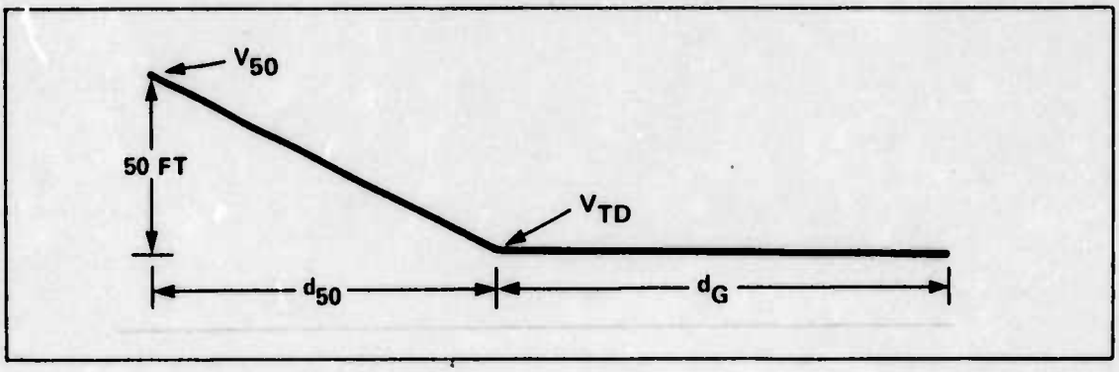

Figure 4.4.6-1. Flight Path in Landing

Other safety factors to account for are nonoptimum weather conditions and variations in pilot technique. Increasing the calculated landing distance by 2/3 to obtain the runway required for the aircraft is common design practice (Ref. 33, Ch. 2, p. 13).

The descent distance is calculated by using the relationship: change in kinetic energy minus potential energy equals retarding force times distance:

so that: $\frac{1}{2}\ GW/g\ (V_{50}^2 - V_{TD}^2) + 50\ GW = F\ d_{50}$

where: g = gravitational constant
V_{50} = velocity at 50 ft altitude = 1.30 V_{SO}
V_{TD} = velocity at touchdown = 1.15 V_{SO}
d_{50} = horizontal distance required to descend 50 ft
V_{SO} = stall velocity

therefore: $$d_{50} = \frac{GW}{F}\left(\frac{V_{50}^2 - V_{TD}^2}{2g} + 50 \right)$$

$F = D$

$GW = Lift$

thus: $$d_{50} = L/D\ \left(\frac{V_{50}^2 - V_{TD}^2}{2g} + 50 \right) \qquad (4.4.6\text{-}1)$$

Ground deceleration distance, $d_G = V_{TD}^2/2a$ (4.4.6-2)

where: a = average deceleration, which is a function of brakes and wheel sizes. For a conventional brake design an average deceleration of 6 ft/sec^2 can be obtained. (Ref. 33, Ch. 2, p. 14)

$$V_{SO} = [\ 2\ GW/(\rho\ S_T\ C_{LMAX})\ ]^{1/2} \qquad (4.4.1\text{-}1)$$

where: C_{LMAX} is with full flaps

and: landing field required = $(d_{50} + d_G)\ 1.67$ (4.4.6-3)

if approach angle is small: R/D at touchdown = $V_{TD}\ (50/d_{50})$ (4.4.6-4)

and R/D for approach will be restricted to 500 fpm maximum.

4.4.7 AIRCRAFT PERFORMANCE: Figure 4.4.7-1 summarizes the point design aircraft performance parameters, which were determined by the methods outlined in this section.

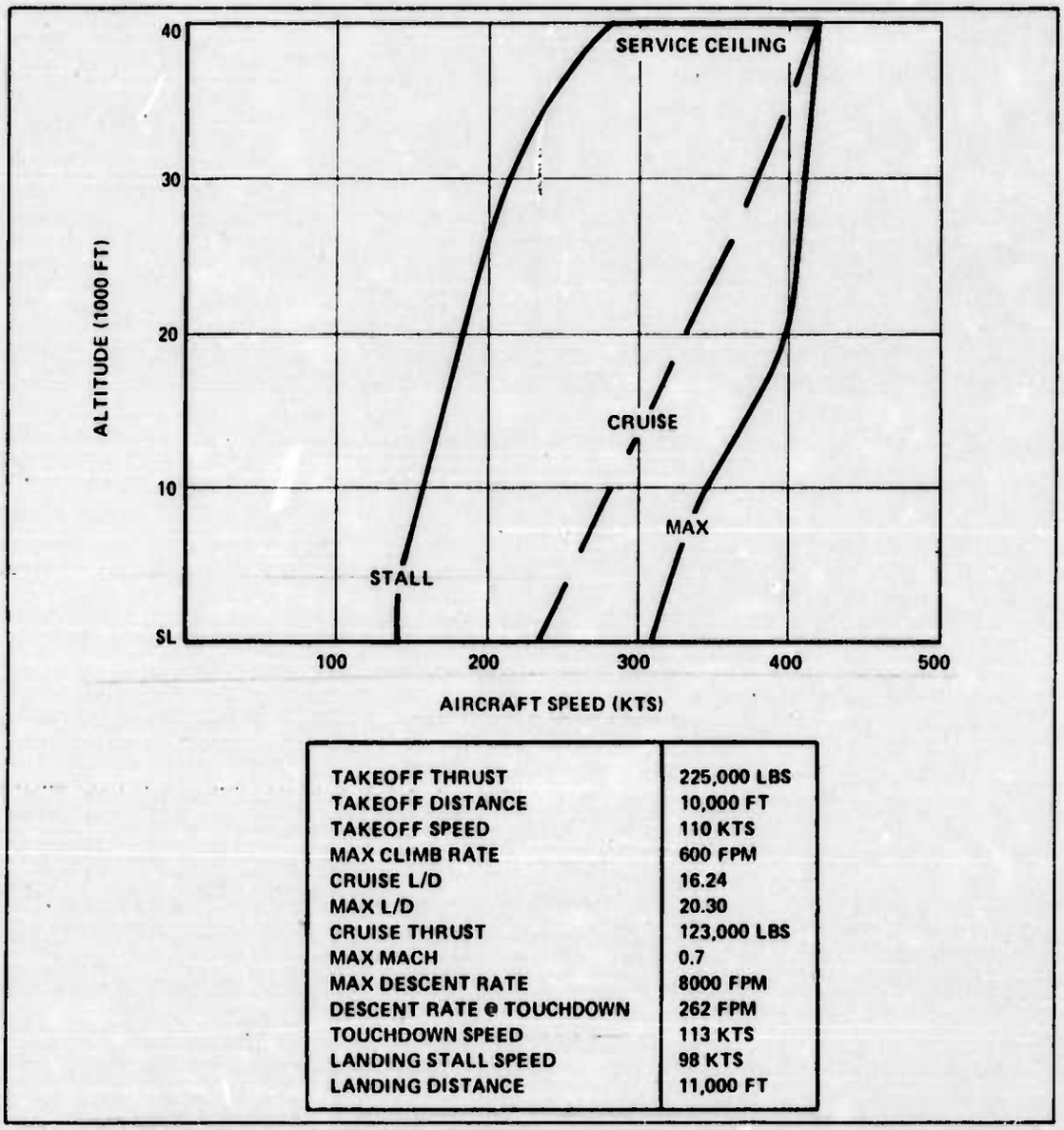

TAKEOFF THRUST	225,000 LBS
TAKEOFF DISTANCE	10,000 FT
TAKEOFF SPEED	110 KTS
MAX CLIMB RATE	600 FPM
CRUISE L/D	16.24
MAX L/D	20.30
CRUISE THRUST	123,000 LBS
MAX MACH	0.7
MAX DESCENT RATE	8000 FPM
DESCENT RATE @ TOUCHDOWN	262 FPM
TOUCHDOWN SPEED	113 KTS
LANDING STALL SPEED	98 KTS
LANDING DISTANCE	11,000 FT

Figure 4.4.7-1. Nuclear Powered Aircraft Performance — 2,000,000 lbs Gross Weight

The flight envelope, for a clean aircraft flying straight and level, was determined as outlined in Sections 4.4.4 and 4.4.5. The maximum speed is a result of the total thrust available (Section 4.4.2) and the airfoil limitations (Section 4.3.4).

Takeoff distance is nearly the same as landing distance, which is to be expected since every landing is made at almost maximum gross weight. The landing deceleration is with normal braking only. The use of a drag chute or thrust reversers could reduce the landing distance by 1500 to 2000 ft (Section 4.4.6).

4.5 AIRCRAFT RECOMMENDATIONS

These recommendations are presented as a guide for additional efforts in airborne nuclear power application. The recommendations cover only major areas of aircraft feasibility and are considered to be the most prominent recommendations of the aircraft section.

4.5.1 CHEMICAL CAPABILITY: The requirement for a nuclear powered aircraft to takeoff, land, and have limited cruise on chemical power is a limiting factor on the feasibility of the aircraft. The required chemical fuel weight subtracts directly from the aircraft's potential payload.

Additional studies should be made in both safety and operational areas to evaluate the need for a chemical capability.

4.5.2 COMPOSITE WEIGHT SAVINGS: The use of composite materials in airframe construction offers a potential weight savings of up to 40% of the structural weight. However, this weight reduction is based on projections for small aircraft for the 1990-2000 state-of-the-art. Additional technology and cost feasibility studies should be made into composite materials applications for large aircraft construction.

4.5.3 REACTOR MOUNTING AND GROUND HANDLING: The reactor and its associated equipment will approach a weight of 900,000 lbs (Sections 5, 6, and 7). This size, in addition to the associated radiation hazard, creates problems never before encountered. The reactor should be removable for servicing because of the layered construction of the reactor and the radiation hazard. A method of heat removal will also have to be devised due to the large amount of thermal energy produced for an extended period of time after reactor shutdown. The containment vessel-supporting structure interface should be the subject of careful study.

Most attempts at containment vessel design to date have relied on a flexible spherical shell that acts as a kinetic energy absorber in the event of a crash. The semi-rigid mounting of the containment vessel in the airframe requires that the containment vessel be made more rigid. This conflict of design requirements must be resolved so that containment vessel integrity is maintained during dynamic loading.

These problem areas should be completely identified and investigated from all aspects including:

1) reactor operating restrictions
2) further analyses of the reactor mounting system, both inflight and landing integrity and ground removal

4.5.4 AIRCRAFT LANDING SYSTEMS: The aircraft landing system becomes increasingly critical as the aircraft gross weight increases; a 2,000,000 lb gross weight may be the upper limit for conventional land based landing systems (Ref. 40). Other types of systems may have to be developed for aircraft in excess of this gross weight.

Further studies should be initiated to investigate the advantages of surface effects or water landing systems for large gross weight aircraft.

4.5.5 AIRCRAFT CONFIGURATION: The majority of effort in this study was spent with a canard configured vehicle. Certainly before any final conclusions can be reached about the feasibility of a nuclear powered airplane, detailed analyses of the several configurations given cursory review in this study should be completed to determine which one would provide the best overall weapon system.

SECTION 5
NUCLEAR REACTOR

5.0 INTRODUCTION

5.0.1 APPROACH: The approach taken in the nuclear reactor analysis was to present and use, without verification, the designers' data for three specific reactor designs. The designers' data for each reactor were applied to the aircraft and mission to assess the feasibility of that particular combination.

In some cases, simplistic modeling was used to assess an off-point design feature of a reactor. An example of this was an attempt to assess potential weight savings through reduced radiation shielding.

The three reactors considered include two gas cooled designs and one liquid-metal cooled design. One of the gas cooled designs is the Westinghouse Astronuclear Laboratory's Low Specific Weight Powerplane, which was based on the nuclear rocket program (NERVA) technology and mobile reactor design work performed for the Navy. Design data for this reactor was proprietary and, thus, much of it was not released, but sufficient parametric data for this study were made available (Ref. 175).

The other gas cooled design was taken from *Aircraft Nuclear Propulsion: A New Look in 1971*, a doctoral dissertation prepared by King L. Mills at the University of Virginia (Ref. 122).

The liquid-metal cooled design is, again, by the Westinghouse Astronuclear Laboratory. The design, NERVA II, was an extensive analysis performed for the Air Force in 1969, and provides complete design data for a point design with parametric data for off-point designs. The NERVA II liquid metal reactor information is presented in Volume II of this study.

5.0.2 TECHNOLOGY: The energy available from a nuclear reactor is in the form of heat, which is extracted by a coolant loop and used to perform work. To maximize the efficiency of such a thermodynamic cycle would require maximizing the operating temperature. In the case of the nuclear aircraft propulsion system, this maximum temperature is limited to approximately 1800°F by metallurgical restrictions in the heat exchangers.

However, even at the 1800°F temperature, the corrosive effects of the coolant rule out the use of anything but helium or liquid-metal cooled reactors (Ref. 100, p. 78-80).

In addition to the desirability of utilizing a high temperature system, a high core power density is desirable to improve lifetime and decrease the system weight.

The necessity of a high power density system becomes evident when a long life fuel element is desired. A low power density fuel element operated at a high power level would obviously have a limited life, but the problem is severely compounded by the fact that the total fuel burned is only a fraction of the total fuel required to make the system operate. This stems from constraints, both nuclear and physical, that will not allow 100% burnup of the available fuel.

The nuclear constraint is the fact that there must be enough fuel present to insure, with probability equal to one, that one of the neutrons released from a fission will produce another fission. When the amount of fuel present becomes too low, and the probability that the released neutrons will produce another fission becomes less than one, the chain reaction ceases.

The physical constraint arises from the fact that the fission fragments, especially the gases, produce a pressure buildup in the fuel element which may cause failure. The fission fragments may also change the structure of the fuel lattice, but in either case only a portion of the fuel may be burned before material failure occurs. When material failure of the fuel element occurs, there exists the possibility of a release of fission fragments into the reactor system's coolant loop.

Liquid-metal cooled systems have demonstrated the capability for high power densities in the Experimental Breeder Reactor — two at 890 watts/cc (Ref. 100, p. 348), and the Enrico Fermi Reactor at 460 watts/cc (Ref. 100, p. 342). However, they have not utilized the temperatures required for the airborne propulsion system. Helium cooled systems have been operated at high temperatures, but not at high power densities; however, the hydrogen cooled NERVA reactor used both high temperature (4500°R) and high power density (4000 watts/cc) (Ref. 172, p. 7).

The relative safety of the helium and liquid-metal systems will have to be studied closely, but some general points can be made.

Helium is chemically inert, cannot be activated by radioactivity and is graphite moderated. Helium cooled reactors are very stable (Ref. 100, p. 409). Also, in the event of a loss of helium coolant, the reactor afterheat can probably be removed by pumping air, at atmospheric pressure, through the core.

On the other hand, the liquid-metal coolants are highly active and react violently with air and water, and do become activated by neutrons. Also, the ability to provide an emergency coolant in the event that the liquid-metal loop is lost is questionable.

Because of the low density of helium, it must be highly pressurized to keep the coolant flow velocity at an acceptable level. Even at high pressure, the pumping power required to circulate the helium is considerable. It will be shown in Section 7 that the pumping power required for helium is approximately 10 times that required for liquid-metal.

Some liquid-metals will be in a solid state at ambient temperatures so that a phase change will be necessary before the system can be used. A heating system would have to be provided to accomplish this phase change.

This section of the report is divided into four main parts. The first part presents reactor design requirements; the second part presents the reactor designs; the third part presents an evaluation of the reactors; and, the fourth part presents ideas on possible reactor weight savings.

5.1 REACTOR DESIGN REQUIREMENTS

5.1.1 POWER REQUIREMENTS: The reactor power comes from energy released by fissioning nuclear fuel. For Uranium 235, this energy is approximately 200 million electronvolts (Mev) per fission. Most of this energy goes into the kinetic energy of the fission fragments and is quickly converted to heat in the surrounding media. The thermal reactor power which must be generated in this manner is determined by the power requirement of the aircraft and the efficiency of the power conversion system.

With the thrust requirement established in Section 4, and the engine and heat transfer system designs given in Sections 6 and 7, respectively, the reactor power requirements were determined to range from 475 to 700 MW thermal (MW(th)).

5.1.2 ENVIRONMENTAL REQUIREMENTS: A portion of the energy given up by fissioning and radioactive decay escapes the reactor core as nuclear radiation. The potentially harmful effects of this radiation require that special attention be given to protection of the crew, the general populace, and the aircraft structure. This section considers only the radiation emissions associated with normal operations. Emissions associated with accidents are discussed in Section 8.

5.1.2.1 THE CREW: In order to establish radiation design criteria for the crew, it was assumed that both the flight and ground crews would be classified as radiation workers. This establishes a maximum legally allowable radiation dosage of 5 rem/yr, which is further restricted in that no more than 3 rem may be received in any one quarter (Ref. 47, p. 53).

It was also assumed that the aircrew would be available for one flight per month, for ten months per year. The other two months were excluded to account for leave and uncertainties such as illness. The mission requirements call for a maximum of 14 days per flight which gives the following maximum hourly dose rate:

$$(5 \text{ rem/yr})(1 \text{ yr}/3360 \text{ flt hrs}) = 1.49 \text{ mrem/flt hr}$$

The maximum allowable ground crew dose rate was based on a duty schedule that assumed 30 days of leave per year, a five day work week, and an eight hour workday. This gives 1916 working hours per year, or a maximum allowable dose rate of:

$$(5 \text{ rem/yr})(1 \text{ yr}/1916 \text{ work hrs}) = 2.61 \text{ mrem/work}$$

It is recognized that these maximum allowable dose rates are average figures based on uniform exposure to radiation and can be exceeded for periods of time provided that the maximum cumulative dose limits are not exceeded.

5.1.2.2 THE GENERAL POPULACE: The radiation standards applicable to light water reactors were assumed to be applicable to the nuclear powered aircraft, thus limiting the radiation exposure of any person in the general populace to 5 mrem/yr (Ref. 46, p. 467). Whereas, in a ground based nuclear power plant, the only radiation that the general populace is exposed to is that received from the effluents that reach the plant perimeter, there is no such

fixed perimeter for the aircraft. Therefore, if the aircraft flies closely enough, the general populace may be exposed to direct radiation from the reactor as well as radiation from the effluents. This analysis considers the exposure to both direct radiation and effluents.

5.2 REACTOR DESIGNS

5.2.1 WESTINGHOUSE HIGH TEMPERATURE GAS REACTOR: The Westinghouse high temperature gas reactor (WHTGR) was designed for mobile application and uses pressurized helium as a coolant. The fuel elements are uranium carbide dispersed in graphite; the radiation shielding layers are tungsten, zirconium hydride, and lithium hydride; and the containment vessel is a layer of Haynes 188 (Ref. 176). Figure 5.2.1-1 shows a preliminary drawing of a 275 MW(th) WHTGR (Ref. 176).

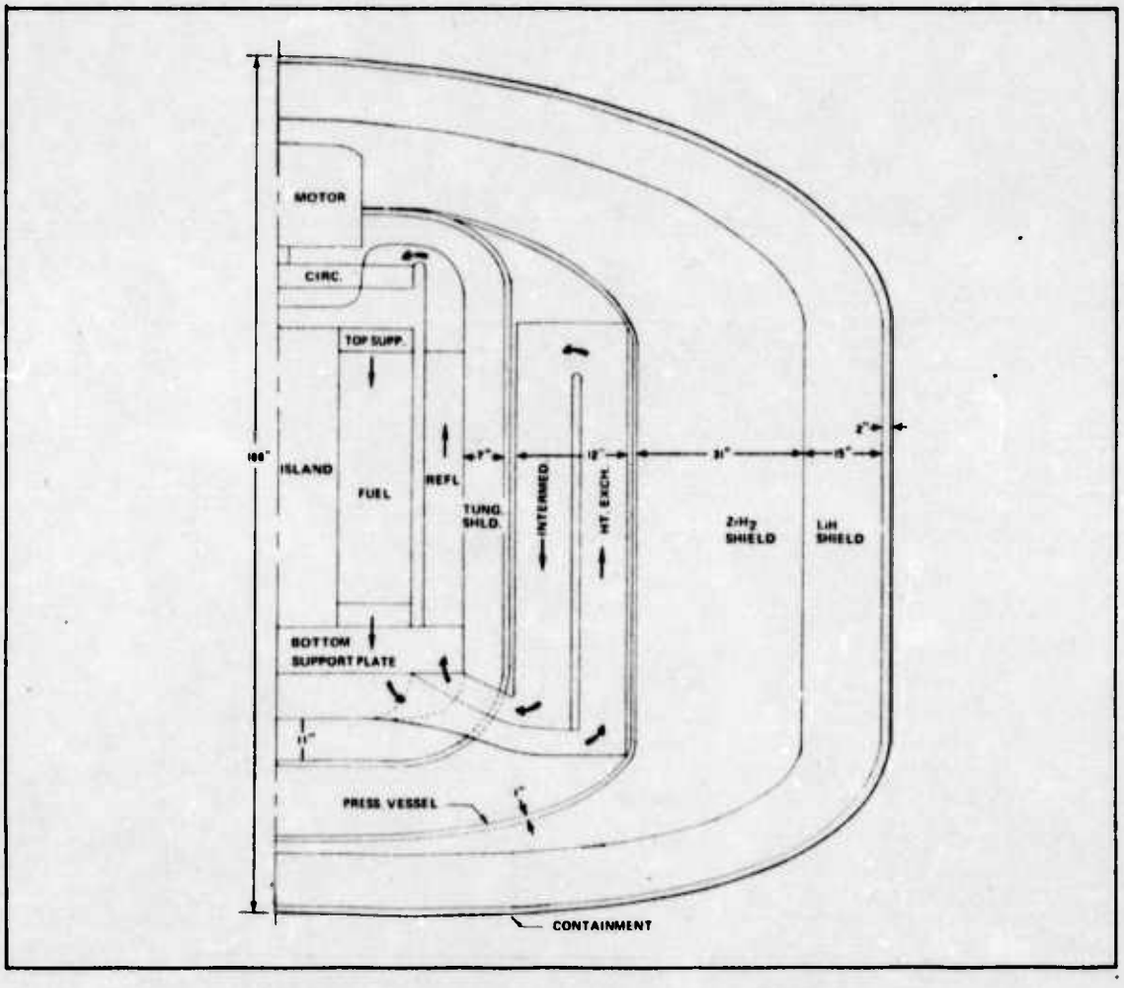

Figure 5.2.1-1. Preliminary Drawing — WHTGR

Figures 5.2.1-2 through 5.2.1-8 show the results of preliminary design analysis performed by Westinghouse Corporation. Figure 5.2.1-2 shows the reactor coolant outlet temperature versus the intermediate heat exchanger outlet temperature. A heat exchanger temperature of 2260°R (1800°F) requires a reactor outlet temperature of approximately 2360°R.

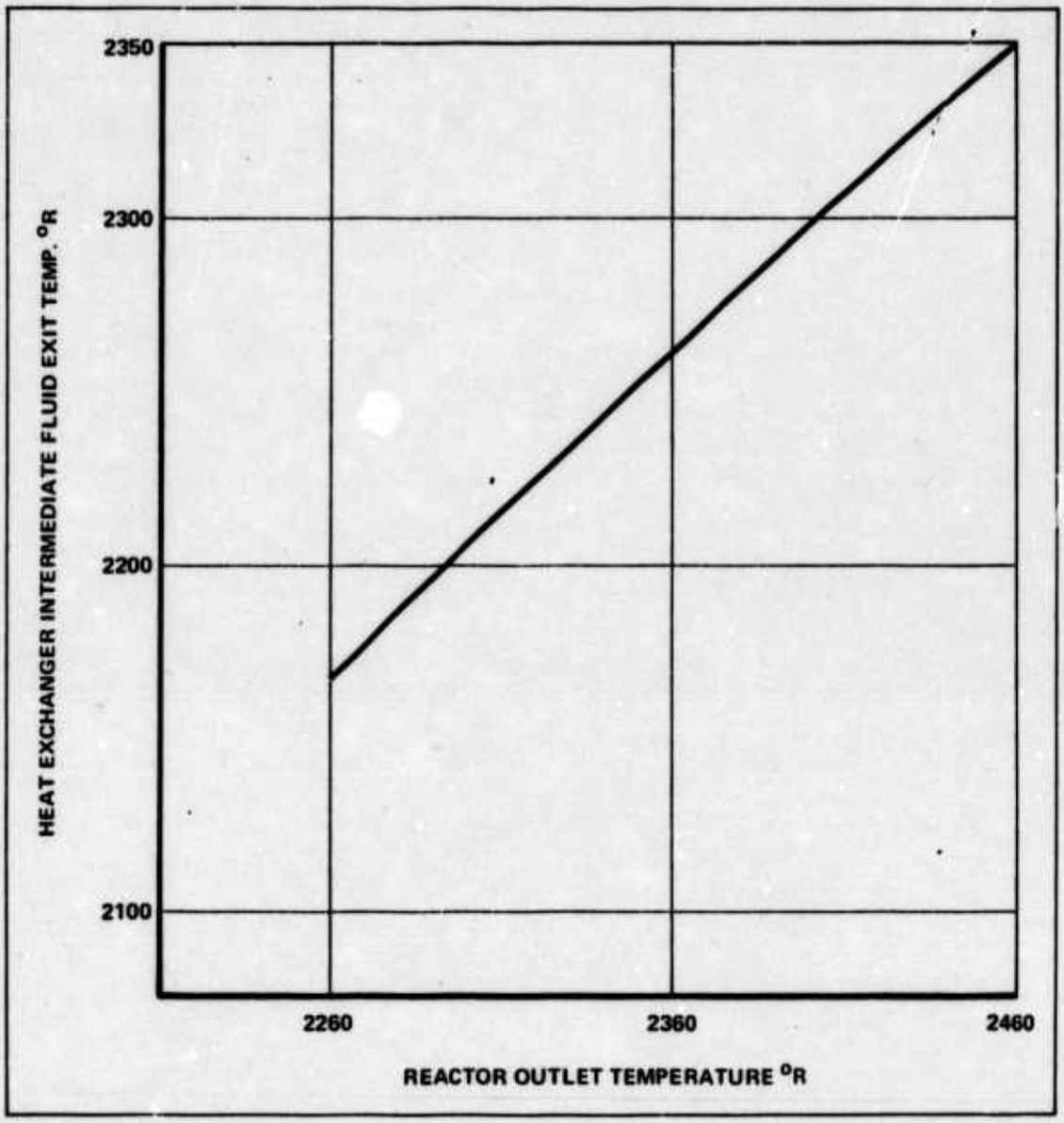

Figure 5.2.1-2. WHTGR Temperature vs Heat Exchanger Temperature

Shown in Figures 5.2.1-3 through 5.2.1-5 are the effects on reactor weight of various power levels, core lifetimes, and core power densities (Ref. 190). The 313 mg/cc fuel density of Figure 5.2.1-3 is presently obtainable; the 400 mg/cc of Figure 5.2.1-4 could be obtained with minimal development; and, the 500 mg/cc of Figure 5.2.1-5 could be obtained with extensive fuel bead development (Ref. 190, p. 54).

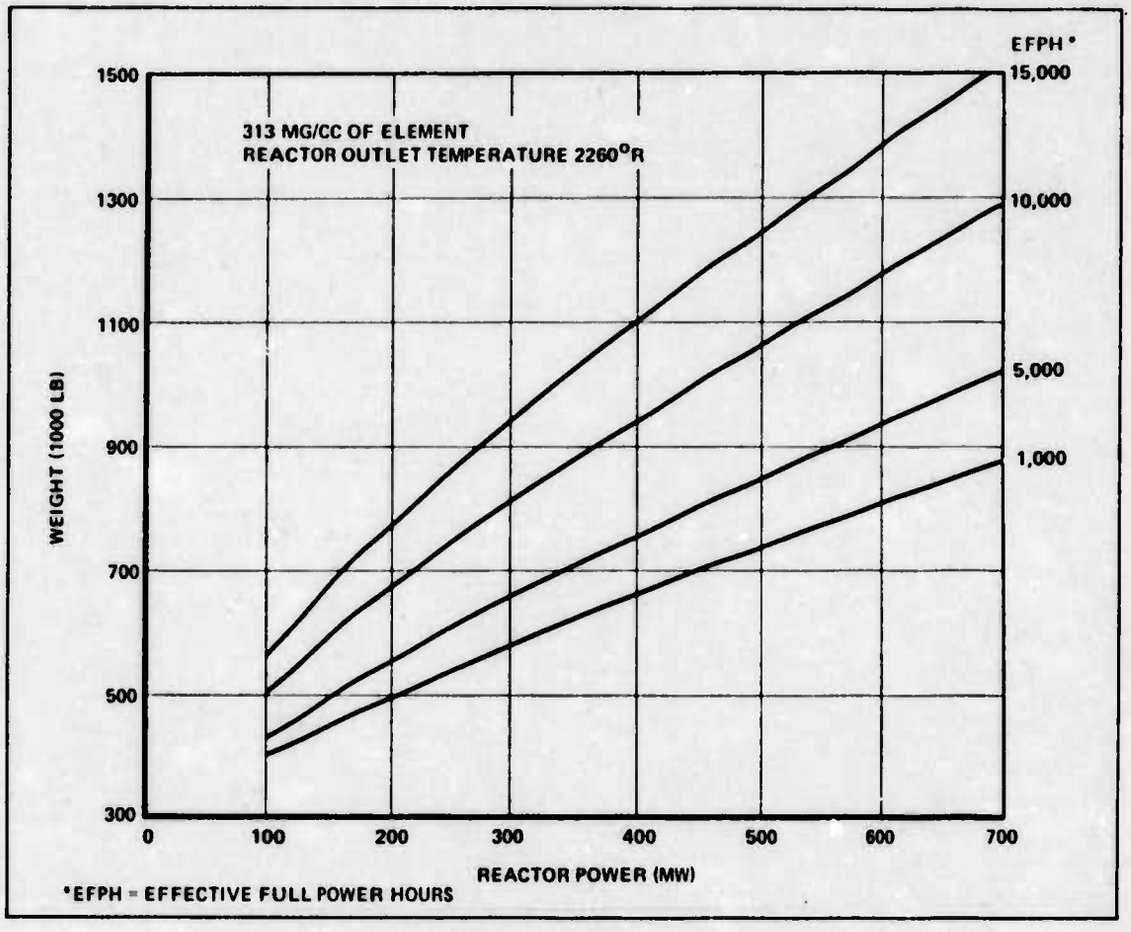

Figure 5.2.1-3. WHTGR Reactor Power vs Reactor Weight

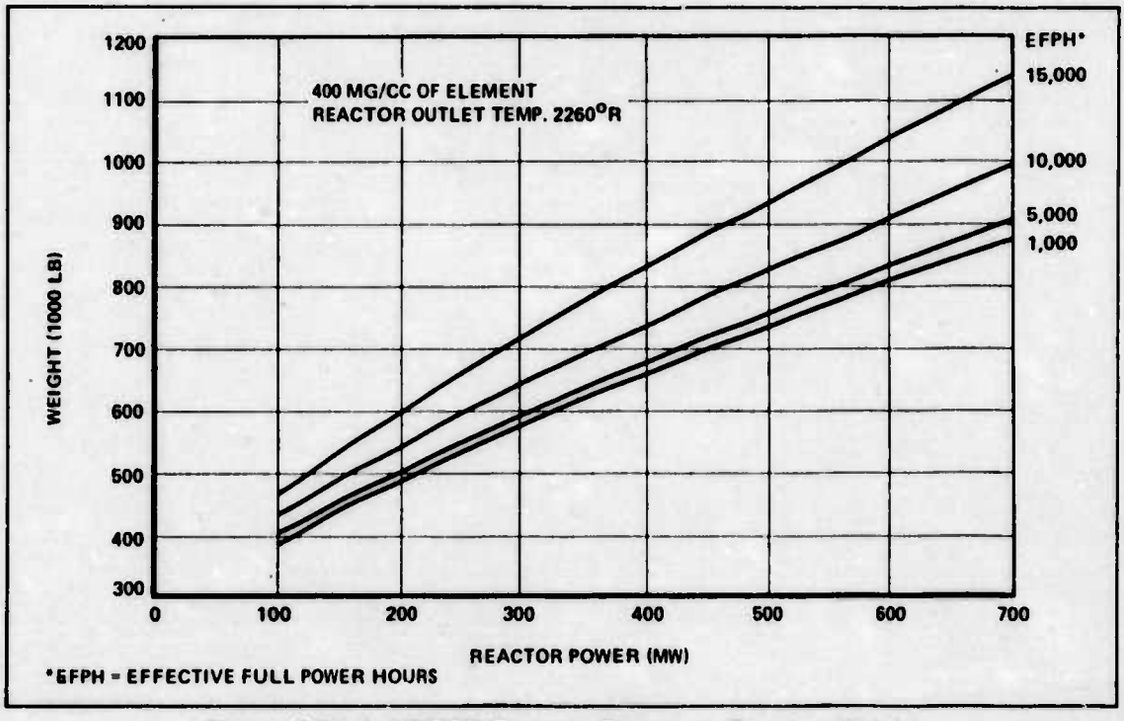

Figure 5.2.1-4. WHTGR Reactor Power vs Reactor Weight

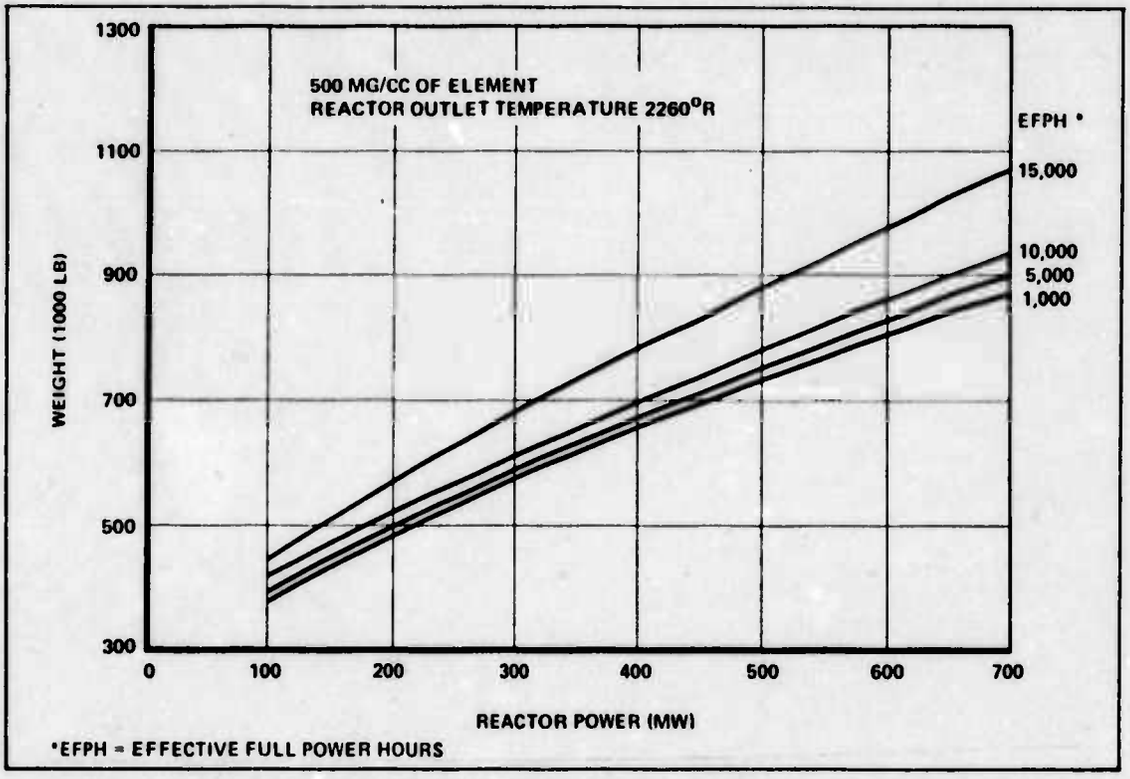

Figure 5.2.1-5. WHTGR Reactor Power vs Reactor Weight

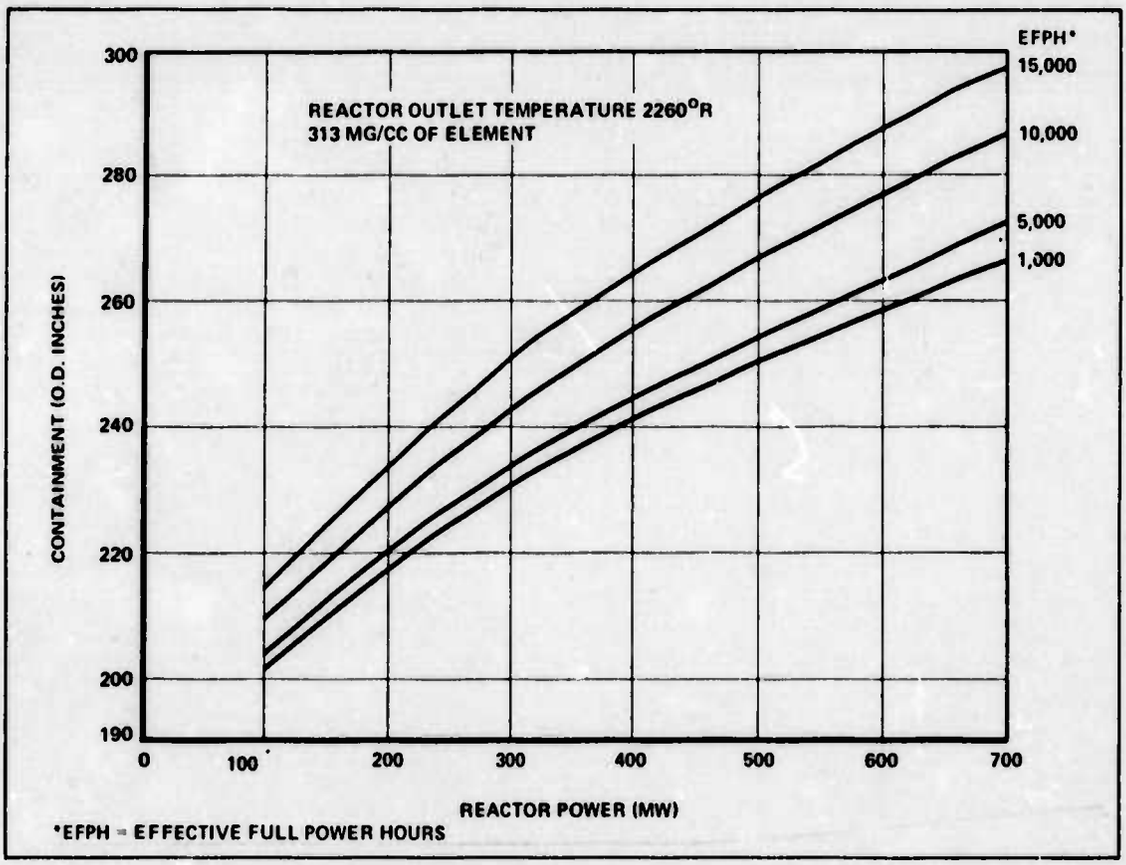

Figure 5.2.1-6. WHTGR Reactor Power vs Outer Diameter

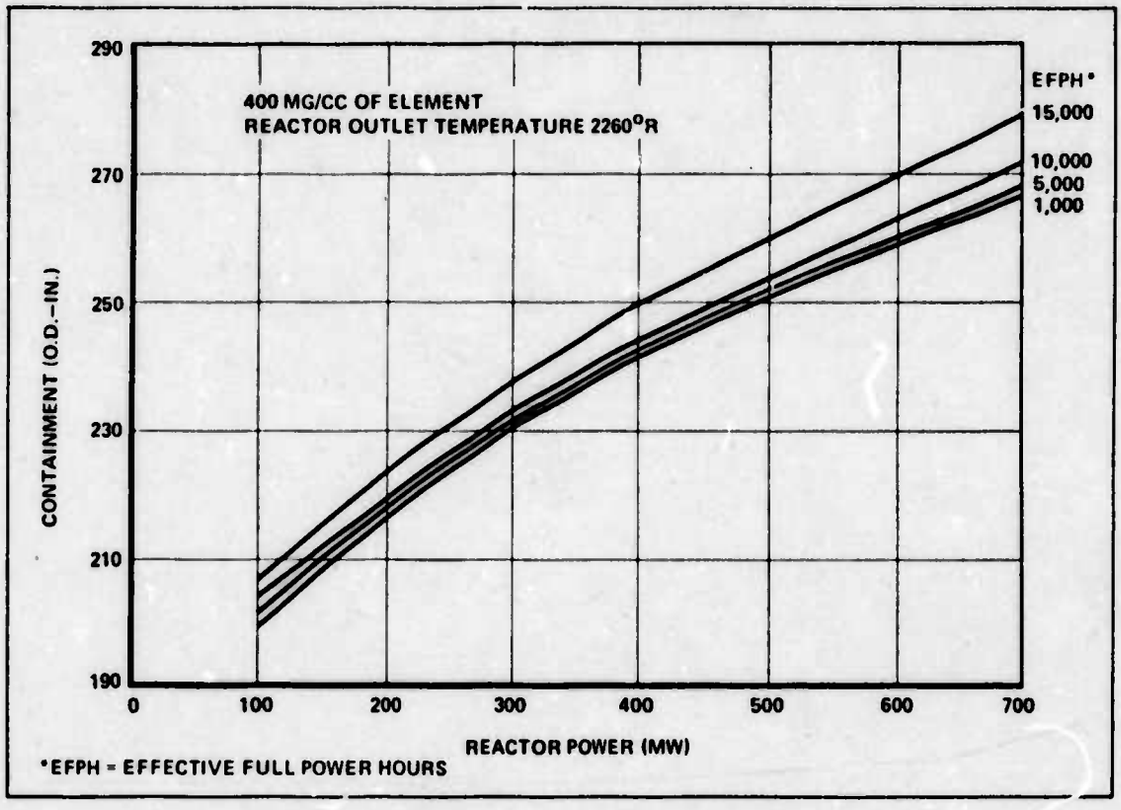

Figure 5.2.1-7. WHTGR Reactor Power vs Outer Diameter

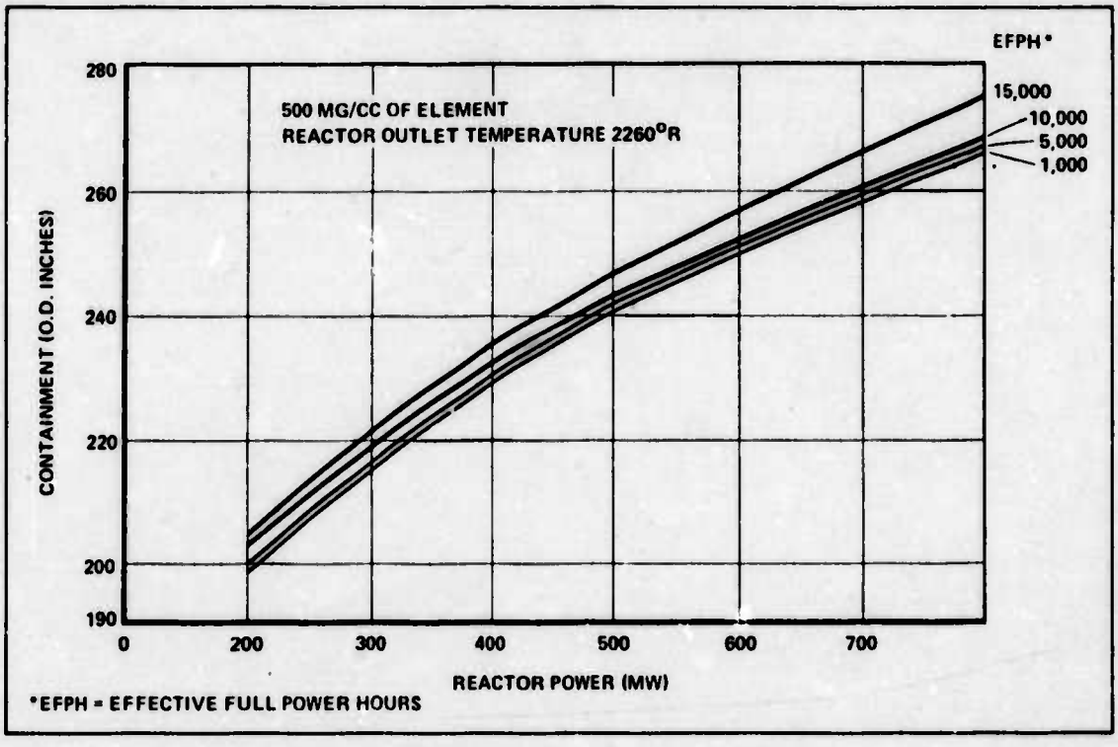

Figure 5.2.1-8. WHTGR Reactor Power vs Outer Diameter

It can be seen that increasing the fuel density from 313 mg/cc to 400 mg/cc, for a 10,000 hour lifetime core at a 700 MW power level would decrease the system weight by approximately 300,000 lbs.

The effects of changing core lifetime can be seen, as an example, by considering the 400 mg/cc core (Figure 5.2.1-4). At 700 MW(th), an increase from 5,000 to 10,000 hrs of lifetime increases the weight by approximately 70,000 lbs.

The effect of reactor power on reactor weight is a nearly linear relationship in the range of interest (475-700 MW(th)). Figure 5.2.1-4 shows a weight of approximately 800,000 lbs at 475 MW(th), and approximately 980,000 lbs at 700 MW(th) for a 10,000 hour core lifetime.

Figures 5.2.1-6 through 5.2.1-8 show the reactor containment vessel outer diameter versus the reactor power. Figure 5.2.1-7 (400 mg/cc) shows a containment vessel outer diameter of approximately 273 in. for a 700 MW(th) reactor with a 10,000 hr core.

Shown in Table 5.2.1-1 is a sample weight breakdown for a 275 MW(th) reactor (Ref. 190). Figure 5.2.1-9 depicts a revised graph of reactor power versus reactor weight. This figure is for a 400 mg/cc, 10,000 hr fuel element, and shows weights for different values of intermediate heat exchanger effectiveness (Ref. 177). Revised data for other fuel loadings and core lifetimes were not available at the time this publication was written.

TABLE 5.2.1-1.
COMPONENT WEIGHTS FOR A 275 MW(TH) WHTGR

REACTOR AND TUNGSTEN SHIELD	123,600
REACTOR PRESSURE VESSEL AND CONTAINMENT	19,440
EXTERNAL SHIELD	313,700
INTERMEDIATE HEAT EXCHANGER	32,240
POWERPLANT, CONTAINMENT AND AUXILIARY SYSTEM	105,800
CICULATORS AND PIPING	19,080
NUCLEAR MODULE TOTAL	615,860

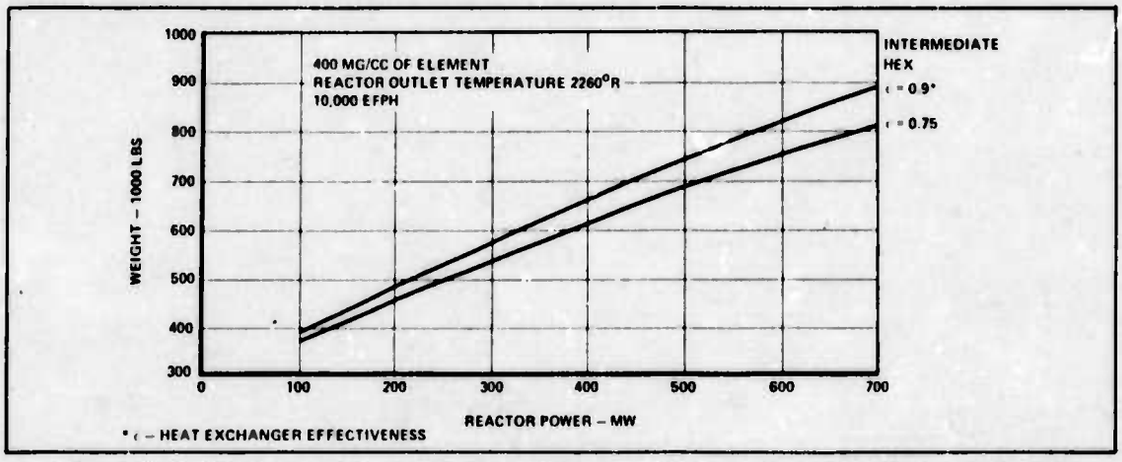

Figure 5.2.1-9. Westinghouse Revised Reactor System Weight vs Reactor Power

Table 5.2.1-2 shows gamma ray dosages predicted at the distance and direction from the reactor shown. The axial direction is toward the aircraft nose, and the radial direction is toward the fuselage skin. It can be seen that the dose rate in the axial direction is 5 mrem/hr, 20 ft from the reactor (Ref. 175).

TABLE 5.2.1-2.
WESTINGHOUSE HIGH TEMPERATURE GAS REACTOR
GAMMA RADIATION DATA (REF. 175)

DISTANCE (FT)	DIRECTION	DOSE RATE (MILLIREM/HR)
20.0	AXIAL	5.00
20.0	RADIAL	400.00

5.2.2 MILLS HIGH TEMPERATURE GAS REACTOR: The Mills High Temperature Gas Reactor (MHTGR) is also helium cooled and was designed specifically for airborne nuclear propulsion. It was point designed for a power level of 200 MW(th) with a 3000 hr core lifetime. The fuel element is uranium carbide dispersed in carbon with tungsten and lithium hydride for shielding. Figure 5.2.2-1 shows a cutaway diagram of the reactor reproduced from Mills' dissertation (Ref. 122).

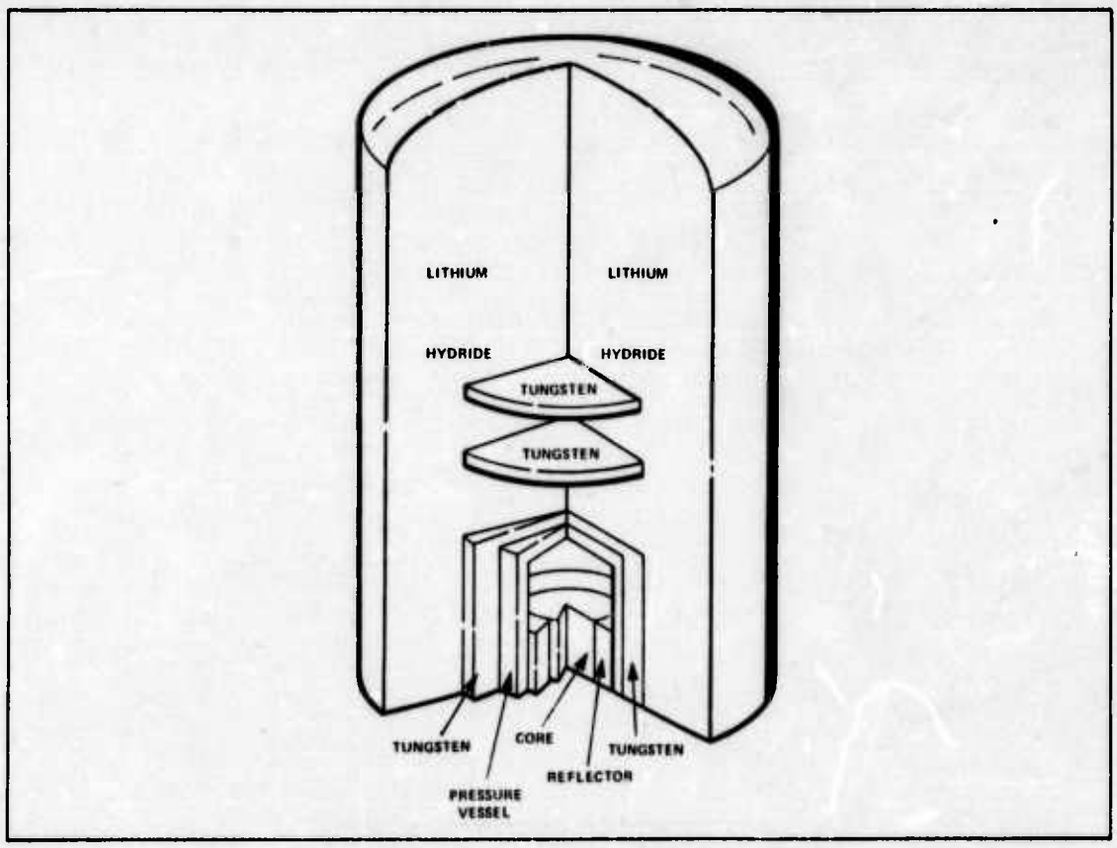

Figure 5.2.2-1. Cutaway Drawing of MHTGR

The MHTGR was designed without an intermediate heat exchanger using a single helium coolant loop, and without a containment vessel. For this analysis, an intermediate heat exchanger was added outside the lithium hydride shield, with a 2 in. thick containment vessel outside the heat exchanger.

Table 5.2.2-1 shows a breakdown of component weights as predicted by Mills (Ref. 122,p. 138), and Table 5.2.2-2 shows some of the reactor dimensions. As before, axial dimensions are in the direction of the aircraft nose, and radial dimensions are in the direction of the fuselage skin.

TABLE 5.2.2-1.
COMPONENT WEIGHTS FOR 200 MW(TH) MHTGR

CORE	1964.5
REFLECTOR	2224.1
PRESSURE VESSEL	9668.7
TUNGSTEN SHIELD	121383.4
LITHIUM HYDRIDE SHIELD	52864.9
	188124.6

TABLE 5.2.2-2. DIMENSIONS OF MHTGR

CORE	RADIUS	14.47	REF. 122, P. 39
	HEIGHT	38.95	REF. 122, P. 39
PRESSURE VESSEL THICKNESS		3.50	
TUNGSTEN SHIELDING THICKNESS	RADIAL	9.24	REF. 122, P. 134
	AXIAL	10.97	REF. 122, P. 95
LITHIUM HYDRIDE SHIELDING THICKNESS	RADIAL	27.60	REF. 122, P. 97
	AXIAL	63.98	REF. 122, P. 95
OVERALL SYSTEM	RADIUS	62.20	REF. 122, P. 98
	HEIGHT	204.7	REF. 122, P. 98

Table 5.2.2-3 gives gamma ray dosages as predicted by Mills. The dose rate in the axial direction is given as 2.199 mrem/hr at 21.98 ft from the reactor (Ref. 122,p. 133).

TABLE 5.2.2-3. MILLS HIGH TEMPERATURE GAS REACTOR GAMMA RADIATION DATA (REF. 122, P. 133)

DISTANCE (FT)	DIRECTION	DOSE RATE (MILLIREM/HR)
22.0	AXIAL	2.20
5.5	RADIAL	8.33×10^4

5.2.2.1 MILLS REACTOR MODIFIED: In order to use the MHTGR design, it was necessary to add an intermediate heat exchanger and a containment vessel, and scale the system to the desired power levels. In order to do these with reasonable accuracy, it was necessary to develop a model that would predict the volumes and weights of the MHTGR design with acceptable accuracy. That was accomplished by modeling the reactor as concentric right circular cylinders. In that fashion, the predicted weight was found to be 202,500 lbs, which is within 7.7% of the 188,124 lbs given by Mills. Table 5.2.2.1-1 shows the breakdown of weights predicted by the model including the added heat exchanger and containment vessel.

TABLE 5.2.2.1-1.
MHTGR WEIGHT ESTIMATION AT 200 MW(TH)

	OUTER RADIUS (IN.)	OUTER HEIGHT (IN.)	TOTAL VOLUME ($IN.^3$)	SECTION VOLUME ($IN.^3$)	SECTION DENSITY ($LB/IN.^3$)	SECTION WEIGHT (LBS)
CORE	14.47	38.95	2.562×10^4	2.562×10^4	0.07665	1.964×10^3
VOID	15.05	38.95	2.771×10^4	2.09×10^3	—	—
REFLECTOR	20.05	38.95	4.919×10^4	2.418×10^4	0.09062	1.946×10^3
VOID	21.54	49.53	7.219×10^4	2.3×10^4	—	—
PRESSURE VESSEL	25.04	56.53	1.113×10^5	3.911×10^4	0.3299	1.290×10^4
TUNGSTEN	34.28	78.47	2.896×10^5	1.783×10^5	0.6973	1.243×10^5
LITHIUM HYDRIDE	61.88	206.43	2.483×10^6	2.193×10^6	0.02801	6.142×10^4
SUB-TOTAL						2.025×10^5
HEAT EXCHANGER	61.88	220.70	2.655×10^6	1.723×10^5	—	2.6×10^4
CONT. VESSEL	63.88	224.70	2.880×10^6	2.25×10^5	0.3299	7.422×10^4
TOTAL						3.027×10^5

The volume of the added heat exchanger was found by linearly scaling the heat exchanger volume as a function of reactor power. The base volume and power were taken from Section 7 of this report and are given as 190.8 ft^3 at 574 MW(th). An additional 50% was added as void to compute the volume of space required for mounting the heat exchanger. In this manner, the volume of space required for heat exchanger addition is given as:

$$V = \frac{P}{574}(190.8)(1.5)$$

V = volume of heat exchanger required at power level P

The weight of the added heat exchanger was also found by linear scaling. In the heat transfer equation $Q = \rho VAC_p \Delta T$, (ρ = density, V = velocity, C_p = specific heat, ΔT = temperature differential, A = area) if all quantities on the right side of the equation are held constant except area, the area varies linearly with power. It was assumed that volume was a linear function of area, and that weight was a linear function of volume, so that:

$$W_2 = \frac{P_2}{P_1} W_1$$

W_2 = heat exchanger weight at power level two
W_1 = heat exchanger weight at power level one
P_2 = power level two
P_1 = power level one

The base values were taken from Section 6 of this report as 65,000 lbs at 500 MW(th). This yields:

$$W_2 = \frac{P_2}{500} (65{,}000)$$

In order to scale the MHTGR to the higher power levels required for this report, it was assumed that the core power density was constant such that core volume varies linearly with power. Additionally, the ratio of core height to radius was kept constant so that:

$$\frac{h}{r} = \frac{38.95}{14.47} = 2.691$$

h = height of core

r = radius of core

With these assumptions,

$$\frac{P_1}{P_2} = \frac{V_1}{V_2} = \frac{r_1^2 h_1}{r_2^2 h_2}$$

$$r_2 = r_1 \left(\frac{P_2}{P_1} \right)^{1/3} = 14.47 \left(\frac{P_2}{200} \right)^{1/3}$$

$h_2 = 2.691\ r_2$

P_1 = power level one

P_2 = power level two

V_1 = volume of core at power level one

V_2 = volume of core at power level two

r_1 = radius of core at P_1

r_2 = radius of core at P_2

h_1 = height of core at P_1

h_2 = height of core at P_2

With the relationships thus established, the volumes and weights for the reactor can be calculated at any power level. Shown in Tables 5.2.2.1-2 and 5.2.2.1-3 are the computed weights for 574 and 700 MW(th) power levels. The three values of total weight computed at 200, 574, and 700 MW(th) were used to plot the power versus weight curve shown in Figure 5.2.2.1-1.

It may be noted that the WHTGR is substantially heavier than the MHTGR. This is due to the much heavier shielding used in the WHTGR. The shielding differences yield considerable differences in radiation dosages as will be discussed in Section 5.3.

5.2.3 WESTINGHOUSE LIQUID METAL REACTOR: See Volume III.

TABLE 5.2.2.1-2.
MHTGR WEIGHT ESTIMATION AT 574 MW(TH)

	OUTER RADIUS (IN.)	OUTER HEIGHT (IN.)	TOTAL VOLUME ($IN.^3$)	SECTION VOLUME ($IN.^3$)	SECTION DENSITY ($LB/IN.^3$)	SECTION WEIGHT (LBS)
CORE	20.56	55.33	7.347×10^4	7.347×10^4	0.07665	5.361×10^3
VOID	21.14	55.33	7.768×10^4	4.210×10^3	—	—
REFLECTOR	26.14	55.33	1.187×10^5	4.102×10^4	0.09062	3.717×10^3
VOID	27.63	65.91	1.580×10^5	3.930×10^4	—	—
PRESSURE VESSEL	31.13	72.91	2.219×10^5	6.390×10^4	0.3299	2.108×10^4
TUNGSTEN	40.37	94.89	4.865×10^5	2.637×10^5	0.6973	1.838×10^5
LITHIUM HYDRIDE	67.97	222.81	3.233×10^6	2.747×10^6	0.02801	7.694×10^4
HEAT EXCHANGER	67.97	256.82	3.727×10^6	4.495×10^5	—	7.462×10^4
CONT. VESSEL	69.79	260.82	3.990×10^6	2.630×10^5	0.3299	8.676×10^4
TOTAL						4.522×10^5

TABLE 5.2.2.1-3.
MHTGR WEIGHT ESTIMATION AT 700 MW(TH)

	OUTER RADIUS (IN.)	OUTER HEIGHT (IN.)	TOTAL VOLUME ($IN.^3$)	SECTION VOLUME ($IN.^3$)	SECTION DENSITY ($LB/IN.^3$)	SECTION WEIGHT (LBS)
CORE	21.96	59.12	8.596×10^4	8.596×10^4	0.07665	6.588×10^3
VOID	22.54	59.12	9.436×10^4	8.400×10^3	—	—
REFLECTOR	27.54	59.12	1.408×10^5	4.644×10^4	0.09062	4.208×10^3
VOID	29.03	69.70	1.845×10^5	4.370×10^4	—	—
PRESSURE VESSEL	32.53	76.70	2.549×10^5	7.040×10^4	0.3299	2.322×10^4
TUNGSTEN	41.77	98.64	5.406×10^5	2.857×10^5	0.6973	1.992×10^5
LITHIUM HYDRIDE	69.37	226.60	3.425×10^6	2.884×10^6	0.02801	8.078×10^4
HEAT EXCHANGER	69.37	266.44	4.028×10^6	6.031×10^5	—	9.100×10^4
CONT. VESSEL	71.37	270.44	4.327×10^6	2.990×10^5	0.3299	9.864×10^4
TOTAL						5.035×10^5

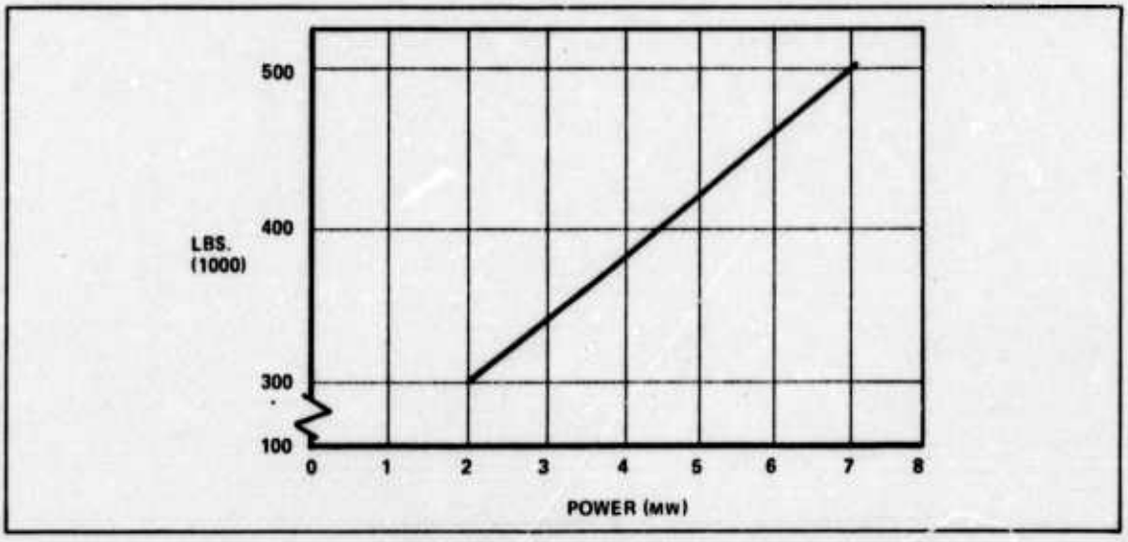

Figure 5.2.2.1-1. MHTGR Reactor Power vs Reactor Weight

5.3 EVALUATION OF THE REACTORS

5.3.1 ENVIRONMENTAL ASPECTS: The environmental effects of the two gas reactors were analyzed using the designers' gamma radiation data which are reproduced in Table 5.3.1-1. All neutrons are assumed to be absorbed by the LiH shield. Dose rate is given as a function of distance from reactor center and direction of the radiation. The longitudinal direction is along the axis of the aircraft's fuselage (tail to nose). The radial direction is perpendicular to the fuselage axis.

TABLE 5.3.1-1. REACTOR RADIATION DATA

REACTOR	DOSE RATE (MREM/HR)	DIRECTION	DISTANCE (FT)
MILLS (REF. 122, P. 133)	2.20	LONGITUDINAL	22.0
MILLS (REF. 122, P. 133)	8.33×10^4	RADIAL	5.5
WESTINGHOUSE (REF. 175)	5.00	LONGITUDINAL	20.0
WESTINGHOUSE (REF. 175)	400.00	RADIAL	20.0

5.3.1.1 THE CREW: Because the reactors were designed with dose rates above the 1.49 mrem/hr requirement of this study, the crew must be located farther from the reactor than the distances associated with the designers' dose rates. This increased separation decreases the dose rate due to spherical divergence of the radiation. Murray's *Introduction to Nuclear Engineering* gives the relationship between dose rates and gives distance as (Ref. 129, p. 254):

$$R_2 = (D_1/D_2)^{1/2} R_1$$

D_1 = dose rate at first distance

D_2 = dose rate at second distance

R_1 = distance at D_1

R_2 = distance at D_2

For the MHTGR the dosage was given as 2.20 mrem/hr at 22.0 ft. If the crew is to get no more than 1.49 mrem/hr, spherical divergence is used to determine the closest distance they can come to the reactor.

$$R_2 = \left(\frac{D_1}{D_2} \right)^{1/2} R_1$$

$$R_2 = \left(\frac{2.20}{1.49}\right)^{1/2} 22 \text{ ft}$$

$$R_2 = 26.73 \text{ ft}$$

Another option would be to design the aircraft so that the crew was to be allowed closer than this for a carefully measured time. They then must spend enough time in an area far enough removed so that they average 1.49 mrem/hr. The number of flights per year as a function of distance from the core center is presented in Figure 5.3.1.1-1. As can be seen, the canard design would allow a crew member to fly for an entire year with a large safety margin. A conventional aircraft design, however, would allow the crew member only about five flights per year which would result in a much larger crew force.

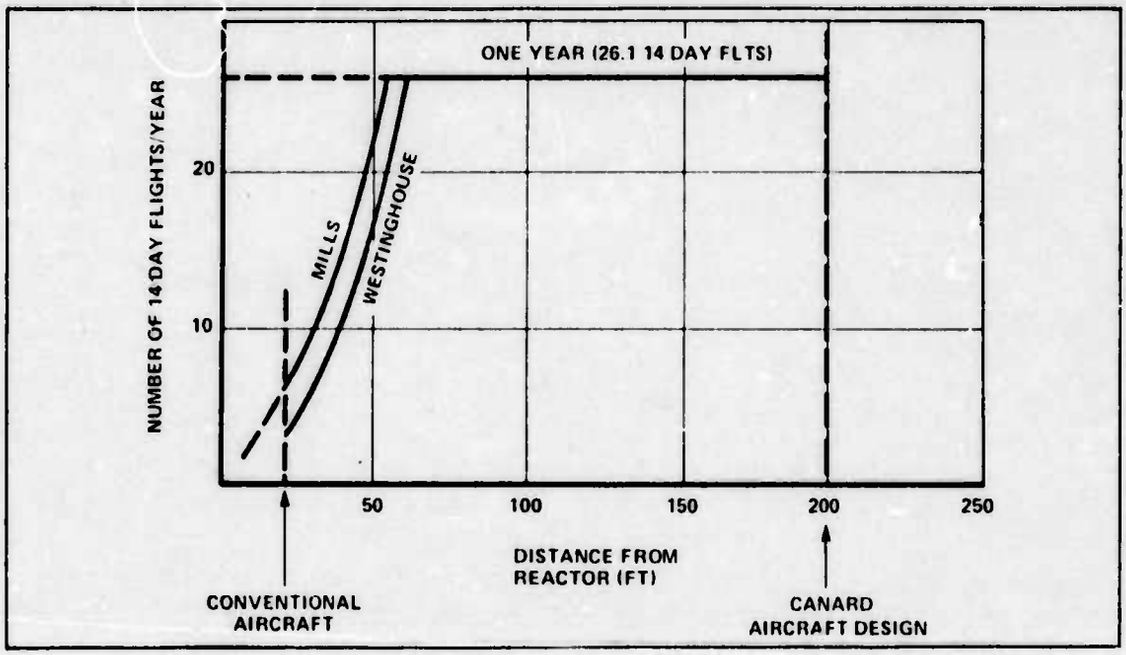

Figure 5.3.1.1-1. Flights per Year

Perpendicular to the aircraft longitudinal axis, the MHTGR has a dose rate of 8.33 x 10^4 mrem per hr at the reactor shield (Ref. 122, p. 199). One minute walking through this area would mean a crew member would receive 950 mrem or the dose allotted for two trips. Unless additional shielding is added, this restricts crew passage from fore to aft of the reactor sections for an entire flight.

The ground crew were also considered radiation workers and this same radiation restriction applied. Considering the 2.61 mrem/hr requirement and the radial radiation of both reactors, the distances the ground crew would have to be removed, if the reactor were in operation, were computed:

Westinghouse Reactor:

$$\left(\frac{400 \text{ mrem/hr}}{2.61 \text{ mrem/hr}}\right)^{1/2} 20 \text{ ft} = 248 \text{ ft}$$

Mills Reactor:

$$\left(\frac{8.33 \times 10^4 \text{ mrem/hr}}{2.61 \text{ mrem/hr}}\right)^{1/2} 5.5 \text{ ft} = 983 \text{ ft}$$

The above results show that ground operation of either reactor would have to be restricted. The MHTGR would have much greater restrictions than those imposed on the Westinghouse Reactor.

5.3.1.2 THE GENERAL POPULACE: The effects on the general populace that were analyzed were those due to effluent and direct radiation. Both effects were modeled on a conservative basis. When reactor power level was required for calculation, it was assumed to be the largest power level required in this study (700 MW).

It was assumed that the effluent release was directly proportional to the operating power level and the helium cooled Peach Bottom Reactor (115 MW(th)) was used as a reference point for effluent release (Ref. 100, p. 429). Peach Bottom's effluent release was 0.003% of that permissible for noble and activation gases and 0.6% of that permissible for halogens and particulates (Ref. 46, p. 255).

Effluent radiation was modeled in two ways. All 60 aircraft were considered (1) to be on the ground, and (2) airborne. For the case of the aircraft on the ground, two cases were considered: (1) the aircraft uses only chemical power for takeoff and landing, in which case, the reactor is not operated within 30 minutes of home station; and (2) the aircraft uses nuclear power for takeoff and landing.

For the first case of effluent radiation with all 60 aircraft on the ground and chemical power used for takeoff and landing, the power level of the reactor can be determined from the Way-Wigner formula (Ref. 49, p. 1-37):

$$P = Po\ (0.0622)\ (t_2^{-.2} - (t_1 + t_2)^{-.2})$$

P_0 = original power level
t_1 = operating time in seconds before shutdown
t_2 = time in seconds since shutdown

For an initial power level, $P_0 = 700$ MW, $t_1 = \infty$, and $t_2 = 1800$ seconds (30 minutes), the power for a single aircraft is found to be 9.71 MW. For the entire fleet of 60 aircraft, the power level is 60 x 9.71 = 583 MW.

Comparing this power level to the Peach Bottom Reactor yields:

$$\left(\frac{583}{115}\right)(0.003\%) = 0.015\% \text{ of the allowed effluents for noble and activation gases}$$

$$\left(\frac{583}{115}\right)(0.6\%) = 3.0\% \text{ of the allowed effluents for halogens and particulates}$$

Thus, the effluent radiation for this case is negligible.

For the case of nuclear powered takeoff and landing, the effluent radiation must be calculated for the 30 min assumed to be required for aircraft warmup, taxi, takeoff, and initial climb.

The mission length was specified at 336 hrs; therefore, the above 30 min is 0.14% of the mission time. For 60 aircraft 8.93% of the 700 MW would be used during the 30 min. This equates to 62.5 MW of stationary reactor power. Thus, the effluent radiation is again negligible for this case.

Finally, effluent radiation was considered with all 60 aircraft airborne, the reactor power level is assumed to be at full power (700 MW), and the time of exposure is taken as the time that the aircraft is within 7 nm of base.

The approach and climb speeds are given in Section 4 as 113 and 150 knots, respectively. This yields a time spent within 7 nm of base of

$$7/113 + 7/150 - 0.1086 \text{ hrs}$$

The total time airborne for a 14 day mission is 336 hours; therefore, the aircraft is within 7 nm of base 0.1086/336 = 0.032% of the time that it is airborne.

If the fleet of 60 aircraft were airborne 100% of the time, only 60 x 0.032% = 1.9% of the time would be spent within 7 nm of the base. The average power level in this case would be

$$700 \times 0.019 = 13.5 \text{ MW}$$

so that, for all cases, the effluent radiation is negligible.

The exposure of the general populace to direct radiation was examined for three cases. The first case considers radiation from aircraft on the ground where chemical power is used for takeoff and landing and the reactor is not operated within 30 min of home station. The second case considers radiation from aircraft on the ground where nuclear power is used for takeoff and landing, and the third case considers radiation from airborne aircraft. Each case was considered using a mission time of 1.2×10^6 seconds and the two limits of utilization rate of 0.7 and 0.16 as established in Section 2.

For these two utilization rates, the time spent on the ground between flights is:

$$\frac{1.2 \times 10^6}{0.7}(0.3) = 5.18 \times 10^5 \text{ seconds for 0.7 utilization rate}$$

$$\frac{1.2 \times 10^6}{0.16}(0.84) = 6.35 \times 10^6 \text{ seconds for 0.16 utilization rate}$$

For the first case, of aircraft on the ground and using chemical for takeoff and landing, the Way-Wigner formula can again be used to determine the average power levels:

$$\bar{P}_{.7} = \frac{P_0 (0.0622) \int_{1800}^{5.18 \times 10^5} t_2^{-0.2}\, dt_2}{5.18 \times 10^5}$$

$$\bar{P}_{.16} = \frac{P_0 (0.0622) \int_{1800}^{6.35 \times 10^6} t_2^{-0.2}\, dt_2}{6.35 \times 10^6}$$

The average number of planes on the ground (NP) is expressed as the fleet size times one minus the utilization rate:

$NP_i = (1\text{-}i)60$

$NP_{.7} = (1\text{-}0.7)60 = 18$

$NP_{.16} = (1\text{-}0.16)60 = 50.4$

The total average power from the aircraft on the ground is:

$P = P\,NP$

$P = 18(1.34) = 68.06$ MW

$P_{.16} = 50.4(0.272) = 119.4$ MW

Since the average power level for aircraft on the ground is greatest for the 0.16 utilization rate, only that case will be considered further.

The dose rate for a given reactor is proportional to the power level in the following manner:

$$\frac{P_1}{P_2} = \frac{D_1}{D_2}$$

P_1 = power level one

P_2 = power level two

D_1 = dose rate at power level one

D_2 = dose rate at power level two

Using the radial radiation data from Table 5.3.1-1, the dose rate for both reactors was calculated:

$$\text{MHTGR: } D_2 = \left(\frac{119.4}{700}\right)(8.33 \times 10^4) = 1.42 \times 10^4 \text{ mrem/hr}$$

$$\text{Westinghouse: } D_2 = \left(\frac{119.4}{700}\right)(400) = 68.2 \text{ mrem/hr}$$

where: D_2 is the dose rate for the average 119.4 MW of reactor power.

The maximum dose rate to the general populace must be 5 mrem/yr (5.71×10^{-4} mrem/hr) or less. Therefore, the distance the aircraft must be removed from the general populace is:

$$\text{MHTGR: } \left(\frac{1.42 \times 10^4}{5.71 \times 10^{-4}}\right)^{1/2} 5.5 \text{ ft} = 27{,}500 \text{ ft}$$

$$\text{Westinghouse reactor: } \left(\frac{68.2}{5.71 \times 10^{-4}}\right)^{1/2} 20 \text{ ft} = 6912 \text{ ft}$$

For the second case, radiation from nuclear powered takeoff and landing, the 30 min of warmup, taxi, takeoff, and climb under full reactor power was used to estimate radiation effects on the general populace. Again, for a worst case model, all 60 aircraft at the same base, a utilization rate of 0.7, and the populace remaining at the same location were assumed. The 0.7 utilization rate and the 60 aircraft fleet size again resulted in 1100 flights/year out of the base. Using the radial radiation data from Table 5.3.1-1 the total dose per year was plotted as a function of distance (Figure 5.3.2-1), such that:

$$\text{Total dose} = (d_1)\left(\frac{R_1^2}{R_2^2}\right) t\,NF$$

where: D_1, R_1 are defined in Table 5.3.1-1

R_2 = distance from aircraft

t = time of reactor operation at full power (assume 30 min)

NF = number of flights per year

As can be seen from Figure 5.3.1.2-1, the general populace must remain at least 2¾ miles from the Mills Reactor and about ¾ mile from the Westinghouse Reactor. Again, the Mills Reactor is more restrictive than the Westinghouse Reactor.

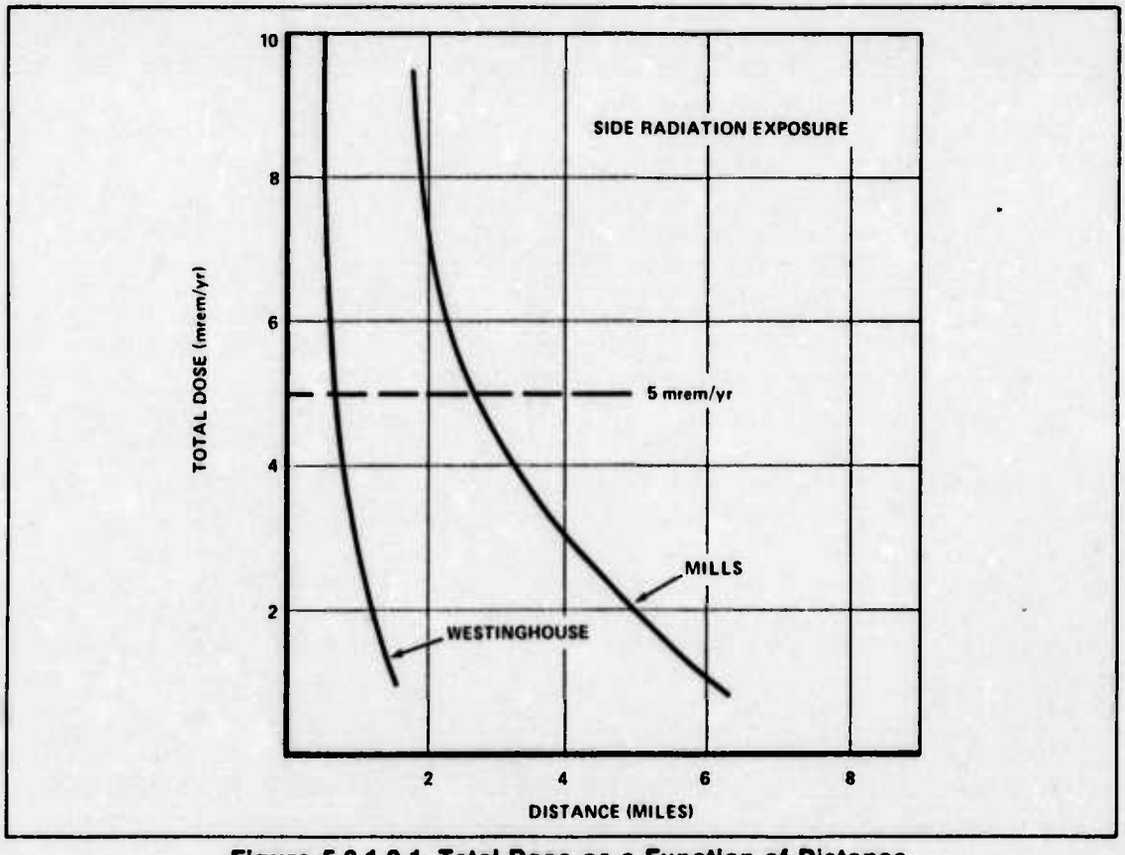

Figure 5.3.1.2-1. Total Dose as a Function of Distance from Full Power Reactor

For the third case, which considers the radiation from airborne aircraft, the minimum separation between the general populace and the aircraft was computed as a function of the number of missions flown per year. It was assumed that only one takeoff and landing would be made per mission, and that, in the long run, the aircraft would fly over the populace on either end of the runway an equal number of times. Therefore, since the aircraft flies slower on approach for landing than on climb after takeoff, it is the worst case, and is the case analyzed here.

The time spend over any area was found using the geometric model in Figure 5.3.1.2-2.

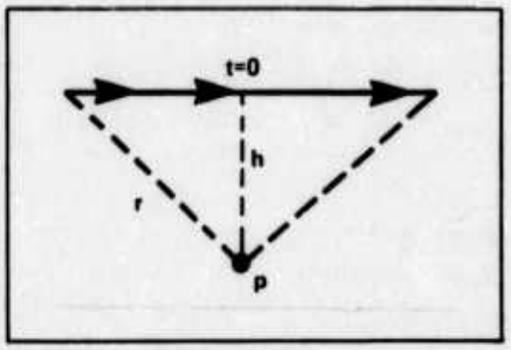

Figure 5.3.1.2-2. Geometric Model

The aircraft is assumed to be flying straight and level and will come no closer than h ft to the point p. With V as the velocity of the aircraft, the total dose (D_T) at the reference distance, D_1, may be found:

$$\frac{d\,Dt}{dt} = \frac{D_1 h^2}{r^2}$$

$$D_T = \int_{-\infty}^{\infty} \frac{D_1 h^2}{r^2}\, dt = \frac{2 D_1 h}{V}$$

The total dose received is expressed as the dose rate times the time interval (2 h/V) over which it is received.

Using spherical divergence, the total dose received at a distance R_2 is:

$$D_T = \frac{R_1^2}{R_2^2} \frac{2 D_1 h}{V}$$

where: D_T = total dose received

D_1 = dose rate at reference distance

R_1 = reference distance

R_2 = distance at which D_T is received

h = aircraft altitude

V = aircraft velocity

Substituting R_2 for h and rearranging terms:

$$R_2 = 2 \frac{R_1^2}{D_T} \frac{D_1}{V}$$

However, this is for each flight and, therefore, must be adjusted for the number of flights per year. Again assume the worst case of a utilization rate of 0.7 and all 60 aircraft pass over the point, p. Therefore the number of flights per year would be 1100 over p.

Thus: $R_2 = 2\,NF \frac{R_1^2}{D_T} \frac{D_1}{V}$

where: R_2 = minimum altitude separation for a total dose D_T

NF = number of flights per year

With D_T = 5 mrem/yr for the general populace and V = 113 kts during the landing phase. The altitude separation of the aircraft and populace was calculated for both reactors using radial radiation data from Table 5.3.1-1.

Thus: MHTGR: R_2 = 1614 ft

Westinghouse: R_2 = 90 ft

Thus, an aircraft equipped with a Mills Reactor cannot descend lower than 1614 ft over the general populace with the reactor at full power, if all aircraft were stationed at the same base. However, if the fleet were dispersed at three bases, this distance would decrease to 538 ft.

Thus, a reactor that gives safe operation for the flight crew will not present a radiation hazard, due to overflight, to the general populace. Nuclear powered landing and takeoff will pose no problem for the Westinghouse Reactor, but based on spherical divergence only, the general populace must be removed three to five miles from the parking ramp for the KLM Reactor.

These distances assumed that the air would not interact with the gamma rays. When the distance traveled through air is a few hundred feet, this is not a bad assumption. When the distance involves thousands of feet, this is no longer a valid assumption. When the thickness of the air is 4000 ft, the attenuation is greater than 10^{-4}. This would make the dose rate equivalent to that of Section 5.1.2.2. For this reason, 4000 ft is assumed to be the maximum distance required for the general populace removal for the KLM Reactor.

5.4 POTENTIAL WEIGHT SAVINGS

The nuclear powered aircraft does not have a viable payload using the basic reactor system weights when the aircraft is assumed to have sufficient fuel for takeoff and landing on chemical fuel only, and a 1000 nm emergency cruise capability. Because a substantial portion of the total aircraft weight is propulsion system weight, the propulsion system, especially the reactor, is a natural area of interest for attempted weight savings.

It was pointed out in Section 5.2.1 that increasing the core fuel density offered potential weight savings. The WHTGR designs predict approximately 300,000 lbs savings for a fuel loading increase from 313 mg/cc to 400 mg/cc. However, the relationship is highly non-linear since a further increase from 400 mg/cc to 500 mg/cc only saves approximately 70,000 lbs.

Higher operating temperatures would be expected to yield weight savings; however, the limitation in this case is not in reactor technology, but rather in heat exchanger materials. Thus, developments in metals technology must precede any increase in operating temperatures.

Since a substantial part of the reactor weight is in shielding material, and since there was as much as 300,000 lbs difference in shielding weights between the MHTGR and the WHTGR, reduced shielding weights were investigated for potential weight savings.

The two gas reactors considered in this section employ considerably different shielding designs in that the MHTGR uses much less shielding in the radial direction than does the WHTGR. Large weight savings are obtained, but at the expense of greatly increased radiation levels (see Table 5.3.1-1). In addition to this consideration, the possibilities of saving weight by maintaining large separation distances between the reactor and the crew and by increasing the dose rate, but letting the crew fly less often, were considered.

5.4.1 SEPARATION DISTANCE: The aircraft design presented in Section 4 shows that a separation of 200 ft between the crew and the reactor can be achieved. This separation allows reduced shielding to maintain the dose rate at the maximum allowable value of 1.49 mrem/hr.

The radiation dose rates of Table 5.3-1 and Eq. 5.3.1.1-1 were used to determine the separation required to achieve 1.49 mrem/hr for the basic reactor designs. This yields:

$$\text{WHTGR: } R = \left(\frac{5}{1.49} \right)^{1/2} (20) = 36.63 \text{ ft}$$

$$\text{MHTGR: } R = \left(\frac{2.2}{1.49} \right)^{1/2} (22) = 26.73 \text{ ft}$$

R = separation distance for 1.49 mrem/hr

By setting the radiation levels at these distances equal to the radiation level at 200 ft, new values of shielding thickness can be solved for. In this analysis, shielding thickness in the

radial direction was kept constant, and only the shielding in the direction of the crew was reduced.

The equation for radiation density is given by (Ref. 49, p. 7-61):

$$I' = \frac{S \exp(-\mu t)}{4\pi R^2}$$

I' = radiation density
S = point source strength
μ = linear attenuation coefficient
R = distance from source

Letting

$$\frac{S \exp(-\mu t)_1}{4\pi R_1^2} = \frac{S \exp(-\mu t)_2}{4\pi R_2^2}$$

$$(\mu t)_2 - (\mu t)_1 = 2 \ln (R_1/R_2)$$

The term (μt) is of the form

$$(\mu t) = \sum_j (\mu_j t_j)$$

μ_j = linear attenuation coefficient of the jth shielding material

t_j = thickness of the jth shielding material

In this analysis, only the tungsten thickness was varied, so that:

$\mu_W t_{W2} = \mu_W t_{W1} + 2 \ln (R_1/R_2)$
μ_W = linear attenuation coefficient for tungsten
t_{W1} = tungsten thickness for distance R_1
T_{W2} = tungsten thickness for distance R_2

$$t_{W2} = t_{W1} + \frac{2}{\mu_W} \ln (R_1/R_2)$$

Using the value of μ for tungsten and gamma rays at 1 Mev gives μ = 1.263/cm (Ref. 49, p. 7-112), so that:

$$t_{W2} = t_{W1} + 1.583 \ln (R_1/200)$$

WHTGR: $t_{W2} = 17.78 + 1.583 \ln (36.63/200) = 15.09$ cm = 5.94 in.

MHTGR: $t_{W2} = 27.86 + 1.583 \ln (26.73/200) = 24.67$ cm = 9.71 in.

In order to compute the weight savings for the WHTGR, it was necessary to model the reactor geometry. A model that produces reasonable accuracy in predicting the weight is one of concentric spheroidal shells. The spheroid volume is given by $V = 4/3\ \pi$ ABC, where A, B, and C are dimensions as shown in Figure 5.4.1-1. In this case, B and C are equal dimensions.

Applying this model to the WHTGR at 275 MW(th) yields the values tabulated in Table 5.4.1-1, and a total weight of 6.509 x 10^5 lbs which is within 6% of the 6.16 x 10^5 lbs predicted by Westinghouse (Figure 5.2.1-4).

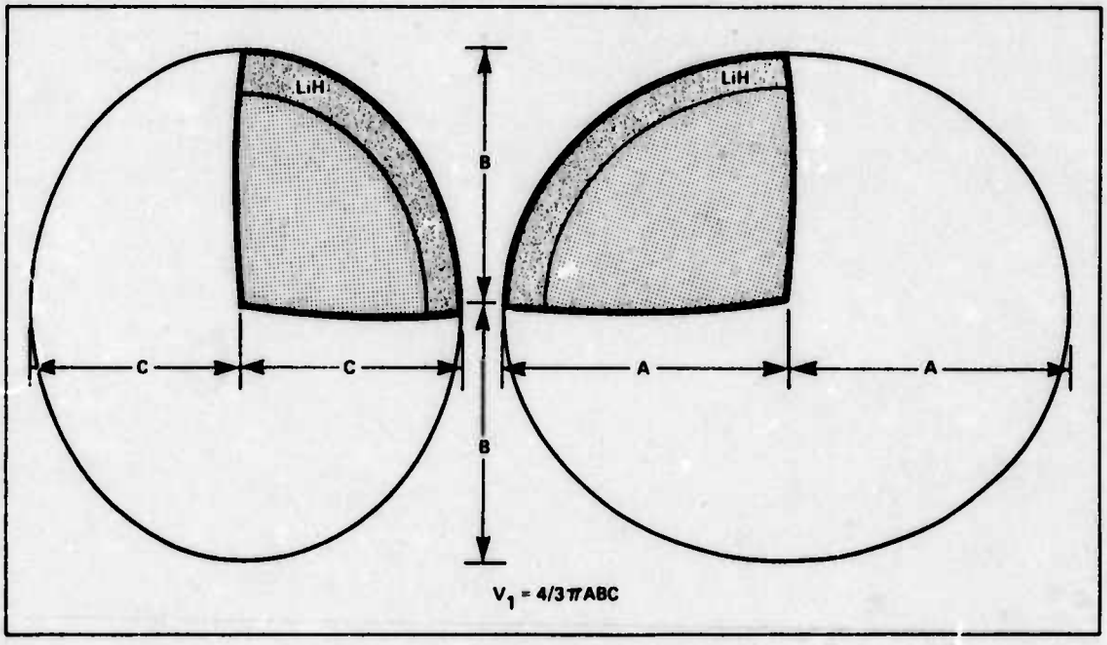

Figure 5.4.1-1. Spheroid Volume

TABLE 5.4.1-1.
WHTGR WEIGHT ESTIMATION FOR 275 MW(TH)

	A (IN.)	B (IN.)	TOTAL VOLUME ($IN.^3$)	SECTION VOLUME ($IN.^3$)	SECTION DENSITY ($LB/IN.^3$)	SECTION WEIGHT (LB)
CONTAINMENT VESSEL	116	94	4.293 X 10^6	2.520 X 10^5	0.3299	8.313 X 10^4
LITHIUM HYDRIDE	114	92	4.041 X 10^6	1.185 X 10^6	0.02801	3.391 X 10^4
ZIRCONIUM HYDRIDE	99	83	2.856 X 10^6	1.539 X 10^6	0.2027	3.119 X 10^5
HEAT EXCHANGER	68	68	1.317 X 10^6	5.499 X 10^5	—	3.575 X 10^4
PRESSURE VESSEL	56	57	7.621 X 10^5	3.970 X 10^4	0.3299	1.309 X 10^4
TUNGSTEN	55	56	7.224 X 10^5	2.495 X 10^5	0.6973	1.739 X 10^5
CORE	48	48.5	4.729 X 10^5			
TOTAL						6.509 X 10^5

The same model applied to the WHTGR at 700 MW(th) yields the values given in Table 5.4.1-2. Shielding reduction was then applied to this 700 MW(th) model to assess the potential weight savings. The weights for the reduced shielding model are given in Table 5.4.1-3. The difference in weights between the two models is approximately 21,000 lbs.

TABLE 5.4.1-2.
WHTGR WEIGHT ESTIMATION FOR 700 MW(TH)

	A (IN.)	B (IN.)	TOTAL VOLUME ($IN.^3$)	SECTION VOLUME ($IN.^3$)	SECTION DENSITY ($LB/IN.^3$)	SECTION WEIGHT (LB)
CONTAINMENT VESSEL	136	116	7.665×10^6	3.710×10^5	0.3299	1.223×10^5
LITHIUM HYDRIDE	134	114	7.294×10^6	1.799×10^6	0.02801	5.038×10^4
ZIRCONIUM HYDRIDE	119	105	5.495×10^6	2.510×10^6	0.2027	5.087×10^5
HEAT EXCHANGER	88	90	2.985×10^6	1.289×10^6	—	9.100×10^4
PRESSURE VESSEL	72	75	1.696×10^6	6.800×10^4	0.3299	2.243×10^4
TUNGSTEN	71	74	1.628×10^6	4.430×10^4	0.6973	3.089×10^5
CORE	64	66.5	1.185×10^6			
TOTAL						1.104×10^6

TABLE 5.4.1-3.
WHTGR WEIGHT ESTIMATION FOR 700 MW(TH)
REDUCED SHIELDING

	A (IN.)	B (IN.)	TOTAL VOLUME ($IN.^3$)	SECTION VOLUME ($IN.^3$)	SECTION DENSITY ($LB/IN.^3$)	SECTION WEIGHT (LB)
CONTAINMENT VESSEL	134.93	116	7.604×10^6	3.690×10^5	0.3299	1.217×10^5
LITHIUM HYDRIDE	132.93	114	7.236×10^6	1.790×10^6	0.02801	5.013×10^4
ZIRCONIUM HYDRIDE	117.93	105	5.446×10^6	2.497×10^6	0.2027	5.061×10^5
HEAT EXCHANGER	86.93	90	2.949×10^6	1.278×10^6	—	9.100×10^4
PRESSURE VESSEL	70.93	75	1.671×10^6	6.700×10^4	0.3299	2.210×10^4
TUNGSTEN	69.93	74	1.604×10^6	4.190×10^5	0.6973	2.921×10^5
CORE	64.00	66.5	1.185×10^6			
TOTAL						1.083×10^6

The same approach was used for the MHTGR. The concentric right circular cylinder model of Section 5.2.2.1 was used, and the weights for the MHTGR at 700 MW(th) and with reduced tungsten shielding are given in Table 5.4.1-4. This compares to the original weights given in Table 5.2.2.1-2 to show a weight savings of approximately 10,000 lbs.

5.4.2 CREW RATIO: The basic assumptions regarding crew duty were given in Section 5.1.2.1. If the number of crews were doubled so that they flew half as much, the dose rate could be increased. Assuming a direct proportionality:

$$\frac{D_1}{D_2} = \frac{N_1}{N_2}$$

D = dose rate

N = number of crews

TABLE 5.4.1-4.
MHTGR WEIGHT ESTIMATION FOR 700 MW(TH)
REDUCED SHIELDING

	RADIUS (IN.)	HEIGHT (IN.)	TOTAL VOLUME ($IN.^3$)	SECTION VOLUME ($IN.^3$)	SECTION DENSITY ($LB/IN.^3$)	SECTION WEIGHT (LB)
CORE	21.96	59.12	8.596×10^4	8.596×10^4	0.07665	6.588×10^3
VOID	22.54	59.12	9.436×10^4	8.400×10^3	—	—
REFLECTOR	27.54	59.12	1.408×10^5	4.644×10^4	0.09062	4.208×10^3
VOID	29.03	69.70	1.845×10^5	4.370×10^4	—	—
PRESSURE VESSEL	32.53	76.70	2.549×10^5	7.040×10^4	0.3299	2.322×10^4
TUNGSTEN	41.77	96.12	5.268×10^5	2.719×10^5	0.6973	1.895×10^5
LITHIUM HYDRIDE	69.37	224.08	3.387×10^6	2.858×10^6	0.02801	8.005×10^4
HEAT EXCHANGER	69.37	263.92	3.989×10^6	6.020×10^5	—	9.100×10^4
CONTAINMENT VESSEL	71.37	267.92	4.287×10^6	2.980×10^5	0.3299	9.831×10^4
TOTAL						4.928×10^5

But, the dose rate ratio can also be expressed as:

$$\frac{D_1}{D_2} = \frac{S \exp(-\mu t)_1}{S \exp(-\mu t)_2}$$

$$(\mu t)_2 = (\mu t)_1 + \ln (D_1/D_2) = (\mu t)_1 + \ln (N_1/N_2)$$

Again, considering only the tungsten:

$$t_{W2} = t_{W1} + \frac{1}{\mu} \ln (N_1/N_2)$$

Letting $N_1 = 1$ be the base as defined in Section 5.1.2.1, the number of crews (N_2) required to effect the same weight savings found in Section 5.4.1 can be found:

$$N_2 = \exp(-\mu(t_2 - t_1))$$

WHTGR: $N_2 = \exp(-1.263(15.09 - 17.78)) = 29.88$

MHTGR: $N_2 = \exp(-1.263(24.67 - 27.86)) = 56.20$

Thus, it is concluded that saving weight by increasing the number of available crews is not a viable option.

SECTION 6
ENGINES

6.0 INTRODUCTION

6.0.1 BACKGROUND: The use of a nuclear power plant for aircraft propulsion is not a new concept. One of the first studies in this area was the Lexington Project (LEXP-1) prepared for the Atomic Energy Commission in 1948. A good review of that report and subsequent work may by found in Armbruster (Ref. 8).

This study uses some of the basic concepts previously employed but takes into account the present state of the art and estimated furture capabilities.

Table 6.0.1-1 lists the symbols that will be used in this section.

TABLE 6.0.1-1 TABLE OF SYMBOLS

A	AREA (FT^2)
c_p	SPECIFIC HEAT OF PRESSURE (BTU/LB°R)
F	THRUST (LBF)
g	PROPORTIONALITY CONSTANT (32.2 FT-LB/LB-SEC^2)
HP	HORSEPOWER
k	$\frac{\gamma-1}{\gamma}$
$\dot{m}$	MASS FLOW RATE (LBM/SEC)
P	STATIC PRESSURE (LB/FT^2)
P_t	TOTAL PRESSURE (LB/FT^2)
q	HEAT ADDITION (BTU/LB)
R	GAS CONSTANT, R_{air} = 53.35 LB-FT/LBM°-R
r	RADIUS (FT)
r_p	PRESSURE RATIO
s	ENTROPY (BTU/LBM)
T	STATIC TEMPERATURE (°R)
T_t	TOTAL TEMPERATURE (°R)
T_{ta}	OUTLET TEMPERATURE OF REGENERATOR ON COMPRESSOR SIDE (°R)
T_{tb}	OUTLET TEMPERATURE OF REGENERATOR ON TURBINE SIDE (°R)
V_e	EXIT VELOCITY (FT/SEC)
V_O	FLIGHT VELOCITY (FT/SEC)

TABLE 6.0.1-1. TABLE OF SYMBOLS (CONTINUED)

	W	WORK (BTU/LBM)
	$\dot{W}$	WORK (BTU/SEC)
	X	$= (r_p)^k$
	Z	TEMPERATURE RATIO OF TURBINE INLET TEMPERATURE TO COMPRESSOR INLET TEMPERATURE
	α	ALPHA, TOTAL CYCLE TEMPERATURE RATIO
	β	BETA, BYPASS RATIO
	χ	CHI, EXPANSION RATIO = $r_p^{\ k} - 1$
	δ	DELTA, PRESSURE RATIO P_{tx}/P_{ts1}
	Δ	DELTA, PERCENT DIFFERENCE
	η	ETA, EFFICIENCY
	η_r	RAM EFFICIENCY
	η_R	REGENERATOR EFFECTIVENESS
	η_{th}	THERMAL EFFICIENCY
	γ	GAMMA, RATIO OF SPECIFIC HEATS
	θ	THETA, TEMPERATURE RATIO, (T_{tx}/T_{ts1})
SUBSCRIPTS		
	1,2,3,4,5,e	ENGINE STATION IDENTIFICATION
	0	AMBIENT CONDITIONS
	c	COMPRESSOR, CORE
	F	FACE
	f	FAN
	I	IDEAL
	n	NET
	sl	SEA LEVEL STATIC
	t	TURBINE
	x	STATION
	β	BYPASS
SUPERSCRIPT		
	'	ACTUAL

6.0.2 PROPULSION CONCEPTS: There are many engine concepts but the three most common, shown in Figure 6.0.2-1, are turboprop, turbofan, and turbojet.

The basic differences between these concepts may be seen from the thrust equation:

$$\text{gross thrust} = F_g = \frac{\dot{w}_{air}}{g} V_j$$

where:

$\dot{w}_{air}$ = mass flow of air Lb/sec

g = proportionality constant, 32.2 $\frac{\text{Lb-ft}}{\text{Lb}_f\text{-sec}^2}$

V_j = increment of velocity added to W_{air} by propulsive system

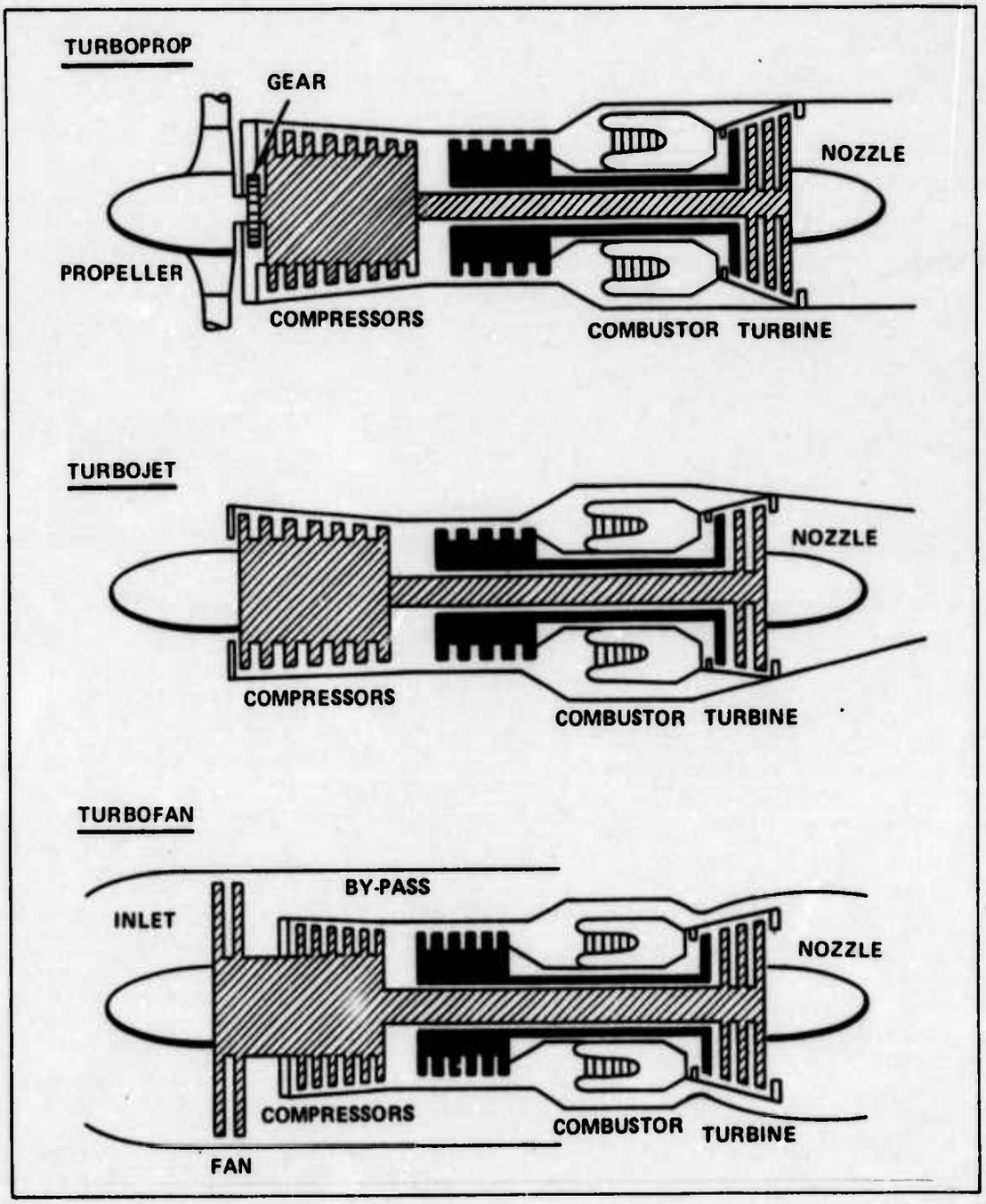

Figure 6.0.2-1. Three Basic Engine Concepts

In principle, then:

1) The turboprop accelerates a large amount of air through a small velocity increment.

2) The turbofan accelerates a medium amount of air through a medium velocity increment.

3) The turbojet accelerates a small amount of air through a large velocity increment.

This mass-velocity relationship may be seen in Figure 6.0.2-2.

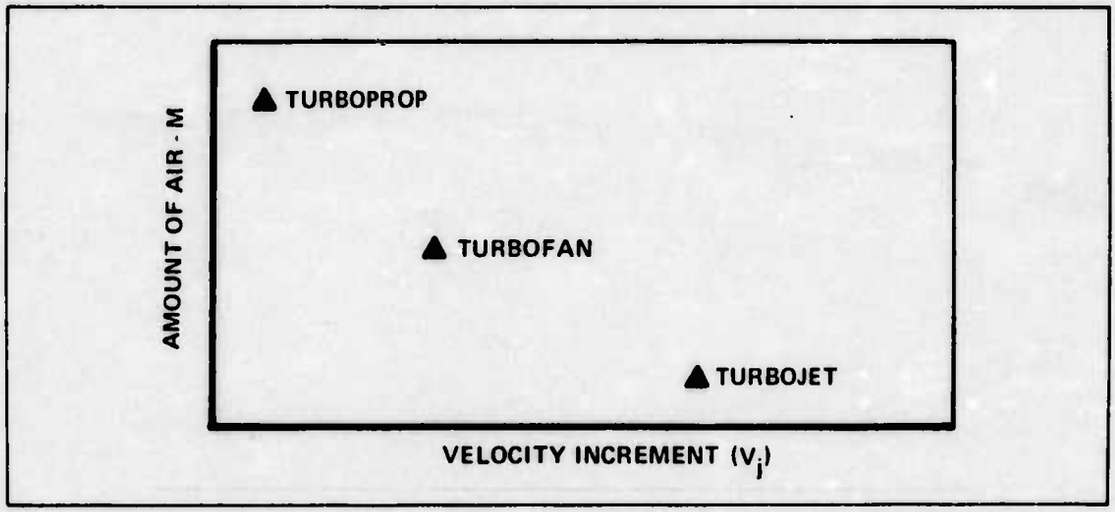

Figure 6.0.2-2. Comparison of Turboprop, Turbofan, and Turbojet Air Mass-Velocity Relationship

6.0.3 SAFETY: The influence of safety considerations today as compared to those in 1948 (Ref. 8) have changed considerably and have thus changed design concepts and considerations. The importance of safety is emphasized and discussed in Section 8.

6.0.4 STATE-OF-THE-ART ASSESSMENT: Recalling the thrust requirements presented in Section 4, and the reactor size and weight relations in Section 5, along with the requirements for a heat exchanger, a heuristic comparison of the three propulsion concepts is presented in Table 6.0.4-1 which is based on References 84; 58; 31, p. 16-499; and 171.

6.0.5 NUCLEAR CYCLES: Two basic methods in which nuclear power may be used in the engine are:

1) *Open Cycle* — The reactor is located within the engine and the air from the compressor passes directly over the reactor and is then expanded over the turbine to the exhaust (Figure 6.0.5-1).

2) *Closed Cycle* — A heat exchanger which contains a hot working fluid that passes through the reactor is located in the engine. Air enters the engine and, after leaving the

compressor, passes over the heat exchanger where energy is added and then expands over the turbine and out the exhaust (Figure 6.0.5-2).

TABLE 6.0.4-1. STATE-OF-THE-ART ASSESSMENT OF PRESENT ENGINE CONCEPTS

PROPULSION CONCEPT	PRESENT CAPABILITIES	RISK
TURBOPROP	A. 30,000 LB THRUST AT SEA LEVEL B. MOST EFFICIENT CYCLE IN SPEED RANGE UP TO 350 MPH	VERY HIGH AS GEAR BOX TECHNOLOGY AND PROPELLER SIZE WOULD HAVE TO BE INCREASED THREEFOLD TO PROVIDE THE REQUIRED THRUST.
TURBOJET	A. 35,000 LB THRUST AT SEA LEVEL B. HIGHEST SPECIFIC THRUST IN SPEED REGIME OF 500-700 MPH	MODERATE RISK BECAUSE ENGINE CORE SIZE WOULD HAVE TO INCREASE SIGNIFICANTLY TO PROVIDE NECESSARY THRUST.
TURBOFAN	A. 51,000 LB THRUST AT SEA LEVEL B. HIGHEST PROPULSIVE EFFICIENCY IN SPEED REGIME OF 500-700 MPH	LOWEST RISK BECAUSE OF AVAILABLE EXPERIENCE WITH HIGH THRUST, HIGH BYPASS ENGINES. LEAST AMOUNT OF ADAPTATION.

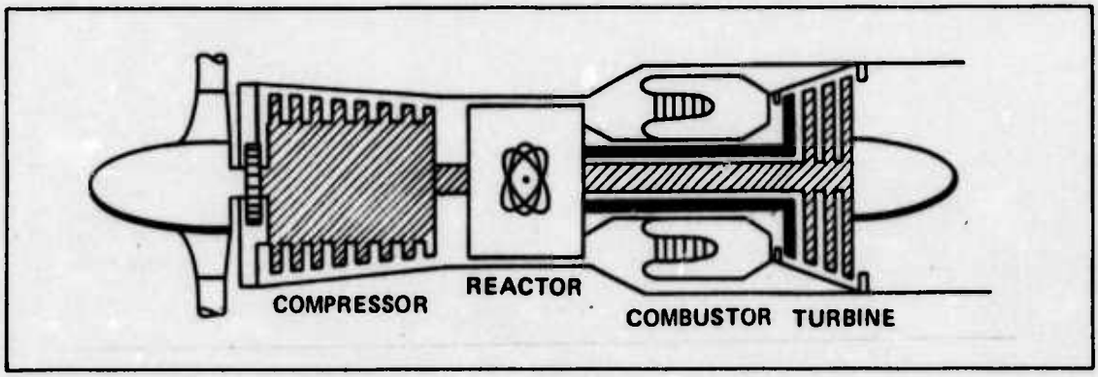

Figure 6.0.5-1. Open Cycle Air Turboprop

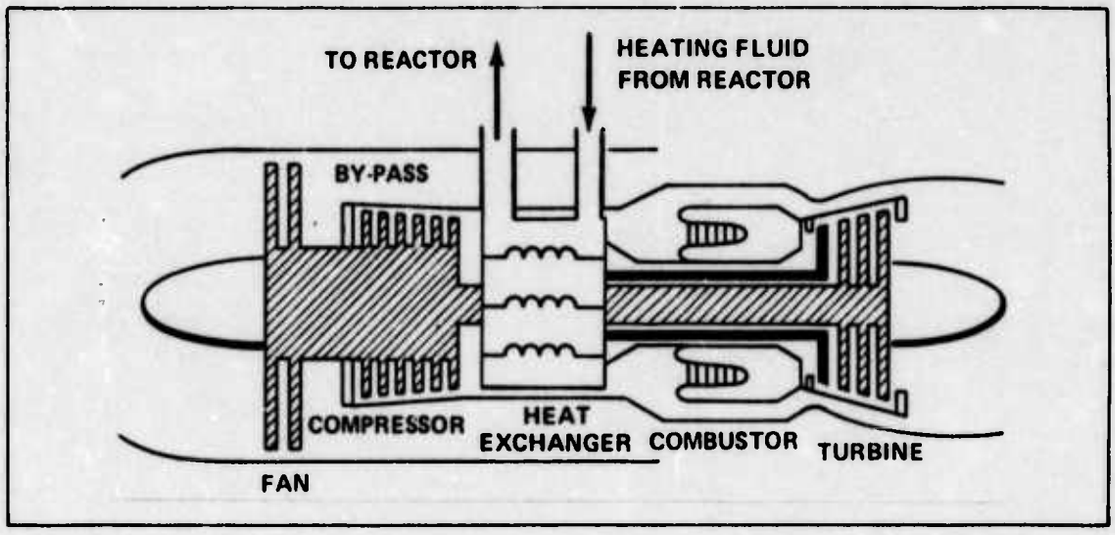

Figure 6.0.5-2. Closed Cycle Turbofan

6.0.6 NUCLEAR POWERED ENGINE SYSTEM CONCEPTS: Three concepts were selected and an analysis of each system in terms of thrust, reactor requirements, and total system weights was performed.

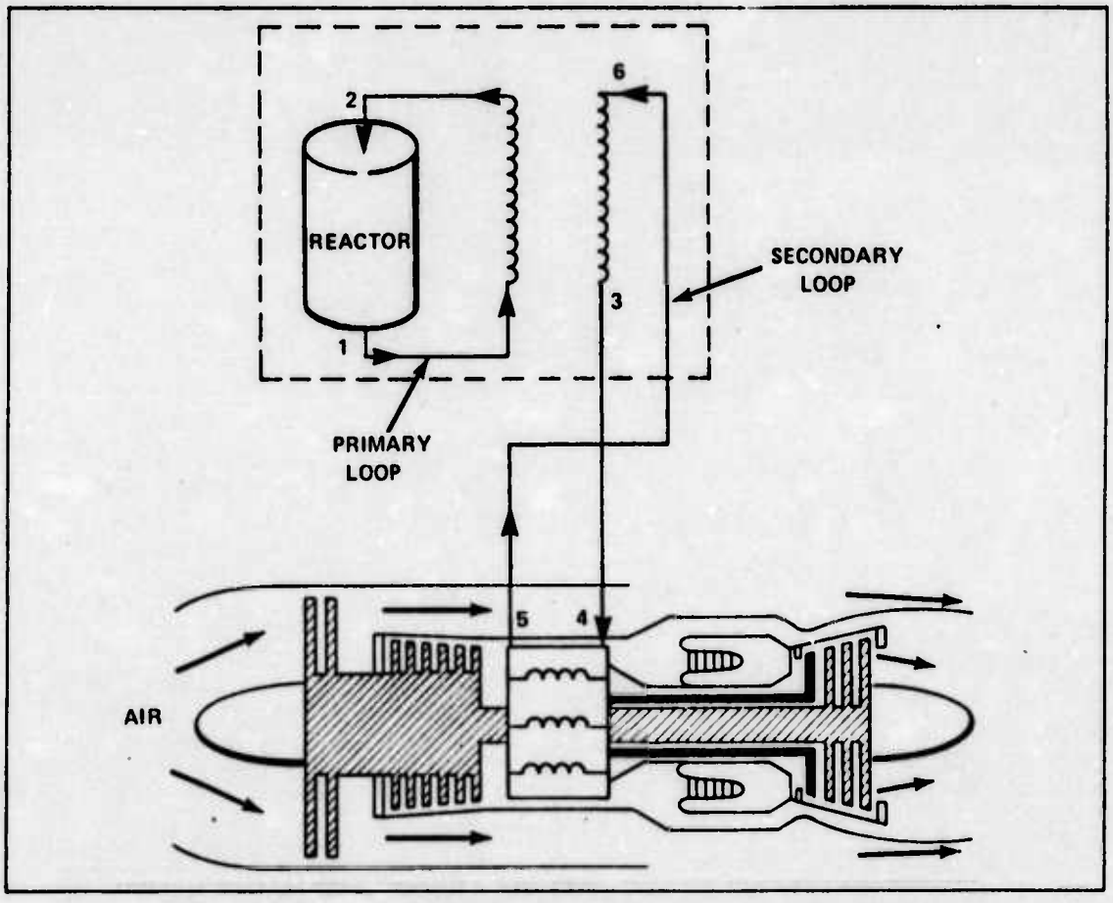

Figure 6.0.6-1. Indirect Cycle, Heat Exchanger Turbofan Engine

The first system will be called the indirect cycle, i.e., an open-closed cycle. Figure 6.0.6-1 shows a primary and a secondary heating loop. The primary loop (1-2) is located within the reactor containment vessel; the secondary loop leaves the reactor from Station 3 and enters the engine heat exchanger in Station 4. Air is heated between stations 4 and 5 and the heating fluid returns to the reactor heat exchanger at Station 6. This is an indirect cycle because the hot fluid is indirectly the working fluid of the engine whereas the air is the primary working fluid for the engine.

Within this system concept there is the option of having either dual-mode or a dedicated nuclear powered engine. The dual-mode engine offers the ability of operating on JP-4 fuel. A brief heuristic comparison of these two engines is presented in Table 6.0.6-1.

TABLE 6.0.6-1. COMPARISON OF DEDICATED VS DUAL-MODE NUCLEAR POWERED ENGINES

	DEDICATED	DUAL-MODE
WEIGHT/ENGINE	BASE	6% HIGHER BECAUSE OF COMBUSTOR WEIGHT AND INTERFACING.
THRUST/ENGINE	BASE	3-4% LESS BECAUSE OF ADDITIONAL PRESSURE LOSS IN COMBUSTOR.
RELIABILITY	HIGHER	LOWER
MAINTAINABILITY	HIGHER	LOWER BECAUSE OF THE ADDITIONAL COMPLEXITY OF TWO SYSTEMS.

The second system concept, the direct cycle in which the helium primary working fluid is expanded over the turbine, is depicted in Figure 6.0.6-2. As with the indirect cycle, there are two coolant loops in this system. The primary loop is from Station 1 to 2, as shown in Figure 6.0.6-1; the secondary goes from the secondary reactor heat exchanger at Station 3 (Figure 6.0.6-1) to Station 4, as shown in Figure 6.0.6-2, and is expanded over the turbine. The hot helium then passes through a regenerator located within the engine and on to a heat rejection heat exchanger. Helium returns to the compressor at Station 6, is compressed up to the required system pressure, and leaves the compressor at Station 7 to return to the reactor heat exchanger at Station 8. Work is extracted off the turbine to drive the compressor and the fan.

The third system is referred to as a two gas turbine generator or central turbine system. Instead of a gas turbine generator in each engine with helium expanding over it as in the second system concept, there are two gas turbine engines located adjacent to the reactor and the power generated for driving the ducted fans is transmitted via shafts. These shafts are contained within each wing and the horsepower required to drive the ducted fan is removed by means of gears and transmission devices. These gears are also restricted by present state-of-the-art as are the turboprop gears. Section 6.2.7 gives further details concerning the required gear technology. Each turbine is part of a two loop coolant system which operates identically to that for the independent turbine system. Figure 6.0.6-3 presents this system concept.

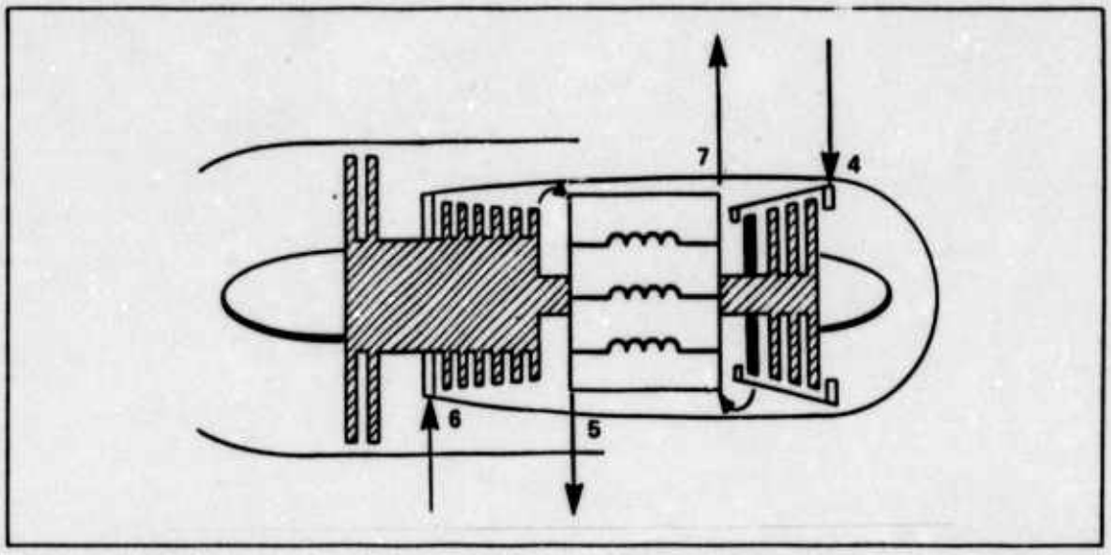

Figure 6.0.6-2. Closed Loop Independent Turbine System with Helium Expanded Directly Over the Turbine

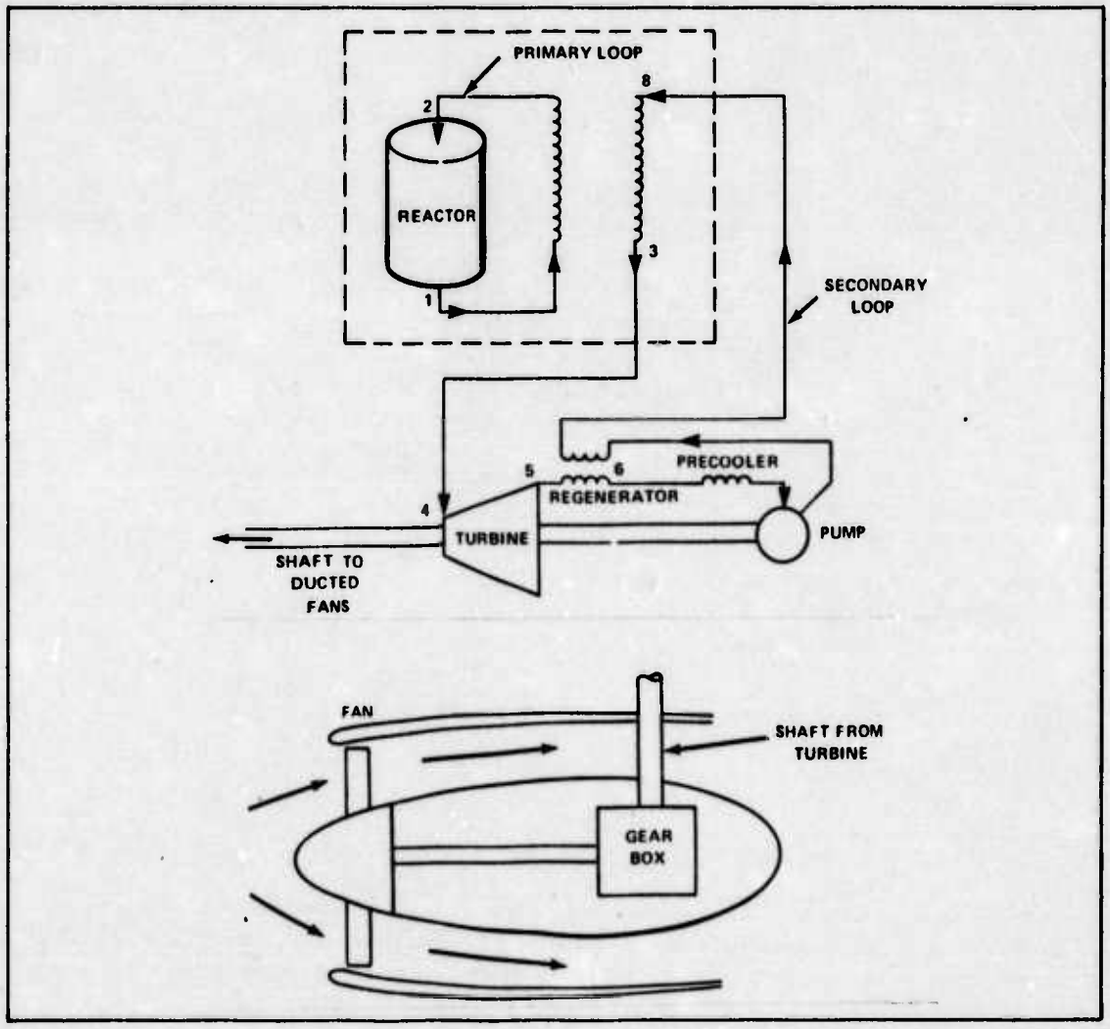

Figure 6.0.6-3. Direct Cycle Central Turbine Ducted Fan

A summary outline of the three systems studied in this report is presented in Figure 6.0.6-4.

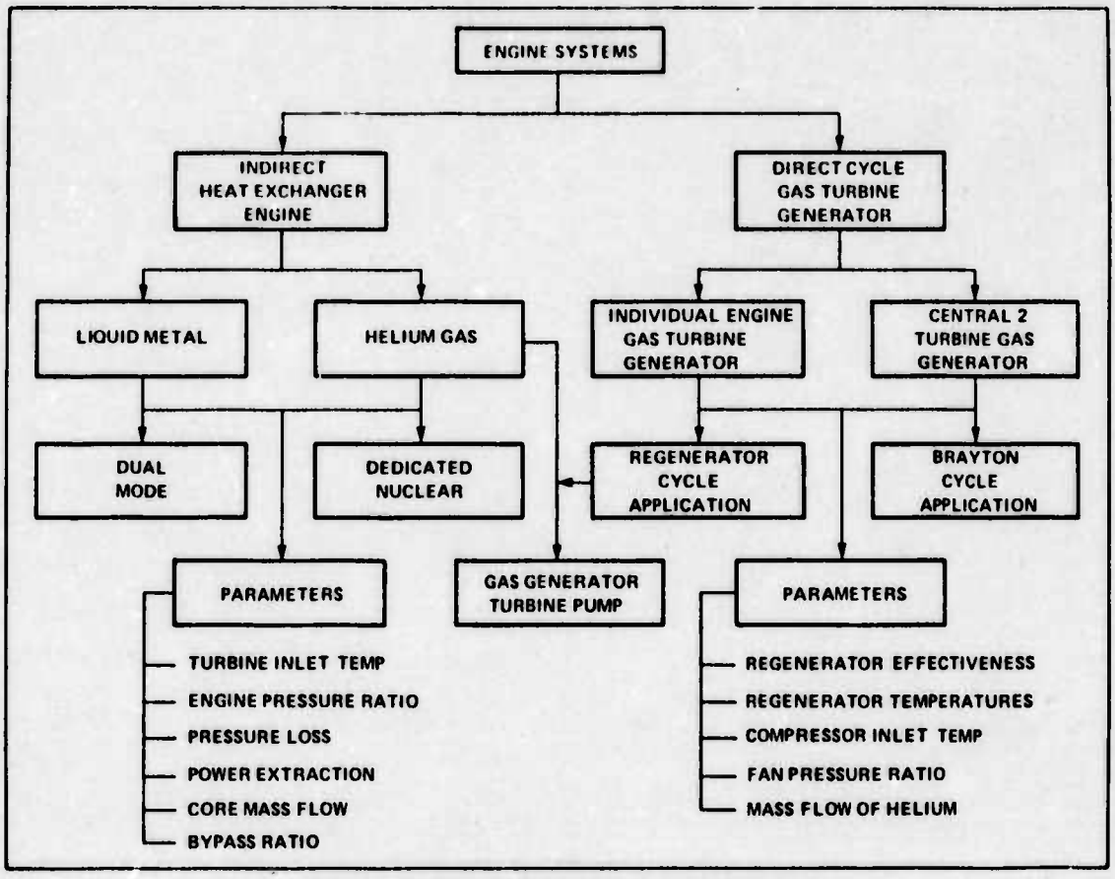

Figure 6.0.6-4. Engine Systems Summary

The system described as the gas turbine generator-pump was a system studied for the helium gas reactor using a regenerator cycle in order to drive the pump used to pump the helium in the primary and secondary coolant loops. This system is described more fully in Section 6.2.8.

6.0.7 DESIGN CONSTRAINTS: The constraints placed upon the three nuclear powered engine concepts were driven primarily by:

1) reactor size
2) reactor temperatures
3) material limitations of heat exchangers

These limitations affect:

1) compressor outlet temperature
2) turbine inlet temperature
3) mass flow allowable through engine core
4) pressure losses
5) pumping power requirements

Table 6.0.7-1 lists the design constraints for design operation at 30,000 ft and at a flight speed of approximately 596 ft/sec. With these design constraints in mind, the problem was to maximize the thrust for minimum system weight.

TABLE 6.0.7-1. DESIGN CONSTRAINTS

CONSTRAINT	DEDICATED	DUAL-MODE	DIRECT	DUCTED FAN (2 TURBINE SYSTEM)
MASS FLOW OF AIR THROUGH CORE LB/SEC	200	200	N/A	N/A
MASS FLOW OF AIR THROUGH FAN LB/SEC	NL[1]	NL[1]	NL[2]	NL[2]
MASS FLOW OF HELIUM OVER TURB. LB/SEC	N/A	BN/A	50-100	250-350
TURBINE INLET TEMPERATURE R	1960	1960	2060	2060
COMPRESSOR OUTLET TEMPERATURE R	1060	1060	600-1000	600-1000
PRESSURE LOSSES %	5-11	11-16	1-2	.5-2
PUMPING POWER [4]	500-1000	500-1000	N/A[3]	N/A[3]

NL[1] - NO LIMITATION. WILL BE SHOWN TO BE A FUNCTION BYPASS RATIO AND OTHER VARIABLE IN SECTION 6.2.

NL[2] - NO LIMITATION. IS A FUNCTION OF FAN PRESSURE RATIO AND WORK AVAILABLE TO THE FAN AND WILL BE DISCUSSED IN SECTION 6.2

N/A[3] - NOT APPLICABLE AS THE PUMPING POWER IS INHERENTLY ENCOMPASSED WITHIN THE SYSTEM DESIGN.

4 - PUMPING POWER IS THE HORSEPOWER REQUIRED TO PUMP THE COOLANT IN THE SECONDARY LOOP.

The mass flow of air through the engine was selected based on tradeoffs between: pressure loss the air experiences passing through the heat exchanger and combustion section; the heat exchanger size, weight, and packaging; and the thrust produced. Section 7.4.12 gives a more detailed account of this tradeoff.

The turbine inlet temperature limit was based on metallurgical and lifetime considerations. A 10,000 hr heat exchanger lifetime can be achieved only by air side temperatures in the 1960°R to 2060°R range (Ref. 107). This study used the more conservative 1960°R for the base engine and a sensitivity analysis of engine thrust to turbine inlet temperature was preformed (Section 6.1.7).

The compressor outlet temperature is driven by the amount of energy the heat exchanger can provide, the amount of core air flow to be heated, and the turbine inlet temperature. For a given amount of available input energy and air flow, the turbine inlet temperature will decrease as the compressor temperature decreases.

6.1 INDIRECT CYCLE

The indirect cycle or heat exchanger turbofan engine operates on the Brayton cycle. A description of the Brayton cycle is discussed in terms of a temperature-entropy (T-S) diagram. The derivations of several of the optimum equations are presented in Appendix 6.2.

Recalling the input conditions for engine for operation at 30,000 ft:

1) Compressor outlet temperature $T_{t_3} = 1060°R$
2) Mass flow of air through engine core $\dot{m}_c = 200$ lb/sec
3) Turbine inlet temperature $T_4 = 1960°R$
4) Horsepower required for pumping HP = 500-1000 hp/engine
5) Pressure loss in heat exchanger ΔP = 6-16%

Using these conditions the following parameters were varied to maximize the thrust:

1) Fan pressure ratio (R_{Pfan})
2) Core pressure ratio (P_{pcore})
3) Bypass ratio (β)

A computer program titled *Design Point Turbine Engine Performance Program* (Ref. 192) was used for the study of the indirect heat exchanger engine. The design point was chosen at 30,000 ft at flight speed of approximately Mach 0.6. The 30,000 ft altitude was chosen over a lower one because of the compressor exit temperature requirements determine the number of compressor stages and the engine compressor pressure ratio required. A simplified diagram of the methodology used in this analysis and a simplified block diagram of the computer program are presented in Appendix 6.3.

6.1.1 CYCLE ANALYSIS: The processes of the Brayton cycle (simple cycle) are depicted in the T-S diagram in Figure 6.1.1-1 and may be described as:

1-2 Compression (compressor process)
2-3 Heat addition
3-4 Expansion (turbine process)
4-1 Heat rejection (exhaust system)

The processes shown in Figure 6.1.1-1 are considered ideal because there is no accounting for the efficiency of the processes. An ideal compression process occurs isentropicly, i.e., reversible adiabatic. Also, the pressure ratio across the compressor equals the pressure ratio across the turbine. The ideal cycle assumes no pressure loss while adding heat, i.e., the

pressure at Station 3 equals the pressure at Station 2. With these in mind, the equations which may be used for the ideal Brayton cycle are as follows.

1) Pressure ratio of the cycle

$$r_p = \frac{P_{t_2}}{P_{t_1}} \qquad (6.1.1\text{-}1)$$

2) Overall cycle temperature ratio

$$Z = \frac{T_{t_3}}{T_{t_1}} \qquad (6.1.1\text{-}2)$$

where: T_{t_3} = turbine inlet temperature

T_{t_1} = compressor inlet temperature

3) Ideal work of the compressor per pound of working fluid

$$W_c = c_p (T_{t_2} - T_{t_1})$$

$$W_c = c_p T_{t_1} (r_p^{\,k} - 1) \qquad (6.1.1\text{-}3)$$

where $k = (\gamma - 1)/\gamma$

4) Heat supplied per pound

$$q = c_p (T_{t_3} - T_{t_2}) \qquad (6.1.1\text{-}4)$$

5) Ideal turbine work per pound

$$W_t = c_p T_{t_3} \left(1 - \frac{1}{r_p^{\,k}} \right) \qquad (6.1.1\text{-}5)$$

6) Net work or useful work

$$W_n = W_t - W_c$$

$$W_n = c_p (T_{t_3} - T_{t_2}) \left(1 - \frac{1}{r_p^{\,k}}\right) \qquad (6.1.1\text{-}6)$$

7) Thermal efficiency for ideal engine

$$\eta_{thi} = 1 - \left(\frac{1}{r_p^{\,k}}\right) \tag{6.1.1-7}$$

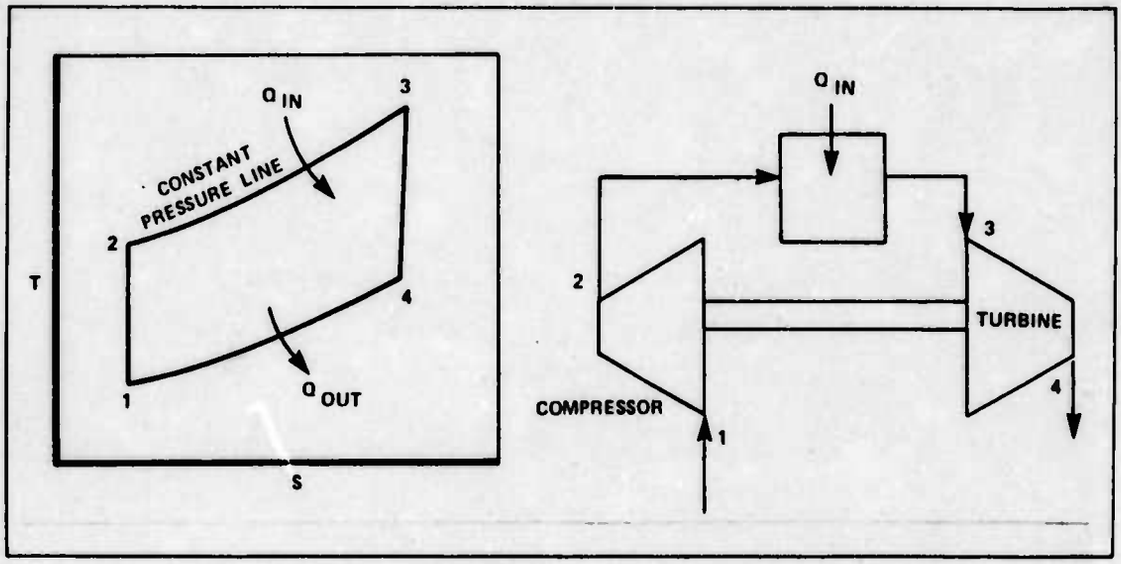

Figure 6.1.1-1. T-S Diagram of Ideal Brayton Cycle

Since optimum pressure ratios and cycle temperatures for maximum net work and thermal efficiency were desired, Eqs. 6.1.1-1 through 6.1.1-8 were used in maximizing net work and thermal efficiency by taking the derivatives of each with respect to pressure ratio and temperatures and setting the result equal to zero. The complete derivation is shown in Appendix 6.2. The results are given by Eqs. 6.1.1-9 through 6.1.1-12.

8) Net work for a non-ideal cycle

$$W_t = c_p\, T_{t_3}\, \eta_t \left(1 - \frac{1}{r_p^{\,k}}\right)$$

$$W_n = c_p\, T_{t_3}\, \eta_t \left(1 - \frac{1}{r_p^{\,k}}\right) - \frac{c_p\, T_{t_1}}{\eta_c}\left(r_p^{\,k} - 1\right) \tag{6.1.1-8}$$

9) Optimum pressure ratio for max net work (non-ideal cycle)

$$r_{pw} = (Z\, \eta_t\, \eta_c)^{\frac{1}{2k}} \tag{6.1.1-9}$$

10) Compressor outlet temperature for maximum net work given T_{t_1} and T_{t_3}

$$T_{t_2} = (T_{t_1} T_{t_3})^{1/2} \qquad (6.1.1\text{-}10)$$

11) Optimum pressure ratio corresponding to maximum efficiency

$$r_{p\,\eta\,max} = \left(\frac{b - \sqrt{b^2 - 4ac}}{2a} \right)^{\frac{1}{2k}} \qquad (6.1.1\text{-}11)$$

where:

$$a = (\eta_t - 1) Z + 1$$

$$b = 2\eta + Z$$

$$c = [\,(1 - \eta_c)\eta_t + \eta_c \eta_t Z\,]\, Z$$

12) Thermal efficiency with compressor and turbine efficiency

$$\eta_{th} = \frac{\eta_t Z \left(1 - \frac{1}{X}\right) - \frac{1}{\eta_c} (X - 1)}{Z - \left(\frac{X-1}{\eta_c} + 1\right)} \qquad (6.1.1\text{-}12)$$

where:

$$X = r_p^{\,k}$$

To give the reader a better understanding of the relationship between the T-S diagram and the actual engine, Figure 6.1.1-2 illustrates both, with the stations on each identically numbered. A general comparison will be given by explaining the working process as it moves simultaneously through each illustration. This will be followed by a description of each station along with the essential equations and their results.

The pressure rise from 1 to 2 is a result of ram pressure rise. The fan compresses the total air flow, 2 to 2.5. The compressor further compresses the core (gas generator) air from 2.5 to 3. Heat is added between 3 and 4, at approximately constant pressure. The high temperature, high pressure gas is expanded over the turbine which produces work required by the fan and compressor. The nozzle converts the remaining enthalpy energy of the core gas flow and the enthalpy energy of the bypass into thrust. Station e will correspond to station ef if subcritical nozzle flow exists.

For the study of a turbofan engine studied in this section, the stations corresponding to Figure 6.1.1-2 are:

1) Station 1 — defined by altitude conditions at 30,000 ft; $T_{t_1} = 412°R$, $P_{t_1} = 629.7$ psf.

2) Station 2 — From Hesse and Mumford (Ref. 69, p. 103), an inlet recovery factor was obtained from Figure 5.3 for temperature and pressure such that $T_{t_2} = 442°R$ and $P_{t_2} = 722.9$ psf.

3) Station 3 — The compressor outlet temperature T_{t_3} = 1060°R. The compression ratio needed to arrive at this temperature will consist of that produced by the fan (Station 2 to 2.5) coupled with the pressure ratio across the high pressure compressor (HPC) (Station 2.5 to 3). At this point the following assumptions were made: the turbine and compressor efficiencies (N_{t_1} N_C) were assumed to be, respectively, 0.9 and 0.88. These are present state-of-the-art figures considered reasonable by several authors including Hosney (Ref. 77), Robson (Ref. 149), Vincent (Ref. 186), and Hesse (Ref. 69). Allowing for the inefficiency of the compressor which will raise the compressor outlet temperature above that for an equivalent isentropic compression ratio, gives the required engine pressure ratio (at 30,000 ft) to be:

$$r_{p\ \text{required}} = 16.8$$

However, recalling Eq. 6.1.1-9 that the optimum pressure ratio for maximum net work:

$$r_{p\ wn\ max} = \left(\frac{T_{t_4}}{T_{t_1}} \eta_t \eta_c \right)^{\frac{1}{2k}}$$

$$r_{p\ wn\ max} = 10.19$$

where γ is the ratio of specific heat and at 1060°R = 1.4.

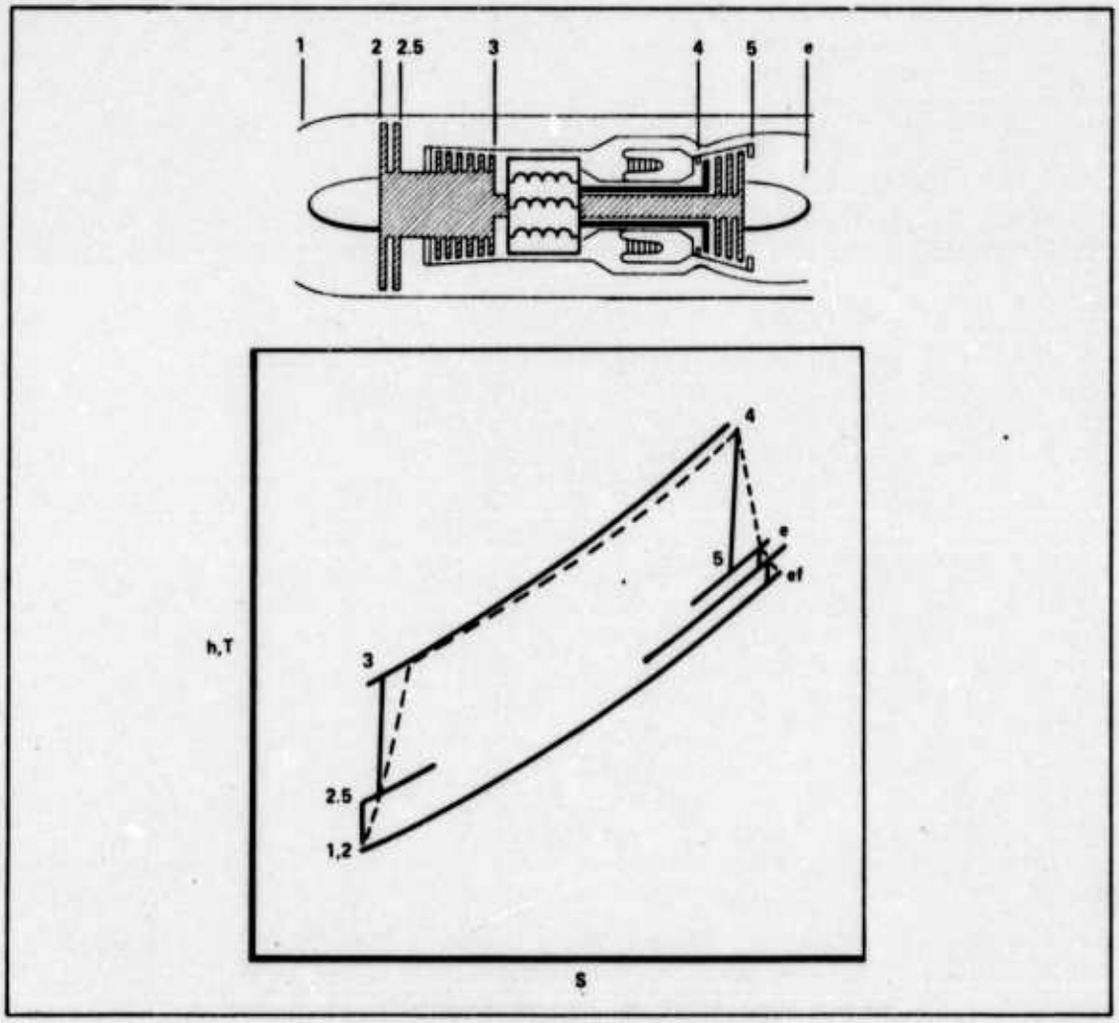

Figure 6.1.1-2. T-S Diagram of Brayton Cycle for Turbofan Engine

Which says the engine is operating approximately 65% above optimum pressure ratio for maximum net work. Using Eq. 6.1.1-12, it may be seen that

$$\eta_{thi} = 0.55$$

for the actual case, i.e. where $R_p = 16.8$, but that

$$\eta_{th} = 0.48$$

for the case of optimum pressure ratio for maximum net work.

4) Station 4 — $T_{t_4} = 1960°R$. The temperature was established by the material limitations of the heat exchanger discussed in Section 6.0.

5) Station 5 — The temperature and pressure at the turbine exit are dependent upon pressure drop across the high pressure turbine and the pressure drop required across the fan turbine. From the procedures outlined in Hesse (Ref. 69, p. 265-272) the turbine exit temperature is calculated to be $T_{t_5} = 1288°R$ and the exit temperature = 1073°R. A sample calculation for the turbofan engine is presented in Appendix 6.4.

6.1.2 OVERALL ENGINE PRESSURE RATIO (R_p): The overall engine pressure ratio is made up by two components:

1) the fan pressure ratio R_{pfan}

2) high pressure compressor pressure ratio R_{pHPC}

It was pointed out in the previous section that the overall engine pressure ratio must be 16.8 at the cruise design point, which must be obtained through some combination of R_{pf} and R_{pc}. Presently high bypass ratio engines deliver 75-85% of their thrust by the fan and typical fan pressure ratios vary from 1.2 - 1.8. There are higher fan pressure ratios and a recent study by NASA for a fan pressure ratio of 2.8 may be found in Reference 144. For various size engines the fan pressure ratio was varied from 1.2 - 2.0. The high pressure compressor (HPC) pressure ratio was varied from 8.0 - 14.0, giving a range for overall pressure ratio of 9.6 to 28.0, in order to test the sensitivity of thrust to Rp. For a lower pressure ratio, the reactor must provide more energy, and for higher pressure ratios it must provide less heating energy per pound of flow. Figure 6.1.2-1 is an example of the analysis for bypass ratio $\beta = 4.0$. The cases for $\beta = 6.5$ & 8.0 may be found in Appendix 6.5. In this portion of the study, cases were also run where the fan tip would produce a higher pressure ratio than the fan hub. It was found that, for some cases, the net thrust was higher than if the fan were equally loaded throughout the span.

6.1.3 BYPASS RATIO (β): The bypass ratio is the rate of the amount of air passing through the bypass channel ($\dot{m}_\beta$) to that air which passes through the core of the engine ($\dot{m}_c$). Because the core flow is 200 lb/sec the total mass flow into the engine ($\dot{m}_{total}$) and must be varied simultaneously. These two parameters establish the size of the engine. For this analysis the bypass ratio was varied from 4.0 to 11.0 which gives a total mass flow variation of 1000 to 2400 lb air/sec. For each β the fan and HPC pressure ratios were varied with the results as pointed

out in Section 6.1.2. By using the thrust from Figure 6.1.2-1 and corresponding figures for different bypass ratios (See Appendix 6.5), an overall engine pressure ratio of 16.8, as determined in Section 6.1.1, Figure 6.1.3-1 was compiled. Thus, for a given fan pressure ratio an optimum engine can be obtained. For example, for a fan pressure ratio of 1.4 the maximum thrust would be 15,800 lbs with a corresponding bypass ratio of approximately 7.0 (Figure 6.1.3-1).

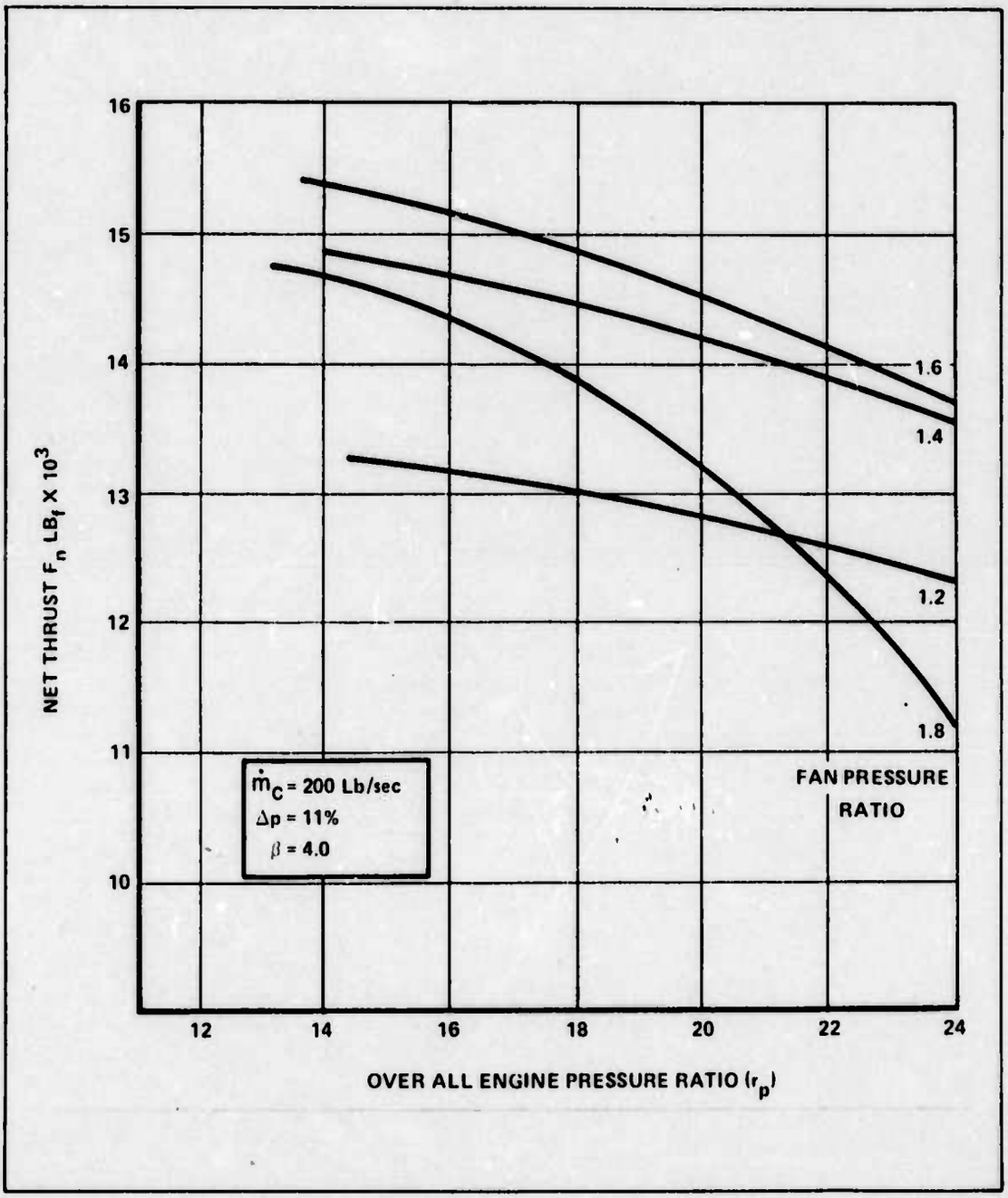

Figure 6.1.2-1. Comparison of Thrust for Various Overall Engine Pressure Ratios and Fan Pressure Ratio for Bypass Ratio = 4.0 and a Core Mass of 200 lb/sec

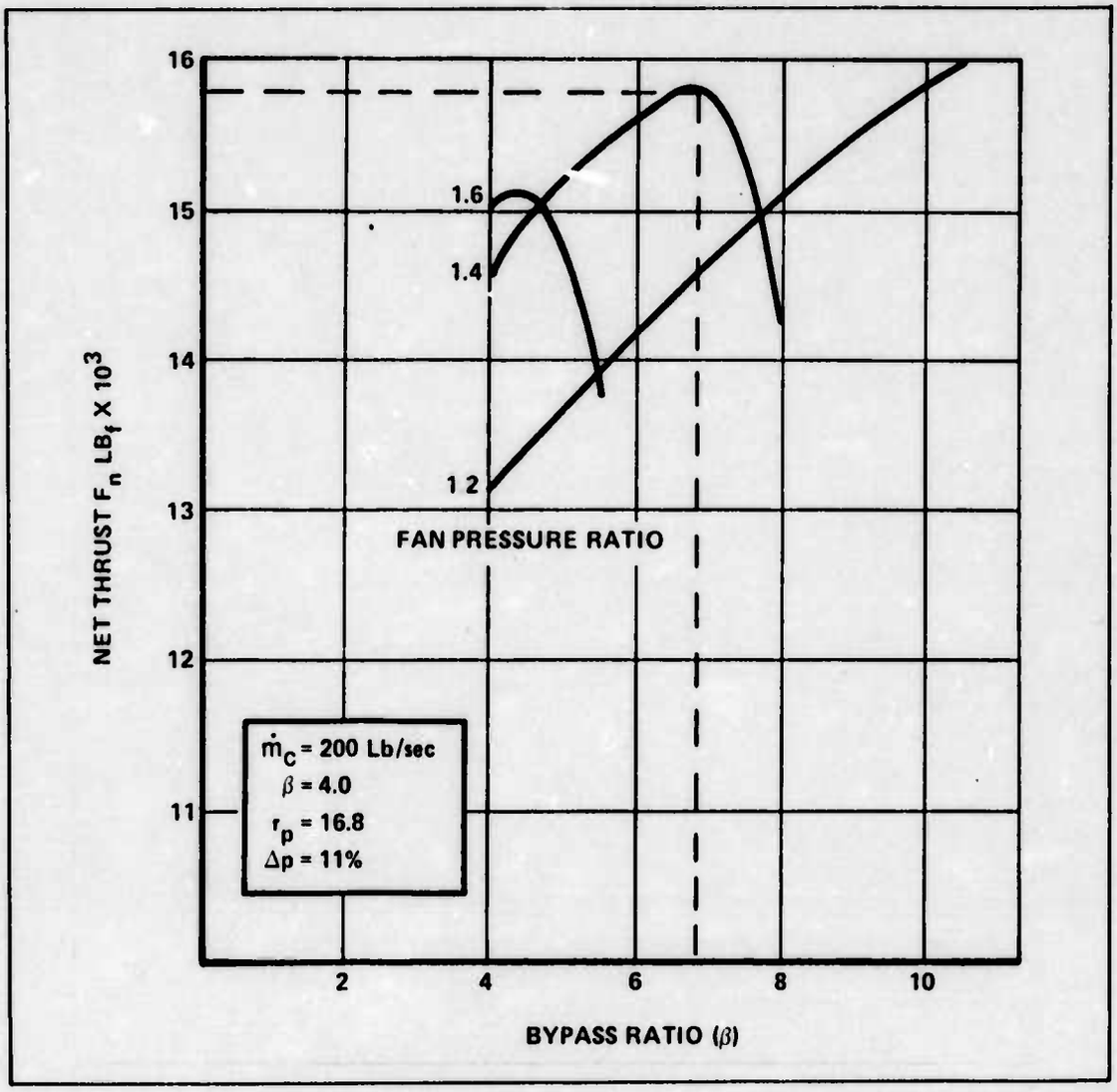

Figure 6.1.3-1. Comparison of Net Thrust for Various Bypass Ratios Having an Overall Engine Pressure Ratio = 16.8 and Core Mass Flow of Air = 200 lb/sec

6.1.4 HORSEPOWER REQUIREMENTS: The horsepower requirements for the system are divided into three main areas:

1) auxiliary power for the aircraft 100-300 hp/engine
2) power required to operate pumps located in the primary coolant loops, 4000 - 23,000 hp (liquid metal - helium gas)
3) power required to operate pumps in the secondary coolant loops, 150 - 1000 hp/engine (liquid metal - helium gas).

One of the reasons for the high horsepower requirements for the helium system is a result of high pressure losses encountered in the reactor and heat exchangers (Ref. 176). Section 7.5 discusses the working fluid circulation with respect to the heat transfer system. Two possible means of providing this pumping power are: (1) Extraction of horsepower off the engines; and (2) Use of a direct drive gas generator turbine-pump system.

Program CARPET (Ref. 192) was used to evaluate the relationship for horsepower extraction to drive the pumps to that of the net thrust produced. The analysis was performed for various bypass ratios and fan pressure ratios at design altitude and with an overall engine pressure ratio of 16.8. Figure 6.1.4-1 illustrates the effects of horsepower extraction for a bypass ratio (β) of 4.0. The data for β = 6.5 and 8.0 are located in Appendix A.6.5. Using 500 hp extraction as the requirement for a liquid metal heat exchanger turbofan engine, the net thrust for various bypass ratios at design altitude are presented in Figure 6.1.4-2. Using the same 1.4 fan pressure ratio example as used in Section 6.1.3, notice that the net thrust has now dropped to 14,100 lbs with a bypass ratio of 5.5.

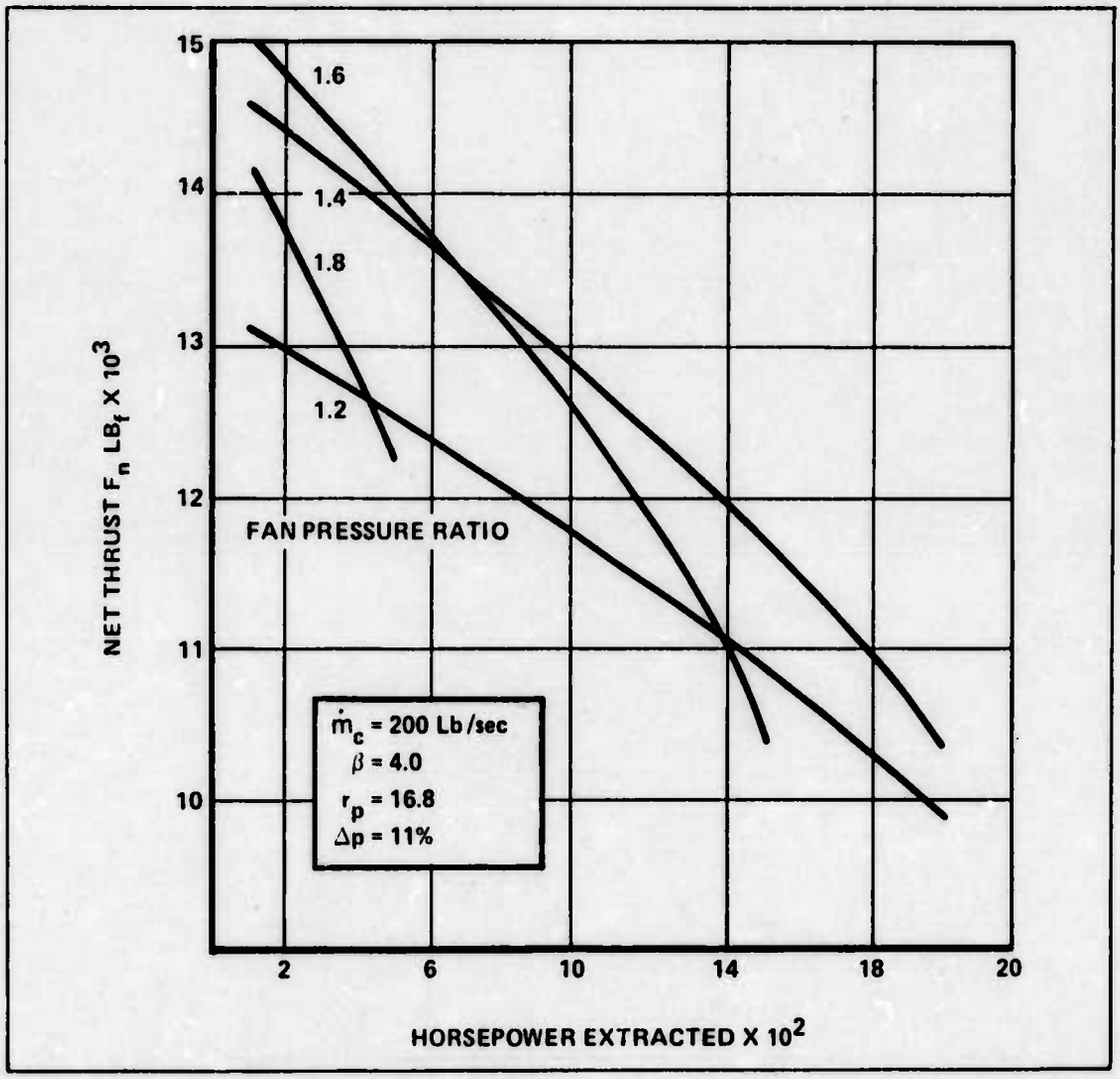

Figure 6.1.4-1. Net Thrust as a Function of Horsepower Extracted Off the Engine for Various Fan Pressure Ratios; Bypass Ratio = 4.0 with an Overall Engine Pressure Ratio of 16.8 and a Core Mass Flow of 200 lb/sec

The use of a direct drive turbine-pump system would alleviate the horsepower extraction requirement on the engines of the helium gas heat exchanger turbofan engine. This would allow a 20% to 24% increase in thrust. A detailed discussion of the turbine-pump system is presented in Section 6.2.8, along with alternative combinations of meeting horsepower requirements.

6.1.5 PRESSURE LOSSES ($\triangle P$): It was found that the pressure losses of air increased significantly as the mass flow got above 200 lb air/sec. (This is discussed further in Section 7.) The pressure loss through the heat exchanger is estimated as approximately 6% (Section 7.1.12). If the dual mode concept is used, then there will be an additional pressure loss (Refs. 77, p. 253; 47), due to the combustor region, in the order of 4 to 6%. For this analysis, 6% pressure loss was assumed for a dedicated nuclear engine and 11% pressure loss was assumed for the dual mode engine. Figure 6.1.5-1 presents an example of the effects of pressure loss for β = 4.0 and fan pressure ratio = 1.6. For this particular engine the loss in thrust is approximately 86 lbs per percent increase in pressure loss.

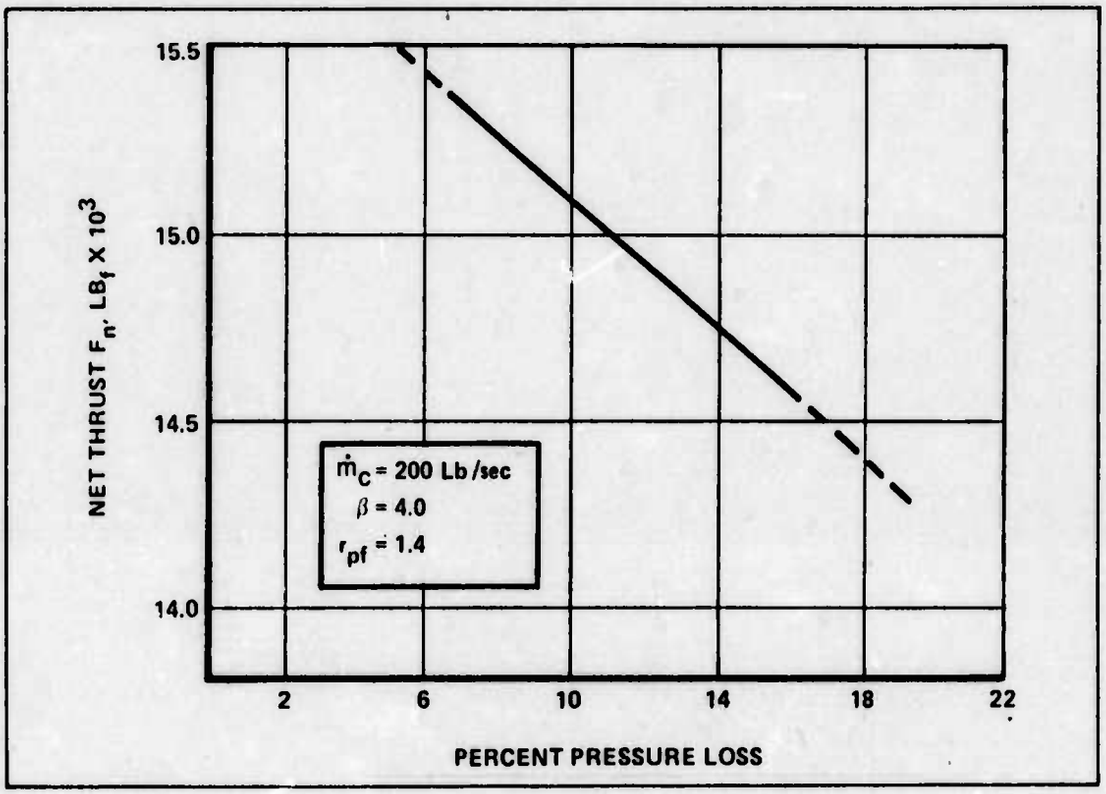

Figure 6.1.5-1. Pressure Loss Effects of Net Thrust Where Bypass Ratio = 4.0, Overall Engine Pressure Ratio = 16.8, Fan Pressure Ratio = 1.6, and Core Mass Flow is 200 lb/sec

6.1.6 CORE MASS FLOW ($\dot{m}_c$): Variations in core mass flow can greatly affect the net thrust. There are two reasons for this. One is because the increase in core flow increases the amount of net work available to drive the fan, as may be seen from Eq. 6.1.1-8:

$$W_n = \dot{m}_c c_p \left[T_{t_4} \eta_t \left(1 - \frac{1}{X_t}\right) - \frac{T_{t_1}}{\eta_c} (X_c - 1) \right]$$

Second, it contributes directly to the net thrust equation as an increase of the core mass flow which is exiting at a high velocity (See Appendix 6.4).

One case was evaluated where the total mass flow was 1000 lb air/sec. Figure 6.1.6-1 compares the cases for m_{c_1} = 200 lb air/sec and m_{c_2} = 250 lb air/sec where the pressure loss for both engines was 11%. Figure 6.1.6-2 shows how this engine can easily handle horsepower

requirements at 11% △P. Figure 6.1.6-3 depicts the effect of pressure loss increases for a higher mass flow engine.

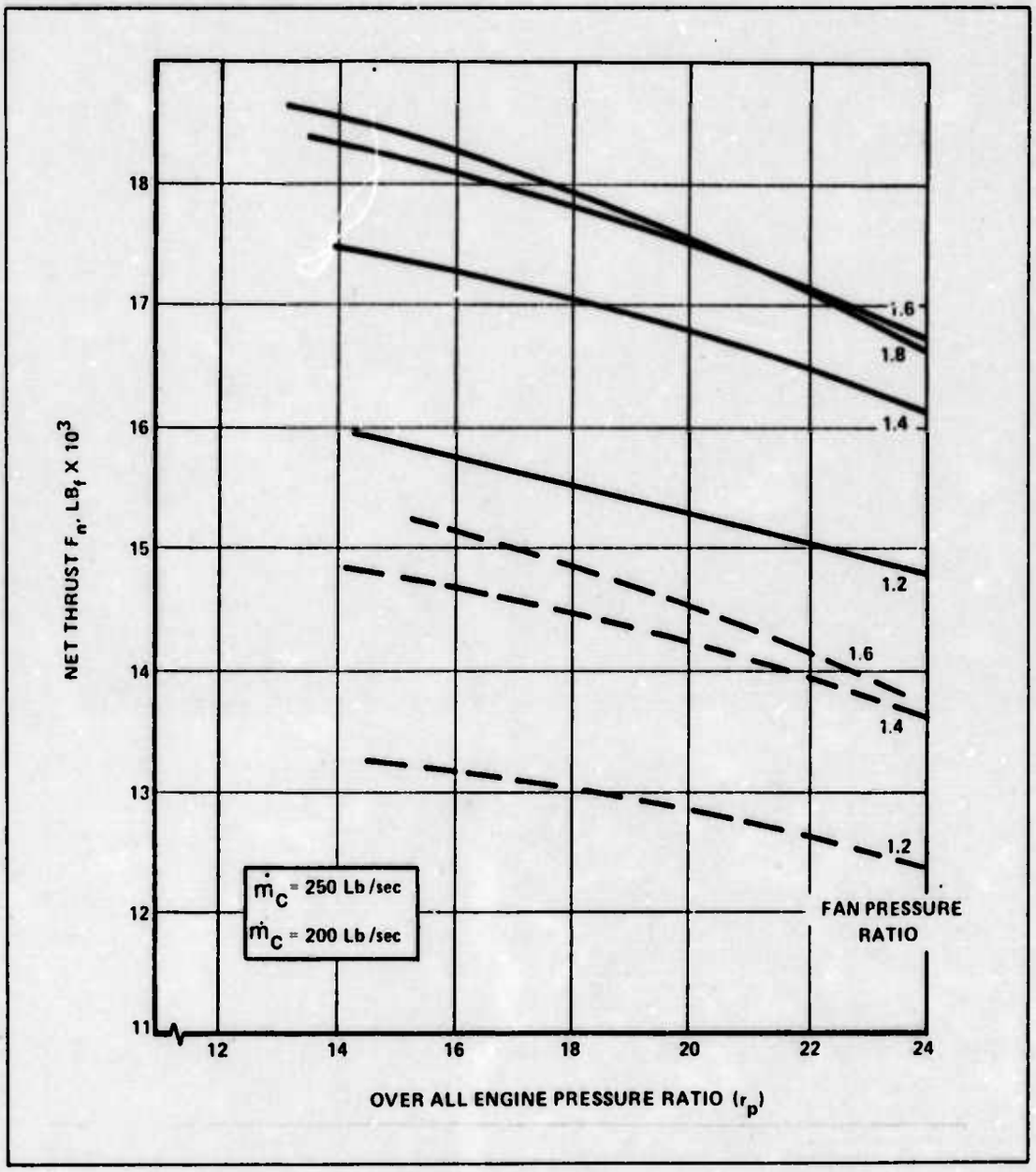

Figure 6.1.6-1. Comparison of Increased Mass Flow of Air Through the Core on Net Thrust for Various Fan Loading and Overall Engine Pressure Ratios, with Bypass Ratio = 4.0

The CF6-50 or the JT9D-7 engines are presently designed to handle a mass flow of approximately 110 to 150 lb air/sec at 30,000 ft (Refs. 171 and 60). This points out one disadvantage of increasing the mass flow to 250 lb air/sec, in that the core size would have to be 1.67 to 2.3 times today's largest engine core.

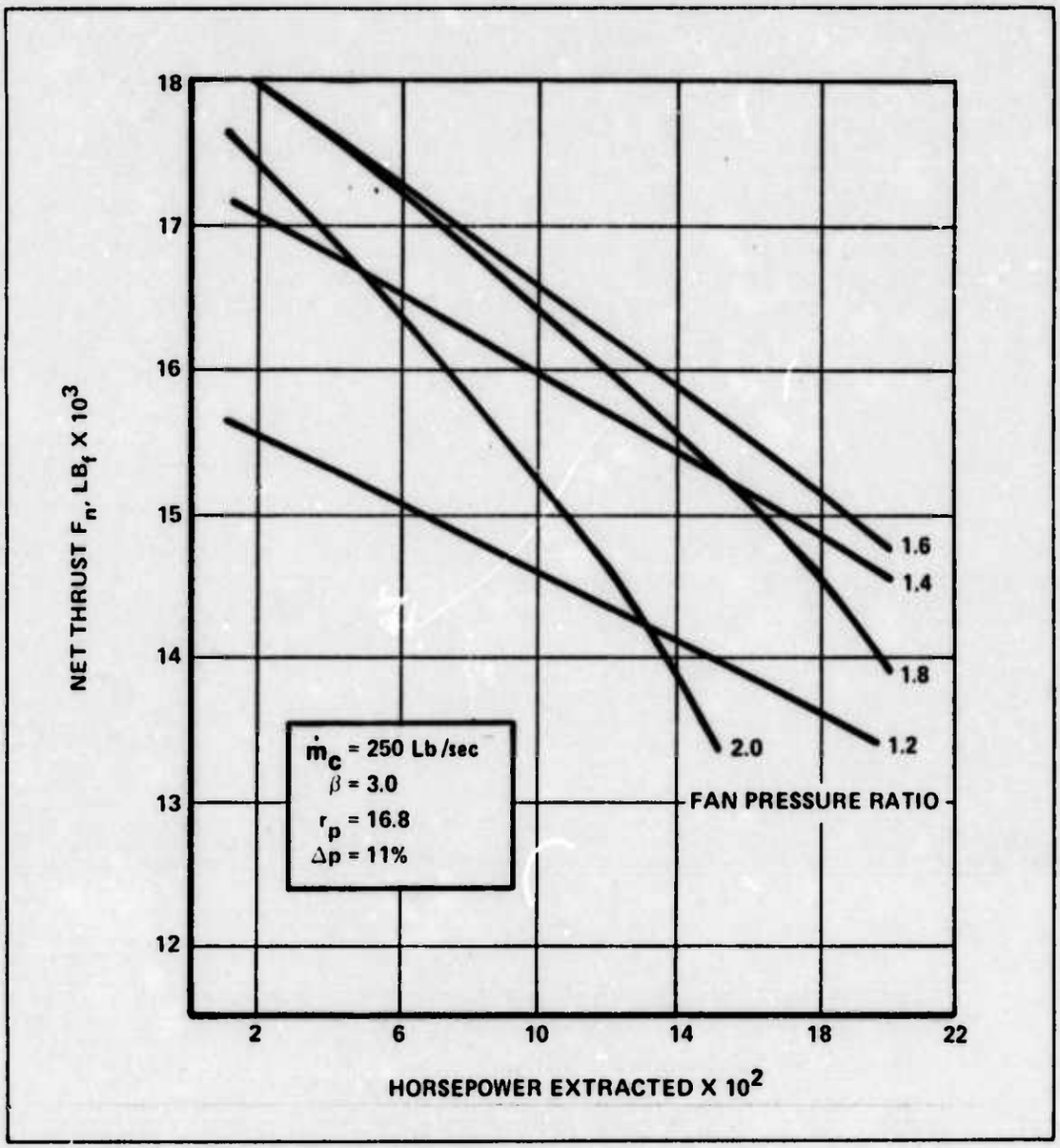

Figure 6.1.6-2. Effect of Horsepower Extraction on Net Thrust Where Bypass Ratio = 3.0, Core Mass Flow is 250 lb/sec, and Overall Engine Pressure Ratio is 16.8

6.1.7 TURBINE (T_{t_4}) AND BYPASS STREAM (T_{ef}) TEMPERATURES: It can be seen from Eq. 6.1.1-5 that turbine work is proportional to the turbine inlet temperature, T_{t_4}. Similarly, Eq. 6.1.1-8 shows that the net work is equal to the turbine work minus the compressor work. Thus, increasing the turbine inlet temperature will have a proportionate effect on the amount of net work available and, thus, the thrust. With this thought in mind, a sensitivity analysis was performed to show the variation in the net thrust for an increase or decrease in turbine inlet temperature. The results of the analysis for one particular engine are presented in Figure 6.1.7-1. However, there are no projections for increasing the turbine inlet temperature above the 1960°R for a heat exchanger engine. To put these temperatures in perspective to JP-4 engines, the CF6-50C has a turbine inlet temperature of 2410°R (Ref. 60, p. 14).

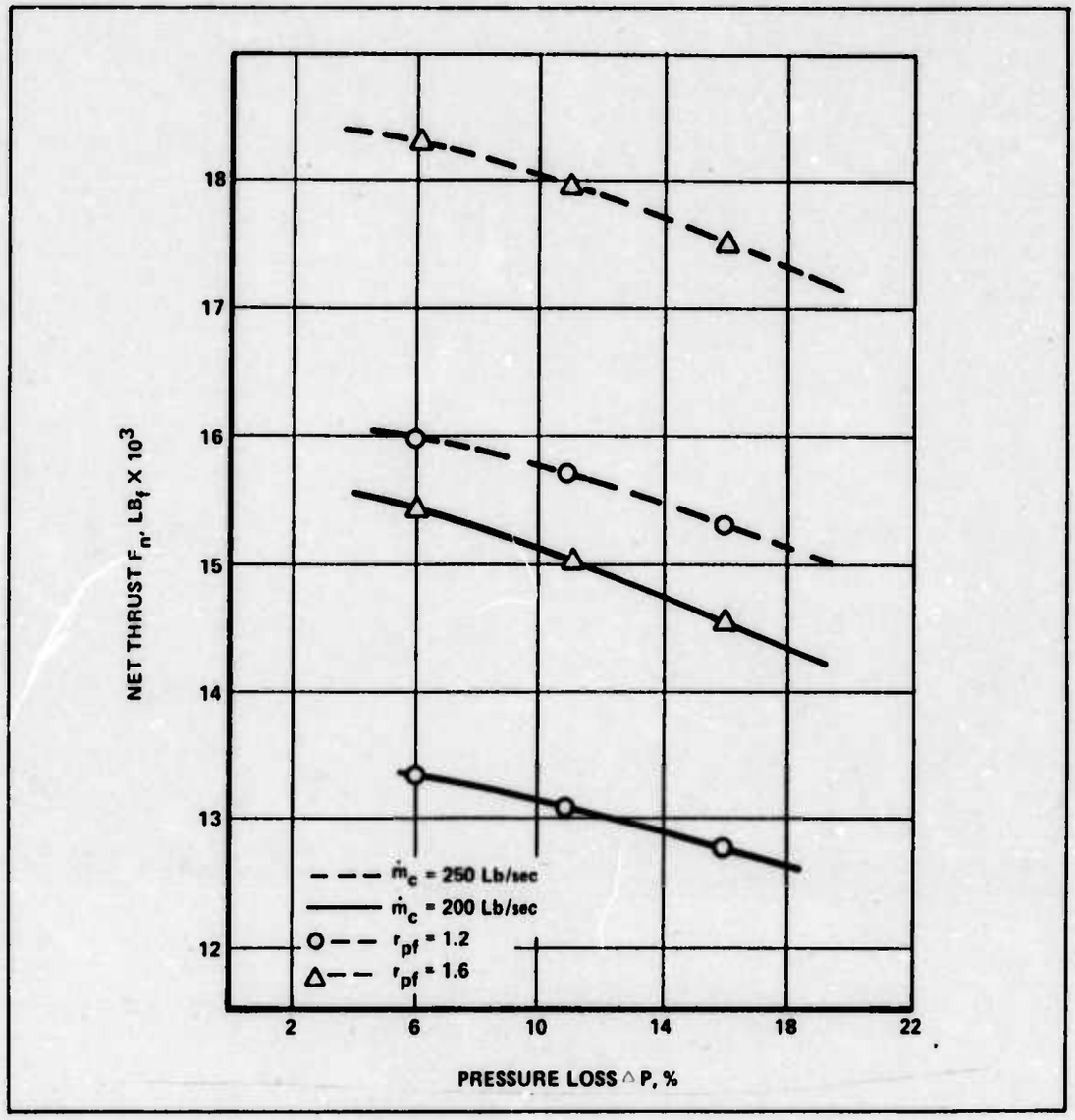

Figure 6.1.6-3. Pressure Loss Effects on High Core Mass Flow Engine Thrust with Overall Engine Pressure Ratio = 16.8, Bypass Ratio = 3.0 ($\dot{m}_c$ = 250 lb/sec), 4.0 ($\dot{m}_c$ = 200 lb/sec)

A preliminary investigation was performed in terms of a cycle analysis with respect to heating the air stream in the bypass. The temperature was increased from 2 to 32%, depending on the base temperature which is established by the fan pressure ratio. These percentage increases gave an exit temperature range of 520 to 620°R. The pressure loss was assumed for this analysis to be on the order of 5 to 10%. Figure 6.1.7-2 shows the interrelationship between percent change in net thrust and percent change in bypass air temperature (Tef) for two bypass ratios and fan pressure ratios. It can be seen from this figure that a larger percent heat addition is required than the percent of pressure drop in the system. The higher the fan pressure ratio, the less heat addition required to get an increase in thrust. Regarding bypass ratio (β), Figure 6.7.1-2 shows that as β increases, a larger percent increase in net thrust is obtainable for the same percent increases in bypass air temperature; however, it must be kept

in mind that any energy put into the bypass air will require the reactor to be larger so long as T_{t_4} is to remain constant at 1960°R. In order to add this energy, it may be required to build heavy, bulky heat exchangers which might increase the pressure drop in the bypass stream above 5%.

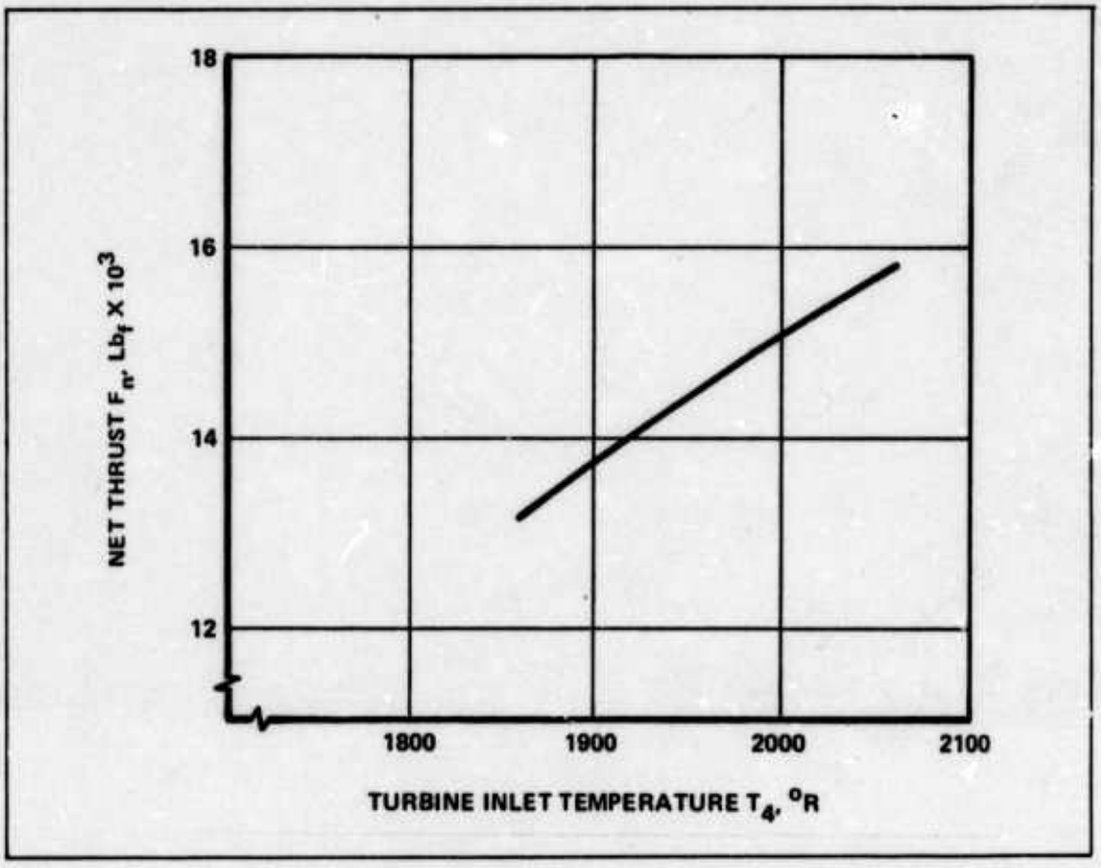

Figure 6.1.7-1. Turbine Inlet Temperature Effects on Thrust Where Bypass Ratio = 4.0, Fan Pressure Ratio = 1.4, and Overall Engine Pressure Ratio is 16.8

6.1.8 ENGINE SIZING: One of the relationships used in sizing an engine is the ratio of weight flow to unit frontal area:

$$\frac{\dot{m}\sqrt{\theta}}{A_F\,\delta}$$

where θ and δ are correction factors for the temperature and pressure differences between a given station x and sea level static conditions. They are given by θ equals temperature at station x divided by standard day sea level temperature and δ equals the pressure at station x divided by the standard day sea level pressure. Johnson, in NASA SP-36 (Ref. 85, p. 22b), derives an equation for this ratio which relates it to Mach number. Figure 6.1.8-1 is taken from Johnson's study.

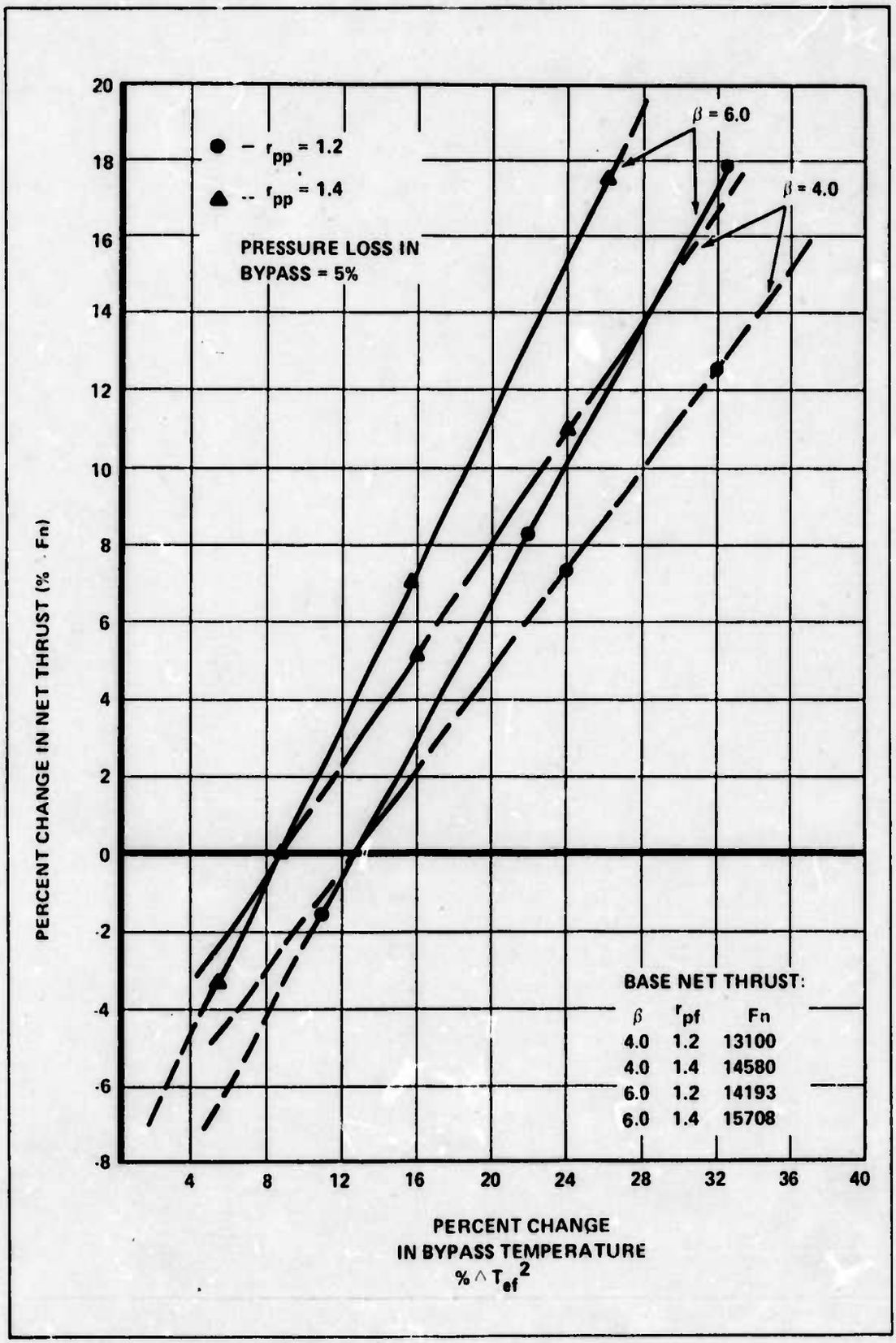

Figure 6.1.7-2. Bypass Heat Addition

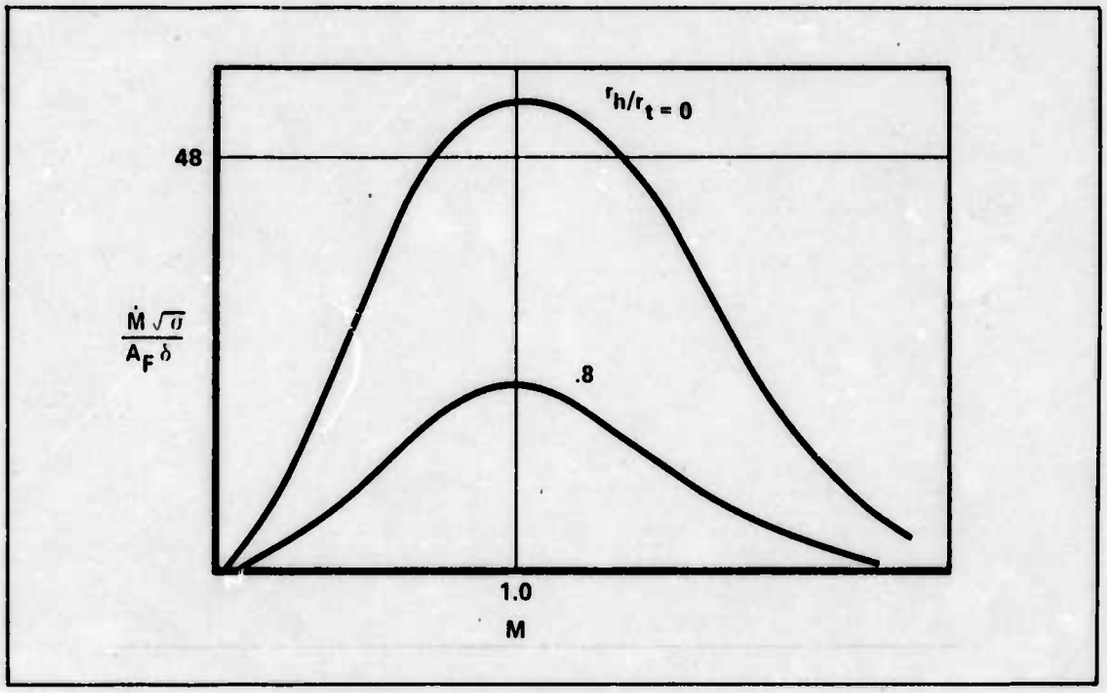

Figure 6.1.8-1. Mass Flow per Unit Frontal Area as a Function of Mach Number and Hub-Tip Radius

Using data from Keenan and Kayes (Ref. 88) for temperatures and pressures and at 30,000 ft, Mach = 0.6, the following calculations were made:

$$P/P_t = 0.784 \qquad T/T_t = 0.9328 \qquad P = 629 \text{ lb/ft}^2 \qquad T = 412^\circ R$$

$$\delta = \frac{\frac{629}{0.784}}{2.110} = 0.38 \qquad \sqrt{\theta} = \left(\frac{\frac{412}{0.9320}}{519} \right)^{1/2} = 0.92$$

1) Inlet: $r_h/r_t = 0.0$

$$A_I = \frac{\dot{m}\sqrt{\delta}}{42.8} = 0.0576\,\dot{m} \qquad (6.1.8\text{-}1)$$

2) Fan: assume $r_h/r_t = 0.4$ and $M = 0.3$ at the fan. And assuming 100% recovery and using isentropic relationships

$$\delta = 0.53 \qquad \sqrt{\theta} = 0.933$$

$$A_F = \frac{\dot{m}\,(0.933)}{0.53\,(22)} = 0.0799\,\dot{m} \qquad (6.1.8\text{-}2)$$

3) Compressor: using $M = 0.4$ and $r_h/r_t = 0.4$

$$\frac{W\sqrt{\theta}}{A\,\delta} \simeq 27$$

gives

$$A_c = 116\ \dot{m}_c \qquad (6.1.8\text{-}3)$$

4) Turbine: assume $r_h/r_t = 0.6$ and $M = 0.6$

$$\frac{A_{Ft}}{A_{Ft}} = \frac{\left(\frac{\dot{m}\sqrt{\theta}}{A_f \delta}\right)_c}{\left(\frac{\dot{m}\sqrt{\theta}}{A_f \delta}\right)} \frac{1}{\frac{P_c}{P_t}\frac{T_t}{T_c}} \Rightarrow \frac{A_{Ft}}{A_{Fc}} = \frac{27}{26}\ \frac{1}{2.15} = 48 \Rightarrow A_{Ft} = 0.056\ \dot{m}_c \qquad (6.1.8\text{-}4)$$

The mass flow of the engine core for the turbofan engine with a bypass ratio (β) is given by

$$\dot{m}_c = \frac{\dot{m}_{TOTAL}}{1 + \beta}$$

Figure 6.1.8-2 shows the effect of increasing the total mass flow of air through the fan on the diameter. For the set amount of 200 lb air/sec through the core, then:

1) area of the compressor face = 23.2 sq ft or 5.43 ft diameter
2) area of the turbine face = 11.2 sq ft or 3.78 ft diameter

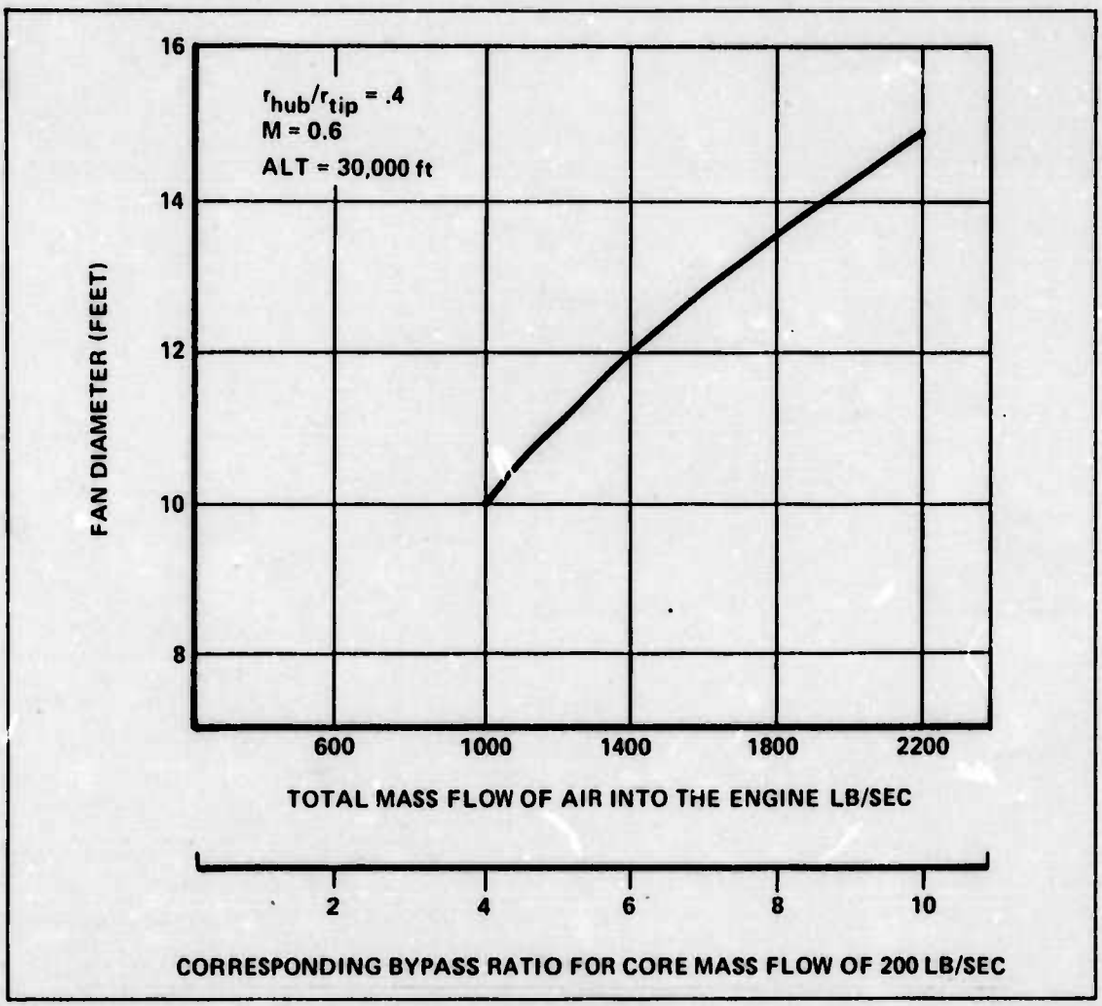

Figure 6.1.8-2. Functional Relationship Between Mass Flow and Fan Diameter

The weight estimate of the turbofan engine is based on a least squares fit on 27 types of turbofan engines. The engines were those of Pratt and Whitney and General Electric, with and without afterburners (AB). The least squares fit of the data are presented in Figure 6.1.8-3. The equation for that line is

$$\text{engine weight} = \exp\left[\frac{\ln(\text{engine SLS thrust}) + 0.889}{1.295}\right] \qquad (6.1.8\text{-}5)$$

Note: the engine thrust is the rated sea level static thrust of the engine. Instead of using the equation to estimate the weight a good first approximation would be to use a 5.5:1 thrust to weight ratio for high bypass, ($\beta \geq 4.0$), high thrust (FN ≥ 30,000) turbofan engines. For smaller engines a first approximation would be 4.5:1. These estimates do not include thrust reversers, which on the CF6-50 engine weight approximately 2000 lbs (Ref. 60, p. 26).

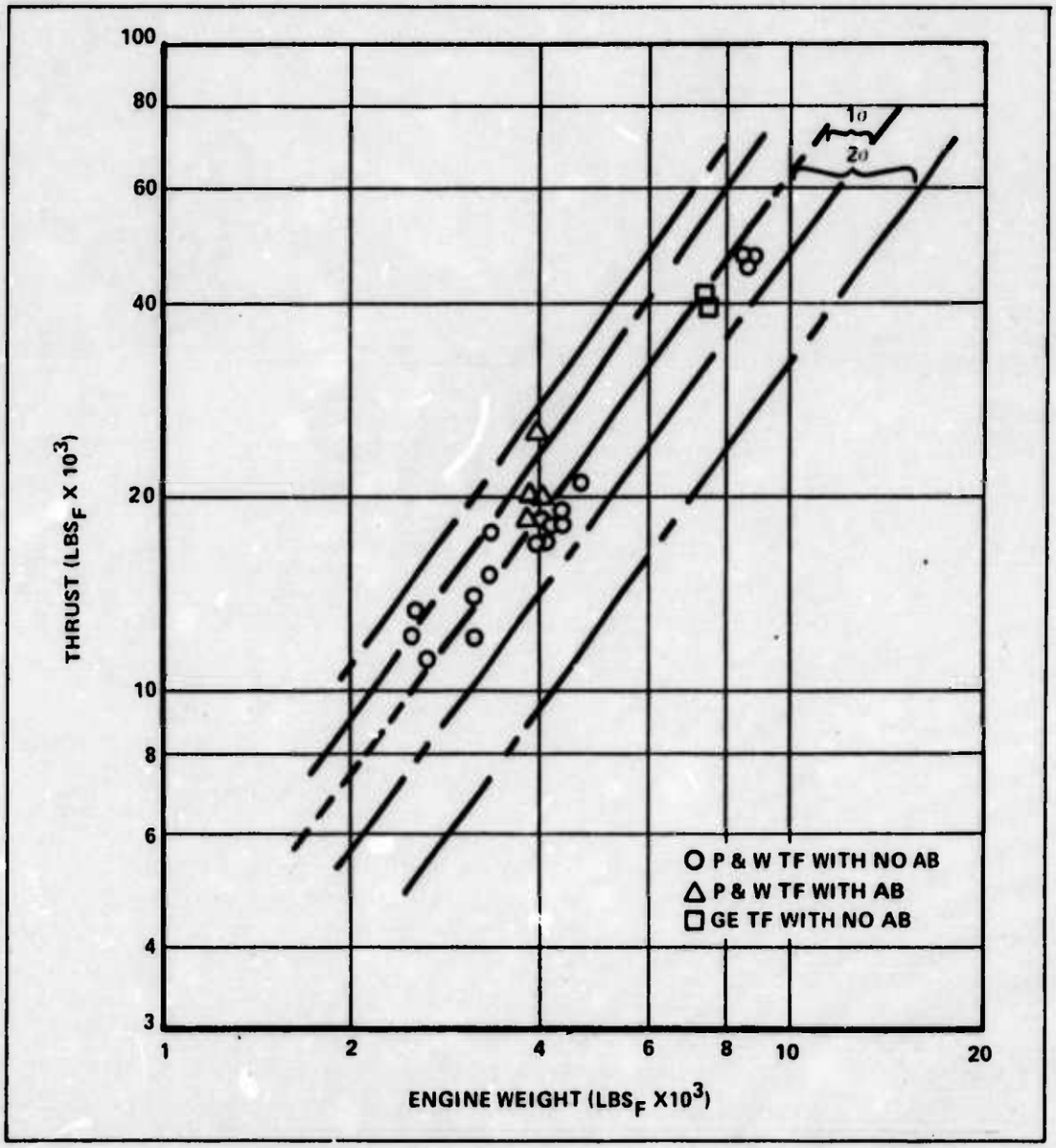

Figure 6.1.8-3. Sea Level Static Thrust to Weight Relationship

For the engine in this study, the derived equation was used to estimate the basic weight of the engine, not including the heat exchanger or thrust reversers. In estimating the weight of the dedicated nuclear engine, approximately 5% of the basic weight is taken off to account for the combustor weight (Ref. 47). The thrust used in the equation is based on the estimated thrust that an equivalent JP-4 engine at sea level could produce. For the engine with a bypass ratio = 4.0 and a total mass flow of 2600 lb/sec air at sea level, the estimated thrust for a JP-4 engine of the same size is approximately 100,000 lb. This gives the base engine weight used in this study as 14,400 lbs for a dual-mode engine.

6.1.9 OFF-DESIGN CONSIDERATIONS: The uniqueness of this problem cannot be overemphasized, in that a standard JP-4 engine can increase the working capability of its turbine to meet the increasing work requirements of the engine as the aircraft descends in altitude. It meets this requirement primarily by adding more fuel to increase the turbine inlet temperature (See Eq. 6.1.1-5). The increase in work requirement is a result of the increasing mass flow into the engine (as a result of increasing density) as well as increasing pressure and temperature at

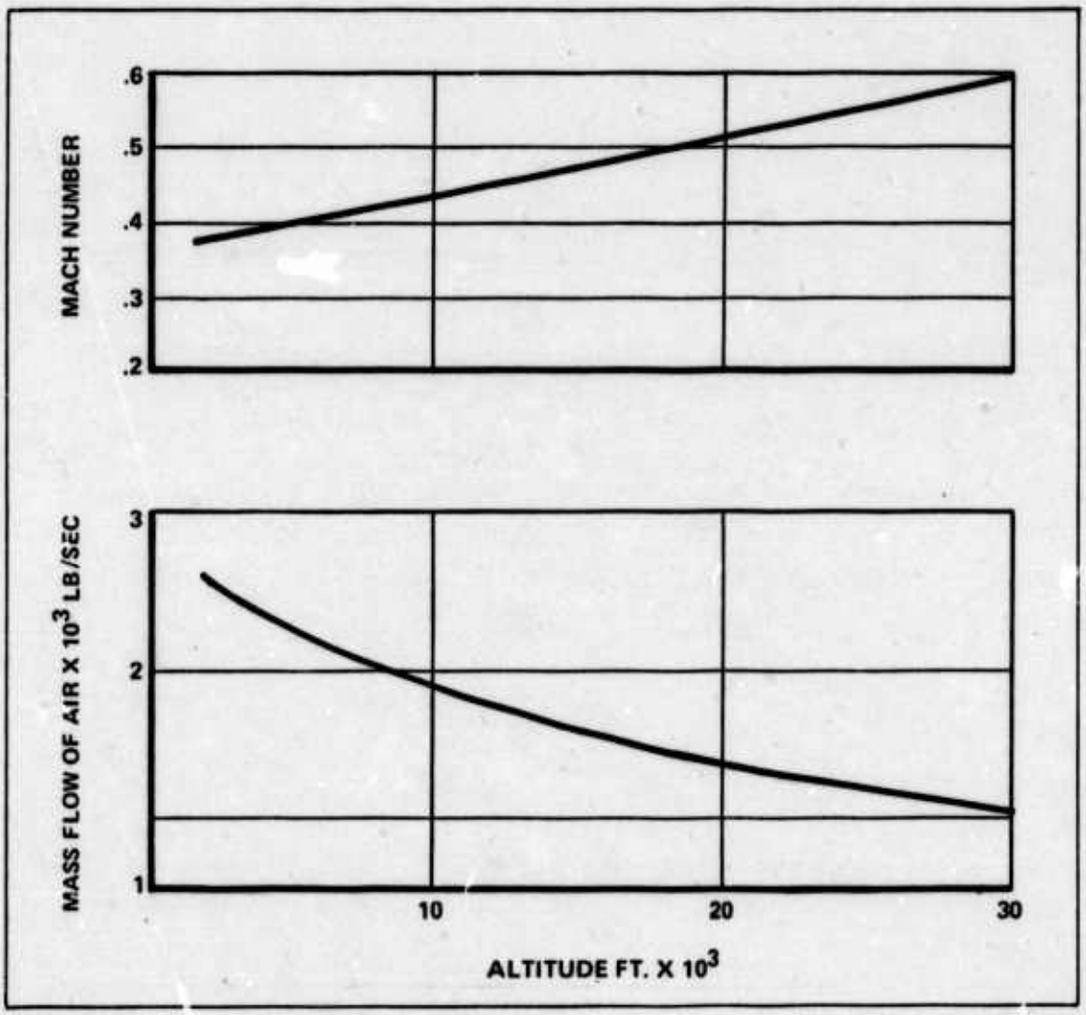

Figure 6.1.9-1. Mach Number and Inlet Air Mass Flow for Various Altitudes Based on Bypass Ratio = 4.0 at 30,000 ft and Core Mass Flow of 200 lb/sec

the inlet. The work increase can be seen by considering Eqs. 6.1.1-3 and 6.1.1-6. Eq. 6.1.1-6 can be also written as

$$W_c = \frac{\dot{m}_c\, c_p\, T_{t_2}}{\eta_c} \left[r_{pc}{}^{k} - 1 \right]$$

$$W_F = \frac{\dot{m}_f\, c_p\, T_{t_2}}{\eta_F} \left[r_{pf}{}^{k} - 1 \right] \qquad (6.1.1\text{-}6[a])$$

However, for the nuclear engine, the working medium is limited because of pressure losses and energy input limitations. For the nuclear engine, the fan work, given by Eq. 6.2.1-6, increases by decreasing altitude as the mass flow has doubled by the time you get to sea level, and the temperature T_{t_2} hasundergone a 30% increase as well. On the other hand, themass flow through the engine core is kept constant so the high pressure compressor (HPC) work

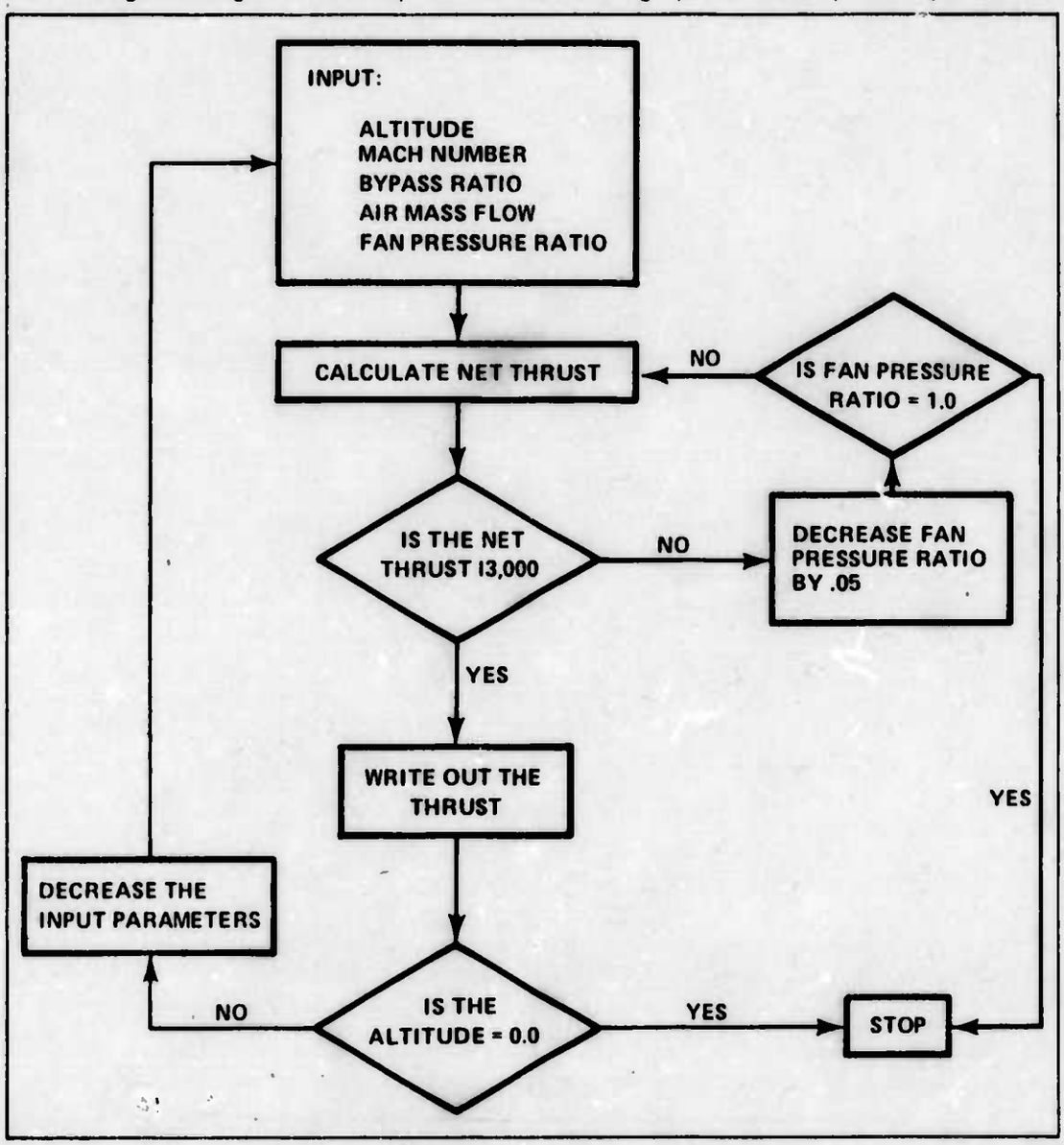

Figure 6.1.9-2. Off-Design Method of Analysis

remains approximately constant, exempting the effect of temperature. In the turbine however, as depicted by Eq. 6.1.1-5:

$$W_t = \dot{m}_c \, c_p \, T_{t_4} \left[1 - \frac{1}{r_p^{\,k}} \right]$$

$\dot{m}_c$ and T_{t_4} remain constant and thus the work available to the engine is constant. With this in mind and remembering that the program which was used, CARPET (Ref. 192), is a point design program, the following procedure was employed in the off-design analysis:

1) Corrected airflows for various altitudes were estimated as presented in Figure 6.1.9-1. The method used for inlet mass flow determination is the same as that presented in Engine Sizing. Figure 6.1.9-2 shows a block diagram of the process used where 13,000 lbs thrust was set as a minimum required net thrust/engine to keep the aircraft in the air. The data, as presented in Figure 6.1.9-3, show some thrust outputs for several altitudes. These are not optimum thrust values for each altitude but were generated only to establish some limits on engine requirements.

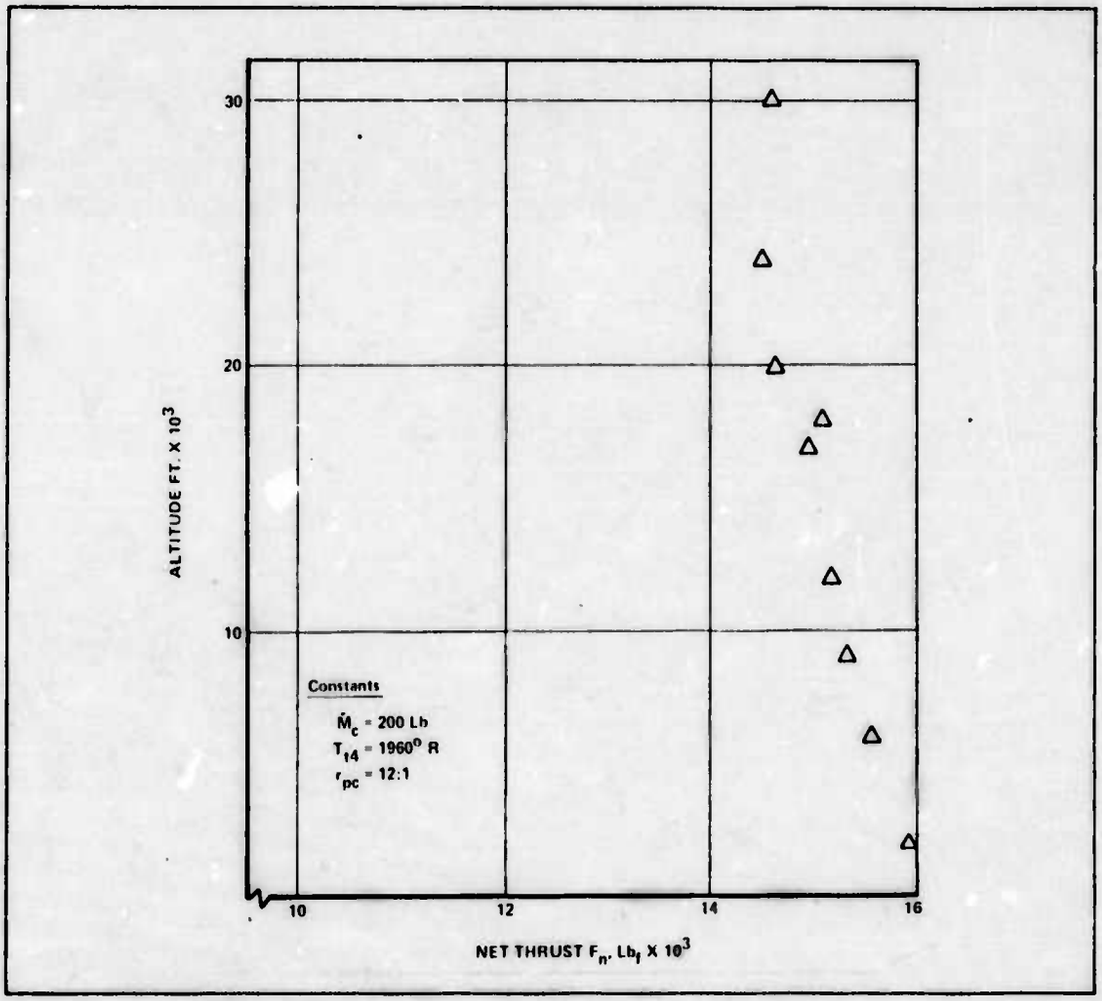

Figure 6.1.9-3. Thrust vs Altitude for Off-Design Analysis

It was found that the fan pressure ratio must vary from 1.4 to 1.15, i.e., it would require a variable pitch fan. The variable pitch fan on a high bypass high thrust engine has not been built but is presently under investigation by General Electric (Ref. 115). The bypass ratio must also vary from 4.0 to 11.0. The bypass ratio may actually be varied by a controllable core exhaust nozzle. Using engine sizing techniques it was estimated that the turbine nozzle diameter would have to vary by approximately 30% to change the bypass ratio as desired. Variable exit nozzles are used today, and a 30% variation is not beyond the capability of today's technology (Ref. 138).

6.1.10 RESULTS AND RECOMMENDATIONS: The interrelationship between the engine parameters studied in this section and their effects on net thrust are presented in Figure 6.1.10-1 and Figure 6.1.10-2 for the base engine which is defined by the following:

1) Total mass flow ($\dot{m}_{total}$), 1000 lb/sec
2) Bypass ratio (β), 4.0, this gives core mass flow ($\dot{m}_c$) of 200 lb/sec
3) Power extraction, 100 HP
4) Total pressure loss in engine core prior to turbine (ΔP), 11%
5) Turbine inlet temperature (T_{t_4}), 1960°R
6) Overall engine pressure ratio (r_p), 16.8:1
7) Fan pressure ratio (r_{pf}), 1.4:1
8) Net thrust (F_n), 14,580 lbs

These figures are representative relationships for larger bypass ratio engines which maintain a constant core mass flow ($\dot{m}_c$) of 200 lb air/sec, i.e., these figures illustrate general trends between engine parameters and net thrust.

Figure 6.1.10-1 presents two important observations. First, there is a fan pressure ratio for a given bypass ratio which predicts the maximum net thrust possible for that engine. For the base engine, this optimum fan pressure ratio is 1.6. Second, it emphasizes the importance of turbine inlet temperature as this parameter provides the largest percent increase in thrust for a given percent increase in a single parameter.

Figure 6.1.10-2 emphasizes three points. First, increasing horsepower extraction requirements for other than the fan reduces the net thrust significantly, and this relationship is sensitive to the fan pressure ratio. Second it should be pointed out that the curve for core mass flow is based on 11% pressure loss which implies that for $\dot{m}_c$ = 250 Lb/sec, it is strictly a dedicated nuclear engine (Section 6.1.6). In order to evaluate the increase in net thrust for increased mass flow the $\dot{m}_c$ = 200 Lb/sec and ΔP = 6% should be compared to $\dot{m}_c$ = 250 Lb/sec and ΔP = 11%. Using this argument the increase in net thrust is 15.5%. The third point is that decreasing the overall engine pressure ratio increases thrust at the expense of increasing reactor power requirements provided one is to maintain the turbine inlet temperature at 1960°R.

Table 6.1.10-2 summarizes the percent effects of these parameters for the base engine.

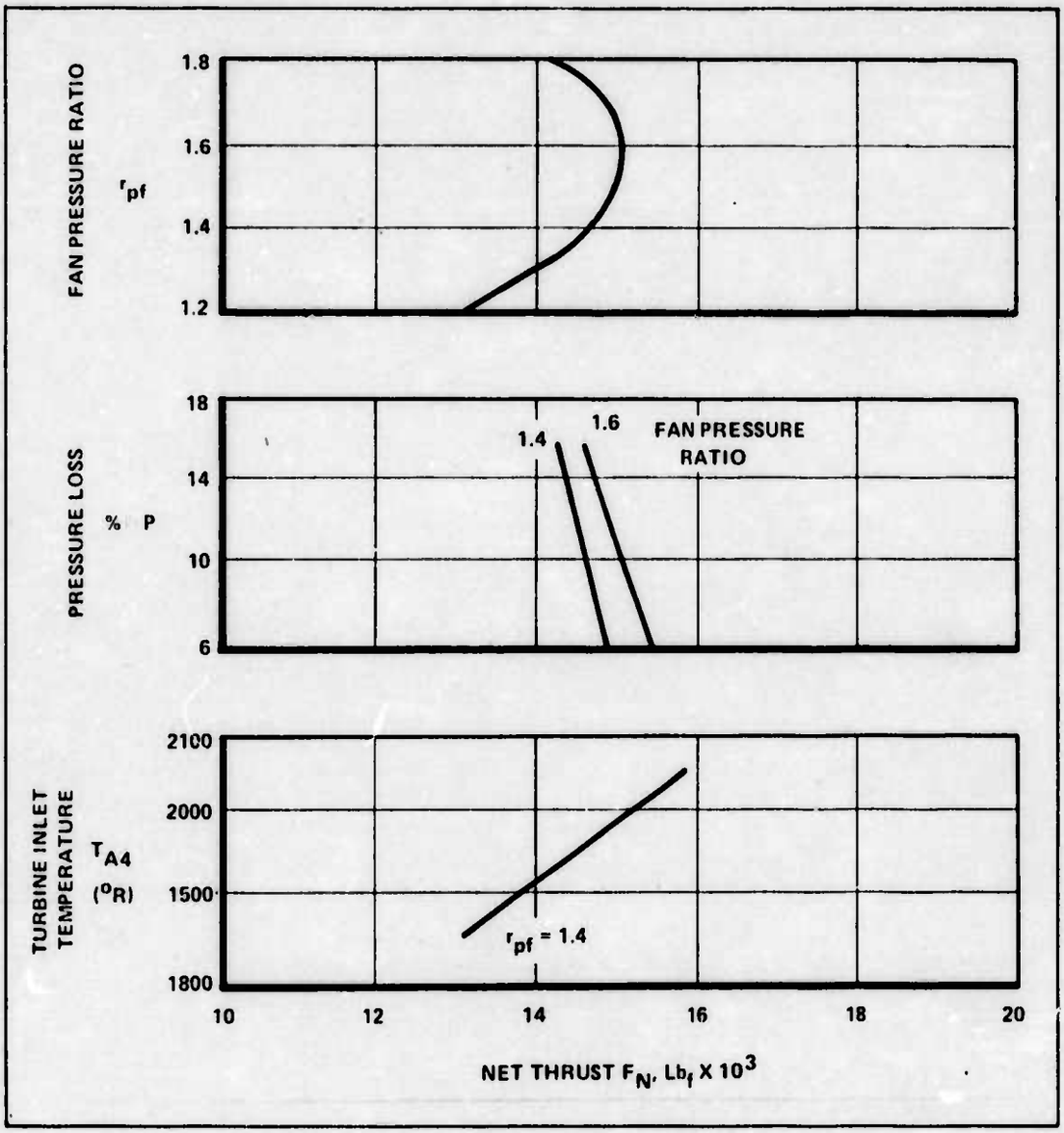

Figure 6.1.10-1. Effects of Three Engine Parameters on Net Thrust

The first design parameter set for the liquid metal system engine was the fan pressure ratio. From Figure 6.1.4-2, the reader can see that the 1.4 fan pressure ratio gives the highest thrust, 14,250 lbs. The maximum point of the curve also sets the bypass ratio at 5.5. Entering the graph in Figure 6.1.8-2 with the bypass ratio of 5.5 results in a fan diameter of 11.3 feet. Eq. 6.1.8-8 used with the thrust yields a basic weight of 14,000 lbs. The weight was scaled upward for an engine with a bypass ratio of 5.5 in the following manner:

Basic weight	14,400
-10% Cowling	1,440
Engine wt without Cowling:	12,960

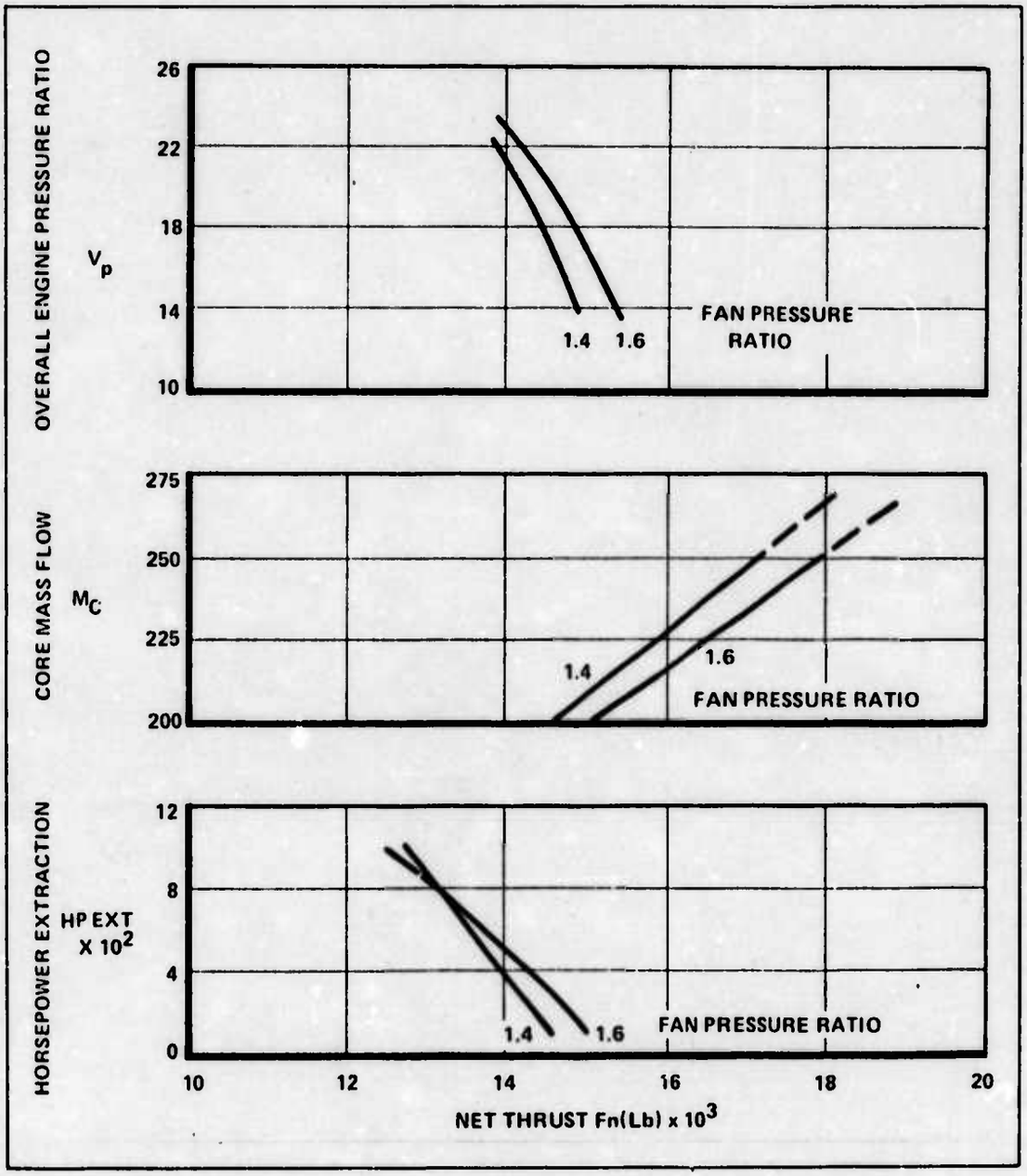

Figure 6.1.10-2. Effects of Three Engine Parameters on Net Thrust

Scale factor for cowling of 1.25 base on area ratio of 5.5 to 4.0 bypass ratio engines. New cowling weight = 1800 lbs. The scale factor for the fan = 1.11, which is based on ratio of fan diameters. This yields a fan weight of 1595. Thus the total engine weight is 16,400 lbs, including the combustor. Subtracting 5% of the basic engine weight from this total gives a dedicated nuclear engine of 5.5 bypass ratio of 15,600 lbs.

Table 6.1.10-1 presents a summary of engine design parameters. The engines shown here have the thrust necessary to power a 2,000,000 lb aircraft cruising at Mach 0.6 at 30,000 ft. The data are presented for the dual mode and dedicated nuclear engines using either helium gas

or liquid metal in the heat exchangers. Not that the difference between those two systems is the horsepower pumping requirement of 1300 hp/eng for the helium loop vs 500 hp/eng for the liquid metal system.

TABLE 6.1.10-1. EFFECTS OF ENGINE PARAMETER VARIATION ON THE NET THRUST OF THE HEAT EXCHANGER TURBOFAN ENGINE

BASE ENGINE: TOTAL MASS FLOW, 1000 LB/SEC; OVERALL ENGINE PRESSURE RATIO, 16.8; TURBINE INLET TEMPERATURE, 1960°R; POWER EXTRACTION, 100; HP PRESSURE LOSS, 11%

PARAMETER	RANGE	% CHANGE	NET THRUST RANGE (10^3)	% CHANGE IN NET THRUST
FAN PRESSURE RATIO	1.2-1.6	33.3	13.1-15	+14.50
POWER EXTRACTION (HORSEPOWER)	100-1000	900	14.6-13.8	-5.5
PRESSURE LOSS (%)	6-16	167	14.9-14.2	-4.7
CORE MASS FLOW (LB/SEC)	200-500	25	14.5-17.2	+18.6
TURBINE INLET TEMPERATURE (R)	1860-2060	10.8	13.1-15.8	+20.6
FAN TIP PRESSURE RATIO	1.4-1.5	7.1	14.6-15.0	+2.74
OVERALL PRESSURE RATIO	16-18	80	14.9-13.5	-8.8

Based upon the analysis of this system concept of using a heat exchanger inside a turbofan engine for heating up the working medium (air) the following recommendations are:

1) Further investigation should be made into heat exchanger design with regard to lowering the engine pressure loss so that higher core mass flows can be used with the end results of greater thrust.

2) The possibility of heating up the bypass flow would increase the thrust significantly provided the pressure losses due to heat exchanger interferences are small. A more detailed study of the flow passage and the heat exchanger air interfacing would have to be accomplished to determine the potential increase in thrust from bypass heating.

3) Improve the material limitations of the heat exchanger in order to increase the turbine inlet temperature.

TABLE 6.1.10-2. SUMMARY OF ENGINE DESIGN PARAMETERS

HELIUM ENGINE (1300 HP)	DUAL MODE	DEDICATED
BYPASS RATIO	4	4
PRESSURE LOSS (%)	11	6
FAN PRESSURE RATIO	1.4	1.4
NET THRUST (LB)	12,100	12,600
DIAMETER (FT)	10.1	10.1
WEIGHT (LBS)	14,400	13,700
NUMBER ENGINES REQ (2 MIL)	11.4	10.95
THRUST/MEGAWATT	254	265
LIQUID METAL ENGINE (500 HP)		
BYPASS RATIO	5.5	5.5
PRESSURE LOSS (%)	11	6
FAN PRESSURE RATIO	1.4	1.4
NET THRUST (LB)	14,250	14,750
DIAMETER (FT)	11.3	11.3
WEIGHT (LBS)	16,400	15,600
NUMBER ENGINES REQ (2 MIL)	9.68	9.36
THRUST/MEGAWATT	300	310

6.2 DIRECT CYCLE

Two system concepts considered use the direct or closed cycle. Both employ helium gas expanded over a turbine. In one case, each fan is driven by a gas turbine, i.e., each is a ducted engine (Figure 6.0.6-2). The other system concept employs two gas turbine engines centrally located around the reactor (Figure 6.0.6-3). Power is extracted from these engines by long shafts going out to gear boxes in the wings which transmit the power to the ducted fans.

The direct cycle can employ either the Brayton cycle as discussed in Section 6.1.2 or the regenerative cycle which will be discussed in this section.

A computer program was written to determine the thrust for the ducted fan engine. A flow diagram of the computer program is presented in Appendix A.6.6.

The flight conditions were the same as those used for the indirect cycle engine.

6.2.1 REGENERATIVE CYCLE: The regenerative cycle depicted in Figure 6.2.1-1 is a cycle in which a heat exchanger is used to recover heat from the gas leaving the turbine and to deliver

it to the gas leaving the compressor. The processes depicted in the T-S diagram may be described as:

1-2 Isentropic compression (compressor process)
2-a Heat exchange (regenerator)
a-3 Heat addition (reactor heat exchanger)
3-4 Expansion (turbine process)
4-b Heat exchange (regenerator)
b-1 Heat rejection (rejection heat exchanger)

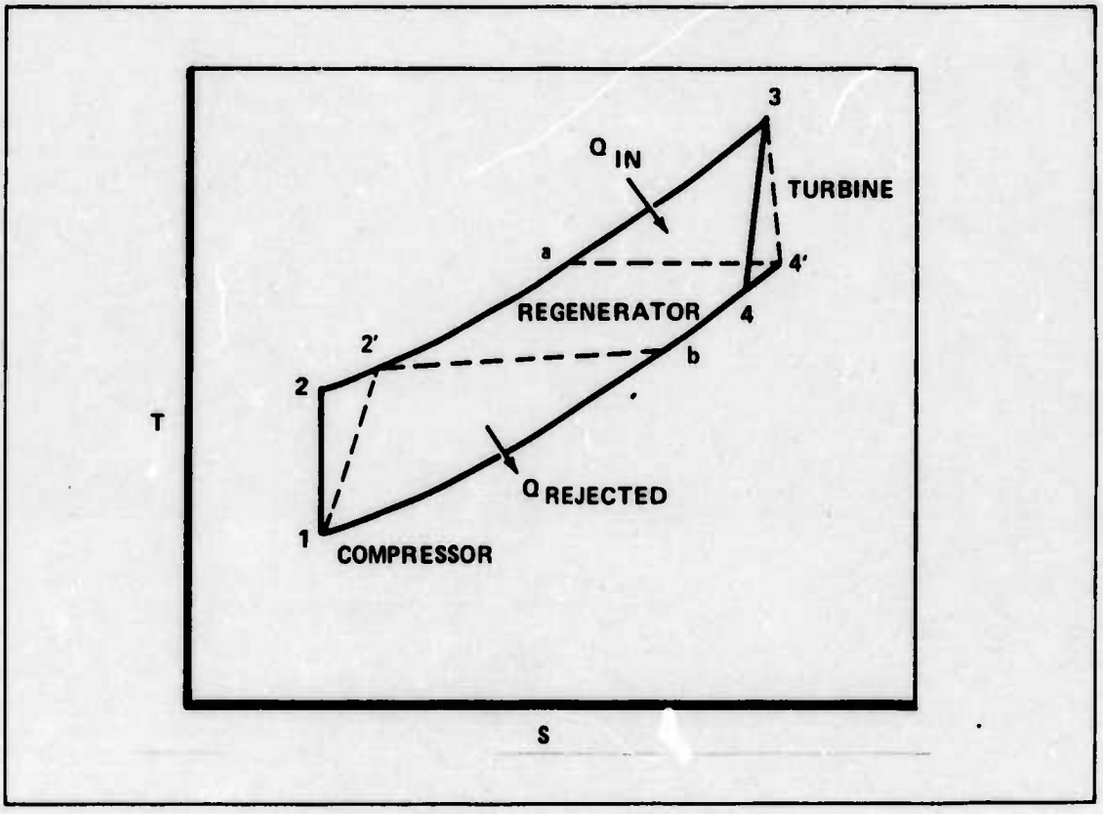

Figure 6.2.1-1. Regenerative Cycle

A schematic diagram of the regenerative cycle is presented in Figure 6.2.1-2, with numbering scheme corresponding to the T-S diagram. This cycle is designed to improve the economy of the turbine plant by reducing the energy input requirements of the fuel (reactor). The equations used in the analysis of this cycle are presented below. Several of the equations are derived in Appendix A.6.7.

1) Station 1. Compressor inlet temperature (T_{t_1}) is dependent upon the amount of heat that the system can reject.

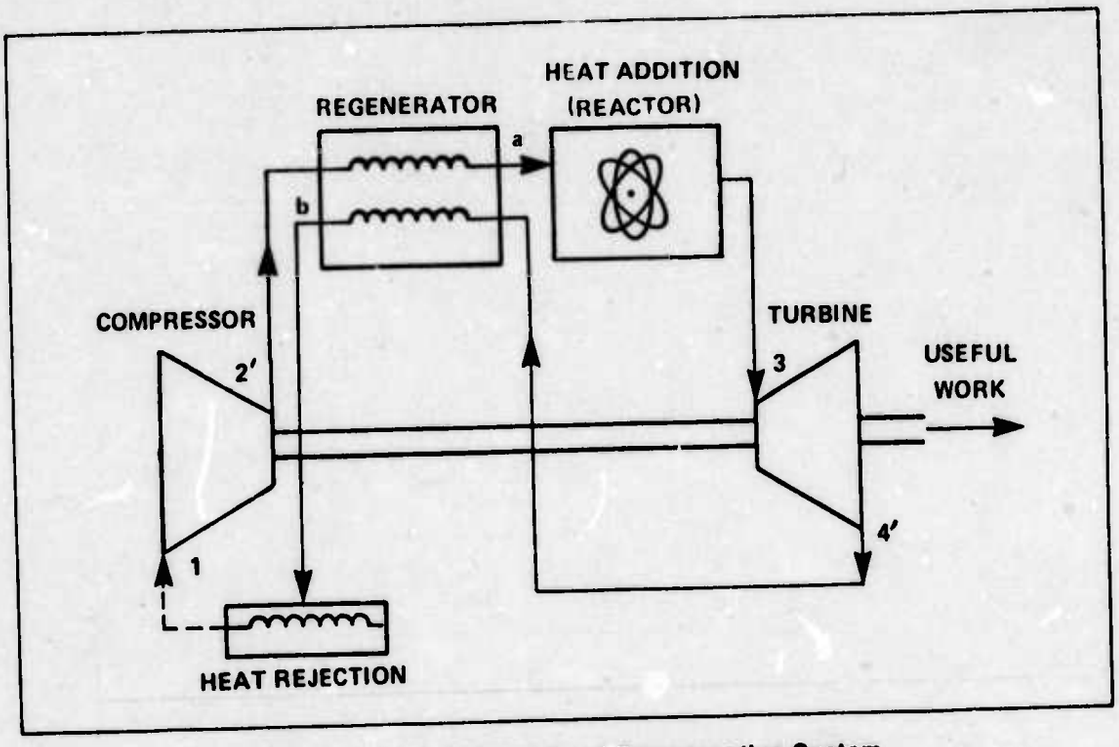

Figure 6.2.1-2. Schematic of Regenerative System

2) Station 2. Compressor outlet temperature (T_{t_2}) may be found from:

$$T_{t_2} = T_{t_1} \left(\frac{P_{t_2}}{P_{t_1}} \right)^k \qquad \text{ideal} \qquad (6.2.1\text{-}1)$$

$$T_{t_{2'}} = \frac{T_{t_1}}{\eta_C} [X_C - 1] + T_{t_1} \qquad (6.2.1\text{-}2)$$

The compressor work is given by:

$$W_C = \frac{c_p T_{t_1}}{\eta_C} [X_C - 1] \qquad (6.2.1\text{-}3)$$

3) Station a. Regenerator outlet temperature (T_{ta}) on the compressor (or cold) side. This temperature may be found from

$$T_{ta} = \eta_R [T_{t_{4'}} - T_{t_{2'}}] + T_{t_{2'}} \qquad (6.2.1\text{-}4)$$

where:

$$\eta_R = \frac{T_{ta} - T_{t2'}}{T_{t4'} - T_{t2'}}$$ is the regenerator effectiveness

T_{t4} is the temperature out of the turbine (actual, not ideal)

4) Station 3. Turbine inlet temperature (T_{t3}) is defined by the reactor heat exchanger limitations to be 2060°R (1600°F).

5) Station 4. Turbine outlet temperature is found by

$$T_{t4} = \frac{T_{t3}}{X_t}$$ isentropic (6.2.1-5)

where:

$$X_t = \left(\frac{P_{t3}}{P_{t4}} \right)^k$$

For the ideal system with no pressure losses in the regenerator or piping, then, $X_t = X_c$. For the non-ideal situation, i.e., the real process, the turbine outlet temperature, is given by

$$T_{t4'} = T_{t3} - \eta_t T_{t3} [1 - 1/X_t]$$ (6.2.1-6)

The turbine work is defined by

$$W_t = \eta_t c_p T_{t3} [1 - 1/X_t]$$ (6.2.1-7)

6) Station b. Regenerator inlet temperature (T_{tb}) on the turbine or (hot) side.

$$T_{tb} = T_{t4'} - \eta_R [T_{t4'} - T_{t2'}]$$ (6.2.1-8)

The ideal thermal efficiency of the regenerative cycle is given by

$$\eta_{thi} = 1 - \frac{T_{t1}}{T_{t3}} r_p^k = 1 - \frac{X}{Z}$$ (6.2.1-9)

The optimum regenerative (heat exchanger) effectiveness (efficiency) is given by

$$\eta_{ROPT} = \frac{Z\,(Z-v) - \dfrac{X^2}{\eta_C\,\eta_t}\,(ZY-1)}{Z^2 + Z - \dfrac{2X^2Y}{\eta_C\,\eta_t} + \dfrac{X^2}{\eta_C\,\eta_t}\,(Z+1) - 2\,vZ} \qquad (6.2.1\text{-}10)$$

The derivation of Eq. 6.2.1-10 and 6.2.1-11 are similar to those for the Brayton cycle and may be found in Hosney (Ref. 77).

where $Z = T_{t_3}/T_{t_1}$, $Y = [\,1 - \eta_t\,(1 - 1/X)\,]$

$$v = \frac{X-1}{\eta_C} + 1, \quad X = r_p^{\,k}, \quad k = (\gamma - 1)/\gamma$$

The thermal efficiency for optimum η_R is given by

$$\eta_R = 1 - \frac{(ZY-1) - \eta_R\,(ZY-v)}{(Z-v) - \eta_R\,(ZY-v)} \qquad (6.2.1\text{-}11)$$

A computer program was written to evaluate the regenerative cycle for various values of Z and r_p. Input parameters were $\eta_t = 0.9$ and $\eta_C = 0.88$. A general performance of the cycle is depicted in Figure 6.2.1-3.

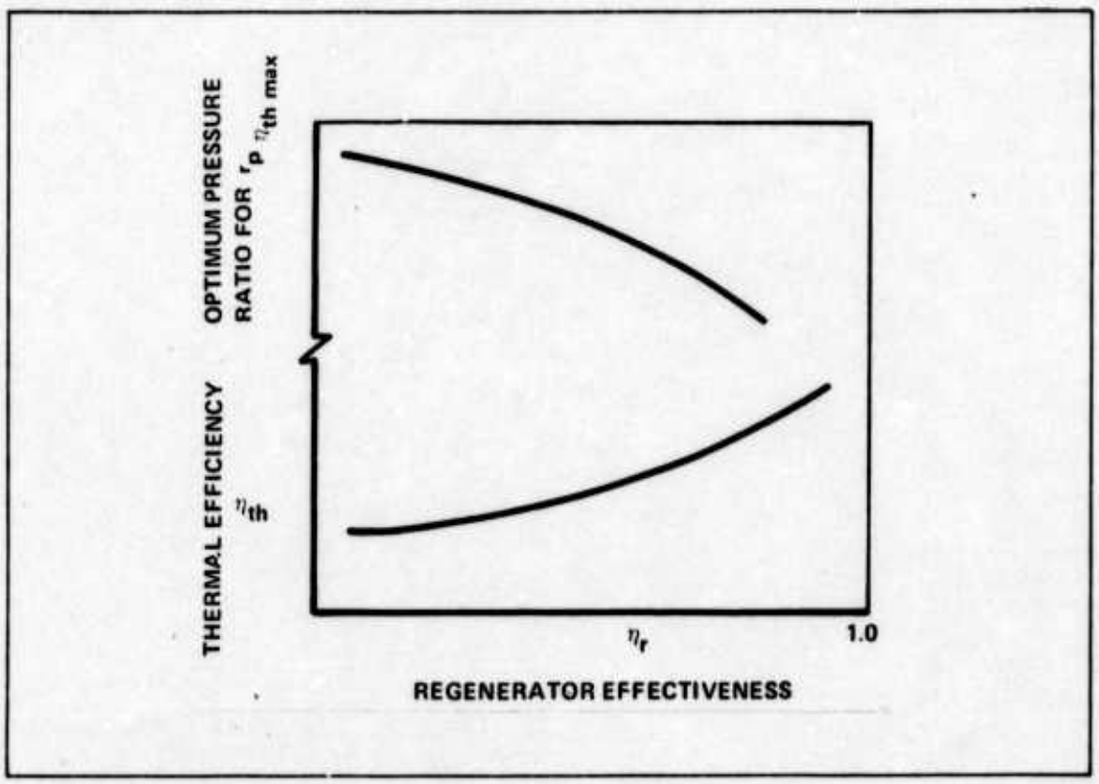

Figure 6.2.1-3. Pressure Ratio and Thermal Efficiency of Regenerative Cycle

The one portion which doesn't show up in this T-S diagram of Figure 6.2.1-1 is the work done by the fan as in the Brayton cycle, Station 2-2.5. The work of the fan (W) is found from

$$W_f = W_n = W_t - W_c$$

$$W_f = c_{p\ helium}\left[\ \eta_t\ T_{t_3}\ \left(1 - \frac{1}{X_t}\right) - \frac{T_{t_1}}{\eta_c}\ (X_c - 1)\right] \qquad (6.2.1\text{-}12)$$

Accounting for the mass flow of the helium and noting that

$$W_f = \frac{\dot{m}_{air}\ c_{pair}\ T_{t_5}}{\eta_f}\ |\ X_F - 1\ |$$

where T_{t_5} is the total temperature at the face of the fan, then equating the two expressions for W_F:

$$\frac{\dot{m}_{air}\ c_{pair}\ T_{t_5}\ |\ X_f - 1|}{\eta_f} = \dot{m}_{helium}\ c_{p\ helium}\ \left[\ \eta_t\ \ T_{t_3}\left(1 - \frac{1}{X_t}\right) - \frac{T_{t_1}}{\eta_c}\ (x_{\ c} - 1)\ \right]$$

(6.2.1-13)

From this equation it can be seen that the mass flow of air $\dot{m}_a$ is inversely proportional to fan pressure ratio function $(X_f - 1)$ for a given amount of work available, i.e.:

given $\quad W_f = W_t - W_c$

then $\quad \dot{m}_{air} \propto \frac{1}{X_f - 1}$

$$\dot{m}_{air} = \frac{K}{X_f - 1}$$

where

$$K = \frac{W_f\ \eta_f}{C_{pair}\ T_{t_5}} \qquad (6.2.1\text{-}14)$$

This relationship is pointed out in Figure 6 2.1-4.

Hesse and Mumpford give an expression for the critical pressure ratio of nozzle flow as

$$\frac{P_{ambient}}{P_{t\ exit}} = \left[\frac{2}{\gamma + 1}\right]^{\frac{\gamma}{\eta_n\ (\gamma - 1)}}$$

(Ref. 69, p. 131)

or

$$= \left[\ \frac{2}{\gamma + 1}\ \right]^{\frac{1}{k\ \eta_n}}$$

With a nozzle efficiency η_n of 0.98 this ratio equals 0.495. Thus a sonic nozzle (Mach = 1.0 at exit plane) will occur if the ambient to exit pressure ratio is less than 0.495.

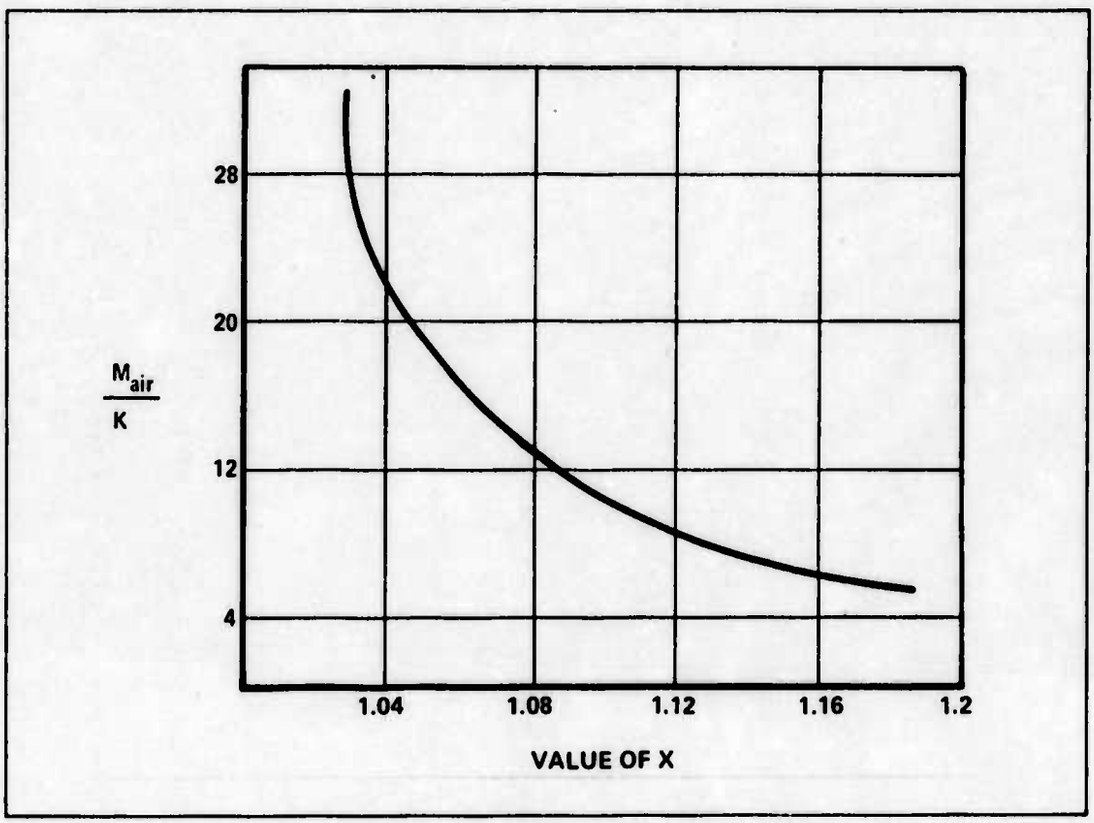

Figure 6.2.1-4. Pressure Ratio Function vs Mass Flow of Air

For design conditions at 30,000 ft and Mach = 0.6, this corresponds to a fan pressure ratio of 1.77, or Xf = 1.18.

6.2.2 HELIUM MASS FLOW: The helium mass flow for the independent ducted fan concept was varied between 50 and 110 lb helium/sec. The central gas turbine generator concept was investigated for $\dot{m}_{helium}$ between 250 and 350 lb He/sec. These mass flow ranges were chosen in order to compare these two systems concepts with the indirect cycle engines which have a 70 lb He/sec/engine. The impact of helium mass flow is most emphasized by Eq. 6.2.1-13 where the work of the fan becomes a linear function of $\dot{m}_{helium}$ if temperature and pressure ratios are held constant.

6.2.3 FAN PRESSURE RATIO: The fan pressure ratio was varied from 1.2 to 3.0, assuming a fully expaned nozzle. For fan pressure ratios above 1.77, a sonic nozzle analysis was also performed. Due to this relationship between mass flow and inlet size which was presented in Section 6.1.8, a higher fan leading in this analysis would allow a smaller engine for a given amount of work available to the fan. The fully expanded nozzle produces more thrust but requires a convergent-divergent nozzle for high fan pressure ratios.

6.2.4 REGENERATIVE CYCLE APPLICATION: Initially the regenerative cycle was studied using ideal conditions, i.e.:

1) $P_{t_2}/P_{t_1} = P_{t_3}/P_{t_4}$
2) Isentropic processes

while varying:

1) η_R = .75 to .9
2) T_2 = 600°R to 1000°R
3) T_a = 1300°R to 1600°R
4) R_{pf} = 1.2 to 3.0

It appears as though the most practical regenerator effectivenss for an airborne application is around $\eta_R = 0.75$. Increasing η_R increases the size and this relationship is discussed in Section 7. This is compared to $\eta_R = 0.9$ or better for ground base operations or seagoing vessels which can carry the additional weight. In this study, $\eta_R = 0.75$ will receive the largest emphasis.

The lower the value of T_{t_2}, the less work the compressor requires for a given pressure ratio and thus the more energy available for thrust. This point is dramatically emphasized in Figure 6.2.4-1.

Decreasing T_{ta} below 1500°R increases the required energy output of the reactor but decreases the regenerator weight. Increasing T_{ta} above 1500°R decreases the required output of the reactor but increases the weight of the regenerator. From Figure 6.2.4-1, it may be seen that the slope of the line for T_{t_2} = 43.0 lb/°R. Thus for a 100 degree change in T_{ta}, the thrust will change by 4300 lbs, which is quite significant. The sensitivity of thrust to the mass flow of helium was also evaluated and a compilation of the relationships between T_{ta}, T_2, and m_{helium} for $\eta_R = 0.75$ and $R_{pfan} = 1.6$ is presented in Figure 6.2.4-2. The reason $R_{pfan} = 1.6$ was chosen is pointed out by Figure 6.2.4-3, which shows that this is the optimum pressure ratio for this system. This optimum pressure ratio is the same for T_{t_2} = 1000°R as well as for all mass flow rates of helium. These studies were for an ideal (isentropic) process. In order to study the real processes the following parameters were taken into consideration.

1) pressure losses ≃ 2%
2) efficiency of the compressor ($\eta_c = 0.88$) and turbine ($\eta_t = 0.9$)
3) limitations on compressor inlet temperature T_{t_1}.

The effects of the first two considerations are strictly an increase in the work required to drive the compressor, which in turn reduces the thrust. However, the third consideration, T_{t_1}, has multiple significant effects. If the system is designed for altitudes of 30,000 ft, it is possible to design the system for T_{t_1} = 500°R with $\eta_R = 0.75$ but to lower that engine to 2000 ft altitude where the outside temperature is higher, then it becomes impossible to reject the energy the system was designed for as Tambient > 500°R. To keep the same inlet temperature to the compressor is effectively asking η_R to increase, which is increasing area and weight of the system beyond feasibility. A more detailed discussion of this weight relationship is presented in Section 7. The other option is to design the system so that a high inlet temperature at 30,000

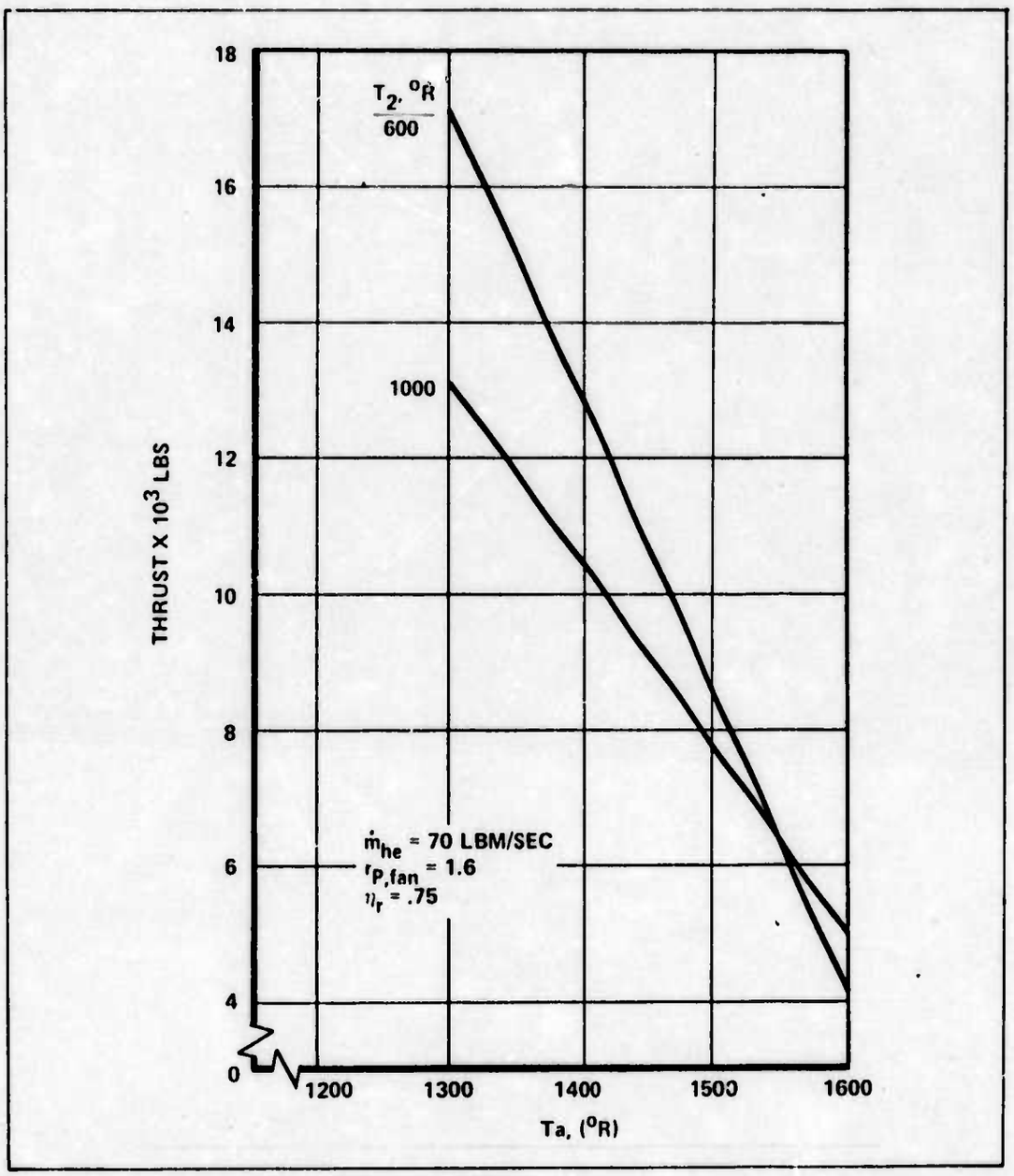

Figure 6.2.4-1. Thrust as a Function of Compressor and Regenerator Temperature

ft is employed and can still be obtained at lower altitude by increasing the area and weight of the rejection heat exchanger. The temperature chosen to meet this second option was T_{t_1} = 700°R(240°F) which, at sea level, still allows a temperature differential across the rejection heat exchanger of approximately 170°R. This still requires increasing the area of the heat exchanger just to maintain its level of efficiency. An additional constraint is the regenerator outlet temperature T_{t_a} which was set at a minimum of 1350°R by the heat exchanger limitations in the reactor. Figures 6.2.4-4 and 6.2.4-5 show the optimum conditions for T_{t_1} = 500 and 700°R. As it turns out, the optimum conditions for T_{t_1} = 500 R are not reached for η_R = 0.75 because of the temperature differential ΔT allowed across the reactor heat exchanger.

However, even at non-optimum, that cycle would produce more work/lb than the cycle employing T_{t_1} = 700°R.

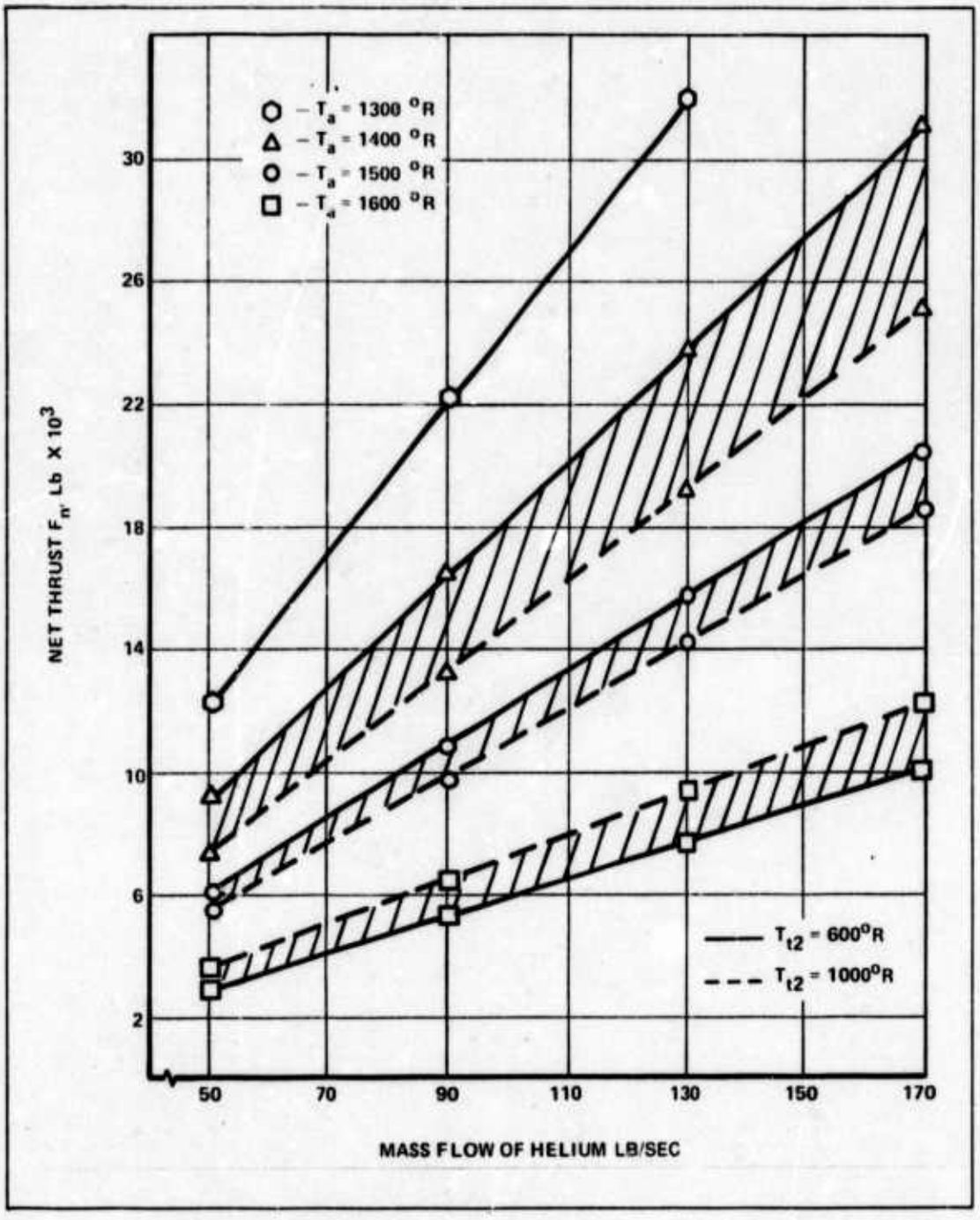

Figure 6.2.4-2. Net Thrust for Ideal Cycle Analysis

Using the program outlined in Appendix A.6.6, the thrust for various temperature cycles was determined. It was found that a system designed with T_{t_1} = 700°R would not produce enough thrust with the total mass flow of helium being limited to 700 lb/sec. Figure 6.2.4-6 shows that, for a minimum thrust/engine of approximately 14,000 lb, a 2,000,000 lb aircraft at 30,000 ft

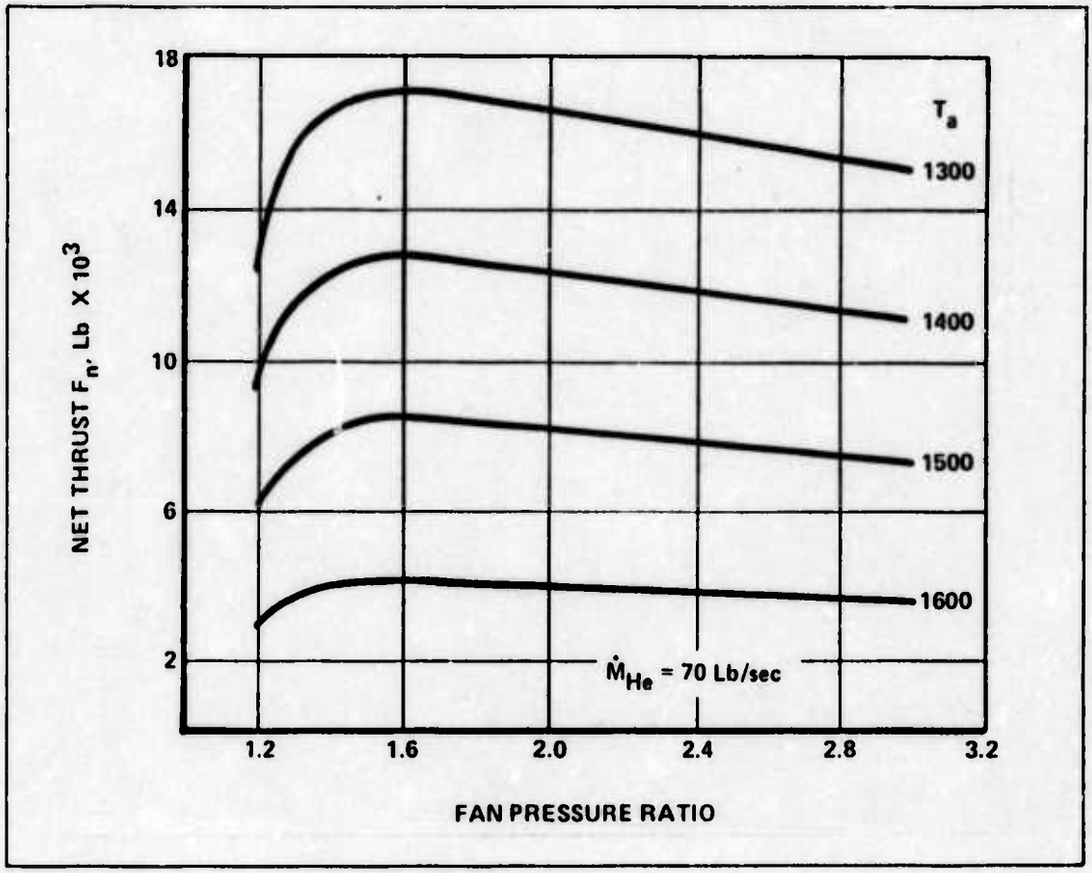

Figure 6.2.4-3. Optimum Fan Pressure Ratio for Maximum Net Thrust Within Given Temperature Limitations

requires a net work output/engine of 275 BTU/lb. This network output completely eliminates the cycle in which T_{t_1} = 700°R. It also eliminates any cycle combination which has a recuperator outlet temperature T_{ta} = 1500°R and η_R = 0.75 (Figures 6.2.4-4 and 6.2.4-5). This implies the need for a bigger reactor to utilize this cycle for the propulsion requirements established.

However, if the mission required only high altitude operation, in which case T_{t_1} could be designed to 500°R, then the thrust requirement could be obtained with the reactor the same size and η_R = 0.75 the reactor increasing by around 10%, i.e., approximately 550 MW.

6.2.5 BRAYTON CYCLE APPLICATION: In studying the application of the Brayton cycle to the direct system (closed cycle) concept, the equations presented in Section 6.1.1 were used. This cycle was looked at because it tends to produce more work/lb than the regenerative cycle, but at a lower efficiency. Figure 6.2.5-1 presents a compilation of variables based on non-ideal study parameters, i.e., pressure losses and inefficiencies. As can be seen from this figure, the net work is low; this is a result of the temperature limitations within which the cycle must operate, specifically, the required compressor outlet temperature. As mentioned in the previous section, a minimum of 275 BTU/lb is required to meet the thrust requirements and, as can

be seen from Figure 6.2.5-1, this would be possible if the system could be designed for a compressor inlet temperature $T_{t_1} = 550°R$. As mentioned earlier, to provide an inlet temperature of 550°R a larger heat exchange would be required than that needed for the regenerative cycle which produced the same network.

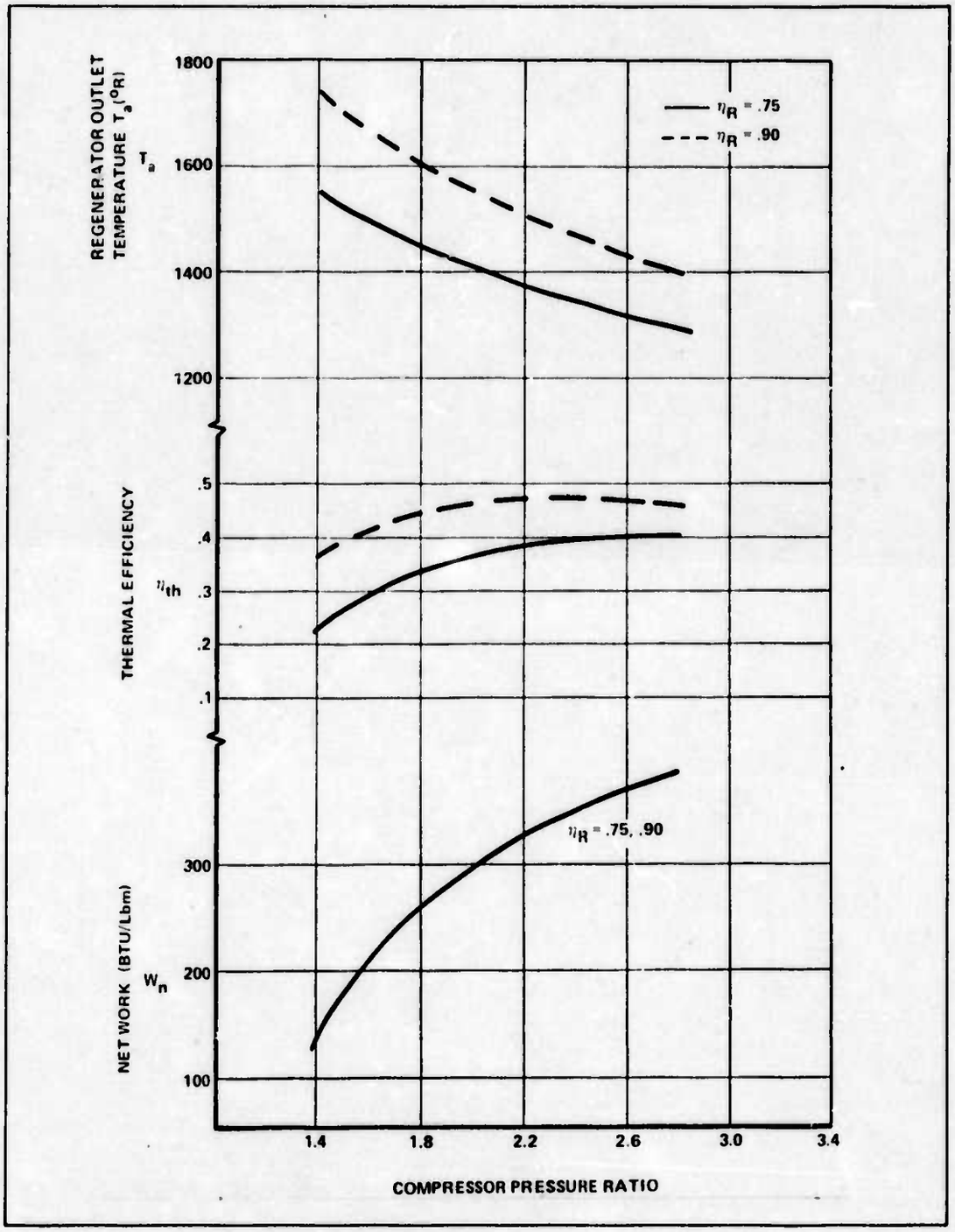

Figure 6.2.4-4. Regenerative Cycle Designed with $T_{t_1} = 500$ R

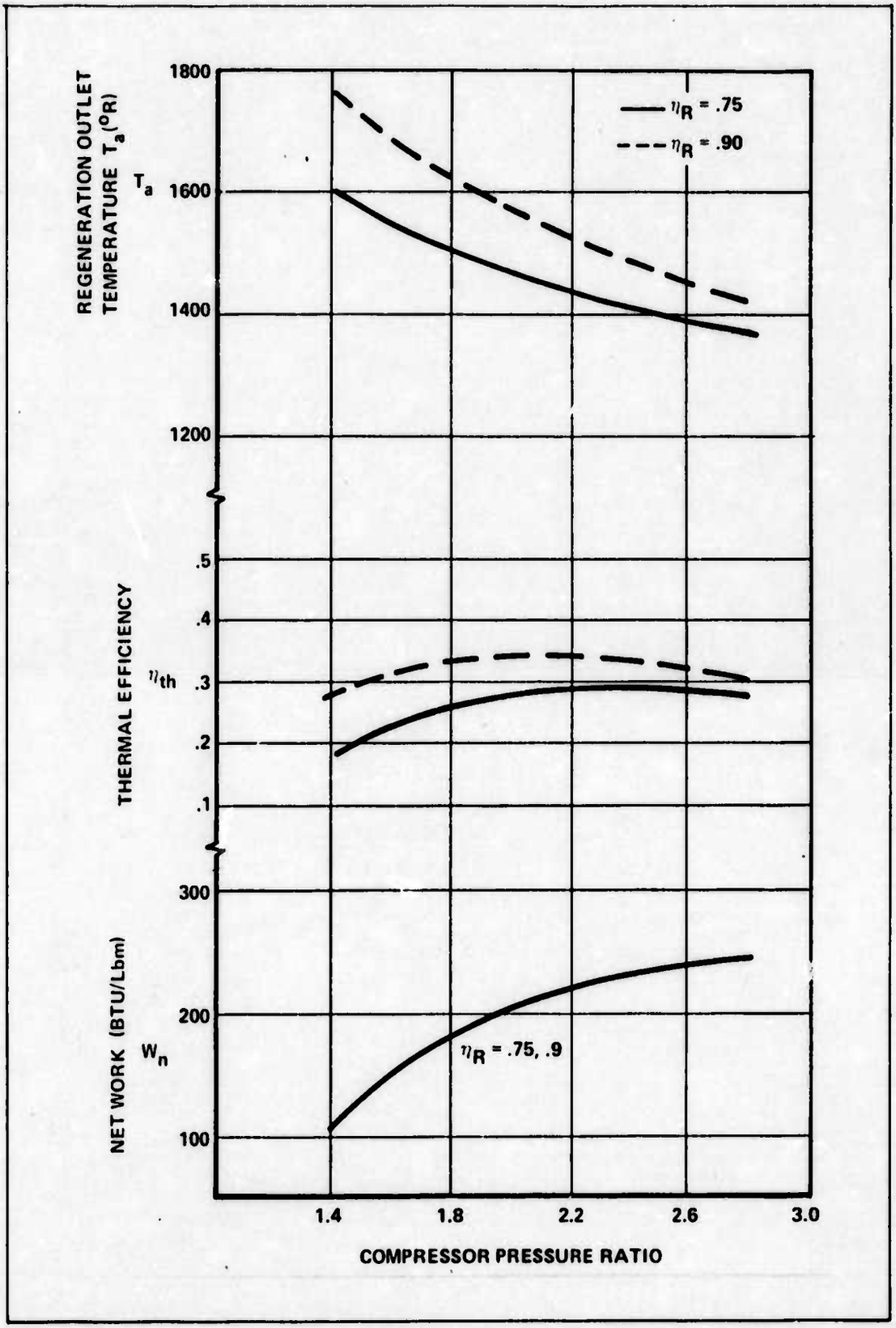

Figure 6.2.4-5. Regenerative Cycle Designed with T_{t_1} = 700 R

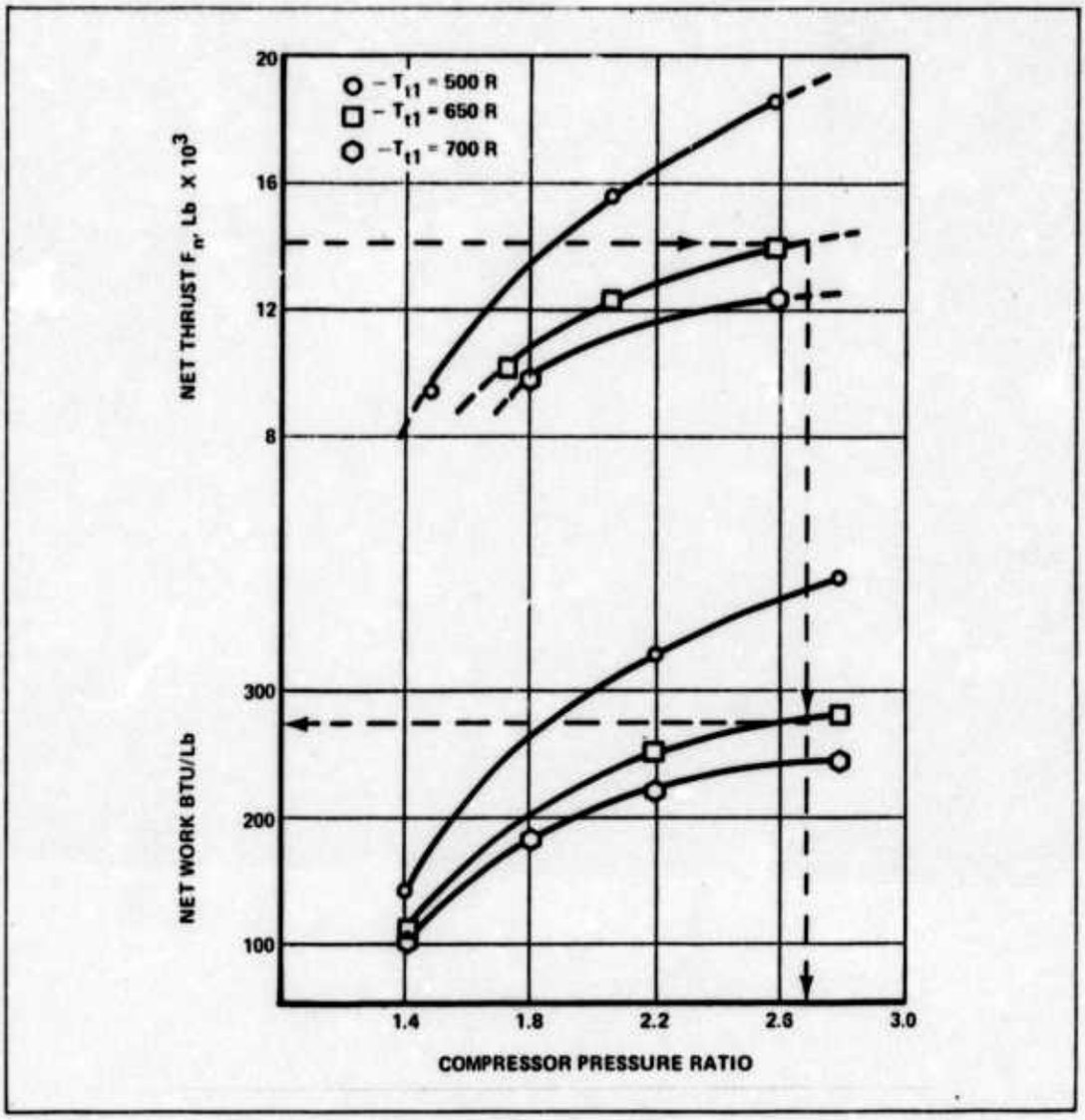

Figure 6.2.4-6. Thrust as a Function of Pressure Ratio and Work/lb (Thrust Based on 70 lb/sec of Helium and Fan Pressure Ratio of 1.6)

6.2.6 CENTRAL TURBINE SYSTEM: Recall this system as described in Section 6.0.6, in which two turbines are located near the reactor and transmit the power to turn a ducted fan engine by means of shafts through the wings. Gear boxes are used to extract the horsepower for the fans. With this system in mind, the mass flow of the helium over each turbine would be as much as 350 lb/sec to put it on a comparative basis with the indirect cycle. Using the cycle studies performed in Sections 6.2.4 and 6.2.5, and using the network available from the systems, an estimated thrust can be obtained. If mechanical efficiency of the gears can be assumed to be $\eta_{mech} = 0.98$, then the horsepower available to the ducted fans will be dependent upon the system design, i.e., the number of gearing mechanisms required. If the engines are located in the wing and the shafts pass through the engines, then one gear box would be required to turn each fan. If the engines are located below the wings, then two gear boxes would be required. A basic assumption underlying this system concept is that lightweight gear boxes would be able

to handle the horsepower required by the fans. Just as for the turboprop the gear boxes would have to handle two to four times the horsepower of today's aircraft gear boxes.

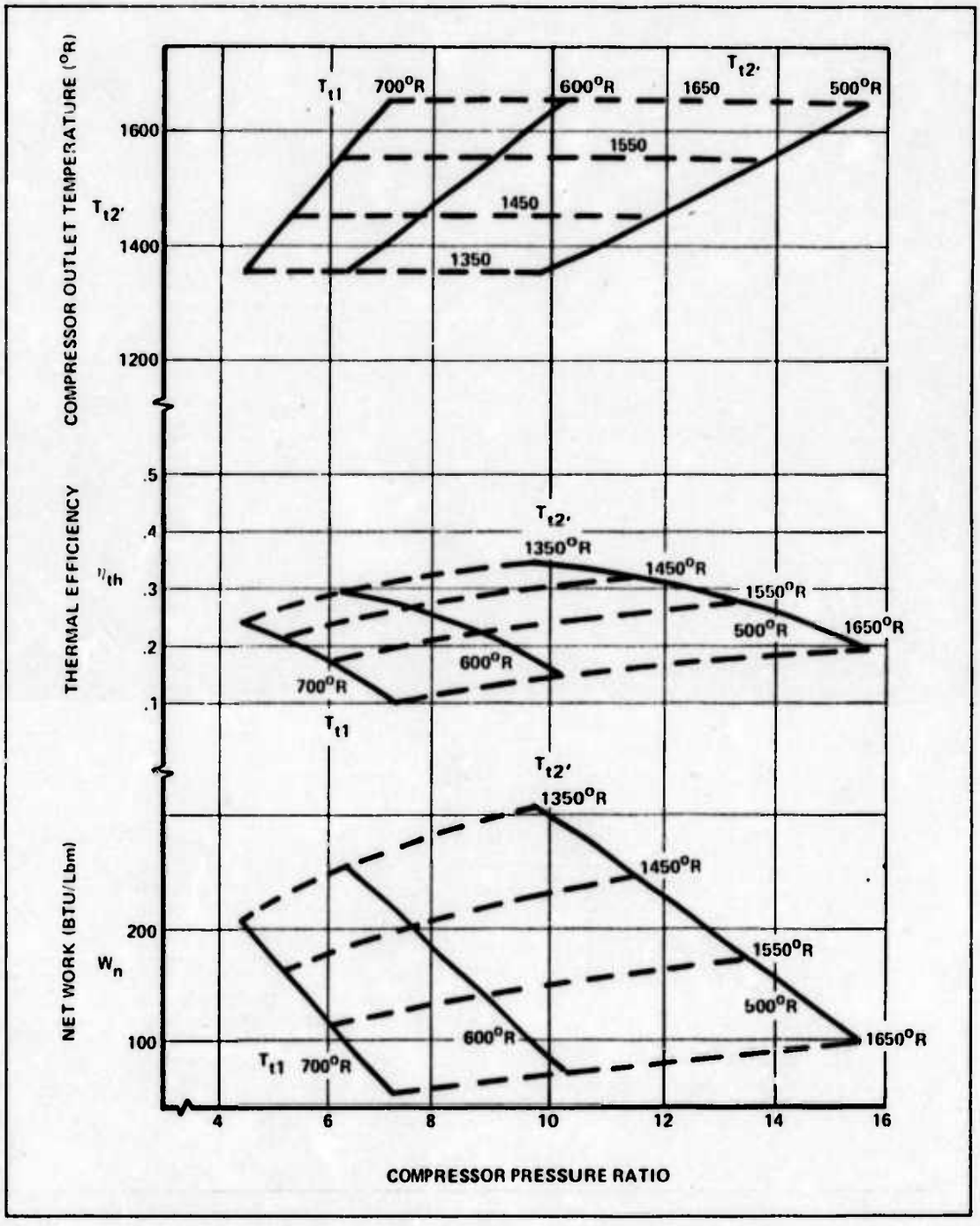

Figure 6.2.5-1. Brayton Closed Cycle Thermodynamic Analysis

6.2.7 SYSTEM SIZING: The method used for approximating the system weights for the independent turbine and central turbine concepts is to give only a "ball park" estimate, because of a lack of available data on weight breakdown on engine components. Based on Reference 47, the following method was employed.

The engine components were divided into five parts, with the following percent weight ranges:

1) fan 5 to 10%
2) compressor 25 to 35% (depending on number of stages)
3) combustor 5 to 7%
4) turbine 25 to 35% (dependent on number of stages)
5) cowling, auxiliary power, struts, etc., 15 to 40%

Using the CF6-50B as a base engine because it is a large engine which has the following characteristics (Ref 60):

1) net sea level static thrust 50,000 lbs
2) dry weight of 8225 lbs not including thrust reversers
3) fan diameter approximately 8 ft

Several weight estimation techniques were considered; however, after discussion with Dr. Elrod (Ref. 47), it was decided to use a weight/hp assessment in estimating the system weights. Using the base engine above, the assumptions used were:

COMPONENT	%	WEIGHT	HORSEPOWER	WT/HP
Fan	10	822	27,000	0.03
Compressor	30	2468	70,000	0.035
Combustor	5	411	-	-
Turbine	30	2468	100,000	0.025
Other	25	2056	-	-

In considering the central turbine system, a gearing mechanism was required. The T34P7 turboprop engine was used as a base engine. It weighs 2670 lbs and delivers 6500 hp (Ref. 171). The gearing mechanism was estimated as 20% of the weight (Ref. 47), thus giving a wt/hp) gear $\cong$ 0.08.

Table 6.2.7-1 presents a listing of engine sections and weight estimates for several engine systems. This table is based on data for where the mass flow of helium is 70 lb/sec and fan pressure ratio is 1.6. An additional weight to consider for the independent gas turbine generator system is the weight of the regenerator and the heat exchanger included with each engine. The weights for these components are determined in Section 7. For the central turbine concept, the weight of the regenerator and the weight of the rejection heat exchanger for each turbine would be approximately five times the weight of the regenerators and heat exchangers used in the independent turbine engine system. These weights are also presented in Section 7.

6.2.8 PRIMARY AND SECONDARY LOOP TURBINE PUMPS: As mentioned in Section 6.1, approximately 23,000 hp is needed to drive the primary coolant fluid through the reactor and the reactor heat exchangers. The system studied to provide this horsepower is one in which a turbine, compressor, and heat exchanger are located within the reactor containment vessel.

TABLE 6.2.7-1 ENGINE SYSTEM WEIGHT COMPARISON

TYPE SYSTEM	COMPONENT	HORSEPOWER	WEIGHT (LBS)	SYSTEM WT FOR:
1	FAN	39830	1194	
	COMPRESSOR	31325	1096	
	TURBINE	71155	1779	
	OTHER	—	3042	7111/ENG
				71,100/AIRCRAFT*
2	FAN	25062	751	
	COMPRESSOR	40990	1434	
	TURBINE	66052	1651	
	OTHER	—	2878	6714/ENG
				67,140/AIRCRAFT*
3	FAN	398300	5975	
	COMPRSSOR	313250	5475	
	TURBINE**	726071	9076	
	GEARS	398300	15932	
	OTHER	—	15210	51672/TURBINE
				103,344/AIRCRAFT

1 - REGENERATIVE CYCLE WITH T_{t1} = 650 AND R_p = 2.7 INDEPENDENT TURBINE

2 - REGENERATIVE CYCLE WITH T_t = 700 AND R_p = 2.4 INDEPENDENT TURBINE

3 - REGENERATIVE CYCLE WITH T_{t1} = 650 AND R_p = 2.7 CENTRAL TURBINE

* - WEIGHT IS BASED ON 10 ENGINE AND EXCLUDES HEAT EXCHANGER WEIGHT.

** - TURBINE HORSEPOWER OUTPUT REQUIREMENT BASED ON COMPRESSORS, FAN AND A MECHANICAL EFFICIENCY OF THE GEAR OF 0.98.

The pump is driven by direct drive shaft off the turbine. The system employing one turbine to drive the circulator is depicted in Figure 6.2.8-1. The regenerative cycle is used because the net work output, i.e., BTU/lb is greater than that of the Brayton cycle. The following parameters were used in the pump system design:

1) Recuperator output temperature on compressor side T_{ta} = 1538°R
2) Turbine inlet temperature T_{t_3} = 2060°R
3) Compressor inlet temperature T_{t_1} = 650°R

The assumptions used in the analysis were:

1) Recuperator effectiveness η_R = 0.789

2) Pressure loss in turbine-compressor system ΔP = 2%.

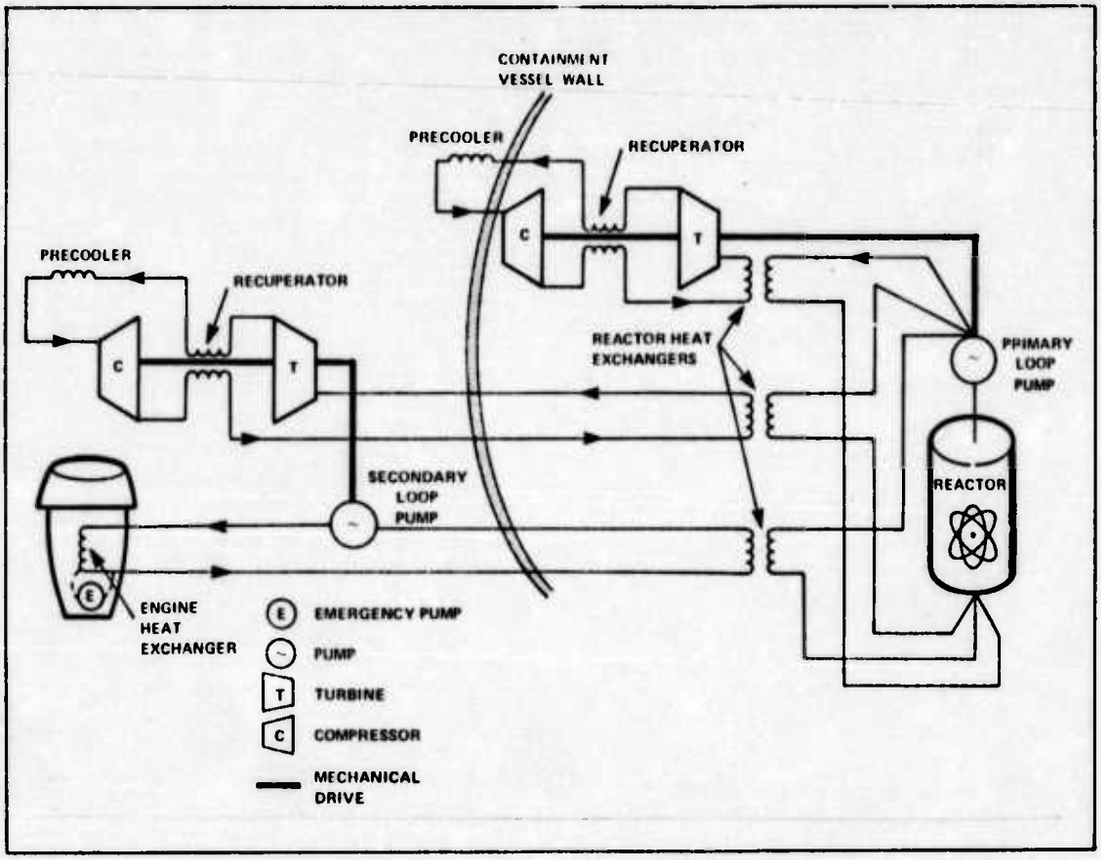

Figure 6.2.8-1. Indirect Cycle Gas Circulation System

With these constraints the maximum horsepower was found to be 25,300 hp for mass flow of helium, $\dot{m}_{helium}$ = 90 lb/sec. This may be seen from Figure 6.2.8-2 in which the network is around 199 BTU/lb, i.e.,

$$W_h = \begin{cases} 199\ \dot{m}_{helium} \\ 281.5\ \dot{m}_{helium} \end{cases}$$

The reactor output may be expressed as:

$$Q = 0.68\ \dot{m}_{helium}$$

Using the continuity equation:

$$\dot{m} = \rho\, A\, V \qquad (6.2.8\text{-}1)$$

Assuming the mass flow to be 840 lb/sec in the primary loop the system specifications may be determined. (The 840 lb/sec is based on 70 lb/sec going to each of the ten engine heat exchangers, 90 lb/sec to the primary pump system, and 50 lb/sec to the secondary pump system.) Table 6.2.8-1 presents a summary of the system specifications which employs a turbine-pump system for both the primary and secondary coolant loops.

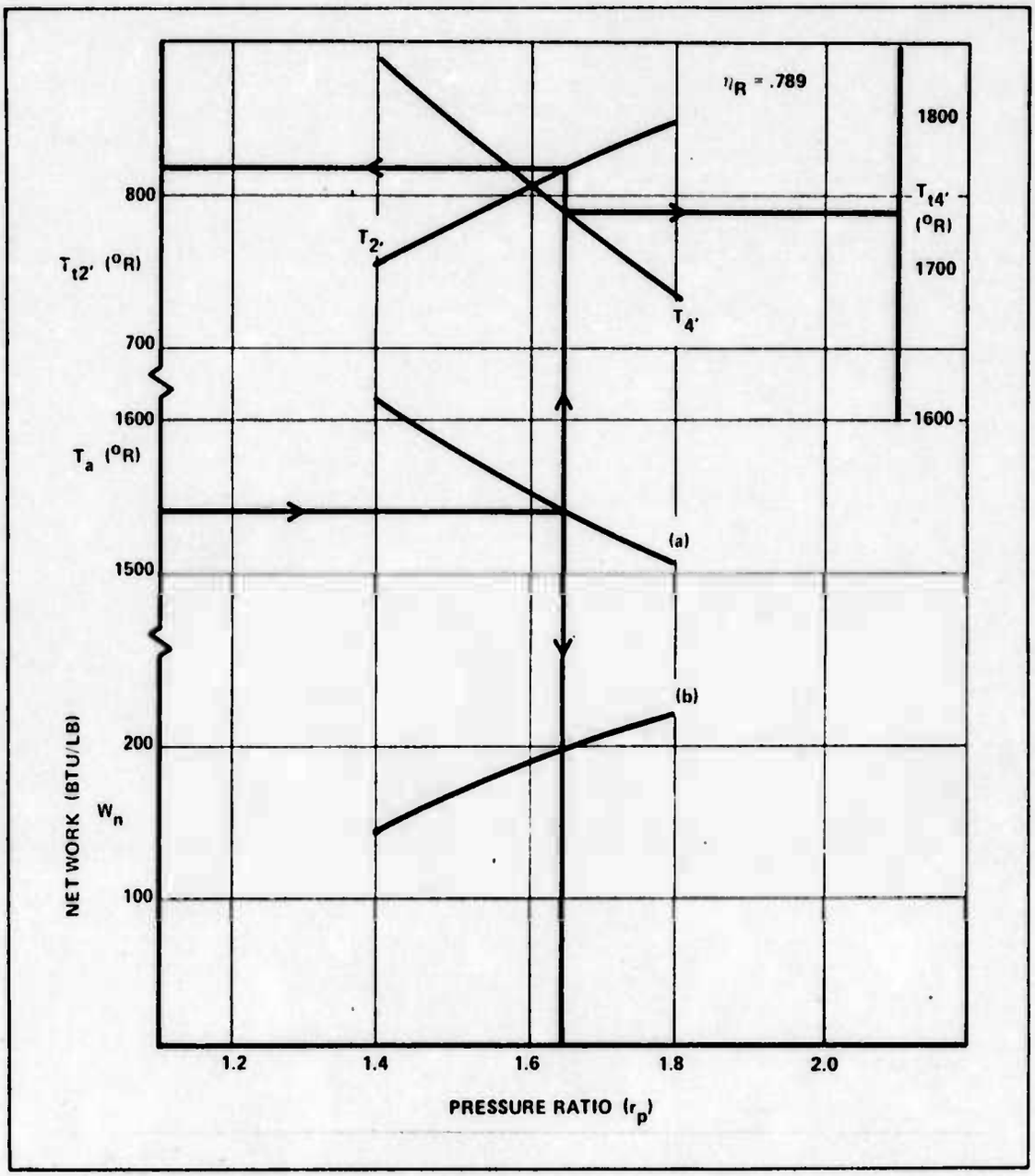

Figure 6.2.8-2. Gas Turbine Generator-Pump Cycle Analysis

Having these turbine systems to produce horsepower allows various system combinations to evaluate optimize on in terms of weight and reliability. Some of these options for the indirect heat exchanger engine system are:

1) Having the engines produce the horsepower necessary for the secondary coolant flow while a direct drive turbine is used inside the reactor for the primary coolant loop.

2) Having a direct turbine-pump system for the primary and secondary coolant loops. Within this option is also the option for increasing the reliability by having:

(a) Two turbines driving two circulators within the primary loop. They would be operating at half maximum capacity so that, in case one turbine-pump system fails, then the other would be able to do all the work.

(b) Two turbines would drive pumps located on each of the ten engine systems. Again the turbine would operate at half maximum capacity.

TABLE 6.2.8-1 TURBINE-PUMP PARAMETERS

REGENERATOR EFFECTIVENESS	**0.789**
COMPRESSOR INLET TEMPERATURE	**650°R**
COMPRESSOR OUTLET TEMPERATURE	**813°R**
REGENERATOR OUTLET TEMPERATURE T_a	**1541°R**
TURBINE INLET TEMPERATURE T_{t4}	**2060°R**
TURBINE OUTLET TEMPERATURE T_{t5}	**1736°R**

	PRIMARY COOLANT LOOP	SECONDARY COOLANT LOOP
TURBINE DIAMETER (IN.)	**12.2**	**9.2**
NET HP AVAILABLE	**25,335**	**14,075**
COMPRESSOR DIAMETER (IN.)	**7.0**	**6.0**
CIRCULAR DIAMETER (IN.)	**31.75**	**10.0**

3) Using direct turbines to drive the primary and secondary coolant system with horsepower extraction backup available on each engine. This would provide the horsepower for the secondary loop pumping power requirements if the gas turbine pump system fails.

6.2.9 RESULTS: For the analysis of the direct cycle independent turbine the following criteria as previously established were:

1) Mass flow of helium ($\dot{m}_{helium}$) = 70 lb/sec/turbine

2) Minimum temperature of the secondary coolant returning to the reactor heat exchanger (T_{ta}) = 1350 R.

In order to provide a cruise thrust of 140,000 lbs plus have a turbine to drive the primary coolant loop, two possible systems are:

1) The case where T_{t_1} = 700°R on the engine system and using the turbine-pump developed in Section 6.2.8. The mass flow of helium would be 930 lb/sec with a reactor size of approximately 744 MW.

2) The case where Tt_1 = 650 R on the engine system and the turbine pump. The mass flow of the helium would be 770 lb/sec with a reactor size of approximately 700 MW.

It was found that the Brayton cycle was not competitive for this engine system concept because the net work it could produce was on the order of 25% less than the regenerative cycle for comparable reactor power.

The central two-turbine concept appears infeasible in comparison to the independent turbine concept because the system weight is on the order of 40 to 50% greater.

Table 6.2.9-1 presents a summary of the design cycles using regeneration, for the independent turbine system with a turbine-pump arrangement for the primary loop pumping requirements. The results are based on design conditions at 30,000 ft at a flight speed of 596 ft/sec.

TABLE 6.2.9-1. REGENERATIVE ENGINE PARAMETERS

T_{t_1} (°R)	650	650	700
η_R	0.75	0.789	0.75
T_a (°R)	1350	1367	1411
MW/ENG	65.1	63.6	
F_n (LBS)	14,000	14,000	12,000
F_n/MW	215	220	206
ENG WT (LBS)	7100	7100	6700

6.3 SUMMARY

6.3.1 RESULTS: Four systems were considered in this section of the report:

1) Indirect cycle heat exchanger turbofan engine using
   (a) Liquid metal coolant
   (b) Helium gas coolant

2) Direct cycle ducted fan engine which is divided into
   (a) Independent gas turbine generator concept
   (b) Central two gas turbine generator concept

The first two systems, 1 (a) and (b) were evaluated by the use of CARPET, a design point program (Ref. 192). These are basically turbofan engines with a heat exchanger located between the compressor and the turbine. They may have a combustor section as well. A

sensitivity analysis was performed, and the results were plotted comparing the net thrust of these engines to:

1) Pressure ratio: fan, gas generating core and overall

2) Turbine inlet temperature

3) Pressure loss in the heat exchanger and or combustor

4) Horsepower extraction for pumping the primary and secondary coolant loops.

5) The amount of core mass flow, i.e., the amount of air passing through the core for various bypass ratios.

A computer program was written (See Appendix A.6.6 for flow diagram) to evaluate systems 2 (a) and (b) which are basically ducted fan operated by closed cycle gas turbine generators. Helium is expanded over a turbine and the net work produced, i.e., after power is taken off to run the compressor, is used to drive a ducted fan. The Brayton and regenerative cycles were used in the analysis.

Several driving factors for both systems (1) and (2) were:

1) thrust/megawatt
2) engine weight including heat exchanger
3) horsepower requirements

The thrust/MW ranged from 220 for the direct cycle ducted fan using the regenerative cycle to 310 for the liquid metal heat exchanger turbofan engine.

The engine weight was driven primarily by the heat exchanger weight, which comprised from 35% to 65% of the total engine system weight. The total engine weight, including heat exchanger (and regenerator for the regenerative direct cycle), ranged from 26,600 lbs for the liquid metal heat exchanger turbofan engine to 35,000 lbs for the helium gas heat exchanger turbofan engine.

The horsepower requirements are divided into that needed for:

1) auxiliary power 100 to 300 hp
2) primary coolant pumping power requires 2000 to 23,000 hp
3) secondary coolant pumping power requires 1200 to 10,000 hp

Several alternatives to meet this pumping requirement are presented in Section 6.2.8. The pumping power is greatest for the helium cycle, i.e., a total of 33,000 hp which requires on the order of 81 MW. The liquid metal system, on the other hand, would require on the order of 4000 hp which corresponds to approximately 10 MW. Table 6.3.1-1 presents a summary of five possible engine systems which were studied in this section. Table 6.3.1-1 presents only the dedicated nuclear engines for the indirect cycle. Section 6.1.10 presents a more detailed

TABLE 6.3.1-1. ENGINE SYSTEM SUMMARY

	HELIUM ENG 1300 HP	HELIUM ENG 200 HP EXT	LIQ METAL 500 HP EXT
INDIRECT CYCLE			
BYPASS RATIO	4.0	6.0	5.5
PRESSURE LOSS (DEDICATED)	6%	6%	6%
THRUST (LBS)	12,600	15,200	14,750
THRUST/MW	254	320	310
NUMBER ENGINES	12	10	10
ENGINE WT	14,720	16,300	15,600
TURBINE-PUMP SYSTEM WT (LBS)	11,020	18,000	—
TURBINE-PUMP MW REQT	61.2	95.2	—
TOTAL MW REQ	631	574	475
TOTAL ENGINE SYSTEM WT (LBS)	187,640	181,000	156,000
DIRECT CYCLE			
COMPRESSOR INLET TEMP °R	650	700	
FAN PRESSURE RATIO	1.6	1.6	
COMPRESSOR PRESSURE RATIO	2.7	2.4	
NET THRUST	14,000	12,000	
NET THRUST/MW	220	205.9	
NUMBER ENGINES	10	12	
ENGINE WEIGHT (LBS)	7111	6714	
TURBINE PUMP SYS WT (LBS)	12,000	10,000	
TURBINE PUMP MW REQ	63.6	58	
TOTAL MW REQ	700	754	
TOTAL ENGINE SYS WT (LBS)	83,110	90,568	

comparison of the dual vs dedicated nuclear engines using helium or liquid metal heat exchangers.

6.3.2 CONCLUSIONS:

1) From Table 6.3.1-1 it can be seen that the direct cycle ducted fan engine weighs 45% less than the indirect liquid metal engine and 55% less than the indirect helium heat exchanger engine.

2) The direct cycle ducted engine requires 10 to 22% more MW than the indirect helium heat exchanger engine and 47% more MW than the indirect liquid metal heat exchanger engine.

3) If the indirect cycle helium concept is employed a 4% engine weight savings and a 9% reactor power saving is possible if the secondary coolant loop is pumped by a central pump rather than engine driven pumps.

6.3.3 RECOMMENDATIONS

6.3.3.1 INDIRECT CYCLE: Several ways which might increase the thrust of the heat exchanger engines are:

1) Further investigation should be made into heat exchanger design with regard to lowering the engine pressure loss so that higher core mass flows can be used with the end results of greater thrust.

2) The possibility of heating up the bypass flow would increase the thrust significantly, provided the pressure losses due to heat exchanger interferences are small. A more detailed study of the flow passage and the heat exchanger air interfacing would have to be accomplished to determine the potential increase in thrust from bypass heating.

3) Investigation of improving the material limitations of the heat exchanger in order to increase the turbine inlet temperature.

6.3.3.2 DIRECT CYCLE: The direct engine system employing the regenerative cycle would be highly competitive with the liquid metal heat exchanger engine if the net thrust/MW could be increased by

1) Design the regenerative cycle for high altitude cruise missions so that the compressor inlet temperature can be reduced by 15% and the thrust increased on the order of 35%. A tradeoff would have to be performed between heat exchanger and regenerator weight increases for this additional thrust.

2) A critical evaluation of pumping requirements in the primary loop to determine means of reducing pumping power requirements and thus releasing that reactor power for propulsion or weight reduction.

SECTION 7
HEAT TRANSFER

7.0 INTRODUCTION

The purpose of the heat transfer analysis is to examine several possible means by which the thermal energy developed in a nuclear reactor may be transferred to the air mass flow through the core of the turbofan engine. Since this analysis is searching for designs that are acceptable for use in airborne systems, size and weight parameters will carry increased importance. It is understood that these parameters vary inversely with other parameters, such as costs of development and fabrication factors. However, since this is primarily a feasibility study for a nuclear powered aircraft system, the study does not attempt to optimize or perform in-depth tradeoff analyses on these conflicting parameters. Rather, its main objective is to credibly establish the feasibility of a theoretical heat transfer system that is capable of providing sufficient energy to the engines to power the design point aircraft. It is hoped that the results of this analysis will then act as an incentive to increase efforts toward optimization of the parameters it has identified as the feasibility driving parameters, as well as those that have been subordinated.

Another non-quantitative factor that figured heavily in the initial design options for the heat transfer system was safety. Although a single-loop heat transfer system was more efficient than a multiple-loop system, it was decided that the analysis would ignore the single-loop system strictly on qualitative environmental safety considerations. Since this system is expected to operate in an airborne environment complete with turbulence and constant vibration stresses, the analysis assumed the probability of a coolant loop leak to be high enough that specific precautions would have to be included to prevent contamination of the surrounding environment by the inadvertent release of radioactive particles. This pointed the methodology to the double-loop system that is used as the basic design point; it is illustrated in Figure 7.0.1.1-1. In this system, not only the reactor is enclosed in the containment vessel, but the entire primary coolant loop and the reactor heat exchangers as well. Thus, any leakage of the coolant from the primary loop, during normal operation, has no significantly probable means of escaping into the environment. Even in the event of a crash, fast-acting valves in the secondary loop, located in the containment vessel wall, close to prevent any leakage of radiation to the environment. Details on the valves are included in Section 7.6.

This analysis attempts not to optimize strictly for the sake of heat transfer. It tries to evaluate the system with a broader view that incorporates both the demands of the heat transfer system on the reactor as well as the demands on the heat transfer system by the engine. In short, it attempts to remain within the "systems concept" as much as possible. In order to maintain this broad approach to the heat transfer problem, it was necessary to carry many additional parametric variables through the methodology calculations. It is believed that the efforts involved in maintaining them throughout will give to the individual readers interested only in the behavior of certain specific parameters, a better understanding of exactly how the system as a whole responds to specific attempts to optimize only a selected portion of the system. In keeping with this idea, the methodology used in this section is

designed to show basically how the heat transfer system fits into the overall powerplant system. To accomplish this, first, a description and illustration of the components of the various heat transfer system configurations that were considered to show how the heat transfer system interfaces with the engine and the reactor is given. The two systems that are considered in this report are the direct cycle configuration and the indirect cycle configuration. Second, the heat transfer fluid parameter calculations in both configurations are made. Heat transfer fluids that are considered are helium and the sodium-potassium compound, NaK. The specific NaK compound contains 44% potassium by weight. The following three sections involve developing the reactor heat exchanger size and weight parameters, the secondary loop piping specifications, and the engine heat exchanger parameters in the various combinations of the two configurations and the two heat transfer mediums. The last section, which contains the results and comparisons of the analysis in a synoptic format, is intended to show how the overall heat transfer system parameters vary according to the various combinations of configurations and fluid mediums.

TABLE 7.0-1 SYMBOLS LIST

MAIN SYMBOLS LIST	
A	HEAT TRANSFER SURFACE AREA
A_{fr}	HEAT EXCHANGER FRONTAL AREA
A_t	CROSS SECTIONAL AREA OF 1 TUBE
b	FIN HEIGHT
c_p	SPECIFIC HEAT
C	CAPACITY RATE OF HEAT EXCHANGER (C = mcp)
D	DIAMETER, OUTSIDE DIAMETER
D_h	HYDRAULIC DIAMETER
d	DISTANCE
d_{fin}	FIN DIAMETER
d_i	INSIDE DIAMETER
d_j	JAMESON DIAMETER
f	FRICTION FACTOR
G	MASS FLUX OF HEAT TRANSFER FLUID
g	GRAVITATIONAL PROPORTIONALITY CONSTANT
H	INLET VELOCITY HEAD
h	HEAT TRANSFER COEFFICIENT
K	PRESSURE LOSS COEFFICIENT
k	THERMAL CONDUCTIVITY
L	FLOW LENGTH

TABLE 7.0.1 SYMBOLS LIST (Continued)

ℓ	TUBE LENGTH
MW	MEGAWATTS
$\dot{m}$	MASS FLOW RATE
N	NUMBER
N_{tu}	NUMBER OF TRANSFER UNITS
v	VELOCITY
GREEK SYMBOLS	
α	RATIO OF TOTAL TRANSFER AREA ON ONE SIDE OF HEAT EXCHANGER TO THE TOTAL VOLUME OF THE HEAT EXCHANGER
Δ	DENOTES DIFFERENCE
δ	DISTANCE BETWEEN FINS
ε	HEAT EXCHANGER EFFECTIVENESS
η_f	FIN EFFECTIVENESS
η_o	OVERALL SURFACE EFFECTIVENESS
ν	KINEMATIC VISCOSITY
σ_H	HOOP STRESS
Σ	RATIO OF FREE-FLOW AREA TO FRONTAL AREA
μ	DYNAMIC (ABSOLUTE) VISCOSITY
ρ	DENSITY
SUBSCRIPTS	
1,2,3,4	PIPE RADII OR STATIONS IN HEAT TRANSFER SYSTEM
a	AIR
av	AVERAGE
h	HELIUM
c	CONCENTRIC PIPE
e	ENGINE
min	MINIMUM
max	MAXIMUM
p	PRIMARY LOOP
I	INSULATION
s	SECONDARY LOOP

TABLE 7.0.1 SYMBOLS LIST (Continued)

E	ENGINE HEAT EXCHANGER
R	REACTOR HEAT EXCHANGER
t	TUBE(S)
Pl	PIPE
f	FILM
y	PER PASS THROUGH HEAT EXCHANGER

7.0.1 HEAT TRANSFER SYSTEMS DESCRIPTIONS: In the basic turbofan engine, heat energy is transferred to the core air mass flow via the combustion process which uses a chemical fuel as the energy source. The overall powerplant system of the nuclear powered aircraft replaces the chemical energy source with a nuclear reactor, providing sufficient thermal energy to the core air mass flow to produce the desired thrust from the engine. The heat transfer system is defined as a subsystem of the overall powerplant system which has the responsibility of transferring this thermal energy from the reactor to the engine core air mass flow. The overall powerplant system can be depicted in a simplified energy flow diagram as in Figure 7.0.1-1.

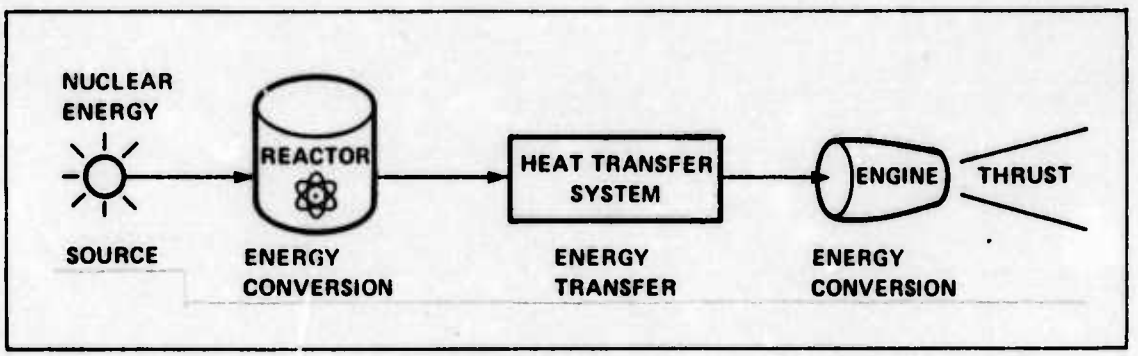

Figure 7.0.1-1. Energy Flow

The three basic major subsystems of the powerplant system are: (1) the reactor, which converts the nuclear energy to thermal energy; (2) the heat transfer system, which extracts this energy from the reactor and transports it to the engines; and (3) the engines themselves, which convert this thermal energy into mechanical and kinetic energy to produce the desired thrust. This section deals in detail with only the heat transfer system.

7.0.1.1 THE INDIRECT CYCLE HEAT TRANSFER SYSTEM: The indirect cycle utilizes a secondary heat transfer loop to extract the energy from the reactor coolant and transfer it to the engine core air mass flow. This energized core air then is expanded across the turbine in the engine to produce the energy to drive the compressor and the bypass fan and to

produce a thrust as the end product. The basic two-loop, indirect cycle heat transfer system is composed of these four primary subsystems:

1) primary reactor coolant loop
2) reactor heat exchanger
3) secondary heat transfer loop
4) ergine heat exchanger

These subsystems are physically related, as shown in Figure 7.0.1.1-1.

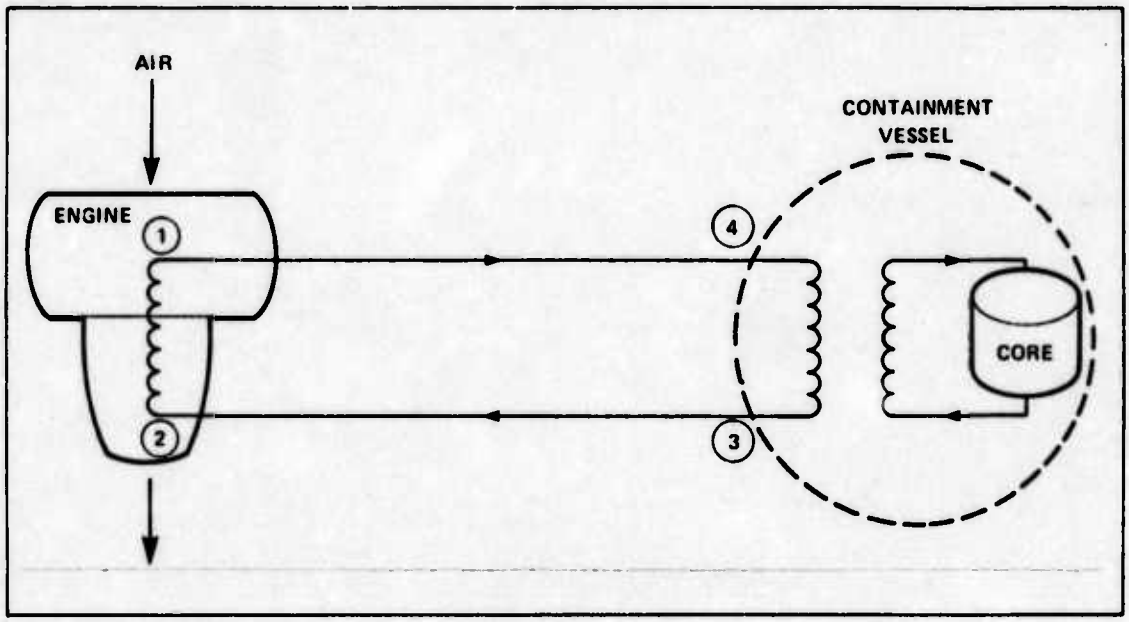

Figure 7.0.1.1-1. Two-Loop Indirect Cycle System

The primary reactor coolant loop consists of a network of pumps and piping that conducts the coolant fluid through the reactor core where thermal energy is absorbed. From here the fluid moves to the primary side of the reactor heat exchanger, where it releases this energy, and finally moves back to the reactor to absorb more heat. This entire primary coolant loop, including all required pumps and valves, is physically located inside the reactor containment vessel.

The reactor heat exchanger is the means by which the thermal energy of the primary loop fluid is transferred to the secondary loop heat transfer fluid. This subsystem also is located entirely within the reactor containment vessel. The reactor heat exchanger is described in more detail in Section 7.2.

The secondary heat transfer loop is the network of pumps and pipes containing the secondary heat transfer fluid. The primary reason that this loop is inserted into the heat transfer system is to reduce the probability of a release of radioactive reactor coolant and/or radioactive fission fragments to the surrounding environment in the event of a reactor coolant system leak. The secondary coolant loop absorbs heat in the secondary side of the reactor

heat exchanger and transports this through the piping network to the secondary side of each engine heat exchanger where the thermal energy is released. The coolant flow then returns to the reactor heat exchanger to be reenergized. With the exception of the secondary side of the reactor heat exchanger, the secondary coolant loop is located entirely outside the containment vessel. That portion located inside the containment vessel can be isolated by fast acting valves, which are described in Section 7.6. The engine heat exchanger, which transfers the thermal energy of the secondary loop fluid to the engine core air mass flow, is described in detail and illustrated in Section 7.4.

7.0.1.2 DIRECT CYCLE HEAT TRANSFER SYSTEM: The direct cycle heat transfer system differs from the indirect cycle heat transfer system primarily in that there is no heat exchanger in the engine to transfer energy from the heat transfer fluid to the air. In fact, the direct cycle does not use air as the working medium in the engine core because, in the direct cycle, the gaseous heat transfer medium in the secondary loop is itself expanded directly across a turbine and recovered. The energy extracted from this heat transfer fluid by the turbine is then used to drive a compressor and the bypass fan. The fan produces thrust and the compressor repressurizes the gaseous heat transfer fluid prior to going back to the reactor heat exchanger for additional thermal energy. This basic two-loop direct cycle heat transfer system is composed of five major subsystems:

1) primary reactor coolant loop
2) heat exchanger
3) secondary heat transfer loop
4) recuperator
5) precooler

These subsystems are physically related to the reactor and the engine subsystems as shown in Figure 7.0.1.2-1.

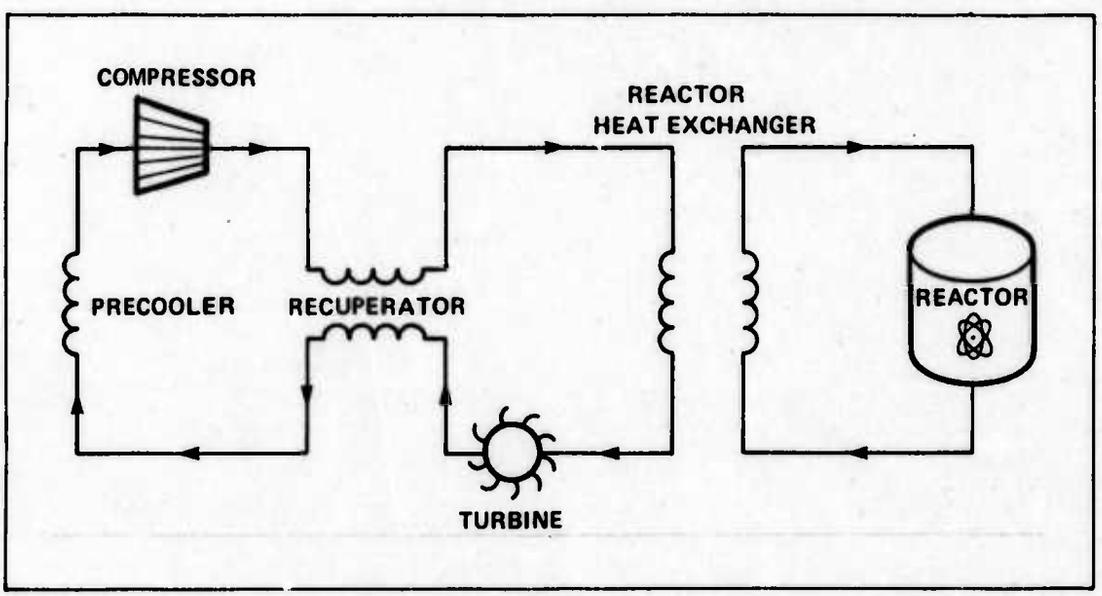

Figure 7.0.1.2-1. Two-Loop Direct Cycle System

The primary reactor coolant loop and the reactor heat exchangers serve the same purpose and are correlated as described in the previous section on the indirect cycle heat transfer system. The secondary loop serves the same function as the indirect cycle configuration also, in that it conducts the heat transfer fluid from the reactor heat exchanger out to the engine. Here the similarity ends. When the hot gaseous heat transfer fluid arrives at the engine, it is expanded directly across the turbine where a portion of its total thermal energy is extracted. After this expansion, the heat transfer fluid goes to the recuperator where it releases some more of its thermal energy. The recuperator is a heat exchanger that utilizes the gaseous heat transfer fluid coming off the turbine as its hot side fluid and the recompressed heat transfer fluid coming off the compressor as its cold side fluid. Thus thermal energy is transferred from the turbine outlet to the compressor outlet fluid. After the secondary fluid leaves the reuperator it goes to the precooler, which is also a heat exchanger, where it transfers the remaining thermal energy necessary to close the modified Brayton regeneration cycle. A detailed description of the secondary loop heat transfer process in the engine is presented in Section 7.4.2. From the precooler, the fluid proceeds to the compressor where a portion of the energy extracted at the turbine is reinstated. This is accomplished by the actual work done by the compressor on the gas. After leaving the compressor, the fluid goes back through the recuperator to gain yet more thermal energy prior to returning to the reactor heat exchanger for completion of the reheating process.

Another design option of the direct cycle heat transfer system that will be presented involves the same principles of operation just described, except that the secondary loop heat transfer fluid that exits the reactor heat exchanger is not routed out to each engine for turbine expansion. This option involves the use of two larger turbines located adjacent to the reactor containment vessel. The hot secondary loop coolant fluid is expanded across these turbines, recovered, and reprocessed for reheating. The two turbines use the energy derived from the heat transfer fluid to drive rotating shafts that are mechanically connected to the engines via a reduction gearbox assembly. The engines in this configuration are of the ducted-fan type.

7.0.2 POINT DESIGN SELECTION: There are many different types, shapes, and sizes of heat exchanger designs, and many piping options to consider, including material, configurations, etc. Thus, the first problem to be faced in the analysis of the heat transfer system was the establishment of a design point. As research progressed, the reasons established in Sections 7.0 and 7.1.0 rapidly became visible and pointed the study effort toward a design point which uses an indirect cycle, High Temperature Gas Reactor (HTGR) System with helium as the coolant and heat transfer medium. Consequently this system was used as the basic energy source system upon which the heat transfer system analysis would be accomplished. With the HTGR system as the energy source, and the two-loop indirect cycle system described earlier as the initial heat transfer system configuration, the total design point package was complete from the energy source to the engine heat exchanger. It should also be noted by the reader that this design point and other initializing assumptions, and parameters yet to be defined, are basically within the state-of-the-art in their particular areas today. The analysis purposely avoided extrapolating parameters into the future in order to exclude as much technological risk as possible from the results of the study.

7.1 HEAT TRANSFER FLUID PARAMETERS

There has been much experimentation on various materials for use as a heat transfer medium. Some of these work well in certain situations and others do not. The suitability of a particular material will depend on many variables. Some of the more important factors that need to be evaluated are:

1) the thermal properties of the material as they affect the temperature regime in which this material can be used.

2) the corrosion properties the material exhibits on the containing materials.

3) the power requirements necessary to circulate the fluid.

4) heat-transfer coefficients which affect the size of the heat exchanger.

5) the hazards involved and safety precautions that must be evaluated in the operating environment.

6) overall economic costs versus the benefits of the material.

7.1.1 HELIUM: In this study, helium was selected as the primary point design heat transfer medium, based primarily on the following reasons. Safety consideration showed that since helium does not activate, the danger of radioactive release is reduced. Also, helium remains stable in the high temperature region in which the reactor core operates. Helium exhibits favorable corrosion properties on most common containing vessel materials. The hazards and safety precautions required with helium are less than with many other common heat transfer mediums, particularly the liquid metals. The penalties weighed against these benefits were a higher pumping power requirement for gaseous helium and poorer heat transfer properties which result in larger heat exchanger requirements.

7.1.1.1 HELIUM INDIRECT CYCLE: The methodology of the heat transfer systems analysis was developed using helium as the heat transfer medium. This basic methodology was then reapplied to analyze the heat transfer system configurations using another heat transfer fluid, specifically the liquid metal compound, NaK. The two heat transfer fluid properties that need to be defined first are the mass flow rate of the fluid and the temperature of this fluid at the various points around the heat transfer system. The starting point was as explained previously at the engine/heat transfer system interface. At this interface, the following parameters of the engine core air mass flow have been established.

- Air Mass flow rate = 200 lb/sec
- Engine heat exchanger air inlet temperature = 600°F
- Engine heat exchanger air outlet temperature = 1500°F

The 900°F air temperature change across the engine heat exchanger and the 200 lb/sec mass flow rate are sufficient to produce the design point thrust as developed in Section 6. Using the

specified engine core air mass flow rate and the specific heat of air, the capacity rate of the air was defined as:

$$C_a = \dot{m}_a c_{pa}$$

where $\dot{m}_a$ = engine core air mass flow rate

c_{pa} = specific heat of air

Now form the ratio of the capacity rates of air on the one side of the engine heat exchanger and the helium on the other side.

$$\frac{C_a}{C_s} = \frac{\dot{m}_a c_{pa}}{\dot{m}_s c_{ph}}$$

If now a specific value is assigned to this ratio, the equation can be solved for $\dot{m}_s$, the mass flow rate of the helium in the secondary heat transfer loop. Initially, C_a / C_s was assigned an arbitrary value but, after the methodology was complete, this value was then iterated from 0.10 to 1.0 before the value of 0.58 was settled on as the optimal value for this particular system. These calculations and the rationale behind the value selected are performed in Section 7.4.1. When $C_{hs} = .58$ is used, the helium mass flow rate becomes

$$\dot{m}_s = \frac{\dot{m}_a c_{pa}}{(C_a/C_s)(c_{ph})} = 70 \text{ lb/sec}$$

The secondary loop helium inlet temperature can be calculated using the heat exchanger efficiency equation.

$$\varepsilon = \frac{\text{actual heat transferred}}{\text{maximum possible heat transfer}} \qquad \text{(7.1.1-2) (Ref. 74, p. 308)}$$

By the definition of C_s, the air side engine heat exchanger has the minimum capacity rate. Therefore, the maximum possible heat transfer would occur if the air underwent the maximum temperature change present in the heat exchanger. Therefore, using the basic heat flow equation

$$q = \dot{m} c_p \Delta T \qquad \text{(7.1.1-3) (Ref. 129, p. 186)}$$

where q = heat transfer rate

ΔT = temperature change of the fluid

$\dot{m}$ = fluid mass flow rate

The maximum possible heat transfer is defined as

$$q_a = \dot{m}_a c_{pa} (T_{s_1} - T_{a_1})$$

The actual heat transferred then is defined using the actual temperature change of the air.

$$q_a = \dot{m}_a \, c_{pa} \, (T_{a_2} - T_{a_1})$$

Thus, the effectiveness is the ratio of these two quantities of heat transfer.

$$\varepsilon = \frac{\dot{m}_a \, c_{pa} \, (T_{a_2} - T_{a_1})}{\dot{m}_s \, c_{ph} \, (T_{s_1} - T_{a_1})} \qquad (7.1.1\text{-}4)$$

This yields $T_{S1} = 1600°F$.

Based on research of prior studies of heat exchangers, and conversations with several heat transfer authorities, the study assumed an engine heat exchanger effectiveness, ε, of 90%. (Refs. 70,111,176). When this is substituted in Eq. 7.1.1-4 the equation can be solved for T_{S1}, the secondary loop helium temperature at the inlet side of the engine heat exchanger. The same equation in a different form can be solved for the secondary loop helium temperature coming out of the engine heat exchanger. The different form involved uses the heat transferred from the helium as the numerator of the effectiveness equation. This calculation is as follows:

$$\varepsilon = \frac{\dot{m}_s \, c_{ph} \, (T_{s_1} - T_{s_2})}{\dot{m}_a \, c_{pa} \, (T_{s_1} - T_{a_1})} \qquad (7.1.1\text{-}5)$$

Rearranging variables and solving for T_{S2} yields:

$$T_{s_2} = 1078°F$$

Using Eq. 7.1.1-3 and these inlet and outlet temperatures, the total power transferred from the helium to the air can be calculated.

$$\begin{aligned} q &= \dot{m}_s \, c_{ph} \, (T_{s_1} - T_{s_2}) \\ &= 4.5 \times 10^4 \text{ BTU/sec} \\ &= 47.48 \text{ megawatts (MW)} \end{aligned}$$

Thus, this is the power required to be delivered to the engine heat exchanger by the heat transfer fluid. This will produce the desired 900°F temperature change in the 200 lb/sec core air mass flow.

Now the inlet and outlet temperatures of the helium can be summed and then divided by two to get an average helium temperature in the engine heat exchanger. Assuming that the helium

behaves as an ideal gas, use the average helium temperature expressed in the Kelvin scale in the Ideal Gas Law equation. This equation when solved for the helium density is

$$\rho = \frac{P}{RT} \qquad (7.1.1\text{-}6)$$

Assuming an operating helium pressure in the secondary loop of 1800 psi yields an average helium density of

$$\rho_{es} = .373 \text{ lb/ft}^3$$

Summarizing up to this point, the methodology has utilized an established air mass flow rate of 200 lb/sec, an air temperature change from 600°F to 1500°F, a capacity rate ratio of 0.58 and an engine heat exchanger effectiveness of 90%. These parameters define the required secondary loop helium mass flow rate of 69.41 lb/sec with an engine heat exchanger inlet temperature of 1600°F and outlet temperature of 1078°F, and an average helium density of .373 lb/cu ft. in the engine heat exchanger. These heat transfer fluid parameter values provide 47.48 MW of power to the core air mass flow.

The next heat transfer fluid parameters to be considered are the temperatures of the fluid at the inlet and outlet of the reactor heat exchanger. To calculate these, however, the heat loss in the piping that connects the engine heat exchangers and the reactor heat exchanger must be considered since the physical distance separating them is significant, particularly for the outboard engines.

Before the thermal energy loss in the pipes can be calculated, several limiting parameters must be defined. The first of these is the maximum amount of radial pipe heat loss that will be allowed. In all the cases it was assumed that 0.1% of the thermal energy being transferred to the air by the helium is the maximum amount of radial heat loss that will be allowed. The primary external means of control over the radial heat loss is the type and thickness of insulation around the pipes. Also, a certain amount of control can be exercised with internal parameters such as flow velocity and/or fluid temperatures and piping material thermal conductivity. The other parameter that must be defined is the ambient external air temperature that will be surrounding the outer circumference of the pipe insulation. This temperature is defined to be -70°F since this would be about the coldest temperature that would be expected in the wing after an extended period of flight at altitude. The coldest temperature was purposely chosen so that the radial temperature differential between the bulk fluid in the pipe and the ambient air would be large. This would provide a "worst case" condition for the analysis. The third parameter to be defined is the maximum allowable surface temperature of the outer edge of the insulation layer. This is assumed to be 100°F to preclude any thermal burning of wires and/or other problems developing from high heat sources.

With these parameters defined, the basic heat transfer equations can be used to equate the radial heat loss to the longitudinal heat loss. This allows the solution for T_{S4}, the

helium temperature at the outlet of the secondary loop side of the reactor heat exchanger and T_{S3} the helium temperature at the inlet of the secondary loop side of the reactor heat exchanger. The next step involves using these two temperatures with T_{S1} and T_{S2} to derive the longitudinal average temperature of the secondary loop supply line helium and the return line helium. These average fluid temperatures can then be used to calculate the actual radial heat loss and the maximum surface temperature at the outer edge of the insulation layer.

If either of these parameters then exceeds its assumed maximum value, the insulation thickness is increased, T_{S3} and T_{S4} are recalculated using the new radial heat loss value, and the entire calculation is reiterated to define another maximum surface temperature and radial heat loss. This process is continued until the insulation is thick enough to keep the radial heat loss and maximum insulation surface temperatures within the maximum design limits. Appendix A.7.1 contains a complete sample set of calculations concerning the radial heat loss of the pipes and the other associated parameters. Specifically, there are 47.48 MW being transferred to the air from the secondary loop helium in each engine heat exchanger and the total pipe loss per engine is less than 0.05 MW. Thus the radial thermal energy loss that results is negligible when compared to the amount of thermal energy being transferred to the air.

The temperature, T_{S4}, at the outlet of the secondary loop side of the reactor heat exchanger is 1600°F and the temperature, T_{S3}, at the inlet of the secondary loop side of the reactor heat exchanger is 1078°F. Now that the temperatures are defined on the secondary loop side of the reactor heat exchanger, the next parameters which need to be defined are the temperatures on the primary loop side and the mass flow rate of the heat transfer fluid in the primary loop.

The reactor heat exchangers are of the basic plate-fin design. This design was selected since it presented a very compact heat transfer package and the overall size and weight of the containment vessel was sensitive to the heat exchanger size. A capacity rate ratio of 1 was selected for this heat exchanger since the plate thickness was very thin, and equal dynamics on both sides would minimize the stresses imposed on it. The effectiveness of this heat exchanger design was initially assumed to be 75%. The effectiveness equation, Eq. 7.1.1-2, can now be used in the same manner as in the engine heat exchanger temperature calculations to determine the primary loop side inlet and outlet temperatures of the primary loop helium. The results of these calculations are $T_{p1} = 1775°F$ and $T_{p2} = 1252°F$. The mass flow rate in the primary loop can be determined by assuming that the difference in the C_{ph} values between the primary loop and the secondary loop are negligible and by using the capacity rate ratio of 1. These conditions then define the primary mass flow rate equal to the secondary mass flow rate.

Since the reactor heat exchangers are in the containment vessel, piping losses between them and the reactor are assumed negligible. Therefore T_{p1} can be equated to the reactor outlet temperature and T_{p2} equated to the reactor inlet temperature. These temperatures along with the primary loop mass flow rate are the interfacing parameters of the heat transfer system and the reactor.

Figure 7.1.1.1-1 is a summary of the fluid parameters for the two-loop indirect cycle system using helium as the heat transfer fluid.

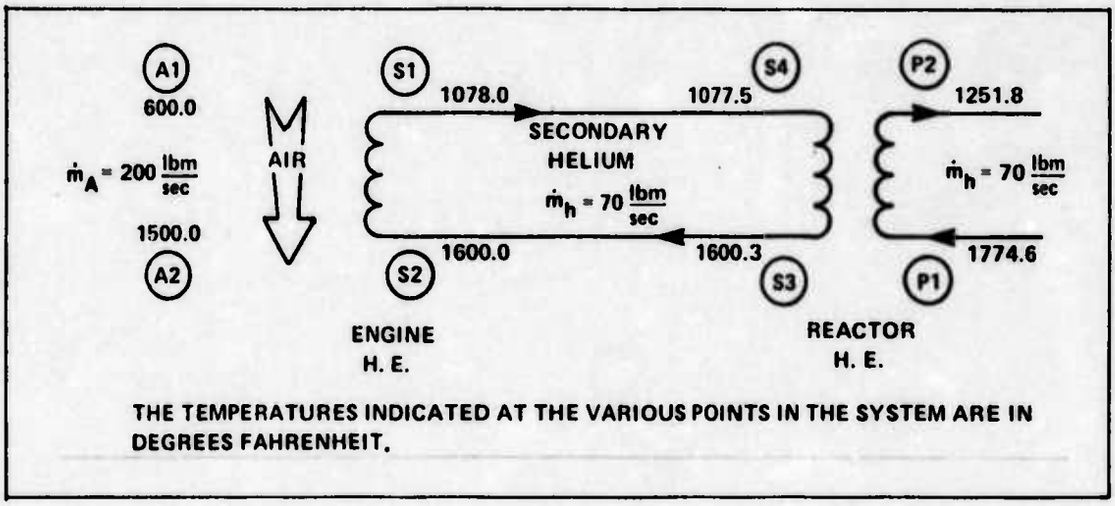

Figure 7.1.1.1-1. Helium Parameters

7.1.1.2 HELIUM DIRECT CYCLE: Figure 7.1.1.2-1 illustrates the direct cycle system that will be analyzed. Initializing temperature values that are underlined once are derived in Section 6.2. Values that are underlined twice are assumptions that already have or will be explained in this section.

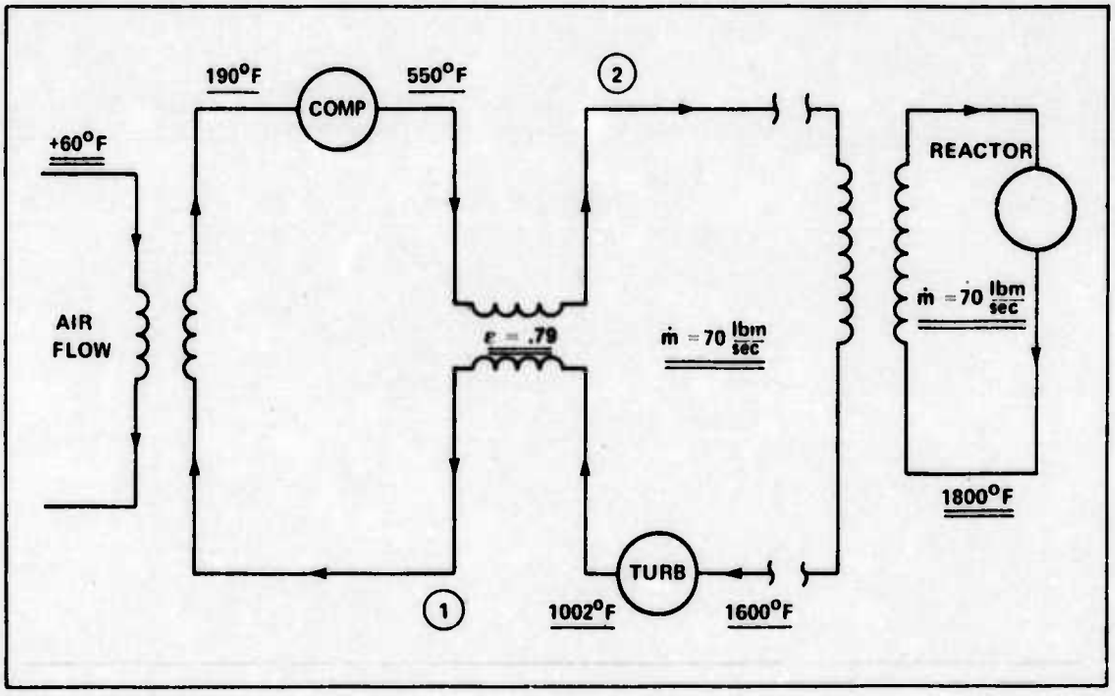

Figure 7.1.1.2-1. Direct Cycle

The outside ambient air temperature of +60°F is assumed for reasons explained in Section 7.4.2. Also, the value of the engine heat exchanger effectiveness is calculated in that section. The secondary loop heat transfer fluid mass flow rate is assumed to be 70 lb/sec, as in the indirect cycle.

The first two heat transfer fluid parameters to be calculated are those of the recuperator outlet temperature on the turbine side and on the compressor side. This is done using Eq. 7.1.1-2, an assumed recuperator effectiveness of 79%, and the turbine and compressor outlet temperatures shown on Figure 7.1.1.2-1 and derived in Section 6.2. These temperature values are:

$$T_1 = 645°F$$
$$T_2 = 907°F$$

where T_1 = recuperator outlet temperature on the turbine side
T_2 = recuperator outlet temperature on the compressor side

Assuming negligible pipe losses in the secondary loop, a maximum reactor output temperature of 1800°F, and a capacity rate ratio of 1, the effectiveness of the reactor heat exchangers can be calculated using Eq. 7.1.1-2. This turns out to be 77% for this direct cycle system. The last parameter to be defined for the heat transfer fluid is the outlet temperature of the reactor heat exchangers. This is 1107°F. Figure 7.1.1.2-2 is a diagram of the direct cycle engine system with all the flow rate and temperature data shown.

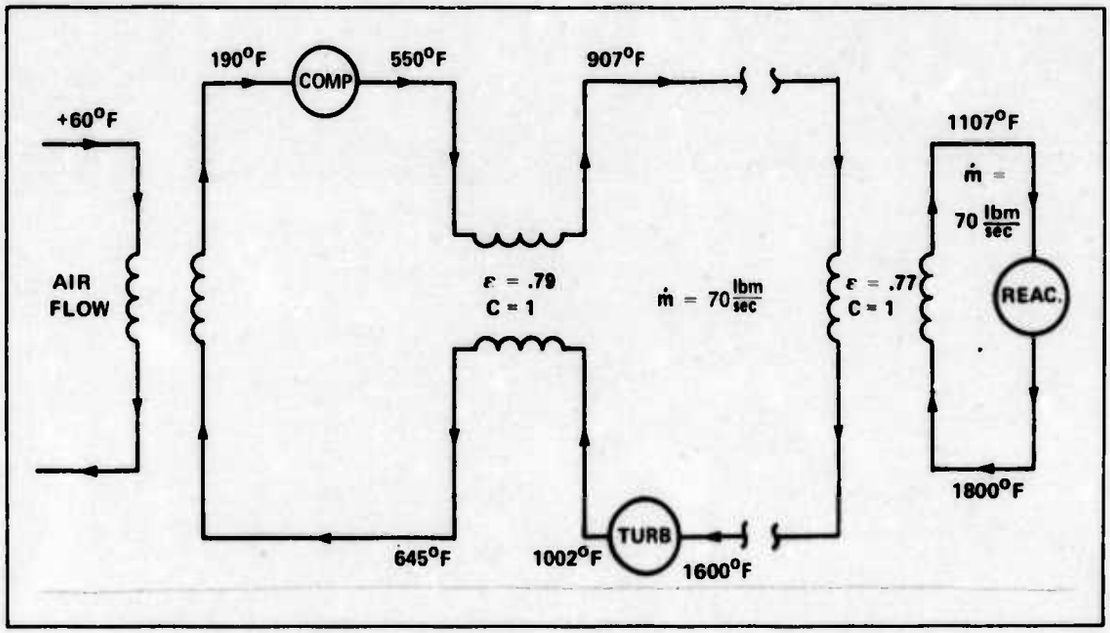

Figure 7.1.1.2-2. Direct Cycle Helium Parameters

Now that the heat transfer fluid parameters are defined, it is possible to calculate the reactor output. Using Eq. 7.1.1-3 this turns out to be 63.6 MW. Of this total, 41.74 MW are transferred to the air in the precooler and lost from the system. Additionally, note that for the same reactor output temperature and primary loop mass flow rate, the overall power required from the reactor is approximately 25% greater for the direct cycle. This increased power requirement will bear directly on the size and weight of the reactor and containment vessel.

7.1.2 NaK INDIRECT CYCLE: The identical methodology used in the helium analysis was used to analyze an indirect cycle system using NaK as the reactor coolant and secondary heat transfer fluid. The specific physical properties and flow parameters that were changed to their appropriate values for NaK are listed in Table 7.1.2-1. Figure 7.1.2-1 presents the temperatures and mass flow rates that resulted from this analysis. Notice that the maximum temperature required is over 100°F less than in the helium system which produced the same 47.48 MW at the engine interface.

TABLE 7.1.2-1. PHYSICAL PROPERTIES OF HELIUM AND NaK

PARAMETER	UNITS	HELIUM	NaK
SPECIFIC HEAT (Cp)	BTU/LB°F	1.242	.249
KINEMATIC VISCOSITY (ν)	SQ FT/SEC	8.3×10^{-5}	2.34×10^{-6}
ABSOLUTE VISCOSITY (μ)	LB/SEC FT	3.1×10^{-5}	1.08×10^{-4}
DENSITY (ρ)			
(SECONDARY SIDE)	LB/FT^3	0.373	46.2
(REACTOR SIDE)	LB/FT^3	0.340	46.2
THERMAL CONDUCTIVITY (k)			
(SECONDARY SIDE)	BTU/HR FT°F	0.330	15.39
(REACTOR SIDE)	BTU/HR FT°F	0.355	15.39
CAPACITY RATIO		0.58	0.22
SECONDARY LOOP HEAT EXCHANGER FLUID VELOCITY	FT/SEC	100	. 20
PIPE FLUID VELOCITY (υ))	FT/SEC	400	20

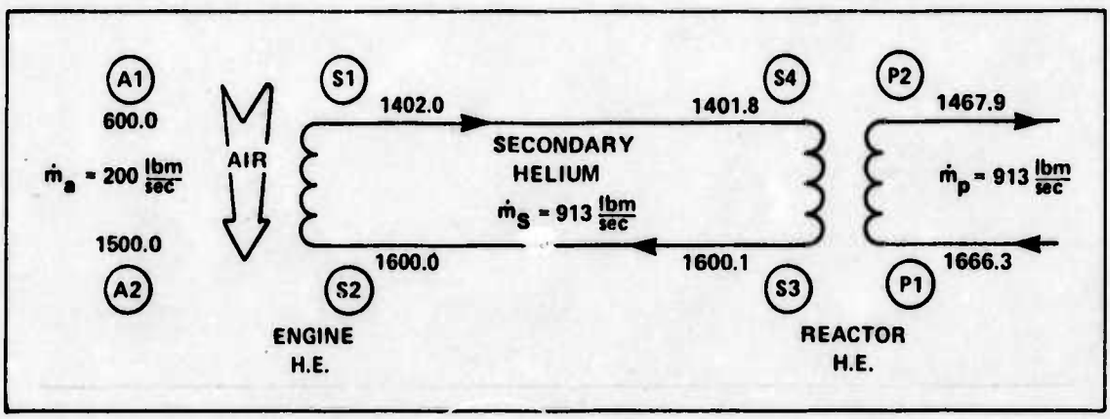

Figure 7.1.2-1. NaK Parameters

7.2 THE REACTOR HEAT EXCHANGER

The sum of the power required by the engine heat exchangers and the pipe losses yields 47.48 MW of power required to be transferred from the primary loop to the secondary loop to provide the 900°F temperature change in the engine core air mass flow. This task belongs to the reactor heat exchanger. Assuming there are 10 engines, the total reactor output requirement will be 475 MW. For safety reasons, this study considered a separate reactor heat exchanger for each engine. Each of these heat exchangers will be physically located within the reactor containment vessel. This will increase the overall power plant system safety margin since it provides that if a break or leak should occur on the primary loop side of an individual reactor heat exchanger, there will only be a requirement to shut down that particular engine. The calculations in Section 7.1.1.1 have quantitatively defined the parameters of temperature and mass flow rates for both heat transfer loops. The objective of this section is to use these parameters to define the reactor heat exchangers in terms of the physical parameters of size and weight. Also, the pressure losses experienced by the heat transfer fluid as it transits the heat exchanger cores will be calculated. The size and weight of these heat exchangers not only add themselves into the overall aircraft gross weight, but since they are located inside the containment vessel, their size directly affects the diameter of the containment sphere and hence they also geometrically affect the gross weight. In keeping with this idea, the reactor heat exchanger design was selected from the Kays and London compact heat exchanger studies (Ref. 87). It is of the basic plate-fin design and is illustrated in Figure 7.2-1. The plate-fin design was selected since by the very nature of its construction, it is possible to achieve a very large area compactness or heat transfer area available per unit of volume. There is more flexibility in the overall heat exchanger design using this construction since the two fluid sides are independent of one another and the most suitable type of extended (finned) surface can be chosen for each of the fluids.This is not possible with the circular-tube-bank surfaces where, for example, the choice of flow normal to a bank of tubes for one fluid automatically fixes the flow geometry for the other fluid.

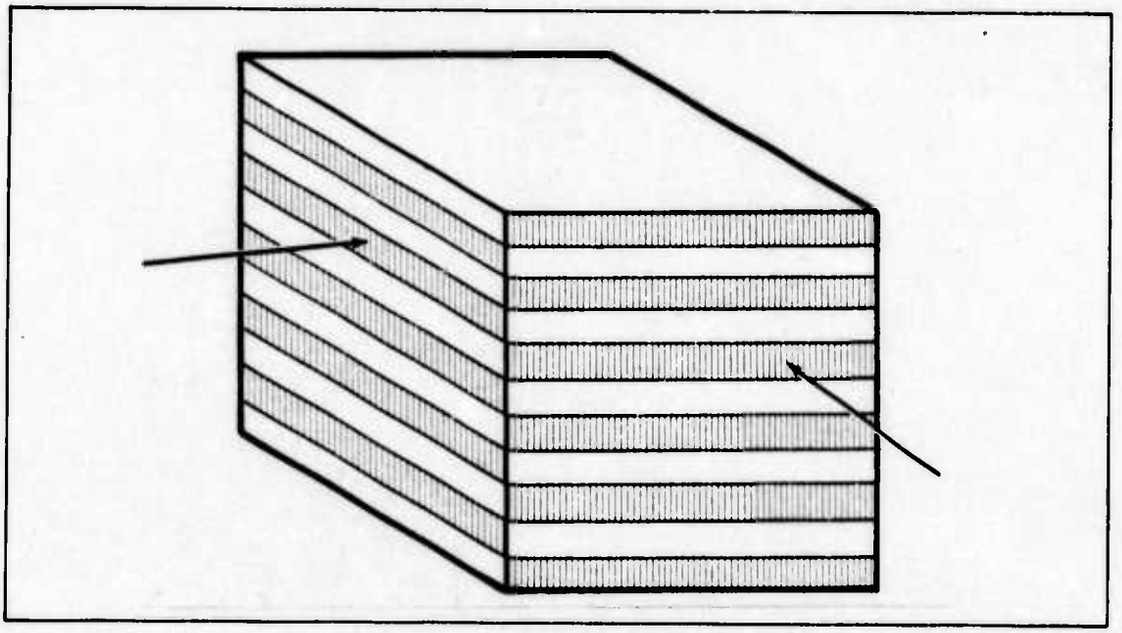

Figure 7.2-1. Reactor Heat Exchanger Core

7.2.1 DESIGN PARAMETERS OF REACTOR HEAT EXCHANGER: The plate-fin heat exchanger is constructed in a sandwich configuration with the primary and secondary loop fluids flowing in alternate layers. In the calculations, it is assumed that this heat exchanger is manifolded in a cross-flow configuration for basic header and manifold design simplicity considerations. Although it is possible to manifold this type heat exchanger in a more thermally efficient combination crossflow/counterflow configuration, there was not enough actual design data available to perform the required calculations for comparison. In this section, the key heat exchanger parameters of volume, weight, and fluid pressure loss will be calculated for helium and NaK.

7.2.1.1 HELIUM SYSTEM: In order to calculate the total reactor heat exchanger volume required, the mass flow rate of the heat transfer fluid in the secondary loop must be used to define the flow area required in the heat exchanger. Before this calculation can be performed, a fluid velocity must be defined. For any given mass flow rate, a direct relationship exists between the helium velocity and the pumping power required to drive the helium through the heat exchanger core. This relationship shows that the pumping power varies as the cube of the velocity as is defined by the following equation.

$$\text{Pumping power} = f \rho \frac{L}{D_h} A \frac{v^3}{2g}$$

where: f = friction factor

ρ = helium density

L = flow length

D_h = hydraulic diameter

A = free flow area

However, by combining Eq. 7.1.1-3 and Eq. 7.2.1-1, it can be seen that the heat transfer rate also varies with the velocity according to the following relationship.

$$q = \rho A v c_p \Delta T$$

where ΔT = temperature change in the helium resulting from transiting the heat exchanger.

A = free-flow area

The objective in the heat exchanger is to obtain a high heat transfer rate while maintaining the required pumping power at an acceptable level. Based on this consideration and on Ref. 70, a velocity of 100 ft/sec was selected as the design point helium velocity in the heat exchanger core. The flow area is defined using this velocity and the previously calculated values of the secondary loop heat transfer fluid parameters.

$$\text{Flow area} = \frac{\dot{m}_s}{\rho_{es}\, v_{es}}$$

where v_{es} is the velocity of the heat transfer fluid through the secondary loop side of the engine heat exchanger core.

This defines the required free flow area that must be presented to the secondary loop helium at the entry face of the heat exchanger core. At this point, it seems that a tabulation of the required heat exchanger core geometry specifications is necessary. These specifications have been extracted from Ref. 87 and consolidated in Table 7.2.1.1-1 for reference. These geometry specifications form, in a large part, the basis of the subsequent heat exchanger calculations.

TABLE 7.2.1.1-1. CORE GEOMETRY SPECIFICATIONS

NOMENCLATURE	SYMBOL	VALUE
PLATE MATERIAL	HAYNES 188	
PLATE SPACING (FT)	b	0.00833
PLATE THICKNESS (FT)	t	0.001
FINS PER INCH	N	46.45
FIN THICKNESS (IN.)	S	0.002
FIN AREA/TOTAL AREA	F	0.837
HEAT TRANSFER AREA/VOLUME BETWEEN PLATES (SQ FT/CU FT)	β	1332.5
HYDRAULIC DIAMETER (FT)	D_H	0.002643
HYDRAULIC RADIUS (FT)	R_H	0.000661

Once the flow area for the secondary helium flow has been established, the ratio of the free-flow area to the frontal area on the secondary loop side of the heat exchanger core, Σ, can be calculated

$$\Sigma = \frac{b\,\beta\,R_h}{2b + 2t} \qquad \text{(7.2.1-2) (Ref. 87, p. 36)}$$

Then the frontal area of the heat exchanger exposed to the secondary loop helium can be defined using

$$A_{fr} = \frac{\text{free-flow area}}{\Sigma} \qquad \text{(7.2.1-3) (Ref. 87, p. 36)}$$

Also needed is the ratio of the total heat transfer area on one side of the heat exchanger to the volume of the entire heat exchanger core

$$\alpha = \frac{\Sigma}{R_h} \qquad \text{(7.2.1-4) (Ref. 87, p. 36)}$$

Now using α and Σ, it is possible to calculate the heat transfer area available to the secondary loop helium based on an assumed flow length, L.

$$\text{heat transfer area available} = \alpha L A_{fr}$$

The value of L is initially chosen arbitrarily but will eventually be iterated to its final value by the equation of the required heat transfer area to the available heat transfer area. To compute the actual heat transfer area required for the heat exchanger, it is necessary to calculate the overall heat transfer coefficient of the heat exchanger. This is accomplished by first calculating the mass flux and the Stanton number which, in turn, define the film conductance coefficient for the helium on on both sides of the heat exchanger.

The Stanton number, N_{st}, can be calculated by using the heat transfer parameter, $N_{st}Pr^{2/3}$. To calculate this parameter first requires the determination of the Reynolds number for the helium flow on the secondary side of the heat exchanger, Re_s.

$$Re_s = \frac{\rho_{RS}\, v_{RS}\, D_h}{\mu_h} \qquad \text{(7.2.1-5)}$$

Use this value of Re_s and the Prandtl number (Pr) for helium defined at the average helium temperature on the secondary side to determine the Stanton number.

$$N_{st} = \frac{.0288}{(Re_s)^{.2}\,(Pr_s)^{2/3}} \qquad \text{(7.2.1-6) (Ref. 74, p. 148)}$$

Now using N_{st}, the unit film conductance for the helium on the secondary side of the heat exchanger can be calculated.

$$h_s = N_{st}\, \rho_{RS}\, v_{RS}\, c_{ph} \qquad \text{(7.2.1-7) (Ref. 87, p. 254)}$$

Both sides of this heat exchanger are using the same fluid and mass flow rates through the same core geometry and over equal flow lengths. Thus, by assuming that the higher average helium temperature on the primary loop side has insignificant effects on the specific heat, the Prandtl number, and the absolute viscosity coefficient, the actual difference between the unit film conductances on either side of the heat exchanger will be negligible. There is a significant density change, but this can be compensated for by increasing the velocity so that the mass flow rates remain equal on both sides. This maintains equal mass flux on either side. Therefore, the value calculated for h_s can be equated to h_p. When both film conductances are defined, the overall heat transfer coefficient for the heat exchanger can be calculated.

$$\frac{1}{U_R} = \frac{1}{\eta_o\, h_s} + \frac{1}{Z(\eta_o\, h_p)}$$

In this equation, η_o is the overall heat transfer surface effectiveness and is calculated using the methodology in Ref. 87, p.14. By entering Figure 7.2.1.1-1 with the capacity rate ratio and the heat exchanger effectiveness, the N_{tu} can be determined. This yields $N_{tu} = 4.50$. With this value and the definition of N_{tu}, the heat transfer area required can be calculated.

$$\text{Area required} = \frac{N_{tu}\, \dot{m}_s\, c_{ph}}{U_R} \qquad \text{(7.2.1-9)}$$

Once both the heat transfer area available and the heat transfer area required are calculated, the two are compared. The initial value of the flow length that was arbitrarily selected earlier is now adjusted as required to insure that the area available is at least as large as the area required. This adjustment was accomplished in a computer program and the resulting flow length was 3.23 feet. Once the flow length and heat transfer area available are finalized, the total heat exchanger volume can be calculated.

$$V_R = \frac{\text{heat transfer area available}}{\alpha} \qquad \text{(7.2.1-10)}$$

The next physical parameter desired is the heat exchanger weight. To make this definition, the ratio of volume of metal to total heat exchanger volume must be calculated. This can be accomplished using the ratio of fluid free flow area to frontal area. Also, since the heat exchanger is constructed in a cross flow configuration with equal flow lengths, and of the same plate-fin geometry, this ratio will be the same on both the secondary and primary sides.

Using Eq. 7.2.1-2, the value of Σ is calculated to be approximately 0.40. This means that 40% of the frontal area on that particular side is void. Since the layers are symmetric, 40% of the alternate layer is also void. Thus, there will be a total void volume of 80% which establishes 20% metal volume for the heat exchanger. Using this, the actual weight of the heat exchanger core can be calculated.

$$W_R = 0.2\,\rho_m\,V_R \qquad (7.2.1\text{-}11)$$

where: ρm = Density of heat exchanger metal

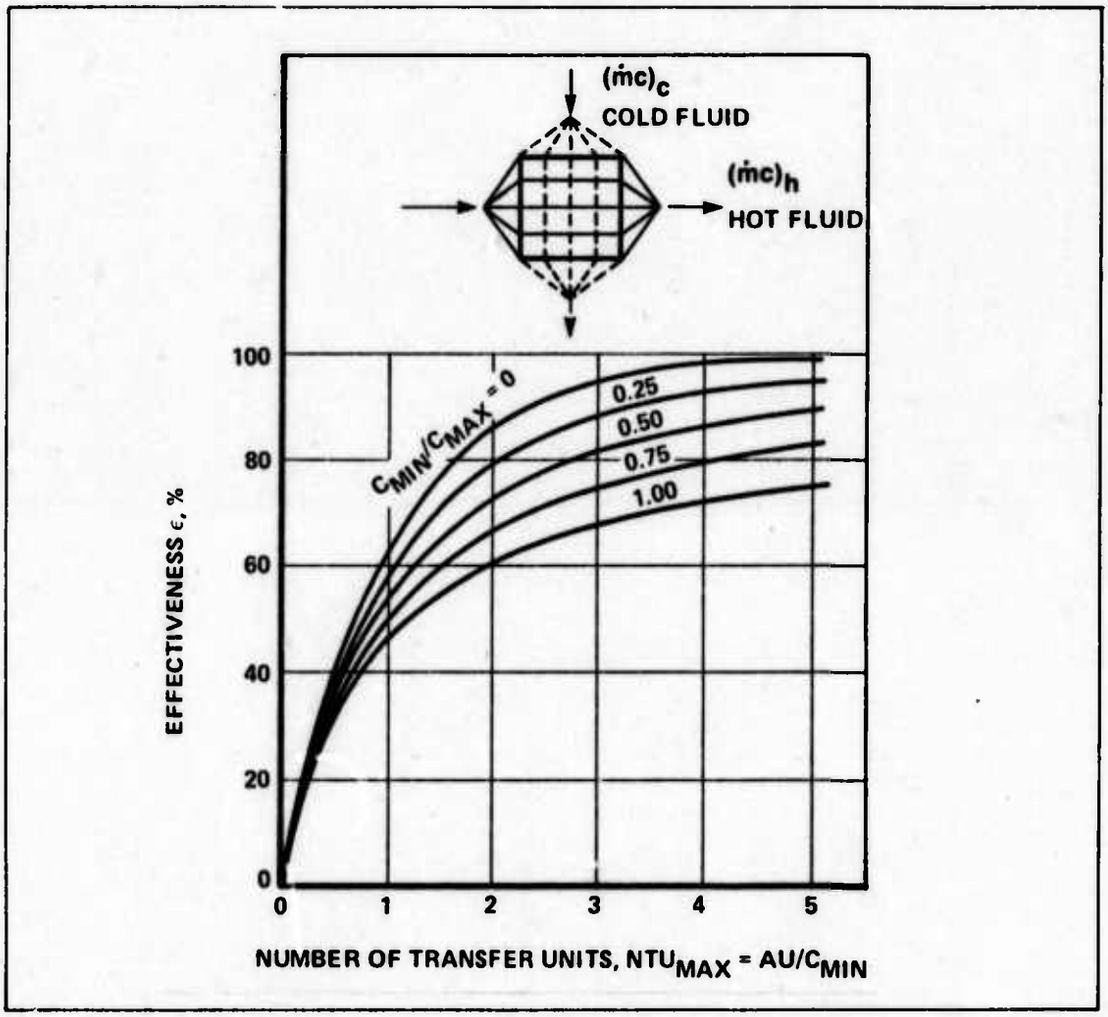

Figure 7.2.1.1-1. Effectiveness for Cross-Flow Exchanger with Fluids Unmixed (Ref. 74, p. 313)

This weight does not include any allowance for outer core support structure, headers, or manifolds. To maintain comparative uniformity, this study used the same approximation that was established in the General Electric report (Ref. 111, p. 48, 233) as an additional weight factor. This results in 12% of the core weight as containment and supporting structure weight. The header and manifold weights comprised 33% of the supported heat exchanger. The

combination of these yields a total heat exchanger package weight equal to 1.49 times the core weight. The resulting weights are tabulated in Table 7.2.1.1-2.

TABLE 7.2.1.1-2. HEAT EXCHANGER PARAMETERS

PARAMETER	HELIUM	NaK
CAPACITY RATE RATIO	0.58	0.22
ENGINE CORE AIR MASS FLOW (LB/SEC)	200	200
ENGINE CORE AIR MASS (°F)	900	900
SEC & PRI LOOP MASS FLOW (LB/SEC)	70	913
MAX TEMPERATURE OF HEAT TRANSFER FLUID (°F)	1775	1666
PRI & SEC LOOP PRESSURE	1800	130
PIPE DIAMETER (IN.)	10	13
NUMBER OF TUBES REQUIRED IN ENGINE HEAT EXCHANGER	9792	4032
TUBE LENGTH (IN.)	21	23.7
NUMBER OF BANKS OF TUBES	34	14
WEIGHT OF ENGINE HEAT EXCHANGER (LBS)	20,600	9300
VOLUME OF REACTOR HEAT EXCHANGER (CU FT)	15.72	3.8
WEIGHT OF REACTOR HEAT EXCHANGER (LB)	2700	650
PRESSURE DROP IN FLUID (PSI)	14.1	24
SEC. LOOP TOTAL		
PRI LOOP HEAT EXCHANGER CORE	7.3	13
SEC LOOP PUMPING POWER (HP)		
2-PIPE	681	121
CONCENTRIC	782	123

The next parameter to be calculated is the pressure drop of the helium as it transits the heat exchanger core. To accomplish this, the friction factor must first be defined.

$$f_{RS} = 0.184\ (Re_S)^{-0.2} \qquad 0(7.2.1\text{-}12)\ \text{(Ref. 129, p. 191)}$$

Using this friction factor and previously calculated parameters, the pressure drop can be determined.

$$\Delta P_{RS} = f_{RS}\, \rho_{RS}\, \frac{L}{D_h}\, \frac{v_{RS}^2}{2g} \qquad (7.2.1\text{-}13)\ \text{(Ref. 74, p. 163)}$$

To find the total pressure drop across the secondary side of the heat exchanger, the pressure drop incurred in the manifolds must also be included. This pressure drop is defined as follows:

$$\Delta P_{ms} = 0.595\, \rho_{RS} \frac{v_{RS}^2}{2g} \qquad \text{(7.2.1-14) (Refs. 111, p.229, 59, p. 161)}$$

Due to the higher average helium temperature on the primary side of the reactor heat exchanger, there is a significant density change if 1800 psi is maintained as the operating pressure. This primary side density can be calculated using the ideal gas law. In order to maintain equal mass flow rates on both sides, the velocity of the helium in the primary loop must be increased to compensate for the decreased density. The magnitude of this velocity increase is approximately 10% over the secondary side velocity. The friction factor remains constant on both sides since the Reynolds number is primarily sensitive to mass flow rate per unit area and not just to velocity alone. Therefore, $f_{Rs} = f_{Rp}$. Thus, using the recalculated values for the density and velocity, the primary side core pressure drop can be calculated using Eq. 7.2.1-13. Add the manifold pressure loss defined by Eq. 7.2.1-14 evaluated with the primary side density and velocity to the primary side core pressure drop to get the total primary side pressure drop. These pressure loss values are tabulated in Table 7.2.1.1-2.

Once the pressure drop is defined, the pumping power can be calculated.

$$\text{Pumping power} = \Delta P_{RS} A_f v_{RS} \qquad \text{(7.2.1-15) (Ref. 129, p. 223)}$$

7.2.2 LIQUID METAL REACTOR HEAT EXCHANGER: The analysis of the same design reactor heat exchanger was also performed using NaK as the heat transfer fluid in both loops. The specific NaK compound used was composed of 44% by weight of Potassium. The initial difference in the analysis involved changing the physical property values of helium to those of NaK. A summary of these values for helium and NaK is listed, for comparison purposes, in Table 7.1.2-1. It was also assumed that the NaK maintained constant density on both sides of the heat exchanger. Another change required in the NaK system was the use of a different capacity rate ratio at the engine heat exchanger. This ratio was derived from the liquid metal system developed in Ref. 111. Once these parameters were changed, the same methodology was used in the reactor heat exchanger except for the calculation of the Stanton number. To calculate N_{St} for a liquid metal, a different relationship is required since there is a significant conductive component as well as the convective component to consider. This difference can be incorporated into the calculation of the Nusselt number.

$$N_{Nu} = 7 + (0.025)(Re\ Pr)^{0.8} \qquad \text{(Ref. 74, p. 180)}$$

Then, using the definition of the Stanton number, N_{st} can be calculated.

$$N_{st} = \frac{N_{Nu}}{Re\ Pr} \qquad \text{(Ref. 74, p. 136)}$$

Once these parameters were changed, the same methodology was used and the same key parameters defined. Table 7.2.1.1-2 summarizes these.

7.3 PIPING SPECIFICATIONS

The piping in the secondary loop is required to conduct the heat transfer fluid from the containment vessel out to the engines. The maximum temperature of this fluid is approximately 1600°F in the helium system and this occurs at the outlet side of the reactor heat exchanger. The maximum temperature of the return fluid occurs at the outlet of the engine heat exchanger in the indirect cycle and at the recuperator outlet in the direct cycle. This temperature is approximately 1100°F. At ordinary temperatures, the stress-strain relations of most engineering metals are independent of the duration of the loading. The temperature regime that we are operating at in the pipes is approximately half the melting point temperature of the metals. In this temperature region, the metal deformation under constant load increases significantly with time. This time-dependent deformation property is called *creep* and it becomes the dominant factor to be considered in long duration, high temperature strength of materials analyses. For this reason, this study and the studies of Westinghouse and General Electric (Refs. 163 and 111), have used the creep-rupture stress defined at a 10,000 hour lifetime as the primary material selection criterion. Based on the temperatures stated, Haynes 188 alloy was selected as the material for the heat transfer fluid supply pipe. The 10,000 hour creep-rupture stress value for this alloy at 1600°F is approximately 6000 psi. For the return line at 1100°F, Inconel 718 was selected as the pipe material. Inconel 718 has a creep-rupture stress at 10,000 hours at 1100°F of approximately 90,000 psi.

Using these two materials, this section will analyze two different piping configurations. The first configuration uses two pipes, one as the supply line to carry the heat transfer fluid out to the engine, and the other as the return line. Both pipes are insulated with a sufficient thickness of alumina-silica blanket to insure that the maximum temperature occuring at the outer edge of the insulating material is less than or equal to 100°F. To simplify the calculations, and since the insulation weight was not a significant driving force of the overall aircraft weight, only a single layer of a single material was used for the insulation calculations. The actual thickness calculations can be found in Appendix A.7.1.

The second configuration uses a concentric arrangement where the supply pipe is inside a larger diameter return line (See Figure 7.3.2-1). Only the outside pipe is insulated in this configuration and the same 100°F temperature limit is used. The parameters of interest in the analysis of these two systems are the overall pipe weight, the heat transfer fluid pressure loss, and the pumping power required. Since the helium system operates at a higher pressure than the NaK system, and since the gas flow will produce a higher pumping power requirement, the helium system is used as the vehicle in defining the methodology of the pipe analysis.

7.3.1 TWO-PIPE CONFIGURATION: The first parameter that must be defined is the pipe inside radius. The mass flow rate of the helium as defined in Section 7.1.1 is 70 lb/sec. The two parameters of pipe weight and pressure loss are inversely related to each other relative to the heat transfer fluid velocity. For a given mass flow, as velocity increases, the pipe weight decreases since the cross sectional flow area required decreases. However, as the velocity increases, the pressure loss incurred by the heat transfer fluid increases, and since the pumping power is proportional to the pressure loss, it increases also. The relationship of these parameters with increasing velocity is shown in Figure 7.3.1-1. The point of crossing of the two curves yields the velocity where the combination of pumping power and pipe radius are minimized and this value is used in the analysis as the velocity of the helium in the pipes. This velocity in the supply line is 400 fps. Using this velocity, the required inner radius of a circular pipe can be defined using Eq. 7.2.1-1.

$$R_1 = \sqrt{\frac{\dot{m}_s}{\pi \rho_{hs} v_{hs}}}$$

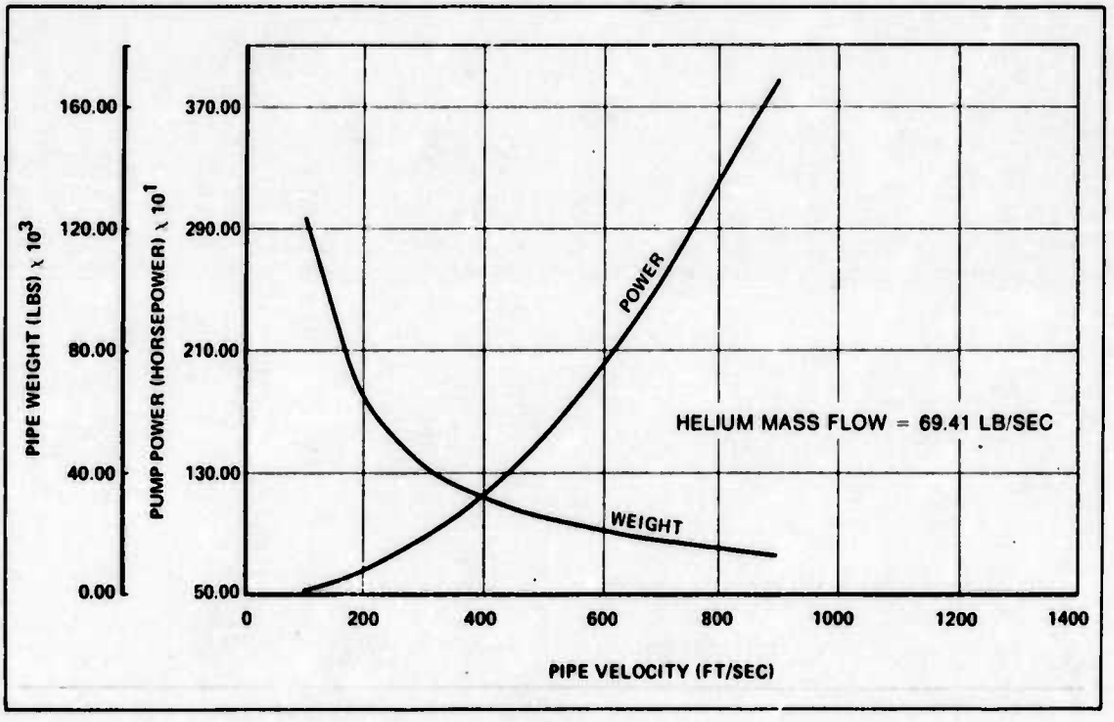

Figure 7.3.1-1. Pipe Velocity vs Pipe Weight and Pump Power

Using the creep-rupture stress at 10,000 hrs as the working stress, and the helium operating pressure of 1800 psi, the outer radius can be calculated using

$$R_2 = R_1 \sqrt{\frac{\text{stress} + \text{pressure}}{\text{stress} - \text{pressure}}}$$

The difference yields the thickness of the pipe as follows:

Pipe thickness = 1.68 in.

Using this, the cross sectional area of metal can be calculated. The length of the pipe is calculated as the total length of pipe required to supply and return the heat transfer fluid from all the engines. The pipe length parameters are calculated using the geometry implied by the following assumptions (Ref. Section 4.2.2):

1) Engine diameter = 14 ft
2) Number of engines = 10
3) 31 ft from containment vessel wall to outside edge of inboard engines
4) No separation between engines on each wing

This total supply piping length required is 285 ft. Using this length and the metal cross sectional area, the total weight of the supply pipes is defined by

Weight = area x length x density

For the helium case, this is approximately 65,000 lbs. The next step is to use the same length for the return pipes, but using the physical properties of Inconel 718 to define the thickness and density.

The strength of Inconel 718 operating at 70 lb/sec and 1100°F allows the use of the thin-walled cylinder equation to define the pipe thickness. The theoretical justifications for this can be found in Reference 15, p. 14-16. In this, the creep-rupture stress is used as the limiting value for the tangential stress component.

$$\text{Thickness} = \frac{\text{Pressure x inner radius}}{\text{Tangential Stress}}$$

Thus, the weight of the return pipe for the helium is approximately 3000 lbs. Therefore for the two-pipe configuration, the weight of piping required, sans insulation weight considerations, is 68,000 lbs.

The calculation of the second parameter of interest, the pressure loss of the heat transfer fluid in the pipes, begins with Eq. 7.2.1-11 to determine the Reynolds number of the pipe fluid flow. For helium, this is 3.7×10^6 and is in the turbulent flow region. Then use

$$f_{Pl} = 0.184\ (Re_{Pl})^{-0.2} \qquad (7.3.1\text{-}1)\ (Ref.\ 129, 191)$$

to determine the friction factor, f_{PI}. Once this is determined, the pressure drop is defined by

$$\Delta P_{PI} = f_{PI} \rho_{hs} \frac{L}{D_{PI}} \frac{v_{PI}^2}{2g} \qquad \text{(7.3.1-2) (Ref. 74, 163)}$$

For the helium system in the two-pipe configuration, the total supply line pressure drop equals 2 psi per engine. In a similar manner, but using an increased density due to the cooler operating temperature, and a reduced velocity to maintain a constant mass flow rate, the total return line pressure drop is calculated to be 1.9 psi per engine. Thus the pumping power required for the supply and return lines can be calculated using

$$\text{Pumping power} = \Delta P_{PI} A_{PI} v_{PI} \qquad \text{(7.3.1-3) (Ref. 129, 223)}$$

where A_{PI} = cross sectional flow area in the pipes.

This results in a supply line requirement of 965 hp, and a return line requirement of 796 hp, which yields an average pipe pumping requirement of 176 hp per engine.

7.3.2 CONCENTRIC CONFIGURATION: In this configuration, the analysis again uses Haynes 188 as the pipe material for the supply line and Inconel 718 for the return line. Figure 7.3.2-1 illustrates a cross sectional view of the concentric pipe configuration. In this configuration, there is a transfer of thermal energy from the supply fluid through the pipe wall to the return fluid. This changes the heat transfer fluid temperatures at the heat exchanger inlets and outlets. The methodology to solve for these new temperatures begins with the same airside parameters at the engine heat exchanger. Specifically, the air inlet temperature is 600°F, the air outlet temperature is 1500°F, and the air mass flow is 200 lbs/sec. Using these values and Eq. 7.1.1-2, the secondary loop helium inlet temperature is calculated to be 1600°F. By equating the heat transferred to the air, to the heat released by the secondary loop heat transfer fluid, the secondary loop outlet temperature can be calculated to be 1082°F. Then, if the radial heat loss experienced by the supply fluid as it transits the supply pipe is equated to the radial heat gained by the return line fluid, the secondary loop fluid temperatures at the inlet and outlet of the reactor heat exchanger can be calculated.

Secondary loop helium inlet = 1148°F
Secondary loop helium outlet = 1666°F

Once these temperature values are defined, Eq. 7.1.1-2 can again be used assuming a capacity rate ratio of 1 and a 75% effective reactor heat exchanger to define the primary loop heat transfer fluid temperatures. The primary loop inlet temperature

Primary loop helium inlet = 1839°F
Primary loop helium outlet= 1321°F

ASSUMPTIONS:

1 – MASS FLOW RATE EQUAL
2 – MAX WORKING STRESS
INNER PIPE – HAYNES 188-6000 PSI
OUTER PIPE – INCONEL 718-90,000 PSI
3 – TOTAL CONCENTRIC PIPE LENGTH – 285 FT

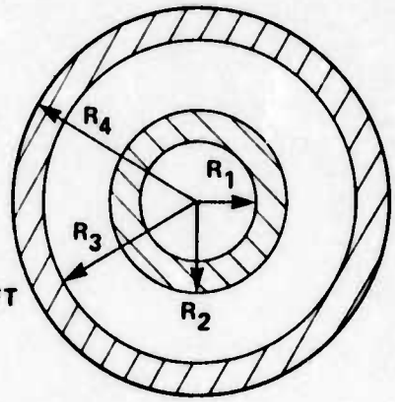

Figure 7.3.2-1. Concentric Pipe Cross Section

To remain within the 1800°F temperature restriction, there are two alternatives. The first is to change the effectiveness of the reactor heat exchanger to 79%. This will increase the overall volume and weight, but will yield a maximum primary loop inlet temperature of 1800°F. The other alternative is to keep the secondary loop mass flow rate at 70 lb/sec and increase the primary loop mass flow rate to 76 lb/sec. This will result in an overall additional mass flow rate of 60 lb/sec required to be pumped through the primary loop and the reactor. This is almost equal to the mass flow requirement that would result from the addition of another engine. To find the weight of the concentric pipe system, begin by using the thin-walled cylinder equation to define the outer pipe thickness since the ratio of the diameter to thickness is greater than 10.

$$\text{Pipe thickness} = \frac{PR_3}{\sigma_{\text{tangential}}}$$

where: P = internal operating pressure

This results in a wall thickness of 0.13 in. Using a total pipe length of 285 ft, the outer pipe weight is 5331 lbs. For the inner pipe, using Haynes 188 at a negligible pressure differential and an assumed thickness of 1/8", the weight is 4150 lbs. The 1/8" thickness is assumed in order to provide a margin for the corrosive effects caused by the flow of the heat transfer fluid on both sides of this pipe. Thus in the concentric configuration, the total pipe weight is 9481 lbs.

The calculation of the pressure loss in this configuration required only the additional calculation of the pressure change for the return line since the supply line pressure change will be the same as in the two-pipe configuration. The outer pipe presents an enlarged surface area of

contact to the heat transfer fluid. To compute the Reynolds number of the flow in the return line requires that an hydraulic diameter be calculated

$$\text{Hydraulic Diameter} = \frac{4A}{P}$$

(Ref. 87, p.7)

where A = Cross sectional flow area
P = Wetted perimeter

Solving this equation using the helium system pipe parameters results in an hydraulic diameter of 0.290 ft. Using this, the Reynolds number and the friction factor can be calculated. The Reynolds number in the outer pipe is 1.40×10^6 which confirms turbulent flow conditions. The pressure drop is calculated using Eq. 7.3.1-1, which results in:

$$\Delta P_{PI} = 6.23 \text{ psi}$$

Using this, the pumping power required in the outer pipe can be calculated using Eq. 7.3.1-3. This calculation yields 2370 hp. Thus the total pumping power required by the concentric pipe configuration is the sum of the inner pipe pumping power, which is equal to the supply line requirement in the two-pipe configuration, plus 2370.

TABLE 7.3.2-1. PIPE PARAMETER SUMMARY

	TWO-PIPE	CONCENTRIC
WEIGHT (LBS)		
HELIUM	67,982	12,217
NaK	12,149	13,734
PRESSURE DROP (PSI/ENGINE)		
HELIUM	3.9	8.2
NaK	0.7	1.5
PUMPING POWER (HP/ENGINE)		
HELIUM	176.1	333.5
NaK	4.0	7.6

Total concentric pipe pumping power = 3335 hp

A summary comparison of the key parameter values for the concentric and the two-pipe configuration are shown in Table 7.3.2-1.

Note that the pressure drop and the pumping power figures for the concentric pipe configuration do not include any allowance for supporting structures between the inner and outer pipes. These structures will increase the stated values. This study did not do an in-depth analysis of available or projected pump hardware. However in Section 6.2 the specific weight of comparable turbomachinery is developed for gas applications and in Section 7.5 for liquid metal applications.

7.4 ENGINE HEAT EXCHANGERS

The heat exchangers in the secondary coolant loop are varied in functional uses. In the indirect cycle, the heat exchanger transfers heat from the coolant or working fluid to the air passing through the turbofan engine. It, in effect, replaces the chemical fuel as the heat source. The secondary loop of the direct cycle contains two heat exchangers. One is similar to the indirect cycle heat exchanger in that it transfers heat to the air. It is used to dump heat to lower the compressor inlet temperature, thus raising the thermal efficiency. The second heat exchanger in the secondary loop of the direct cycle is the recuperator. It exchanges heat between the working fluid, after it leaves the turbine, and the same fluid after it leaves the compressor. This enables the working fluid to enter the primary heat exchanger at a higher temperature, therefore requiring less reactor power to heat the fluid to its required output temperature. Two heat exchangers were designed for the indirect cycle since both liquid metal and helium were compared as the working fluid. In the direct cycle system which expands high temperature helium over a turbine, the heat exchangers were designed for the same mass flow so that a comparison between the direct and indirect cycles could easily be made.

7.4.1 INDIRECT CYCLE HEAT EXCHANGERS

7.4.1.1 LIQUID METAL SYSTEM: In April 1974, the Air Force Aero Propulsion Laboratory received from the General Electric Company, Energy Systems Program, the final report on a study entitled *Liquid Metal-to-Air Heat Exchanger Design Study* (Ref. 111). The heat exchanger was designed to use a sodium-potassium liquid metal mixture for its working fluid and transfer enough heat to power a 60,000 lb takeoff thrust turbofan engine. The engine would be used to power a 1,000,000 lb/gross weight nuclear powered aircraft. In addition, the heat exchanger was engineered to have a 10,000 hour lifetime. The results of the contactor study were reviewed to determine their suitability for the aircraft in this design study. After the review and a conference with the contractor, it was decided to use the contractor designed heat exchanger for the liquid metal system and then design a comparable heat exchanger for the high temperature gas system.

A summary of the General Electric report shows their heat exchanger, which was engineered to have an effectiveness of 90%, is a wrap-around, cross-counterflow, finned-tube

design. The 0.25 inch outside diameter tubes have 30 fins per inch and are fabricated from Haynes Alloy No. 188 (Ref. 111, p. 33).

Figure 7.4.1.1-1 shows the general arrangement of the heat exchanger. Air from the engine compressor would enter from the center and flow radially outward through the heat exchanger. Figures 7.4.1.1-2 through 7.4.1.1-4 depict the geometry of the heat exchanger. Table 7.4.1.1-1 gives the construction parameters. The integration of the heat exchanger with a 60,000 lb takeoff thrust class turbofan engine and the air flow through the engine and heat exchanger are shown in Figures 7.4.1.1-5 and 7.4.1.1-6.

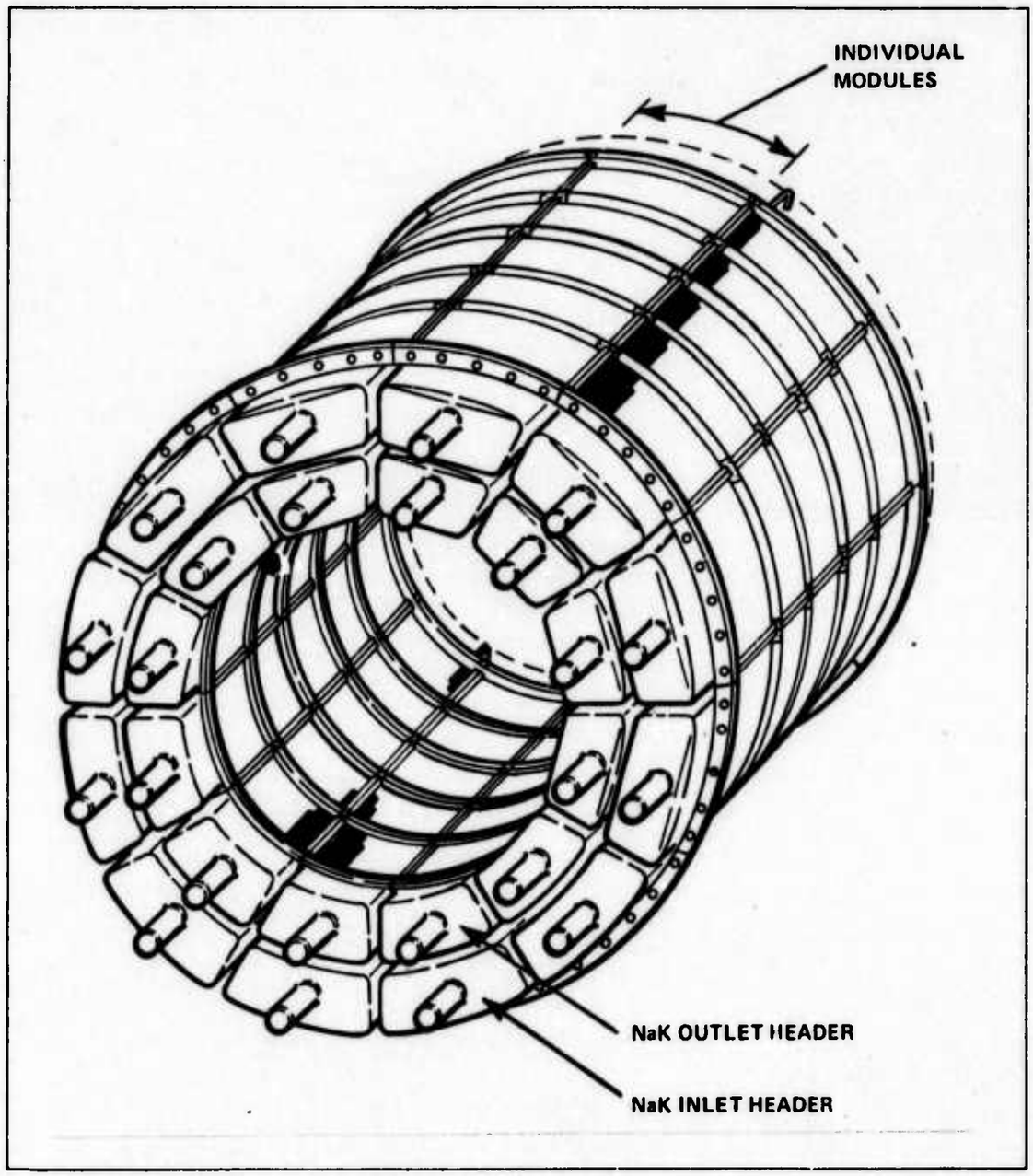

Figure 7.4.1.1-1. Wrap Around Heat Exchanger Assembly (Ref. 111, p. 69)

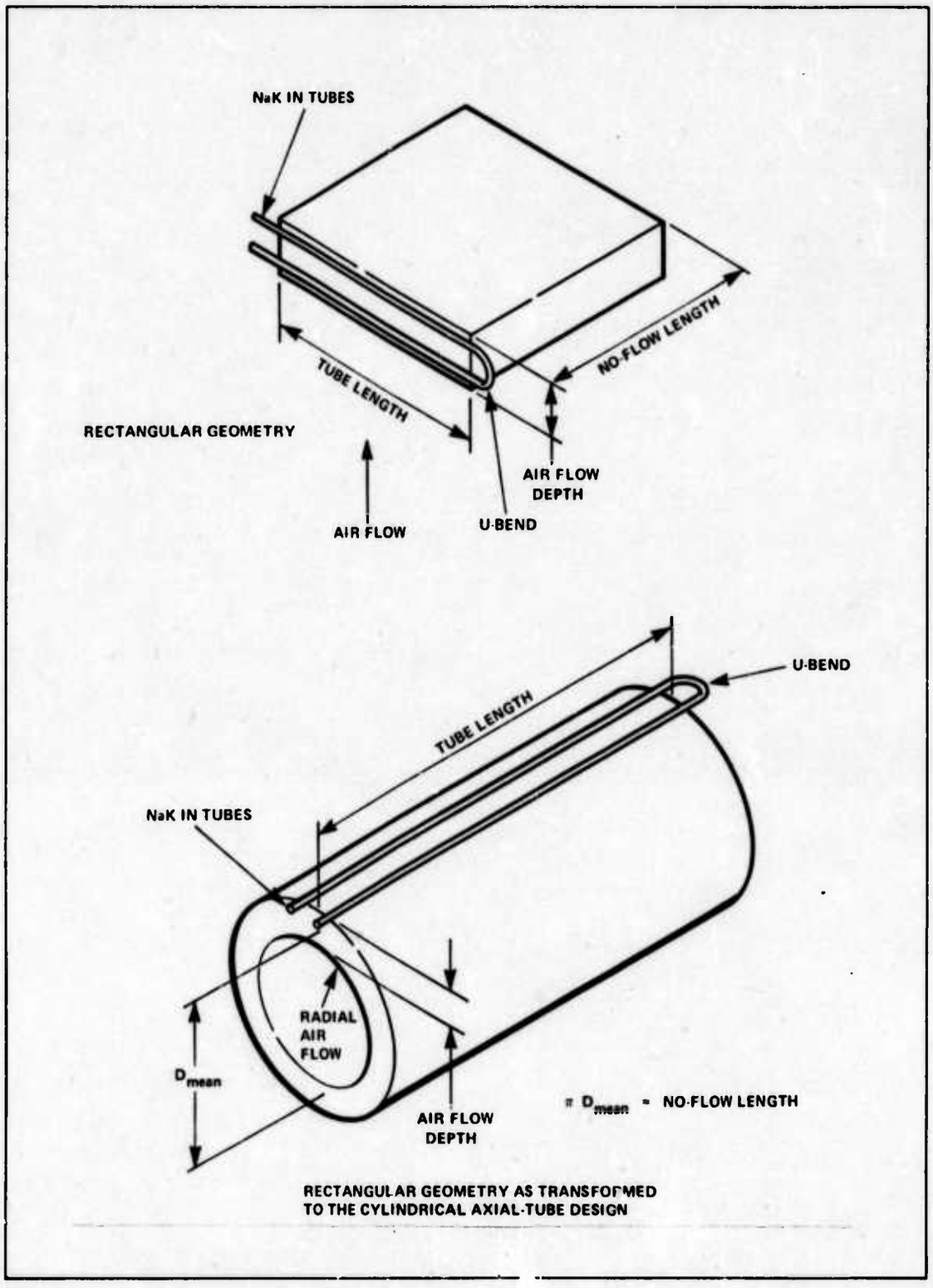

Figure 7.4.1.1-2. Cross-Counterflow Arrangements with Two Passes on the NaK Side (Ref. 111, p. 95)

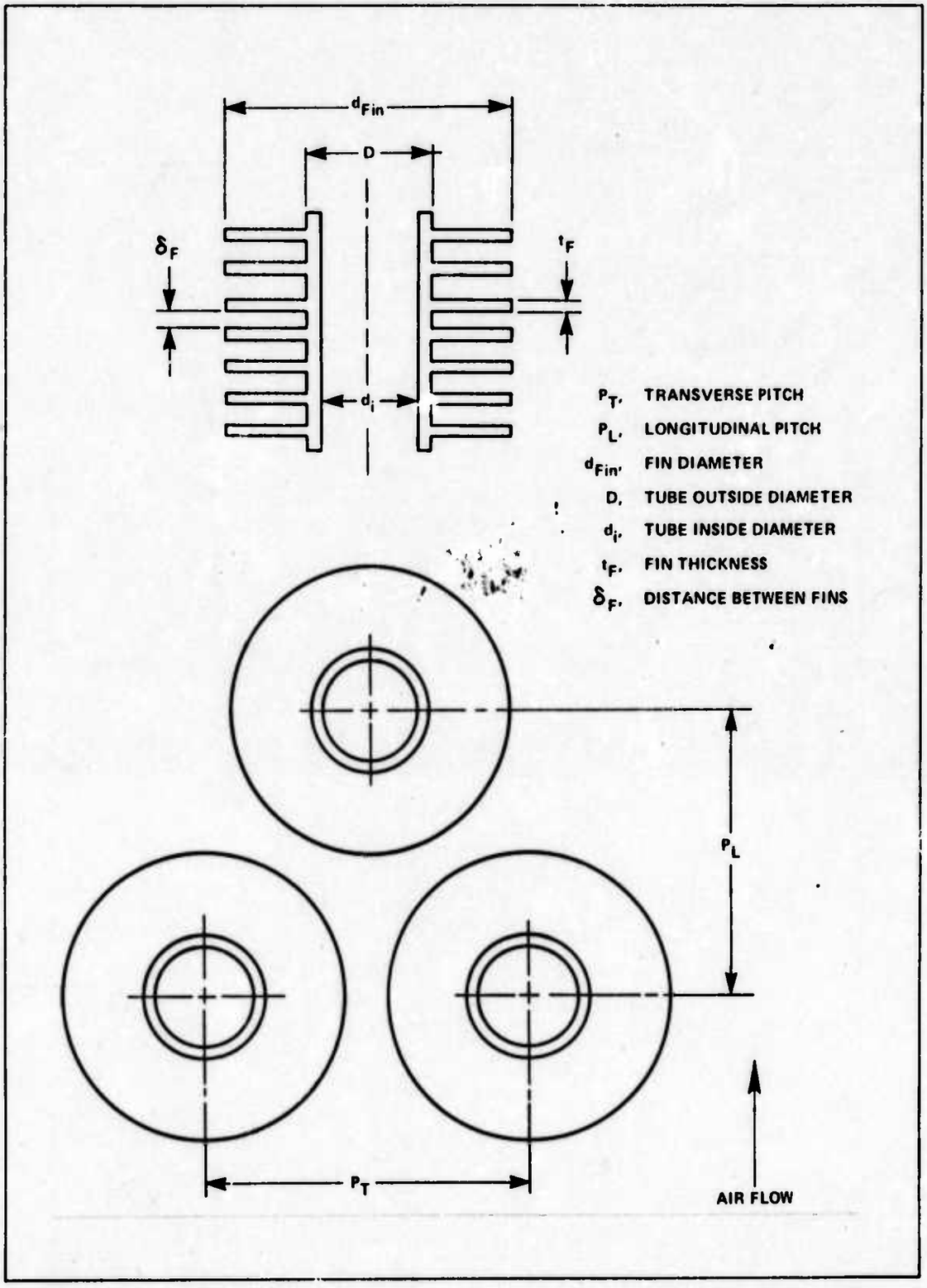

Figure 7.4.1.1-3. Geometry of Helical Disc Fins on Round Tubes (Ref. 111, p. 97)

The weight added to the engine for the complete heat exchanger assembly is given in the following breakdown (lbs):

Finned Tube Heat Exchanger	7000
Inlet Manifold	800
Outlet Manifold	900
Header Ducts	600
Total	9300

(Ref 111, p.48)

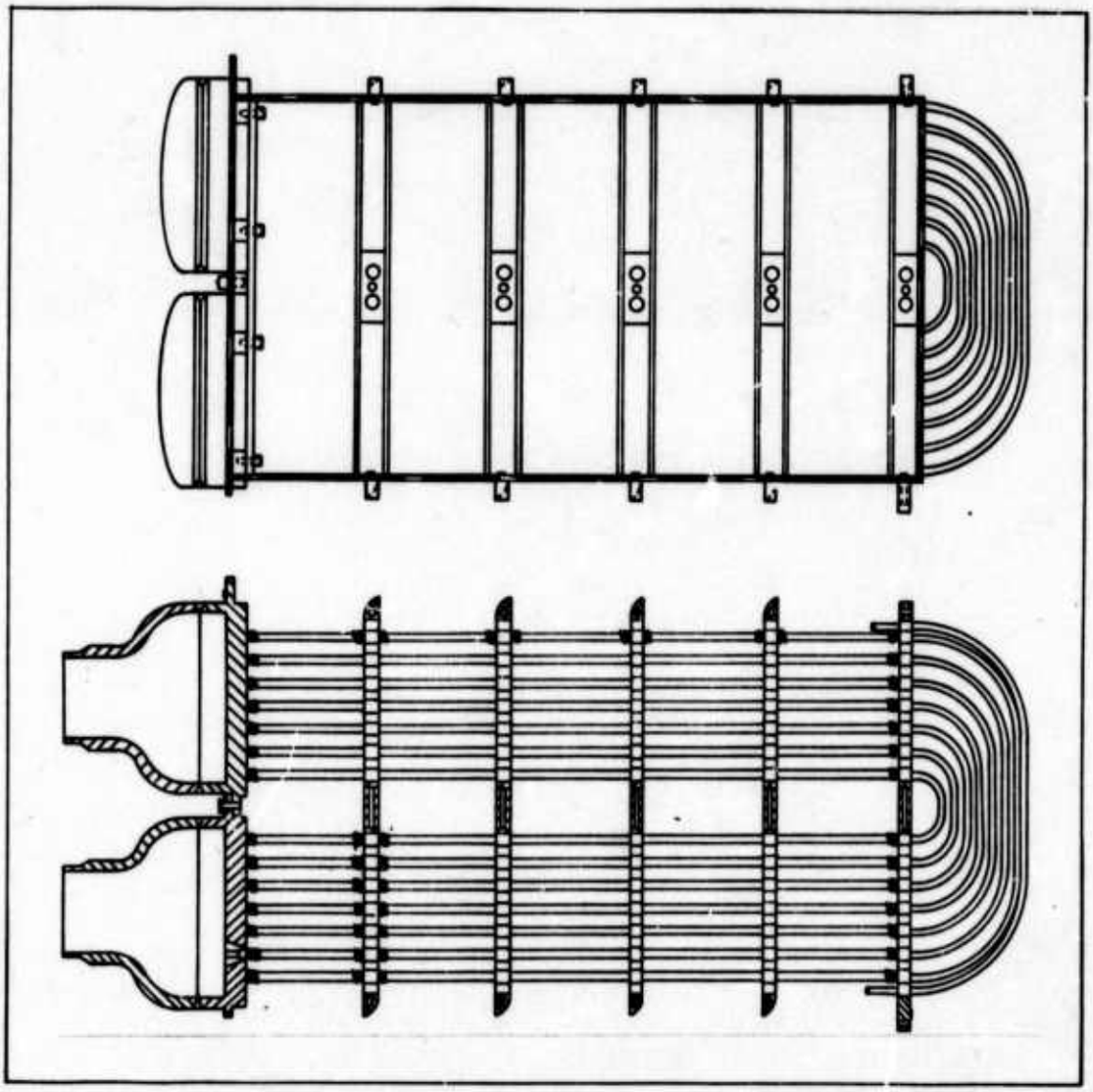

Figure 7.4.1.1-4. Cross Sectional View of U-Tube Arrangement (Ref. 111, p. 29)

TABLE 7.4.1.1-1. HEAT EXCHANGER CONSTRUCTION PARAMETERS

(REF. 111, P. 33)

CONFIGURATION	STAGGERED ARRAY
TUBE SIZE (IN.)	0.25 OD
WALL THICKNESS (IN.)	0.031
AVERAGE TRANSVERSE TUBE PITCH (P_T) (IN.)	0.625
LONGITUDINAL TUBE PITCH (P_L) (IN.)	0.45
FIN CONFIGURATION	30 FINS/IN. X 0.010 IN. THICK
FIN DIAMETER (d_{fin}) (IN.)	0.44
MATERIAL	HAYNES ALLOY-188
NUMBER OF TUBES	4032
AIR FLOW LENGTH OF TUBES (IN.)	23.7
PRESSURE DROP (PSI)	10.67
WEIGHT OF HEAT EXCHANGER (LBS)	9300

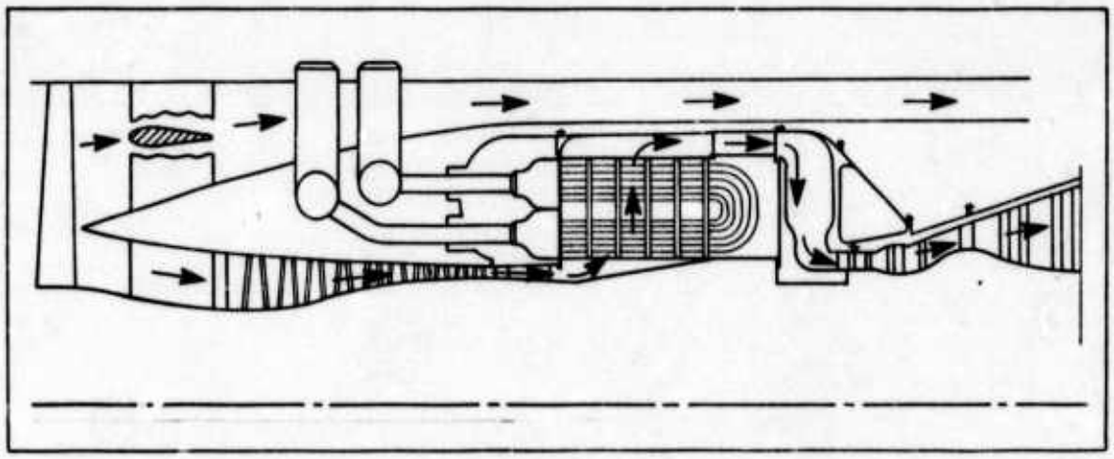

Figure 7.4.1.1-5. Air Flow through Nuclear Engine (Ref. 111, p. 269)

7.4.1.2 HIGH TEMPERATURE GAS SYSTEM: For the design of the helium gas heat exchanger, it was decided to use the same basic layout as the liquid metal heat exchanger. Due to the different working fluids with their different specific heats, a direct conversion of the liquid metal heat exchanger to helium was found to be impossible, therefore a complete redesign was undertaken.

In the design of the gas heat exchanger, several variable conditions had to be considered. The three major ones were air mass flow through the heat exchanger, the capacity ratio of the heat exchanger, and the velocity (v_t) of the gas through the tubes which make up the heat exchanger.

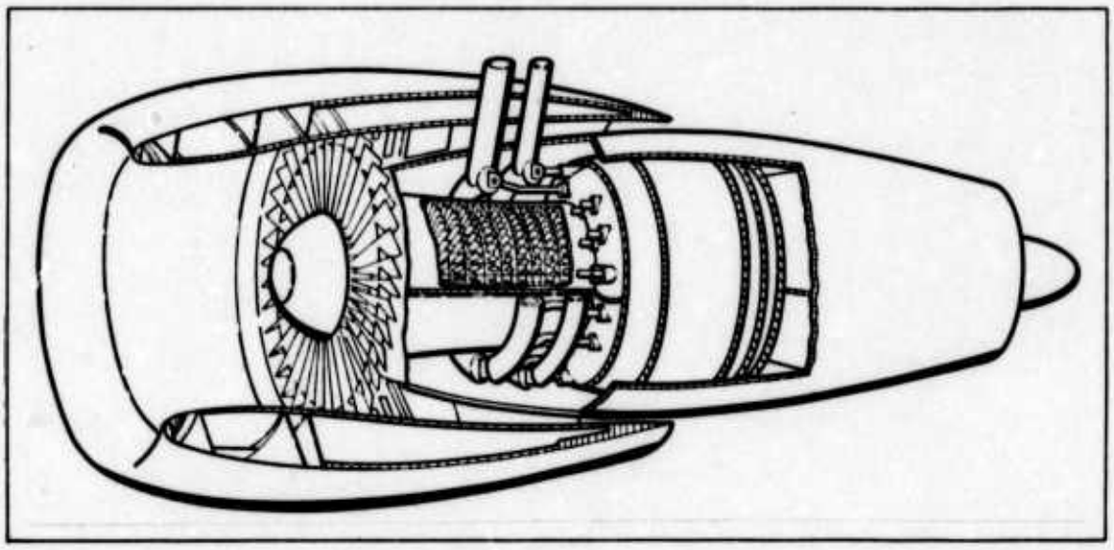

Figure 7.4.1.1-6. Nuclear Turbofan Engine Layout Showing Heat Exchanger Manifolds (Ref. 111, p. 69)

To limit the major variables to two, the velocity of the working fluid in the heat exchanger was assumed to be 100 fps, since this velocity should give a low pressure loss. (Ref. 70). Further, to make a comparison with the liquid metal heat exchanger, a similar air mass flow of 200 lb/sec was initially assumed. The air mass flow would later be varied from 175 lb/sec to 350 lb/sec to determine the optimum flow.

Using the same Haynes Alloy No. 188 tubing as the liquid metal heat exchanger with an inside diameter 0.188 in., a tube cross sectional area (A_t) was calculated to be 0.028 sq in.

The mass flow through one tube equals the total helium mass flow as calculated in Section 7.0, divided by the number of tubes (N_t):

$$\dot{m}_t = \dot{m}_h / N_t \qquad (7.4.1\text{-}1)$$

And the mass flow is also defined by:

$$\dot{m}_t = \rho A_t v \qquad (7.4.1\text{-}2)$$

where: ρ = density of helium

Equating Eq. 7.4.1-1 and Eq. 7.4.1-2 and rearranging terms yields:

$$N_t = \frac{\dot{m}\, h}{\rho\, v_t\, A_t} \qquad (7.4.1\text{-}3)$$

A preliminary analysis of the system using a mass flow that transferred an amount of heat equivalent to the liquid metal system yielded over 9000 tubes. This would make the gas heat exchanger over twice as thick as the liquid metal one and too large to install in an engine of similar size as the one used in the liquid metal system.

To maintain a feasible diameter, it was decided to lengthen the engine and install two heat exchangers, each one a mirror image of the other and each approximately the same size of the liquid metal heat exchanger. Figure 7.4.1.2-1 shows the arrangement of the heat exchangers. Note that they are fed by a common manifold placed between the two heat exchangers.

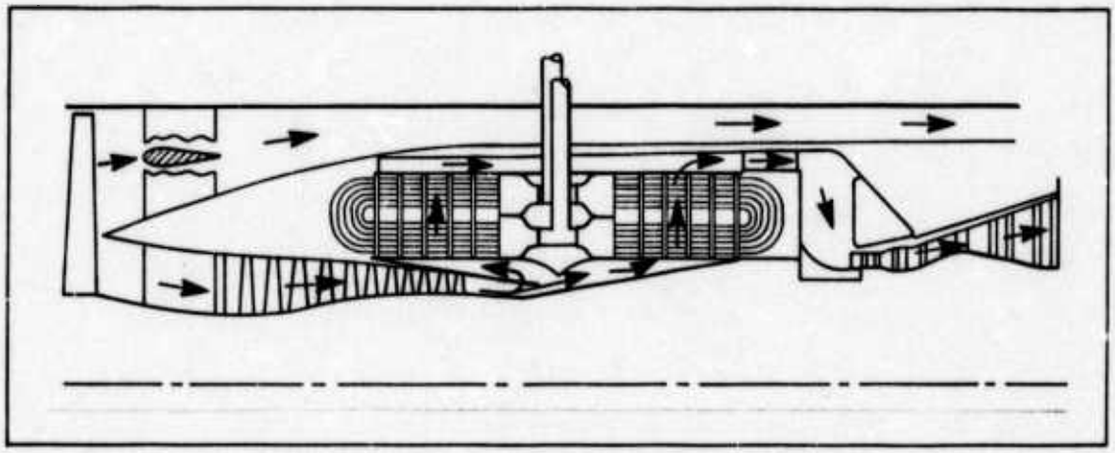

Figure 7.4.1.2-1. Helium Heat Exchanger Engine

Once the general configuration of the heat exchanger was determined, the remaining heat transfer parameters could be calculated. From Eq. 7.2.1-7 the overall heat transfer coefficient is:

$$\frac{1}{U} = \frac{1}{h_h} + \frac{1}{h_a}$$

where: h_h = heat transfer coefficient of the helium side of the heat exchanger
h_a = heat transfer coefficient of the air side of the heat exchanger

The heat transfer coefficient, h_h, for turbulent, convective heat transfer is given in Holman (Ref. 74) as one term in the definition of the dimensionless group, the Nusselt number.

$$Nu = \frac{hd}{k}$$

where d is the inside diameter of the tube
k is the thermal conductivity of the fluid.

To confirm that the flow was in fact turbulent, a check of the Reynolds number was performed. Holman states that if the Reynolds number given by

$$Re_h = \frac{\rho v d_i}{\mu} \qquad (7.4.1\text{-}5)\ (Ref.\ 74,\ p.\ 128)$$

is greater than 2300, the flow is usually turbulent. Using the following values, ρ_h = 0.373 lb/cu ft, $\mu_h = 310 \times 10^{-7}$ lb/sec ft, and a velocity of 100 fps, the Reynolds number was computed to be 18,600. This is well within the turbulent region.

The empirical formula for Nusselt number recommended by Dittus and Boelter and presented in Holman is:

$$Nu = 0.023\ Re^{0.8}\ Pr^{0.4} \qquad (7.4.1\text{-}6)\ (Ref.\ 74,\ p.\ 176)$$

where Pr is the Prandtl numner of helium.

Equating Eqs. 7.4.1-4 and 7.4.1-6 and solving for h yields:

$$h_h = \frac{0.023\ Re^{0.8}\ Pr^{0.4}\ k}{d_i} \qquad (7.4.1\text{-}7)$$

The helium side heat transfer coefficient h_h was then computed to be 1257 BTU/hr·ft²·°F.

The air side heat transfer coefficient was calculated using data from Manson (Ref. 106) for finned tube heat exchangers which related Reynolds number to the dimensionless j-factor. The j-factor is defined as:

$$j = \frac{h\ Pr^{2/3}}{c_p\ G_{max}} \qquad (7.4.1\text{-}8)\ (Ref.\ 106,\ p.\ 157)$$

Rearranging terms gives a relationship for the air side heat transfer coefficient.

$$h_a = \frac{j\ c_p\ G_{max}}{Pr^{2/3}} \qquad (7.4.1\text{-}9)$$

where: c_p = specific heat of air

G_{max} = maximum mass flux of air between tubes = mass flow of air divided by the flow area between the tubes (A_f).

To calculate the flow area (A_f), one must know the length of the tubes (ℓ) and the distance between them. Refer to Figure 7.4.1.2-2 for an illustration of the area. At this point, however, the tube length is not known. If the flow area were known, the mass flux and the air side heat transfer coefficient (h_a) could be calculated. With h_a and the previously calculated h_h, the overall heat transfer coefficient could be calculated. From this, the heat transfer surface area and then the tube length may be determined. Thus a paradox emerges: the tube length is used to calculate the tube length.

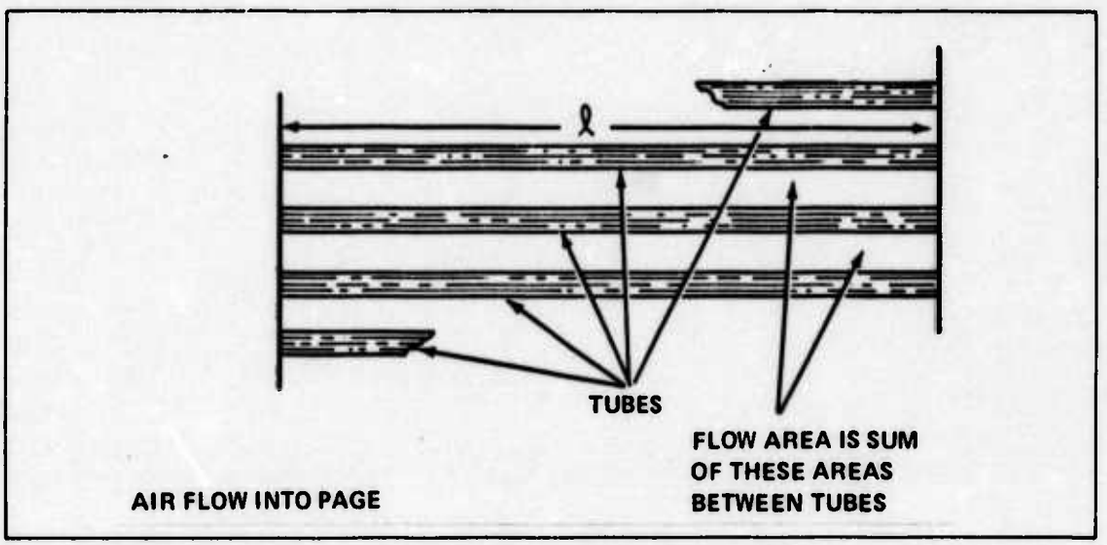

Figure 7.4.1.2-2. Section of Heat Exchanger Looking in Direction of Air Flow

This discrepancy was resolved by assuming an initial value for the tube length (x) of 25 in. then completing the calculations through the determination of the tube length (ℓ). x and ℓ were compared and if there was greater than 1 in. difference, 1 in. was added to or subtracted from x and the calculations made again until there was less than 1 in difference. This iterative process was performed by a computer. The logic diagram for the process is in Appendix 7.2.

Manson's data relating Reynolds number for air flow over banks of finned tubes to j-factor was found by Marvin to fit a straight line in the Reynolds number region in question (Ref. 111, p. 106). The following relationship was then derived:

$$j = \exp [-1.874 - 0.353 \ln (Re)] \qquad (7.4.1\text{-}10)$$

The Reynolds number Manson used was determined by the following:

$$Re = \frac{G_{max} d_j T_{av}}{\mu_f T_f} \qquad (7.4.1\text{-}11)$$ (Ref. 106, p. 105)

where: T_{av} is the average temperature

T_f is the film temperature

μ_f is the viscosity of the air on the fins at the film temperature

d_j is the Jameson diameter, an equivalent diameter for finned tubes. Jameson defines this diameter as:

$$d_j = D + \frac{2b(b + t)}{\delta + 2b + t} \qquad \text{(7.4.1-12) (Ref. 106, p. 85)}$$

where b = fin height
D = outside diameter of tube
δ = distance between fins
t = fin thickness

Using the tube and fin dimensions from Table 7.4.1.1-1, Jameson diameter was calculated to be 0.0283 in.

Standard equations for average and film temperature were used.

$$T_{av} = \frac{(T_{s_1} + T_{s_2})}{2} - \Delta T_{lm} \qquad \text{(7.4.1-13) (Ref. 70)}$$

$$T_f = \frac{T_{s_1} + T_{s_2} - \Delta T_{lm}}{2} \qquad \text{(7.4.1-14) (Ref. 70)}$$

where: T_{S1}, T_{S2} = inlet and outlet helium temperatures

and ΔT_{lm} = log mean temperature difference

$$\Delta T_{lm} = \frac{(T_{s_2} - T_{a_1}) - (T_{s_1} - T_{a_2})}{\ln \left[(T_{s_2} - T_{a_1}) / (T_{s_1} - T_{a_2}) \right]} \qquad \text{(7.4.1-15) (Ref. 74, p. 235)}$$

The temperatures were calculated to be: ΔT_{lm} = 242.°F, T_{av} = 1097°F, and T_f = 1218°F.

After several iterations to match the assumed tube length to the actual tube length so that the flow area could be accurately determined, G_{max} was computed to be 12.7 lb/sec-sq ft and the Reynolds number 11,850. With these factors determined, the j-factor could be calculated. It was found to be 0.00415.

The air side heat transfer coefficient given by Eq. 7.4.1-9, $h_a = jc_p G_{max}/Pr^{2/3}$, was then calculated. With h_a and the already calculated h_h, the overall heat transfer coefficient U (Eq. 7.2.1-7) was calculated. The results of these calculations were:

h_a = 81.6 BTU/hr-sq ft-°F

U = 76.1 BTU/hr-sq ft-°F

The remaining heat transfer parameters were calculated using the number of transfer units (Ntu) — effectiveness method described in Kays and London (Ref. 87). The number of transfer units is a nondimensional expression giving the relative heat transfer size of the heat exchanger and is defined by:

$$Ntu = \frac{AU}{C_{min}} \qquad \text{(7.4.1-16) (Ref. 87, p. 15)}$$

where: A = heat transfer surface area

C_{min} = minimum capacity rate of heat exchanger and given by $C = \dot{m}c_p$. In this case $C_{min} = \dot{m}_a c_{pa}$.

and U = overall heat transfer coefficient.

Figure 7.4.1.2-3 shows the asymptotic character of the relationship between effectiveness and Ntu for given capacity ratios (C_{min}/C_{max}). When the number of transfer units is small the effectiveness is low, and when the number of transfer units is large the effectiveness approaches asymptotically a limit which is determined by the flow arrangement and the thermodynamic characteristics of the heat exchanger (Ref. 87, p. 15).

For most heat exchangers a closed form solution is impossible and experimental data must be used for the design. In the case of cross-flow heat exchangers with the fluids unmixed, however, a closed form solution is possible. The solution and equations as presented in Kays and London were used. (Ref. 87, p. 19). They first define a nondimensional parameter Γ to simplify their equations.

$$\Gamma = 1 - \exp\left(- Ntu_y \frac{C_{min}}{C_{max}} \right) \qquad \text{(7.4.1-17) (Ref. 87, p. 19)}$$

where: Ntu_y is number of transfer units per pass.

The effectiveness per pass (ε_y) is then expressed in terms of Γ.

$$\varepsilon_y = 1 - \exp\left(- \Gamma \frac{C_{max}}{C_{min}} \right) \qquad \text{(7.4.1-18) (Ref. 87, p. 19)}$$

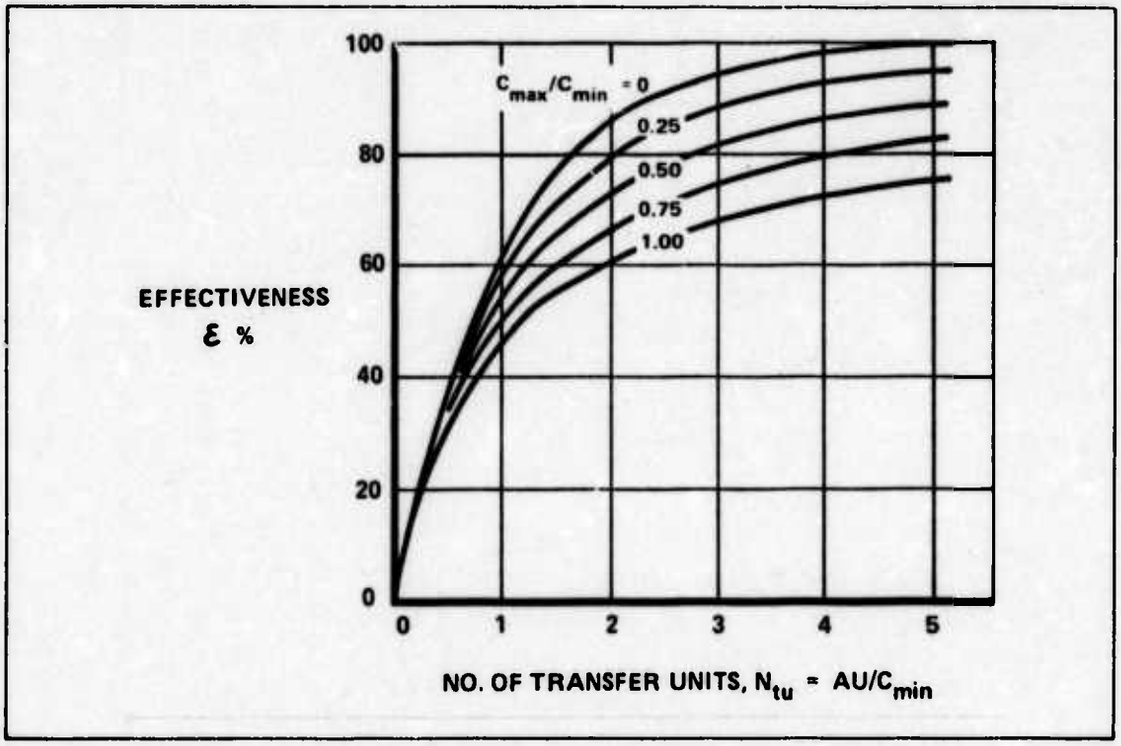

Figure 7.4.1.2-3. Effectiveness — N_{tu} Relationship (Ref. 87, p. 51)

For multi-pass heat exchangers, the relationship between the effectiveness (ε) and the effectiveness per pass is given by:

$$\varepsilon = \frac{\xi^2 - 1}{\xi^2 - \frac{C_{min}}{C_{max}}} \qquad (7.4.1\text{-}19)$$ (Ref. 87, p. 20)

where:

$$\xi = \sqrt{\frac{1 - \varepsilon_y \frac{C_{min}}{C_{max}}}{1 - \varepsilon_y}} \qquad (7.4.1\text{-}20)$$

Solving Eq. 7.4.1-20 for ξ gives:

$$\varepsilon_y = \frac{1 - \xi}{\frac{C_{min}}{C_{max}} - \xi} \qquad (7.4.1\text{-}21)$$

Rearranging terms in Eq. 7.4.1-18 yields:

$$\Gamma = -\frac{C_{min}}{C_{max}} \ln (1 - \varepsilon_y) \qquad (7.4.1\text{-}22)$$

Similarly, with Eq. 7.4.1-17:

$$Ntu_y = -\frac{C_{max}}{C_{min}} \ln (1 - \Gamma) \qquad (7.4.1\text{-}23)$$

And finally for the 2-pass heat exchanger:

$$Ntu = 2\, Ntu_y \qquad (7.4.1\text{-}24)$$

Equations 7.4.1-20 through Eq. 7.4.1-24 are used to calculate Ntu for a given effectiveness and capacity ratio. With this information, the determination of the heat transfer surface area and hence the tube length (ℓ) is possible. At this point, the computer iteration was begun until the correct value for ℓ was found.

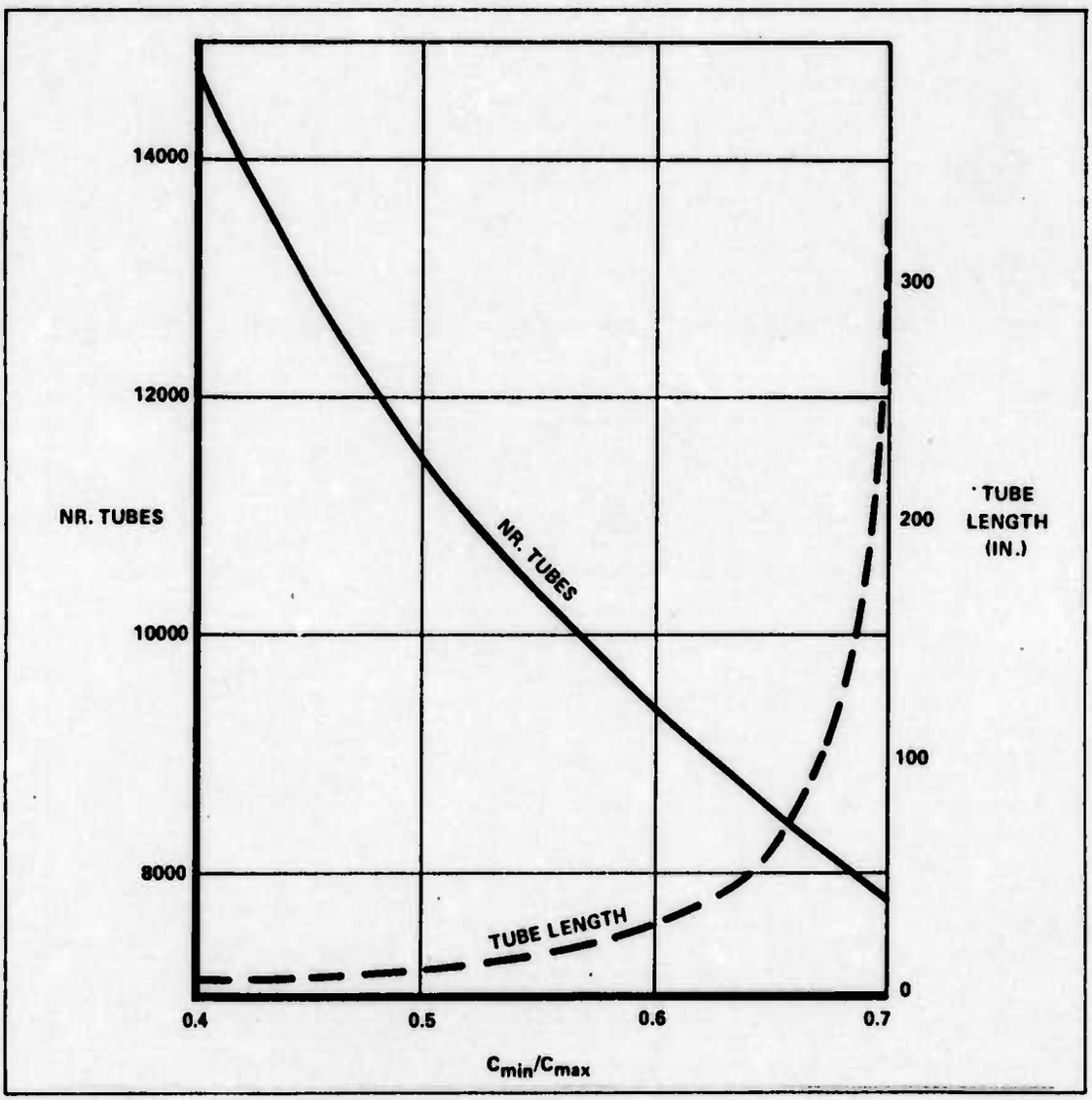

Figure 7.4.1.2-4. Capacity Ratio Variations

The heat transfer parameters for the gas heat exchanger have now been determined. However, these are for one case only, using assumed values for capacity ratio and air mass flow. The next step was to optimize these two parameters.

Computations were made for 31 different capacity ratios from 0.4 to 0.7 while holding air mass flow constant at 200 lb/sec. Figure 7.4.1.2-4 shows graphically the number of tubes and the tube length for each capacity ratio.

To keep each half of the gas heat exchanger approximately the same size as the liquid metal heat exchanger (4032 tubes, 23.7 in. long), the design goal became 8064 tubes each 23.7 in. long. A capacity ratio of 0.58 gave the closest results: 9792 tubes each 21 in. long.

Next, with the capacity ratio held fixed at 0.58, the air mass flow was varied from 200 lb/sec to 300 lb/sec. Figure 7.4.1.2-5 shows the change in number of tubes and tube length with variations in air mass flow. At mass flows greater than 200 lb/sec, the number of tubes increases rapidly beyond the design goal. For this reason, the air mass flow was tentatively placed at 200 lb/sec. A check of the air side pressure drop will be used to finally fix the figure.

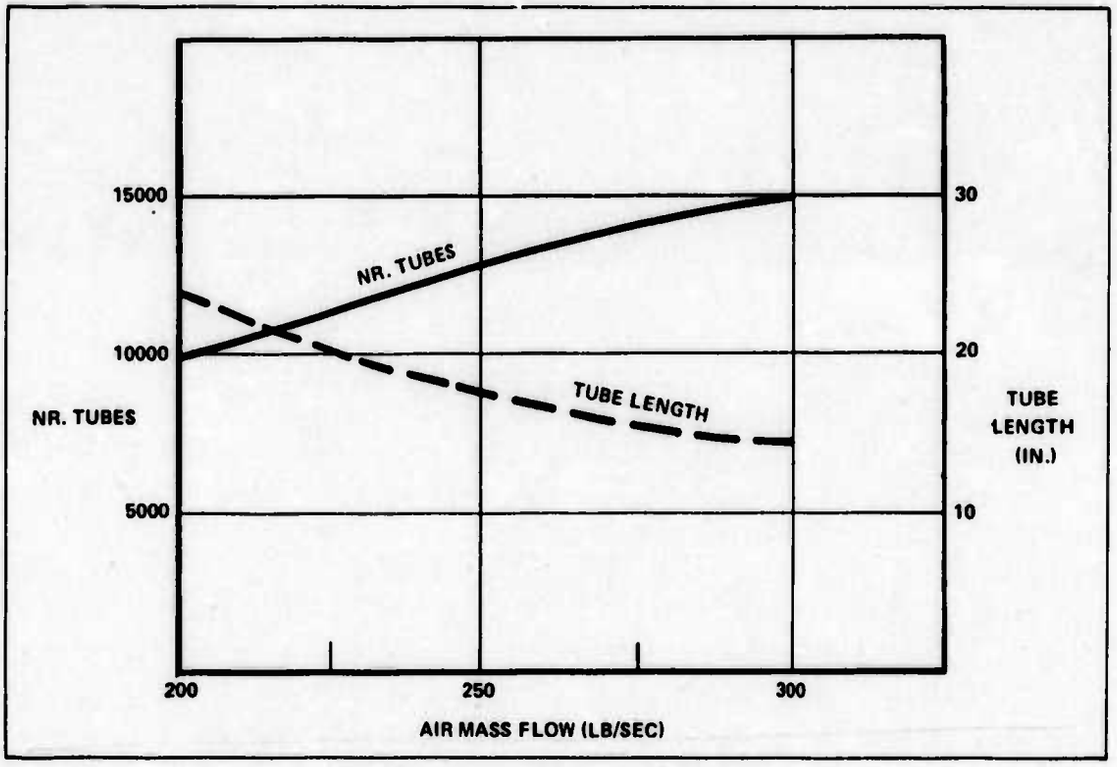

Figure 7.4.1.2-5. Air Mass Flow Variations

Determining the air side pressure drop first involved finding the friction factor (f_a) of the air over the finned tubes. Manson used empirical data to relate Reynolds number to friction factor across finned tubes. The relationship derived was:

$$f_a = \exp [- 0.755 - 0.16 \ln (Re)] \qquad (7.4.1\text{-}25)\ (\text{Ref. } 106, \text{ p. } 157)$$

Manson used the same expression for the Reynolds number in this case as he did for the j-factor, $Re = G_{max} d_j T_{av}/\mu_f T_f$ (See Eq. 7.4.1-11). The air side friction factor was determined to be 0.105. His expression for pressure drop was taken from Jameson's extensive research on finned tube heat exchangers.

$$\Delta P_a = f_a \left[2.324 \left(\frac{b}{\delta} \right)^{0.4} \left(\frac{1}{\sqrt{\frac{P_T}{D} - 1}} + \frac{1}{\sqrt{\frac{P_L}{D} - 1}} \right) \right] N_b \frac{(G_{max})^2}{2 \rho_a g}$$

(7.4.1-26) (Ref. 106, p. 111)

where: N_b is the number of banks of tubes the air passes over. P_T and P_L are the transverse and longitudinal pitch of the tubes (Refer to Fig. 7.4.1.1-3)

ρ_a is the average air density in the heat exchanger core.

This pressure drop was calculated to be 2.5 psi.

To complete the airside pressure drop calculations, the pressure drop for the inlet and outlet headers must be determined. London, with Klopfer and Wolf, has made theoretical studies with extensive experimental verification in the field of oblique flow headers for heat exchangers (Ref. 101). Figure 7.4.1.2-6 illustrates a heat exchanger with an oblique flow header configuration. Their study indicates that a shaped inlet header is the best since it provides the most uniform flow distribution in addition to a constant pressure drop across the heat exchanger core. They further indicate that a box exit header has the smallest pressure drop for any given exit area. Their equation for the total header pressure drop is:

$$\Delta P_h = \left[1.467 \frac{\rho_i}{P_o} \left(\frac{E}{F} \right)^2 + 1 \right] H \qquad (7.4.1\text{-}27)\ (\text{Ref. } 101, \text{ p. } 274)$$

where: ρ_i and ρ_o are the inlet and outlet air densities.

E/F is the ratio of the depths of the shaped inlet header and the box outlet header.

and H is the inlet velocity head. The inlet and exit dimensions used were taken from Marvin's heat exchanger study for a similar sized engine (Ref. 111, p. 223). They were: E = 3 in., and F = 4 in.

The standard equation for velocity head was used.

$$H = \frac{\rho v^2}{2g} \qquad (7.4.1\text{-}28)\ (\text{Ref. } 59, \text{ p. } 161)$$

Using 0.1869 lb/cu ft, the engine compressor outlet air density as the header inlet density, the velocity head was calculated to be 1.21 psi. The header pressure drop was then calculated to be 2.97 psi. The sum of this pressure drop with the core pressure drop of 2.5 psi gives a total air side pressure drop of 5.47 psi.

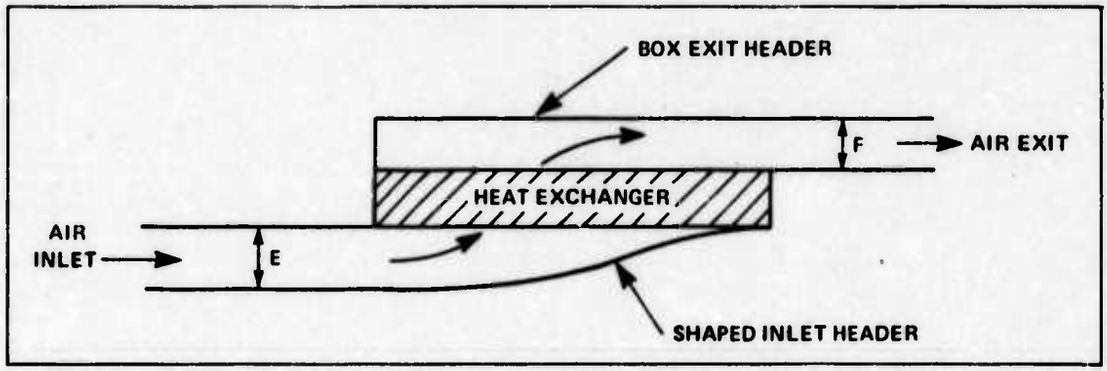

Figure 7.4.1.2-6. Schematic of Shaped Inlet Header with a Box Exit Header

Figure 7.4.1.2-7 shows the airside pressure drop as a percent of the compressor outlet pressure for the range of air mass flow variations. As indicated in Section 6.1.6, a 6% pressure drop was desirable. This occurs at approximately 200 lb/sec mass flow. In addition, as the mass flow increases above 200 lb/sec the percent pressure drop climbs quickly into an infeasible region. Thus, 200 lb/sec mass flow was chosen as optimal.

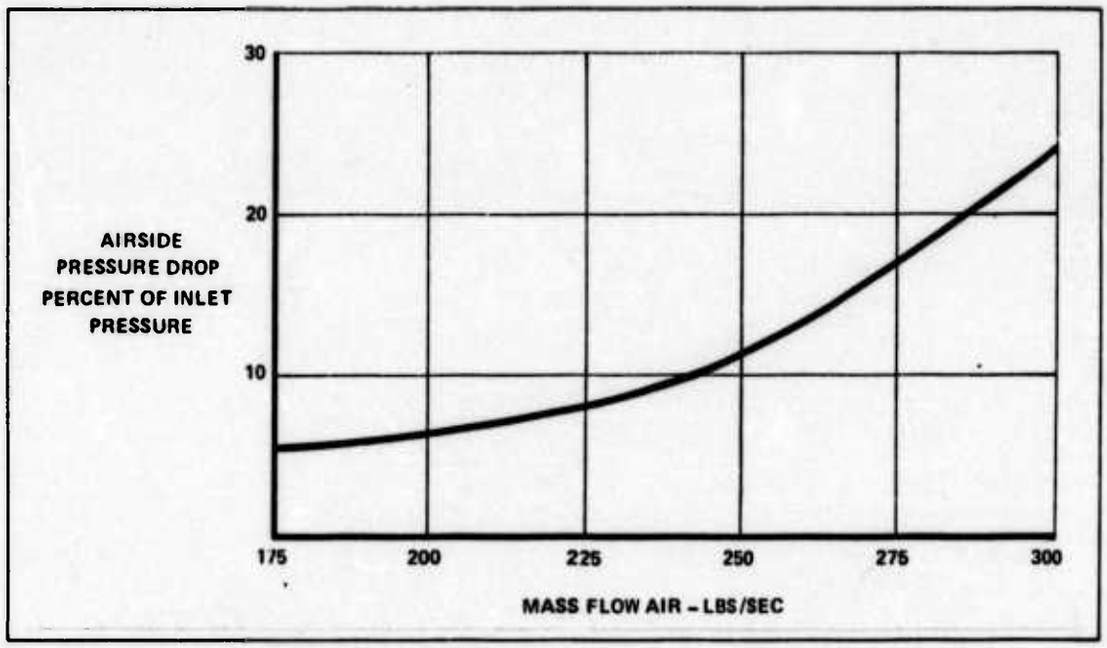

Figure 7.4.1.2-7. Mass Flow Air (lbs/sec)

With the air mass flow and capacity ratio determined, the helium mass flow may be determined and the sizing of the heat exchanger completed. The helium mass flow is given by:

$$0.58 = \frac{C_{min}}{C_{max}} = \frac{C_{air}}{C_{helium}} = \frac{\dot{m}_a c_{pa}}{\dot{m}_h c_{ph}}$$

Rearranging terms yields:

$$\dot{m}_h = \frac{\dot{m}_a\, c_{pa}}{0.58\, c_{ph}}\, 69.4 \approx 70 \text{ lb/sec}$$

The final sizing of the heat exchanger then yielded twin heat exchanger assemblies, each with 4896 finned tubes 21 in. long.

The heat transfer parameters were computed in their final form and are tabulated in Table 7.4.1.2-1.

TABLE 7.4.1.2-1. HEAT TRANSFER PARAMETERS

ε	0.9
ε_y	0.74
Γ	0.778
N_{tu}	5.19

The heat transfer surface area required was found using Eq. 7.4.1-16, Ntu = AU/Cmin. Solving for the area yields A = Ntu Cmin/U. In his calculation of surface area, Marvin used a 15% Ntu safety factor to account for any unknown losses (Ref. 111, p. 36). This safety factor was applied and yields a design Ntu of 5.97. A slightly larger surface area results. The heat transfer surface area is then:

$$A = (5.97)(200)(0.25)(3600)/76.1 = 14{,}120 \text{ sq ft}$$

The final piece of information needed to complete the design of the heat exchanger was the helium side pressure drop. This will be used later to calculate the pumping power required. The major pressure losses are due to the long, small diameter tubes. Minor losses are due to the bends in the tubes and the expansion of the gas in the manifolds.

The standard formula for pressure drop in a tube was used.

$$\Delta P_t = f_t \frac{\ell}{d_i} \rho_h \frac{v^2}{2g} \qquad \text{(7.4.1-29) (Ref. 74, p. 179)}$$

where: f_t is the friction factor in the tubes.
ℓ is total tube length

The Reynolds number in the tube was first computed with Eq. 7.4.1-5 to determine whether the flow was laminar or turbulent. A Reynolds number of 1.89×10^4 indicated that the flow was turbulent.

Next, the Karman-Nikuradse Equation for turbulent flow friction factor in circular tubes as presented in Murray was used (Ref. 129, p. 191).

$$f_t = 0.184\ Re^{-0.2} \qquad (7.4.1\text{-}30)$$

The friction factor was computed to be 0.0257. The pressure drop is then 2.85 psi.

The pressure drop due to the bends in the tubes was calculated by using the loss coefficient (K_b) for a medium sweep bend. From Streeter (Ref. 168) $K_b = 0.75$. Therefore:

$$\Delta P_b = K \rho_h \frac{v^2}{2g} \qquad (7.4.1\text{-}31)\ (\text{Ref. 168, p. 187})$$

The pressure drop due to the bends was computed to be 0.3 psi.

Marvin calculates the total manifold pressure drop to be:

$$\Delta P_m = 0.595\ h_i \qquad (7.4.1\text{-}32)\ (\text{Ref. 111, p. 229})$$

where: h_i is the velocity head at the inlet manifold given by Eq. 7.4.1-28.

$h_i = \rho v^2/2g$

The computation for h_i yielded 0.4 psi which gave a $\Delta P_m = 0.24$ psi.

The separate pressure drops and the total pressure drop for the gas heat exchanger is given in Table 7.4.1.2-2.

TABLE 7.4.1.2-2. HELIUM SIDE PRESSURE DROP

TUBES	**2.85**
BENDS	**0.29**
MANIFOLDS	**0.24**
ΔP_{TOTAL} (PSI)	**3.38**

A conference with Marvin's liquid metal heat exchanger design team indicated that reasonable weight estimates for tne gas heat exchanger could be determined by scaling the weights of the liquid metal heat exchanger less the coolant weight (Ref. 107). The ratio of the number of tubes (9792/4032 = 2.43) was used as the scaling factor on the mounting and

support structure header ducts, and manifolds. The tube length was also used in the calculation of the weight of the finned tube assembly. The weight breakdown is shown in Table 7.4.1.2-3.

TABLE 7.4.1.2-3. GAS HEAT EXCHANGER WEIGHTS (LBS)

FINNED TUBE ASSEMBLY	15,100
HEADER DUCTS	1,500
MANIFOLDS	4,000
TOTAL	20,600

A summary of the major heat exchanger parameters is shown in Table 7.4.1.2-4

TABLE 7.4.1.2-4. PARAMETERS FOR TWO ASSEMBLY HIGH TEMPERATURE HELIUM GAS HEAT EXCHANGER

CAPACITY RATIO	0.58
AIR MASS FLOW (LB/SEC)	200
HELIUM MASS FLOW (LB/SEC)	70
NUMBER OF FINNED TUBES (PER ASSEMBLY)	9792 (4896)
AIR FLOW LENGTH OF TUBES (IN.)	21
PRESSURE DROP (PSI)	3.38
TOTAL WEIGHT (LBS)	20,600

7.4.2 DIRECT CYCLE HEAT EXCHANGERS: There are two heat exchangers associated with the engines in the direct cycle system. The recuperator transfers heat from the working fluid, after it leaves the turbine, back to the working fluid after it leaves the compressor. The second heat exchanger is a helium-to-air heat exchanger that is used to cool the helium before it enters the compressor. Figure 7.1.1.2-3 shows the working fluid flow through the two heat exchangers. For convenience, it will be referred to as the precooler. Figure 7.4.2-1 shows a possible arrangement of the heat exchangers in a pylon mounted direct cycle system engine.

A second type of direct cycle arrangement is possible. One or two centralized turbines may be used and located near or inside the reactor containment vessel with the power mechanically transmitted to fan type engines. The direct cycle individual turbine propulsion system will be discussed first.

7.4.2.1 INDIVIDUAL TURBINE ENGINE

7.4.2.1.1 RECUPERATOR: Since the recuperator has the same working fluid flowing on both sides of it, by definition the capacity ratio is 1. The recuperator uses the working fluid after it leaves both the compressor and the turbine, thus it should be located near them to minimize heat losses. This places it very near or within the engine. In either case, compactness

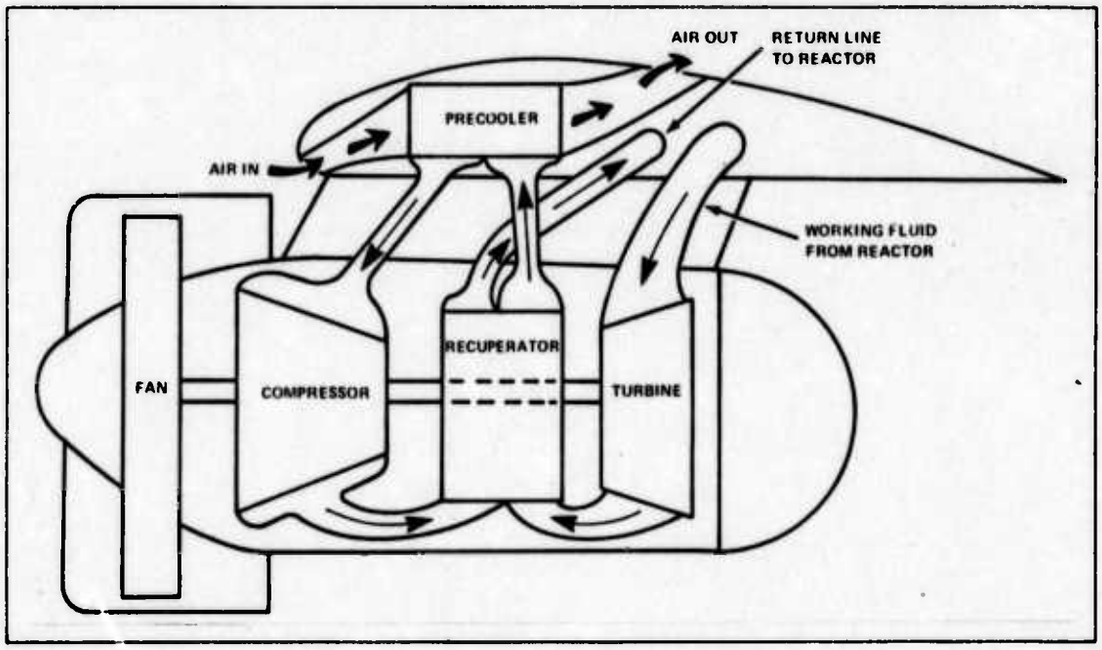

Figure 7.4.2-1. Direct Cycle System Engine

is desired. Compactness and a capacity ratio of 1 are also design features of the reactor heat exchanger; therefore it was decided to use the same design for the recuperator as was used

TABLE 7.4.2.1-1. RECUPERATOR SPECIFICATIONS

HEAT EXCHANGER TYPE	PLATE FIN
CAPACITY RATIO	1.0
MASS FLOW (BOTH SIDES) (LB/SEC)	70
PLATE SPACING (IN.)	0.1
FINS/INCH	46.45
FLOW LENGTH (FT)	3.8
HEAT TRANSFER SURFACE AREA (SQ FT)	10,675
HEAT EXCHANGER VOLUME (CU FT)	17.9
PRESSURE DROP (PSI)	
TURBINE SIDE	16.9
COMPRESSOR SIDE	14.5
HEADERS	0.3
TOTAL	31.7
WEIGHT (LBS)	
PLATE FIN ASSY	2050
MOUNTING HARDWARE	250
HEADERS	750
TOTAL	3050

for the gas reactor heat exchanger. The design is a cross-flow, finned-plate design with an effectiveness (ε) of 0.75. The only difference in the two designs was the input temperatures

with the reactor heat exchanger naturally having higher temperatures. The cooler temperature of the working fluid results in a greater density than that of the helium in the reactor heat exchanger. This, in turn, dictates a smaller cross sectional flow area ($A = \dot{m}/\rho v$). To obtain the required heat transfer surface area with the reduced flow area it was necessary to use a longer flow length. The longer flow length yielded a sharp increase in pressure drop which directly increases pump power. The solution to this was to reduce the velocity an amount proportional to the increase in density to keep the cross sectional flow area approximately the same as that of the reactor heat exchanger.

The temperatures from Section 7.1.1.2 were used with the equations from Section 7.2.1 to calculate the heat exchanger parameters with the exception of the header pressure drop. Like the indirect cycle engine heat exchanger, shaped inlet and box outlet headers were specified. Refer to Section 7.4.1.2 for the complete description of the headers and the associated equations. Table 7.4.2.1-1 gives the recuperator parameters.

7.4.2.1.2 PRECOOLER: The precooler is a helium-to-air heat exchanger that appears to be similar to the indirect cycle engine heat exchanger. Its function is slightly different, however.

In the system, there are four temperatures, inlet and outlet helium temperature and inlet and outlet air temperatures. The indirect cycle heat exchanger maintains a constant outlet air temperature while the precooler must maintain a constant outlet helium temperature. In the indirect cycle the inlet air, which comes from the engine compressor, has a relatively constant temperature. On the other hand, the inlet air temperature of the precooler varies with the outside air temperature. This variance in the outside air temperature can be from - 70°F at the 40,000 ft service ceiling to 60°F in the 3000 to 5000 ft range. If the mission of the nuclear airplane required it to cruise only at high altitude, the precooler could be designed using the colder - 70°F air as the heat sink. Since the ASW mission requires a variable altitude, the precooler had to be designed for the lower altitude and the warmer 60°F air. The warmer heat sink will naturally take a larger heat exchanger than one designed for the colder, higher altitude.

As the aircraft climbs into colder air the heat exchanger will become more effective and therefore lower the helium outlet temperature. Since this temperature is also the direct cycle compressor inlet temperature, it must be maintained constant. One system that would do this is an air modulation device that would decrease the amount of the air flow in an amount proportional to the lowering temperature so that the helium outlet temperature would remain constant. Temperature sensing of the helium would be used to control the closing of the heat exchanger air inlet to accomplish this.

The design of the precooler followed the procedures outlined in Section 7.4.1.2 with a few exceptions. First, using an approximate flow area of 13 sq ft and a low altitude velocity of 575 ft/sec, the air mass flow was calculated to be approximately 400 lb/sec. This means that the

air side capacity rate ($C = \dot{m}c_p$) is greater than the helium side capacity rate (100 BTU/sec-°F vs 87 BTU/sec-°F). The equation for effectiveness of the heat exchanger, Eq. 7.1.1-2

$$\varepsilon = \frac{C_{hot}}{C_{min}} \frac{T_{hot,\,in} - T_{hot,\,out}}{T_{hot,\,in} - T_{cold,\,in}}$$

shows that the effectiveness is predetermined by the fixing of the helium outlet temperature (190°F). That is, all the values in the equation are known. And since the hot side capacity rate is the minimum capacity rate, the effectiveness is the ratio of the temperature differences.

In the indirect cycle engine heat exchanger, however, the hot or helium outlet temperature was not fixed. This allows the designer the flexibility of choosing the effectiveness. Recall that an effectiveness of 0.9 was chosen for the indirect cycle heat exchanger. The temperatures required for the precooler, when used in Eq. 7.1.1-2, on the other hand, dictate an effectiveness of 0.72.

One other change is necessary due to the switch of the minimum capacity rate from the cold side to the hot side. The non-dimensional parameter, Γ, depends on which capacity rate is minimum. Equation 7.4.1-20 now becomes:

$$\Gamma = -\frac{C_{min}}{C_{max}} \ln\left(1 - \varepsilon_y \frac{C_{min}}{C_{max}}\right) \qquad \text{(7.4.2-1) (Ref. 87, p. 19)}$$

All other equations remain unchanged and the results of the precooler calculations are shown in Table 7.4.2.1-2 through Table 7.4.2.1-5.

The precooler would naturally not be arranged in a wraparound configuration like the engine heat exchanger. A rectangular array would be the most compact arrangement. With the same transverse and longitudinal pitch as the engine heat exchanger, the overall heat exchanger, less headers, would measure 15 ft long, 1.5 ft high, and 2.55 ft deep. Figure 7.4.2.1-1 illustrates the precooler.

TABLE 7.4.2.1-2. PRECOOLER PARAMETERS

HEAT EXCHANGER TYPE	**FINNED TUBE**
EFFECTIVENESS	**0.789**
CAPACITY RATIO	**0.87**
AIR MASS FLOW (LB/SEC) (VARIABLE)	**400**
HELIUM MASS FLOW (LB/SEC)	**70**
NUMBER OF FINNED TUBES	**8064**
AIR FLOW LENGTH OF TUBES (IN.)	**10**
PRESSURE DROP (PSI)	**3.03**
TOTAL WEIGHT (LBS)	**10,500**

TABLE 7.4.2.1-3. PRECOOLER WEIGHTS

	(LBS)
FINNED TUBES	2,800
MOUNTS AND SUPPORTS	3,100
HEADERS	1,200
MANIFOLDS	3,400
	10,500

TABLE 7.4.2.1-4. HEAT TRANSFER PARAMETERS

ε	0.78
ε_y	0.61
Γ	0.877
N_{tu}	4.2

TABLE 7.4.2.1-5. PRESSURE DROPS (PSI)

TUBES	2.26
BENDS	0.43
MANIFOLD	0.34
TOTAL	3.03

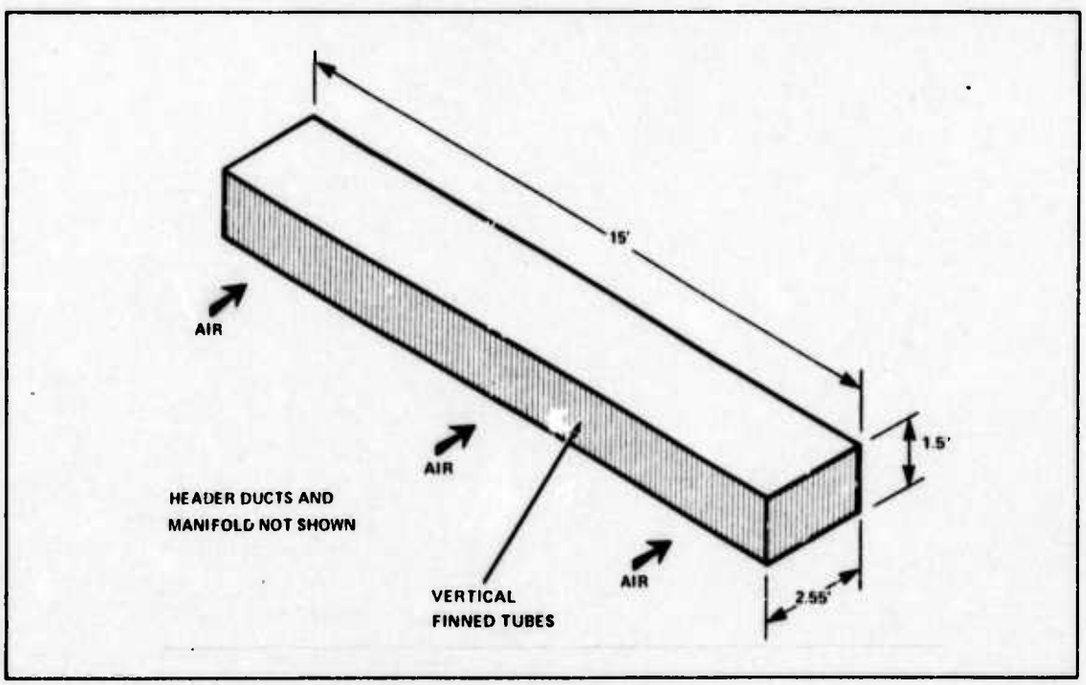

Figure 7.4.2.1-1. Precooler

7.4.2.2 CENTRAL TURBINE ENGINE: The central turbine was an attempt to increase efficiency by centralizing the turbine, compressor, and heat exchangers and using mechanical drives for ducted fan type engines. It was determined in Section 6 that, although the basic idea of centralization had promise, the weight of the gearing and drive shafts was prohibitive. For comparison purposes, however, the heat transfer system design was completed using the procedures presented in Section 7.4.2.1. The results are shown in Tables 7.4.2.2-1 and 7.4.2.2-2.

TABLE 7.4.2.2-1. PRECOOLER SPECIFICATIONS

CAPACITY RATIO	0.87
AIR MASS FLOW (LB/SEC)	2000
HELIUM MASS FLOW (LB/SEC)	350
NUMBER OF FINNED TUBES	40,320
AIR FLOW LENGTH OF TUBES (IN.)	10
PRESSURE DROP (PSI)	3.03
TOTAL WEIGHT (LBS)	52,500

TABLE 7.4.2.2-2. RECUPERATOR SPECIFICATIONS

HEAT EXCHANGER TYPE	PLATE FIN
CAPACITY RATIO	1.0
MASS FLOW (BOTH SIDES) (LB/SEC)	350
PLATE SPACING (IN.)	0.1
FINS/INCH	46.45
FLOW LENGTH (FT)	3.8
HEAT TRANSFER SURFACE AREA (SQ FT)	53,375
HEAT EXCHANGER VOLUME (CU FT)	89.5
PRESSURE DROP (PSI)	
TURBINE SIDE	16.9
COMPRESSOR SIDE	14.5
HEADERS	1.5
TOTAL	32.9
WEIGHT (LBS)	
PLATE FIN ASSY	10,300
MOUNTING HARDWARE	1,300
HEADERS	3,800
TOTAL WEIGHT (LBS)	15,400

7.5 WORKING FLUID CIRCULATION

The pumping power required to circulate the two working fluids, NaK and helium, are quite different. The liquid metal has small horsepower requirements and may easily be

pumped by mechanical pumps weighing on the order of 0.8 lbs/hp (Ref. 102, p. 191). In addition, the pumping requirements of the two different cycles, the indirect and the direct cycles, are different. The primary loops of the two cycles are virtually the same; however, the secondary loops bear no resemblence to each other. The secondary loop of the direct cycle is self pumping — the compressor acts also as a circulator, while the secondary loop of the indirect cycle engine requires pumping.

For either system, Murray in *Introduction to Nuclear Engineering* (Ref. 129) gives the following expression for pump power

$$\text{Power} = \Delta PAv/550 \qquad (7.5\text{-}1)$$ (Ref. 129, p. 223)

where ΔP is pressure drop
A is cross sectional area
v is fluid velocity
550 is horsepower conversion factor

Using the pressure drop and area for the liquid metal system shown in Table 7.2.1.1-2, with the NaK velocity of 20 fps, yields a system power of 121 hp per engine or 1210 hp for the 10 engine aircraft. The pumps may be mechanically driven or, in the case of the reactor loop, be driven by a small turbine using bleed air from the engines. In either case, the pump power requirements in terms of weight and horsepower are quite small and the engine thrust lost due to the horsepower removed to perform the pumping as extracted from Figure 6.1.4-1 is 500 lbs thrust per engine. The same may not be said for the helium gas system.

Velocities and heat exchanger cross sectional areas are both much larger in the gas system. (Compare 100 fps to 20 fps and 272 sq in. to 112 sq in.) A review of Eq. 7.5-1, Power = $\Delta PAv/550$, shows that the power requirements will indeed increase.

TABLE 7.5-1. PUMP POWER REQUIRED

PRIMARY (REACTOR) LOOP POWER (HP)	
REACTOR	**18,700 (REF. 176)**
HEAT EXCHANGER (PRI SIDE)	**3,630**
PIPES, MANIFOLD	**300**
TOTAL	**22,680 HP**
SECONDARY LOOP (HP PER ENGINE)	
REACTOR HEAT EXCHANGER	**299**
PIPES	**317**
ENGINE HEAT EXCHANGER	**166**
TOTAL	**782**

Since the velocity varies in different sections of the gas system, the horsepower requirements for each must be calculated individually and then summed for the total power requirement. The horsepower requirements are shown in Table 7.5-1. These indicate that a large system will be needed for circulation. In fact, when the secondary loop is pumped from engine driven pumps, Figure 6.1.4-1 indicates an approximate 2500 lb thrust loss and, if an attempt is made to derive the power for both loops from the engines, they would be unable to produce any thrust.

The mechanics of the pumping system were discussed in Section 6.2.8. The heat transfer requirements and heat exchanger design will be detailed in this section.

7.5.1 PRIMARY LOOP PUMPING SYSTEM HEAT EXCHANGERS: The pumping system is a direct cycle turbine system which drives a circulator pump. Refer to Figure 7.5.1-1 for an illustration of the system. As indicated in Section 6.2.8, the turbine circulation system produces in excess of 25,000 hp. This is more than the 23,000 hp required to power the primary loop.

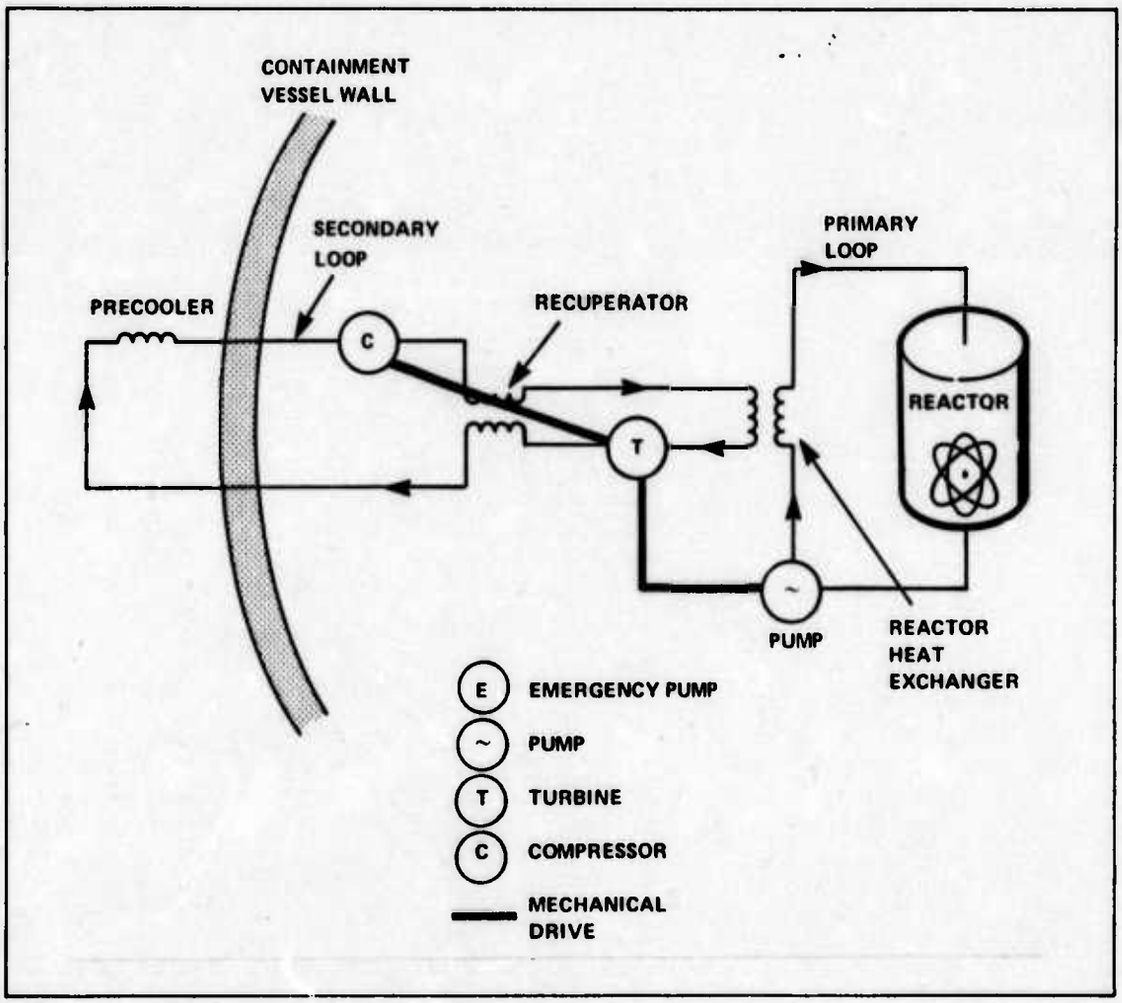

Figure 7.5.1-1. Primary Loop Pumping System

The heat exchangers are similar to the heat exchangers in the direct cycle engine system. They differ only in the secondary side reactor heat exchanger temperatures. In the pump system, the temperatures were matched to those of the heat exchanger engines so that the inlet and outlet temperatures of all the heat exchangers connecting the primary and secondary loops would be the same. Figure 7.5.1-2 shows a comparison of the temperatures.

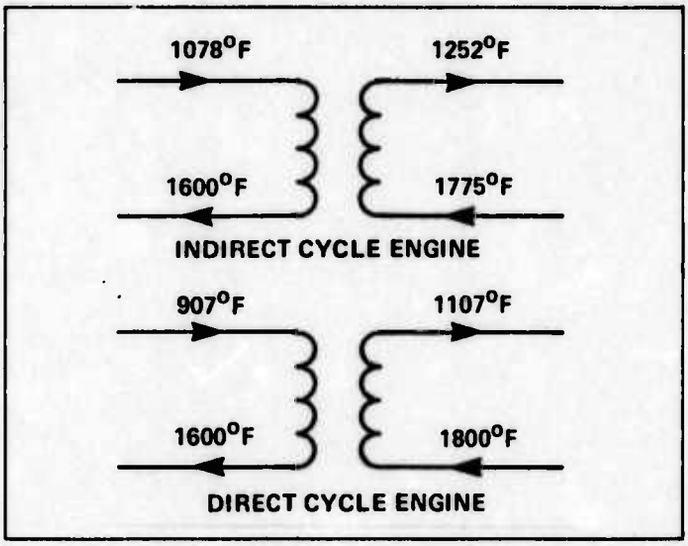

Figure 7.5.1-2. Reactor Heat Exchanger Temperatures

The recuperator was designed using the temperatures for the indirect cycle engine. The design procedure described in Section 7.4.2.1.1 was employed. Table 7.5.1-1 summarizes the pump system recuperator parameters.

TABLE 7.5.1-1. PRIMARY PUMP SYSTEM RECUPERATOR PARAMETERS

HEAT EXCHANGER TYPE	PLATE FIN
CAPACITY RATIO	1.0
MASS FLOW (LB/SEC)	90
PLATE SPACING (IN.)	0.1
FINS/INCH	46.45
FLOW LENGTH (FT)	3.8
HEAT TRANSFER SURFACE AREA (SQ FT)	13586
HEAT EXCHANGER VOLUME (CU FT)	22.8
PRESSURE DROP (PSI)	
HEAT EXCHANGER	34.5
HEADERS	0.5
TOTAL	35.0
WEIGHT (LBS)	
PLATE FIN ASSY	2600
MOUNTING HARDWARE	300
HEADERS	1000
TOTAL	3900

The precooler was designed in the same manner as detailed in Section 7.4.2.1.2. The compressor inlet temperature of 190°F is the same as the direct cycle engine precooler and the discussion in that section concerning the process of maintaining that temperature constant applies here, also. Table 7.5.1-2 gives the precooler parameters.

TABLE 7.5.1-2. PRIMARY PUMP SYSTEM PRECOOLER PARAMETERS

HEAT EXCHANGER TYPE	**FINNED TUBE**
EFFECTIVENESS	**0.74**
CAPACITY RATIO	**0.87**
AIR MASS FLOW (LB/SEC)	**515**
HELIUM MASS FLOW (LB/SEC)	**90**
NUMBER OF FINNED TUBES	**7776**
AIR FLOW LENGTH OF TUBES (IN)	**5**
PRESSURE DROP (PSI)	
TUBES	**2.5**
BENDS	**0.7**
MANIFOLDS	**0.6**
TOTAL	**3.8**
WEIGHT (LBS)	
FINNED TUBES	**1350**
MOUNTS & SUPPORTS	**1500**
HEADERS	**1150**
MANIFOLDS	**3300**
TOTAL	**7200**

7.5.2 SECONDARY LOOP PUMPING SYSTEM HEAT EXCHANGERS: The secondary loop requires much less pumping power than the primary loop. Whereas the primary loop has a reactor with limited volume to pump through, the secondary loop has, besides its turbine and compressor, only heat exchangers to pump through. The heat exchangers may have their flow area increased to slow the velocity and lower the pump power. Figure 7.5.2-1 depicts the secondary loop pump system. It also is a direct cycle turbine system producing over 14,000 hp, which is coupled to a circulator pump. Engine driven pumps may be used to circulate the working fluid but the power required to drive them reduces the thrust from approximately 15,000 lbs to 12,500 lbs. Section 6.2.8 has a more complete description of the various pumping systems. In addition, that section compares the ratio of the total engine thrust produced to the total reactor power required for each system.

Both the recuperator and the precooler were designed using the techniques and constraints presented in the previous section. Tables 7.5.2-1 through 7.5.2-2 show the parameters of the two heat exchangers.

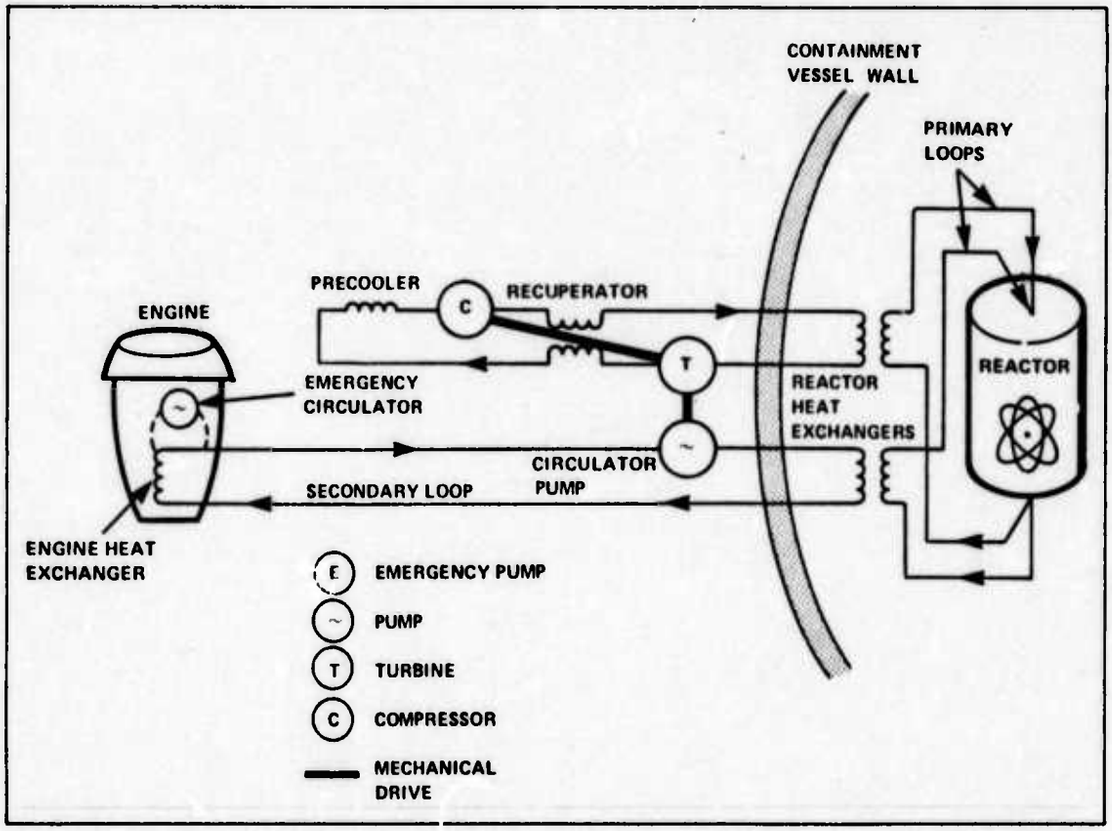

Figure 7.5.2-1. Indirect Cycle Engine and Secondary Loop Pumping System

TABLE 7.5.2-1. SECONDARY PUMP SYSTEM RECUPERATOR PARAMETERS

HEAT EXCHANGER TYPE	PLATE FIN
CAPACITY RATIO	1.0
MASS FLOW (LB/SEC)	50
PLATE SPACING (IN.)	0.1
FINS/INCH	46.45
FLOW LENGTH (FT)	3.8
HEAT TRANSFER SURFACE AREA (SQ FT)	7548
HEAT EXCHANGER VOLUME (CU FT)	12.7
PRESSURE DROP (PSI)	
HEAT EXCHANGER	34.5
HEADERS	0.5
TOTAL	35.0
WEIGHT (LBS)	
PLATE FIN ASSEMBLY	1400
MOUNTING HARDWARE	200
HEADERS	500
TOTAL	2100

TABLE 7.5.2-2. SECONDARY PUMP SYSTEM PRECOOLER PARAMETERS

HEAT EXCHANGER TYPE	FINNED TUBE
EFFECTIVENESS	0.74
CAPACITY RATIO	0.87
AIR MASS FLOW (LB/SEC)	286
NUMBER OF FINNED TUBES	5184
AIR FLOW LENGTH OF TUBES (IN.)	8
PRESSURE DROP (PSI)	
TUBES	1.9
BENDS	0.5
MANIFOLDS	0.4
TOTAL	2.8
WEIGHT (LBS)	
FINNED TUBES	1400
MOUNTS & SUPPORTS	1600
HEADERS	800
MANIFOLDS	2200
TOTAL	6000

7.5.3 PUMPING SYSTEM SUMMARY: When the whole indirect cycle system is integrated, the combined mass flow is 840 lb/sec, that is, the 10 engines at 70 lb/sec each plus the 90 lb/sec and 50 lb/sec for the two pumping systems. This is approximately the same as powering 12

TABLE 7.5.3-1. PUMP POWER AND WEIGHT REQUIREMENTS

LOOP PUMP POWER (HP)	
PRIMARY LOOP	
REACTOR	18,700
12 HEAT EXCHANGERS	4,300
PIPES, ETC.	400
	23,400
SECONDARY LOOP	
12 REACTOR HEAT EX.	3600
PIPES	3800
12 ENGINE HEAT EX.	2000
	9400
WEIGHT ADDED TO SYSTEM (LBS)	
LIQUID METAL	≈ 2000
INDIRECT CYCLE HELIUM	24,600
DIRECT CYCLE HELIUM	22,900

engines but having only 10 produce thrust. The direct cycle system requires the equivalent of 11 engines and 770 lb/sec mass flow.

A final tabulation of the power required for the various loops is shown in Table 7.5.3-1. In both cases there is sufficient power to pump the systems: 25,000 hp is available for the primary loop and 14,000 hp is available for the secondary loop. Also shown is the heat transfer system weight added.

In addition to the weight and extra horsepower required, these pumping systems generate a requirement for additonal reactor output. The indirect cycle helium system has a total mass flow 840 lb/sec instead of 700 lb/sec. Using equation 7.1.1-3, $Q = \dot{m}c_p\Delta T$ with $c_p = 1.242$ BTU/lb-°F and a ΔT from Figure 7.5.1-2 of 522°F, the total reactor output now required is 574 MW. Similarly, for the direct cycle system with m = 770 lb/sec and $\Delta T = 693$°F, the reactor output becomes 700 MW.

7.6 FAST ACTING VALVES

The Nuclear Power Systems Branch, Nuclear Safety Division, AFWL, is concentrating its effort on nuclear safety. At present, the Air Force is investigating the use of a hardened sphere on a nuclear powered aircraft to contain the reactor, its shielding, and primary coolant. The lines carrying heat exchanger fluid to the engines from the reactor vessel must pierce the sphere wall. In the event of an accident, these ports must be quickly sealed, and remain sealed during and after an accident to preclude radioactive material from contaminating the environment. This study has attempted to ascertain the feasibility of developing a lightweight fast-acting safety valve to seal the coolant lines emanating from a reactor used to power an aircraft.

Research to determine past efforts in the design of this type safety valve for an aircraft reactor was disappointing. The only study uncovered was a research report accomplished by Sandia Laboratories (Ref. 154) for the Nuclear Power Systems Branch, Nuclear Safety Division, AFWL. This report was admittedly a cursory effort to apply Sandia Laboratories' expertise in underground nuclear test containment to aircraft reactor containment (Ref. 153). The study proposed four designs and recommended the design with the best reliability of remaining sealed after a crash. This proposed design is in Figure 7.6-1.

The valve operates by employing the basic principle of a mandrel/sleeve. The pin, acting as a mandrel, is driven into the smaller bore of the housing, whereupon the outer diameter of the pin becomes compressively loaded. At the same time, the inner diameter of the housing expands elastically, and after the pin stops, it is this interference fit that keeps the pin in the sealed position.

The author of the report mentions that he is cognizant of the fact that the reactor package should be as light as possible to increase aircraft payload. On the other hand, the study admittedly did not consider weight reduction as a design parameter. The interference of the pin over the entire length of travel (excluding the first 2 in.), and the fact that the pin is a solid piece of metal requires an explosive package capable of generating a constant pressure of

40,000 psi on the pinhead. This requires a pressure chamber with a wall thickness of 11.37 in. and weighs approximately 13,000 lbs. Consequently, the overall valve weight approaches 23,000 lbs, with a net increase of weight to the reactor vessel of 17,000 lbs per valve. Should 10 nuclear engines be required, each engine would utilize two of these valves, thus increasing the reactor weight by 340,000 lbs, or 17% of the weight of a 2,000,000 lb aircraft must be reserved for reactor safety valves.

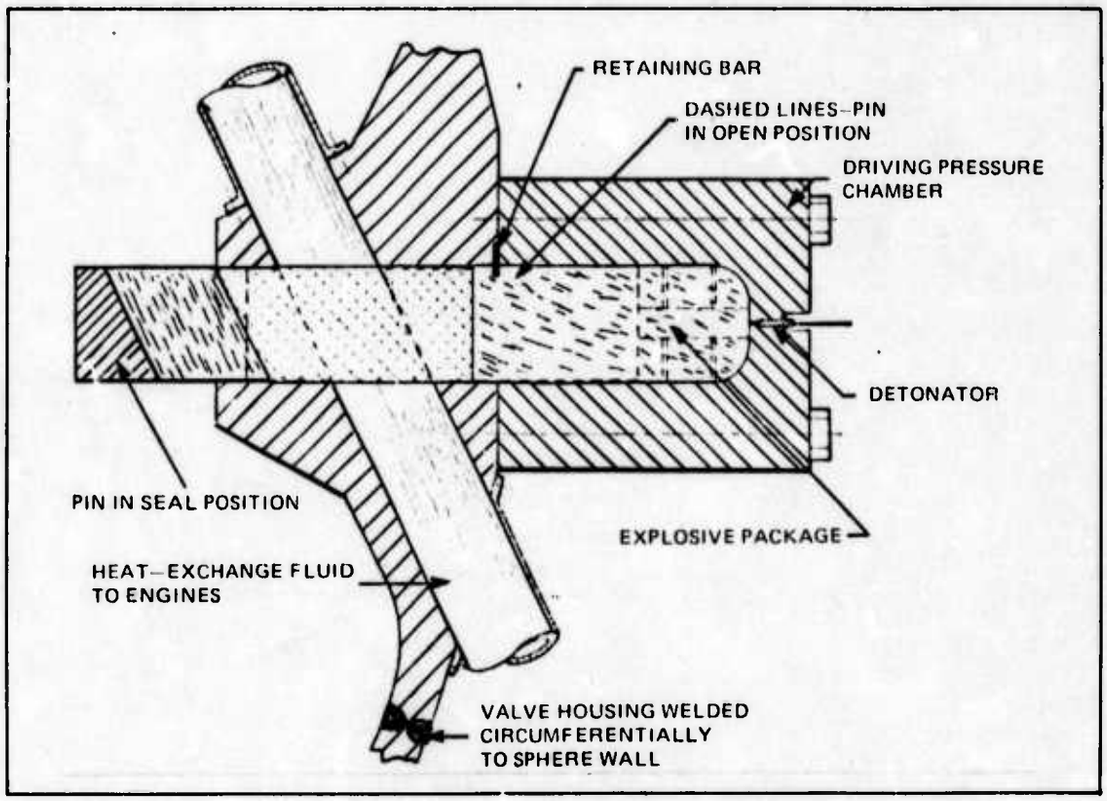

Figure 7.6-1. Sandia's Proposed Design (Ref. 154)

Because of the large percentage of the gross weight being allocated to safety valves under this design, it was necessary to contemplate additional feasible concepts in an effort to reduce the valve weight.

7.6.1 DESIGN PARAMETERS: This study essentially used the same design parameters as Sandia Laboratories. The line diameter required to penetrate the vessel was 10 in. The impact velocity was 1000 ft/sec based on a report by NASA (Ref. 55, p. 1) on data from 96 major accidents occurring before 1965 and involving multi-engine jet aircraft. The in-flight structural failure accident had a maximum impact velocity of 1000 ft/sec. The vessel was assumed to decelerate to zero velocity in 10 ft, based on a technical report by Capt. Holton on impact tests of simulated nuclear containment vessels (Ref. 75). The required valve closure time is 50 msec, which is the same closure time Sandia used; but, as will be shown, this is really a conservative estimate when the impact velocity is 1000 ft/sec. And, finally, the normal operating temperature was 1600°F and a normal working pressure of 1500 psi as opposed to 1200°F and 1500 psi for the Sandia valve.

7.6.2 DESIGN PROPOSALS: The study proposes two designs which are derivatives of the Sandia valve. These valves are named the slide valve and the pin valve and are drawn to a scale of 1 in. to 30 in. in Figures 7.6.2-1 and 7.6.2-2, respectively. The incorporated modifications decreased the mass of the moving mechanism, thus decreasing the mass of the receptacle. A substantial weight savings in the pressure chamber is a complementary weight savings due to the decreased mechanism weight. In addition, a smaller interference fit than the 0.020 in. diameter interference proposed by Sandia was required. These are sumarized in Table 7.6.2-1. For both cases, the valve is constructed of Haynes Alloy 188 with a weight of 0.33 lbs/cu in. The approach used to determine the results was to assume that the holding force required on the movable mechanism in the closed position was equal to the force applied at impact. This study looked only at forces applied along the axis of the movable mechanism.

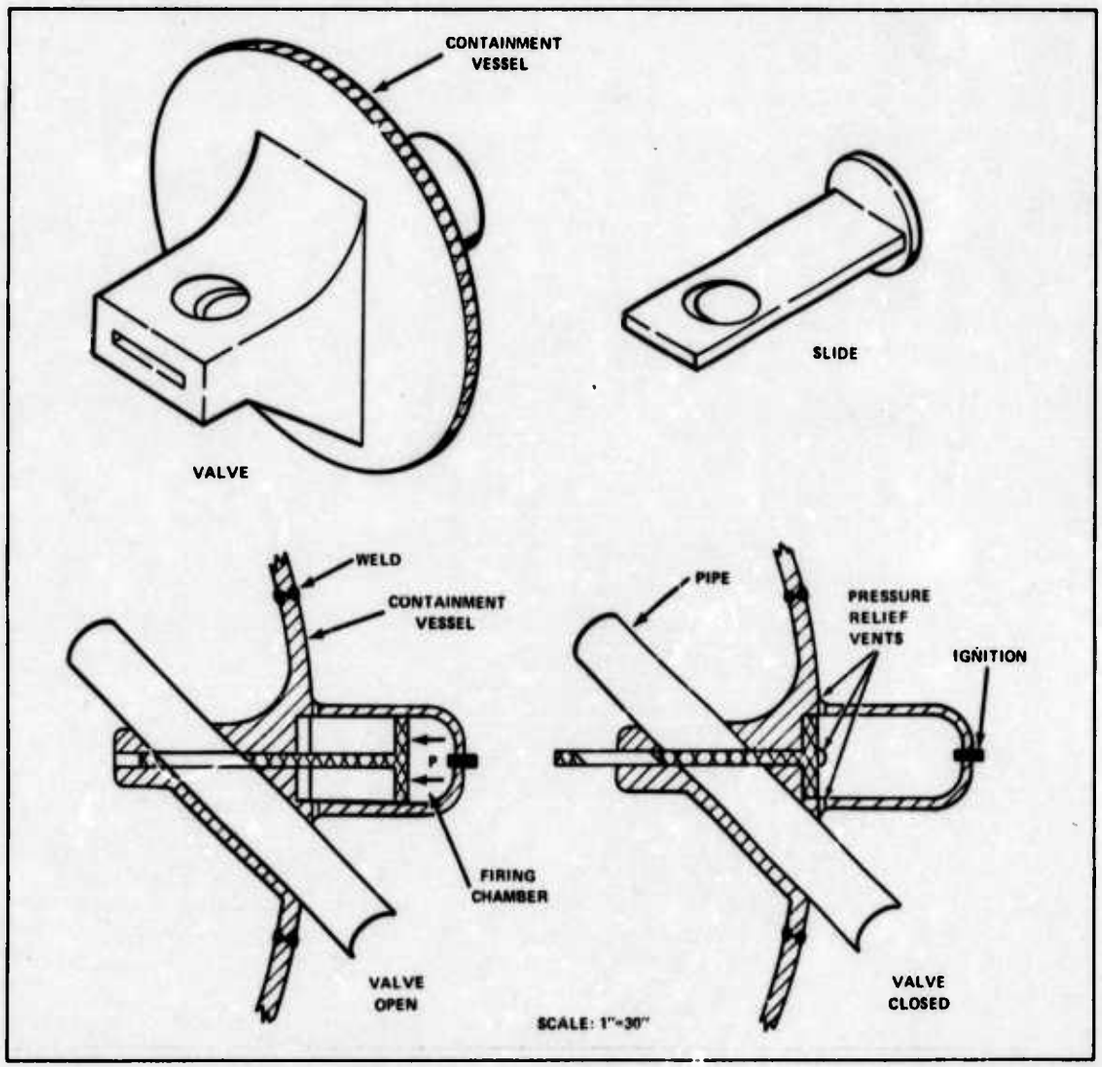

Figure 7.6.2-1. Proposed Slide Valve

Since $v^2 = 2\,ad$

where $v^2 = 1000$ ft/sec

$d = 10$ ft

therefore $a = 1500$ g

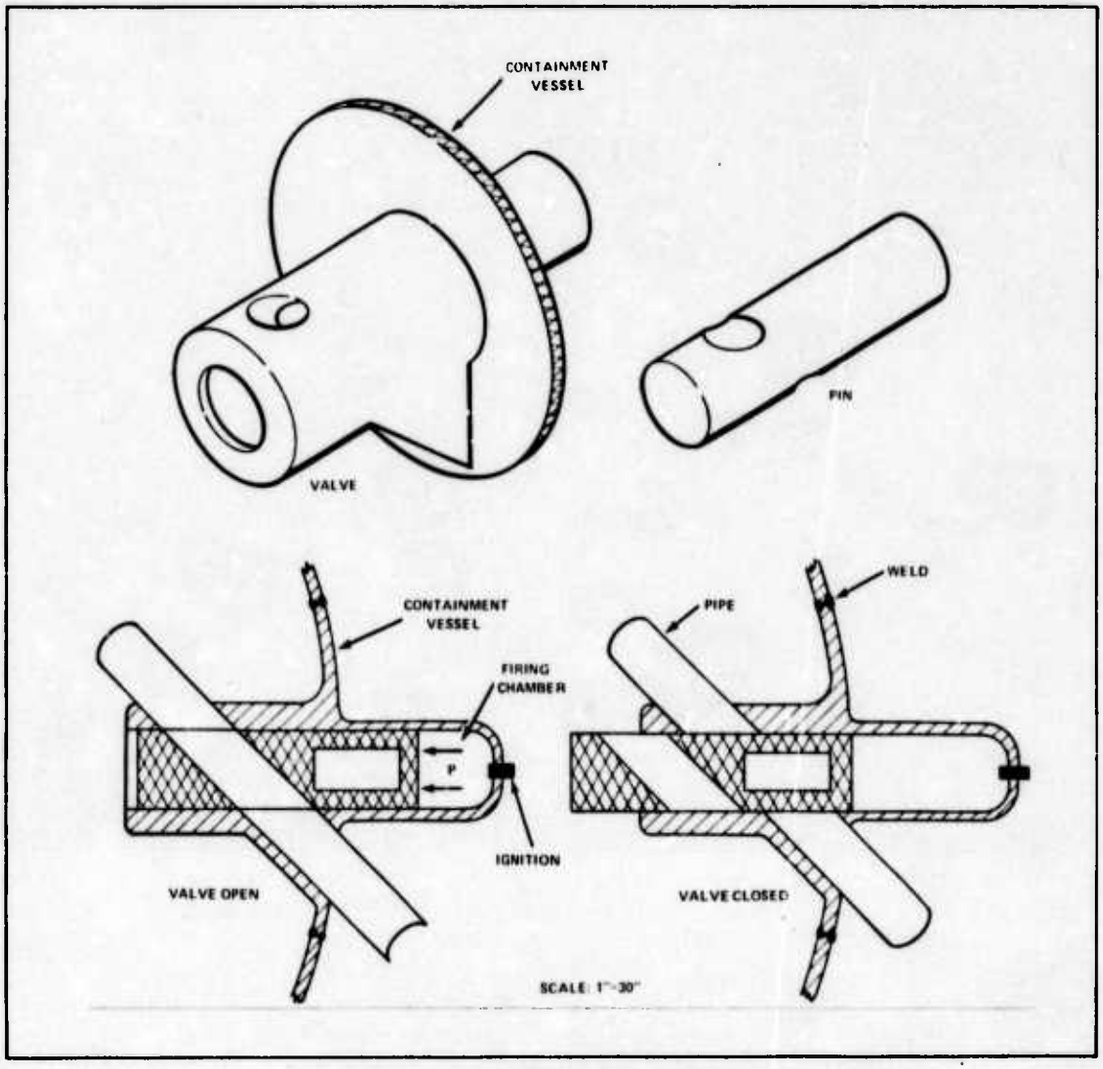

Figure 7.6.2-2. Proposed Pin Valve

Knowing the acceleration, the force required to keep the mechanism in the closed position is obtained from

$$F = \dot{m}a \qquad (7.6.2\text{-}1)$$

where $\dot{m}$ = mass of the mechanism
$a = 1500\ g$

The pressure required to sustain this force is

$$F = PAf \qquad (7.6.2\text{-}2)$$

where F = results from Eq. 7.6.2-1
A = area over which pressure is applied
* f = friction factor = 0.2

*Friction factors of 0.09 to 0.5 may be achieved depending on the finish. (Ref. 113, p. 135).

TABLE 7.6.2-1. SLIDE VALVE AND PIN VALVE RESULTS FOR 10 IN. DIAMETER FLUID LINE

	SLIDE	PIN
WEIGHT OF RECEPTACLE (LBS)	2100	3500
WEIGHT OF SLIDE/PIN (LBS)	450	1340
WEIGHT OF FIRING CHAMBER (LBS)	215	700
WEIGHT OF BRACE (LBS)	1800	850
TOTAL WEIGHT (LBS)	4565	6390
SLIDE/PIN LENGTH (IN.)	40	40
FIRING CHAMBER LENGTH (IN.)	30	30
FIRING CHAMBER WALL THICKNESS (IN.)	0.5	1.5
DESIGN STRESS LEVEL EXCLUDING FIRING CHAMBER (PSI)	40,000	40,000
DESIGN STRESS LEVEL OF FIRING CHAMBER (PSI)	65,000	65,000
EXPLOSIVE CHARGE REQUIRED (PSI)	3,700	11,000
TIME OF CLOSURE (MSEC)	7.5	7.5
FORCE FIT REQUIRED (IN.)	*	0.01

* 0.01 IN. ON SIDES AND 0.001 IN. ON TOP AND BOTTOM OF SLIDE.

With this pressure, the necessary thickness of the receptacle can be determined. For the slide valve Eq. 7.6.2-3 was used to determine the necessary thickness, while Eq. 7.6.2-4 was used to determine the outer radius, and ultimately the required thickness of the pin sleeve.

For rectangular plates with rigidly supported edges:

$$\sigma = \frac{L^2 W^2 P}{2 t^2 (L^2 + W^2)} \qquad (7.6.2\text{-}3)$$

where
- t = thickness
- σ = 40,000 psi which is the ultimate tensile stress for Haynes Alloy 188 with a safety factor of 2
- L = length
- W = width
- p = applied pressure

For thick-walled cylinder:

$$\sigma = p \left(\frac{r_2^2 + r_1^2}{r_2^2 - r_1^2} \right) \qquad (7.6.2\text{-}4)$$

where
- r_1 = outer radius of receptacle
- r_2 = inner radius of receptacle = pin radius
- p = applied pressure
- σ = 40,000 psi which is the ultimate tensile stress for Haynes Alloy 188 with a safety factor of 2.0

The pressure in the gun barrel or pressure chamber can be calculated using Eq. 7.6.2-2 without a friction factor. With this pressure, the thickness of the pressure chamber wall can be obtained by the following thin wall cylinder equation

$$\sigma = \frac{pr}{t}$$

where
- t = thickness of wall
- r = inner radius
- p = applied pressure
- σ = 65,000 which is the ultimate yield stress for AISI 4340 steel with a safety factor of 2.0.

The interference fit can be calculated using the following logic:

$$\epsilon = \frac{\sigma}{E}$$

where
- ϵ = strain
- E = modulus of elasticity for the material
- σ = applied stress

and

$$\epsilon = \frac{E}{L}$$

- ϵ = strain
- e = change in length
- L = length

therefore:

$$e = \frac{L\sigma}{E}$$

And finally the time of closure is calculated from

$$d = 1/2\ at^2$$

where
- t = time of closure
- a = acceleration
- d = distance traveled

A summary of the results of applying the foregoing equations to the two proposed designs is contained in Table 7.6.2-1. The figures shown are for a valve of the size required to close a 10 in. diameter fluid line.

7.6.3 ORIFICE REDUCTION TO SAVE WEIGHT: In an attempt to reduce valve weight by reducing the size of the orifice, a computation was made to determine the amount of additional pump horsepower required. It was felt that the pressure drop could be kept to a reasonable amount if the orifice reduction did not raise the Mach number over 0.9 (Ref. 194).

The Crane Company, in its Technical Paper No. 10 (Ref. 35), indicates that the pressure drop due to a sudden contraction is

$$K_1 \rho \frac{v^2}{2g}$$

where K_1 is the resistance coefficient due to sudden contraction and the pressure drop for a sudden expansion is

$$K_2 \rho \frac{v^2}{2g} \qquad \text{(Ref. 35, A26)}$$

where K_2 is the resistance coefficient due to sudden expansion. Due to the short distance between the contraction and the enlargement, K_2 was doubled (Ref. 194). If $K_2' = 2K_2$

Then

$$\Delta P = (K_1 + K_2') \rho \frac{v^2}{2g} \qquad (7.6.3\text{-}1)$$

The piping which carries helium at 400 fps is 10 in. in diameter. When the area is reduced so that the velocity is approximately Mach 0.9, the diameter is 7 in. That is $d_1 = 7$ in. and $d_2 = 10$ in. The ratio d_1/d_2 is the 0.7. Figure 7.6.3-1 reproduced from the Crane Company Technical Paper No. 10 (Ref. 35) shows K_1 to be 0.22 and K_2 to be 0.26. $K_2' = 2K_2 = 0.52$.

From Eq. 7.6.3-1

$$\Delta p = (0.22 + 0.52)(0.373)(400)^2/(2)(32.2)(144) = 4.76 \text{ psi}$$

Murray's expression for the power required to pump the working fluid through a nuclear power loop is

$$\text{Power} = \Delta PAv/550 \qquad \text{(Ref. 129, p. 223)}$$

where: A is the cross sectional area

and: v is fluid velocity

This yields a delta power of 229 hp.

7.6.4 SUMMARY: The overall conclusion on the safety valve is that it can be accomplished with a far less weight than the Sandia Report proposes. The study's best estimate for such a valve is the range of 4000-8000 lbs. Should a more comprehensive study be undertaken, transverse loads on the valve must be addressed

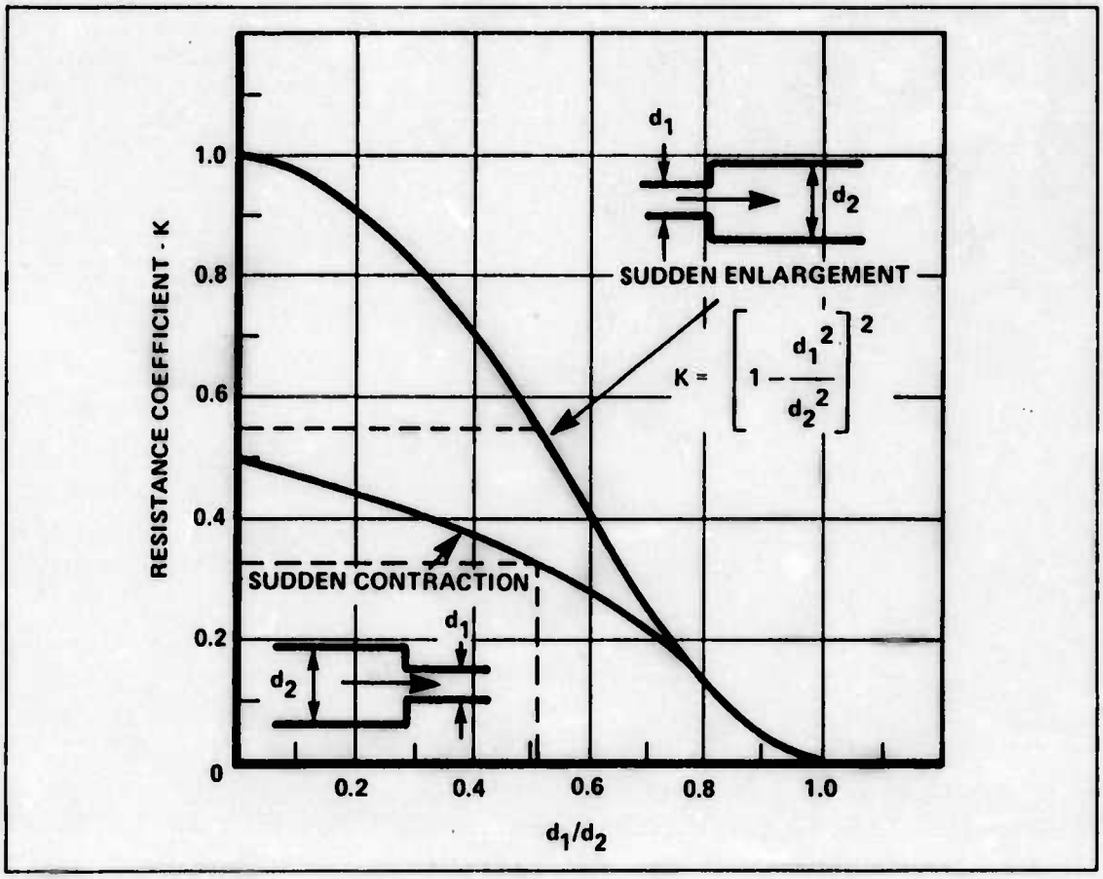

Figure 7.6.3-1. Resistance Due to Sudden Enlargements and Contractions (Ref. 35, A26)

Figure 7.6.4-1 is empirically derived from relationships in Section 7.6.2 showing the weight of a valve vs the pipe diameter.

7.7 RESULTS AND COMPARISONS

In this section two different systems, each with two variations have been analyzed. The indirect cycle heat transfer system was analyzed with two different working fluids, helium and NAK, and the direct cycle system in individual and central turbine forms. In addition, two types of pipes were also analyzed, individual pipes and concentric pipes. The same reactor heat exchanger sufficed for all the designs. Finally, three different types of fast-closing safety valves were discussed: one designed by the Sandia Corp. and two designs proposed by this design study.

The results of the heat transfer system designs and analyses were then compared. The lightest components were used to "build" each system so that the best possible comparison could be made.

In the liquid metal system, the lighter two-pipe configuration was used with the slide type valves, the General Electric designed engine heat exchanger (Ref. 111), and the reactor heat exchanger proposed by this study. Both the indirect and direct cycle helium systems were constructed from the lighter concentric pipe arrangement with the slide type valves and the

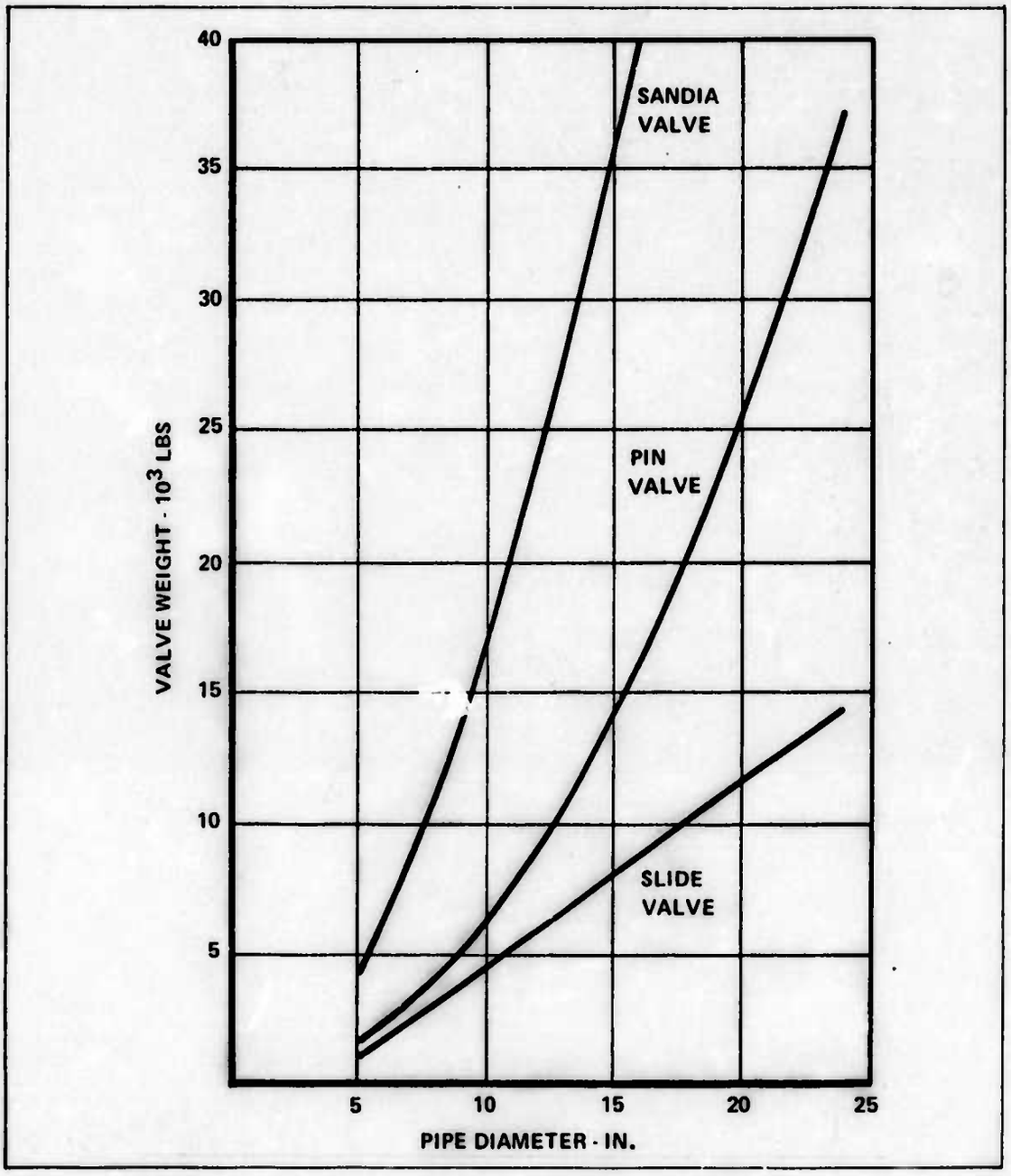

Figure 7.6.4-1. Valve Weight as a Function of Pipe Size

heat exchangers designed in this section. The indirect cycle system used engine heat exchangers as well as the heat exchangers for the primary and secondary circulation systems. The direct cycle system needed only the primary loop circulation system heat exchangers added to its normal heat exchangers.

Table 7.7-1 shows a weight breakdown comparison of the systems. It should also be stated that thrust was used as the common denominator of the comparison, that is, all systems shown produce virtually the same amount of output thrust. They do not, however, have the same reactor power requirements. The weights of the heat transfer systems should not be

used alone to decide which type of system is preferable. Taken with the corresponding engine and reactor weight they may be used as one of the major decision factors.

TABLE 7.7-1. WEIGHT AND POWER COMPARISONS

	INDIRECT CYCLE		DIRECT CYCLE
	LIQUID METAL	HELIUM	
WEIGHT (LBS)			
HEAT EXCHANGERS	99,500	257,600	178,800
VALVES	136,000	81,600	74,800
PIPES	12,100	12,200	12,200
COOLANT	27,000	100	100
TOTAL	274,600	350,900	269,500
REACTOR POWER (MW)	478	574	700

7.7.1 CONCLUSIONS

1. The direct cycle heat transfer system is the lightest weight system. The slight weight advantage it has over the liquid metal indirect cycle system (263,400 vs 274,600) is due to the much heavier liquid metal working fluid and the lighter valves used with the smaller diameter helium pipes.

2. Although the direct cycle system has a small weight advantage with respect to the heat transfer system, it requires nearly one and one-half times the reactor output to produce the same thrust, (700 MW compared to 475 MW).

3. The pumping system for the helium working fluid requires an inordinate amount of power; in the indirect cycle this is 0.95 MW or 20% additional power, the equivalent of two extra engines.

4. The concentric pipe configuration produces significant weight savings over the conventional two parallel pipes (12,200 lbs vs 68,000 lbs). The weight savings are not gained without problems in the areas of fabrication, suspension of the inner pipe, and pumping power.

5. Weight should not be the only criterion used to decide the best system. The relative safety of the two working fluids should also be considered. The liquid metal is a highly active material which can become radioactive. The helium gas, while it cannot become radioactive, is under an extremely high pressure, 1800 psi.

7.7.2 AREAS RECOMMENDED FOR FURTHER STUDY

1. Studies and experimentation in high temperature metallurgy should be conducted with the goal of producing significant increases in heat exchanger working temperature to the

point that they are comparable with the turbine inlet temperatures of state-of-the-art turbofan engines.

2. Long concentric pipes should be investigated and experiments performed to determine the optimal design and location of the inner pipe suspension as well as the pressure loss caused by the suspension. The test environment would have to simulate the conditions of vibration and bending which the pipe would be subject to in an aircraft wing.

3. A safety analysis should be performed to determine the relative hazards of each working fluid in the event of an accident or a heat transfer system malfunction involving the escape of working fluid. The study should address hazards to both the crew and the public.

SECTION 8
SAFETY ANALYSIS

8.0 INTRODUCTION

8.0.1 BACKGROUND: The current interest in the possible use of nuclear propulsion for aircraft is a natural outgrowth of numerous changes which have taken place since the shutdown, in 1961, of the Aircraft Nuclear Propulsion Development Program. There have been large increases in the size of aircraft, growing scarcity of fossil fuels, numerous technological advances in nuclear energy systems, and a significant easing of design performance parameters in that there is no longer a requirement for supersonic capability. These changes have tended to increase the feasibility of a nuclear powered airplane, but throughout the same time period other changes have occurred which have tended to decrease the feasibility of such an airplane.

In particular, there is an increasingly persistent question of the impact of a system on the environment and public safety. In aviation, a relatively mild departure from the norm, the supersonic transport created substantial public concern over possible environmental effects, and in the nuclear energy industry there is an unabated concern over the environmental effects of nuclear plants.

8.0.2 OBJECTIVE: The question of public safety was deemed to be of prime importance and concern, therefore one objective of this study was defined as determining the feasibility of a nuclear powered aircraft from the standpoint of public risk.

8.0.3 OVERVIEW OF METHODOLOGY: Individual risk was defined to be the probability, per year, that any person in the U.S. would be killed by a release of radioactive material from a nuclear powered airplane. The individual risk is expressed as

$$\text{INDIVIDUAL RISK} = \frac{\text{SOCIETAL RISK}}{\text{TOTAL U.S. POPULATION}}$$

where societal risk is the expected number of deaths per year and is expressed as

$$\text{SOCIETAL RISK} = \frac{\text{NUMBER OF ACCIDENTS}}{\text{YEAR}} \times \frac{\text{NUMBER OF DEATHS}}{\text{ACCIDENT}}$$

The number of accidents per year is the mean or expected value of an accident probability distribution which was derived by a probabilistic assessment of the failure modes of a nuclear powered aircraft using an Event Tree/Fault Tree methodology.

The number of deaths per accident is an expected value of a probability distribution of number of deaths which was derived by simulation techniques using random dispersal of radioactive material into areas of random population density.

It was recognized very early that a precise determination of such probabilites was impossible. First, a nuclear powered airplane is still in a broad conceptual phase. Engineering details and diagrams are yet to be formulated, as are the development and testing of hardware. Second, data for components and systems performing similar functions are diverse and scarce. Therefore, the technique employed was one of trying to find bounds within which the true probability lay and against which acceptance criteria could be applied.

This section is organized into two main parts. The first, *Release Probability*, details the development of the probability of a release of radioactive material; the second, *Release Consequences*, details the development of the probability of any number of deaths given that a release of radioactive material has occurred.

The mission duration, for which an upper limit of approximately two weeks has been established, was chosen to be 330 hrs. The basic reactor system configuration chosen for the modeling and calculations presented in this section is a 574 MW, gas cooled reactor supplying coolant to 10 engines. The effects of using a liquid-metal coolant in the basic configuration are discussed and the results of calculations for different power levels are presented.

Throughout this study, extensive use was made of a recent Atomic Energy Commission report, *Reactor Safety Study*, WASH-1400 (Ref. 185). WASH-1400 is a probabilistic risk assessment of ground based nuclear power generating systems and much of the methodology and data contained therein were used for this study. In particular, much of the release probability modeling closely parallels that of WASH-1400, and the release consequence portion involves validation and direct use of models and methodology contained in that report.

Extensive use was also made of a computer program called SIMPAK (Ref. 27), which generates probability distributions from raw input data and uses random sampling from those distributions to perform any arithmetic operation in a Monte Carlo simulation.

8.1 RELEASE PROBABILITY

8.1.1 EVENT TREES: The Event Tree is a tool frequently employed in system analysis. It is, in essence, a means of bookkeeping and provides a pictorial representation of the various ways in which an event can occur. In general (See Figure 8.1.1-1) an Event Tree is drawn with an initiating event on the left, the outcome on the right, and, in between, the various protective functions of engineering safety features designed to prevent the undesired outcome from occurring. At each decision point, success of the safety feature is denoted by an upward path and failure by a downward path. The various paths on the tree then represent the various ways in which the postulated initiating event can lead to the outcome.

Not all sequences on the Event Tree terminate in an undesired outcome. In general, the first sequence, in which all safety features operate, does not yield an undesired outcome, and the last sequence, in which all safety features fail, does yield an undesired outcome. All other sequences must be analyzed for the particular system in question to determine whether or not a sequence leads to an undesired outcome.

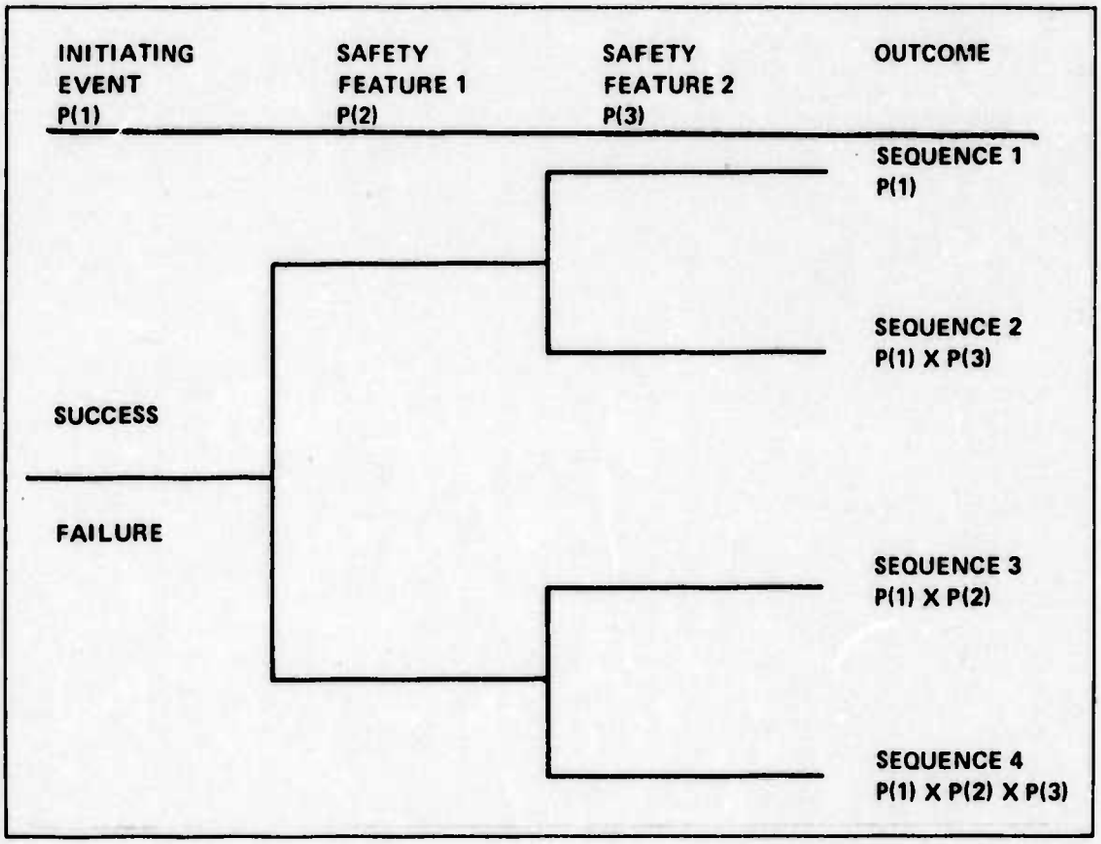

Figure 8.1.1-1. Event Tree Construction

By establishing the probability of occurrence of the various events on the tree, the probability of any sequence of events can be calculated. In Figure 8.1.1-1, the probability of occurrence of the initiating event is denoted as P(1) and the conditional probabilities of failure of safety features 1 and 2 are denoted P(2) and P(3), respectively. The probability of occurrence of sequence 3, for example, is given as the probability that the initiating event occurs times the probability that safety feature number 2 fails, or P(1) x P(2). It should be noted that, to be absolutely correct, the sequence 3 probability should contain the term 1-P(3), so that

$$P(\text{sequence 3}) = P(1) \times P(2) \times (1-P(3))$$

However, in this study, all probabilities used were significantly less than 10^{-1} (generally less than 10^{-3}) so that all (1-P) terms were treated as unity.

In most instances, it was not possible to determine a single value for the probability of failure at the Event Tree decision points but, rather, it was necessary to establish a confidence interval of values. That is, using fault trees and other analytical techniques coupled with Monte Carlo simulation, a probability distribution of probabilities was generated for each decision point. It was then possible to state, with confidence, the interval within which the true probability of failure lay. For this study, the 5th and 95th percentiles of the probability distributions were chosen as the bounds for a 90% confidence interval. For example, if the

probability values at the 5th and 95th percentiles were 10^{-3} and 10^{-1}, respectively, it can be stated with 90% confidence that the true probability value lies between 10^{-3} and 10^{-1}.

Once the probability distribution of probabilities was generated for each decision point on the tree, a probability distribution of probabilities was computed for each sequence by randomly selecting a failure probability from each decision point and multiplying the appropriate values for each sequence. This process was repeated 500 times to form a random set of values for each sequence which was then statistically summarized as a probability distribution. From the distribution for each of the sequences which results in a release of radioactive material, the 5th, 50th, and 95th percentiles are presented as the low, median, and high release probabilities, respectively

For this study, the undesired outcome of an accident sequence was defined to be a release of radioactive material. Three initiating events were postulated: (1) Crash, (2) Transient, and (3) Loss of Coolant. The Impact and Transient Event Trees are shown in Figures 8.1.3.8-1 and 8.1.4.6-1, respectively, and the formulation of the three accident probabilities are discussed in detail in Sections 8.1.3, 8.1.4, and 8.1.5.

8.1.2 FAULT TREES: In some cases, it was convenient to employ a technique known as Fault Tree analysis to determine the failure probability associated with Event Tree decision points. A Fault Tree is a schematic representation of the reliance of a system on its various components, constructed by connecting the components via AND/OR logic symbols.

The use of AND logic on the Fault Tree is shown in Figure 8.1.2-1a. The tree shows a two component system that fails only if components 1 and 2 fail. In Figure 8.1.2-1b, the use of OR logic is shown in a system that fails if either component 1 or component 2 fails.

To allow the computation of the system failure probabilities, the following relationships are established:

For the AND logic of Figure 8.1.2-1a

$$P(\text{system failure}) = P(1) \times P(2)$$

For the OR logic of Figure 8.1.2-1b

$$P(\text{system failure}) = P(1) + P(2) - P(1) \times P(2)$$

where P(1) and P(2) denote the failure probabilities of components 1 and 2 respectively. For those cases where all Ps are less than 0.1, the product terms become insignificant compared to the summation terms and can generally be disregarded without significant loss of accuracy. In that case, the equation for OR logic becomes simply a sum of component failure probabilities.

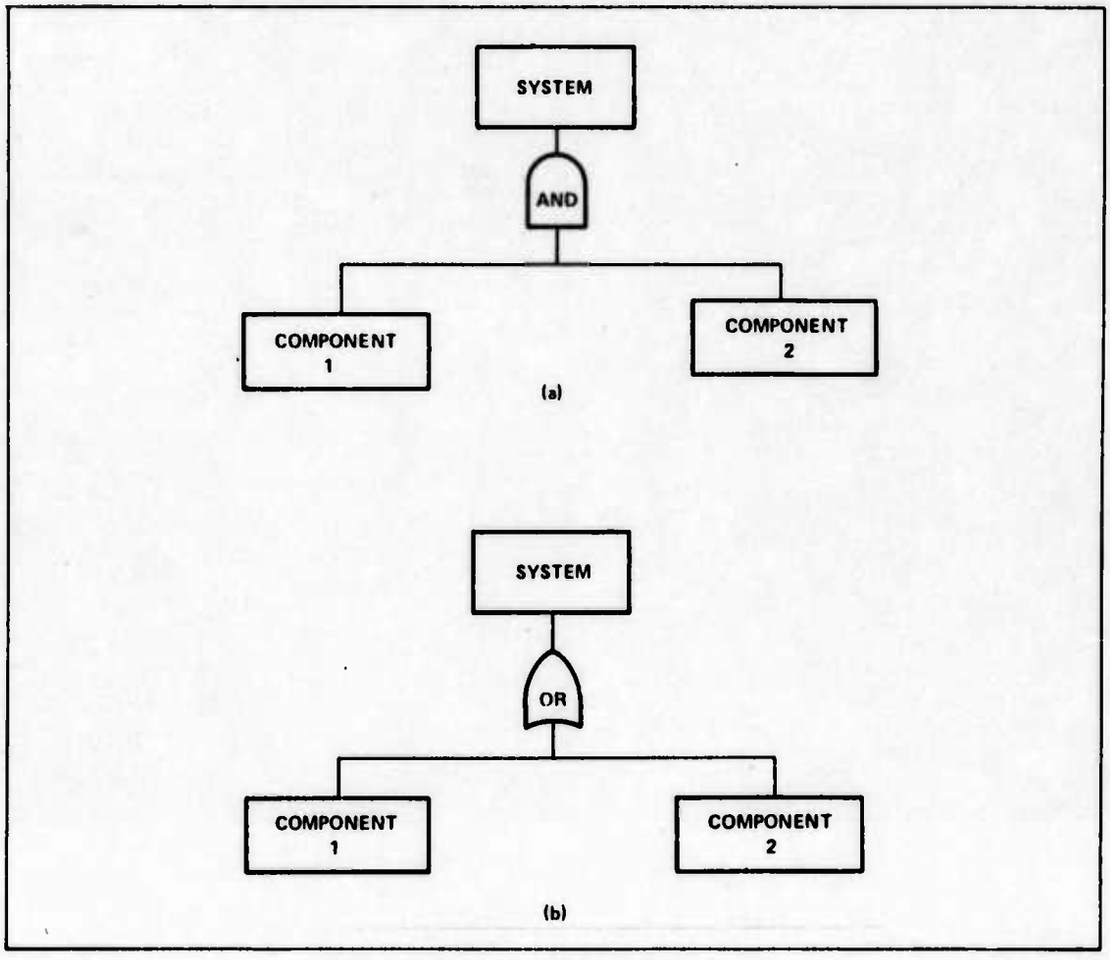

Figure 8.1.2-1. Fault Tree Construction

In general, for an N component system connected by AND logic:

$$P(\text{system failure}) = \prod_{i=1}^{N} P_i \qquad (8.1.2\text{-}1)$$

and for an N component system connected by OR logic:

$$P(\text{system failure}) = \sum_{i=1}^{N} P_i \qquad (8.1.2\text{-}2)$$

The component failure probabilities for the Fault Trees were computed using the negative exponential probability distribution formulation,

$$P(\text{component failure}) = P = 1 - \exp(-\lambda t) \qquad (8.1.2\text{-}3)$$

where λ is the component failure rate in failures per hour and t is the operating time of the component in hours.

The negative exponential probability distribution is widely employed in reliability analysis for predicting component or system failures, but is subject to a requirement that the failure rate be constant. Figure 8.1.2-2 shows a typical complex equipment failure rate (λ) as a function of operating time (Ref. 13, p. 33). It is characterized by a useful life period of constant failure rate, and burn-in and wearout periods of higher failure rates.

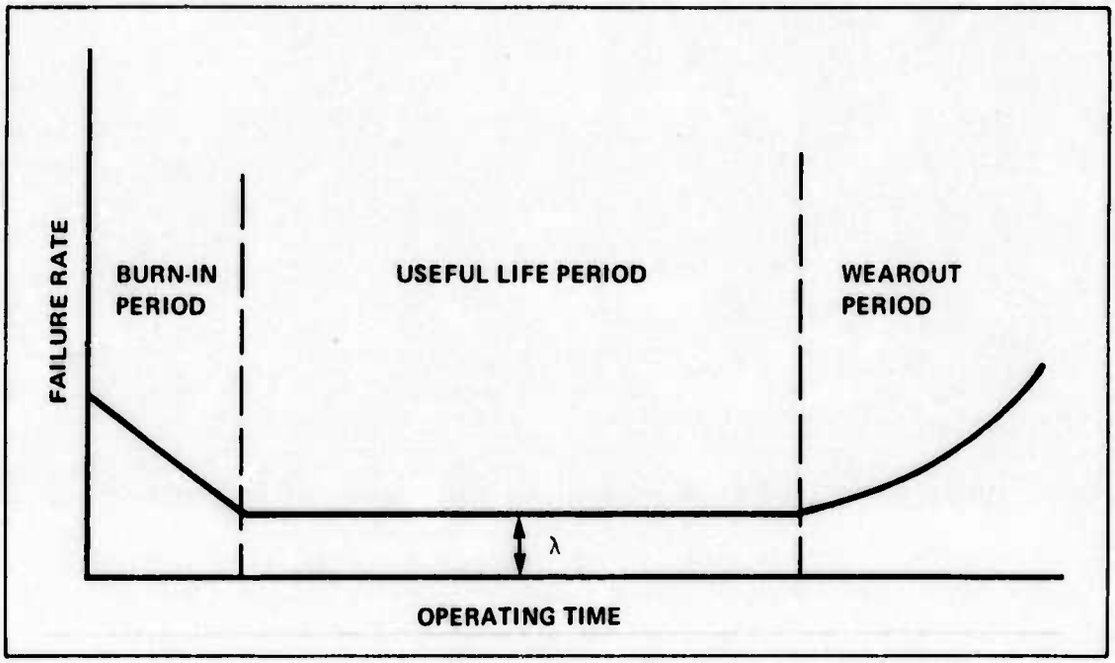

Figure 8.1.2-2. Typical Failure Rate Pattern of Complex Equipments

The burn-in period is a period in which the weaker, substandard components representing manufacturing defects fail. The wearout period is a period in which components begin to fail due to the specific cause-factor, wear. The useful life period in which failures occur by chance, or a random occurrence of some cause-factor (Ref. 13, p. 32-35; 28, p. 72; 140, p. 67-75).

By using burn-in and preventive replacement techniques, a system can be maintained so that the failures occur by chance. That is, by burning in components before use and replacing components before they fail by wearout, the system can be maintained in the useful life period characterized by a constant failure rate.

An assumption has been used throughout this study that systems or components related to safety would be maintained in such a manner, thus permitting the use of the negative exponential function.

It was mentioned in the Event Tree analysis, Section 8.1.1, that it was generally not possible to establish a single valued estimate of the probability of failure at the Event Tree decision points. This fact stems from the nature of the failure rates available for computation

of the Fault Tree and other probabilities. The failure rate estimates are often based on a very limited number of failures and are taken from a variety of sources. These two facts contribute to a wide variance in statistical estimates of failure rates which led to a decision to utilize Monte Carlo simulation to solve the Fault Trees and the Event Trees.

Figure 8.1.2-3 shows a sample Fault Tree of six components connected by a combination of AND/OR logic indicators. The system failure probability is solved as:

$$P(T) = (P(1) + P(2)) \times (P(3) + P(4)) + P(5) + P(6)$$

Each component on the tree has an associated operating time and a range of failure rates. Monte Carlo solution is accomplished by selecting a random value of the failure rate from each of the failure rate distributions, solving the failure probability for each of the components on the tree, and then solving the expression for P(T). Five hundred values of P(T) were generated

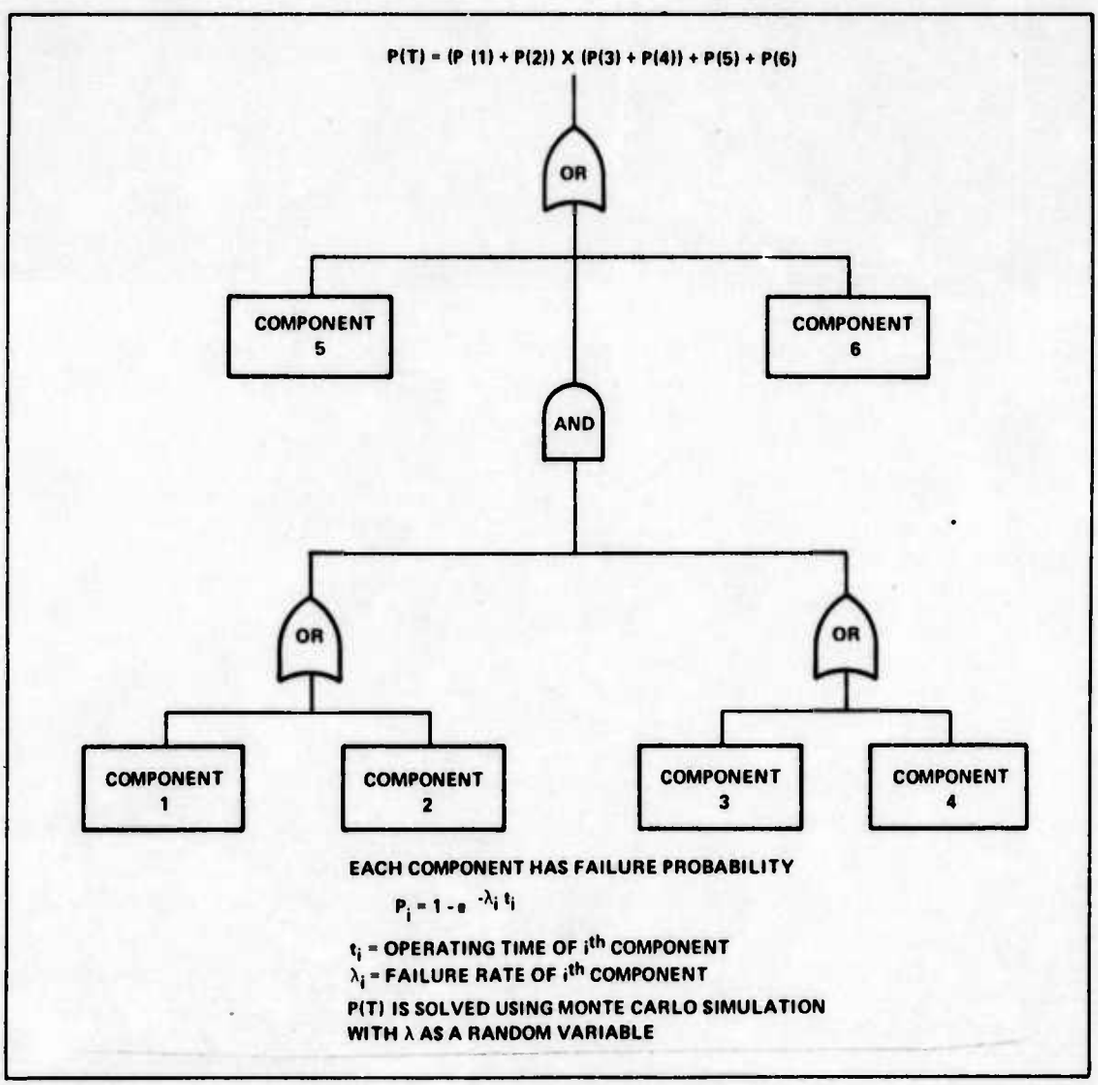

Figure 8.1.2-3. Fault Tree Solution

by iteratively solving the tree with random values of the failure rates, and the 500 values of P(T) were then summarized statistically to arrive at a probability distribution of P(T). This distribution of P(T) was then used as an input in the solution of the Event Tree.

8.1.3 IMPACT EVENT TREE: The Impact Event Tree was formulated to describe those accidents (release of radioactive material) which might occur as a result of crashes or mid-air collisions. The initiating event was denoted as crash, and the tree was developed under the assumption that the aircraft is in a crash mode (impending crash) or has already crashed. The Impact Event Tree is shown in Figure 8.1.3.8-1, and is discussed in Sections 8.1.3.1 through 8.1.3.7.

8.1.3.1 CRASH: Aircraft crash is the initiating event for the Impact Event Tree and is defined to include only those accidents which occurred during an in-flight phase of operation.

The model used for describing crash probability was the negative exponential formula given in Eq. 8.1.2-3 where λ is the loss rate in crashes per flight hour and t is the mission time of 330 hours (Ref. 29, p. 46).

The loss rate was taken from the USAF Accident Bulletins (Ref. 183) for 1961 through 1973. It was desired to restrict attention to large multi-engine aircraft, but to include aircraft that had missions involving some tactical maneuvering such as descent to low altitude with subsequent climb back to cruise altitude. The aircraft selected under these criteria were all aircraft in the two major categories, bomber and cargo. The loss rate for each of the 13 years was computed by dividing the total number of bomber and cargo crashes by the total bomber and cargo flying hours. The 13 estimates of loss rate so derived were tested statistically and found to be normally distributed with mean = 1.46×10^{-5} and standard deviation = 0.348×10^{-5} (Appendix A.8.1.1.1).

Five hundred random selections of loss rate were taken from the loss rate distribution and used with Eq. 8.1.2-3 to generate the distribution of crash probabilities summarized in Table 8.1.3.1-1.

TABLE 8.1.3.1-1. CRASH PROBABILITY DISTRIBUTION PER FLIGHT

PROBABILITY		
LOW	**MEDIAN**	**HIGH**
3.07×10^{-3}	4.83×10^{-3}	6.55×10^{-3}

Table 8.1.3.1-1 is interpreted in the following manner. There is a 90% confidence that the probability of crash for a 330 hour mission lies between 3.07×10^{-3} and 6.55×10^{-3}.

8.1.3.2 ELECTRIC POWER: The first safety feature on the Impact Event Tree is electric power, and its probability is defined as the conditional probability that electrical

power will be failed given that the aircraft is about to crash. The electric power safety feature was placed on the tree at this point because of the dependence of subsequent safety features on the availability of electrical power.

The probability of electrical power failure was determined by the use of the Fault Tree shown in Figure 8.1.3.2-1. Major components of electrical power are the aircraft primary electrical system, an auxiliary generator dedicated to reactor control, monitor, and safety functions, and battery power dedicated to emergency functions.

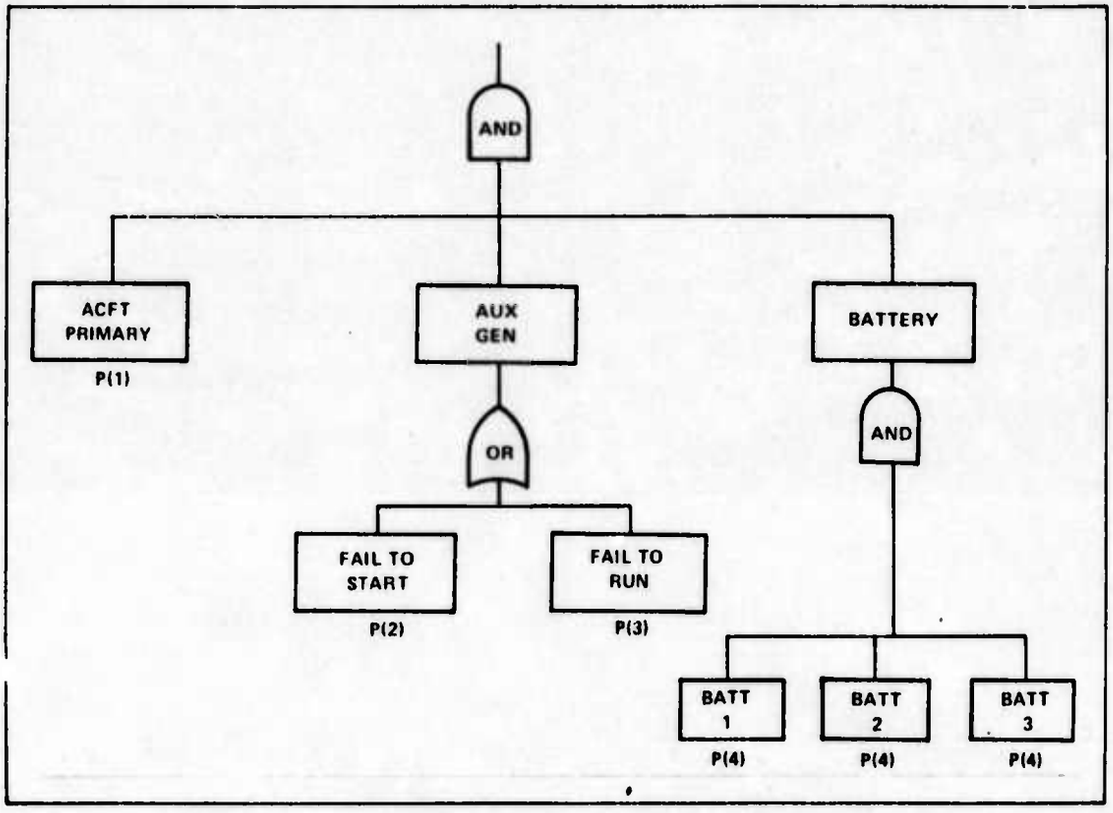

Figure 8.1.3.2-1. Electrical Power Failure Fault Tree

The data used for the components of the tree are given in Appendices A.8.1.2.1 and A.8.1.3.1 and the probability of electrical power failure is given by

$$P(\text{electric failure}) = P(1) \times (P(2) + (P(3)) \times (P(4))^3 \qquad (8.1.3.2\text{-}1)$$

P(1) = failure probability of primary electrical system
P(2) = probability auxiliary generator will fail to start
P(3) = probability auxiliary generator will fail to run
P(4) = probability batteries will fail

The probability that the aircraft electrical system fails is a conditional probability based on historical crash data. The auxiliary generator and battery probabilities were computed using the negative exponential formula. Operating time for the auxiliary generator is the

time from loss of aircraft electrical power until the crash occurs and a value of 10 minutes was used. All other probabilities use mission time of 330 hours.

The distribution of probabilities of electrical power failure is summarized in Table 8.1.3.2-1.

TABLE 8.1.3.2-1. ELECTRICAL POWER FAILURE PROBABILITY DISTRIBUTION

PROBABILITY		
LOW	**MEDIAN**	**HIGH**
3.98×10^{-15}	2.48×10^{-13}	1.84×10^{-11}

8.1.3.3 PRE-IMPACT SENSING: The second safety feature shown on the Impact Event Tree is pre-impact sensing and has as its purpose initiation of reactor shutdown and closure of safety valves prior to impact. The feature works by predicting impact based on inputs of aircraft altitude, attitude, and flight dynamics.

The pre-impact sensing system is dependent on the availability of electrical power, therefore no decision point was allowed for this function on the branch which depicts failure of electric power.

The probability of pre-impact sensing failure was determined by the use of the Fault Tree shown in Figure 8.1.3.3-1. The major components of the tree are an impact prediction computer and equipment to sense altitude, attitude, airspeed, and vertical velocity.

The data used are given in Appendix A.8.1.3.1 and the Fault Tree was solved using the equation:

$$P(\text{pre-impact sensing failure}) = (P(1))^2 + (P(2))^2 + (P(3))^2 \qquad (8.1.3.3\text{-}1)$$

P(1) = failure probability of impact prediction computer
P(2) = failure probability of air data system
P(3) = failure probability of inertial data system

The negative exponential formula was used for all component failure probabilities with operating time equal to 330 hours.

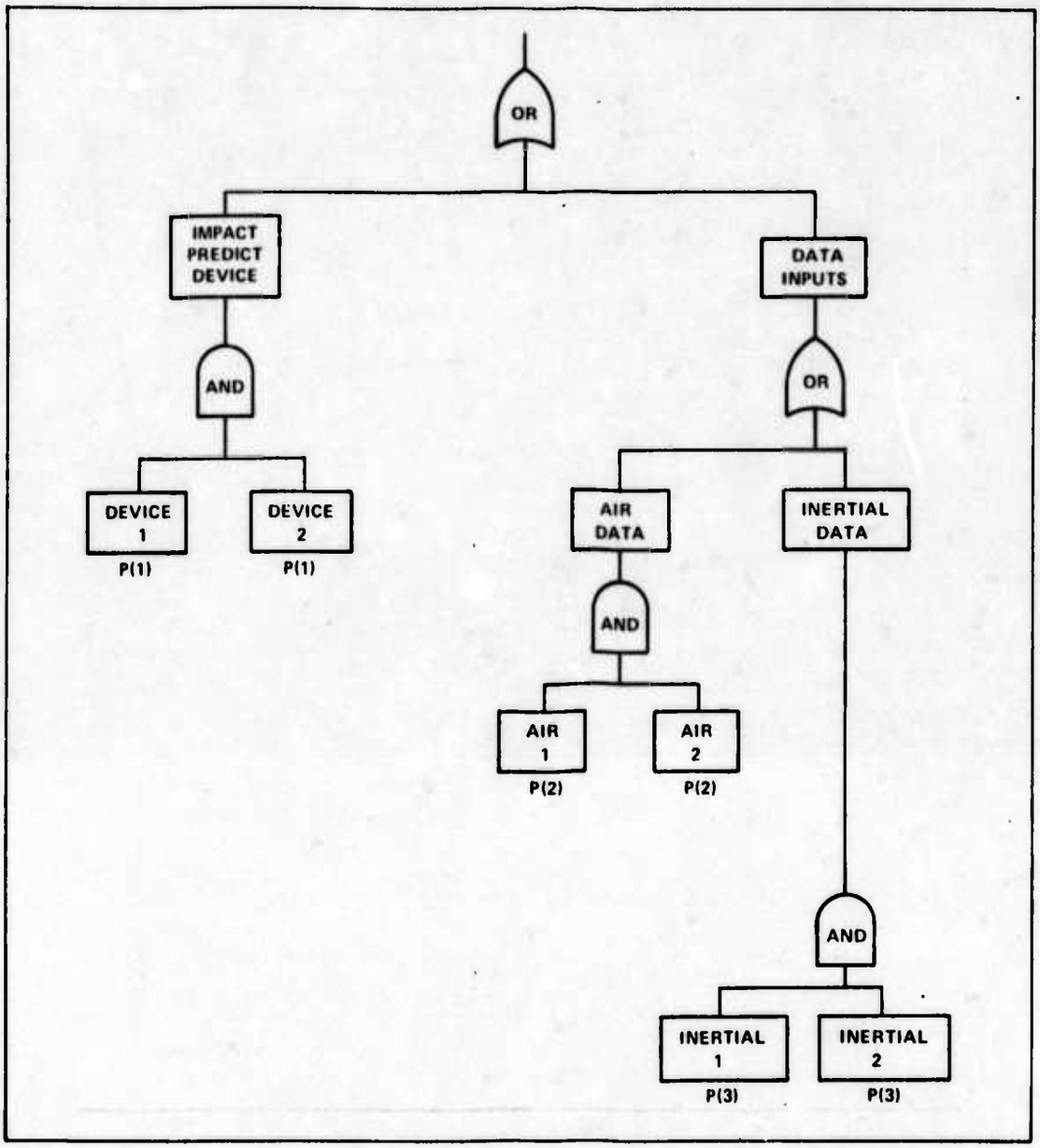

Figure 8.1.3.3-1. Pre-Impact Sensing Fault Tree

The distribution of probabilities of pre-impact sensing failure is summarized in Table 8.1.3.3-1.

TABLE 8.1.3.3-1. PRE-IMPACT SENSING FAILURE PROBABILITY DISTRIBUTION

PROBABILITY		
LOW	**MEDIAN**	**HIGH**
1.11×10^{-7}	8.18×10^{-7}	9.02×10^{-6}

8.1.3.4 REACTOR SHUTDOWN: The third safety feature shown on the Impact Event Tree is reactor shutdown. It follows pre-impact sensing since pre-impact sensing has, as one of its functions, shutdown of the reactor.

The probability that the reactor will fail to shut down is conditioned on the prior events. Thus, the failure probability increases with the loss of pre-impact sensing and increases further with the loss of electric power. Therefore, solution of the Event Tree requires three different probabilities for the reactor shutdown event.

The probability of the reactor failing to shut down was computed using the Fault Tree shown in Figures 8.1.3.4-1a-d. Figure 8.1.3.4-1a depicts the two major ways of shutting down the reactor. The normal means of reactor shutdown is by rotation of the control drums to effect neutron capture. The backup or emergency method of shutdown is by flooding the reactor core with boron.

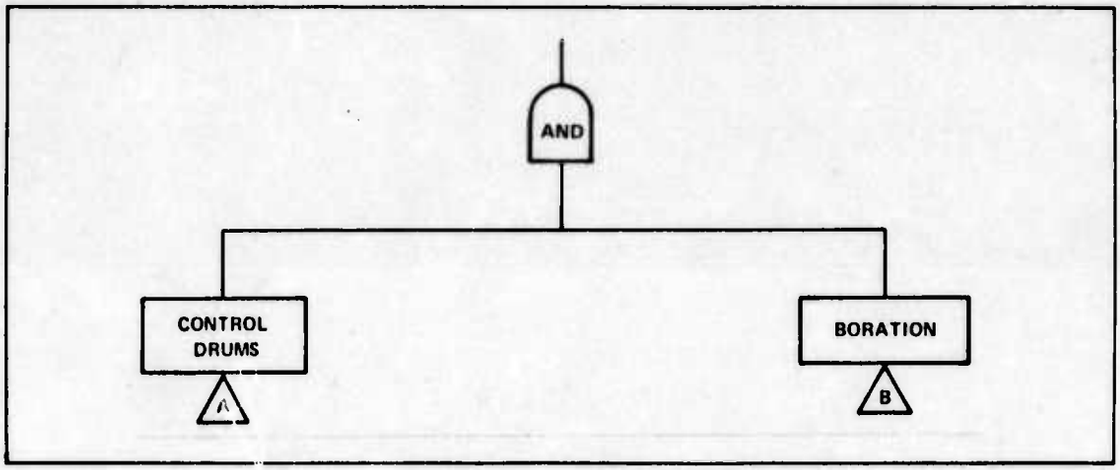

Figure 8.1.3.4-1a. Reactor Shutdown Fault Tree

Figure 8.1.3.4-1b shows the control drum mechanism, and was computed in three different ways. When electrical power was available and the pre-impact sensor was operating, a shutdown signal was assumed to be received and the impact sensor was neglected. The resulting expression for the probability of control drum failure is

$$P_C = P(1) \times P(2) \qquad (8.1.3.4\text{-}1)$$

P(1) = probability of control drum failure
P(2) = probability of control drum drive failure

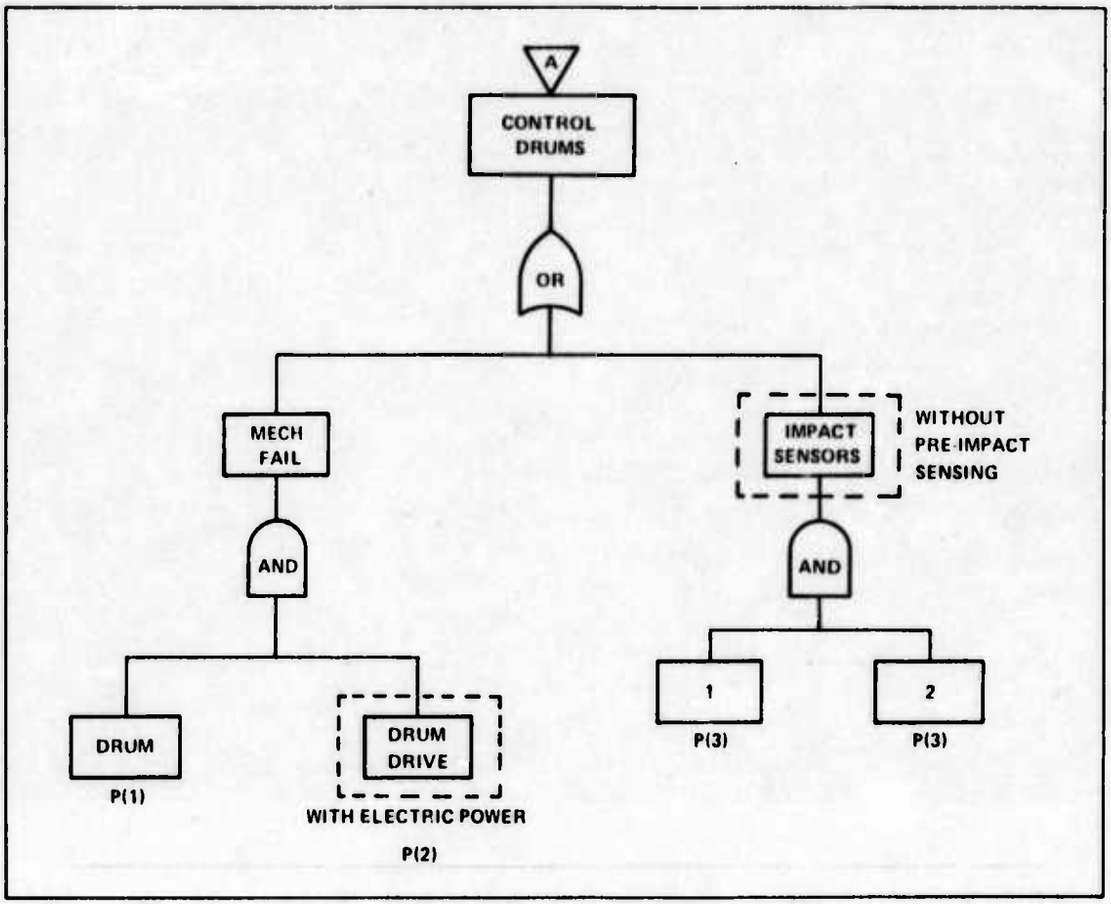

Figure 8.1.3.4-1b. Reactor Shutdown Fault Tree

When electric power was available and the pre-impact sensor was failed, the shutdown signal was assumed to come from the impact sensor, and the failure probability is given by

$$P_C = P(1)\,P(2) + (P(3))^2 \qquad (8.1.3.4\text{-}2)$$

P(3) = probability of impact sensor failure

When electric power was failed, the impact sensor and the electrically driven drum drive were excluded and the drum was considered to rotate by spring action. The probability of failure in this case is given by

$$P_C = P(1) \qquad (8.1.3.4\text{-}3)$$

The formulations in Eqs. 8.1.3.4-1 through 8.1.3.4-3 express the probability that no control drum rotates to the shutdown position. During steady state operation, a single control

drum rotated to the shutdown position is sufficient to shut down the reactor. However, in order to eliminate the hot side/cold side effect that could occur if a single drum rotated to shutdown, a more conservative approach was used.

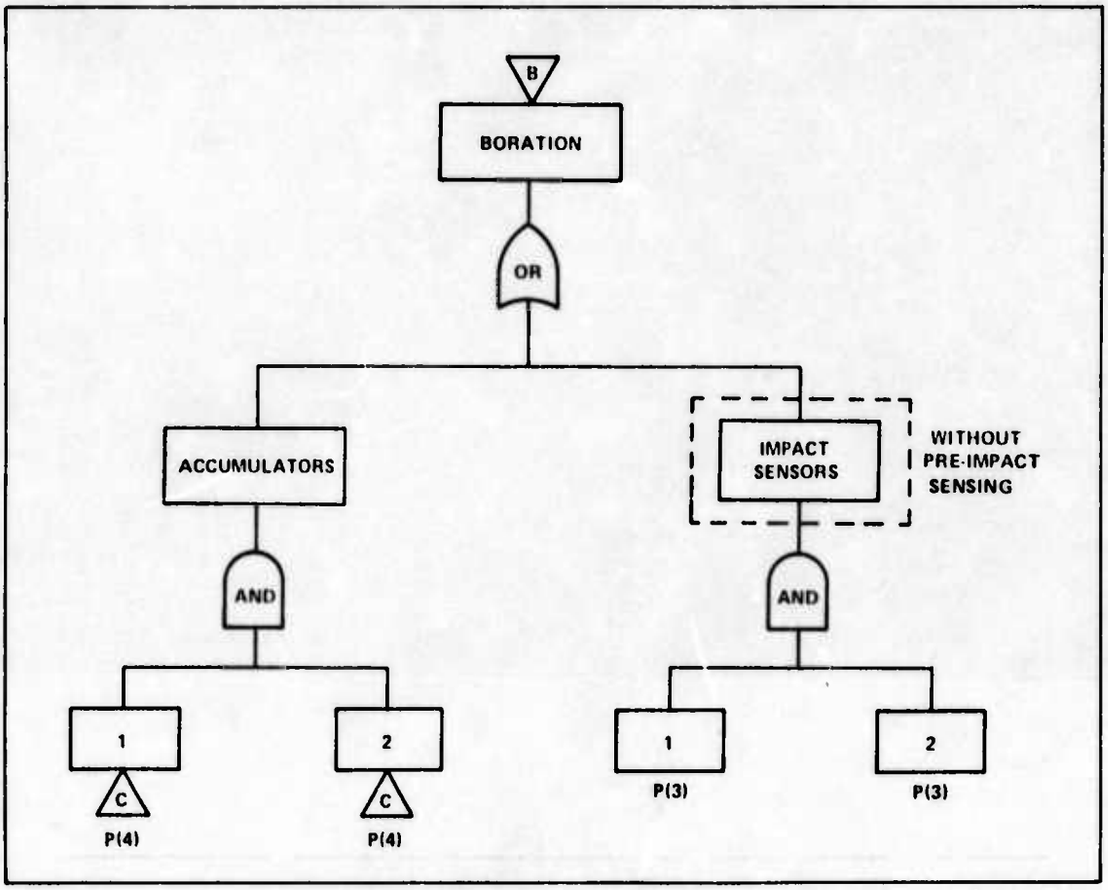

Figure 8.1.3.4-1c. Reactor Shutdown Fault Tree

Figure 8.1.3.4-2 depicts the reactor core with the 24 surrounding control drums. For this study, the circular core zone was divided into six equal segments containing four control drums each. Control drum failure was then defined as the failure to get at least one drum in each of the six segments rotated to the shutdown position. The control drum failure probability is given by

$$P(\text{control drum failure}) = 6(P_C)^4 \qquad (8.1.3.4\text{-}4)$$

where P_C denotes the failure probability of a single drum.

Figure 8.1.3.4-1d depicts a portion of the boration system. The system relies on electrical power and the failure probability was computed for the two cases of pre-impact sensor operating or failed. In the first case, the impact sensor was excluded and the failure

probability was computed for the accumulators of which there are two, and either of the two can perform the function alone.

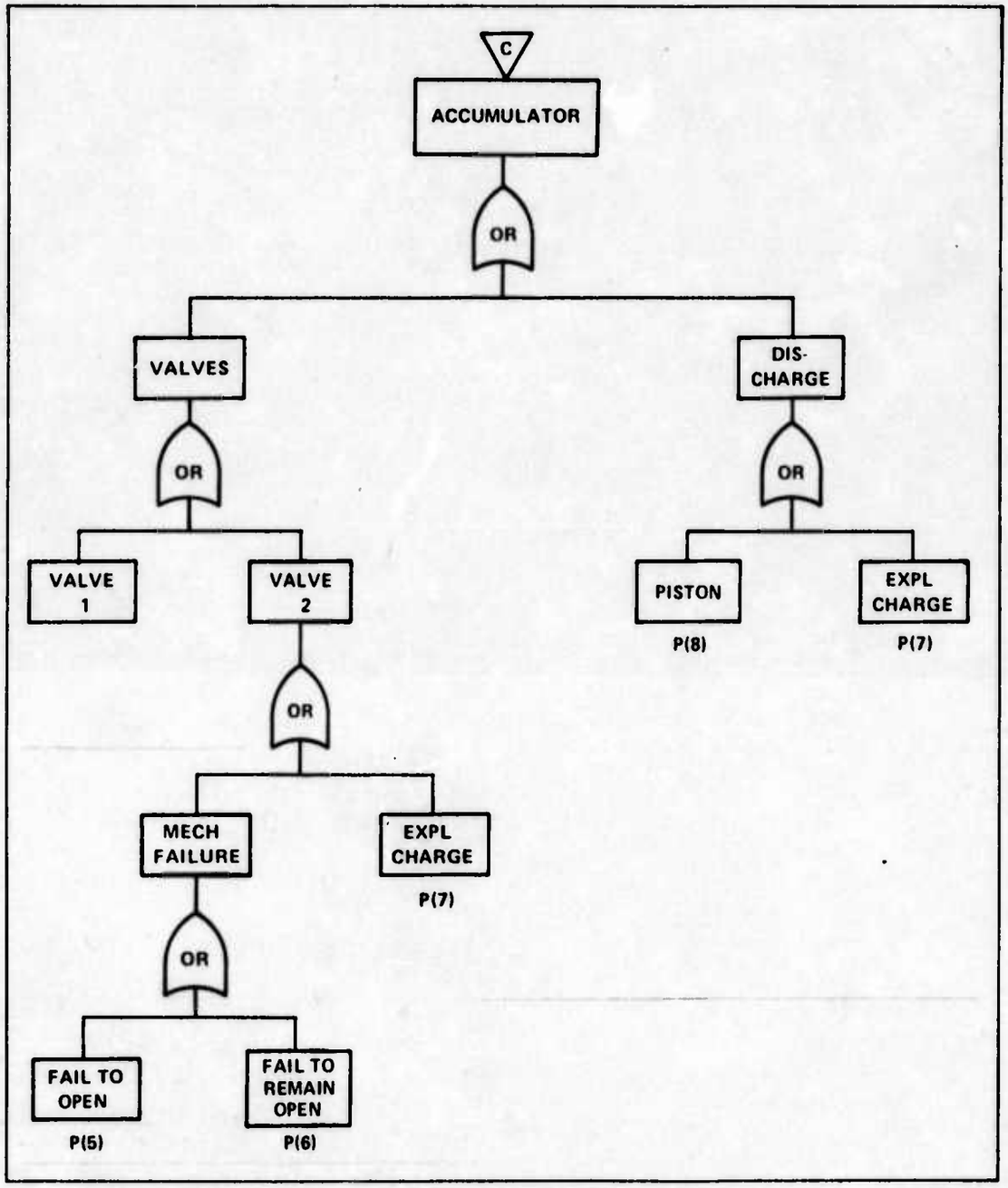

Figure 8.1.3.4-1d. Reactor Shutdown Fault Tree

The accumulator (Figure 8.1.3.4-1d) is a storage container for boron and is isolated from the reactor core by two isolation valves connected in series. To get boron to the core, both isolation valves must be driven open by an explosive force and must then remain open. With the valves open, the boron is expelled from the container by an explosively driven piston.

The expression for accumulator failure is given by

$$P(4) = (P(5) + P(6) + P(7))^2 + P(8) + P(7) \qquad (8.1.3.4\text{-}5)$$

P(5) = probability valve fails to open
P(6) = probability valve fails to remain open
P(7) = probability of explosive charge failure
P(8) = probability accumulator piston fails

and the expression for boration failure is given by

$$P(\text{boration failure}) = (P(4))^2 \qquad (8.1.3.4\text{-}6)$$

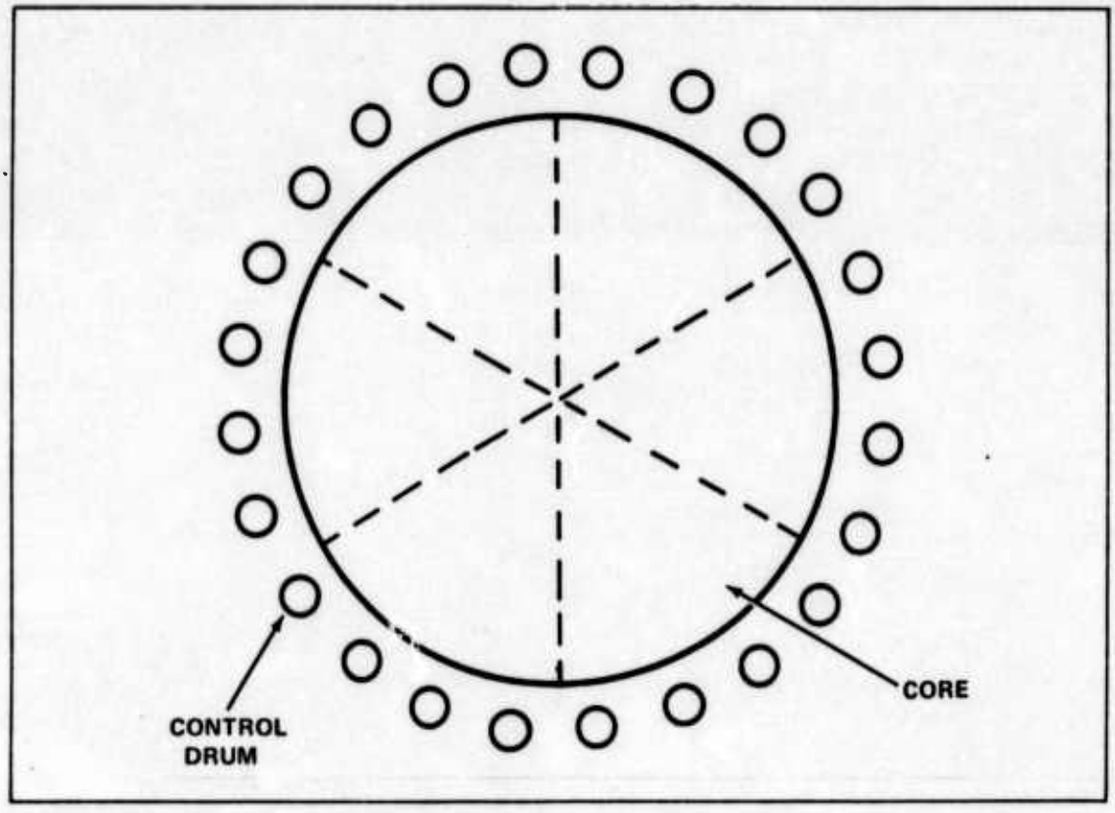

Figure 8.1.3.4-2. Reactor Control

In the second case, where the pre-impact sensor is failed, the impact sensor was included and the expression for boration failure becomes

$$P(\text{boration failure}) = (P(4) + P(3))^2 \qquad (8.1.3.4\text{-}7)$$

The overall expression for the probability of reactor shutdown failure is then given by

P(reactor shutdown failure) = P(control drum failure) x P(boration failure) (8.1.3.4-8)

All component failure probabilities were computed using the negative exponential formula given in Eq. 8.1.2-3. For the time dependent components, mission time of 330 hours was used. Several of the components have failure rates given in failures per demand. For those cases, the number of demands was set equal to one, and the negative exponential failure probability equation has the form

$$P = 1 - \exp(-\lambda)$$

The data used to solve the Fault Tree are given in Appendix A.8.1.3.1, and the resulting distributions of reactor shutdown failure are summarized in Table 8.1.3.4-1.

TABLE 8.1.3.4-1. REACTOR SHUTDOWN FAILURE PROBABILITY DISTRIBUTIONS

DECISION POINT	PROBABILITY		
	LOW	MEDIAN	HIGH
WITH ELECTRIC POWER AND PRE-IMPACT SENSING	4.85×10^{-23}	5.83×10^{-21}	6.04×10^{-19}
WITH ELECTRIC POWER	4.88×10^{-23}	6.19×10^{-21}	6.04×10^{-19}
WITHOUT ELECTRIC POWER	6.84×10^{-17}	6.36×10^{-15}	6.26×10^{-13}

8.1.3.5 SAFETY VALVES: Safety valves, the fourth safety feature on the Impact Event Tree, are intended to isolate the contents of the containment vessel from the environment by sealing the containment vessel pipe penetrations in any accident which could allow the radioactive core material to escape.

The safety valves are dependent on electrical power for their operation, thus no decision point was allowed where electrical power was failed. Because the probability of failure of the valves is also dependent on pre-impact sensing, two computations of valve failure probability were required: one for pre-impact sensing operative and one for pre-impact sensing failed.

The probability of failure of the safety valves was computed using the Fault Tree shown in Figure 8.1.3.5-1. To be successful, each valve must close and remain closed; to close, an explosive charge must fire properly. For the case of pre-impact sensing operative, the

probability of valve failure is given by

$$P(\text{valve failure}) = N \times (P(1) + P(2) + P(3)) \qquad (8.1.3.5\text{-}1)$$

P(1) = probability valve fails to close
P(2) = probability valve fails to remain closed
P(3) = probability of explosive charge failure

N = total number of safety valves

and where pre-impact sensing is failed, the probability of valve failure is given by

$$P(\text{valve failure}) = N \times (P(1) + P(2) + P(3)) + P(4) \qquad (8.1.3.5\text{-}2)$$

P(4) = probability impact sensor fails

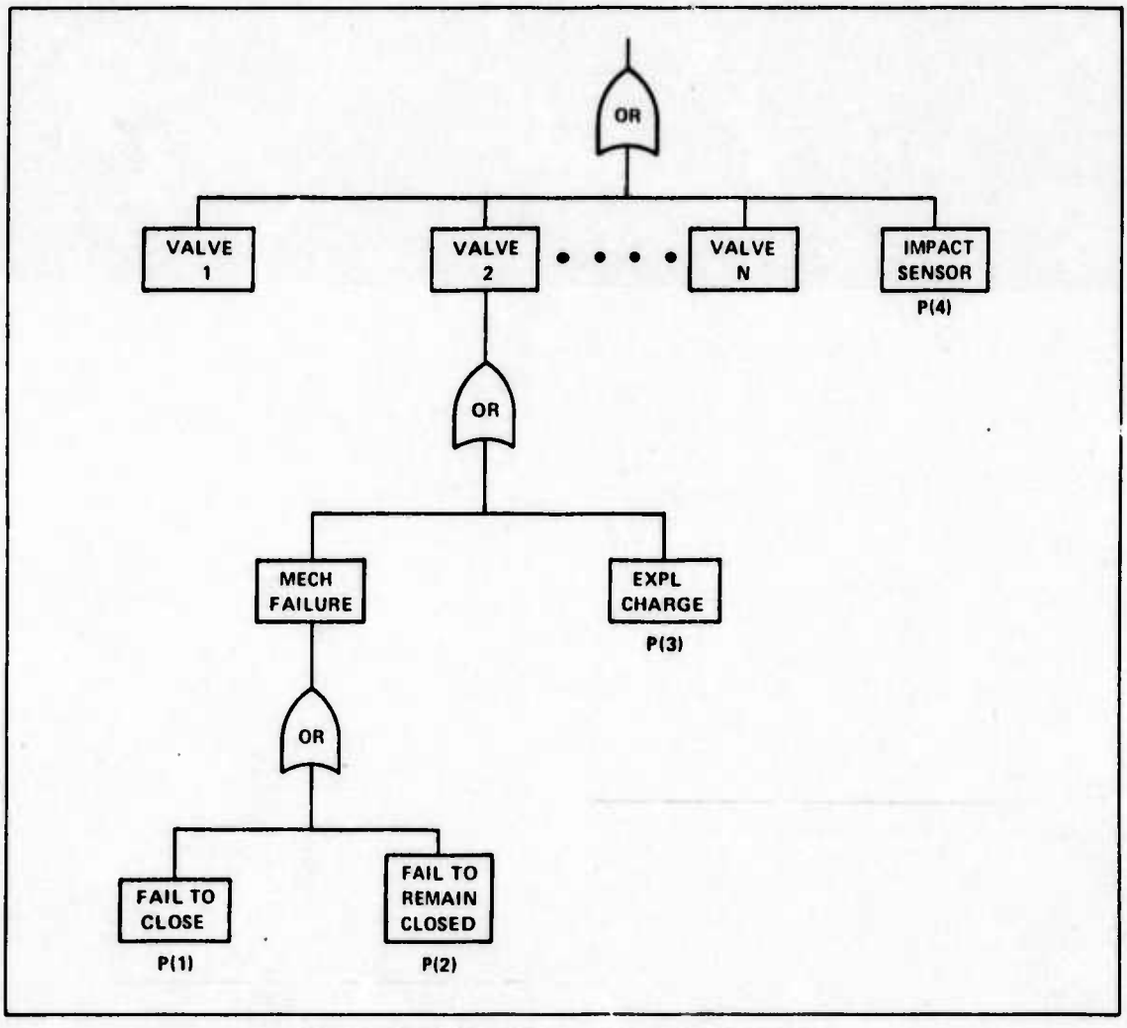

Figure 8.1.3.5-1. Safety Valve Fault Tree

For this analysis, the aircraft was taken to have 10 engines with 1 delivery and 1 return pipe between the reactor and each engine, giving a requirement for 20 safety valves at the containment vessel. The effect of different numbers of valves is considered in Section 8.1.3.8, *Impact Event Tree Results and Sensitivity Analysis*.

The failure probabilities for the components on the safety valve Fault Tree were computed using the negative exponential formula of Eq. 8.1.2-3. The failure rates are all given in failures per demand, and the number of demands was set equal to one in all cases.

The data used in the solution of the safety valve Fault Tree are given in Appendix A.8.1.3.1 and the resulting distributions of failure probabilities are summarized in Table 8.1.3.5-1.

TABLE 8.1.3.5-1. SAFETY VALVE FAILURE PROBABILITY DISTRIBUTION

DECISION POINT	PROBABILITY		
	LOW	MEDIAN	HIGH
PRE-IMPACT SENSOR OPERATE	3.77×10^{-3}	9.72×10^{-3}	2.34×10^{-2}
PRE-IMPACT SENSOR FAILED	3.77×10^{-3}	9.74×10^{-3}	2.34×10^{-2}

8.1.3.6 IMPACT INTEGRITY: The fifth safety feature shown on the Impact Event Tree is impact integrity. Its corresponding failure probability is defined as the probability that the containment vessel will sustain a rupture on the outer wall as a result of crash impact.

It was assumed that, in any of the impact sequences, core melt would occur and that radioactive material would be dispersed throughout the containment vessel so that any containment vessel opening results in a release of radioactive material. Under this assumption, if any safety valve is open, integrity of the containment vessel is violated, therefore no decision is allowed for impact integrity.

Impact rupture tests of simulated containment vessels have been conducted by the National Aeronautics and Space Administration (NASA) and the Air Force Weapons Laboratory (AFWL) (Refs. 144 and 75). Those tests simulated containment vessels of approximately 500,000 lbs impacted into concrete obstacles. The results of those tests were modeled in Appendix A.8.1.4.1 to yield a probability of failure as a function of impact speed which is normally distributed with a mean of 954 ft/sec and standard deviation of 88 ft/sec. The normal distribution Z statistic is expressed as

$$Z = \frac{X - \text{mean}}{\text{standard deviation}}$$

where X is the value of the random variable. Z is then the entering argument for normal probability tables to determine the probability associated with the value of X. In this case, the Z

statistic is given as

$$Z = \frac{S - 954}{88} \qquad (8.1.3.6\text{-}1)$$

where S denotes impact speed. The expected deformation of a 20 ft diameter containment vessel is approximately 7.5 ft (Ref 83, p. 63).

Tests were also conducted by NASA to simulate burial of a containment vessel impacted against soil (Ref. 143), the results of which are discussed in Appendix A.8.1.4.2. The resulting empirical equation (Eq. A.8.1.4.2-1) predicts a depth of burial of 48 ft for a 20 ft diameter 500,000 lb containment vessel, and 68 ft for a 20 ft diameter 1,000,000 lb containment vessel, where impact velocity is 1000 ft/sec.

An approximation of

$$F = MV \frac{\Delta V}{\Delta X}$$

can be used to estimate the forces on the containment vessel at impact. By letting $V = \Delta V$ and ΔX = deformation of containment vessel and target, a conservative estimate of the velocity needed for the force of an impact against soil to equal the force of an impact against concrete can be made. Let

$$M \frac{V_C^2}{\Delta X_C} = M \frac{V_S^2}{\Delta X_S} \qquad (8.1.3.6\text{-}2)$$

$$\frac{V_C^2}{7.5} = \frac{V_S^2}{48}$$

$$V_S = 2.5\, V_C \qquad (8.1.3.6\text{-}3)$$

V_S = soil impact velocity
ΔX_S = soil impact deformation
V_C = concrete impact velocity
ΔX_C = concrete impact deformation

A similar form of analysis was used to extrapolate the effect of doubling the weight of the containment from 500,000 lbs to 1,000,000 lbs. Let

$$\frac{M V_1^2}{\Delta X_1} = \frac{2M V_2^2}{\Delta X_2} \qquad (8.1.3.6\text{-}4)$$

$$\frac{V_1^2}{48} = \frac{2 V_2^2}{68}$$

$$V_2 = 0.841 V_1 \qquad (8.1.3.6\text{-}5)$$

V_1 = Soil impact velocity for 500,000 lb containment vessel

V_2 = Soil impact velocity for 1,000,000 lb containment vessel

ΔX_1 = Soil impact deformation for 500,000 lb containment vessel

ΔX_2 = Soil impact deformation for 1,000,000 lb containment vessel

Eqs. 8.1.3.6-1 and 8.1.3.6-5 were used to estimate a probability distribution for impact of a 1,000,000 lb containment vessel against a hard (concrete) surface. The resulting distribution has Z statistic

$$Z = \frac{S - 802}{74} \qquad (8.1.3.6\text{-}6)$$

Eqs. 8.1.3.6-6 and 8.1.3.6-3 were used to estimate a probability distribution for impact of a 1,000,000 lb containment vessel against a soft (soil) surface. The resulting distribution has Z statistic

$$Z = \frac{S - 2005}{185} \qquad (8.1.3.6\text{-}7)$$

The methodology of Appendix A.8.1.4.1 and the impact speed distributions of Appendix A.8.1.1.2 were used to obtain impact rupture probabilities for both soft and hard surface impacts. The probability of rupture given a soft surface impact is given as

P(rupture| soft surface impact) =
P(rupture| soft surface airport crash) X
P(airport crash) +
P(rupture| soft surface cruise crash) X
P(cruise crash)

and the probability of rupture given a hard surface impact is given by

P(rupture| hard surface impact) =
P(rupture| hard surface airport crash) X
P(airport crash) +
P(rupture| hard surface cruise crash) X
P(cruise crash)

and the resulting probabilities are

P(rupture| soft surface impact) = 2.72×10^{-6}
P(rupture| hard surface impact) = 0.0425

To accurately describe the probability of rupture given an impact, it would be necessary to determine the probabilities of soft and hard surface impacts. There was no known way to quantify these probabilities, but it can be qualitatively argued that more of the earth's surface is composed of soft soil than rock, concrete, etc. Therefore, in the Monte Carlo technique of solving the Impact Event Tree, the lower probability of rupture associated with a soft surface impact was favored by letting the soft and hard surface probabilities be the endpoints of a beta probability distribution skewed toward the soft surface impact rupture probability. The range of possible outcomes that could be achieved by different skewing is discussed in Section 8.1.3.8, *Impact Event Tree Results and Sensitivity Analysis.*

The distribution of probabilities of impact integrity failure is summarized in Table 8.1.3.6-1.

TABLE 8.1.3.6-1. IMPACT INTEGRITY FAILURE PROBABILITY DISTRIBUTION

PROBABILITY		
LOW	**MEDIAN**	**HIGH**
3.89×10^{-3}	**1.41×10^{-2}**	**3.32×10^{-2}**

Two additional factors which can bear on the probability of impact integrity failure have not been included in this analysis. The first of these is the effect of welding safety valves into the containment vessel wall, and the second is the effect of the energy absorbed by the aircraft structure during crash deformation. The first of these factors could tend to increase the failure probability while the second is expected to decrease it. It is believed that these two factors together make the probabilities used in this study somewhat conservative, i.e., higher than actual.

8.1.3.7 POST-IMPACT INTEGRITY: The sixth safety feature shown on the Impact Event Tree is post-impact integrity, a measure of the ability of the containment vessel to withstand the afterheat transient without meltthrough or creep rupture.

The model used for describing the probability of failure is the Arrhenius model (Ref. 157, p. 453-455)

$$P = 1 - C_1 \exp\left(\frac{-C_2}{T}\right) \qquad (8.1.3.7\text{-}1)$$

where P denotes the probability of failure, C_1 and C_2 are constants, and T is the stress parameter temperature.

The temperature, T, is taken from the heat transfer equation

$$q = h\,A\,\Delta\,T \qquad (8.1.3.7\text{-}2)$$

where q is the heat flow from the containment vessel to the air, h is the heat transfer coefficient, A is the area of the containment vessel exposed to air cooling, and T is the temperature differential between the surface of the containment vessel and the surrounding air (Ref. 74, p. 11).

The heat transfer coefficient is determined from (Ref. 74, p. 221)

$$G_r\,P_r = \frac{P_r\,g\,B\,\Delta\,T\,r^3}{(\nu)^2}$$

G_r = Grashoff number

P_r = Prandtl number

g = gravitational constant

$$B = \frac{1}{T_{abs}}$$

$$T_{abs} = \frac{T_s + T_a}{2} + 460$$

T_s = surface temperature of containment vessel

T_a = ambient air temperature

ν = kingmatic viscosity of air

r = radius of containment vessel

$\Delta T = T_s - T_a$

For $T_a = 100°F$ and $T_s \geq 500°F$

$$G_r P_r \geq \frac{32.2 \times 400 \times 10^3 \times 0.712}{760 \times (1.56 \times 10^{-4})^2} \geq 4.95 \times 10^{11}$$

For $G_r P_r \geq 10^9$, $h = 0.205 (\Delta T)^{.33}$ (Ref. 74, p. 219)

therefore

$$q = 0.205 A(\Delta T)^{1.33}$$

$$(\Delta T)^{1.33} = \frac{\text{constant}}{A}$$

The area of the containment vessel exposed to ambient air cooling is given by

$$A = D(D-H) \qquad (8.1.3.7\text{-}3)$$

where D = diameter of containment vessel

H = depth of burial of containment vessel

and

$$(\Delta T)^{1.33} = \frac{\text{constant}}{D(D-H)}$$

$$(\Delta T) = \frac{\text{constant}}{(D-H)^{0.75}} \qquad (8.1.3.7\text{-}4)$$

Substitution of Eq. 8.1.3.7-4 for T in Eq. 8.1.3.7-1 yields

$$P = 1 - C_1 \exp(- C_2 (D-H)^{0.75}) \qquad (8.1.3.7\text{-}5)$$

where H, the depth of burial of the containment vessel, is a random variable as formulated in Appendix A.8.1.4.2.

Afterheat transient analysis, reported in References 83 and 145, indicates an ability to survive the afterheat transient provided the containment vessel is not buried more than 50%. In a telephone conversation (Ref. 76), Major Holton, AFWL, characterized 50% burial as the maximum depth that current materials would allow to prevent meltthrough.

In order to evaluate the constants in Eq. 8.1.3.7-5, the values

$$P = 0 \text{ at } H = 0$$
$$P = 1 \text{ at } H = 10$$

were assumed and the final expression for the probability of failure was determined to be

$$P = 1 - 1.38 \times 10^{-10} \exp\left(2.4(D-H)^{0.75}\right) \qquad (8.1.3.7\text{-}6)$$

A distribution of probabilities of post-impact integrity failure was formed by iteratively solving Eq. 8.1.3.7-6 with random values of H. That distribution is summarized in Table 8.1.3.7-1.

TABLE 8.1.3.7-1. POST-IMPACT INTEGRITY FAILURE PROBABILITY DISTRIBUTION

PROBABILITY		
LOW	**MEDIAN**	**HIGH**
0.056	**0.642**	**1.0**

The results are expected to be somewhat conservative since the depth of burial calculations were based on an unenclosed containment vessel. It is believed that, in most cases, the depth of burial would be lessened by the aircraft structure.

8.1.3.8. IMPACT EVENT TREE RESULTS AND SENSITIVITY ANALYSIS: The results of the Impact Event Tree sequence calculations are shown in Table 8.1.3.8-1 where the sequence numbers correspond to those shown in Figure 8.1.3.8-1. There are 16 sequences, of which two, sequences 1 and 8, do not result in a release of radioactive material. The remaining sequences determine the net probability of release and are clearly dominated by sequences 2, 3, and 4. These sequences range from four to six orders of magnitude higher in probability than the next highest sequence on the tree.

In considering the sensitivity of the results to the input data and assumptions, only the dominating sequences were analyzed. The remaining sequence probabilities were considered to be low enough to merit no further consideration.

TABLE 8.1.3.8-1. IMPACT EVENT TREE SEQUENCE PROBABILITIES

SEQUENCE	PROBABILITIES		
	LOW	MEDIAN	HIGH
SEQUENCE 1			
SEQUENCE 2	1×10^{-3}	3×10^{-3}	5×10^{-3}
SEQUENCE 3	6×10^{-5}	1×10^{-4}	3×10^{-4}
SEQUENCE 4	2×10^{-5}	5×10^{-5}	2×10^{-4}
SEQUENCE 5	2×10^{-24}	3×10^{-23}	7×10^{-20}
SEQUENCE 6	6×10^{-25}	1×10^{-24}	2×10^{-21}
SEQUENCE 7	3×10^{-26}	5×10^{-25}	1×10^{-21}
SEQUENCE 8			
SEQUENCE 9	3×10^{-10}	3×10^{-9}	1×10^{-7}
SEQUENCE 10	1×10^{-11}	1×10^{-10}	7×10^{-9}
SEQUENCE 11	5×10^{-12}	9×10^{-11}	5×10^{-9}
SEQUENCE 12	1×10^{-30}	5×10^{-28}	1×10^{-24}
SEQUENCE 13	4×10^{-32}	2×10^{-29}	4×10^{-26}
SEQUENCE 14	2×10^{-32}	8×10^{-30}	1×10^{-26}
SEQUENCE 15	1×10^{-16}	1×10^{-14}	1×10^{-12}
SEQUENCE 16	4×10^{-31}	1×10^{-27}	3×10^{-24}

The first effect considered was that of mission time. Safety valves, impact integrity, and post-impact integrity are not functions of mission time. Electric power, pre-impact sensing, and reactor shutdown are functions of mission time, but their contributions to the dominating sequences are of the form (1-P) and P is less than 10^{-7}, so an approximation of unity was used.

The only significant effect that mission time has relative to the dominating sequences is the effect on crash probability. The effect of time on crash probability is such that a one order of magnitude decrease in time, from 330 hrs to 33 hrs, yields a one order of magnitude decrease in crash probability, and therefore a one order of magnitude decrease in any sequence probability. The same magnitudes are true for changes in crash rate.

The probability of release of sequence 4 can be affected by variance in the safety valve probability. Due to the heavy weight of the valves, improving reliability by redundancy is not a feasible consideration. A reduction in the number of valves results in some improvement. For example, the median failure probability for 20 valves is 9.72×10^{-3}, but for 10 valves it is 4.86×10^{-3}. For a 20 valve configuration, a one order of magnitude improvement in release probability can be achieved with a 90.3% reduction in valve failure rate.

The effect of deleting the safety valves is to assure an avenue of escape for the radioactive material, thus eliminating the questions of impact and post-impact integrity. The release probability then equals the crash probability, an increase of almost two orders of magnitude.

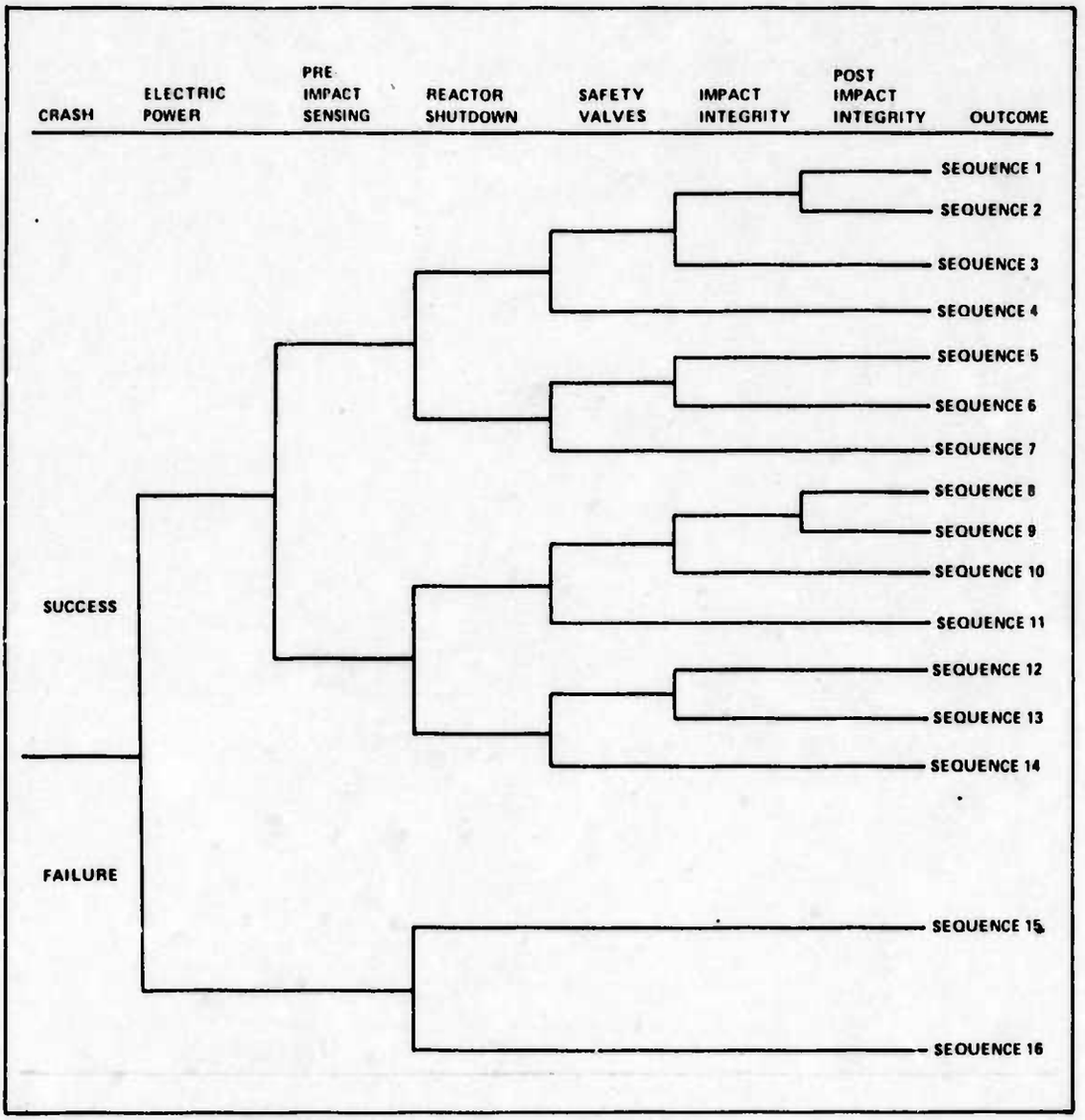

Figure 8.1.3.8-1. Impact Event Tree

The probability of release of sequence 3 is affected by the probability of impact integrity. As discussed in Section 8.1.3.6, the impact integrity failure probability varies over a range of approximately 10^{-6} to 10^{-2}, dependent on the assumptions made about the nature of the surface impacted. An assumption of impact only against soft soil would decrease the sequence 3 probability by approximately three orders of magnitude.

The probability of release of sequence 2 is affected by post-impact integrity. A variety of models might be chosen to describe post-impact integrity, but the most clear cut functional relationship is between failure probability and temperature. Of the variables involved in a given accident, the one that most affects the cooling rate, and hence the temperature, of the containment vessel is the degree to which the containment vessel is buried in soil.

Some study of the optimization of post-impact integrity versus weight may be possible in that increasing the number or thickness of layers of lithium hydride or tungsten would tend to impede the meltthrough for a given accident, but the weight to area ratio increases, thereby increasing the depth of burial and the probability of failure.

8.1.4 TRANSIENT EVENT TREE: The Transient Event Tree is used to describe those accidents which occur as a result of transient imbalances in the rates of heat generation and heat removal, but not including the imbalance resulting from a total loss of coolant. The transient condition can be caused by either a surge in power generation or a reduction of cooling capacity. The Transient Event Tree is shown in Figure 8.1.4.6-1 and is discussed in Sections 8.1.4.1 through 8.1.4.6.

8.1.4.1 TRANSIENT: The initiating event for the Transient Event Tree is denoted as transient and was defined in Section 8.1.4. The model used to describe the transient probability was the negative exponential formula given in Eq. 8.1.2-3, where λ denotes the transient rate in occurrences per hour and t is the mission time of 330 hrs.

The transient rate is discussed in Appendix A.8.1.3.2 and the distribution of transient probabilities is summarized in Table 8.1.4.1-1.

TABLE 8.1.4.1-1. TRANSIENT PROBABILITY DISTRIBUTION

PROBABILITY		
LOW	**MEDIAN**	**HIGH**
0.164	**0.336**	**0.648**

8.1.4.2 ELECTRIC POWER: The first safety feature on the Transient Event Tree is Electric Power. It was placed first because all subsequent safety features are affected by the availability of electrical power.

The probability of failure of electrical power was computed using the fault tree shown in Figure 8.1.4.2-1. The major sources of electrical power are the primary aircraft system and

an auxiliary generator system. The primary aircraft electrical power system was assumed to have 10 generators (one per engine) and 10 associated generator subsystems. The 10 systems were treated as being independent, with a requirement that all 10 systems fail before the primary aircraft system was treated as failed. The auxiliary generator is the emergency power system dedicated to reactor monitor, control, and safety functions.

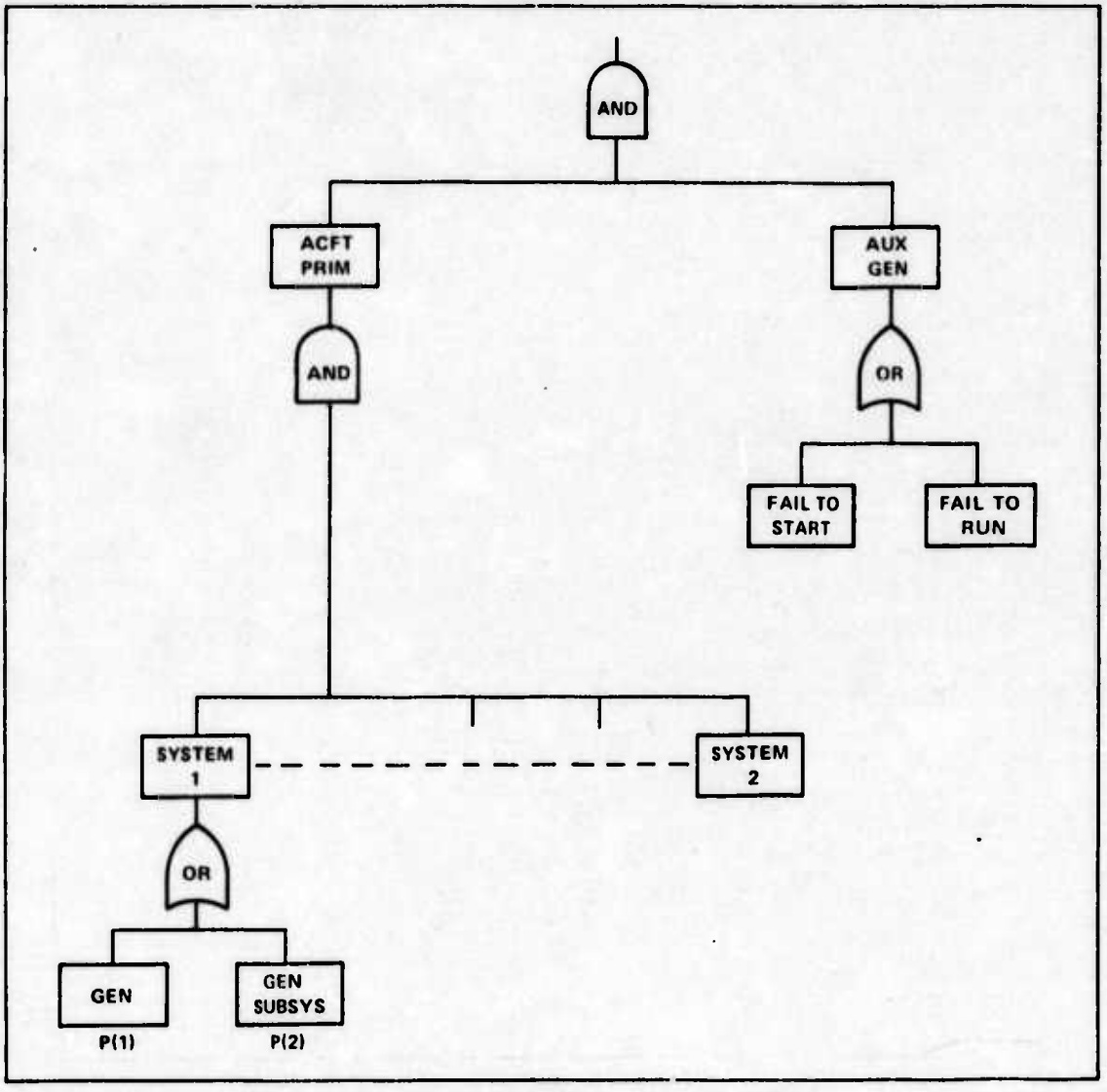

Figure 8.1.4.2-1. Electrical System Fault Tree

The data used to solve the Fault Tree are given in Appendices A.8.1.2.1 and A.8.1.3.1 the probability of electrical power failure is given by:

$$P = (P(1) + P(2))^{10} \times (P(3) + P(4))$$

where P(1) = failure probability of aircraft generator
P(2) = failure probability electrical subsystem
P(3) = auxiliary generator failure to start probability
P(4) = auxiliary generator failure to run probability

In solving the negative exponential failure probability, operating time was assumed to be 10 hrs for the auxiliary generator and 330 hrs for all other components. The 10 hrs was based on an assumption that, if auxiliary generator power was required for operation, a landing would be made within 10 hours.

The distribution of electrical power failure probabilities is summarized in Table 8.1.4.2-1.

TABLE 8.1.4.2-1. ELECTRIC POWER FAILURE PROBABILITY DISTRIBUTION

PROBABILITY		
LOW	**MEDIAN**	**HIGH**
3.60×10^{-10}	7.26×10^{-7}	2.48×10^{-5}

8.1.4.3 REACTOR SHUTDOWN: The second safety feature on the Transient Event Tree is reactor shutdown. The failure probabilities used are those derived in Section 8.1.3.4 for reactor shutdown with electric power and without electric power.

8.1.4.4 HEAT REMOVAL: The third safety feature on the Transient Event Tree is heat removal and the associated probability is defined as the probability that the normal reactor cooling system will fail to provide adequate cooling.

The demand for heat removal capacity is dependent on whether or not the reactor is shut down. Therefore, two probabilities of failure were required for the heat removal safety feature: one for reactor operating, and one for reactor shutdown.

The heat removal system is comprised of two main subsystems. The primary subsystem circulates coolant between the reactor core and the primary heat exchangers located inside the containment vessel. Pumping power for the primary loops is provided by two turbine driven circulators. The secondary subsystem circulates coolant between the primary heat exchanger and the engines. Pumping power for the secondary loops is provided by 10 engine driven pumps.

The heat removal system can fail if either the primary or the secondary subsystems fail, and the expression for the probability of heat removal failure is

$$P = P(\text{primary subsystem failure}) + P(\text{secondary subsystem failure}) \qquad (8.1.4.4\text{-}1)$$

The primary subsystem consists of two turbine driven circulators, operating in parallel, to circulate the coolant through the 10 primary heat exchangers. Either circulator loop can supply sufficient coolant flow for normal, full power operation, and one of the circulator loops

fails if either the circulator or the turbine fails. The probability of failure of one of the circulator loops is given as

$P(1) = P(2) + P(3)$
$P(2)$ = turbine failure probability
$P(3)$ = circulator failure probability

The secondary subsystem consists of 10 independent loops with each containing three major components for reliability analysis. These components are the engine, the pump, and the associated piping. One of the loops can fail if any of the three major components fails. The probability of failure of one of the loops is

$P(4) = P(5) + P(6) + P(7)$ (8.1.4.4-2)
$P(5)$ = engine failure probability
$P(6)$ = engine driven pump failure probability
$P(7)$ = pipe failure probability

The probability of failure of all of the components used in the heat removal system was computed using the negative exponential formula given in Eq. 8.1.2-3 with time equal to mission time of 330 hrs.

In order to determine the overall failure probability, it was necessary to determine the number of primary or secondary loops that could fail before the system failed.

Considering first the case of the reactor operating,

$Q = \dot{m} \times c_p \times (T_{c\ out} - T_{c\ in})$ (8.1.4.4-3)
Q = heat flow (BTU/sec)
$\dot{m}$ = coolant mass flow (lb/sec)
c_p = specific heat (BTU/lb–°F)
$T_{c\ out}$ = coolant temperature leaving the cold side of the heat exchanger
$T_{c\ in}$ = coolant temperature entering the cold side of the heat exchanger

(Ref. 129, p. 187)

$$\varepsilon = \frac{T_{c\,out} - T_{c\,in}}{T_{h\,in} - T_{c\,in}}$$

ε = heat exchanger effectiveness

$T_{h\,in}$ = coolant temperature entering hot side of heat exchanger

(Ref. 87, p. 15)

$$\dot{m} = \frac{Q}{c_p \times \varepsilon \times (T_{h\,in} - T_{c\,in})}$$

From the heat exchanger design, Section 7.1.1.1

ε = 0.75
$\dot{m}$ = 700 lb/sec
Q = 450,000 BTU/sec
c_p = 1.242 BTU/lb–°F
$T_{c\,in}$ = 0.1078°F

$$\dot{m} = \frac{483091}{T_{h\,in} - 1078}$$

The coolant mass flow of 700 lb/sec gives 70 lb/sec for each of the 10 secondary coolant loops.

$\dot{m} = 70 \times (10 - K)$
K = number of loops failed

$$K = 10 - \frac{6901}{T_{h\,in} - 1078} \qquad (8.1.4.4\text{-}4)$$

The minimum melt temperature encountered in the loop is approximately 2460°F (HA piping material). Using 2460°F as the maximum $T_{h\,in}$ yields K = 5.

For the primary subsystem, 700 lb/sec of coolant flow can be handled by either of the two circulators, therefore both circulators must fail before the system fails.

The result is that, with the reactor operating, both primary loop circulators or more than five secondary loops must fail before a melt temperature is reached. The probability of losing both primary loop circulators and more than five secondary loops was defined to be the probability of failure of the heat removal system given that the reactor is operating.

The binomial probability formula was used to determine the failure probability.

$$P(\text{subsystem failure}) = \sum_{x}^{M} \frac{N!}{(N-x)!\,x!} P^{x}(1-P)^{N-x} \qquad (8.1.4.4\text{-}5)$$

N = total number of loops
x = number of loops failed
P = probability of failure of one loop

$$P(\text{primary subsystem failure}) = \sum_{x=2}^{2} \frac{2!}{(2-x)!\,x!} P(1)^{x}(1-P(1))^{2-x}$$

$$= (P(1))^{2} \qquad (8.1.4.4\text{-}6)$$

$$P(\text{secondary subsystem failure}) = \sum_{x=6}^{10} \frac{10!}{(10-x)!\,x!} P(4)^{x}(1-P(4))^{10-x}$$

$$= 126\,P(4)^{10} - 560\,P(4)^{9} + 945\,P(4)^{8} - 720\,P(4)^{7} + 210\,P(4)^{6} \qquad (8.1.4.4\text{-}7)$$

In the second case, where the reactor is shut down, the heat generation is less than 5.7% of the full power heat generation (Ref. 62, p. 105) thus requiring not more than 5.7% of full power coolant flow. One secondary loop carries 10% of normal full power mass flow, therefore sufficient heat removal capability will exist in the secondary subsystem if at least one loop remains operational.

For the primary subsystem, however, the circulators are failed since the turbines shut down when the reactor shuts down. The mass flow of coolant required to insure that all parts of the system remain below melt temperature can be found from Eq. 8.1.4.4-3. Using a maximum temperature of 2460°F, and Q = 0.057 x 450,000 yields a mass coolant flow requirement less than 2.8% of full power coolant flow.

The relatively small circulating system required to remove this afterheat could be powered by the aircraft primary electrical system or an auxiliary generator. However, for this analysis, no consideration was given to such a system.

The afterheat transient analyses performed by NASA and AFWL (Refs. 83 and 145) predict survival for unburied containment vessels and it was assumed that sufficient cooling would occur by ambient air cooling and natural circulation of the primary loop coolant to prevent meltthrough. Under this assumption, sequences 4 and 6 of the Transient Event Tree (Figure 8.1.4.6-1) are treated as having no release of radioactive material. Sequences 5 and 7 reflect the failure of the secondary subsytem and because of this reduced cooling capability, the possibility of a meltthrough was allowed and the sequence probabilities were computed. The heat removal failure probability for these cases is the probability that no secondary loops operate, or

$$P(\text{secondary subsystem failure}) = P(4)^{10} \qquad (8.1.4.4\text{-}8)$$

For those cases where it was assumed that no release of radioactive material would occur, the effects of an opposite assumption (release assured) is discussed in Section 8.1.4.6, *Transient Event Tree Results and Sensitivity Analysis*.

The failure data for the turbine was taken from Reference 52, p. 114. The failure rate is given as 1.03×10^{-4} failures per hour. The methodology of Reference 185, Appendix III, (also see Appendix Section A.8.1.1.1, *Crash Rates*) was used to generate a log-normal distribution of failure rates with lower and upper bounds one order of magnitude less than and greater than, respectively, the rate given above.

The data used to solve the failure probabilities of the remainder of the heat removal system are given in Appendices A.8.1.2.2 and A.8.1.3.1 and the distributions of heat removal failure probabilities are summarized in Table 8.1.4.3-1.

TABLE 8.1.4.3-1. HEAT REMOVAL FAILURE PROBABILITY DISTRIBUTIONS

DECISION POINT	PROBABILITY		
	LOW	MEDIAN	HIGH
REACTOR OPERATE	6.89×10^{-4}	8.64×10^{-2}	3.87×10^{-1}
REACTOR SHUTDOWN	2.80×10^{-17}	5.00×10^{-15}	1.24×10^{-4}

8.1.4.5 SAFETY VALVES: The fourth safety feature shown on the Transient Event Tree is safety valves. The valves are dependent on electrical power, so no decision point exists on the branch with electrical power failed. On the branch with electrical power, but reactor failed to shut down, core melt does not occur if heat removal functions, and meltthrough occurs regardless if heat removal is failed. If electrical power is available and the reactor is shut down, core melt does not occur if heat removal functions, but core melt does occur if heat removal fails. Thus, there is only one logical decision point for safety valves. The failure probabilities used are those developed in Section 8.1.3.5.

With the safety valves closed, the only way a release can occur is by meltthrough or creep rupture. The afterheat transient analyses performed by NASA and AFWL (Refs. 83 and 145) predict survival for unburied containment vessels, and it was assumed that sufficient ambient air cooling, would occur to prevent a release of radioactive material. The effects of an opposite assumption (that a meltthrough or creep rupture would occur) is discussed in Section 8.1.4.6.

8.1.4.6 TRANSIENT EVENT TREE RESULTS AND SENSITIVITY ANALYSIS: The results of the Transient Event Tree sequence calculations are shown in Table 8.1.4.6-1. Of the nine sequences, five do not result in a release of radioactive material. Sequence 3 clearly dominates the tree, being at least five orders of magnitude higher in probability than the next highest sequence.

TABLE 8.1.4.6-1. TRANSIENT EVENT TREE SEQUENCE PROBABILITIES

SEQUENCE	PROBABILITY		
	LOW	MEDIAN	HIGH
SEQUENCE 1	NO RELEASE	NO RELEASE	NO RELEASE
SEQUENCE 2	NO RELEASE	NO RELEASE	NO RELEASE
SEQUENCE 3	1.44×10^{-10}	1.65×10^{-8}	6.21×10^{-7}
SEQUENCE 4	NO RELEASE	NO RELEASE	NO RELEASE
SEQUENCE 5	1.26×10^{-23}	8.49×10^{-21}	9.04×10^{-19}
SEQUENCE 6	NO RELEASE	NO RELEASE	NO RELEASE
SEQUENCE 7	6.47×10^{-22}	6.69×10^{-13}	6.20×10^{-10}
SEQUENCE 8	NO RELEASE	NO RELEASE	NO RELEASE
SEQUENCE 9	5.89×10^{-24}	4.57×10^{-21}	5.87×10^{-18}

To examine the sensitivity of the dominating sequence to the input data, the appropriate initiating event and decision point probabilities were examined.

For a 100 hour reduction in mission time, the transient probability is reduced by a factor of 0.735, and the heat removal probability is reduced by a factor of 0.236. The sequence 3 probability is reduced by a factor of 0.173. The same factors would apply for a 30% reduction in all component failure rates.

If the assumption of no release for sequences 4 and 6 were reversed, and a release were assumed to occur, the combined probabilities of sequences 4, 5, 6, and 7 would increase from approximately 6×10^{-13} to approximately 2×10^{-7}.

A similar analysis for sequence 2 would increase the combined probabilities of sequences 2 and 3 from approximately 1.6×10^{-8} to approximately 1.5×10^{-6}. Thus, even under the most conservative assumptions, the highest Transient Event Tree probabilities are still approxmiately three orders of magnitude less than the probabilities associated with the Impact Event Tree.

8.1.5 LOSS OF COOLANT: The loss of coolant accident is the design basis accident for Atomic Energy Commission licensing of nuclear power plants and is generally considered to be the worst initiating event possible for nuclear power generating stations (Ref. 185, Appendix I, p. 10).

The loss of coolant accident is defined as a complete loss of coolant. Considering the primary coolant system as consisting of two loops, and the secondary coolant system as consisting of 10 loops, the probability of losing coolant in all primary loops or all secondary loops was computed. Using the highest pipe failure rate given (Ref. 185, Appendix III, p. 19) of 3×10^{-9} failures/hour and the negative exponential formula of Eq. 8.1.2-3, the failure probability was computed to be 9.60×10^{-25}. Using an assumed failure probability of 1×10^{-6}, the required pipe failure rate was computed to be approximately 1×10^{-4} failures/hour, or approximately five orders of magnitude higher than the highest found in historical data.

From these considerations it was decided that the initiating event probability for a loss of Coolant Event Tree would make all sequence probabilities sufficiently low to cause the entire tree to be dominated by the Impact and Transient Event Trees. Therefore, the loss of coolant accident was eliminated from further consideration.

8.1.6 TOTAL RELEASE PROBABILITIES: To arrive at a single or inclusive distribution of probabilities of release of radioactive material, the probability distributions of the various release sequences were summed. The first summation made was for the Impact Event Tree, the second for the Transient Event Tree, and finally a summation of both trees. The results of these summations are presented in Table 8.1.6-1, showing the 5th, 50th, and 95th percentiles and the mean, or expected value, of the probability distributions.

Implicit in the formulations thus far is the fact that all probabilities are on a per flight basis. For comparative purposes used in Release Consequence modeling, it is desirable to express the probabilities on an annual basis. The binomial formula of Eq. 8.1.4.3-6 was used with the number of flights expressed as flights per year.

$$P(\text{release per year}) = 1 - (1 - P)^N$$

N = number of flights per year
P = probability of release per flight

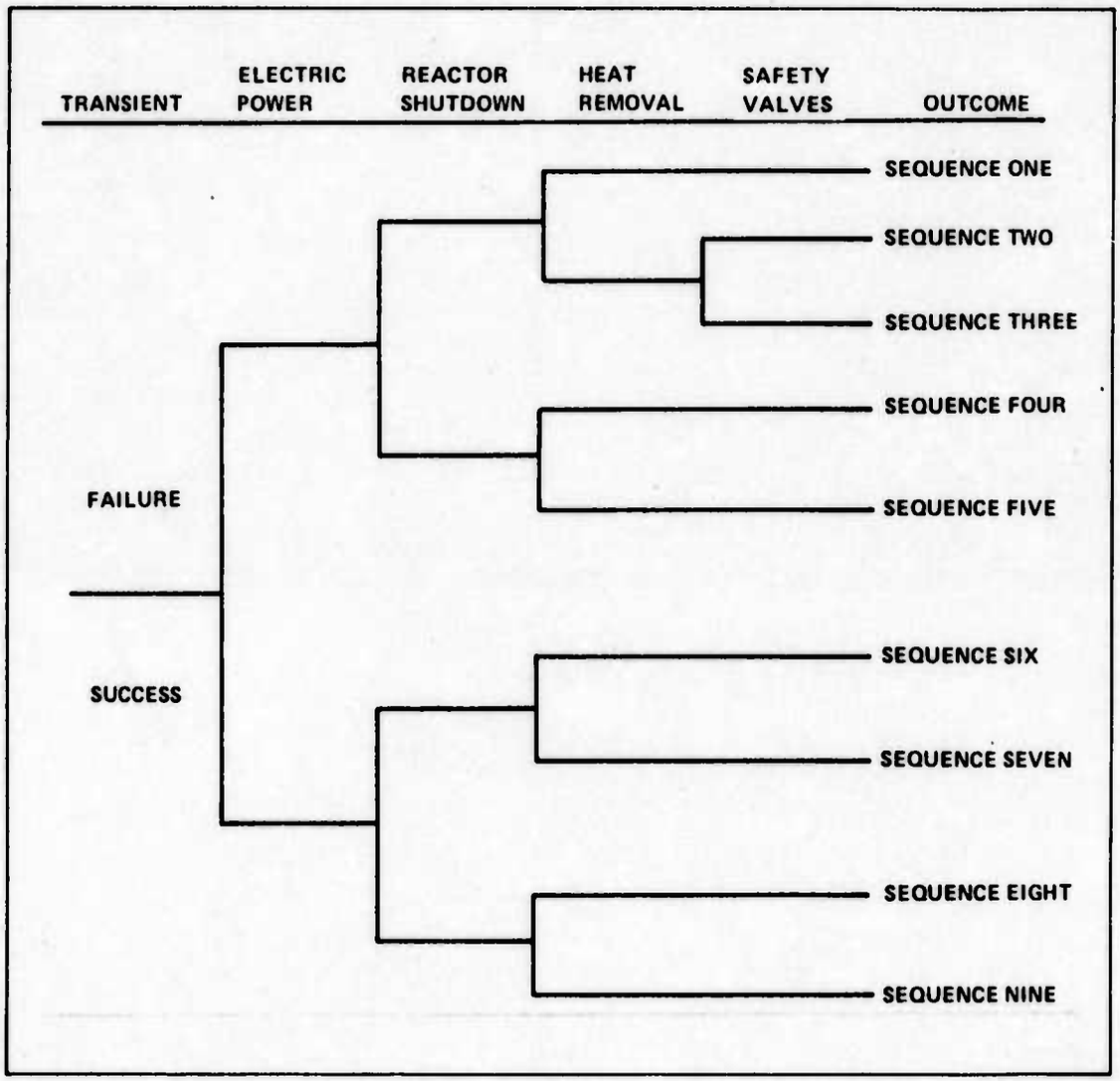

Figure 8.1.4.6-1. Transient Event Tree

TABLE 8.1.6-1. TOTAL RELEASE PROBABILITY PER FLIGHT

SUMMATION	PROBABILITY			
	.05	.50	.95	MEAN
IMPACT TREE	1.86×10^{-3}	3.18×10^{-3}	4.43×10^{-3}	3.18×10^{-3}
TRANSIENT TREE	1.97×10^{-9}	4.90×10^{-8}	1.03×10^{-6}	2.96×10^{-7}
BOTH TREES	1.87×10^{-3}	3.19×10^{-3}	4.43×10^{-3}	3.18×10^{-3}

Using the summation of probabilities for both event trees, the annual release probability was computed for 100, 500, 1000, 1500, and 2000 flights per year. The results showing the 5th, 50th, and 95th percentiles and the mean are summarized in Table 8.1.6-2. For example, at a rate of 1000 flights per year, there is a 90% confidence that the probability of a release of radioactive material lies between 0.821 and 0.990, with a mean, or expected value, of 0.941.

TABLE 8.1.6-2. TOTAL RELEASE PROBABILITY PER YEAR

NUMBER OF FLIGHTS PER YEAR	PROBABILITY			
	.05	.50	.95	MEAN
1	1.87×10^{-3}	3.19×10^{-3}	4.43×10^{-3}	3.18×10^{-3}
100	0.158	0.273	0.371	0.270
500	0.576	0.797	0.901	0.778
1000	0.821	0.959	0.990	0.941
1500	0.924	0.992	0.999	0.982
2000	0.968	0.998	1.000	0.994

8.1.7 APPLICATION OF RESULTS TO A LIQUID-METAL COOLED SYSTEM: Thus far, the safety analysis has assumed a reactor configuration using a gas coolant; however, a liquid-metal coolant is also of interest. Therefore, consideration was given to the applicability of the Impact and Transient Event Tree sequence calculation to a liquid-metal cooled system.

8.1.7.1 APPLICATION OF IMPACT EVENT TREE RESULTS TO A LIQUID-METAL COOLED SYSTEM: For the modeling used to develop the Impact Event Tree, the probabilities of crash, electrical power failure, pre-impact sensing failure, and safety valve failure are independent of the type of coolant used.

The Impact Integrity is assumed to be independent of the type of coolant used since the small mass and volume of coolant, relative to the entire reactor, offers insignificant kinetic energy absorption capability.

The Post-Impact Integrity is assumed to be independent of the type of coolant used since the principal means of preventing meltthrough is to effect a delaying action while the radiation activity decays. The delay in meltthrough is achieved by using high melting point, high specific heat shielding materials, thus requiring a large amount of energy to effect a phase change from solid to liquid. In this fashion, meltthrough is delayed sufficiently long for the heat generated by the radioactive core material to decay to a level less than the heat given up to ambient air, thereby preventing a complete meltthrough. Since the liquid-metal coolant is already in a molten state, its effect on the rate of meltthrough is expected to be negligible.

The only event remaining on the Impact Event Tree is reactor shutdown failure and this event would be affected by using a liquid-metal coolant. Reactor shutdown in the gas system is accomplished by either control drum rotation or boration of the core, but in a liquid-metal system, the core can not be flooded with boron. The effect of this on the values given in Table 8.1.3.8-1, Impact Event Tree Sequence Probabilities, would be to increase the probabilities of sequences 5, 6, 7, 12, and 14 by a factor of approximately 10^8.

The result is that the dominating sequences would remain the same, and the change to the total release probability for the impact event would be negligible.

8.1.7.2 APPLICATION OF TRANSIENT EVENT TREE RESULTS TO A LIQUID-METAL COOLED SYSTEM: For the case of the Transient Event Tree, the probabilities of transient, electrical power failure, and safety valve failure are independent of the type of coolant used.

The heat removal feature could be indirectly affected in that less pumping power is required for liquid-metal and, therefore, more redundancy might be built into the system. However, if the single level of redundancy assumed for the gas system is used for a liquid-metal system, the heat removal failure probability is independent of the type of coolant used.

The reactor shutdown failure probability is affected in the same manner as described in Section 8.1.7.1, so that sequences 5 and 7 in Table 8.1.4.6-1, *Transient Event Tree Sequence Probabilities*, would be increased by a factor of approximately 10^8.

The result, again, is that the dominating sequences would remain the same, and the change to the total release probability for the Transient Event Tree would be negligible.

8.2 CONSEQUENCE MODEL

The consequences of radioactive releases are simply the result of people being affected by the radiation produced by the escaping radioactive materials. The results of a release can be determined from four independent items:

1) magnitude of the release
2) dispersion of the radioactive particles
3) number of people exposed
4) effects of the radiation on these people.

Each of these items can be broken into several alternatives, each having an associated probability. The combination of an alternative from each item forms a sequence of events that has a measurable effect. Since the items are independent, the overall probability for a sequence was the product of the probabilities associated with the alternatives of the sequence. The effect and probability for each sequence can be used to form a cumulative distribution function. Using this function one can find the probability of a specified number of people receiving a lethal dose.

The U.S. Atomic Energy Commission's *Reactor Safety Study* (WASH-1400 Report) extensively studied accidents in immobile nuclear power plants. If a nuclear powered aircraft were to crash, the sequence of events following its radioactive release would be quite similar to a ground accident. Since the situation to be studied was similar to accidents considered in the WASH-1400 report, it was decided to validate the methods of that report. This study chose to validate an accident sequence that had the quickest possible core melt with an available escape route for the radioactive materials. This would be similar to the worst case expected in a crash accident. The main differences in the consequences would be as a result of different power level, population density, and evacuation of the population. Sections A.8.2.1 through A.8.2.4 contain the complete validation of the WASH-1400 consequences model. The only consequence considered in this study was that of deaths which occurred within 30 days of the accident.

8.2.1 MAGNITUDE OF RELEASE: Normally when one considers a nuclear release, one thinks in terms of a bomb. Some of the essentials for such an explosion are present, but this type of detonation is impossible. In the most severe impact considered in this study, the core was compacted but stayed well below the critical level (Ref. 83, p. 208).

The only releases considered in this study were due to core melt. After an impact the core was assumed to stay inside the containment. In this well insulated environment, the core will reach a temperature sufficiently high to melt. As it melts, it releases an amount of radioactive particles that has been determined by experiment (Ref. 185, Appendix VII, p. 12). That was the release of interest in this study.

The magnitude of a radioactive release is governed by the amount of radioactive material available to be released and the timing of the release.

8.2.1.1 AMOUNT OF RADIOACTIVITY AVAILABLE: In a nuclear fission process, an atom of the fuel is split into two new atoms. These are called fission fragments and their decay daughters are called fission products. It was assumed that 1.5 of the new atoms are radioactive. The amount of these fission products is determined by the power and fuel of the nuclear reactor.

For a 574 megawatt reactor the curies available are

$$C_i = \frac{1.5\ (574 \times 10^6 \text{ watts})\ 3.3 \times 10^{10} \text{ fissions/watt-sec}}{3.7 \times 10^{10} \text{ fissions/sec}} = 7.68 \times 10^8 \text{curies}$$

By assuming that when UC_2 melts in an oxidizing atmosphere it releases fission products as does UO_2 (Ref. 136), Table 8.2-1 shows the amount of each isotope released (Ref. 185, Appendix VII, p. 12). These isotopes can escape from the molten core because they are in a gaseous state.

TABLE 8.2-1. AMOUNT OF RADIOACTIVE ISOTOPES RELEASED WHEN FISSIONED UO_2 MELTS

ELEMENT	% RELEASED
Xe, Kr, I, Br	90
Cs, Rb	80
Te, Se, Sb	15
Ba, Sr	10
Ru, Rh, Pd, Mo, Tc	3
Y, La, Ce, Pr, Nd, Pm, Sm, Eu, Np, Pu, Zr, Nb	0.3

Table 8.2-2 shows all of the isotopes available for release in a 3200 megawatt reactor. The amount of curies released was calculated for each isotope in Table 8.2-1 by multiplying the curies available from Table 8.2-2 by the percentage released. The sum of all activity released was 33.6% of that available. The remaining 66.4% stay in molten form in the reactor. Since the percentages of fission products formed in similarly fueled reactors are the same, the activity released in the 574 megawatt reactor would be 33.6% of the fission products available. So the activity of the products available to be released if the reactor operates until just before it melts is:

$$Q = 7.68 \times 10^8 (0.336) = 2.58 \times 10^8 \text{ curies}$$

8.2.1.2 TIMING OF THE RELEASE: After a fission product is manufactured it begins decaying; however, while the reactor is still running, more are produced. This leads to a steady state level of each isotope. After a nuclear reactor is shut down or quits running for any reason, the fission products begin decaying from their steady state level. Since each isotope has a different decay rate, the total activity must be found from a summation of at least 45 isotopes and the isotopes that are formed when they decay. A good approximation of the energy at various times after shutdown can be obtained by using the Way-Wigner formula:

$$E = 13.3\ F \left\{ \frac{1}{(t_2 - t_1)^{0.2}} - \frac{1}{t_2^{0.2}} \right\}$$

where F is fission per sec, t_1 is reactor run time, and t_2 is time of interest from reactor start time.

TABLE 8.2-2. SET OF INITIAL ACTIVITY OF FISSION PRODUCTS USED IN THE WASH-1400 REPORT FOR A 3200 MEGAWATT REACTOR

NUMBER	NAME	SOURCE (CURIES X 10^6)	HALF-LIFE (DAYS)
1	KR-85	0.006	3.900E 03
2	KR-85*	0.26	1.800E-01
3	KR-87	0.52	5.300E-02
4	KR-88	0.76	1.160E-01
5	SR-89	1.1	5.060E 01
6	SR-90	0.052	1.050E 04
7	SR-91	1.3	4.000E-01
8	Y-90	0.052	2.700E 00
9	Y-91	1.4	5.900E 01
10	ZR-95	1.6	6.550E 01
11	ZR-97	1.6	7.000E-01
12	NB-95	1.6	3.500E 01
13	MO-99	1.6	2.800E 00
14	TC-99*	1.4	2.500E-01
15	RU-103	1.0	4.000E 01
16	RU-105	0.58	1.800E-01
17	RU-106	0.19	3.680E 02
18	RH-105	0.58	1.500E 00
19	TE-129	0.28	4.800E-02
20	TE129*	0.10	3.410E 01
21	TE-131*	0.15	1.250E 00
22	TE-132	1.2	3.250E 00
23	I-131	0.85	8.050E 00
24	MI-131	0.85	8.050E 00
25	I-132	1.2	1.000E-01
26	I-133	1.7	8.750E-01
27	I-134	2.0	3.600E-02
28	I-135	1.5	2.800E-01
29	MI-135	1.5	2.800E-01
30	XE-133	1.7	5.300E 00
31	XE-135	0.26	3.800E-01
32	CS-134	0.017	7.520E 02
33	CS-136	0.06	1.290E 01
34	CS-137	0.058	1.100E 04
35	BA-140	1.6	1.280E 01
36	LA-140	1.6	1.660E 00
37	CE-141	1.6	3.280E 01
38	CE-143	1.5	1.370E 00
39	CE-144	1.1	2.850E 02
40	PR-143	1.5	1.360E 01
41	ND-147	0.6	1.100E 01
42	PM-147	0.17	9.600F 02
43	PM-149	0.4	2.200E 00
44	PU-238	0.001	3.200E 04
45	PU-239	0.0001	8.700E 06

By assuming that the reactor has been running for a very long time, compared to the period of interest, energy can be obtained by using another form of the Way-Wigner formula, (Ref. 129, p. 244):

$$E = \frac{13.3\ F}{t^{0.2}}$$

where t is time after shutdown.

This formula shows just how dependent the level of activity is upon time. Since this study was interested in the decay of the activity, the constant (13.3) was dropped because it converted fissions into million electron volts (Mev). The activity relationships were taken to be:

$$A = A_o \left\{ \frac{1}{(t_2 - t_1)^{0.2}} - \frac{1}{t_2^{0.2}} \right\} \qquad (8.2.1\text{-}1)$$

or

$$A = \frac{A_o}{t^{0.2}} \qquad (8.2.1\text{-}2)$$

where A_o is initial activity level.

The second form was used for the 24 hours after reactor shutdown.

8.2.1.3 SUMMARY OF RELEASES: To find out how much time has elapsed between shutdown and escape to the atmosphere, each release must be traced separately. This was done by returning to the event tree developed in Section 8.1.3.

Each release sequence was traced to determine the approximate time the fission products escape after a reactor shutdown. All sequences that ended in a release were grouped into either of two broad categories: immediate or delayed. The immediate release assumed that the core would melt in 30 minutes and have an escape route available to the outside (Ref. 83, p. 105). The 10 sequences included in this category are the ones with containment vessel rupture or safety isolation valve failure. Using Eq. 8.2.1-2, curies for immediate release are:

$$Q = \frac{2.58 \times 10^8}{(1800)^{0.2}} = 5.76 \times 10^7 \text{ curies}$$

The delayed releases assumed the containment vessel would fail in 25.5 days (Ref. 83, p. 110). Only four were included in this category because these sequences required that all safety valves work properly and that the containment vessel remain intact during impact. The

containment vessel was assumed to have finally failed during the after heat transient by either meltthrough or creep rupture. Using Eq. 8.2.1-1, the curies for a delayed release were

$$Q = 2.58 \times 10^8 \left\{ \frac{1}{(2.2 \times 10^6)^{0.2}} - \frac{1}{(3.4 \times 10^6)^{0.2}} \right\} = 1.16 \times 10^6 \text{ curies}$$

The immediate releases clearly dominate the delayed releases by a margin of one order of magnitude. The delayed release allows enough time to evacuate everyone from the threatened area therfore they would not produce any immediate deaths. For these reasons only the immediate release sequence was pursued in depth.

8.2.2 DISPERSION MODEL: As the cloud of radioactive particles is moved from the crash site by the wind, its concentration is changed. The concentration is reduced by the cloud expanding and by minute particles falling from the cloud. The activity of the fission products is constantly decreasing with time, so the level of activity in the cloud is also time varying. This model attempts to determine the concentration of the cloud in curies per cubic meter. This problem is a three dimensional time varying one, but there are approximations available for its solution (Ref. 160, p. 403).

8.2.2.1 CLOUD EXPANSION: A rough estimate of the volume of the cloud as it moves out could be obtained by using the area of a sector of an annulus that expands up at a predetermined rate. A much more accurate model is the Pasquill expression which was used both in the WASH-1400 report and in this study. It is:

$$\chi_{(x)} = \frac{Q}{\sqrt{2\pi}\ \pi\ f \times \sigma_z(x)\ u \exp(h^2/2\ \sigma_z^2)} \qquad (8.2.2\text{-}1)$$

where χ (x) = cloud concentration at radial position x (curie-sec/m^3)

Q = source (curies)
f = angular sector width (fraction of circle)
u = wind velocity (m/sec)
σ_z (x) = standard deviation for vertical diffusion (m)
h = release height (m)

Normally a gas escapes over a period of time that depends upon the type of leak. Instead of forcing an assumption on the period of time over which the leak is spread, the above expression compacts the cloud into one second. For example, if a leak lasted 60 seconds, 1/60th of the cloud would be released each second so the concentration would be 1/60th of the total. When the cloud reaches an individual, he experiences the total cloud over a period of 60 seconds. So instead of dividing by the release period at the start and then multiplying by it later, it is assumed to be one second in length, i.e., it will pass by a point in one second. To make this a valid assumption, no one is allowed to leave or enter the area while the cloud passes.

The angular sector width (f) and the standard deviation for vertical diffusion (σ_z) are dependent upon the stability of the wind. Pasquill grouped wind stabilities into six classifications that range from turbulent (A) to stable (F). Stability classification A means that the cloud expands upward rapidly and has an angular width of 40%. Stability classification F means that the cloud remains narrow (angular width of 7½°) and low to the ground (See Figure 8.2.2-1.). All clouds are assumed to be based on the ground.

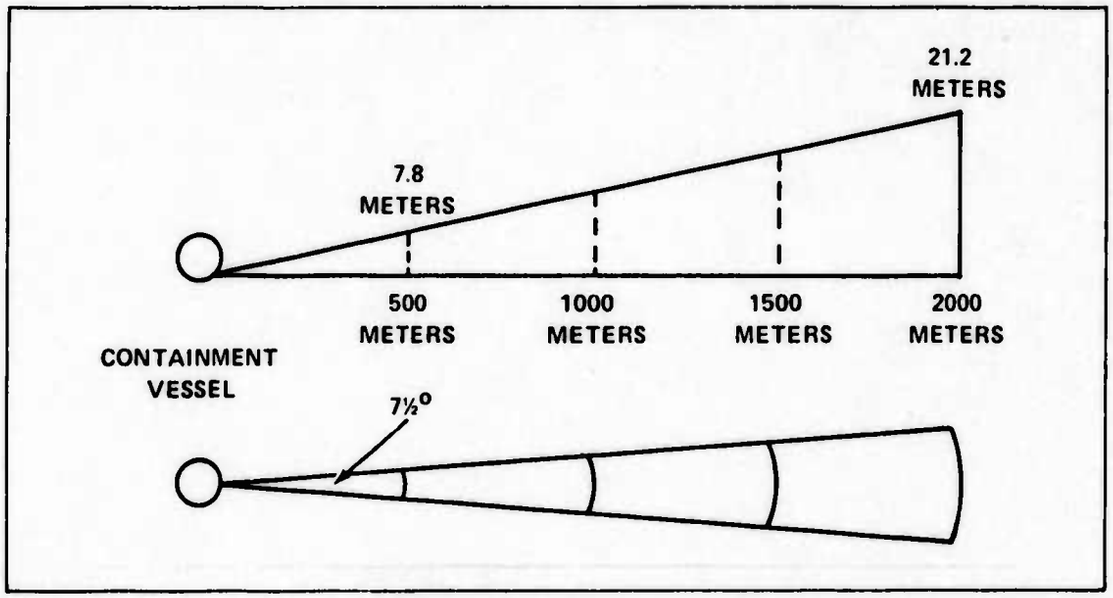

Figure 8.2.2-1. Cloud Expansion Stability Classification: Pasquill F

The standard deviation for vertical diffusion is shown in Figure 8.2.2-2; angular widths are presented in Table 8.2.2.1-1.

TABLE 8.2.2.1-1. ANGULAR WIDTHS FOR PASQUILL'S STABILITY CLASSIFICATIONS

STABILITY CLASSIFICATION	ANGULAR WIDTH (DEGREES)
A	40
B	30
C	20
D	15
E	10
F	7.5

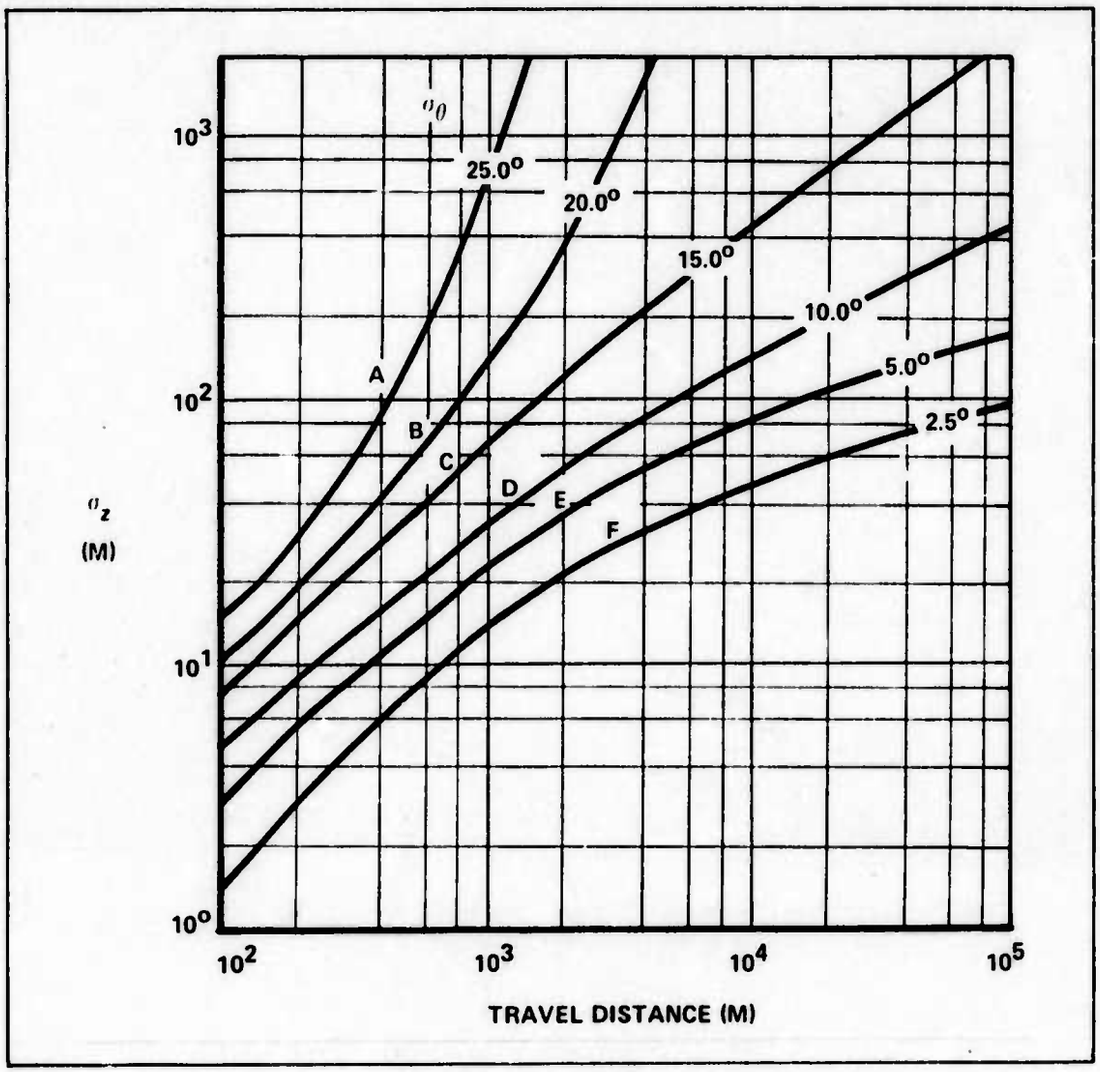

Figure 8.2.2-2. Standard Deviation of the Vertical Concentration Distribution, σ_z, as a Function of Travel Distance from a Continuous Source (A-F are Pasquill's Diffusion Categories) (Ref. 160, p. 409)

8.2.2.2 CLOUD DEPLETION: As the cloud moves along, very small particles are dropped to the ground. Their size determines how fast they fall; the height from which they fall determines how long it takes to reach the ground; and the velocity of the cloud determines the amount that will fall in a specified distance of cloud travel. For this study the area covered by the cloud was divided into 500 meter intervals. The area of each interval was a sector of an annulus (See Figure 8.2.2-1).

The equation used to compute the fraction of the cloud that is deposited in each interval, taken from the WASH-1400 report is:

$$fr_k = \frac{V \, \delta \, X_k}{\bar{Z}_k \, U}$$

where

fr_k = fraction deposited in interval k

$\bar{Z}_k = \sqrt{\pi/2} \, \sigma_z \exp(h^2/2 \, \sigma_z^2)$

V = the particle's falling velocity

δX_k = 500 meters for all k (Ref. 185, Appendix VII, p. 20)

by assuming that the release height is always zero, $z_k = 1.25\sigma_z$.

The falling velocities were assumed to be 0.5 cm/sec for iodine and 0.2 cm/sec for all other particles. These are approximate values and are considered conservative (Ref. 46, p. 109). The total activity released has 23.7% Noble Gas (Xenon and Krypton), 65% iodine, and 11.3% of all others. Substituting the latter two into the previous equation yields:

$$fr_k = \frac{0.65\,(0.005)\,500}{\bar{Z}_k \, U} + \frac{0.113\,(0.002)\,500}{\bar{Z}_k \, U} = \frac{1.39}{\sigma_z \, U} \qquad (8.2.2\text{-}2)$$

To obtain an accurate measure of the total fraction remaining in the cloud the following equation was used from WASH-1400:

$$FM = \exp\left\{ -\sum_{i=1}^{K-1} fr_i \right\} \qquad (8.2.2\text{-}3)$$

This gives the amount of the cloud over the interval k as the negative expotential of the sum of the previous fractions.

The concentration of activity deposited per interval was found by computing the product of the activity (Q) and the fraction deposited in that interval. Then the activity per square meter was found by dividing by the area of the interval.

8.2.2.3 WEATHER MODEL: The weather model adopted for this study was the one developed for WASH-1400 (Ref. 185, Appendix VI, p. 16). The model, an average of the weather from 39 sites spread across the country in 27 different states, was chosen as applicable to this study because it did almost cover the entire U.S., and our mission aircraft could be based almost anywhere in the U.S. The model is shown in Table 8.2.2.3-1.

TABLE 8.2.2.3-1. METEOROLOGICAL PARAMETERS

NUMBER	STABILITY CLASSIFICATION	RELATIVE PROBABILITY	WIND VELOCITY (M/SEC)	SECTOR (FRACTION OF CIRCLE)
1	A	1.02E-02	8.00E-01	1.11E-01
2	A	1.94E-02	2.50E-00	1.11E-01
3	A	1.41E-02	4.50E 00	1.11E-01
4	A	0.96E-02	7.00E 00	1.11E-01
5	B	6.72E-03	8.00E-01	8.30E-02
6	B	0.98E-02	2.50E 00	8.30E-02
7	B	8.10E-03	4.50E 00	8.30E-02
8	B	8.60E-03	7.00E 00	8.30E-02
9	C	1.10E-02	8.00E-01	5.50E-02
10	C	2.95E-02	2.50E 00	5.50E-02
11	C	3.00E-02	4.50E 00	5.50E-02
12	C	2.15E-02	7.00E 00	5.50E-02
13	D	3.23E-02	8.00E-01	4.20E-02
14	D	7.00E-02	2.50E 00	4.20E-02
15	D	7.70E-02	4.50E 00	4.20E-02
16	D	7.20E-02	7.00E 00	4.20E-02
17	E	5.60E-02	8.00E-01	2.80E-02
18	E	0.98E-01	2.50E 00	2.80E-02
19	E	7.96E-02	4.50E 00	2.80E-02
20	E	6.22E-02	7.00E 00	2.80E-02
21	F	7.30E-02	8.00E-01	2.10E-02
22	F	5.91E-02	2.50E 00	2.10E-02
23	F	3.11E-02	4.50E 00	2.10E-02
24	F	2.12E-02	7.00E 00	2.10E-02
25	D(RAIN)	0.91E-01	2.50E 00	4.20E-02

8.2.2.4 SUMMARY OF DISPERSION MODEL: This model can compute the concentration of the cloud after it leaves the reactor by allowing for expansion and depletion. Total cloud activity is a time varying function and therefore reduces the concentration of activity as well. To allow for this reduction, the activity was recomputed at the beginning of each interval and assumed to remain constant over the interval.

The end product of this model is the cloud concentration in curies-seconds per cubic meter. A second product, as found in Section 8.2.2.2, is the concentration of the ground activity from particles which have fallen from the cloud. Figure 8.2.2-3 shows how the cloud concentration varies with various Pasquill stability classifications. Figure 8.2.2-4 shows how the cloud concentration varies with wind velocity within Pasquill stability classification F.

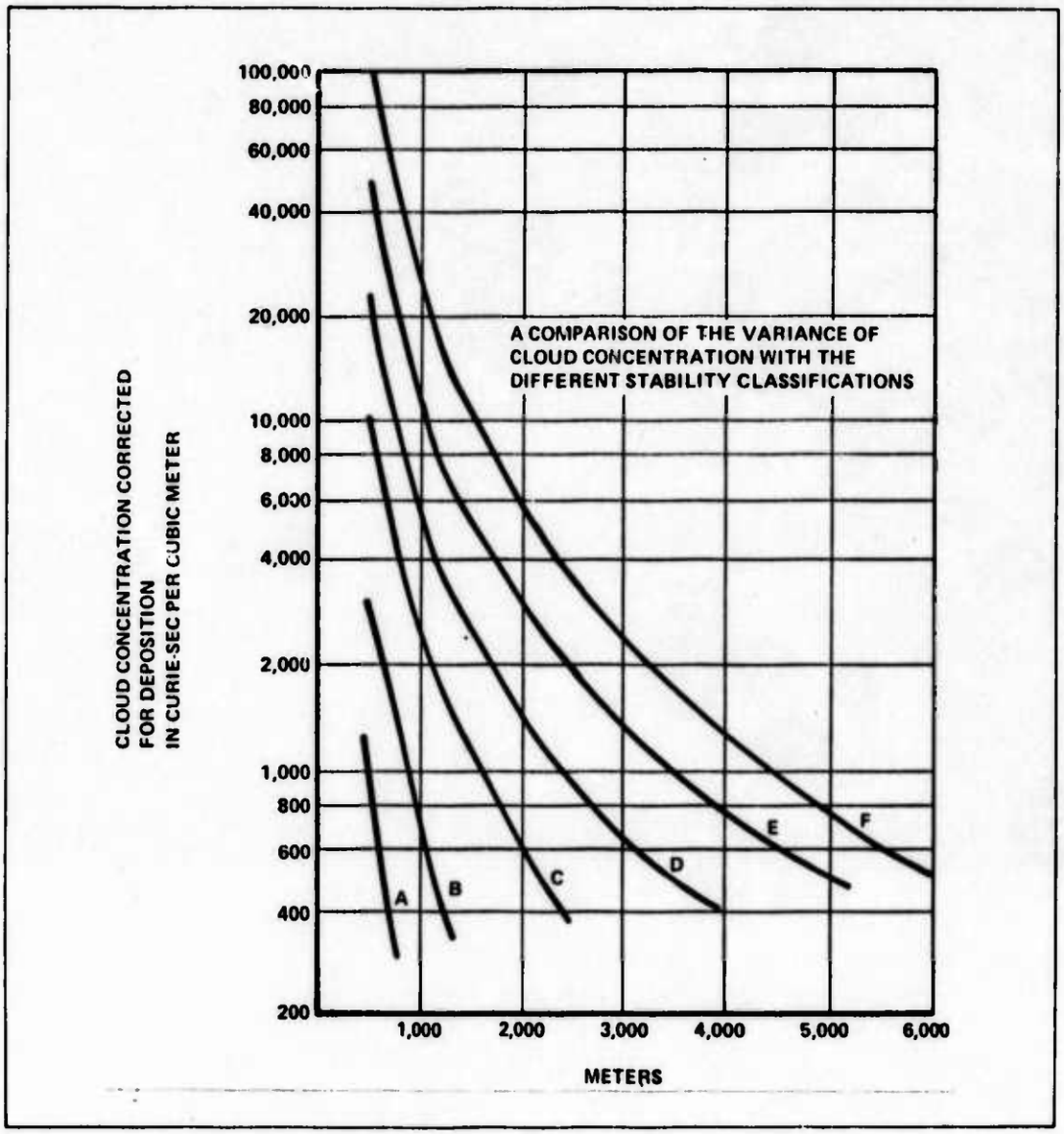

Figure 8.2.2-3. Cloud Concentration Corrected for Deposition

8.2.3 EVACUATION: For this study it was assumed that there would be no prior warning of the aircraft accident and that evacuation would begin at six hours after the crash. The start time was selected by considering the amount of mass communications that are available today to relay emergency information. Surely, the communications media will increase their attempt to reach all the public, as the FAA will continue to increase its ability to keep aircraft under radar control. The combination of the two should be able to pinpoint a crash and broadcast the warning within six hours. After evacuation begins, it was assumed to have a half-life of two hours (Ref. 185, Appendix V1, p. 31). This would mean that, after warning, one half of the population concerned would evacuate in two hours, one half of the remaining would leave in the next two hours, etc. All evacuation should be completed by 24 hours after the accident.

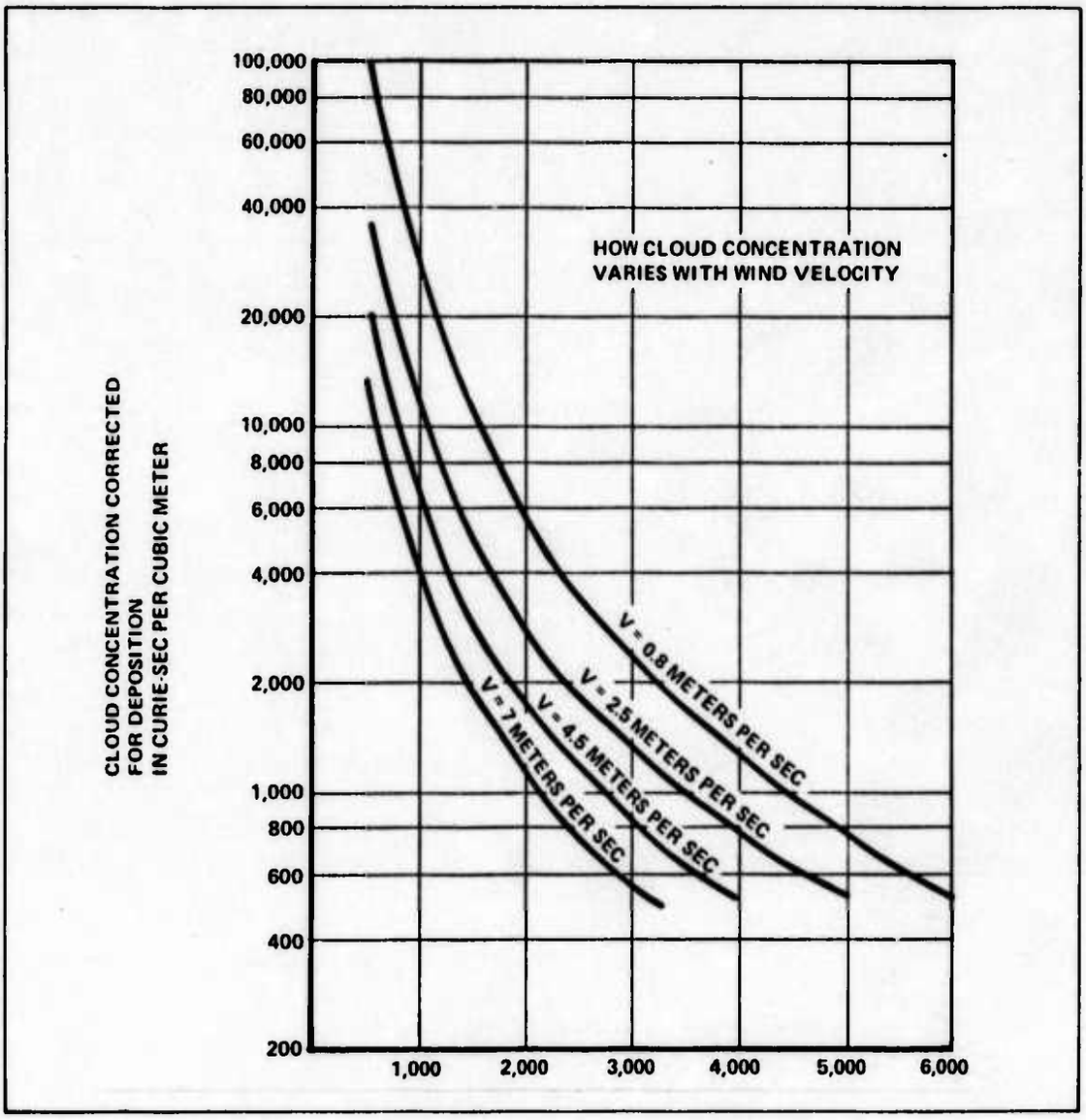

Figure 8.2.2-4. Cloud Concentration Corrected for Deposition (Pasquill Stability Classification F)

8.2.4 HEALTH EFFECTS MODEL: This model, the intermediate step between the Dispersion Model and the Population Model, takes the cloud and the ground concentrations and computes multiplication factors (K factors). The product of a K factor and a population density gives the number of deaths for that particular combination. This study considered only deaths due to a dose to the whole body. The lethal threshold for whole body dose (WBD) was so low that its statistics dominated those of a dose to the gastro-intestinal (GI) tract or lungs. A WBD includes the dose received from a radioactive cloud, from inhaling particles of the cloud, and from particles deposited on the ground. Figure 8.2.4-1 is a simple probability distribution to compute deaths from the dose a person has received. This distribution, used by the WASH-1400 report, was adopted for this study because it is very conservative (Ref. 185, Appendix VI, p. 54). Normally 400 REM is taken as the 50% lethality threshold but this distribution has it as the upper limit (Ref. 46, p. 20).

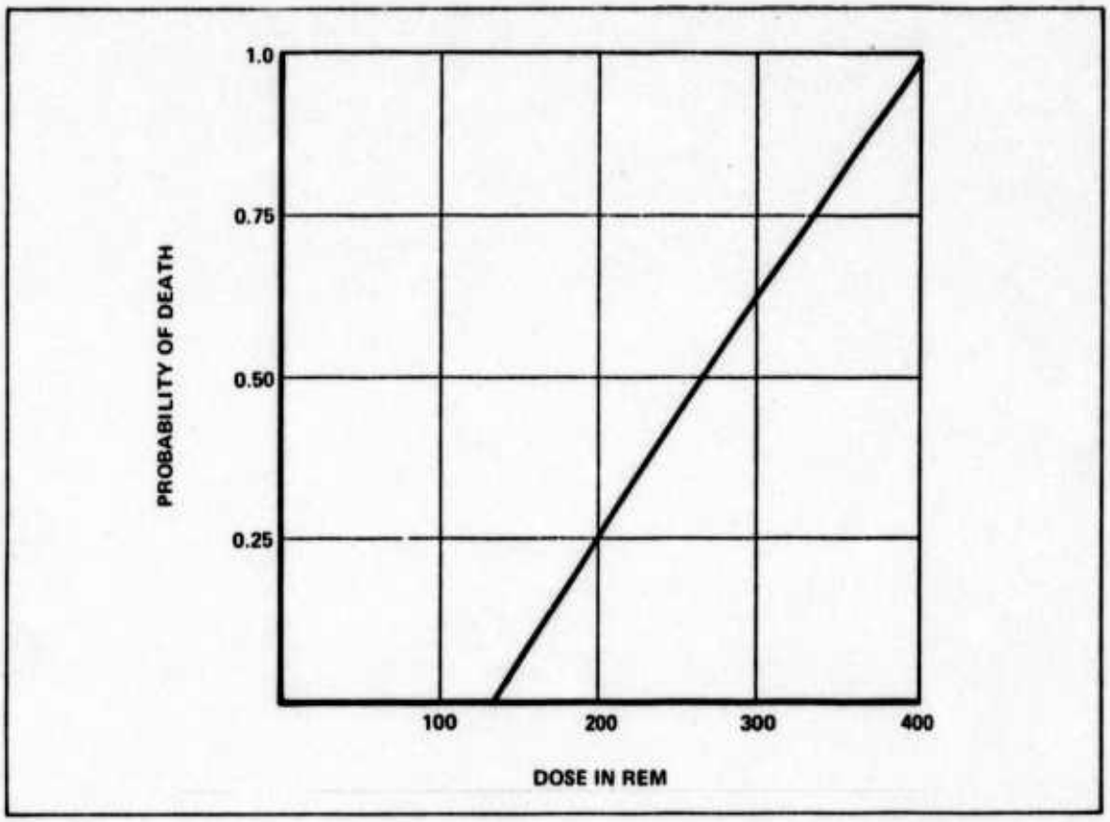

Figure 8.2.4-1. Assumed Probability Distribution for Fatalities vs Radioactive Dose

8.2.4.1 WBD-CLOUD SHINE: When exposed to a radioactive source of any nature, a person will receive a dose of radioactivity depending on the strength of the source and the time exposed. If the source is a cloud, it is referred to as cloud shine. The amount of the dose depends upon the concentration of activity in the cloud and how long it takes the cloud to pass.

Table 8.2.4-1 gives the conversion factors from curie-seconds per cubic meter to REM used by the WASH-1400 report. Several of these values were chosen at random and verified (Ref. 46, p. 93). Each value was multiplied by the percentage it contributed to the total activity and then summed. For example, I_{132} contributes 9.6% of the total activity so it would give a cloud shine dose of (0.55)9.6% = 0.053 REM/curie-sec per cubic meter. The total of the release isotopes was 0.274 REM/curie-sec per cubic meter. Since most people spend a large portion of time in well-protected environments, the dose was reduced by a factor of three, the shelter factor used in the WASH-1400 report which does consider that people will be exposed during evacuation (Ref. 185, Appendix V1, p. 58). The conversion factor becomes

0.0913 REM/curie-sec per cubic meter

TABLE 8.2.4-1. AVERAGE DECAY ENERGIES AND DOSE FACTORS FOR GROUND DEPOSITION AND CLOUD SHINE

NUMBER	NAME	GROUND (REMS/HR)/(CI/m²)	CLOUD REMS/(CI-SEC/m³)
1	KR-85	0.0	0.0
2	KR-85*	3.0	0.036
3	KR-87	10.0	0.36
4	KR-88	30.0	0.42
5	SR-89	0.0	0.0
6	SR-90	0.0	0.0
7	SR-91	14.2	0.16
8	Y-90	0.01	0.002
9	Y-91	0.01	0.002
10	ZR-95	10.0	0.19
11	ZR-97	11.9	0.06
12	NB-95	10.2	0.18
13	MO-99	3.6	0.06
14	TC-99*	2.0	0.035
15	RU-103	7.2	0.11
16	RU-105	9.0	0.20
17	RU-106	3.0	0.05
18	RH-105	1.4	0.005
19	TE-129	1.5	0.018
20	TE-129*	1.5	0.025
21	TE-131*	16.8	0.375
22	TE-132	3.4	0.05
23	I-131	5.6	0.09
24	MI-131	5.6	0.09
25	I-132	34.0	0.55
26	I-133	7.4	0.12
27	I-134	32.0	0.60
28	I-135	24.0	0.42
29	MI-135	24.0	0.42
30	XE-133	1.0	0.007
31	XE-135	3.0	0.060
32	CS-134	24.0	0.36
33	CS-136	30.0	0.46
34	CS-137	8.4	0.13
35	BA-140	4.2	0.06
36	LA-140	30.0	0.52
37	CE-141	1.1	0.016
38	CE-143	4.4	0.085
39	CE-144	0.6	0.004
40	PR-143	0.0	0.0
41	ND-147	2.0	0.045
42	PM-147	0.0	0.0
43	PM-149	0.05	0.012
44	PU-238	0.002	0.0
45	PU-239	0.002	0.0

8.2.4.2 WBD-INHALATION: As the cloud of minute fission products passes along, everyone engulfed in the cloud will inhale a harmful amount that depends upon the concentration of the cloud. This is the largest single contributor to deaths (Ref. 185, Appendix VI, p. 81).

The conversion factor for the WBD due to inhalation is developed using the conversion factors from the WASH-1400 report shown in Table 8.2.4-2. Once again each value was multiplied by the percentage it contributed to the total activity. For example, using I_{132} again, it contributed (130) 9.6% = 11.5 REM/curie. The total of the release was 560 REM/curie. A breathing rate of 2.2×10^{-4} cubic meters per second was assumed and multiplied times the total to complete the conversion factor of 0.12 REM cubic meters/curie-seconds. There is no allowance for shelter in this conversion.

8.2.4.3 WBD-GROUND DEPOSITION: The concentration of particles left by the cloud was computed in Section 8.2.2.4 and its corresponding conversion factor was computed in the same manner as Section 8.2.4.1.

The factor is

4.39 REM square meters/curie-hours

and does include the allowance for shelter.

8.2.4.4 WBD-SUMMATION: To obtain the number of deaths, each interval must be considered separately. The WBD from inhalation and cloud shine could be immediately computed by assuming the cloud concentration remained constant through the interval and that no one left during the cloud passage. The WBD from ground deposition depends almost completely on the evacuation model. All people in an interval received the same dose until after six hours. The 50% of the population who evacuated between the sixth and eighth hours were considered to receive the total WBD for six hours plus an average ground dose for the two hour evacuation period. The 25% who evacuated between the eighth and tenth hours received the WBD for eight hours plus an average dose for the two hour evacuation period. This method was continued until fewer than 1% remained to be evacuated.

With the combination of the percentage of population evacuated in a two hour period and the WBD they received, Figure 8.2.4-1 will yield the percentage who will die. By entering the figure with the dose, the probability is obtained. This is multiplied by the percentage evacuated to obtain the percentage who will die. The percentage of fatalities for each period were totaled to yield the percentage for that one interval.

The percentage for each interval was computed out to the distance where no one was killed. The areas of the affected intervals were totaled to compute the total area in square miles that was affected by that weather classification. Using this total area, the fraction of the total area that each interval contributed was obtained. The product of the interval's fraction of the total area and its percentage of fatalities is that interval's contribution to the total lethal percentage.

TABLE 8.2.4-2. INHALATION DOSE FACTORS (REM/CI) X 10^3

NAME	WBD (30d)
KR-85	0.0
KR-85*	0.0
KR-87	0.0
KR-88	0.0
SR-89	3.90E 00
SR-90	1.60E 00
SR-91	3.52E-01
Y-90	6.00E-01
Y-91	2.60E 00
ZR-95	4.90E 00
ZR-97	3.90E-01
NB-95	2.00E 00
MO-99	6.61E-01
TC-99*	8.40E-03
RU-103	7.71E-01
RU-105	6.44E-02
RU-106	2.85E 00
RH-105	9.75E-02
TE-129	2.00E-02
TE-129*	4.40E 00
TE-131*	7.32E-01
TE-132	1.96E 00
I-131	2.40E 00
OI-131	2.40E 00
I-132	1.30E-01
I-133	5.70E-01
I-134	4.00E-02
I-135	2.90E-01
OI-135	2.90E-01
XE-133	0.0
XE-135	0.0
CS-134	1.50E 01
CS-136	5.50E 00
CS-137	8.20E 00
BA-140	7.20E 00
LA-140	8.35E-01
CE-141	8.10E-01
CE-143	3.37E-01
CE-144	6.60E 00
PR-143	1.13E 00
ND-147	1.16E 00
PM-147	3.60E-01
PM-149	3.11E-01
PU-238	3.04E 02
PU-239	2.83E 02

The lethal percentages for each interval were totaled to compute a lethal percentage for that particular weather classification. This total was called the K factor. When the K factor was multiplied by a population density, the result was a number of deaths for that particular density.

8.2.4.5 K FACTOR FOR F-0.8: The calculation of the worst case K factor is shown to illustrate this procedure. The worst weather conditions considered were those of stability classification F with winds of 0.8 meters per second (1.8 mph). This was chosen for an example because it entails more calculations than some others, so no calculations will be missed. The first interval ends at 500 meters. The cloud starts into this interval at 1800 seconds after shutdown, therefore the activity is found using Eq. 8.2.1-2:

$$Q = A = \frac{A_o}{t^{0.2}} = \frac{2.58 \times 10^8}{(1800)^{0.2}} = 5.76 \times 10^7 \text{ curies}$$

The cloud concentration before depletion is found using Eq. 8.2.2-1

$$\chi_{(0.5)} = \frac{5.76 \times 10^7}{\sqrt{2\pi}\,\pi\,(0.021)\,500\,(7.8)\,0.8} = 111{,}400 \text{ curie-sec per cubic meter}$$

The fraction of the cloud deposited in the interval comes from Eq. 8.2.2-2

$$fr_{(0.5)} = \frac{1.39}{\sigma_z\, U} = \frac{1.39}{7.8(0.8)} = 0.22$$

The fraction of the cloud remaining is from Eq. 8.2.2-3

$$FM_{(1)} = \exp(-0.22) = 0.80$$

Therefore, actually 20% was dropped in the first 500 meters. The WBD is figured using the cloud concentration at the beginning of the interval. Conversion factors for inhalation and cloud shine (computed in Sections 8.2.4.1 and 8.2.4.2) can be added to yield the initial WBD conversion factor of 0.22 REM Cubic meters/curie second. Using this factor the initial WBD is:

$$(111{,}400)\,(0.22) = 24{,}500 \text{ REM}$$

This is obviously well above the lethal threshold.

The total activity deposited in the interval is:

$$5.75 \times 10^7\,(0.20) = 1.15 \times 10^7 \text{ curies}$$

To obtain the activity per square meter, the deposited activity must be divided by the area of the interval. In all but the first interval, the area is found using formula for the area of the sector of an annulus. Activity concentration is:

$$\frac{1.15 \times 10^7}{16363} = 703 \text{ curies per square meter}$$

The WBD from ground deposition for the initial close rate can be found by using the conversion factor computed in Section 8.2.4.3. The WBD — ground deposition is:

$$703\ (4.39) = 3090\ \text{REM per hour}$$

All calculations for the other intervals followed the same pattern, and all people within 4000 meters received a lethal dose.

In the 500 meter interval ending at 4500 meters, the initial WBD was 212 REM with a WBD — ground starting at 15 REM per hour. The WBD — ground decreases to 12 REM per hour at six hours after the accident, 10.6 at 12 hours after, and 9.3 at 24 hours after the accident. The WBD accumulation is displayed in Figure 8.2.4-2.

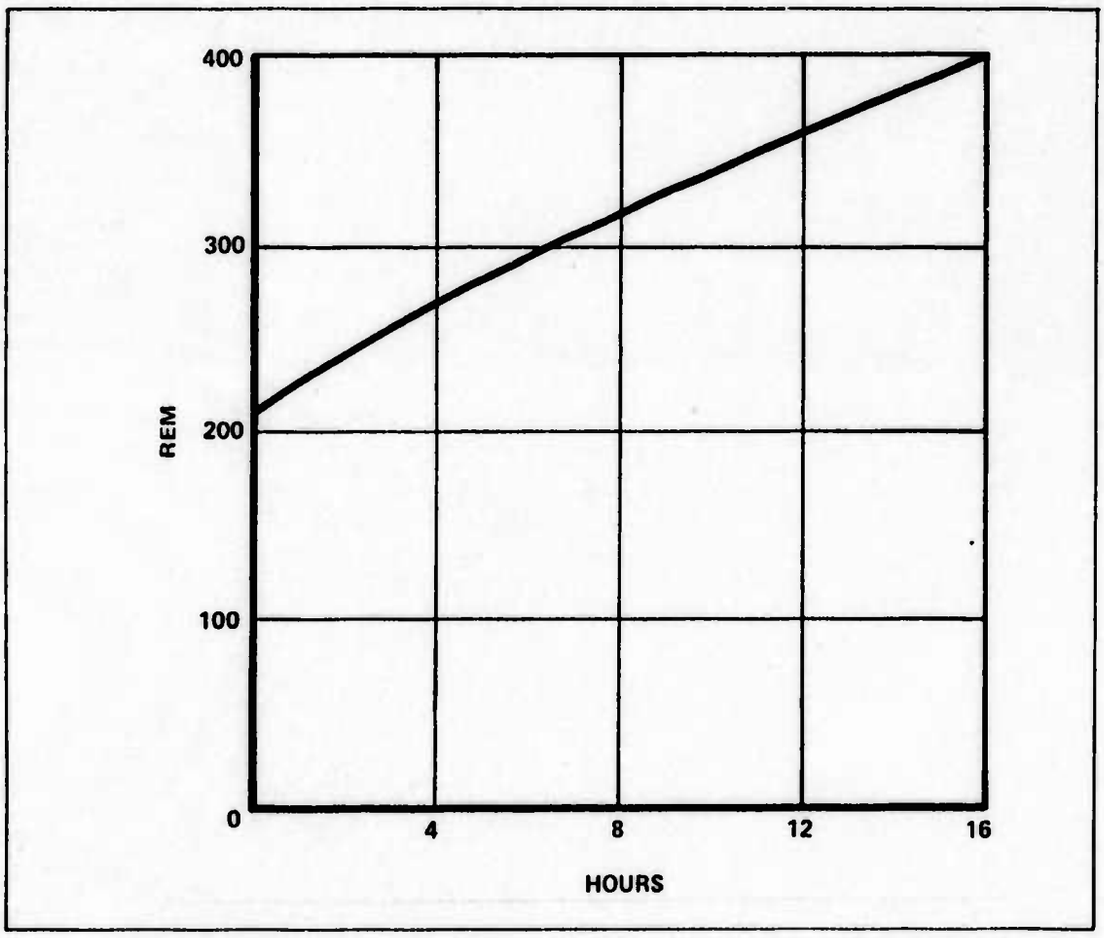

Figure 8.2.4-2. Cumulative Whole Body Dose for the 4500 Meter Interval

All people evacuating in a two hour period are assumed to receive the average dose for that period. In the first evacuation period ending at the eight hour point, the people receive a dose of 303 REM. By entering Figure 8.2.4-1 with this dose, the probability of death is given as 0.64. This can be interpreted to mean that 64% of the people will die.

The evacuation model assumed that 50% of the people leave in the first two hours of evacuation so:

$$(0.50)(0.64) = 32\% \text{ will die}$$

The next two hours shows 25% of the people receiving a dose of 325 REM. Of this 25% evacuated, the lethal fraction is 0.67, which leads to another 17% who will die. Continuing in this manner leads to a total of 65% for this interval.

The lethal area extends out to 6500 meters and covers a total area of 1.07 sq mi. The 500 meter interval ending at 4500 meters contains only 0.10 of this total area. If a uniform population density is assumed, 65% of this fraction will be killed or 6.5% . The area out to the 4000 meter point is 0.36 of the total area and 100% of these people are killed. The 5000 meter interval has 0.11 of the total area with 47% of its people killed for only a 5.2% contribution. By totaling each interval in this manner a sum of 57% was reached, meaning that 57% of the people in an area of 1.07 sq mi will suffer a lethal dose.

The K factor is the product of the two or

$$(0.57)(1.07) = 0.60 \text{ lethal percent} - \text{sq mi}$$

When multiplied times a population density in people per sq mi, this yields a number of people killed for this weather classification. All of the K factors are listed in Table 8.2.4-3.

8.2.5 POPULATION DENSITY MODEL: The nuclear aircraft could conceivably crash anywhere in the U.S., so a population density model of the entire U.S. was constructed. A listing of all towns of over 2500 in the U.S. was obtained from the U.S. Bureau of the Census. This listing contained the number of people, square miles covered, and population density for each town. By subtraction, the area and population not in towns was obtained for each state. It was assumed that these people were uniformly spread throughout the remaining area. By dividing the area of the state by the continental U.S. area, a probability of landing in that state was obtained. This led to a listing of 48 probabilities of crashing into various population densities. Next the towns were grouped by population density. The area for each grouping of population density was divided by the area of the U.S. and added to the list of probabilities and densities. The cumulative distribution function formed from the list is shown in Table 8.2.5-1. The upper limit of the distribution was 10,000 people per sq mi. This cutoff point was chosen because the area covered by densities over 10,000 people per sq mi was found to be only 4.9×10^{-4} of the total U.S. area. Since the area was so small, it was assumed that a nuclear aircraft could be restricted from flying over these areas without affecting its mission accomplishment.

The combination of this cumulative distribution function and the K factors with their associated probabilities yielded a cumulative distribution of deaths given an accident. This distribution is shown in Table 8.2.5-2.

TABLE 8.2.4-3. K FACTORS FOR A 574 MEGAWATT REACTOR

STABILITY CLASSIFICATION	WIND VELOCITY METERS/SEC	K FACTOR
A	0.8	0.04
A	2.5	0
A	4.5	0
A	7	0
B	0.8	0.05
B	2.5	0.03
B	4.5	0.02
B	7	0
C	0.8	0.16
C	2.5	0.04
C	4.5	0.02
C	7	0.02
D	0.8	0.38
D	2.5	0.12
D	4.5	0.05
D	7	0.03
E	0.8	0.52
E	2.5	0.20
E	4.5	0.11
E	7	0.06
F	0.8	0.60
F	2.5	0.37
F	4.5	0.22
F	7	0.13

TABLE 8.2.5-1. POPULATION DENSITY PROBABILITY DISTRIBUTION

PEOPLE PER SQUARE MILE			
0.05	0.50	0.95	MEAN
0.75	10.2	342	113

TABLE 8.2.5-2. FATALITIES PER RELEASE OF RADIOACTIVE MATERIAL PROBABILITY DISTRIBUTION

DEATHS PER RELEASE			
0.005	0.50	0.995	MEAN
0.003	1.20	865	18.9

8.2.6 RISK COMPARISON: The average number of deaths per accident was computed to be 18.9. The number of deaths per year would depend upon the number of flights made by the nuclear aircraft. Using the probability of an accident for a given number of flights shown in Table 8.1.6-2, the deaths per year can be calculated. If 1000 flights were made per year, the mean probability of an accident is 0.941 which gives an average of 17.8 deaths per year. If 2000 flights are made per year, then there would be an average of 18.8 deaths per year. The distributions of deaths per year are shown in Table 8.2.6-1 for three levels of flying activity.

TABLE 8.2.6-1. DEATHS PER YEAR PROBABILITY DISTRIBUTION

	DEATHS PER YEAR			
FLIGHTS PER YEAR	0.005	0.50	0.995	MEAN
1000	< 1	1.13	814	17.9
1500	< 1	1.18	850	18.5
2000	< 1	1.19	860	18.6

TABLE 8.2.6-2. INDIVIDUAL RISK OF ACUTE FATALITY BY VARIOUS CAUSES (U.S. POPULATION AVERAGE 1969)

ACCIDENT TYPE	TOTAL NUMBER FOR 1969	APPROXIMATE INDIVIDUAL RISK ACUTE FATALITY PROBABILITY/YR[1]
MOTOR VEHICLES	55,791	3×10^{-4}
FALLS	17,827	9×10^{-5}
FIRES AND HOT SUBSTANCE	7451	4×10^{-5}
DROWNING	6181	3×10^{-5}
POISON	4516	2×10^{-5}
FIREARMS	2309	1×10^{-5}
MACHINERY (1968)	2054	1×10^{-5}
WATER TRANSPORT	1743	9×10^{-6}
AIR TRAVEL	1778	9×10^{-6}
FALLING OBJECTS	1271	6×10^{-6}
ELECTROCUTION	1148	6×10^{-6}
RAILWAY	884	4×10^{-6}
LIGHTNING	160	5×10^{-7}
TORNADOES	91[1]	4×10^{-7}
HURRICANES	93[2]	4×10^{-7}
ALL OTHERS	8695	4×10^{-5}
ALL ACCIDENTS		6×10^{-4}

[1] BASED ON TOTAL U.S. POPULATION.
[2] (1953-1971 AVERAGE)
[3] (1901-1972 AVERAGE)

This is the risk to all the U.S. society. To determine the individual risk, this is divided by the total U.S. population. For 2000 flights per year, the individual risk would be:

$$\frac{18.8}{201,000,000} = 9.34 \times 10^{-8} \text{ Fatality Probability per year}$$

Without comparison, this figure has little meaning. Table 8.2.6-2 provides a basis for comparison with more normal fatal accident causes. The risk from a nuclear aircraft would fall below that of lightning, tornadoes, and hurricanes. Note that the U.S. population for 1969 was used to make this comparison.

8.2.7 SENSITIVITY: The major assumptions made for this study affect the outcome of the consequences model are core melt time, evacuation time, and the upper limit on the WBD. Each of these was examined as to its impact upon the average number of deaths per accident.

If the core melted in 15 minutes instead of 30 minutes, the curies released would be increased by a factor of 1.15. This would raise the average number of deaths per accident from 18.9 to 21.7.

If the core melted in one hour, the curies would decrease of factor of 1.15. The average number of deaths per accident drops to 16.4.

If the evacuation start were delayed from 6 hours to 12 hours, the average climbs to 25.7 deaths per accident.

The effect of lowering the lethal dose from 400 REM to 200 REM was to raise the average from 18.9 to 33 deaths per accident.

Although these changes could almost double the deaths in the worst case considered, the overall risk to the individual changes very little. The individual still has a slightly greater chance of being killed by a nuclear aircraft than by a meteor.

Even though a coastal airport would most likely be chosen to aid in accomplishing an ASW mission, the base location was not limited for the consequences model. The assumption that the nuclear aircraft will crash only on the U.S. land mass makes the entire model very conservative. The only assumption made that might understate the number of people killed in an accident was the assumption to neglect the fatalities resulting from the aircraft falling upon them.

For a comparison between the effects of an airborne reactor and the effects of a ground reactor, the worst case of the 3200 MW ground reactor from the WASH-1400 report was compared with an airborne reactor of the same power. Using the same population density as the WASH-1400 report, an airborne reactor with the same power would kill 4840 people while the ground reactor would kill only 2300 people. The difference is a result of the evacuation model. The airborne system gives no prior warning and assumes that evacuation would not start until six hours after the accident. The largest reactor considered in this study however was a 700 MW reactor which would kill 1058 people if it fell into an area with a similar population density to the worst case in the WASH-1400 report.

All the consequence calculations have assumed a 574 MW reactor; however, a 475 MW and a 700 MW reactor were also considered in this study. A comparison of the three reactors' effects is shown in Table 8.2.7-1.

TABLE 8.2.7-1. PROBABILITY DISTRIBUTION OF THE THREE REACTORS CONSIDERED

FATALITIES PER RELEASE				
MW	0.005	0.50	MEAN	
475	<1	0.99	716	15.9
574	<1	1.20	865	18.9
700	<1	1.46	1055	23.0

8.3 CONCLUSIONS AND RECOMMENDATIONS

8.3.1 CONCLUSIONS:

1) The overall probability of a release of radioactive material is dominated by the contribution from the crash or impact event. The probability of a release resulting from a crash is approximately three orders of magnitude higher than other accidents.

2) The probability of release of radioactive materials for a crash is dominated by three factors. These are, in ascending order, the probability of failure to seal the containment vessel, the probability of failure to withstand the impact, and the probability of failure to withstand the afterheat transient.

3) A release of radioactive material is not expected to result in large numbers of fatalities. There is a 95% confidence that the number of deaths would be equal to or less than 57, with an expected number of 19.

8.3.2 RECOMMENDATIONS:

1) Further development of containment vessel safety valves should be accomplished, with special attention given to reliability.

2) Further testing or modeling of containment vessel impact survivability should be accomplished. Emphasis should be placed on the effects of valve weldments, pipe penetrations, and other protuberances on the impact survivability of the containment vessel. Additionally, the effects of the aircraft structure and its connection points on the impact survivability of the containment vessel should be investigated.

3) Further investigation of the ability of the containment vessel to survive the post-impact afterheat transient should be performed. The effects of the aircraft structure on the depth of burial of the containment vessel should be studied.

4) Further investigation of the reactor system reliability and its impact upon safety should be performed. Initial investigations indicated the probability of a reactor shutdown due to a transient was 0.3 per flight. This failure rate would have an enormous impact upon mission reliability and safety.

5) Historical aircraft crash data indicate that approximately one half of the accidents occur in close vicinity of the airfield. Further investigation should be conducted into the special equipment and emergency reaction force needed to respond to an accident. Further study should be conducted into the safety implications of having to close or evacuate an airfield after each accident.

8.4 SUMMARY

The feasibility, with respect to public safety, of a nuclear powered airplane has been analyzed using a probabilistic approach to risk assessment. The study was divided into two major areas of analysis or tasks. The first task was an analysis of the probability of a release of radioactive material from a nuclear powered airplane. The second task was an analysis of the consequence, in terms of fatalities, of a release of radioactive material.

The probability of a release of radioactive material was analyzed by first considering the events which could lead to a release, and then analyzing those events with event trees and fault trees.

An aircraft crash was found to be the only event with a significant contribution to the probability of a release of radioactive material.

The probability of a release on a per flight basis is expected, with a 90% confidence, to be between 1.87×10^{-3} and 4.43×10^{-3}. For 1500 flights, the probability is expected to be between 0.924 and 0.999.

An analysis of the consequence of a release of radioactive material was performed for the crash accident only. The Impact Event Tree was analyzed to determine the composition and magnitude of the release. This was then coupled with probabilistic models of atmospheric dispersion and population density to derive a probabilistic assessment of the number of fatalities.

The number of deaths resulting from a release of radioactive material from a crash accident is expected, with a 90% confidence, to be between 1 and 57 deaths.

The results of the probability of release modeling and consequence modeling were then combined to determine the risk to society in terms of fatalities per year. The expected number of deaths for 1500 flights per year was found to be approximately 19.

The individual risk to any member of society can be found by dividing the expected number of deaths by the total U.S. population. For 1500 flights per year, this was found to be 9.2×10^{-8} deaths per person per year, which is less risk than any other known accidents.

SECTION 9

LIFE CYCLE COST

9.0 INTRODUCTION

The cost study was undertaken to provide an initial input to the decisions that will be made concerning the direction of the nuclear aircraft program. It is recognized that in early system stages little information may be available from which to derive a complete cost estimate. However, important decisions must be made early in the life cycle. Therefore, realistic life cycle cost estimates should be made as early as possible and updated continuously as the system progresses and more data are made available.

Of the proposed systems, only those having dedicated propulsion systems will be addressed, i.e., engines which operate exclusively with fossil fuel, and engines which operate exclusively with energy supplied by a nuclear reactor. This is the system which combines a chemical fueled takeoff and landing with a long mission duration. Furthermore, there was no information available for a dual mode engine, and time was not available to attempt a look at its cost.

Since this study of the nuclear powered aircraft did not single out any one gross weight to be optimal, the cost analysis used the 2,000,000 lbs, suggested in Section 4.1.7.2 as a typical gross weight for a nuclear powered aircraft. Pertinent information about this aircraft can be found in Table 9.0-1. Data summarized in this table provide inputs for the following developments.

TABLE 9.0-1. PARAMETERS USED TO ESTIMATE NUCLEAR AIRCRAFT COST

GROSS WEIGHT (LBS)	2.0×10^6
* AMPR WEIGHT (LBS)	666,900
EMPTY WEIGHT (LBS)	1.64×10^6
JP-4 WEIGHT (LBS)	320,000
MAXIMUM SPEED (KTS)	461
MAXIMUM MACH	0.78
NUMBER OF JP-4 ENGINES	6
NUMBER OF NUCLEAR ENGINES	10
JP-4 ENGINE SLS THRUST (LBS)	50,000
** NUCLEAR ENGINE EQUIVALENT SLS THRUST (LBS)	100,000
JP-4 FUEL CONSUMPTION	1300 GAL/HR/ENGINE
REACTOR OUTPUT (MW)	475

* AMPR weight is defined in the *Aeronautical Manufacturers' Planning Report* as the empty weight of the airplane less (1) wheels, brakes, tires, and tubes; (2) engines; (3) starter; (4) cooling fluid; (5) rubber on nylon fuel cells; (6) instruments; (7) batteries and electrical power supply and conversion equipment; (8) electronic equipment; (9) turret mechanism and power operated gun mounts; (10) remote fire mechanism and sighting and scanning equipment; (11) air conditioning units and fluid; (12) auxiliary power plant unit; and (13) trapped fuel and oil, (Ref. 95, p. 5). For this study, AMPR weight was equated to structure weight.

** The nuclear engine actually creates 16,000 lbs of thrust at 30,000 ft, but its equivalent physical size is the same as a 100,000 lb sea level static thrust JP-4 engine.

The life cycle for a nuclear aircraft was assumed to be 10 years, which may seem low if only the amortization of the investment is considered. But, as mentioned in Section 2, a 0.7 utilization rate was chosen to be the upper limit on utilization rate. With this utilization rate, the aircraft would be airborne for approximately 6200 hrs per year. For a 10 year life at this rate, the airframe time would be approximately 62,000 hrs, the most that could be expected of an airframe between the years 1990 to 2000.

The cost analysis will take the form of the outline in Figure 9.0-1, prefaced by the methodology used to determine and sum the inputs. All cost estimates will be in constant 1974 dollars.

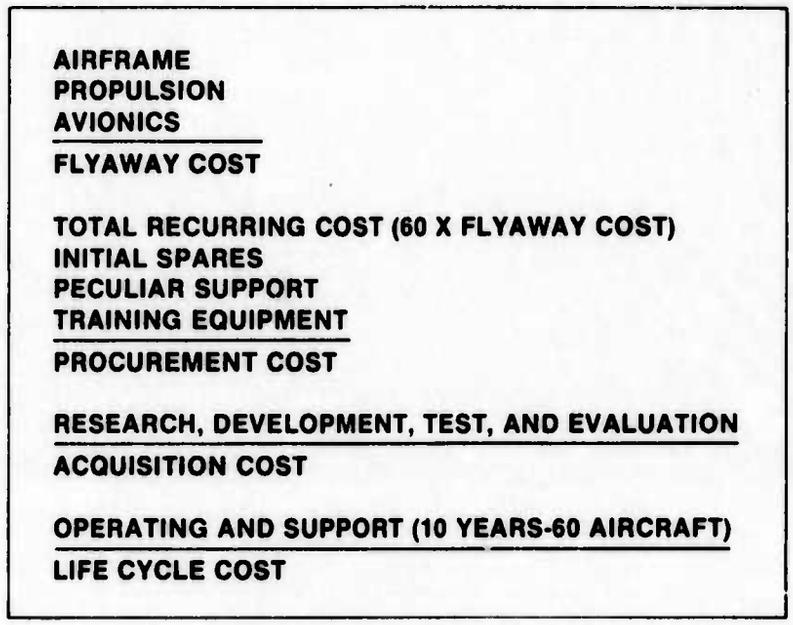

Figure 9.0-1. Cost Outline

9.1 METHODOLOGY

The analysis emphasizes the systems approach to life cycle cost for squadrons of nuclear powered airplanes for the ASW mission. This required a myriad of information, and methods to manipulate this information into meaningful results. Section 9.1.1 discusses the techniques used to obtain the information and is followed by a section on the method used to sum this information.

9.1.1 COST ESTIMATING TECHNIQUES: There are several recognized techniques (Ref. 32) for gathering information for cost estimating: parametric approach; analogy approach; engineering approach; and expert opinion.

The parametric approach is used for cost estimating when system costs can be based only on physical characteristics, performance parameters, and their relationship to highly aggregated component costs. In other words, a functional relationship must be set up between total system cost and various system parameters. Associated with each functional

relationship is the standard error of the estimate which is a measure of the variance about the regression. Also associated with these relationships is the coefficient of determination (R^2) which measures the percentage of variation in actual cost data that is explained by the fitted regression. A value of one for R^2 indicates a perfect correspondence between the actual costs for the observations in the data base and the cost predicted by the model for the same observations. On the other hand, a value near zero implies that the model does not explain variation of the actual data.

The cost estimating technique of analogy is the method of estimating cost by direct comparison with historical information on like or similar systems.

The engineering approach consists of a consolidation of estimates from various separate work segments into a total project estimate. Estimating by engineering methods is based on extensive knowledge of the system characteristics and, hence, is applicable to items at or near the production stage of the life cycle. The engineering approach is therefore not compatible with the nuclear powered aircraft in its present stage of the life cycle and was not used to obtain any of the following estimates.

The expert opinion approach consists of seeking judgments of recognized experts at all phases of the estimating process.

Data obtained from experts were in the form of three values: low, most likely, and high estimates. The low value was presented as a realistic value that, with probability one, the actual value would not be less than this value. The most likely value is the expert's best guess as to what the actual value would be. Finally, the high value was presented as a realistic value that, with probability one, the actual value would not exceed this value.

The parametric, analogy, and expert opinion approaches to cost estimating were used in this study. Figure 9.1-1, extracted from a publication by the Department of the Army (Ref. 32), indicates that during the conceptual stage of a system development, the above mentioned costing methods are, indeed, the appropriate methods to utilize. The "methods" column illustrates the relative relationship among the various cost estimating approaches.

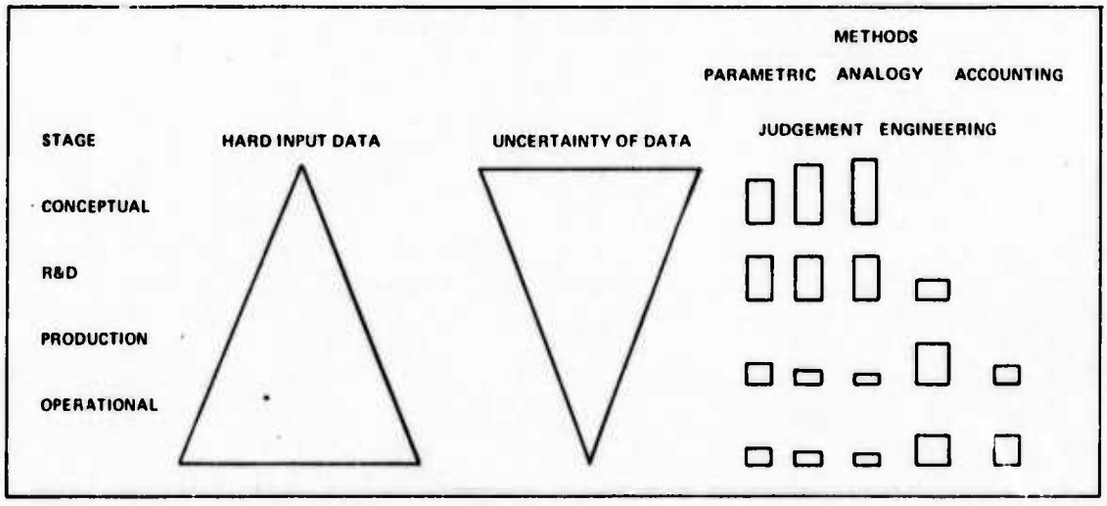

Figure 9.1-1. Relation of Weapon System Stage to Input and Estimating Methods

In the parametric and judgment approaches, ranges of cost estimates were obtained. The range for the parametric approach was plus and minus two times the standard error; for the judgment approach, the range was from the low to the high estimate. It became apparent that some means were necessary to manipulate these data into meaningful output. It was decided to treat these data as observations on continuous random variables. In nearly all cases, the data were skewed either left or right.

Random variables of this type are generally assumed to be either Weibull or Beta-distributed (Ref. 128, p. 1). The difference between these two functions is that the Weibull distribution is infinite at its extremes, whereas the Beta distribution is finite. Because of its finite limits, the Beta distribution was selected as the distribution for this analysis.

The assortment of Beta distributions obtained from this study were then summed using Monte Carlo simulation techniques, in conjunction with the SIMPAK (Ref. 27) computer program developed at Harvard. The Monte Carlo simulation is a method which generates random numbers in the range of a selected probability density function and then develops a cumulative distribution function based on the frequency that the numbers in the range are generated. The SIMPAK computer program was used to accomplish this task. If access to a computer is not readily available, manual means for manipulating random variables can be found in References 128 and 169.

9.1.2 SIMPAK COMPUTER PROGRAM: The SIMPAK program requires that the slope of the cumulative distribution function at the mode (most likely value) or the value of the cumulative distribution function at the median or 50th percentile be known. A method to determine the slope of Beta distribution may be found in Reference 7. This method was discarded in favor of determining the value of the 50th percentile. The median or 50th percentile for the Beta distribution can be approximated by the following equation (Refs. 128 or 169).

$$\text{Median} \simeq \frac{L + 4\,ML + H}{6}$$

where L = lowest value
ML = most likely value
H = highest value

This equation allows data to be inputed into the SIMPAK computer program in the following form:

VALUE	CUMULATIVE PROBABILITY
Low	0.0
Medium	0.5
High	1.0

The nuclear aircraft cost model in its simplest form is:

$$LCC = TRC + IS + RDT\&E + \sum_{i=1}^{10} D_i\,(0\&SC) \qquad (9.1.2\text{-}1)$$

where LCC = Life Cycle Cost
TRC = total recurring cost for 60 aircraft
IS = support and initial spares cost
RDT&E = research, development, test, and evaluation cost
D_i = discount factor for year "i"
O&SC = operating and support cost for 60 aircraft

Each of the above cost categories in the cost model is further divided into subcategories which are discussed in the following paragraphs. The entire life cycle cost model has been developed to accommodate both deterministic and probabilistic parameters. The life cycle cost output is in the form of a cost distribution function in which a maximum, most likely, and a minimum are determined. The costs are distributed over a range of probability from 0 to 1, with quartiles and the mean stated. By treating the life cycle cost in a probabilistic manner, risk and uncertainty are recognized and dealt with in a logical and systematic manner.

Summary figures have cost on the abscissa and cumulative probability on the ordinate. These figures are interpreted to mean that there is zero probability of the cost being less than the smallest indicated cost, i.e., it is certain that the actual cost will not be less than the highest indicated value. For other cumulative probabilities, such as 0.7, the actual cost will have a 70% chance of being less than the value indicated.

9.2 AIRFRAME

The cost of the airframe was obtained using the parametric method of cost estimating relationships. Two reports, Rand R-761-PR, *Cost-Estimating Relationships for Aircraft Airframes*, and Rand WN-8729-PR *Cost-Estimating Relationships for Aircraft Airframes*, (Refs. 95 and 43) provided approaches for determining the airframe cost. It was originally planned to use WN-8729-PR, since it contained the C-5A, which has the largest AMPR weight of the present Air Force fleet (279,000 lbs). It was believed that the relations in this report could be used to extrapolate the cost for an airframe with an AMPR weight of 666,900 lbs. However, a conference with Rand Corporation (Ref. 93) indicated that this was only a *working note* which still contained errors. In addition, one of the study goals was to consider research, development, test, and evaluation (RDT&E) costs, but the *working note* did not provide this information in an accessible form. It was then agreed that the Rand R-761-PR was the better model to use.

Since R-761-PR has a somewhat smaller data base and does not include the C-5A, a determination of how well the model is capable of estimating an airframe outside of its data base was desired. Applying the appropriate parameters for the C-5A into the model, it was determined that the model is capable of estimating the cost of the C-5A airframe within two times the standard error. (Figure 9.2-1). The C-5A airframe is heavier than twice the largest data point in the model's data base. Since the model estimated the C-5A airframe cost, it was felt that it would be able to predict the cost of an airframe for a nuclear powered aircraft with reasonable accuracy.

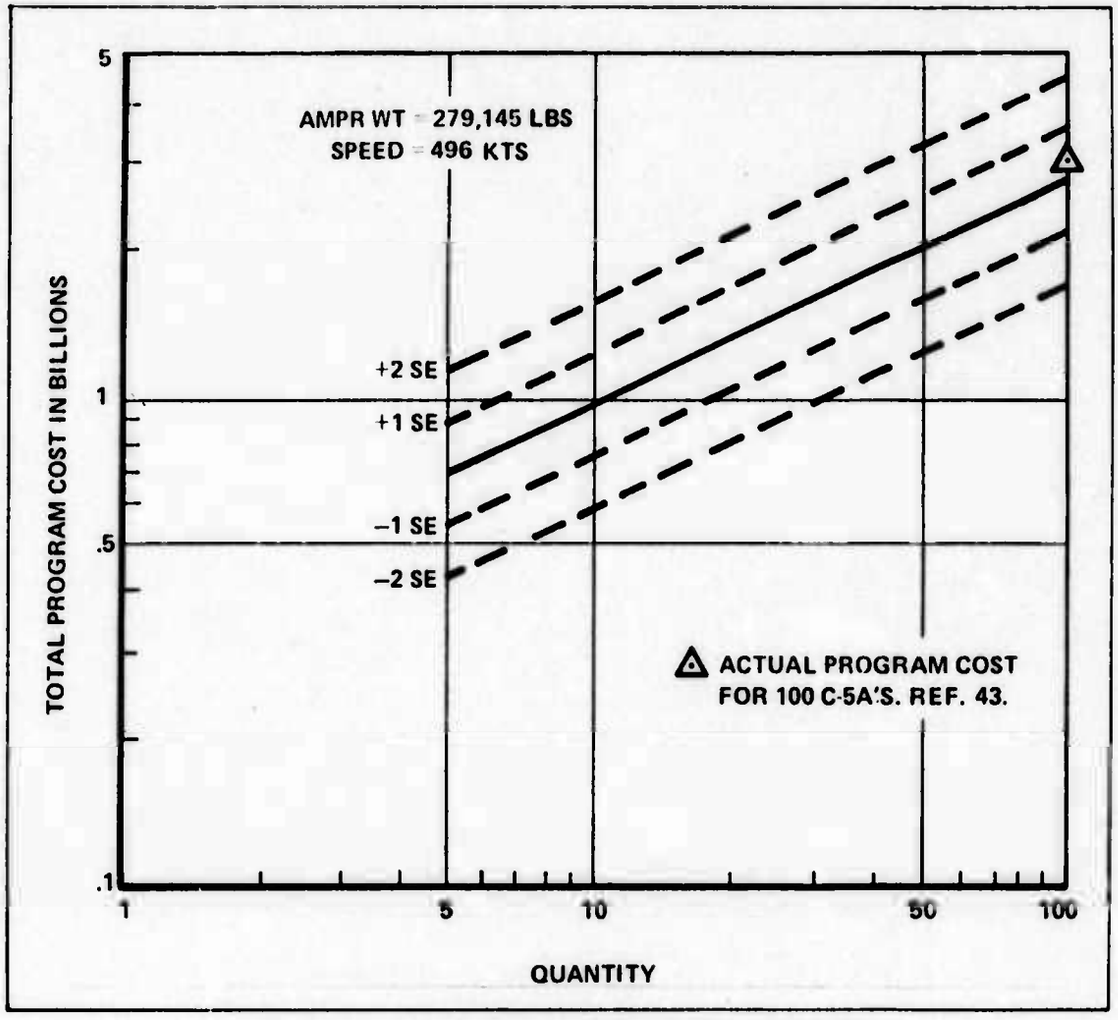

Figure 9.2-1. C-5A Total Program Cost vs Quantity

The equation used to determine the total program cost for the airframes for 60 production units plus one prototype is:

$$\ln TPC = 3.32 + 0.786 \ln A + 100 \ln S + 0.451 \ln Q \qquad (9.2\text{-}1)$$

ln TPC = natural log of total program cost in thousands of 1970 dollars (See Ref. 95 for what is included in TPC.)

A = AMPR weight (lb)
S = maximum speed (kts)
Q = total quantity produced including prototype.

This equation has an R^2 of 0.87, i.e., 87% of the variation in actual cost data is explained by this equation, and standard error of +28%, -27%. Table 9.2-1 was then used to convert the total program dollars into 1974 dollars to obtain the range of costs in Table 9.2-2 of two standard errors on either side of the predicted value. This range of estimated costs includes the

following costs for both production and prototype airframes: flight test, development support, manufacturing labor, manufacturing material, engineering, tooling, and quality control.

TABLE 9.2-1. PRICE INDEX WITH 1974 AS THE BASE YEAR*

YEAR	INDEX	YEAR	INDEX	YEAR	INDEX	YEAR	INDEX
1961	1.355	1966	1.312	1971	1.092	1976	0.941
1962	1.372	1967	1.282	1972	1.054	1977	0.913
1963	1.370	1968	1.250	1973	1.027	1978	0.885
1964	1.366	1969	1.209	1974	1.000	1979	0.858
1965	1.333	1970	1.155	1975	0.970	1980	0.833

* Index obtained from reciprocal of price level index in AFM 173-10.

TABLE 9.2-2. AIRFRAME TOTAL PROGRAM COST

	QUARTILES IN BILLIONS					
COST ELEMENT	0.00	0.25	0.50	0.75	1.00	MEAN
TOTAL PROGRAM COST	2.14	3.87	4.66	5.47	7.24	4.67

The following equations (Ref. 95, p. 29) and their respective standard error of the estimate were used to determine the range of cost for one prototype airframe.

$$\text{Engineering Hours} = 8.634A^{.576}\,S^{.856}\,Q^{.960} \qquad (9.2\text{-}2)$$

$$\text{Development Support \$} = 0.06474A^{.366}\,S^{2.267}\,Q_p^{.485} \qquad (9.2\text{-}3)$$

$$\text{Flight Test Operations} = 0.001244A^{1.160}\,S^{1.371}\,Q_p^{1.261} \qquad (9.2\text{-}4)$$

$$\text{Tooling hours} = 57.335A^{0.466}\,S^{0.633}\,Q_p^{0.482} \qquad (9.2\text{-}5)$$

$$\text{Manufacturing hours} = 0.3019A^{1.118}\,S^{0.410}\,Q_p^{1.366} \qquad (9.2\text{-}6)$$

$$\text{Quality control \$} = 0.13\ (\text{Manufacturing \$}) \qquad (9.2\text{-}7)$$

$$\text{Material \$} = 1.5A^{0.585}\,S^{1.213}\,Q_p^{0.622} \qquad (9.2\text{-}8)$$

where
A = AMPR weight (lbs)
S = maximum speed (kts)
Q_p = number of prototype airframes

The equations yielding dollar values were converted from 1970 to 1974 dollars using Table 9.2-1. Engineering hours, tooling hours, and manufacturing hours were multiplied by $19.50/hr, $13.50/hr, and $11.75/hr, respectively, to obtain 1974 dollar values.* Table 9.2-3 shows the results of applying Eq. 9.2-2 to Eq. 9.2-8 for the nuclear powered prototype.

TABLE 9.2-3. PROTOTYPE AIRFRAME COST FOR A NUCLEAR AIRCRAFT

	MILLIONS		
	LOW	MEDIAN	HIGH
PROTOTYPE ENGINEERING COST	43.9	72.7	102.0
PROTOTYPE DEVELOPMENT SUPPORT COST	2.3	11.0	19.8
PROTOTYPE FLIGHT TEST COST	11.8	36.8	61.9
PROTOTYPE TOOLING COST	14.3	21.7	29.2
PROTOTYPE MANUFACTURING COST	135.0	142.0	149.0
PROTOTYPE QUALITY CONTROL COST	17.5	18.5	19.4
PROTOTYPE MATERIAL COST	4.5	7.5	10.6
TOTAL	229.3	310.2	391.9

The prototype cost distribution was subtracted from the total program cost distribution, and the resulting distribution was divided by 60 to arrive at the average airframe cost for a nuclear powered aircraft (Table 9.2-4). The average cost of one airframe at the 50th percentile is $73.0 million. For comparison purposes, one C-5A airframe has an average cost of $30.6 million (Ref. 170).

TABLE 9.2-4. AVERAGE AIRFRAME COST

	QUARTILES IN MILLIONS					
COST ELEMENT	0.00	0.25	0.50	0.75	1.00	MEAN
AVERAGE AIRFRAME COST	31.6	60.7	73.0	84.7	114	72.6

Eqs. 9.2-2 through 9.2-8 are especially suited for sensitivity analysis. If any one of the independent variables is altered by 10%, the corresponding dependent variable is changed by a factor of 10 times the exponents of the independent variable; e.g., if the AMPR weight were increased by 67,000 lbs, the estimated development support cost would increase by approximately 4%. However, this is only appropriate for small variations in the independent variables.

* Dollar per hour values were extrapolated from charts in Reference 95.

9.3 PROPULSION

This portion of the study deals with the production cost for dedicated fossil fueled engines and dedicated nuclear engines for the 2,000,000 lb aircraft. Appropriate parameters were extracted from Table 9.0-1.

9.3.1 FOSSILE FUELED ENGINES: The production cost for the fossil fueled engines was obtained using the parametric method of cost estimating. The Rand Report R-1288-PR, *Relating Technology to Acquisition Costs: Aircraft Turbine Engines* (Ref. 130), which includes the TF-39, C-5A engine in its data base, was used to obtain cumulative production costs. Figure 9.3.1-1 was obtained by using the following equation:

$$\ln \text{PRQ Cost} = -7.9417 + 0.84172 \ln Q + 0.84755 \ln \text{THRMAX} + 0.21462 \ln \text{Mach.} \quad (9.3.1\text{-}1)$$

where PRQ Cost = Production cost in 1973 millions of dollars
Q = quantity
THRMAX = Maximum SLS thrust
Mach = Maximum Mach number

Two times the standard error of the estimate (+34%, −26%) on either side of the predicted value was used as the range of cost. The 1973 dollars were then converted to 1974 dollars using Table 9.2-1.

Since six fossil fueled engines are required for each airframe, Figure 9.3.1-1 was entered along the abscissa at a quantity of 366 and the appropriate values extracted along the ordinate corresponding to a range for production cost. The SIMPAK computer program divided this range of cost by 61 to arrive at a distribution of costs for the total cost of six fossil fueled engines on each airplane (See Table 9.3.1-1).

TABLE 9.3.1-1. PRODUCTION COST FOR SIX FOSSIL FUELED ENGINES.

	QUARTILES IN MILLIONS					
COST ELEMENT	0.00	0.25	0.50	0.75	1.00	MEAN
SIX FOSSIL FUELED ENG.	3.91	6.78	8.02	9.66	12.7	8.22

The 50th percentile of this cost distribution was then divided by six to arrive at an average cost per engine of $1.34 million. This compared to the average engine cost for the C-5A of $1.21 million (Ref. 170). The fact that these average costs are so close is not surprising because the two engines are in the same thrust category, i.e. 50,000 lbs of thrust for the nuclear aircraft's fossil fueled engine as compared to 47,000 lbs of thrust for the C-5A engine.

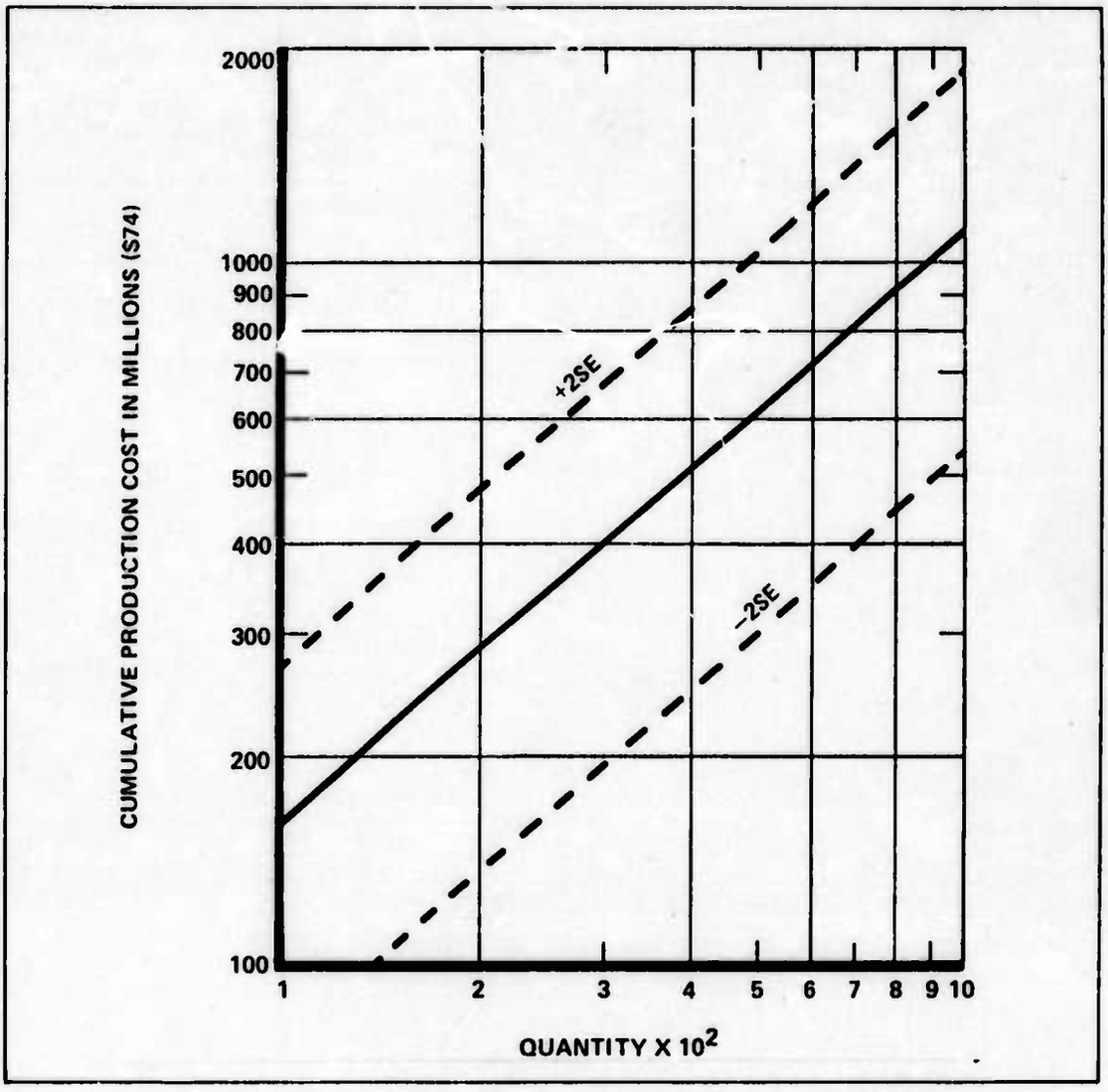

Figure 9.3.1-1. Production Cost for Fossil Fueled Engines in $74 vs Quantity

9.3.2 NUCLEAR ENGINES: The production cost for the nuclear engines was broken into two parts — the engine and the heat exchanger. The first part consisted of determining the cost of an entire engine as though it were really a fossil fueled engine. The validity of this approach lies in the fact that a nuclear engine is essentially a chemical engine with the combustion chamber replaced by a heat exchanger. Once again, the Rand R-1288-PR (Ref. 130) was utilized and, in particular, Eq. 9.3.1-1. However, instead of using actual sea-level-static-thrust as input to the model, the equivalent thrust of a fossil-fueled engine that would have the same physical dimensions as the proposed nuclear engine was used. Figure 9.3.2-1 was constructed in the same way as Figure 9.3.1-1.

Ten nuclear engines are required for each airframe. Therefore, Figure 9.3.1-1 was entered along the abscissa at 610 and the corresponding three values extracted along the ordinate. The SIMPAK computer program divided this range of costs by 61 to arrive at the total cost for nuclear engines per airframe (Table 9.3.2-1).

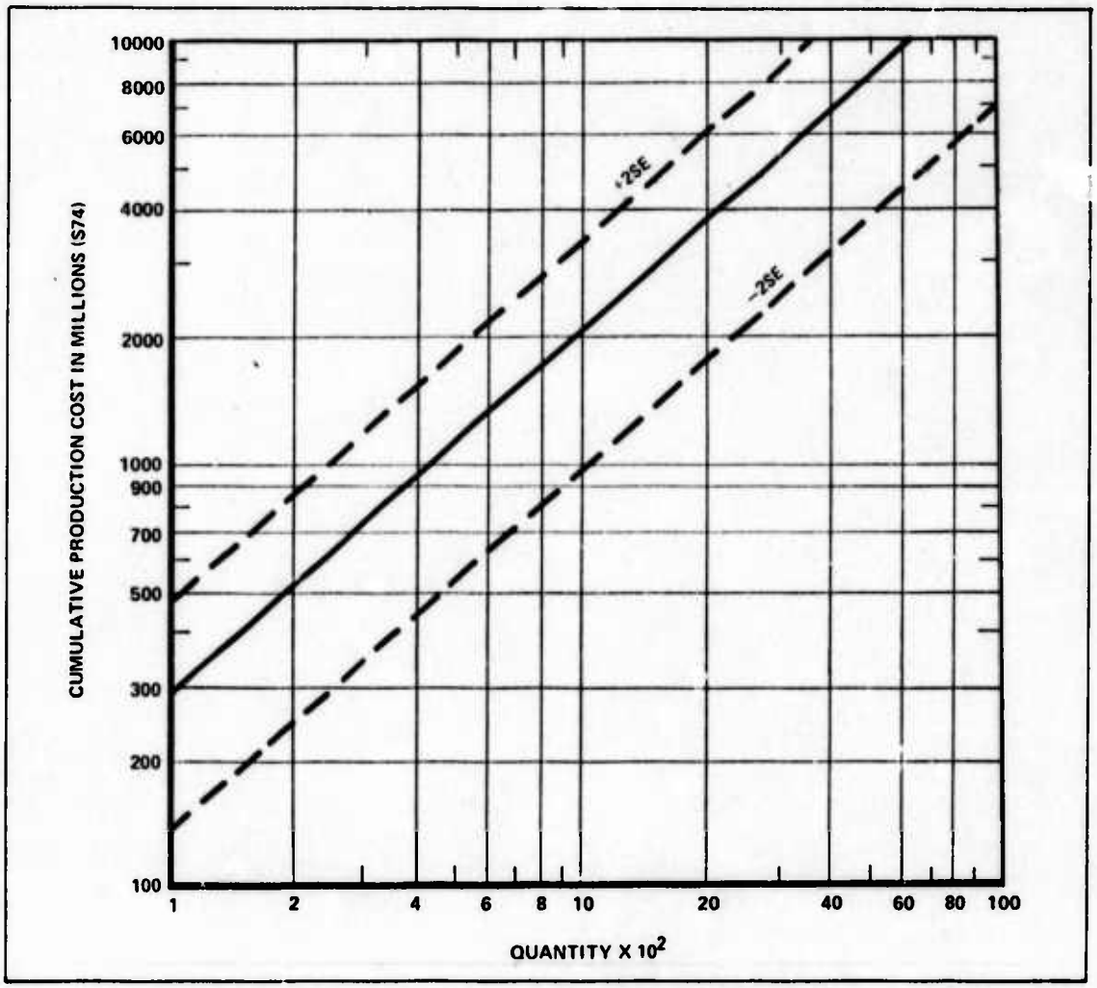

Figure 9.3.2-1. Production Cost for Nuclear Engines in $74 vs Quantity

TABLE 9.3.2-1. PRODUCTION COST FOR TEN NUCLEAR ENGINES

	QUARTILES IN MILLIONS					
COST ELEMENT	0.00	0.25	0.50	0.75	1.00	MEAN
TEN NUCLEAR ENGINES	10.8	18.8	22.2	26.7	35.2	22.7

The 50th percentile of this cost distribution was then divided by 10 to arrive at an average cost per engine of $2.22 million. Obviously, there is no comparison, since there is neither a nuclear engine nor a fossil fueled engine of this thrust category.

The second portion of the determination of the production cost of a nuclear engine is the cost of the heat exchanger. The method used to arrive at this cost was to consult the contractor that proposed the design that is outlined in Section 7.4.1.1 (Ref. 110). The information obtained from the contractor is contained in Table 9.3.2-2, and these values are the range of costs for a quantity of 10 heat exchangers.

TABLE 9.3.2-2. PRODUCTION COST FOR FIRST TEN ENGINE HEAT EXCHANGERS

LOW	MOST LIKELY	HIGH
$0.5 X 10^6	$0.75 X 10^6	$1.0 X 10^6

The contractor also indicated that a 90% learning curve could be expected for a production item, i.e., each time the quantity of heat exchangers is doubled, the cost per item reduces to 90% of its previous cost. Utilizing this information the following equation was developed:

$$y = a\,Q^b$$

y = cumulative average cost

where $b = \frac{\ln 0.9}{\ln 2} = -0.152$

b = slope of the learning curve

Q = quantity

Example: For 10 heat exchangers whose average cost is $100,000

$$100{,}000 = a\ 10^{-0.152}$$

$$\ln 100{,}000 = \ln a - 0.152 \ln 10$$

or

$$\ln a = \ln 100{,}000 + 0.152 \ln 10$$

$$a = 0.142 \times 10^6$$

therefore

$$y = 0.142 \times 10^6\ Q^{-0.152}$$

For $Q = 100$

$$y = 0.142 \times 10^6\ (100)^{-0.152}$$

$$= 7.05 \times 10^4 = \text{cumulative average cost}$$

Total cost for 100 units $= 100\ (7.05 \times 10^4)$

$$= 7.05 \times 10^6$$

The procedure demonstrated in the example was carried out for the three estimates for varying quantities to arrive at Figure 9.3.2-2. This graph was then entered at 610 units along the abscissa and the corresponding range of costs extracted from the ordinate. This range of costs was then divided by 61, yielding the cost of 10 heat exchangers per airframe (Table 9.3.2-3). Dividing the cost at the 50th percentile by 10, the average cost of $40,100 per exchanger is obtained.

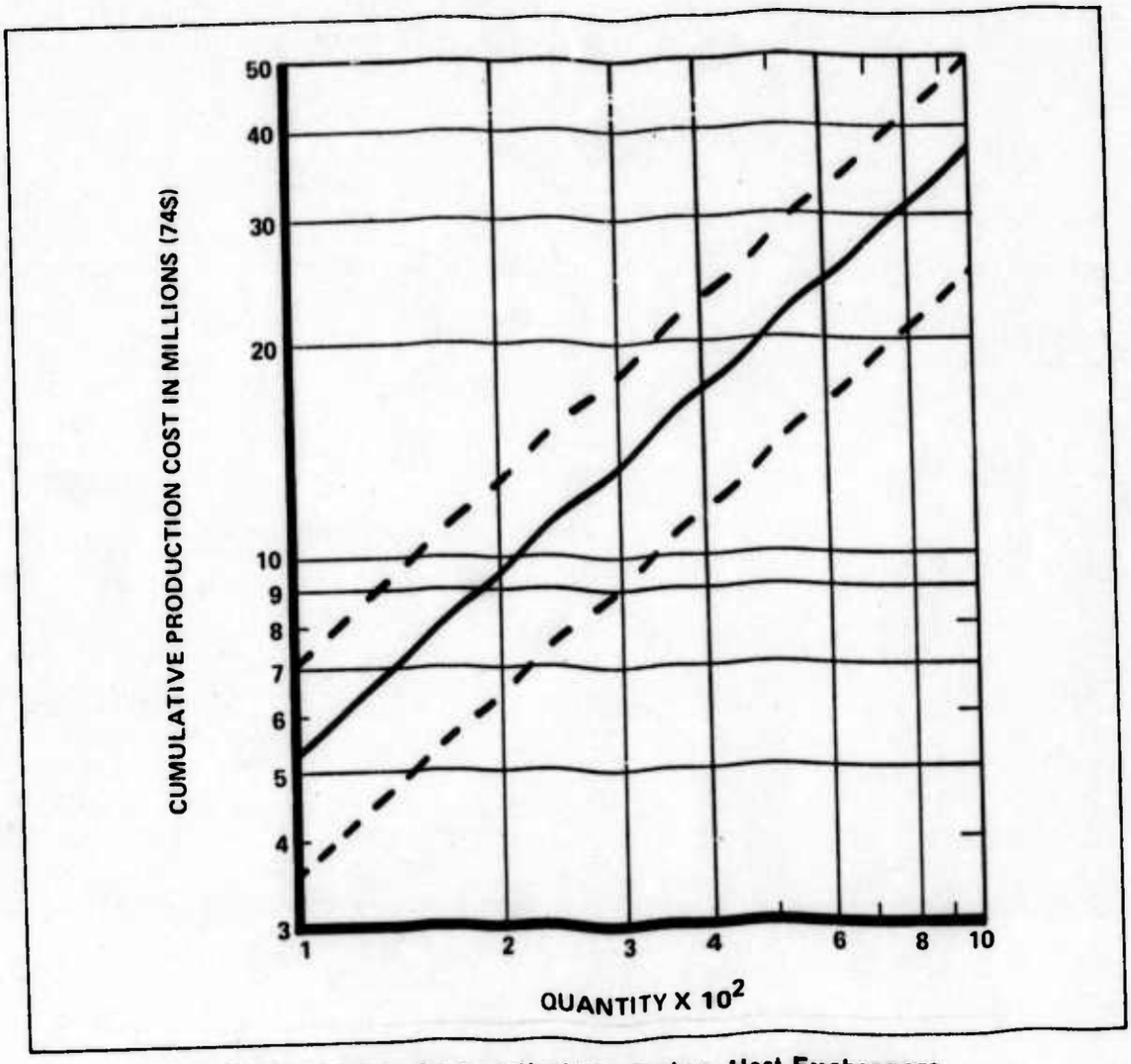

Figure 9.3.2-2. Cost of Nuclear Engine Heat Exchangers for Liquid Sodium System vs Quantity

TABLE 9.3.2-3. PRODUCTION COST FOR TEN NUCLEAR ENGINE HEAT EXCHANGERS

	QUARTILES IN THOUSANDS					
COST ELEMENT	0.00	0.25	0.50	0.75	1.00	MEAN
TEN HEAT EXCHANGERS	274	363	401	443	525	403

Equation 9.3.1-1, which was used to determine the cost of a nuclear engine, included the cost of a traditional combustion section in the engine. It was originally thought that the nuclear engine heat exchanger would be a significant additional cost, over and above the cost for the estimated engine. However, since the cost of the traditional combustion chamber amounts to less than 5% of the total engine production cost (Ref. 61) and the cost for a heat exchanger for the nuclear engine is also less than 5% of the total engine production cost, it is

not expected that the heat exchanger will be an additional cost. Therefore, the costs in Table 9.3.2-1 will be considered to be the total cost to produce engines whose thrust is generated via a heat exchanger.

9.4 REACTOR

The nuclear reactor production cost was obtained by contacting organizations with reactor cost expertise. In addition to the Atomic Energy Commission (AEC), four nuclear reactor contractors were contacted (Ref. Volume II, A.9).

Two contractors and the AEC responded with reactor information, while the third contractor declined input. One of the contractor's input was not a direct reply to the information requested, but rather brochures and unrelated data having no applicability to the design study. Therefore, the production cost for the nuclear reactor was based on figures supplied by AEC and one nuclear reactor contractor. These two replies are maintained with the original copy of this document in the library (AFIT/LB) at The Air Force Institute of Technology, School of Engineering, Wright-Patterson AFB, Ohio.

The bulk of the data supplied by the AEC were actual data from the NERVA Program. No scheme was uncovered to apply this data to the reactor in question. However, in the letter accompanying the NERVA data, the AEC suggested that a helium cooled reactor for the aircraft propulsion having an output power of 200-400 MW would cost $21 million ± 20%. This is quite close to the range of the contractor's estimates and lends validity to their estimates.

The information from the contractor concerning the cost of a gas cooled nuclear reactor is contained in Table 9.4-1. This table excludes the cost of secondary loop coolant which can be obtained for $5/lb (Ref. 176).

TABLE 9.4-1. PRODUCTION COST FOR 200 MW HELIUM COOLED NUCLEAR REACTOR

	ESTIMATE IN MILLIONS OF DOLLARS		
	LOW	MOST LIKELY	HIGH
10,000 EFPH CORE	2.1	3.3	4.5
ENGINEERING, PROCUREMENT, AND SERVICES	4.1	5.0	6.9
REACTOR VESSEL	0.2	0.3	0.4
PRIMARY HEAT EXCHANGER	0.7	1.0	1.5
SHIELDING AND CONTAINMENT	3.6	4.1	6.0
IN-REACTOR STRUCTURES	1.1	1.6	2.1
DUCTING, VALVES, CIRCULATORS, AND POWER SUPPLIES	0.4	0.6	1.0
INSTRUMENTATION, CONTROL, AND RADIATION MONITORING	0.8	1.0	1.5
ALLOWANCES-AUXILIARIES	0.4	0.5	0.7
TOTAL	13.4	17.4	24.6

The data specified pertain to a 200 MW, helium cooled reactor. This was originally the type of reactor that the study group was interested in. However, further study indicated a necessity for a larger reactor (See Section 6.3). Additional consultation with the contractor yielded the following scaling relationship to determine the cost of a larger output helium cooled reactor.

$$\text{New Cost} = \left(\frac{\text{new reactor power}}{\text{old reactor power}} \right)^{0.6} \text{Old Cost} \qquad (9.4\text{-}1)$$

Therefore, a 575 MW, helium cooled reactor would cost 1.88 times the 200 MW cost.

The cost analysis has, however, been assuming a liquid metal (NaK) coolant fluid rather than helium. The contractor's best estimate for this type of reactor, with a 475 MW output, is contained in Table 9.4-2. Costs for other reactor power outputs can be obtained by utilizing Eq. 9.4-1.

TABLE 9.4-2. COST FOR ONE 475 MW LIQUID SODIUM COOLED REACTOR

LOW	MOST LIKELY	HIGH
$29.0 X 10^6	$38.0 X 10^6	53.0 X 10^6

As mentioned in Section 3, it was desired to have triple redundancy for the reactor instrumentation. Therefore, from Table 9.4-1 additional $1.6 million, $2.0 million, and $3.0 million, respectively, were added to the figures in Table 9.4-2.

The summary statistics for the production cost for a 475 MW liquid metal cooled reactor are contained in Table 9.4-3. Included in this cost estimate are 27,000 lbs of seconday loop coolant (Ref. Table 7.7.1) which can be obtained for $7.50/lb (Ref. 176).

TABLE 9.4-3. COST FOR ONE 475 MW LIQUID SODIUM COOLED REACTOR WITH REDUNDANT INSTRUMENTATION

	QUARTILES IN MILLIONS					
COST ELEMENT	0.00	0.25	0.50	0.75	1.00	MEAN
475 MW REACTOR	30.8	38.1	41.5	46.3	56.2	42.4

9.5 ISOLATION SAFETY VALVE

The production cost for isolation safety valves is included in the production cost for the reactor. However, should a design like the Sandia design referenced in Section 7 be required, this is a substantial increase in the size of the valve which should be taken into account in the production cost. This valve has been estimated to increase the weight of the reactor an additional 15,000 lbs/valve.

Discussion with the Division Chief of Test Engineering Division (Ref. 164), Sandia Laboratories, indicated that production cost of a complex valve of this type would be no more than $10/lb and not less than $3/lb, with the most likely cost being about $5/lb. Should a heavy valve like this be required, Table 9.5-1 contains the summary statistics for 20 fast acting safety valves whose median average cost is $82,000.

TABLE 9.5-1. HEAVY SAFETY VALVE COST PER REACTOR

	QUARTILES IN MILLIONS					
COST ELEMENT	0.00	0.25	0.50	0.75	1.00	MEAN
SAFETY VALVE COST	0.95	1.41	1.64	2.08	2.90	1.75

9.6 AVIONICS

As discussed in Section 3, reliability in an avionics system to achieve a long duration mission was accomplished through the use of redundancy. The units or subsystems mentioned in the avionics section are the identical subsystems estimated in this section of the study. The methods used to determine the subsystem costs are a mixture of those mentioned in Section 9.1-1. Some items were estimated by expert opinion and others were considered to be deterministic. The cost of one item, the interference blanker, could not be estimated by any of the avionics references. Rather, it was estimated at $1000/lb, the rule-of-thumb used for costing avionics when no other means are available (Ref. 65).

Table 9.6-1 is a concise listing for an avionics package for a 14 day mission, utilizing a 0.95 reliable system. The distribution of cost for such a system can be found in Table 9.6-2. Cost distributions for other system reliabilities are contained in Appendix A.9.2.

It should be remembered that the required redundancy to obtain a certain reliability was based on an order of magnitude increase in MTBF. This implies that the deterministic costs in Table 9.6-1 should be somewhat increased from today's value to account for a greater MTBF. However, it is assumed that the cost of a system is not increased. This is based on the assumption that by the proposed in-commission date, electronic technology, and manufacturing techniques will have increased the present MTBF failure for a particular unit to 10 times this MTBF and they will have the same cost in 1974 constant dollars. This phenomenon has occurred in the recent past when electronic systems began using transistors in place of vacuum tubes. This increase in reliability was accomplished along with a decrease in the cost of the item.

9.7 FLYAWAY COST

The flyaway cost, as presented in Section 9.0, is the sum of the average airframe cost, the cost of a propulsion system, and the cost of installed avionics. Specifically, the flyaway cost distribution, Figure 9.7-1, for a 2,000,000 lb gross weight aircraft includes a 475 MW liquid metal (NaK) cooled reactor with safety valves, six fossil fueled engines, and 10 nuclear engines, a

TABLE 9.6-1. AVIONICS SUBSYSTEM COST FOR 0.95 RELIABLE SYSTEM

* SYSTEM	QUANTITY REQ.	WT (LBS)	COST IN THOUSANDS	REF.
INERTIAL	18	30	89.6	1
RADAR	6	350	269.	1
DOPPLER	15	15	50.2	1
RADAR ALTIMETER	9	11	7.9	1
ASTROTRACKER	20	100	75.-100.-150.	3
SECURE SPEECH	6	7	4.5	2
HF RADIO	10	54	23.	1
VHF RADIO (SONOBUOY)	13	33	5.5	2
UHF RADIO	13	33	11.6	1
DATA LINK	6	17	20.-40.-60.	2
INTERCOM	4	54	17.6	1
TACAN	10	29	25.	1
ADF	10	15	1.2	1
ILS	6	8	5.4	1
LORAN	10	22	14.	2
IFF	7	22	7.7	1
BEACON	7	3	12.2	1
OMEGA	5	60	15.	2
AIR DATA	4	12	5.6	1
AUTOPILOT	17	61	21.-50.-60.	2
STANDBY ATTITUDE INDICATOR	11	25	5.	3
RHAW	10	85	9.-225.-371.	2
ECM	8	218	116.	2
INTERFERENCE BLANKER	7	5	5.	5
COM/NAV DISPLAYS & CONTROLS	4	15	49.9	1
MTC DISPLAYS & CONTROLS	11	30	6.1	1
AUX DISPLAYS & CONTROLS	11	30	46.9	1
VERTICAL SITUATION DISPLAY	13	43	50.	3
HORIZONTAL SITUATION DISPLAY	13	43	50	3
MAGNETIC ANOMALY DETECTOR	16	—	—	4
AUDIO RECORDER	8	—	—	4
LOW LIGHT TV	20	67	141.1	1
IR	20	67	131.1	1
TACTICAL DISPLAYS	4	80	50.-75.-80.	3
COMPUTER	16	—	—	4
MISC. TAC DISPLAYS & CONTROLS	11	30	46.9	1

* SEE TABLE 3.2.1.4-1 FOR EXPLANATION OF LESS OBVIOUS ABBREVIATIONS

REFERENCE

1. SYSTEM PROJECT OFFICE (REF. 181)
2. CAPT. DARLINGTON (REF. 38)
3. MAJ. GRIMM (REF. 65)
4. MISSION ANALYSIS OF AF ASW CAPABILITY (REF. 152)
5. ESTIMATED AT $1000/LB (REF. 65)

TABLE 9.6-2. COST FOR AVIONICS PACKAGE FOR A 14 DAY MISSION

	QUARTILES IN MILLIONS					
COST ELEMENT	0.00	0.25	0.50	0.75	1.00	MEAN
AVIONICS - 0.95 RELIABLE	19.6	21.4	22.1	27.7	23.8	22.0

0.95 reliable avionics package, and an airframe. For comparison purposes the flyaway cost of the B-1 is currently estimated to be $76 million per aircraft (Ref. 12).

The graph in Figure 9.7-1 is interpreted that the flyaway cost for one aircraft will lie in the range of $127-224 million. The expected cost is $173 million with the median value also being $173 million.

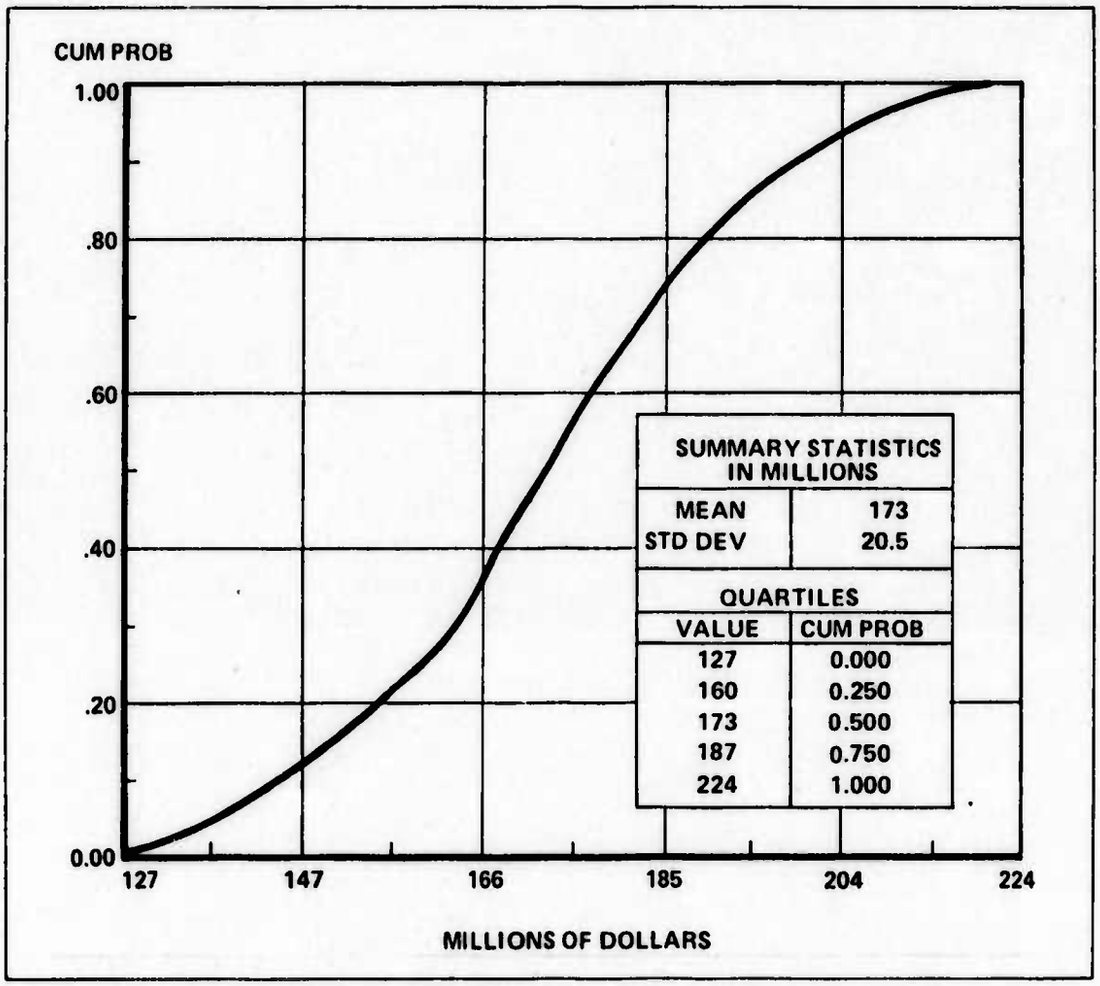

Figure 9.7-1. Flyaway Cost in Millions of $74 vs Cumulative Probability

9.8 TOTAL RECURRING COST

The total recurring cost is the total production cost which can be obtained either by summing up the production costs in Sections 9.3 through Section 9.7 or by multiplying the flyaway cost by 60. Figure 9.8-1 illustrates the cumulative probability distribution curve for the total recurring cost which was obtained by multiplying the flyaway cost by 60.

Figure 9.8-1 is interpreted that the flyaway cost for 60 aircraft lies in the range of $7.76-13.2 billion. The expected and median value is $10.4 billion.

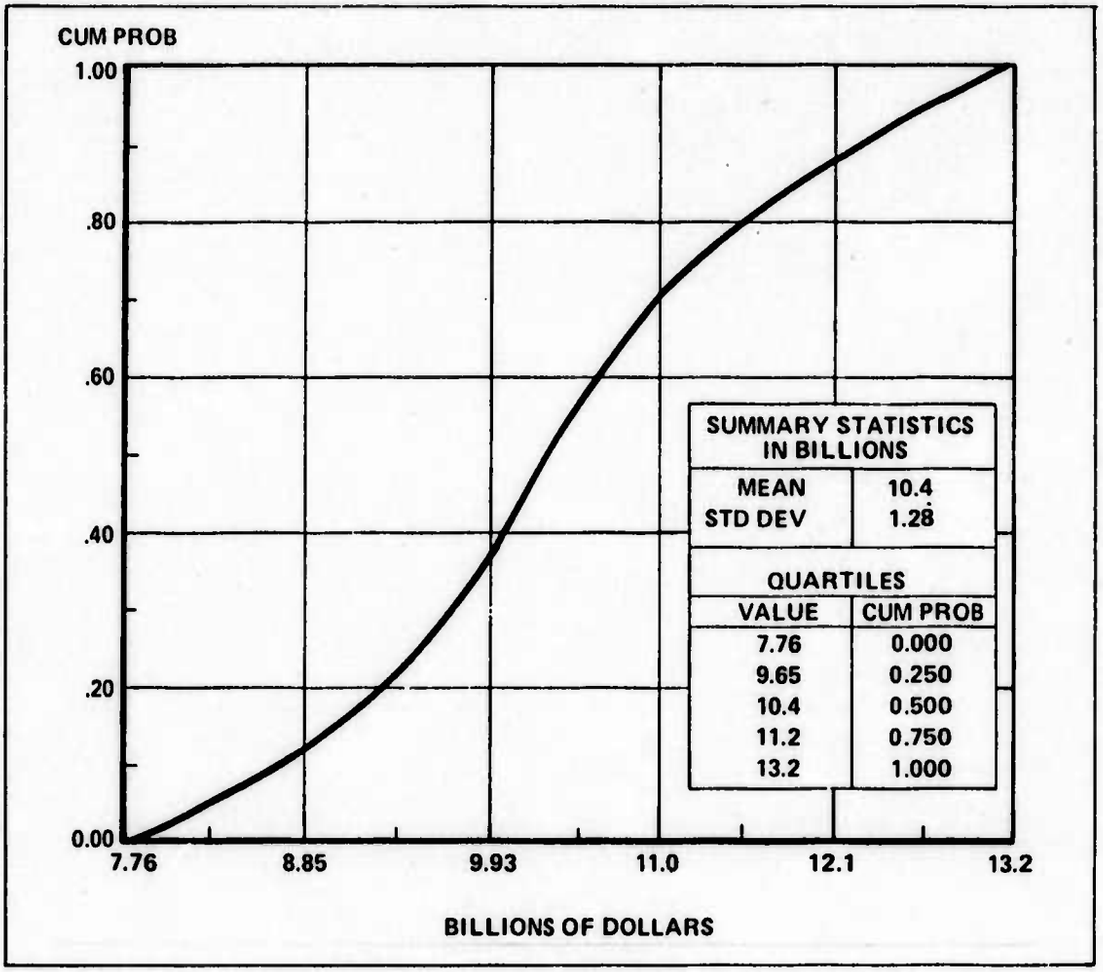

Figure 9.8-1. Total Recurring Cost (Flyaway Cost for 60 Aircraft) in Billions of $74 vs Cumulative Probability

9.9 INITIAL SPARES, PECULIAR SUPPORT, AND TRAINING EQUIPMENT

The cost for initial spares, peculiar support, and training equipment was obtained by taking a percentage of the flyaway cost. This technique is the method currently used by the Air Force Logistics Command (AFLC). As will be seen in Section 9.13, there is also a spares cost associated with the operating and support costs. The cost estimated for initial spares is the cost for spares for the first two years, over and above those spares connected with the annual purchases in operating and support. All new systems use more spares in the beginning of their operation and then level off to a constant or semi-constant quantity (Ref. 12). The initial spares cost is the cost for the extra parts utilized until the system problems are worked out. The peculiar support cost is the cost of aerospace ground equipment (AGE) peculiar to the aircraft, i.e., a crane to lift the heavy reactor from the airplane for refurbishing, tall lifts to inspect the vertical tail, etc. Training equipment cost includes such costs as simulators, or procedure trainers cost, and Technical Orders.

Percentage factors were estimated by Maj. Babbitt of the Logistics Support section of the B-1 SPO (Ref. 12) and are based on an AFLC Standard Factors Percentage dated 8 March 1972. A range of 15% to 70% of the flyaway cost and a most probable of 30% of the flyaway cost were determined to be the appropriate factors. Table 9.9-1 gives the summary statistics for initial spares, peculiar support and training equipment costs for one aircraft. The total cost for these items for the fleet of aircraft appears in Table 9.9-2.

TABLE 9.9-1. INITIAL SPARES, PECULIAR SUPPORT & TRAINING EQ. COST PER AIRCRAFT

	QUARTILES IN MILLIONS					
COST ELEMENT	0.00	0.25	0.50	0.75	1.00	MEAN
IS, PS & TE COST/AIRCRAFT	28.1	47.0	59.2	80.1	138	64.6

TABLE 9.9-2. INITIAL SPARES, PECULIAR SUPPORT & TRAINING EQ. COST FOR FLEET

	QUARTILES IN BILLIONS					
COST ELEMENT	0.00	0.25	0.50	0.75	1.00	MEAN
IS, PS & TE COST FOR FLEET	1.68	2.83	3.54	4.80	8.18	3.87

9.10 PROCUREMENT COST

The procurement cost is the sum of total recurring cost plus the cost of initial spares, peculiar support, and training equipment. The cumulative distribution of the procurement cost is contained in Figure 9.10-1. This graph is interpreted that the procurement cost will lie in the range $10.8-20.3 billion. The expected procurement cost is $14.5 billion with the median being $14.3 billion.

9.11 RESEARCH, DEVELOPMENT, TEST, AND EVALUATION

The costs for RDT&E are segmented into airframes, engines, reactors, and fast acting valves. The estimated costs for these items were obtained by either expert's opinion or by using appropriate cost estimating relationships.

The airframe RDT&E cost was developed using the Rand R-761-PR (Ref. 95). The prototype program is characterized as having no production planning and limited tooling. The development cost for one prototype airframe is contained in Table 9.2-2.

The development costs for the engines employed the techniques contained in the Rand R-1288-PR (Ref. 130) to determine their cost estimates. The cost estimating relationship used for this study was to determine the cost to develop an engine to Model Qualification Test

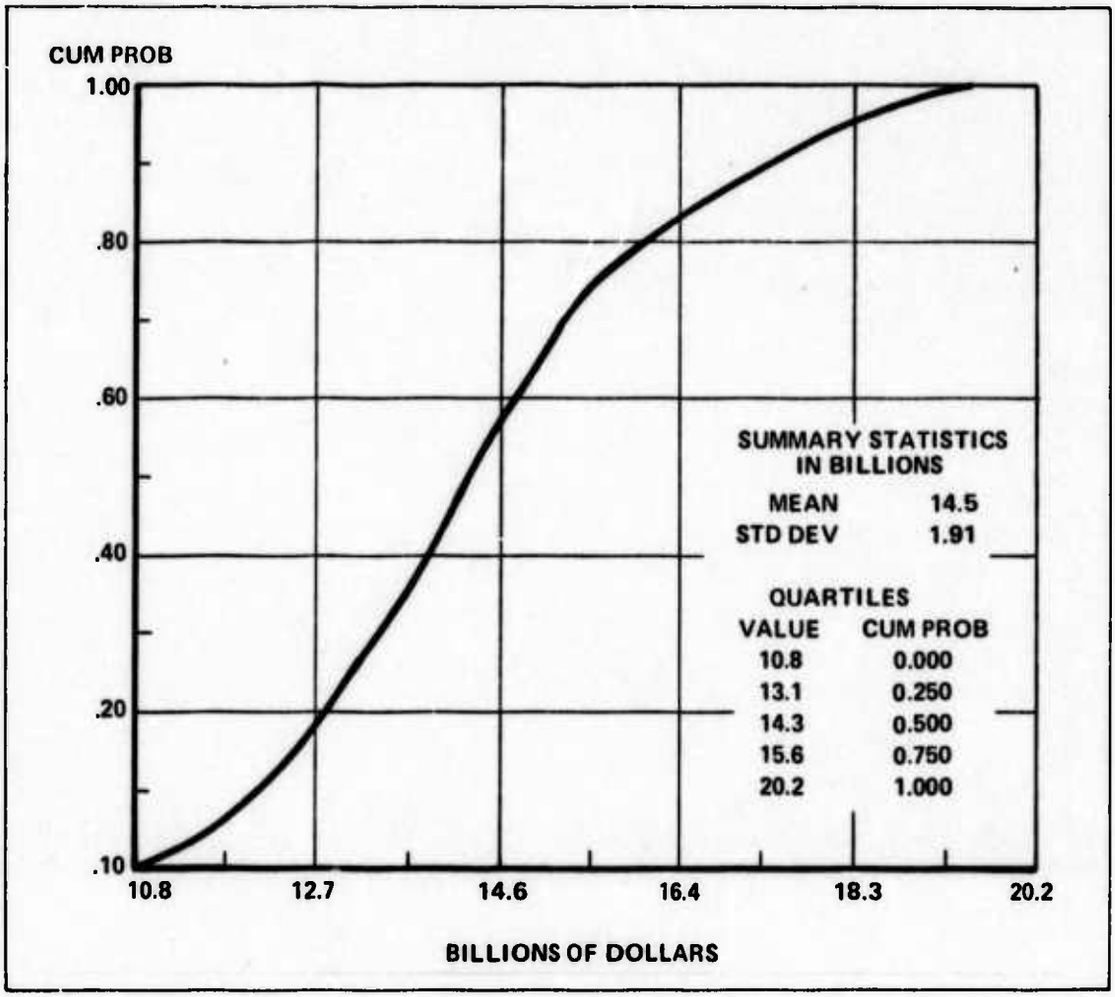

Figure 9.10-1. Procurement Cost in Billions of $74 vs Cumulative Probability

(MQT). The MQT is the final military qualification, normally 150 static test hours after which an engine is considered to be sufficiently developed for installation in a production aircraft. However, this amounts to only a portion of the development cost since development continues throughout the production cycle. A rule of thumb used by industry is that development cost doubles between MQT and 2000 production engines (Ref. 120). Thus, the total development cost is composed of cost to MQT plus a constant times the cost to MQT. The following equation was used to develop the cost to MQT for both the fossil fueled engine and the nuclear engine:

$$\ln DCMQT = -1.0774 + 0.07463\,DT + 0.47611 \ln THRMAX + 0.5112 \ln Mach$$

where DCMQT = development cost to MQT in million 73$
DT = development time in quarters*
THRMAX = maximum SLS thrust
Mach = maximum Mach number

* Twenty-four quarters (six years) is a reasonable time for development of a technologically advanced engine (Ref. 130).

Having calculated the cost to MQT, the 1973 dollars were converted to 1974 dollars using Table 9.2-1 and then the total development cost calculated by:

$$TDC = DCMQT + K \quad (DCMQT)$$

where TDC = total development cost
K = proportion of 2000 production engines.

The results are tabulated in Table 9.11-1.

TABLE 9.11-1. ENGINE DEVELOPMENT COST

	QUARTILES IN MILLIONS					
COST ELEMENT	0.00	0.25	0.50	0.75	1.00	MEAN
FOSSIL FUELED ENG.	60.4	293	399	538	820	415
NUCLEAR FUELED ENG.	255	493	601	743	1030	617

It was decided to consider the heat exchanger for the nuclear powered engine to be an additional cost toward its development cost. The cost estimating relationship was based only on engines with combustion sections and this would have to be a new development with virtually no past experience. Discussions with Aeronautical Systems Division (ASD), Advanced Missions (Ref. 132), indicated that the figure they used in their estimates was $20 million for heat exchanger development. This was then considered to be a deterministic input to the total development cost.

Reactor development cost is based on estimates from the same contractor that supplied reactor production costs in Section 9.4. The contractor's best estimate was $1.4 ± 0 5 billion for a 200 MW reactor. However, because of the range of the estimates, it was assumed that reactor power output had very little impact on this cost and therefore the estimate was also valid for a 475 MW reactor. This assumption was later confirmed during a visit to the contractor's facility.

Finally, the RDT&E cost for the fast acting safety valve was necessary. A conversation with the Chief of Test Engineering Division (Ref. 164), Sandia Laboratories, suggested a figure of $25 million to develop a safe and reliable valve. The reason it is this expensive is because of the required interface with the wall of the containment vessel which is a compound curve. The cost was considered to be deterministic. The summation of all the development costs is contained in Table 9.11-2.

TABLE 9.11-2. TOTAL DEVELOPMENT COST

	QUARTILES IN BILLIONS					
COST ELEMENT	0.00	0.25	0.50	0.75	1.00	MEAN
TOTAL DEV. COST	2.07	2.59	2.78	2.96	3.66	2.79

9.12 ACQUISITION COST

As illustrated in Section 9.0, acquisition cost is defined to be the sum of the procurement cost and the RDT&E cost. The distribution for acquisition cost is contained in Figure 9.12-1. This figure can be interpreted that the acquisition cost will lie in the range $13.7-22.9 billion. The expected acquisition cost is $17.4 billion with the median being $17.0 billion.

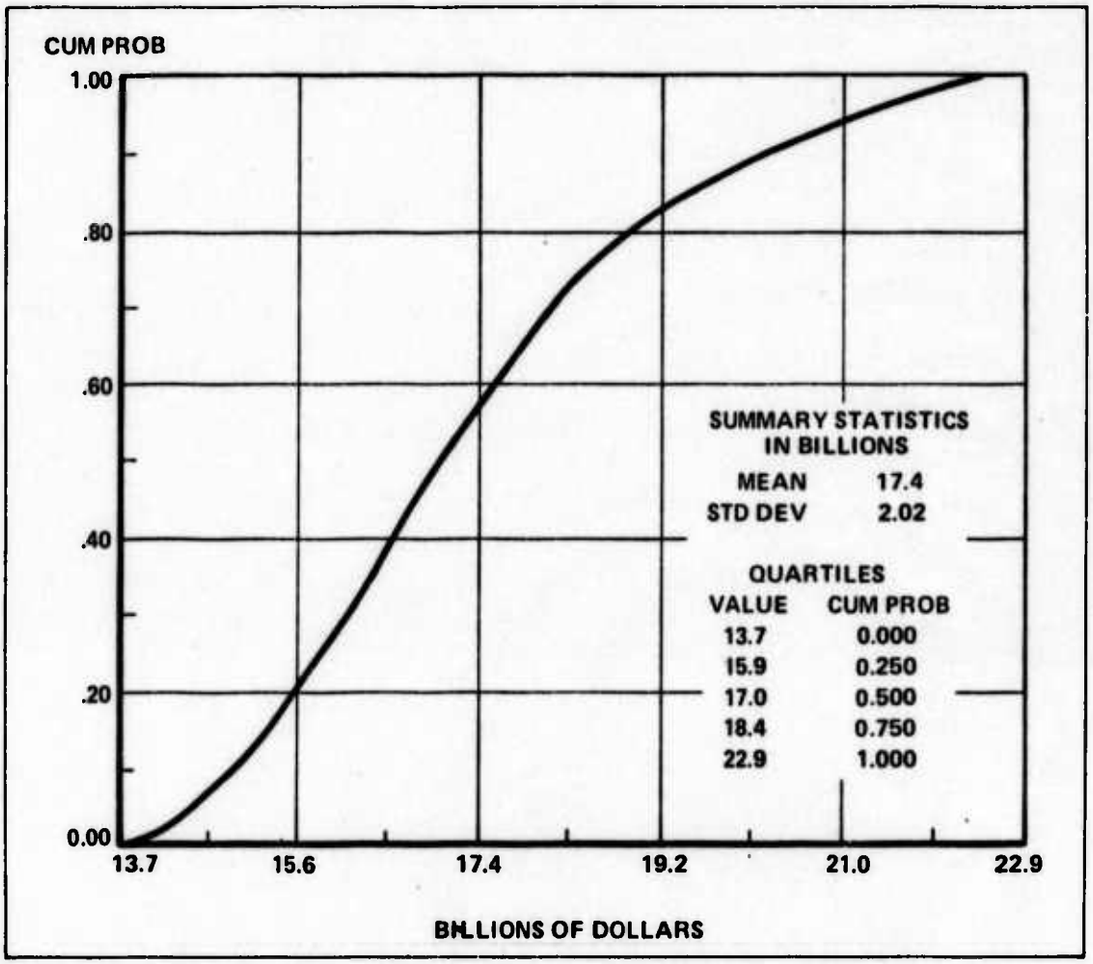

Figure 9.12-1. Acquisition Cost in Billions of $74 vs Cumulative Probability

9.13 TEN YEAR OPERATING AND SUPPORT COST

The intent of this study was to determine a life cycle cost for a fleet of nuclear powered aircraft. A large portion of the life cycle cost is contained in the operating and support (O&S) costs which are recurring costs. The method used to estimate the O&S cost was patterned after the Planning Aircraft Cost Estimating (PACE) Model contained in AFM 173-10. This model has been used to calculate the O&S costs for every type of aircraft squadron in the Air Force. A similar model has been developed by the Cost Analysis Improvement Group (CAIG) for use in preparing new aircraft system operating and support cost estimates for the Defense Systems Acquisition Review Council. Since the two methods are almost identical, the PACE model was arbitrarily chosen to determine the O&S cost for the nuclear powered aircraft.

The PACE model is an organized bookkeeping scheme with which one can arrive at an estimate of the cost to operate one squadron of aircraft. The model has been used to develop a point cost to operate an aircraft squadron. This study, however, used variable inputs with the PACE model to arrive at an overall distribution of O&S costs.

The model is broken down into different cost elements with less obvious elements being defined below (Ref. 5):

Replenishment Spares: This estimate reflects the cost of replenishment spares, components, and repair parts that are identified as investment items and which are obtained as follow-on procurement primarily in support of the flying hour program.

Class IV Mod and Spares: This element estimates the correction of operationally revealed deficiencies.

Common Age and Spares: This element represents the cost of procuring replacement of common ground servicing equipment, maintenance, and repair shop equipment, instruments and laboratory test equipment, and other miscellaneous items including equipment spares.

Primary Program Element: An aggregate of personnel required to make the squadron function properly, i.e., crew, maintenance, munitions, security, and wing/squadron staff.

System Support Material: Material purchased from the System Support division for maintenance of the aircraft. This material includes centrally procured expense items such as non-repairable spares.

General Support Material: Material purchased from the General Support Division. These materials include decentrally managed expense items such as aircraft, electronic and communications repair parts, plus base consumables.

Base Operating Support: This element represents the cost of paying base support personnel needed to handle the workload generated by Squadron Operations.

Depot Maintenance: This element includes the cost of maintenance performed on material requiring major overhaul or complete rebuilding of parts.

Rec/Tech Training: This element represents the cost of paying men in the non-flying training pipeline who will replace personnel who annually attrite from squadron and base service functions.

Inputs used with the PACE Model are contained in Table 9.13-1. The number of aircraft per squadron was arbitrarily chosen to be 20, so that personnel requirements could be compared to existing personnel strengths for large aircraft. The flying hours per aircraft were obtained from Section 2 for the high and most likely values. The low value was chosen to be that of a C-130, which has the highest utilization rate in the Air Force today. The crew ratio was based on a crew being available 10 months of the year and flying two crews per month. This implies

that 2.2 crew years per aircraft year are required for each 14 day mission; the crew ratio is 6.6 times the utilization rate. Items 6 through 14 were obtained from expert opinion (Ref. 12). Items 15, 16, and 17 were extracted from AFM 173-10. The last five items are functional relationships developed by Mr. John Dorsett (Ref. 42). These relationships were developed from the data base that was used to develop inputs in the PACE Model for the Airborne Warning and Control System (AWACS) airplane. The data base included data from ten aircraft including C-5A, C-141, KC-135, B-52H and B-52G.

TABLE 9.13-1. PACE MODEL INPUTS

	LOW	MOST LIKELY	HIGH
1 NUMBER OF AIRCRAFT PER SQUADRON		20	
2 TOTAL FLYING HOURS PER YEAR	1440	4185	6136
3 TOTAL JP-4 FLYING HOURS PER YEAR	13	38	55
4 TOTAL NUCLEAR FUEL HOURS PER YEAR	1427	4147	6081
5 CREW RATIO	1.08	3.15	4.62
6 PRIMARY PROGRAM ELEMENT CIVILIAN	110	167	225
7 PRIMARY PROGRAM ELEMENT OFFICER	180	425	616
8 PRIMARY PROGRAM ELEMENT AIRMAN	1242	2099	2891
9 BASE OPERATING SUPPORT CIVILIAN	65	114	158
10 BASE OPERATING SUPPORT OFFICER	5	9	13
11 BASE OPERATING SUPPORT AIRMAN	190	334	463
12 MEDICAL CIVILIAN	5	9	13
13 MEDICAL OFFICER	18	31	43
14 MEDICAL AIRMAN	6	11	15
15 OFFICER PAY & ALLOWANCES		18,334	
16 AIRMAN PAY & ALLOWANCES		8202	
17 CIVILIAN	6221	11,497	16,671

18 BASE MATERIAL SUPPORT = −780.0 + 154.3 LNGW

19 REPLENISHMENT SPARES FACTOR = 206.6 − 0.426SP + 1.8 AW

20 DEPOT MAINTENANCE/FLYING HOUR FACTOR = − 1270.3 + 351.4 LNAW

21 DEPOT MAINTENANCE/AIRCRAFT = 700.0 − 280.2 LNSP + 276.0 LNAW

22 COMMON AGE FACTOR = EXP | −10.3 −0.3 LNAV +2.3 LNGW|

WHERE:
GW = GROSS WEIGHT
AW = AMPR WEIGHT
SP = MAX SPEED
AV = AVIONICS COST

The input factors were then inserted into the PACE Model to yield the results contained in Table 9.13-2. The model is classified CONFIDENTIAL due to deterministic values associated with some of the relationships and, therefore, is not presented here. However, a copy of the PACE Model relationships can be found in the classified portion of this study, Volume III.

These relations are quite numerous and self-explanatory. An example of one of the relations and the way it was used is provided by the determination of aviation fuel cost:

aviation fuel = (number of hours using aviation fuel) (gallons of fuel used per hour) (fuel cost per gallon) (number of aircraft).

TABLE 9.13-2. PACE MODEL SUMMARY

	MILLIONS				
	0.00	0.25	0.50	0.75	1.00
PRIMARY PROGRAM ELEMENTS					
REPLENISHMENT SPARES	27.6	71.4	96.4	125.0	204.0
CLASS IV MOD PLUS SPARES	27.6	71.4	96.4	125.0	204.0
COMMON AGE PLUS SPARES	27.6	71.4	96.4	125.0	204.0
TOTAL APPROPRIATION 3010	55.3	93.3	119.0	143.0	225.0
CIVILIAN PAY	55.3	93.3	119.0	143.0	225.0
MISC SUPPORT	[illegible]	[illegible]	[illegible]	[illegible]	[illegible]
AVIATION FUEL	0.7	1.6	2.0	2.2	2.8
*NUCLEAR FUEL	42.0	94.2	117.0	140.0	206.0
SYSTEM SUPPORT MATERIAL	42.0	94.2	117.0	140.0	206.0
GENERAL SUPPORT MATERIAL	42.0	94.2	117.0	140.0	206.0
TOTAL APPROPRIATION 3400	64.7	123.0	149.0	175.4	249.7
OFFICER PAY	64.7	123.0	149.0	175.4	249.7
AIRMAN PAY	64.7	123.0	149.0	175.4	249.7
TOTAL APPROPRIATION 3500	17.5	22.4	25.0	27.1	32.7
BASE OPERATING SUPPORT					
CIVILIAN PAY	17.5	22.4	25.0	27.1	32.7
MISC. SUPPORT	17.5	22.4	25.0	27.1	32.7
TOTAL APPROPRIATION 3400	17.5	22.4	25.0	27.1	32.7
OFFICER PAY	17.5	22.4	25.0	27.1	32.7
AIRMAN PAY	17.5	22.4	25.0	27.1	32.7
TOTAL APPROPRIATION 3500	17.5	22.4	25.0	27.1	32.7
TOTAL BOS	4.6	5.6	6.0	6.5	7.5
DEPOT MAINTENANCE					
DEPOT MAINTENANCE	44.0	82.0	99.1	115.0	157.0
PERSONNEL SUPPORT					
MED CIVILIAN PAY	44.0	82.0	99.1	115.0	157.0
PROGRAM VIII MISC SUPPORT	44.0	82.0	99.1	115.0	157.0
MED O&M NON-PAY	44.0	82.0	99.1	115.0	157.0
TOTAL PROGRAM VIII APP 3400	0.7	0.9	0.9	1.0	1.1
OFFICER PAY	0.7	0.9	0.9	1.0	1.1
AIRMAN PAY	0.7	0.9	0.9	1.0	1.1
PCS OFFICER	0.7	0.9	0.9	1.0	1.1
PCS AIRMAN	0.7	0.9	0.9	1.0	1.1
TOTAL PROGRAM VIII APP 3500	3.8	4.7	5.1	5.5	6.4
SIMPAK TOTALS	293.0	401.0	442.0	481.0	608.0

*ADDITION TO PACE MODEL

The input to the model for fuel O&S costs was modified to account for 3 hours of JP-4 fuel use per flight instead of the entire flight using JP-4. The nuclear fuel costs were then added to the model. Nuclear fuel costs were obtained from the following relationship:

$$\text{Nuclear fuel cost} = \left(\frac{\text{hrs used by reactor}}{10{,}000}\right)\left(\frac{\text{reactor cost}}{3}\right)(\text{NR. of ACFT})$$

(Ref. 86)

The results of similar calculations from the PACE Model were then summed and multiplied by the appropriate discount factors for ten successive years. The discount factors used are in Table 9.13-3. The discounted dollars were used because dollars that buy resources today are worth more than dollars tomorrow. Thus, before we can meaningfully add together dollars spent in different periods "we must discount" future dollars, for they are worth less than current dollars. Table 9.13-4 displays the discounted squadron cost.

TABLE 9.13-3. DISCOUNT FACTOR AT 10%

YEAR	FACTOR	YEAR	FACTOR
1	1.0000	6	0.6209
2	0.9091	7	0.5645
3	0.8264	8	0.5132
4	0.7513	9	0.4665
5	0.6830	10	0.4241

The discounted squadron costs were then multiplied by three to account for the fleet of 60 aircraft. This distribution is contained in Table 9.13-5.

TABLE 9.13.4. OPERATING & SUPPORT COST FOR 20 AIRCRAFT, DISCOUNTED OVER 10 YEARS

	QUARTILES IN BILLIONS					
COST ELEMENT	0.00	0.25	0.50	0.75	1.00	MEAN
10 YR. O&S COST FOR 20 AIRCRAFT	2.03	2.73	2.98	3.24	4.02	3.00

TABLE 9.13-5. OPERATING & SUPPORT COST FOR 60 AIRCRAFT, DISCOUNTED OVER 10 YEARS

	QUARTILES IN BILLIONS					
COST ELEMENT	0.00	0.25	0.50	0.75	1.00	MEAN
10 YR. O&S COST FOR 60 AIRCRAFT	6.22	8.24	8.93	9.66	11.8	8.98

9.14 LIFE CYCLE COST

The entire life cycle cost or program cost for a fleet of 60 nuclear powered aircraft is the sum of airframe, propulsion, avionics, peculiar support, and initial spares, RDT&E, and 10 year O&S cost. This cost is estimated in 1974 constant dollars and is contained in Figure 9.14-1. This graph means that the funds that would have to be committed, if a nuclear aircraft program were undertaken, is in the range of $21.5-32.7 billion for the program from birth to death. The expected cost would be $26.4 billion with the median being $26.1 billion.

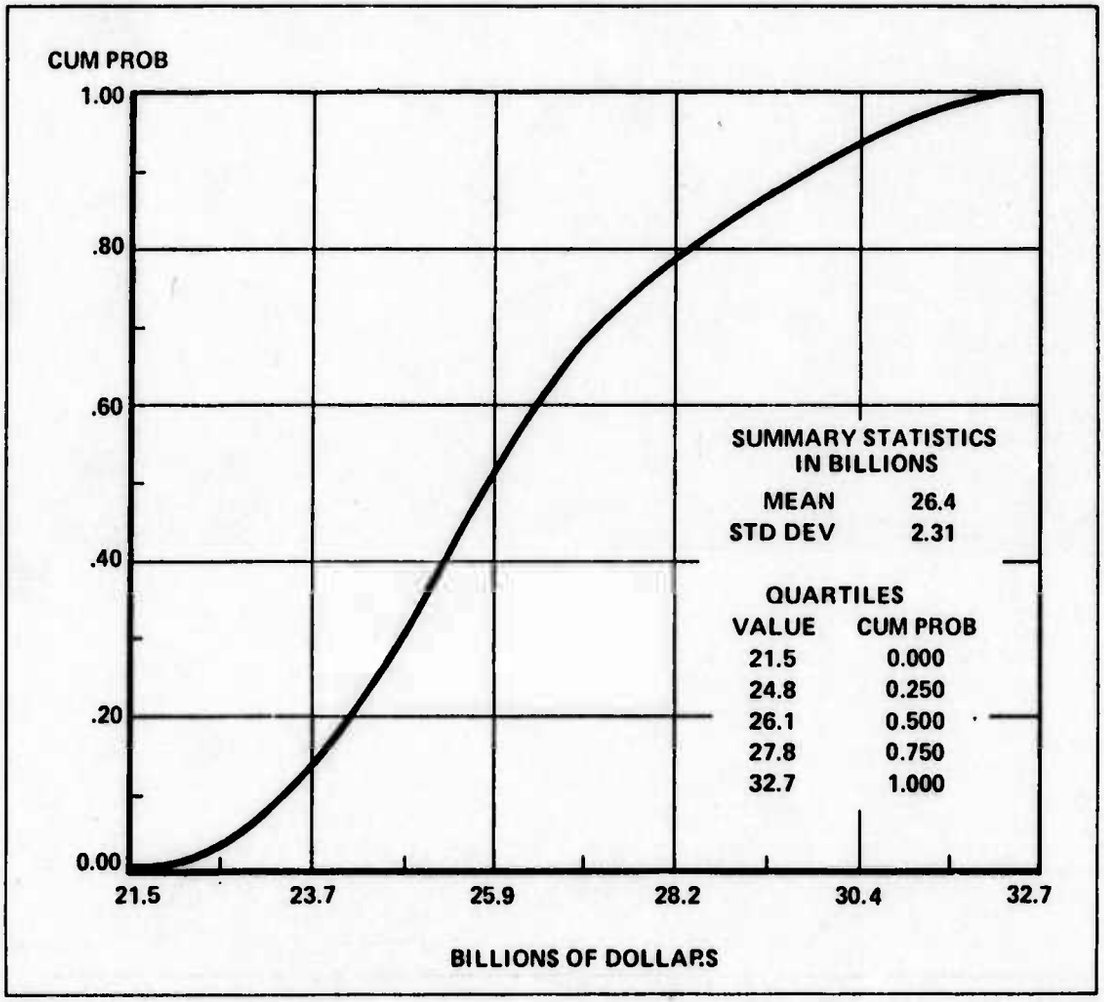

Figure 9.14-1. Ten Year Life Cycle Cost for 60 Production Aircraft vs Cumulative Probability

SECTION 10
SUMMARY

10.1 BACKGROUND

The last major effort to develop a nuclear powered airplane was the Aircraft Nuclear Propulsion (ANP) Development Program which was terminated in 1961. The technology of that decade was such that the program was unable to meet its design objectives, and a nuclear powered airplane was deemed infeasible.

Since 1961, a combination of several factors has caused a renewed interest in the concept of a nuclear powered airplane. First the United States is no longer self sufficient in meeting its energy demand, in that it is now dependent on foreign sources for a major portion of its oil needs. Several alternative forms of energy are being studied in an effort to relieve the dependence on foreign oil, with hydrogen, methane, and nuclear fuels being considered for aircraft propulsion.

Second, significant improvements have been made in nuclear technology since 1961. Of particular importance are developments in high temperature, gas-cooled and liquid metal-cooled reactors, and the production of nuclear fuels with higher power densities and longer lifetimes. Collectively, these developments have given support to the concept of a relatively lightweight nuclear power system that may be used for aircraft power.

Finally, changes in the performance requirements for a nuclear powered aircraft have made feasibility easier to attain. The earlier programs sought an aircraft with supersonic speed capability; however, this capability is no longer a prerequisite. The criteria now simply involve the replacement of fossil fueled aircraft in the performance of Air Force missions.

While these factors have changed so as to support the concept of a nuclear powered airplane, another factor, that of public safety, has changed in exactly the opposite fashion. The public is now acutely aware of the potential hazards of any nuclear power system; therefore, public safety must now be a major design consideration. This concern requires the expenditure of considerable design effort to insure that a nuclear powered airplane does not pose an unacceptable hazard to the public.

The objective of this study was to assess, through a comprehensive systems engineering analysis, the feasibility of applying nuclear propulsion to aircraft in the performance of the Air Force mission.

The specific major areas of study addressed in this report are: (1) mission, (2) avionics, (3) aircraft, (4) propulsion system, (5) safety, and (6) cost. The propulsion system is further divided into three sections: reactor, engines, and heat transfer system. This summary first presents the major details and the results obtained from each section of the report. Next, a systems integration summary is presented which is then followed by the conclusions and recommendations.

10.1.1 MISSION (Section 2): In the early phase of the study, it was determined that a large, subsonic, nuclear powered aircraft could conceivably perform several Air Force missions. These missions were: (1) antisubmarine warfare (ASW), (2) strategic airlift, (3) command and control, (4) airborne warning and control, and (5) airborne missile launch. The ASW mission was chosen as the point design mission because it readily lent itself to the operational nuclear safety considerations and because an aircraft designed for this mission could easily be adapted to perform other missions.

Mission requirements were estimated from an analysis of projected enemy submarine capabilities. Design parameters were developed based on the aircraft performance that was necessary to fulfill the mission requirements. A summary of the aircraft and mission parameters is presented in Table 10.1.1-1. Parameters were selected using the following bases:

1) The two week mission duration is based on human factors. Studies predict that fatigue, boredom, vibration, etc., would impair flight safety after two weeks (Section 2).

2) The crew component of 36 men assumes three shifts of 12 men each, performing mission related jobs for eight hours per day. The 12 man crew is based on Navy studies for an advanced ASW aircraft and is comprised of a four man flight crew and an eight man tactical crew.

3) The 150 to 350 kts airspeeds are based on airspeeds currently used by the Navy during ASW operations. It was anticipated that there would be no significant increase in the speed of a submarine in the time frame addressed in this report. Consequently, current Navy ASW operations speeds were deemed sufficient.

4) The requirement that the aircraft be able to operate from sea level to 30,000 ft is compatible with projected ASW sensor capabilities.

5) The 130,000 to 200,000 lb payload is based on projected weights of avionics and expendables as outlined in Sections 2 and 3.

6) The takeoff and landing distances insure that the nuclear aircraft will be capable of using existing DoD airfields.

7) The nuclear powered aircraft was assumed to have unlimited range, therefore, the radius of action was not of concern in this design study.

8) The fleet size of 60 aircraft is based on an assumption that no more aircraft will be built than the number of Submarine-Launched Ballistic Missile submarines allowed by the Strategic Arms Limitations Talks.

9) It was assumed that at least 20 years would be required to develop a nuclear powered aircraft. The initial operational capability would then occur during the decade of the 1990s.

10) The aircraft lifetime of 62,000 hrs is based on the current high airframe time experience of large commercial transports as discussed in Section 2.

TABLE 10.1.1-1. AIRCRAFT/MISSION PARAMETERS

MISSION DURATION (HRS)	336 (2 WEEKS)
CREW COMPONENT	36 MEN (3 SHIFTS OF 12 MEN)
AIRSPEED (KTS)	150 AT SEA LEVEL 250-350 AT 30,000 FEET
ALTITUDE (FT)	SEA LEVEL TO 30,000
PAYLOAD (LBS)	MINIMUM 130,000 MAXIMUM 200,000
TAKEOFF DISTANCE	CLEAR A 35 FT OBJECT IN 12,000 FEET
LANDING DISTANCE	CLEAR A 50 FT OBJECT AND STOP IN 12,000 FEET
FLEET SIZE	60 AIRCRAFT
IOC	1990-2000
LIFETIME	62,000 FLYING HOURS

10.1.2 AVIONICS (SECTION 3): The avionic equipment required to perform an ASW mission was defined by establishing functional subsystems to meet mission requirements. The mission duration was assumed to be up to 14 days. The problem was to determine the impact on total avionic system weight when redundancy of avionic subsystems was used to achieve a 14 day mission. Weight,volume, power, and reliability estimates were obtained for each avionic subsystem. Assuming an order of magnitude improvement in mean-time-between-failure over present day systems, and by applying redundancy, the overall system weight, volume, and power requirements were estimated as a function of time. These estimates were obtained by minimizing system weight subject to reliability constraints. The method of generalized La-Grange Multipliers was used to accomplish this task. Figure 10.1.2-1 plots the avionic system weight as a function of mission duration, system reliability, and component reliability. The dashed lines in the figure indicate the average number of subsystems which must be connected in parallel in order to meet a specified mission length and reliability. For example, if the total system were specified to be 0.90 reliable over a four day period, then the minimum system weight would be approximately 8,000 lbs. The resulting system has an average quadruple redundancy for each subsystem. Other combinations of redundancy, system reliability, and mission duration can be found in a similar manner. For a 0.95 reliable mission lasting 14 days, the weight, volume, power, and average subsystem redundancy are 28,000 lbs, 600 cu ft, 240 KVA, and 10, respectively. Note that this latter volume is less than 1% of the total aircraft fuselage volume.

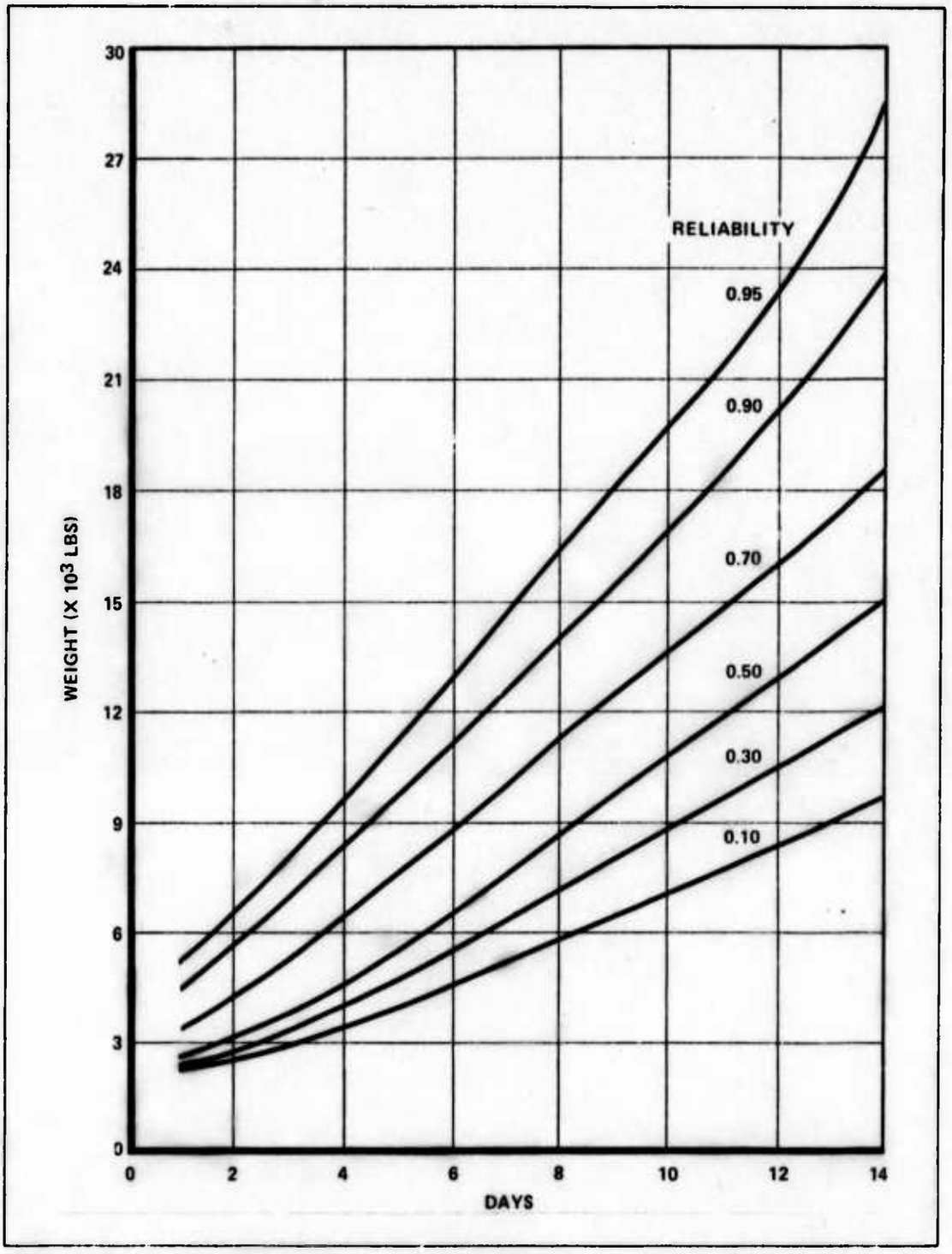

Figure 10.1.2-1. Redundancy Required to Meet System Reliability and Mission Length

10.1.3 AIRCRAFT (Section 4): Standard aerodynamic design analysis was used to determine an aircraft design which would fulfill an ASW mission and use nuclear power to the best advantage. Three factors, taken together, resulted in the selection of an aircraft of two million pounds gross weight for the point design. First, was an assumption that the aircraft's initial operational capability would occur during the decade of the 1990s (Section 2). Based on

empirical technology extrapolations, this time period placed an upper technology limit of 2,000,000 lbs gross weight for the aircraft. Second, was an assumption that the aircraft would operate from existing Air Force runways. This restriction also imposed a 2,000,000 lbs gross weight upper limit with respect to takeoff and landing distance and conventional landing gear capability. Finally, because of the large weight of the nuclear propulsion system (800,000 to 1,000,000 lbs), it was deemed necessary to use the 2,000,000 lbs as the design point gross weight to obtain any payload at all.

After selection of the gross weight, several configurations were considered for the point design aircraft. A canard design was selected as the configuration offering the most advantage. With the selection of the gross weight and configuration, aircraft weight and balance, dimensions and configuration, and performance were estimated.

Both aluminum and advanced composite construction were examined along with the required weight of chemical fuel to determine the weight available for the nuclear propulsion system and the payload. Table 10.1.3-1 summarizes the point design weight and balance for the following four options:

1) Standard aluminum construction and a chemical fuel capability for takeoff, landing, and a 500 to 1000 nm emergency cruise range.

2) Standard aluminum construction, but using a chemical fuel capability to supplement nuclear power only during takeoff and initial climb.

3) Advanced composite construction using the composite offering the best weight-saving potential. Chemical fuel is again used for takeoff, landing, and emergency cruise in this option.

4) The same composite construction as in option 3, but with chemical fuel used only to supplement nuclear power only for takeoff and initial climb.

Table 10.1.3-2 details the dimensions and configurations of the point design aircraft. The 60 lbs/sq ft wing/canard loading was found to be optimum considering the mission requirements, lift-to-drag ratio, and required thrust. This wing loading yields a very large wing and a canard with almost the same area as the C-5A wing. Figure 10.1.3-1 shows a comparison of the point design and a C-5A aircraft.

A performance analysis summarized in Figure 10.1.3-2 yielded the aircraft flight envelope and the takeoff and landing parameters. The flight envelope is for a clean aircraft flying straight and level. Maximum speed is a result of total thrust available and the airfoil selected. Landing distance is nearly the same as takeoff distance which is to be expected since every landing is made at almost maximum gross weight. The landing deceleration calculations assumed normal wheel-braking only.

TABLE 10.1.3-1. AIRCRAFT WEIGHT AND BALANCE SUMMARY — 2,000,000 LB GW

	COMPONENT WEIGHT (LBS)			
	A	B	C	D
WING WEIGHT	267,200	267,200	112,224	112,224
CANARD WEIGHT	31,200	31,200	14,664	14,664
VERTICAL STABILIZER WEIGHT	38,000	38,000	17,860	17,860
FUSELAGE WEIGHT	219,500	219,500	100,970	100,970
LANDING GEAR WEIGHT	111,000	111,000	111,000	111,000
TOTAL STRUCTURAL WEIGHT	666,900	666,900	356,718	356,718
FIXED EQUIPMENT WEIGHT	200,000	200,000	200,000	200,000
CHEMICAL ENGINE WEIGHT	50,000	14,000	50,000	14,000
CHEMICAL FUEL WEIGHT	320,000	80,000	320,000	80,000
TOTAL LESS NUCLEAR PROPULSION SYSTEM & PAYLOAD	1,236,900	960,900	926,718	650,718
AVAILABLE FOR NUCLEAR PROPULSION SYSTEM & PAYLOAD	763,100	1,039,100	1,073,282	1,349,282
CG LOCATION (FT)	265	250	260	255

A - STANDARD ALUMINUM CONSTRUCTION (SEC. 4.3.2) - TAKEOFF WITH CHEMICAL POWER (4.1.3)

B - STANDARD ALUMINUM CONSTRUCTION - TAKEOFF WITH NUCLEAR POWER (SEC. 4.1.3)

C - GRAPHITE/EPOXY ADVANCED CONSTRUCTION (SEC. 4.3.3) - TAKEOFF WITH CHEMICAL POWER

D - GRAPHITE/EPOXY ADVANCED CONSTRUCTION - TAKEOFF WITH NUCLEAR POWER

TABLE 10.1.3-2. AIRCRAFT DIMENSIONS AND CONFIGURATION
2,000,000 LBS GROSS WEIGHT

WING/CANARD LOADING (PSF)	60
ASPECT RATIO	9
TAPER RATIO	0.4
THICKNESS RATIO	0.18
WING QUARTER CHORD LOCATION (FT)	300
WING AREA (SQ FT)	27,800
WING SPAN (FT)	500
WING ROOT (FT)	79
WING TIP (FT)	32
WING MAC (FT)	59
FLAP AREA (% OF WING AREA)	20
SPEED BRAKE AREA (% OF WING AREA)	13
CANARD QUARTER CHORD LOCATION (FT)	60
CANARD AREA (SQ FT)	5600
CANARD SPAN (FT)	225
CANARD ROOT (FT)	36
CANARD TIP (FT)	14
CANARD MAC (FT)	27
VERTICAL TAIL QUARTER CHORD LOCATION (FT)	360
VERTICAL TAIL AREA (SQ FT)	4300
VERTICAL TAIL HEIGHT (FT)	86
VERTICAL TAIL ROOT (FT)	70
VERTICAL TAIL TIP (FT)	30
VERTICAL TAIL MAC (FT)	53
MAX FUSELEGE DIAMETER (FT)	40
FUSELEGE LENGTH (FT)	430
REACTOR LOCATION (FT)	300
REACTOR POWER (MW)	400 — 500
LANDING GEAR LOCATION (FT)	60, 265, & 335
LANDING GEAR LOAD FACTOR (g)	3
NUMBER OF TIRES	36
TIRE SIZE	56 x 16
AIRCRAFT FOOTPRINT (SQ IN.)	8700
AIRCRAFT PRESSURE PRINT (PSI)	230

NOTE: All locations from nose of aircraft.

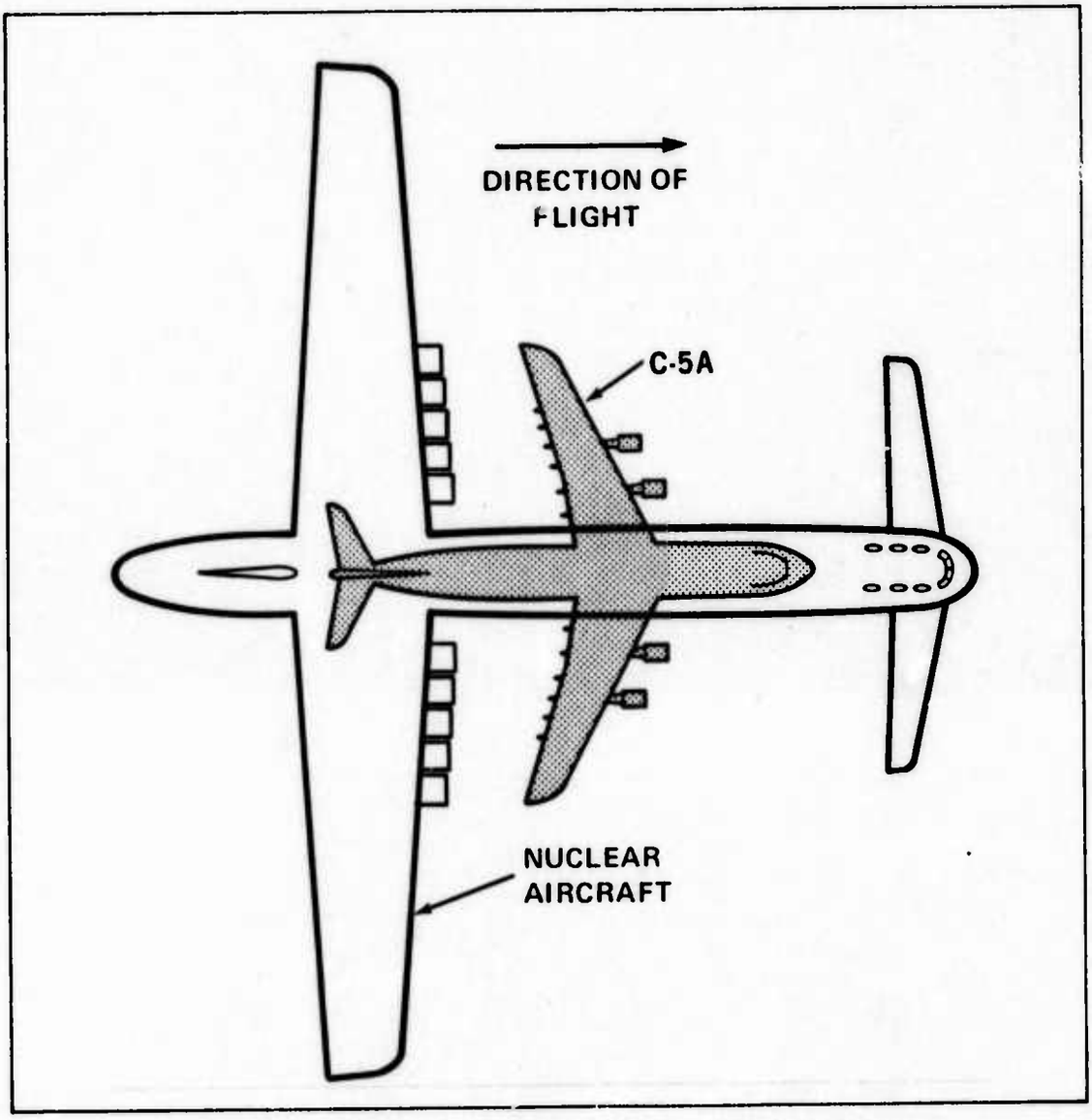

Figure 10.1.3-1. Nuclear Powered Aircraft - C-5A Comparison

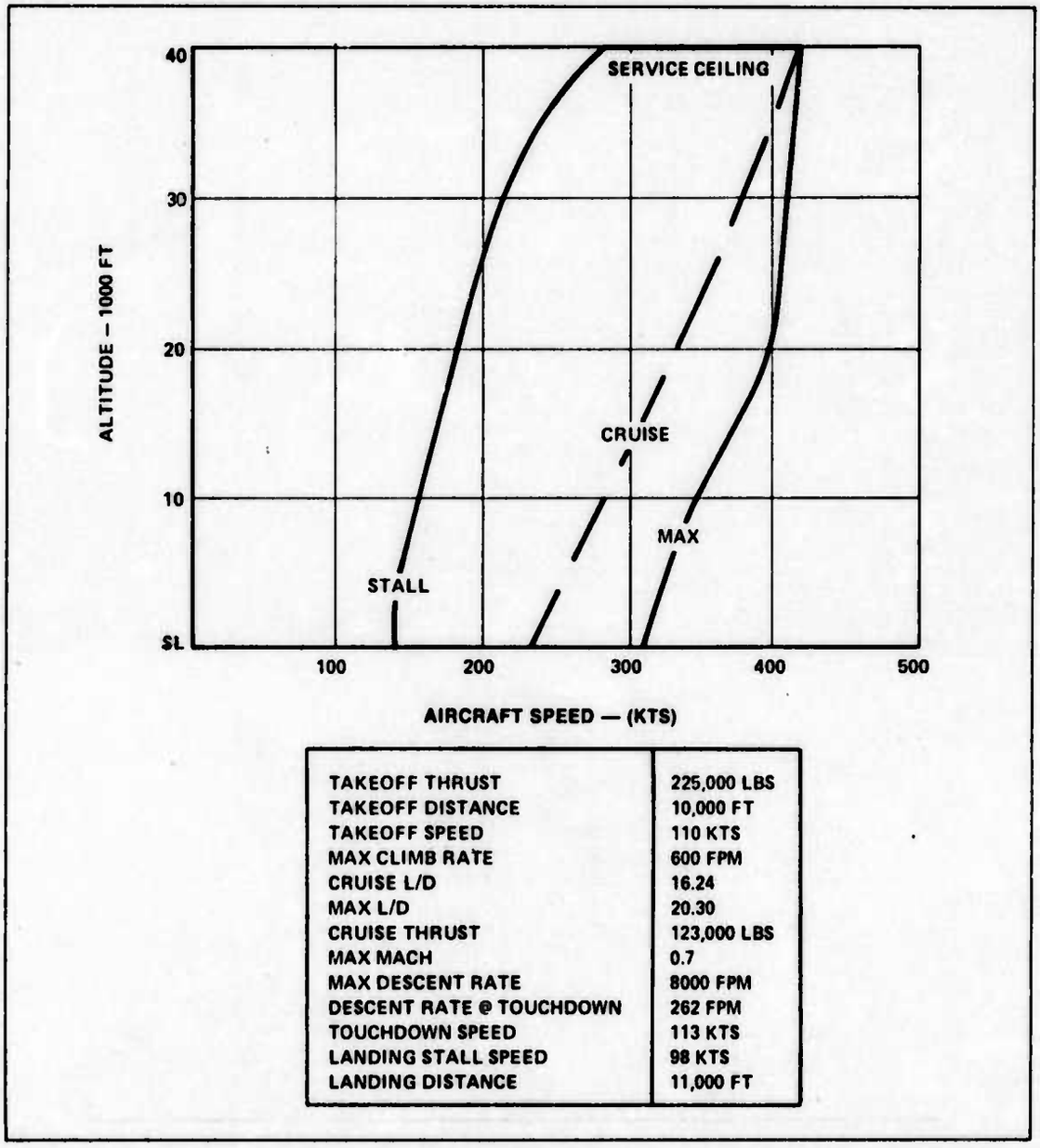

TAKEOFF THRUST	225,000 LBS
TAKEOFF DISTANCE	10,000 FT
TAKEOFF SPEED	110 KTS
MAX CLIMB RATE	600 FPM
CRUISE L/D	16.24
MAX L/D	20.30
CRUISE THRUST	123,000 LBS
MAX MACH	0.7
MAX DESCENT RATE	8000 FPM
DESCENT RATE @ TOUCHDOWN	262 FPM
TOUCHDOWN SPEED	113 KTS
LANDING STALL SPEED	98 KTS
LANDING DISTANCE	11,000 FT

Figure 10.1.3-2. Nuclear Powered Aircraft Performance - 2,000,000 lbs Gross Weight

10.1.4 REACTOR (Section 5): The reactor study assessed the applicability of three different reactor designs to aircraft propulsion by evaluating them in three different areas. First, it was determined whether or not the required reactor power could be achieved and how much the reactor would weigh. Second, the radiation effect on the crew and the public was assessed. Third, off-point design features were analyzed to determine whether or not weight reductions were possible for the configuration used in this study.

The three reactor designs used in the study included two high temperature gas cooled reactors and one liquid metal cooled reactor. The first gas cooled design considered was the "Low Specific Weight Reactor," a 10,000 hr lifetime reactor based on the nuclear rocket (NERVA) technology and designed by the Westinghouse Astronuclear Laboratory. The second gas cooled reactor was a 3000 hr lifetime reactor designed specifically for airborne application by King L. Mills at the University of Virginia (doctoral dissertation). The liquid metal cooled reactor was the NUERA II design by Westinghouse Astronuclear Laboratory, a 10,000 hr lifetime design using sodium-potassium (NaK) as a coolant.

Three different types of propulsion systems were proposed (see Sections 10.1.5 and 10.1.6), each requiring a different reactor power level. The three proposed systems are an indirect cycle liquid metal system, an indirect cycle gas system, and a direct cycle gas system, with power requirements as follows:

Liquid Metal System	475 MW
Indirect Cycle Gas System	574 MW
Direct Cycle Gas System	700 MW

Parametric data supplied by Westinghouse Corporation indicated that both their gas and liquid metal designs would supply the required power. The gas cooled design by Mills was a 200 MW point design, however scaling techniques were applied to scale the reactor to the required power levels.

Shown in Table 10.1.4-1 are the reactor weights for the combinations of reactors and propulsion systems considered in the study. It can be seen that the Mills design is substantially lighter than either Westinghouse design. This is due to two factors: (1) a 3000 hr lifetime vs 10,000 hrs for Westinghouse, and (2) substantially less radiation shielding in the radial direction (perpendicular to direction of crew).

TABLE 10.1.4-1. REACTOR WEIGHTS (LBS)

REACTOR	TYPE PROPULSION SYSTEM AND POWER REQUIRED		
	LIQUID METAL 475 MW	INDIRECT CYCLE GAS 574 MW	DIRECT CYCLE GAS 700 MW
WESTINGHOUSE LIQUID METAL	520,000	—	—
WESTINGHOUSE HIGH TEMP GAS**	—	740,000	810,000
K L MILLS* PROPOSED DESIGN	—	459,000	504,000

*WEIGHTS INCLUDE INTERMEDIATE HEAT EXCHANGER AND 2 IN. CONTAINMENT VESSEL

** 75% EFFECTIVENESS HEAT EXCHANGER

The radiation effect of the reactors was considered for two cases: the crew and the general public. The crews were assumed to be radiation workers and therefore restricted by law to a dose rate of not more than 5 rem per year, nor more than 3 rem in any quarter. It was also assumed that the reactors would have to meet AEC standards for light water reactors, with a maximum exposure of 5 rem/year to the general populace.

As presented in Section 4, the crew in the point design canard-type aircraft will be stationed at least 200 ft from the reactor. Taking into account only spherical attenuation, the crew will receive a dose rate of 0.05 mrem per hour for the Westinghouse reactor and 0.02 mrem per hour for the Mills reactor. Figure 10.1.4-1 shows the number of 14 day flights that the crew is allowed as a function of crew distance from the reactor. Note that with the canard design, the crew could be airborne all year without reaching their maximum allowable dose.

The three reactor designs can operate with the legal limits for the general populace (5 mrem/yr) if no one except the crew is allowed to remain within 4000 ft of the aircraft. The large increase in separation distance required over that of the crew is due to the radiation level in the lateral direction being as much as 6000 times that in the direction of the crew and the dose for the general populace being 1/1000 that of the crew. Figure 10.1.4-2 depicts the 3.5 mrem/hr isodose plot for the Mills reactor. The distance in the direction of the crew is 16 ft while the distance in the lateral direction is 800 ft.

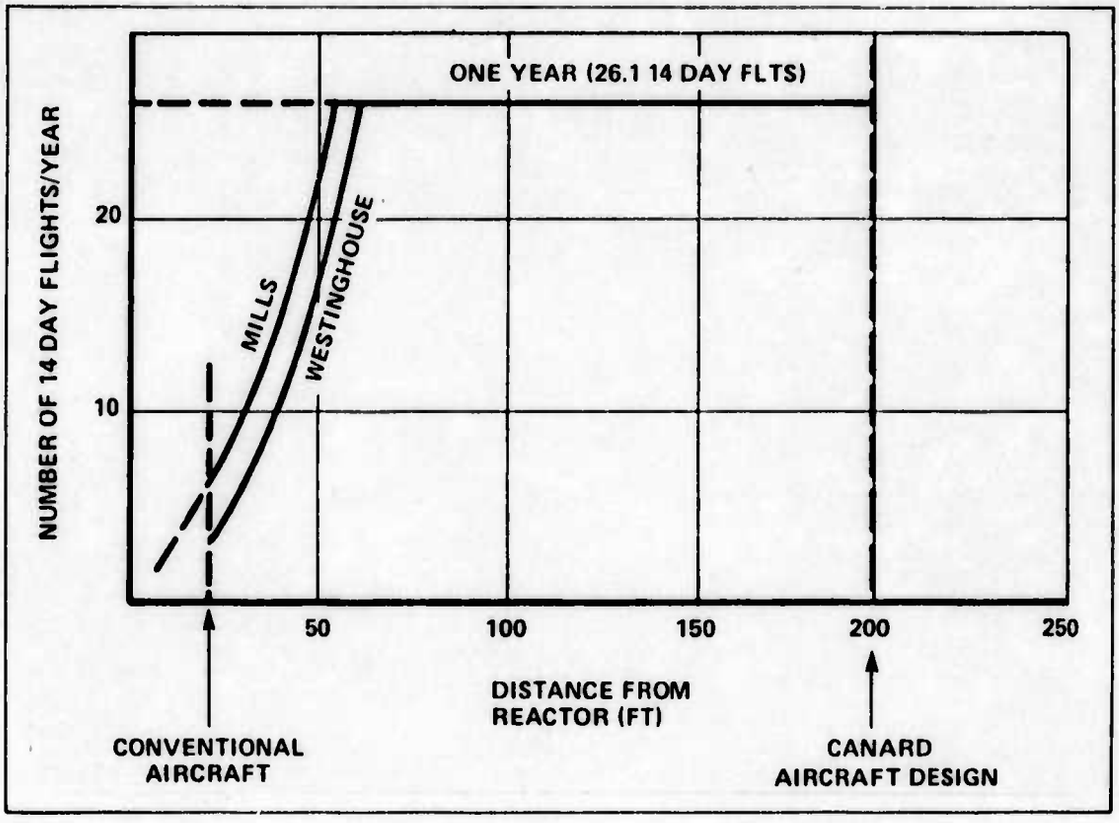

Figure 10.1.4-1. Number of Flights vs Distance from Reactor

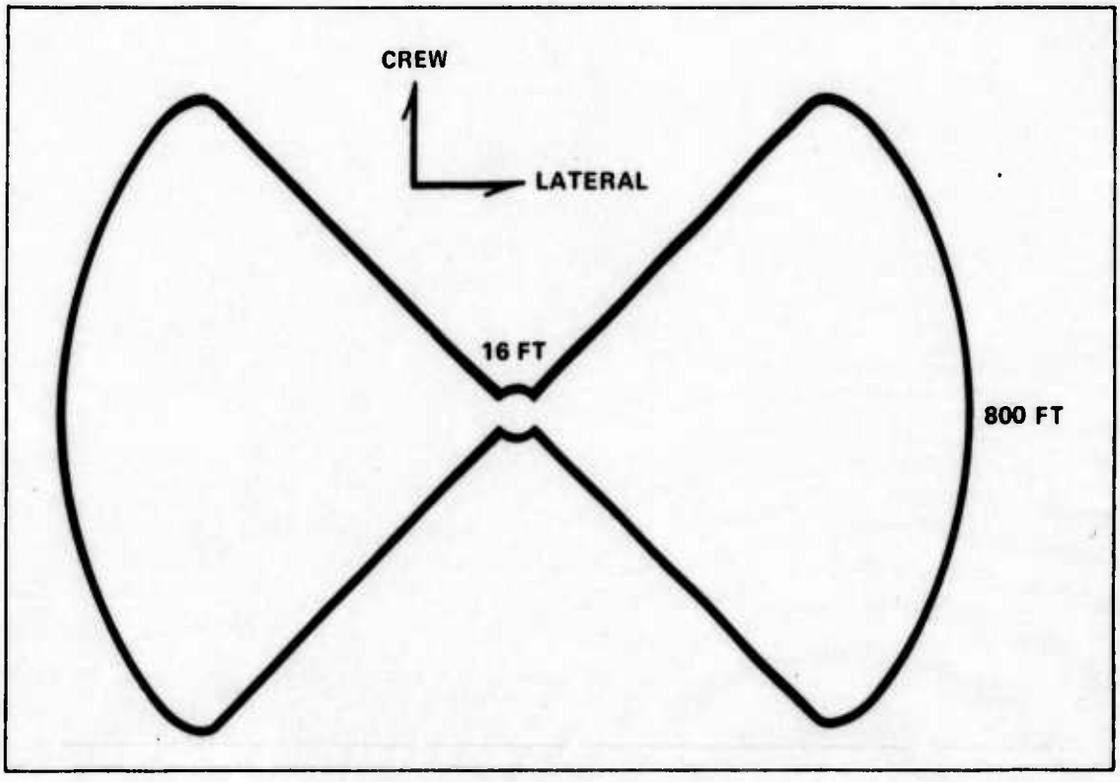

Figure 10.1.4-2. 3.5 Mrem/Hr Isodose

An analysis was performed to determine the amount of weight reduction possible by decreasing the shielding. The crew was assumed to fly ten 14 day flights per year of 1.49 mrem/hr. The shielding of the three reactors was then reduced until the crew would receive this much radiation at 200 ft. The results of the reduction are shown in Table 10.1.4-2.

TABLE 10.1.4-2. REACTOR WEIGHTS: ORIGINAL VS REDUCED SHIELDING

REACTOR	POWER (MW)	ORIGINAL WEIGHT (LBS)	REDUCED WEIGHT (LBS)
WESTINGHOUSE LIQUID METAL	475	520,000	N/A
WESTINGHOUSE GAS	574	740,000	719,000
	700	810,000	789,000
K L MILLS* PROPOSED DESIGN	574	452,000	442,000
	700	504,000	494,000

*WEIGHTS INCLUDE INTERMEDIATE HEAT EXCHANGER & 2 IN. CONTAINMENT VESSEL

The reactor study provided the following information. The nuclear reactors proposed are capable of supplying the power necessary. The weights of the systems can be reduced by redesigning for application to the canard type aircraft.

10.1.5 ENGINES (Section 6): Two turbofan engine concepts using nuclear energy were evaluated. First, an indirect system was considered in which air as the working fluid is heated in a heat exchanger. The heat exchanger is located between the compressor exit and the turbine inlet. The second concept was a direct engine system in which helium is used as the

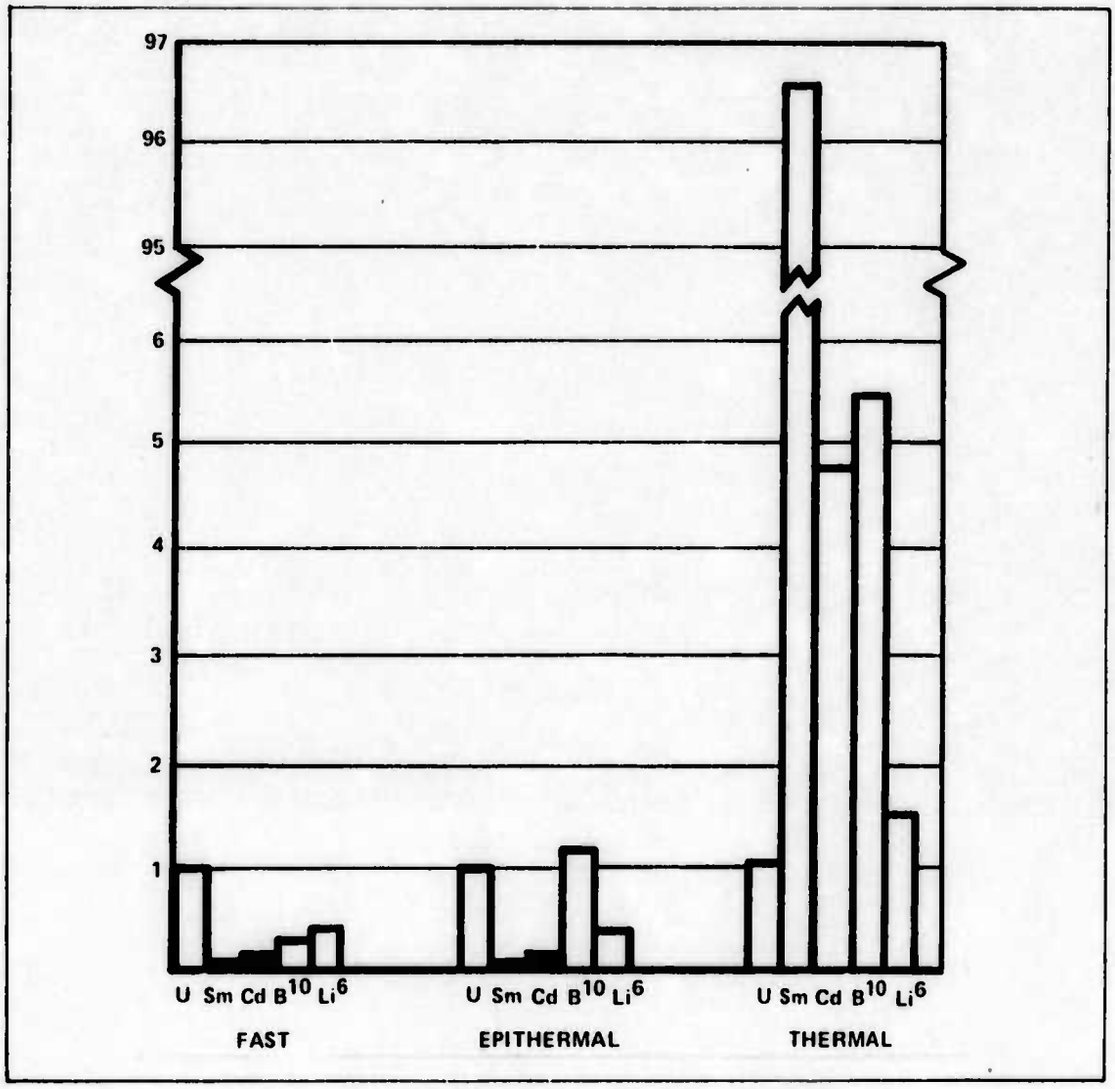

Figure 10.1.4-3. Absorption Cross Section Ratio

working fluid in a closed cycle gas turbine engine, and the net useful work is used to drive a ducted fan.

In the indirect system concept, either a dual mode engine which operates as a heat exchanger turbofan or a JP-4 combustion driven turbofan, or strictly a dedicated nuclear engine may be used.

The direct engine system was considered in two different configurations. One configuration uses a gas turbine generator located in each engine and the other uses two gas turbine generators centrally located in the fuselage. For the central turbine configuration, power is transmitted to the engines via shafts and gear trains housed in the wings. Within this concept, the Brayton cycle and the Brayton cycle with regeneration were evaluated.

A necessary subsystem considered was a gas turbine generator-pump used to pump the helium through the reactor primary coolant loops. A similar subsystem was evaluated for pumping helium gas through the secondary coolant loops to the engines.

A block diagram depicting the organization of the overall engine systems study is shown in Figure 10.1.5-1.

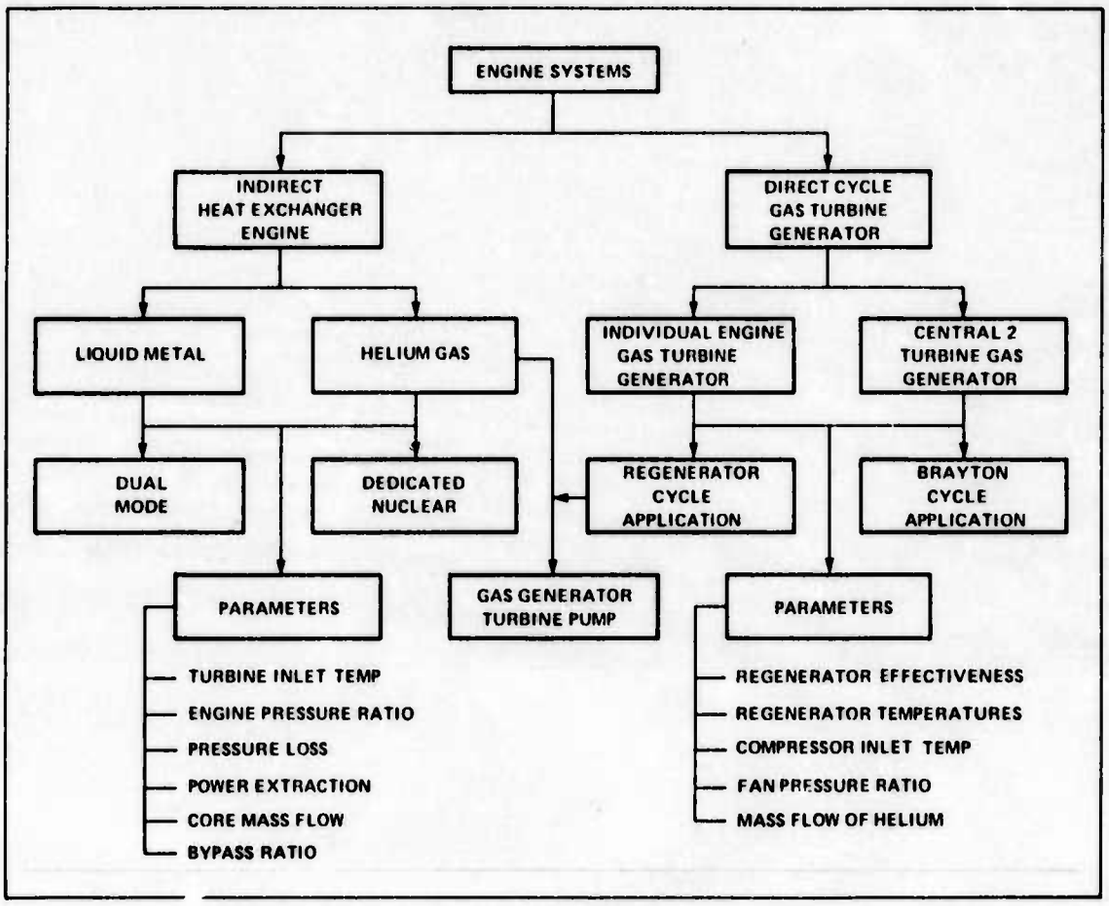

Figure 10.1.5-1. Engine Systems Study Diagram

An example of the effects of the engine parameters investigated on net thrust of the heat exchanger engine is summarized in Table 10.1.5-1. This table is for the base engine which has a bypass ratio of 4.0, engine core mass flow of 200 lbs/sec, and power extraction of 100 horsepower. Similar analysis was performed for several higher bypass ratios and is discussed in Section 6. From Table 10.1.5-1 it may be seen that a 5.1% change in turbine inlet temperature gives the greatest (8.2%) change in net thrust. Changing the bypass ratio will result in a different maximum net thrust at a different fan pressure ratio. A 16.7% decrease in overall engine pressure ratio will net a slight (1.9%) increase in thrust and a small (10%) reduction in compressor weight; however, to maintain the turbine inlet temperature, the reactor would have to be more powerful and therefore heavier. The increase in reactor weight offsets any engine weight saved.

TABLE 10.1.5-1. EFFECTS OF ENGINE PARAMETER VARIATIONS ON THE NET THRUST OF THE HEAT EXCHANGER TURBOFAN ENGINE

BASE ENGINE BYPASS RATIO 4.0 ENGINE CORE MASS FLOW 200 LBS/SEC POWER EXTRACTED 100 HP NET THRUST 14,580 LB			
PARAMETER	**BASE**	**% CHANGE IN PARAMETER**	**% CHANGE IN NET THRUST**
FAN PRESSURE RATIO	1.4	+ 14.3	+3.05
HORSEPOWER EXTRACTED	100.0	+900.0	–5.50
PRESSURE LOSS IN CORE%	11.0	+ 45.5	–2.36
TURBINE INLET TEMPERATURE, °R	1960	+ 5.1	+8.20
OVERALL ENGINE PRESSURE RATIO	16.8	– 16.7	+1.90

The regenerative cycle produced 11 to 25% more work (BTU/lb) than the standard Brayton cycle for the direct system concept. A detailed discussion of these two cycles and their performance is presented in Sections 6.2.4 and 6.2.5. Increasing the regenerative effectiveness from 0.75 to 0.90 would reduce the reactor output requirement by approximately 10%; however, the regenerator weight and volume increase with increasing effectiveness.

Table 10.1.5-2 gives a brief summary of several systems that resulted from this study.

10.1.6 HEAT TRANSFER (Section 7): Three different heat transfer systems were analyzed. Two systems were designed for the indirect cycle engines, one using NaK as a working fluid, and the other using helium gas. A third system was designed for the helium direct cycle engines.

All three systems were designed with similar cross flow, plate-fin reactor heat exchangers, with an effectiveness of 0.75. The reactor heat exchangers for the gas systems used a plate spacing of 0.1 in. with 46 fins/in. and weighed a total of 51,000 lbs. The liquid metal reactor heat exchanger used a plate spacing of .256 in. with 16.96 fins/in. and weighed a total of 6500 lbs.

Both concentric and parallel pipe configurations were analyzed. In the liquid metal system, the type of pipe made no significant difference in weight, but in the gas systems a savings of over 50,000 lbs was possible using the concentric pipes (65,000 lbs vs 12,000 lbs).

TABLE 10.1.5-2. ENGINE SYSTEM STUDY SUMMARY

TYPE ENGINE HORSEPOWER EXTRACTED	HELIUM 1300	HELIUM 200	LIQUID-METAL 500
INDIRECT ENGINE SYSTEM			
BYPASS RATIO	4.0	6.0	5.5
NET THRUST (LB)	12,600	15,200	14,750
NUMBER OF ENGINES	12	10	10
THRUST/MW	254	320	310
ENGINE WEIGHT (LBS)	13,680	16,800	15,600
TURBINE-PUMP WT.	11,000	18,000	—
TUR. PUMP MW REQ.	61.2	95.2	—
TOTAL MW	636	574	475
TOTAL ENG. SYSTEM WT.	18,700	181,000	160,000
DIRECT ENGINE SYSTEM			
NET THRUST (LB)	14,000	11,950	
NUMBER OF ENGINES	10	12	
THRUST/MW	220	206	
ENGINE WEIGHT (LBS)	7,111	6,714	
TURBINE-PUMP WT.	12,000	10,000	
TUR. PUMP MW REQ.	63.6	58	
TOTAL MW REQ.	700	754	
TOTAL ENG. SYSTEM WT.	83,110	90,568	

Although the concentric pipe arrangement offers a weight savings, it presents more problems in the areas of fabrication and inner pipe stability under flow conditions, and additional pumping power. This configuration should be explored in greater depth to determine the magnitude of these problems and their solutions.

The maximum temperature allowed by the design parameters in the heat transfer system was 1800°F. The temperature used was the present state-of-the-art limit in metals designed to operate for long periods at high temperatures. This temperature was used rather than a higher temperature based on anticipated technological breakthroughs in metallurgy. Above 1800°F, the creep-rupture stress value is degraded to the point where the required pipe thicknesses become very large. Consequently, the pipe weight, even in the concentric configuration, becomes impractical. Further study and experimentation in high temperature metallurgy should be accomplished with the goal of increasing the allowable long duration working temperatures.

Two pass cross-counterflow finned-tube heat exchangers were used in the indirect cycle engines. The liquid metal heat exchanger, which was designed by the General Electric Company, Energy Systems Programs, is arranged in a wrap-around configuration and has 4032 finned tubes and weighs 9300 lbs. The gas engine heat exchanger has two heat ex-

changer sections, each one a mirror image of the other, arranged in-line. This was necessary to get the 9792 tubes required within the diameter of the engine. The heat exchanger weighs 20,600 lbs. Section 7.4.1 gives a more complete discussion of these heat exchangers.

The direct cycle engines require two heat exchangers: a recuperator and a precooler. Each recuperator is similar in design to the reactor heat exchanger and weighs 3050 lbs. The precoolers were designed using the same procedures as the indirect cycle engine heat exchangers. They are arranged in a rectangular configuration as opposed to the wrap-around arrangement of the engine heat exchangers. Each precooler weighs 10,500 lbs.

The pumping power required to circulate the two different working fluids is quite different. Liquid metal may easily be pumped at a small cost in horsepower while helium gas required a complex turbine circulation system. In addition, the two different helium systems have different pumping requirements as the direct cycle system is self pumping, while the indirect cycle is not. Both gas systems require a primary loop circulator system of approximately 25,000 hp. The circulator is similar to a direct cycle engine with a helium gas powered turbine turning the circulator pump. This adds over 11,000 lbs to either gas system in additional heat exchanger weight.

The indirect cycle helium system requires a similar, though less powerful, circulator for its secondary or engine loop. (The reactor core has a much higher pump power requirement than does either heat exchanger). The extra heat exchangers required add 8100 lbs to the system weight.

These gas circulation systems not only add heat exchanger and pump weight, they also require additional power from the reactor which necessitates a larger, heavier reactor. Table 10.1.6-1 shows a comparison of the system power required with and without the gas circulators. Refer to Section 5 of this report for the weight comparison.

TABLE 10.1.6-1. GAS CIRCULATION POWER REQUIREMENTS

	POWER REQUIRED FOR ENGINES (MW)	POWER REQUIRED FOR ENGINES & CIRCULATORS (MW)
INDIRECT CYCLE HELIUM GAS SYSTEM	475	574
DIRECT CYCLE HELIUM GAS SYSTEM	636	700

Safety isolation valves are required on all working fluid lines entering and leaving the reactor containment vessel. These valves can add considerable weight to the heat transfer system since there can be as many as 22 pipes going from and to the reactor (indirect cycle, 2-pipe configuration for 10 engines with one circulator pump).

Three valve designs are presented, one by Sandia Corp. and two designs proposed by this study. All the valves are designed to be constructed from Haynes Alloy 188, close in 50 msec, and withstand an axial decelleration of 1500 g's without opening. A summary of weights including safety valves, and reactor power requirements of the three heat transfer systems is presented in Table 10.1.6-2.

TABLE 10.1.6-2. WEIGHT AND POWER COMPARISONS

	INDIRECT CYCLE		
	LIQUID METAL	HELIUM	DIRECT CYCLE
WEIGHT (LBS)			
HEAT EXCHANGERS	99,500	257,600	176,300
VALVES	136,000	81,600	74,800
PIPES	12,100	12,200	12,200
COOLANT	27,000	100	100
TOTAL	274,600	351,500	263,400
REACTOR POWER (MW)	475	574	700

10.1.7 SAFETY (Section 8): Three categories of accidents were used to compute the probability of releasing radioactive material to the environment. These were the Crash Accident, which considers a mid-air collision or ground impact; the Transient Accident which considers all other accidents that result in a demand for reactor shutdown, except for total loss of coolant; and total Loss of Coolant Accident.

The total Loss of Coolant Accident was found to have a probability of occurrence of less than 10^{-25} per flight and was excluded from further consideration because the probability of occurrence was insignificant in comparison to the other accident categories.

The results of the Crash and Transient Accident analyses are summarized in Table 10.1.7-1. As shown, there is 90% confidence that the probability, per flight, of a release of radioactive material lies between 1.87×10^{-3} and 4.43×10^{-3} with a mean, or expected value, of 3.18×10^{-3}.

TABLE 10.1.7-1. TOTAL RELEASE PROBABILITY PER FLIGHT

ACCIDENT CATEGORY	PROBABILITY			
	0.05	0.50	0.95	MEAN
CRASH	1.86×10^{-3}	3.18×10^{-3}	4.43×10^{-3}	3.18×10^{-3}
TRANSIENT	1.97×10^{-9}	4.90×10^{-8}	1.03×10^{-6}	2.96×10^{-7}
TOTAL	1.87×10^{-3}	3.19×10^{-3}	4.43×10^{-3}	3.18×10^{-3}

The crash accident dominates the overall probability of incurring a release of radioactive material, and for that reason, the consequence of a release, in terms of fatalities, was modeled for the crash accident only, using a 574 MW reactor.

TABLE 10.1.7-2. FATALITIES PER RELEASE OF RADIOACTIVE MATERIAL PROBABILITY DISTRIBUTION

DEATHS PER RELEASE				
PROBABILITY	0.005	0.50	0.995	MEAN
DEATHS	0.003	1.20	865	18.9

The results of that analysis, summarized in Table 10.1.7-2, show the number of fatalities resulting from a release of radioactive material. There is a 99% confidence that the number of fatalities lies between 0.003 and 865. The mean, or expected number, is 18.9 fatalities per release of radioactive material.

Table 10.1.7-3 shows a similar analysis, but is given in fatalities per year based on the number of flights per year. For example, for 1000 flights per year, the expected number of fatalities is 17.8.

TABLE 10.1.7-3. DEATHS PER YEAR PROBABILITY DISTRIBUTION

DEATHS PER YEAR				
FLIGHTS PER YEAR	0.005	0.50	0.95	MEAN
1000	<1	1.13	814	17.8
1500	<1	1.18	850	18.5
2000	<1	1.19	860	18.8

The individual risk to any member of society was expressed as the expected number of deaths divided by the total U.S. population. For an expected number of fatalities of 17.8 per year, and a population of 201 million, the individual risk is 8.9×10^{-8} per year. Stated another way, each individual has approximately 1 chance in 11 million, each year, of being killed by a release of radioactive material from a nuclear powered airplane over the continental United States.

10.1.8 LIFE CYCLE COST (Section 9): This study undertook the task of determining the life cycle cost for a nuclear powered aircraft. The life cycle cost for the aircraft included flyaway cost, initial spares, peculiar support and training equipment, research, development, test and evaluation, and, finally, operating and support cost discounted over 10 years. Of the proposed systems, only the 2,000,000 lb aircraft with a dedicated propulsion system was addressed. The study determined the life cycle cost of 60 production airframes and one prototype airframe through the use of cost-estimating relationships, the cost of analogous items, and a best estimate of the cost presented by experts associated with the items in question. The flyaway

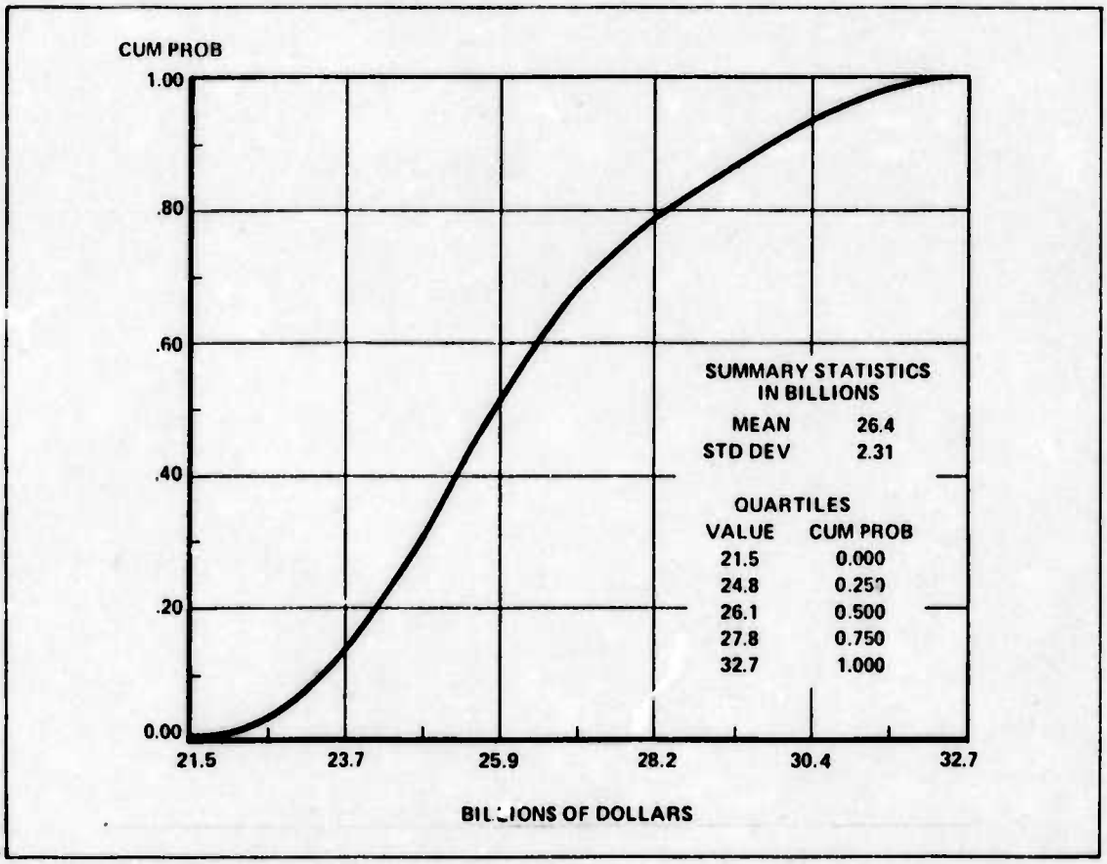

Figure 10.1.8-1. Life Cycle Cost for 60 Nuclear Aircraft - Cumulative Probability

cost was determined to be in the range of $127 - 224 million. Figure 10.1.8-1 illustrates the range of cost for the life cycle of 60 nuclear powered aircraft, i.e., from the birth to the death of the system. Its interpretation is that, if a nuclear aircraft program were undertaken, the life cycle cost would lie in the range of $21.5 - 32.7 billion. The mean or expected life cycle cost would be $26.4 billion with the median being $26.1 billion in 1974 dollars.

10.2 WEAPON SYSTEM

10.2.1 PROPULSION SYSTEM: In the past several years, there has been no large scale integrated systems study performed on an airborne nuclear propulsion system. There have, however, been several studies performed concerning airborne applications of several components of a nuclear propulsion system such as the reactor and dual mode engines. Each of these studies attempted to optimize about one or more parameters peculiar to the component being analyzed. It is important to realize that misleading results can be obtained by this type of subsystem analysis, and that individual components may be less than optimum when the overall nuclear propulsion system is optimized.

The nuclear propulsion system designs in this report utilized reactor data from the Westinghouse Electric Corporation, Astronuclear Division, (Ref. 190), and a doctoral dissertation prepared by K. L. Mills, (Ref. 122), and then used a systems approach to design the engines, heat exchangers, piping, valves, and pumping systems required to complete the propulsion system.

Shown in Table 10.2.1-1 are the propulsion system weights resulting from the eight possible combinations of the reactors, working fluids, and engine types. These weights represent the total propulsion system weights necessary to provide the required cruise thrust for the point design aircraft.

It can be seen that the engines and heat transfer systems are the lightest in the helium-cooled, direct cycle systems, but the lightest gas reactor (442,000 lbs) is the Mills reactor which weighs 78,000 lbs less than the Westinghouse liquid-metal reactor. However, three points must be considered when comparing the Mills and Westinghouse reactor designs:

1) The Westinghouse reactor has a 10,000 hr lifetime compared to the Mills' 3000 hr lifetime. Note that this difference in reactor lifetime will affect other parameters associated with the propulsion system. For instance, the cost data computed in the analysis is based on the 10,000 hr lifetime reactor and does not reflect any changes due to the increased number of reactor refurbishings required by a 3000 hr reactor.

2) The Mills reactor lateral radiation level is about five times that of the Westinghouse reactor.

3) The Mills reactor is a one man design effort and thus, probably, does not incorporate the depth of engineering contained in the Westinghouse effort.

Before a final comparison can be made, however, the total system must be examined with the aircraft and nuclear propulsion system integrated.

TABLE 10.2.1-1. NUCLEAR PROPULSION SYSTEMS

	PROPULSION SYSTEM							
	1	2	3	4	5	6	7	8
THRUST/ENGINE (1000 LB)	14.7	14.3	15.2	14.7	15.2	14.7	14.0	14.0
NUMBER OF ENGINES	10.0	10.0	10.0	10.0	10.0	10.0	10.0	10.0
TOTAL ENGINE WEIGHT (1000 LBS)	156.0	164.0	181.0	188.0	181.0	188.0	83.0	83.0
HEAT TRANSFER SYSTEM WEIGHT (1000 LBS)	275.0	275.0	351.0	351.0	351.0	351.0	270.0	270.0
REACTOR POWER (MW)	475.0	475.0	574.0	574.0	574.0	574.0	700.0	700.0
REACTOR WEIGHT (1000 LBS)	520.0	520.0	719.0	719.0	442.0	442.0	789.0	494.0
TOTAL PROPULSION SYSTEM WEIGHT (1000 LBS)	951.0	959.0	1251.0	1258.0	974.0	981.0	1142.0	847.0

PROPULSION SYSTEM DESCRIPTIONS

1 - NaK / INDIRECT CYCLE / DEDICATED ENGINES / WESTINGHOUSE REACTOR
2 - NaK / INDIRECT CYCLE / DUAL MODE ENGINES / WESTINGHOUSE REACTOR
3 - HELIUM / INDIRECT CYCLE / DEDICATED ENGINES / WESTINGHOUSE REACTOR
4 - HELIUM / INDIRECT CYCLE / DUAL MODE ENGINES / WESTINGHOUSE REACTOR
5 - HELIUM / INDIRECT CYCLE / DEDICATED ENGINES / MILLS REACTOR
6 - HELIUM / INDIRECT CYCLE / DUAL MODE ENGINES / MILLS REACTOR
7 - HELIUM / DIRECT CYCLE / DEDICATED ENGINES / WESTINGHOUSE REACTOR
8 - HELIUM / DIRECT CYCLE / DEDICATED ENGINES / MILLS REACTOR

10.2.2 TOTAL AIRCRAFT SYSTEM: The point design, 2,000,000 lbs gross weight, canard configuration aircraft developed in Section 4 and summarized in Section 10.1.3 was coupled with the six possible propulsion system configurations given in Section 10.2.1 to yield a variety of possible payloads. Specifically, the alternatives include considerations of conventional aircraft construction versus a lighter weight advanced composite construction; pure chemical power for takeoff versus chemically augmented nuclear power; and the eight proposed nuclear propulsion systems.* These alternatives yield 32 possible combinations, the results of which, in terms of available payload, are summarized in Table 10.2.2-1.

Table 10.2.2-1 shows the following major points.

1) A positive payload for a 2,000,000 lbs aircraft cannot be achieved under any of the propulsion system options using conventional aircraft construction and a purely chemical takeoff.

2) A positive payload can be achieved under all the propulsion systems options using advanced composite construction and chemically augmented nuclear takeoff.

3) The highest payload is obtained using the Mills reactor in a direct cycle with advanced composite construction and chemically augmented nuclear takeoff.

4) From a payload standpoint, the worst combination exists when using the Westinghouse reactor in a helium indirect cycle with conventional aircraft construction and a pure chemical takeoff capability.

5) In all propulsion system options, the NaK cooled indirect cycle produces a larger payload than the helium cooled indirect cycle.

6) The direct cycle helium system, when compared with the indirect cycle, produces a larger payload in all aircraft configurations.

7) Using a helium cooled Westinghouse reactor in either direct or indirect cycle, it is necessary to go to advanced composite construction and chemically augmented nuclear takeoff to produce a positive payload.

8) Under all propulsion system options, using chemically augmented nuclear power for takeoff yields a higher payload than pure chemical power for takeoff.

*The chemically augmented, nuclear powered takeoff uses nuclear powered engines plus dedicated chemical engines. The nuclear engines produce cruise thrust corrected from the design point altitude conditions to the ambient air conditions at the departure field. The dedicated chemical engines produce the remainder of the thrust required for takeoff.

TABLE 10.2.2-1. PREDICTED PAYLOAD FOR 2,000,000 LBS GROSS WEIGHT AIRCRAFT

PROPULSION SYSTEM	AIRCRAFT CONFIGURATION A	B	C	D
	PAYLOAD x 10^3LB / PAYLOAD GROSS WT.			
1	-190 / 0	90 / 0.05	120 / 0.06	400 / 0.20
2*	-146 / 0	90 / 0.05	160 / 0.08	400 / 0.20
3	-484 / 0	-214 / 0	-174 / 0	96 / 0.05
4*	-444 / 0	-204 / 0	-134 / 0	106 / 0.05
5	-212 / 0	68 / 0.04	98 / 0.05	378 / 0.19
6*	-114 / 0	126 / 0.06	196 / 0.10	436 / 0.22
7	-380 / 0	-100 / 0	-70 / 0	210 / 0.11
8	-84 / 0	196 / 0.10	176 / 0.09	506 / 0.25
	CONVENTIONAL CONSTRUCTION/ PURE CHEMICAL TAKEOFF	CONVENTIONAL CONSTRUCTION CHEMICALLY AUGMENTED NUCLEAR TAKEOFF	COMPOSITE CONSTRUCTION/ PURE CHEMICAL TAKEOFF	COMPOSITE CONSTRUCTION/ CHEMICALLY AUGMENTED NUCLEAR TAKEOFF

1. NaK / INDIRECT CYCLE / DEDICATED ENGINES / WESTINGHOUSE REACTOR
2. NaK / INDIRECT CYCLE / DUAL MODE ENGINES / WESTINGHOUSE REACTOR
3. HELIUM / INDIRECT CYCLE / DEDICATED ENGINES / WESTINGHOUSE REACTOR
4. HELIUM / INDIRECT CYCLE / DUAL MODE ENGINES / WESTINGHOUSE REACTOR
5. HELIUM / INDIRECT CYCLE / DEDICATED ENGINES / MILLS REACTOR
6. HELIUM / INDIRECT CYCLE / DUAL MODE ENGINES / MILLS REACTOR
7. HELIUM / DIRECT CYCLE / DEDICATED ENGINES / WESTINGHOUSE REACTOR
8. HELIUM / DIRECT CYCLE / DEDICATED ENGINES / MILLS REACTOR

*CHEMICAL ENGINE WEIGHT REMOVED FOR DUAL MODE ENGINE SYSTEMS

Whereas Table 10.2.2-1 compares the different propulsion systems from a payload standpoint, safety considerations must also be taken into account in the overall evaluation. Following is a list of some major points that must be considered:

1) The helium system operates under high pressure (1800 psi) in both the primary and secondary heat transfer loops whereas the NaK system operates at a low pressure (130 psi).

2) The corrosion problems encountered in the NaK system are much more severe than in the helium system.

3) The atomic structure of NaK allows it to become activated, whereas the helium is radioactively inert.

4) While high pressure gas and explosively reacting NaK may be deemed comparably hazardous from a crew safety standpoint, NaK would be much more damaging to the general populace and the environment in the event of a crash.

10.2.3 MISSION APPLICATION: In a chemically powered turbofan engine, the heat is manufactured in the engine by the burning of fuel, whereas in a nuclear engine the heat source is a remotely located reactor. The necessary heat transfer system with at least two heat exchangers is complicated and inflexible with regard to air temperature changes. Changes in altitude, and therefore air temperature, require the indirect cycle engine to vary the nozzle and fan pitch in order to maintain the constant airflow parameters required as the heat exchanger input conditions. If these airflow input conditions are not maintained constant, the heat exchanger is no longer adequate, and the turbine inlet temperature will drop resulting in a loss of thrust. The direct cycle engine has virtually identical problems; it may be designed for a lower altitude and the air flow to its heat exchanger varied, but failing to do so leads to an engine which does not produce the design point thrust.

The mechanical complexity needed to provide constant airflow parameters can alternately be avoided by using chemical power for the off-design altitude portion of the mission. However, this again restricts the aircraft because of the following:

1) The aircraft must replace the chemical fuel consumed in altitude changes. This would require that either the aircraft curtail its mission length and return to base, or that it be refueled in flight.

2) Any supplementary chemical fuel load carried subtracts directly from the payload.

For these reasons, a mission which requires changes in altitude may be less suitable for the application of nuclear power than one which requires that the entire mission be flown at a constant altitude. Table 10.2.3-1 shows the candidate mission requirements for the nuclear aircraft. The above altitude restrictions may severely restrict the nuclear powered aircraft's ASW mission effectiveness. A choice of a mission flown at constant altitude would allow the propulsion system designer to optimize the system at that altitude. Thus, AWAC or C&C may

be more viable candidates. However, both of these missions require extended flight times over populated areas and thus imply increased concerns with respect to safety of the general populace. The AWAC and C&C may require only a few hundred miles of emergency chemical fuel capability. These missions can be flown near their home station and will not require the extended over water range nor require the large chemical fuel reserve that the ASW mission does. This fact results in potentially larger payloads for the AWAC and C&C missions using the same point design aircraft.

TABLE 10.2.3-1. AIRCRAFT PARAMETERS FOR SELECTED MISSIONS

PARAMETER	MISSION				
	ASW	AWAC	C/C	Mx	CARGO
MISSION DURATION	DAYS	DAYS	DAYS	DAYS	HOURS
CREW SIZE (NO. OF MEN)	FLT 4-5 MISSION 6-8	FLT 4-5 MISSION 17	FLT 4-5 MISSION 19	FLT 4-5 MISSION 4-6	FLT 4-5 MISSION 1
AIRSPEED	SUBSONIC	SUBSONIC	SUBSONIC	SUBSONIC	HIGH SUBSONIC
ALTITUDE (FT)	0 to 25,000-35,000	25,000-35,000	25,000-35,000	25,000-35,000	25,000-35,000
PAYLOAD (LBS)	130,000-200,000	91,000 +	200,000 +	400,000	200,000-400,000
FLEET SIZE (NO. OF AIRCRAFT)	60	34	17	25-50	40-81
RANGE/ ENDURANCE	UNLIMITED	UNLIMITED	UNLIMITED	UNLIMITED	UNLIMITED

A COMPLETE EXPLANATION OF THE PARAMETERS IS CONTAINED IN VOLUME III.

10.3 CONCLUSIONS AND RECOMMENDATIONS

The conclusions and recommendations contained in this section of the report are related, primarily, to considerations of system weights and safety, and, as such, represent only the major conclusions and recommendations derived from the nuclear airplane feasibility study. Numerous other conclusions and recommendations may be found in the various sections of the main text.

Although the individual sections of the main report are accurate and largely complete in their own right, it is, nonetheless, true that false or misleading conclusions regarding the feasibility of the nuclear airplane concept can be drawn by considering only isolated portions of this study. It is, therefore, recommended that users of this report consider the report in its entirety before making judgments or decisions regarding nuclear propulsion for aircraft.

10.3.1 AVIONICS: The avionics portion of this study has shown the requirements that are necessary to achieve a specified mission reliability through the use of equipment redundancy only. For example, to achieve 90% reliability requires approximately 4 levels of redundancy for a 96 hr mission, and approximately 10 levels of redundancy for a 336 hr mission.

It was concluded that, while not absolutely essential, alternatives to redundancy for achieving high reliability are desirable, and it is recommended that the option of utilizing an in-flight repair capability be studied to determine its feasibility.

10.3.2 REACTOR: The reactor analysis utilized two reactor design proposals by the Westinghouse corporation and one design proposal by K.L. Mills (doctoral dissertation) in assessing the nuclear airplane concept. Because of the 200 ft minimum separation between the crew and the reactor, which results from the canard configured aircraft used in this study, it was concluded that a potential weight savings exists, through reduced radiation shielding, for all three reactor designs. Reactor weight savings of 10,000 to 21,000 lbs are possible without exceeding the original design specifications for maximum allowable radiation dose rate to the crew. It is, therefore, recommended that any future designs consider the use of large separation distance between the crew and the reactor, and that the reactor be designed for that specific application.

It was also concluded that reactor weight savings of up to 300,000 lbs can be realized through the use of increased power density fuels. Therefore, it is recommended that the development of higher power density fuels be considered as part of any future nuclear aircraft development programs.

Following a reactor shutdown, heat continues to be generated by the decay of radioactive fission products. This reactor afterheat could be as high as 25 million BTU per hr, 30 min after shutdown of a 574 MW reactor. Although this problem was not specifically addressed in this study, it was concluded that a means of removing reactor afterheat during ground operations must be devised.

10.3.3 NUCLEAR PROPULSION SYSTEM: The nuclear propulsion system analysis considered three propulsion system concepts. Both liquid metal and gas-cooled systems were considered, and, for the gas system, both direct and indirect cycle engines were considered. Of these three concepts, the liquid metal-cooled system is considerably lighter. This results from two facts: (1) the reactor, which is the heaviest part of the system, is inherently lighter for a liquid metal coolant than for a gas coolant, and (2) the engines and heat transfer systems for a gas/cooled system are inherently less efficient than for a liquid metal system, thus requiring an even larger reactor.

Shown in Table 10.3.3-1 are some of the weight and power requirements for the three propulsion concepts. It can be seen that, if only the engine weights are considered, the direct cycle helium system is lightest at 83,000 lbs. A similar conclusion is drawn when considering only the heat transfer system where the direct cycle helium system weighs 242,000 lbs. However, when considering only the reactor, the liquid metal system, at 520,000 lbs is substantially lighter than either of the helium systems.

The total propulsion system weights of 1,035,000 lbs for the direct cycle helium system, 1,244,000 lbs for the indirect cycle helium system, and 943,000 lbs for the liquid metal system show the liquid metal system to be substantially lighter than either helium system.

Additionally, if the efficiencies of the helium systems were assumed to equal that of the liquid metal system, so that all systems could use a 475 MW reactor, the reactor for the helium cooled systems would weigh 730,000 lbs versus the 520,000 lbs reactor for liquid metal. In such a case, a helium-cooled system would still weigh at least 112,000 lbs more than a liquid metal-cooled system. Thus, it is concluded that a liquid metal-cooled propulsion system will be substantially lighter than a helium-cooled propulsion system.

However, the relative safety of liquid metal vs gas systems is a question that has not been addressed in this study, and it is recommended that such a study be accomplished before any commitment is made to develop a nuclear powered airplane.

TABLE 10.3.3-1. PROPULSION SYSTEM WEIGHTS AND POWER REQUIREMENTS (2,000,000 LBS AIRCRAFT)

TYPE OF SYSTEM	WEIGHT (LBS)				POWER (MW)	
	ENGINE[1]	HEAT TRANSFER[2]	REACTOR[3]	TOTAL	PUMP	TOTAL
HELIUM DIRECT CYCLE	83,000	242,000	810,000	1,035,000	64	700
INDIRECT CYCLE	181,000	323,000	740,000	1,244,000	95	574
LIQUID METAL	156,000	267,000	520,000	943,000	1.5	475

[1] INCLUDES PUMP WEIGHTS

[2] DOES NOT INCLUDE REACTOR HEAT EXCHANGER WEIGHT

[3] BASED ON WESTINGHOUSE DESIGN WITH REACTOR HEAT EXCHANGER WEIGHT INCLUDED

10.3.4 CHEMICAL PROPULSION SYSTEM: The efficiency of a nuclear propulsion system is such that it will not develop a sufficient thrust for takeoff. Therefore, it is necessary that a chemical fuel propulsion system be incorporated in the aircraft design.

In this design study, two chemical propulsion system requirements were defined for point design calculations. In the first case, it was assumed that only chemical power would be used for takeoff and landing, with an additional requirement for a 1000 nm emergency cruise capability. These criteria led to a chemical propulsion system weighing 320,000 lbs, or 16% of the gross weight of the 2,000,000 lbs point design aircraft.

In the second case, the chemical propulsion system was only required to augment the nuclear propulsion system for takeoff and landing, with no requirement for emergency cruise capability. In this case, the chemical propulsion system weighed 80,000 lbs, or 4% of the aircraft gross weight.

The 80,000 lbs system represents the minimum weight that must be allocated to chemical propulsion requirements since it only supplies the minimum thrust augmentation necessary

for takeoff and landing. Additional requirements for chemical fuel capability must be evaluated in terms of the additional weight imposed.

10.3.5 PAYLOAD: A 2,000,000 lbs aircraft, constructed by conventional construction techniques, and carrying sufficient chemical fuel for takeoff, landing, and emergency cruise (320,000 lbs) cannot achieve a positive payload with any of the nuclear propulsion systems considered in this study. To achieve the required ASW payload (200,000 lbs) under these criteria would require an aircraft with a gross weight in excess of 3,000,000 lbs, assuming that the estimation techniques used in this study are valid for gross weights exceeding 2,000,000 lbs.

A 2,000,000 lbs aircraft, constructed by conventional construction techniques, but with the chemical fuel capability reduced to the minimum necessary for takeoff and landing (80,000 lbs) cannot achieve a positive payload using a helium-cooled nuclear propulsion system. A payload of 90,000 lbs could be achieved by using a liquid metal system.

Expert predictions indicate that airframe weight savings as high as 40% may be realized by advanced composite construction techniques. Based on these predictions, a 2,000,000 lbs aircraft, with a 320,000 lbs chemical fuel system, still cannot achieve a positive payload using a helium-cooled nuclear propulsion system. A payload of 120,000 lbs could be achieved by using a liquid metal system.

A 2,000,000 lbs aircraft, constructed by advanced composite construction techniques, and utilizing an 80,000 lbs chemical fuel system can achieve a positive payload of 96,000 to 210,000 lbs with a helium-cooled nuclear propulsion system, and 400,000 lbs with a liquid metal system.

It is concluded that, in any case, a liquid metal-cooled nuclear propulsion system will yield the largest payload. Additionally, the predicted weight savings to be offered by advanced composite construction techniques indicates that such technology should be pursued if the nuclear airplane is to be feasible. Also, it should be noted that the payload predictions given in this section have incorporated the reactor weight savings discussed previously in Section 10.3.2.

It is recommended that, rather than going to increasingly larger aircraft, a concerted effort be made to reduce both propulsion system and airframe weights in order to make the nuclear powered airplane a more viable concept.

10.3.6 SAFETY: This study has concluded that the overall probability of a release of radioactive material is dominated by the contribution from the crash accident. The probability of a release of radioactive material resulting from a crash is approximately three orders of magnitude higher than all other accidents, and is dominated by three factors. These are, in ascending order of probability, the probability of failure to seal the containment vessel at impact, the probability of failure of the containment vessel to withstand the impact, and the probability of failure of the containment vessel to withstand the afterheat transient.

To date, only one known study of safety valves for sealing containment vessels has been performed. It is recommended that further development of safety valves be accomplished with design objectives of lighter weight and higher reliability.

Previous tests of containment vessel impact survivability used smooth surfaced spheres, free of any structures. It is recommended that further evaluation of containment vessel impact survivability be accomplished with emphasis on the effects of the aircraft structure, valve weldments, pipe penetrations, and other protuberances.

Previous analyses of afterheat transient survival have assumed ideal insulation with no voids, pumps, pipes or heat exchangers. It is recommended that further analysis be performed with consideration given to the effects of the voids and the installed heat transfer equipment.

Of special importance to the survivability of the containment vessel during the afterheat transient is the depth of burial resulting from the crash impact. Previous studies have assumed burial depths for an unenclosed sphere impacted against soil. It is recommended that the effect of the aircraft structure on depth of burial be studied.

A release of radioactive material to the environment is not expected to result in a large number of fatalities. Given that a release occurred from a 574 MW reactor, there is a 95 percent confidence that the number of fatalities would be equal to or less than 52, with an expected number of 19. When a release of radioactive material does occur, it will necessitate the evacuation of a large area until the dose rate from radioactive particles returns to an acceptable level.

Historical aircraft crash data indicates that more than one-half of the crashes will occur in the vicinity of the airport. Therefore, it is recommended that further study be conducted into the safety and operational implications of having to close or evacuate an airport, for up to 90 days, after each crash.

Initial investigations, based strictly on historical data from ground based reactors, indicated a median probability of a reactor shutdown, due to some transient condition, of 0.3 per flight. It was concluded that such a shutdown rate would have an unacceptable impact on safety and mission reliability. Additionally, a premature reactor shutdown on every third flight would substantially increase the estimated life cycle costs from those summarized in Section 10.1.8, and the option of reducing the chemical fuel to the minimum needed for takeoff and landing could not be considered.

It is recommended that a detailed study of reactor systems be performed to insure an acceptable reliability.

BIBLIOGRAPHY

1. Abbot, I. H. and A. E. Von Doenhoff, *Theory of Wing Sections*. New York: Dover Publications, Inc., 1959.

2. Adams, D. F., "High Performance Composite Material Airframe Weight and Cost Estimating Relations," *Journal of Aircraft*, 11: 751-757, December 1974.

3. Aerophysics Research Corp., *Watts – A Computer Program For Weights Analysis of Advanced Transportation Systems, NASA Contractor Report CR-2420. Washington: National Aeronautics and Space Administration, September 1974.*

4. AFM 88-6, *Airfield Pavement Design, General Provisions and Criteria*. Washington: Department of the Air Force, December 1960.

5. AFM 173-10, *USAF Cost and Planning Factors*. Washington: Department of the Air Force, 1 April 1973.

6. Air Force Flight Dynamics Laboratory, *AFFDL Evaluation of the Virtus Concept*. Unpublished report Air Force Flight Dynamics Laboratory, Wright-Patterson AFB, Ohio.

7. Andrews, E. Jr., et al, *Microwave Landing Systems Integration Study*. Wright-Patterson AFB, Ohio: Air Force Flight Dynamics Laboratory, March 1974.

8. Armbruster, C. H., *Literature Survey & Preliminary Study of Potential Nuclear Propulsion Power Conversion System for Aircraft*, AFAPL-TBP-TM-72-20. Turbine Engine Division, AF Propulsion Laboratory, Wright-Patterson AFB, Ohio.

9. Armstrong, R. E. and Koob, S. J., Personal Interview. Wright-Patterson AFB, Ohio: USAF/FDL, Prototype Design Branch, May 1974-January 1975.

10. ASD/XR 74-21, *Advanced Tactical Fighter Target Acquisition and Weapons De' very Study*. Wright-Patterson AFB, Ohio, October 1974.

11. Austin, L. G.,*Fuel Cells*, NASA SP-120. U.S. Government Printing Office, 1967.

12. Babbitt, Major G. T., Personal Interview. Wright-Patterson AFB, Ohio: Directorate of Integrated Logistic Support for B-1, Aeronautical Systems Division (AFSC), 30 October 1974.

13. Bazovsky, I., *Reliability Theory and Practice*. New Jersey: Prentice-Hall, 1961.

14. Beers, Col. K. N., Chief, Medical Office, Aeronautical Systems Division, Personal Interview, Wright-Patterson AFB, Ohio, 25 June 1974.

15. Benham, P. P., *Elementary Mechanics of Solids*. London: Pergamon Press Ltd., 1965.

16. Bisplinghoff, R. L., H. Ashley, R. L. Halfman, *Aeroelasticity*. Reading, Massachusetts: Addison-Wesley Publishing Company, Inc., 1955.

17. Blakley, T. N. Dr., Ohio State University, Reactor Facility, Personal Interview, Columbus,Ohio, 31 October 1974.

18. Blatz, H., *Introduction to Radiological Health*. New York: McGraw-Hill Book Company, 1964.

19. Blizard, E. P., ed., *Reactor Handbook*, Vol. III (Second Edition). New York: Interscience Publishers, 1962.

20. Bonilla, C. F. and T. A. Jaeger, *Nuclear Engineering and Design*, Vol. 26, No. 3, February 1974. Amsterdam: North Holland Publishing Company.

21. Bonilla, C. F. and T. A. Jaeger, *Nuclear Engineering and Design*, Vol. 23, No. 2, November 1972. Amsterdam: North Holland Publishing Company.

22. Bonilla, C. F. and T. A. Jaeger, *Nuclear Engineering and Design*, Vol. 26, No. 1, January 1974. Amsterdam: North Holland Publishing Company.

23. Bonilla, C. F. and T. A. Jaeger, *Nuclear Engineering and Design*, Vol. 25, No. 2, July 1973. Amsterdam: North-Holland Publishing Company.

24. Booton W. C., *et al., A Conceptual Definition Study For A Digital Avionics Information System (Approach 1)*, Technical Report AFAL-TR-73-300. Wright-Patterson AFB, Ohio: Air Force Avionics Laboratory, October 1973.

25. Bridgman, C. J., "The Physics of Nuclear Explosives." Class Notes, Air Force Institute of Technology, 1972.

26. Brodnax C. T., *A Conceptual Study for a Digital Avionics Information System (Approach II)*, Technical Report AFAL-TR-73-427. Wright-Patterson Air Force Base, Ohio: Air Force Avionics Laboratory, March 1974.

27. Buchin, S. I., *Computer Programs for the Analysis of Complex Decision Problems*. Harvard University: January 1969.

28. Calabro, S. R., *Reliability Principles and Practices*. New York: McGraw-Hill, 1962.

29. Chalk, C. R., et al., *Background Information and User Guide for MIL-F-8785B (ASG). Military Specification-Flying Qualities of Piloted Airplanes*, AFFDL-TR-69-72. Wright-Patterson AFB, Ohio: Air Force Flight Dynamics Laboratory, August 1969.

30. Clark A. B. and Disney R. L., *Probability and Random Processes for Engineers and Scientists*. New York: John Wiley & Sons, 1970.

31. Cleveland, F. A., "Size Effects in Conventional Aircraft Design", *Journal of Aircraft*, Volume 7: 483-512 (November-December 1970).

32. Comptroller of the Army, *Costing Methodology Handbook*. Washington: Department of the Army, April 1971. AD 884835.

33. Corning G., *Supersonic and Subsonic Airplane Design*, (3rd ed). Ann Arbor: Braun-Brumfield, Inc. 1960.

34. Cost Analysis Improvement Group, *Operating and Support Cost Estimates: Aircraft Systems*. Washington: Pentagon, May 1974.

35. Crane Technical Paper No. 10., *Flow of Fluids Through Valves, Fittings, and Pipe*. Chicago: The Crane Company, Engineering Division, 1957.

36. Crandall, S. H. and N. C. Dahl, *An Introduction to the Mechanics of Solids*. New York: McGraw-Hill Book Company, Inc., 1959.

37. "CRT TERMINAL is Ruggedized", *Electronics*, 47: 104, 31. October 1974.

38. Darlington, Capt. L., Personal Interview. Wright-Patterson AFB, Ohio: Air Force Avionics Laboratory/AAA-4 (AFSC), 14 November 1974.

39. DH-1-6, *System Safety Design Handbook*, Third Edition. Andrews AFB, Maryland: Headquarters Air Force Systems Command, July 1971.

40. Diggs, K. H., Personal Interview. Wright-Patterson AFB, Ohio: USAF/AFSC/AFFDL, Mechanical Branch, August 1974.

41. Dommasch, D. O., et. al., *Airplane Aerodynamics* (4th Edition). Pitman Publishing Co., c1967.

42. Dorsset, J., Cost Analysis, Telephone Conversation. Washington: Pentagon, AFACMC, 20 January 1975.

43. Dreyfuss, D. J., et. al., *Cost-Estimating Relationships for Aircraft Airframes*, WN8729-PR. Santa Monica, California: The Rand Corporation, June 1974.

44. Dusinberre, G. M., *Heat Transfer By Finite Differences*. New York: International Textbook Co., 1961.

45. Dusinberre, G. M. and J. C. Lester, *Gas Turbine Power*. International Textbook Co., 1958.

46. Eisenbud, M., *Environmental Radioactivity*, (Second Edition). New York: Academic Press, 1973.

47. Elrod, W. C., Associate Professor of Mechanical Engineering, Department of Aeromechanical Engineering, Personal Interviews. January 1974-March 1975.

48. Eshbach, O. W. ed., *Handbook of Engineering Fundamentals*. New York: J. Wiley and Sons Inc., 1963.

49. Etherington, H., *Nuclear Engineering Handbook*. New York: McGraw-Hill Book Company, 1958.

50. Everett, H., "Generalized LaGrange Multiplier Method for Solving Problems of Optimum Allocation of Resources," *Operations Research, 11: 399-417*. May-June 1963.

51. *FAA Statistical Handbook of Aviation*, Department of Transportation/Federal Aviation Administration. Washington: U. S. Government Printing Office, 1969.

52. *Failure Data Handbook for Nuclear Power Facilities*, Vol. 1. Rev. 1. LMEC Memo 69-7. Canoga Park, California: Liquid Metal Engineering Center, June 1970.

53. Faires, V. M., *Thermodynamics*. London: MacMillan Co., 1970.

54. Finch, V. C., *Jet Propulsion Turboprops*. National Press, 1950.

55. Finnegan, P. M., et. al., *Preliminary Impact Speed and Angle Criteria for Design of a Nuclear Airplane Fission Product Containment Vessel*, NASA TM X-2245. Washington: National Aeronautics and Space Administration, May 1971.

56. Flagle C. D., et. al., *Operations Research and Systems Engineering*. Baltimore: The Johns Hopkins Press, 1960.

57. Foster, A. R. and R. L. Wright, Jr., *Basic Nuclear Engineering* (Second Edition), Boston: Allyn and Bacon, Inc., 1973.

58. Garner, C. M., Acting Chief, Engine Branch Propulsion Division, Data Package Request for Large Engine "State-of-the-Art". Letter from ASD/ENJET TO AFAPL/XRHP, 30 November 1973.

59. Gebhart, B., *Heat Transfer*. New York: McGraw-Hill Book Company, Inc., 1961.

60. General Electric, CF6 *High Bypass Turbofan*. Cincinnati, Ohio: General Electric, 1970.

61. Gingrich, T. J., Telephone Conversation. Wright-Patterson AFB, Ohio: Aero Propulsion Laboratory/TBT, 9 January 1975.

62. Glasstone, S., and A. Sesonske, *Nuclear Reactor Engineering*. New York: D. Van Nostrand Company, Inc., 1963.

63. Goldberg, M.D., S. F. Mughabghab, S. N. Purohit, B. A. Magurno, and V. M. May, *Neutron Cross Sections*, BNL 325 (Second Edition), Supplement No. 2, Vol. 11b, Z = 41 to 60. Brookhaven National Laboratory, TID 4500.

64. Goldberg, M. D., S. F. Mughabghab, S. N. Purohit, B. A. Magurno, and V. M. May, *Neutron Cross Sections*, BNL325 (Second Edition) Supplement No. 2, Vol. 11c, Z= 61 to 87. Brookhaven National Laboratory, TID 4500.

65. Grimm, Major R., Personal Interview. Wright-Patterson AFB, Ohio: Comptroller Cost Estimating and Analysis, Aeronautical Systems Division (AFSC), 18 November 1974.

66. Harrison, J. R., *Nuclear Reactor Shielding*. New York. Simmons-Boardman Publishing Corporation, 1958.

67. Headquarters Strategic Air Command, LGMEA, *F-111 Performance Graphs*, Unpublished Computer Program Results. Offutt AFB, Nebraska: October 1973.

68. Heppe R. R., et. al., *S-3A – A New Dimension in Airborne Sea Control*, Technical Paper 74-239, presented at AIAA annual meeting. Burbank, California: Lockheed-California Company, January 1974.

69. Hesse, W. J. and N. V. S. Mumford, Jr., *Jet Propulsion for Aerospace Applications* (Second Edition). Pitman Publishing Corp., 1964.

70. Hitchcock, Dr. J., Professor, Department of Aero Mechanical Engineering, Personal Interview. Wright-Patterson AFB, Ohio: Air Force Institute of Technology, School of Engineering, August 1974 - March 1975.

71. Hoch, S.,*Cost Criteria in Weapon Systems Analysis and Force Studies*, Assistant Secretary of Defense (Comptroller). Washington: August 1965.

72. Hoener, R. E., "The Influence of New Materials on Aircraft Design.", *Agard Conference Proceedings – No. 62 – Preliminary Design Aspects of Military Aircraft*. London: Harford House, March 1970.

73. Hoerner, S. F., *Fluid Dynamic Drag*. Midland Park, NJ: Pub. by author, 1965.

74. Holman, J. P., *Heat Transfer* (Third edition). New York: McGraw-Hill, 1972

75. Holton, R. L., *Impact Test of Simulated Nuclear Containment Vessels*. AFWL TR-72-69. Kirkland AFB, New Mexico: Air Force Weapons Laboratory, June 1972.

76. Holton, R. L., Nuclear Power Systems Branch, Telephone Conversation. Kirkland AFB, New Mexico: Air Force Weapons Laboratory, December 1974.

77. Hosney, A. N., *Propulsion Systems*. Published and distributed by the author. University of South Carolina Engineering, Columbia, South Carolina, 1965.

78. "How to Cost Avionics by the Pound," *Electronics* Vol. 47: 128, September 1974.

79. Howard R. A., *Dynamic Programming and Markov Processes*. New York: John Wiley & Sons, Inc., 1960.

80. Hughes, D. J., B. A. Magurno, and M. K. Brussel, *Neutron Cross Sections*, Supplement Number 1 (Second Edition). Upton, New York: Brookhaven National Laboratory, 1960.

81. Hughes, D. J. and Robert B. Schwartz, *Neutron Cross Sections* (Second Edition). Upton, New York: Brookhaven National Laboratory, 1958.

82. Huseman, R. C., "Barnyard III: A Moments Code for Neutron Cross Section Collapsing with the CDC 6600 Computer." Wright-Patterson, AFB, Ohio: Air Force Institute of Technology, March 1974.

83. *Investigation of Containment Vessel Concepts for Airborne Nuclear Systems*, Vol. 1, AFWL TR-72-239. Kirkland AFB, New Mexico: Air Force Weapons Laboratory, April 1973.

84. Johnson, J. H., Jr., Chief Plans Office, AF Aero Propulsion Laboratory, *State-of-the-Art Assessment of Turbine Engines and Heat Exchangers*. Letter from AFAPL/XP to ASD/XRHP, dated 11 December 1973.

85. Johnson, I. A. and R. O. Bullock, editors, *Aerodynamic Design of Axial Flow Compressors*, NASA SP-36. Washington: Superintendent of Documents, 1965.

86. Jones, A., Personal Interview. Pittsburgh, Pennsylvania: Westinghouse Astronuclear Division, 7 October 1974.

87. Kays, W. M. and A L. London, *Compact Heat Exchangers* (Second Edition). New York: McGraw-Hill, 1964.

88. Keenan, J. H. and J. Kaye, *Gas Tables*. New York: John Wiley & Sons Inc., 1945.

89. Kepler, H. B., Professor, Department of Aero Mechanical Engineering, Personal Interview. Wright-Patterson AFB. Ohio: Air Force Institute of Technology, School of Engineering, 25 October 1974.

90. Kettelle, J. D. "Least-Cost Allocation of Reliability Investment," *Operations Research*, 10 249-265, March-April 1962.

91. Kreith, F. *Principles of Heat Transfer*. New York: International Textbook Co., 1965.

92. Kuethe, A. M. and Schetzer, J. D., *Foundations of Aerodynamics*, (2nd Edition). New York: John Wiley & Sons, 1959.

93. Large, B., Rand Corp., Telephone Conversation. Santa Monica, California: 11 October 1974.

94. Larsen, H. C., Head, Aero Design Center, Air Force Institute of Technology. Personal Interview. Wright-Patterson AFB, Ohio: AFIT, School of Engineering, June 1974-February 1975.

95. Levenson, G. S., *Cost-Estimating Relationships for Aircraft Airframes*. Santa Monica, California: The Rand Corp., February 1972. R-761-PR.

96. "*Light Weight Nuclear Propulsion Presentation*." Westinghouse Astronuclear Laboratory, 13 May 1974 (Proprietary).

97. Lillifors, H. W. "On the Kolmogorov-Smirnov Test for Normality with Mean and Variance Unknown," *American Statistical Association Journal*, 62: 399-401, June 1967.

98. Liquid Metal Engineering Center, *Failure Data Handbook for Nuclear Power Faciiities*. LMEC-Memo-69-7. U.S. Atomic Energy Commission. Canoga Park, California, October 1970.

99. List, B., "Dais: A Major Crossroad in the Development of Avionic Systems," *Astronautics and Aeronautics. 11: 55-61*, January 1973.

100. Loftness, R. L., *Nuclear Power Plants*. New York: D. Van Nostrand Company, Inc., 1964.

101. London, A. L., G. Klopfer, and S. Wolf, "Oblique Flow Headers for Heat Exchangers," *Journal of Engineering for Power 90:* 271-286 (July 1968).

102. Lyon, R. N., *Liquid Metals Handbook*. Washington: U.S. Printing Office, 1952.

103. McAdams, W. H., *Heat Transmission*. New York: McGraw-Hill, 1954.

104. McLain, S. and J. H. Martens, eds., *Radioactivity* (Second Edition). New York: Interscience Publishers, 1964.

105. Maas, R., Preliminary Design, Deputy for Development Planning, ASD, Personal Interview. December 1974.

106. Manson, S. V., "A Study of Finned Tube Gas-to-Liquid Heat Exchangers for Brayton Cycles in Space," NASA CR-459. Washington: National Aeronautics and Space Administration, April 1966.

107. Marring, M. D., A. W. Schnacke, C. W. Deane, J. A. Bond, B. L. Moor, and W. F. Zimmerman, Heat Exchanger Design Team, Personal Interview. Cincinnati, Ohio: The General Electric Co., Energy Systems Programs, 11 September 1974.

108. Marshall J. H. *C-5A Program Command Assessment Review*, Briefing Notes. Wright-Patterson AFB, Ohio: C-5A System Program Director, July 1974.

109. Martin J., *Telecommunications and the Computer*. Englewood Cliffs, NJ: Prentice-Hall, Inc., 1969.

110. Marvin, M., Telephone Conversation. Cincinnati, Ohio: General Electric, Jet Engine Division.

111. Marvin, M. D, J. A. Bond, C. W. Deane, B. L. Moor, A. W. Schnacke, and W. F. Zimmerman, "Liquid Metal-to-Air Heat Exchanger Design Study," AFAPL-TR-74-12. Wright-Patterson AFB. Ohio: Air Force Aero Propulsion Laboratory, April 1974.

112. Maultsby, Capt. W. F. *A Classification and Evaluation of Current Cost Models*. Springfield, Virginia: Clearinghouse, January 1970. AD 863844.

113. Mayer, R., *Mechanical Seals*. New York: American Elsevier Publishing, 1969.

114. Meghreblian, R. V. and D. K. Holmes, *Reactor Analysis*. New York: McGraw-Hill, 1960.

115. Micklos, J., Personal Interview. Dayton, Ohio: Representative for General Electric, 18 December 1974.

116. MIL-A-008861A, *Airplane Strength and Rigidity, Flight Loads*. Wright-Patterson Air Force Base, Ohio: 4950th Test Wing, Engineering Standards Division, 31 March 1971.

117. MIL-A-008865A, *Airplane Strength and Rigidity, Miscellaneous Loads*. Wright-Patterson Air Force Base, Ohio: 4950th Test Wing, Engineering Standards Division, 31 March 1971.

118. MIL-A-008870A, *Airplane Strength and Rigidity, Flutter, Divergence, and Other Aeroelastic Instabilities*. Wright-Patterson AFB, Ohio: 4950th Test Wing, Engineering Standards Division, 31 March 1971.

119. MIL-HDBK-5, *Strength of Metal Aircraft Elements*. Washington: Armed Forces Supply Support Center, March 1959.

120. *Military Equipment Cost Analysis*, Office of the Secretary of Defense (Systems Analysis). Santa Monica, California: The Rand Corporation, June 1971.

121. Miller, F. E. and H. A. Doeringfeld, *Mechanics of Materials*. Scranton, Pennsylvania International Textbooks Co., 1963.

122. Mills, K. L., III, *Aircraft Nuclear Propulsion: A New Look in 1971*. Unpublished dissertation: University of Virginia, June 1972.

123. MIL-STD-756A, *Military Standard Reliability Prediction*. Washington: Defense Supply Agency, May 1963.

124. MIL-T-5041F, *Tire, Pneumatic Aircraft*. Wright-Patterson AFB, Ohio: 4950th Test Wing, Engineering Standards Division, 11 November 1971.

125. Moses, F. and D. E. Kinser, "Optimal Structural Design with Probability Constraints," *AIAA Journal*, 5: 152-158. June 1969.

126. Motorola, *SST-131 Beacon Transponder*, Sales Brochure. Scottsdale, Arizona: Motorola Inc., Military Electronics Division.

127. Muehlbauer, J. C., *Nuclear Power For Aircraft*, LG74ER0068. Report, Lockheed-Georgia Co., Marietta, Georgia May 1974.

128. Murphy, Edward L. Jr., *Statistical Methods of Measuring the Uncertainty of Cost Estimates*. Redstone Arsenal, Alabama: U.S. Army Missile Command, February 1970. AD 718862.

129. Murray, R. L. *Introduction to Nuclear Engineering* (Second Edition). Englewood Cliffs, New Jersey: Prentice-Hall, 1961.

130. Nelson, J. R., *Relating Technology to Acquisition Costs: Aircraft Turbine Engines*, R-1288-PR. Santa Monica, California: The Rand Corp., March 1974.

131. Nicolai, L. M., *Design of Airlift Vehicles*. USAFA: Department of Aeronautics, July 1972.

132. Noggle, L. W., Personal Interview, Wright-Patterson AFB, Ohio. USAF/ASD Deputy for Development Planning, May 1974 - March 1975.

133. Northrop Corporation Electronics Division, Sales Brochure AN/ARN-99(V) Omega System. Hawthorne, California, 1974.

134. *Nucleonics Handbook of Nuclear Research and Technology*. New York: McGraw-Hill, Inc., 1965.

135. Numbers, G., Manager-Product Engineering, Telephone Conversation. Miamisburg, Ohio: Mound Laboratory, 1 November 1974.

136. Parker, G. W., Fast Reactor Safety, Nuclear Engineering Division, Telephone Conversation. Oak Ridge, Tennessee, Oak Ridge National Laboratory, 17 December 1974.

137. Peery, D. J., *Aircraft Structures*. New York: McGraw-Hill, 1950.

138. Pennucci, M., Personal Interview. Wright-Patterson AFB, Ohio: Foreign Technology Division, June 1974 - January 1975.

139. Peoples, J. A. and D. Fieno, "Transport Study of Neutron and Photon Attenuation Through Lithium Hydride and Tungsten Spherical Media." Washington: National Aeronautics and Space Administration, January 1969.

140. Pierschka, E., *Principles of Reliability*. New Jersey: Prentice-Hall, 1963.

141. Povejsil, D. L., *et. al.*, *Principles of Guided Missile Design, Vol. VIII: Airborne Radar*. Princeton, New Jersey: D. Van Nostrand Company, Inc., 1961.

142. Proschan F. and T. A. Bray "Optimum Redundancy Under Multiple Constraints," *Operations Research*, 13: 800-814. September-October 1965.

143. Puthoff, R. L., *A 810 FT/SEC Soil Impact Test of a 2-Foot Diameter Model Nuclear Reactor Containment System*, NASA TM X-68180. Cleveland, Ohio: Lewis Research Center, December 1972.

144. Puthoff, R. L., *High Speed Impact Tests of a Model Nuclear Reactor Containment System*, NASA TM X-67856. Cleveland, Ohio: Lewis Research Center, June 1971.

145. Puthoff, R. L., *Post Impact Behavior, Behavior of Mobile Reactor Core Containment Systems*, NASA TMX 68176. Cleveland, Ohio: Lewis Research Center, June 1972.

146. PWA O.I.200, *The Aircraft Gas Turbine Engine and Its Operation*. East Hartford, Connecticut: United Aircraft Corp., 1952.

147. Quayle R. J., *Operations Research in Reliability*, Unpublished Pamphlet. Wright-Patterson AFB, Ohio: Systems Management Departmen' Air Force Institute of Technology, March 1972.

148. Robinson, G. C., "Emergency Cooling Systems in Gas Cooled Reactors", *Nuclear Safety 6:425-432*. Summer, 1965.

149. Robson, F. L., et. al., *Analysis of Nuclear Propulsion and Power Conversion Systems for Large Subsonic Aircraft*. United Aircraft Research Laboratories, 1972.

150. Rockwell, T., *Reactor Shielding Design Manual*. New York: D. Van Nostrand Company, Inc., 1956.

151. Rugger, Robert S. and W. A. Baser, *Performance of a Highly Loaded Two-Stage Axial Flow Fan*. NASA TMX-3076. Cleveland, Ohio: Lewis Research Center, NASA, June 1974.

152. SAMSO-TR-72-283, *Mission Analysis on Air Force Antisubmarine Warfare (ASW) Capabilities*, Vol. VI. Los Angeles, California: AFSC., June 1974.

153. Scott, W. F., Engineer, Telephone Conversation. Albuquerque, New Mexico: Test Engineering Division, Sandia Laboratories, 13 January 1975.

154. Scott, W. F., *Feasibility Study on Fast-Acting Valves for Airborne Nuclear Containment Systems*. Albquerque, New Mexico: Sandia Laboratories, June 1973.

155. Shapiro, A. H., *Compressible Fluid Flow*, Vol. I. New York: Ronald Press, 1953.

156. Shelly, B., Reliability Engineering Department, Telephone Conversation. Marietta, Georgia: Lockheed-Georgia Company, 30 October 1974.

157. Shooman, M. L., *Probabilistic Reliability: An Engineering Approach*. New York: McGraw-Hill, 1968.

158. Singer Kearfott, *SKD-2100 Doppler Radar System*, Sales Brochure. Little Falls, New Jersey: Singer Kearfott Company.

159. Skolnik M. I., *Introduction to Radar Systems*. New York: McGraw-Hill, 1962.

160. Slade, D. H., ed., *Meteorology and Atomic Energy: 1968*, TID-24190. U.S. Atomic Energy Commission, Oak Ridge, July 1968.

161. Smith, D., "Reactor Pressure Vessel Integrity: Heavy Section Steel Technology Vessel Tests," *Nuclear Engineering*, 19:751-757. September 1974.

162. Spivey W. Z., *Comparison of Reliability Allocation Optimization Methods*, Unpublished Thesis. Wright-Patterson AFB, Ohio:, Air Force Institute of Technology, December 1969.

163. Spurrier, F., Personal Interview. Pittsburgh, Pennsylvania: Westinghouse Astronuclear Division, 13 January 1975.

164. Stather, J., Telephone Conversation. Albuquerque, New Mexico: Sandia Laboratories, 7 December 1974.

165. Stehn, J. R., M. D. Goldberg, B. A. Magurno, and R. Weiner-Chasman, "Neutron Cross Sections," BNL 325 (Second Edition), Supplement No. 2, Vol., I, z = 1 to 20. Brookhaven National Laboratory, TID 4500.

166. Stehn, J. R., M. D. Goldberg, R. Weiner-Chasman, S. F. Mughabghab, B. A. Magurno, and V. M. May, "Neutron Cross Sections," BNL 325 (Second Edition), Supplement No. 2, Vol. III, z = 88 to 98. Brookhaven National Laboratory, TID 4500

167. Storm, E. and H. I. Israel, "Photon Cross Sections from 0.001 to 100 Mev for Elements 1 through 100," LA 3753. Los Alamos Scientific Laboratory of the University of California. TID 4500.

168. Streeter, V. L., *Fluid Mechanics*. New York: McGraw-Hill, 1958.

169. Sutherland, W., *Adding Cost Estimates That Are Not Symmetric About the Most Likely Value*. McLean, Virginia: Research Analysis Corporation. AD 883232

170. Tally, B., Telephone Conversation. Wright-Patterson AFB, Ohio: C-5A System Program Office, Aeronautical Systems Division (AFSC), 15 July 1974.

171. Taylor, J. W. R., ed., *Jane's All The World's Aircraft* (1972-73 Edition), London: Paulton House.

172. *Technical Summary Report of NERVA Program*. Phase 1 NRV & XE. Vol. 1. TNR-230, Westinghouse Astronuclear Laboratory, 15 July 1972.

173. Thompson, R. E., Technical Assistant to Manager, Engineering, Westinghouse Astronuclear Laboratory, Correspondence to Dr. L. W. Noggle, 16 July 1974.

174. Thompson, R. E., Technical Assistant to Manager, Engineering, Westinghouse Astronuclear Laboratory, Correspondence to Dr. L. W. Noggle, 8 August 1974.

175. Thompson R. E. and A. R. Hackl, Westinghouse Astronuclear Laboratory, Personal Interview. 9 August 1974.

176. Thompson, R. E., Technical Assistant to Manager Engineering Astronuclear Laboratory Power Systems, Telephone Conversation. Pittsburgh, Pennsylvania: Westinghouse Astronuclear Laboratory, 17 October 1974.

177. Thompson, R. E., Technical Assistant to Manager, Engineering, Astronuclear Laboratory, Telephone Conversation to Dr. L. W. Noggle, 5 February 1975.

178. Thring, M. W., *Nuclear Propulsion*. Washington: Butterworth, Inc., 1960.

179. Timoshenko, S. P. and J. M. Gere, *Mechanics of Materials*. New York: D Van Nostrand Company, 1972.

180. Timoshenko, S. & J. N. Goodier, *Theory of Elasticity* (Second Edition). New York: McGraw-Hill, 1951.

181. Townsley, R., Personal Interview. Wright-Patterson AFB, Ohio: ASD/B-1 Systems Project Officer, 4 October 1974.

182. Turbo-Three Corporation, *Feasibility Study to Consider an Aircraft for the Air Launch and Air Transportation of the Space Shuttle Orbiter*. Goleta, California: Turbo-Three Corporation, May 1974.

183. *USAF Accident Bulletins*, Norton AFB, California. Directorate of Aerospace Safety, 1961-1973.

184. U.S. Atomic Energy Commission, *Evaluation of High Temperature Gas-Reactors*, WASH 1085. Washington: U.S. Atomic Energy Commission, December 1969.

185. U.S. Atomic Energy Commission, *Reactor Safety Study*, WASH-1400. Washington: U.S. Atomic Energy Commission, August 1974.

186. U.S. Bureau of the Census, *Population of Places of 2,500 or More: 1970 and 1960*, PC (SI)-26. Washington: August 1972.

187. U.S. Bureau of the Census, *Statistical Abstract of the United States: 1973* (94th edition). Washington, 1973.

188. Vincent, E. T., *The Theory and Design of Gas Turbines and Jet Engines*. New York: McGraw-Hill Book Co., 1950.

189. Weick, Fred E. *Aircraft Propeller Design*. New York: McGraw-Hill Book Co., 1930.

190. Westinghouse Electric Corp., *Low Specific Weight Powerplant Data*. Letter to Dr. L. W. Noggle, ASD/XRHP, 16 July 1974.

191. Wills, J. G., *Nuclear Power Plant Technology*. New York: John Wiley & Sons, Inc., 1967.

192. Witherell, Capt. R. E., USAF, Design Point Turbine Engine Performance Program. AFAPL-TR68-88. September 1968.

193. Wolf, J. *Aerospace Structural Metals Handbook* (AFML-TR-68-115) Vol. 4. Traverse City, Michigan: Mechanical Properties Data Center, Belfour Stulen, Inc., 1973.

194. Wright, Dr. H. E., Associate Professor of Mechanical Engineering, Department of Aero Mechanical Engineering, Personal Interview. Wright-Patterson AFB, Ohio: Air Force Institute of Technology, School of Engineering, 25 January 1975.